PB85-186492

Modeling of Auto Exhaust Smog Chamber Data for Ekma Development

Systems Applications, Inc., San Rafael, CA

Prepared for

Environmental Protection Agency
Research Triangle Park, NC

Apr 85

U.S. Department of Commerce
National Technical Information Service
NTIS

PB85-186492

EPA/600/3-85/025
April 1985

MODELING OF AUTO EXHAUST SMOG CHAMBER DATA FOR EKMA DEVELOPMENT

by

G. Z. Whitten
J. P. Killus
R. G. Johnson

Systems Applications, Inc.
101 Lucas Valley Road
San Rafael, CA 94903

Contract No. 68-02-3735

Project Officer

Marcia C. Dodge

Atmospheric Chemistry and Physics Division
Atmospheric Sciences Research Laboratory
Research Triangle Park, North Carolina 27711

ATMOSPHERIC SCIENCES RESEARCH LABORATORY
OFFICE OF RESEARCH AND DEVELOPMENT
U.S. ENVIRONMENTAL PROTECTION AGENCY
RESEARCH TRIANGLE PARK, NORTH CAROLINA 27711

REPRODUCED BY
NATIONAL TECHNICAL
INFORMATION SERVICE
U.S. DEPARTMENT OF COMMERCE
SPRINGFIELD, VA. 22161

TECHNICAL REPORT DATA

(Please read Instructions on the reverse before completing)

1. REPORT NO. EPA/600/3-85/025	2.	3. RECIPIENT'S ACCESSION NO. PB85 186492/AS
4. TITLE AND SUBTITLE MODELING OF AUTO EXHAUST SMOG CHAMBER DATA FOR EKMA DEVELOPMENT		5. REPORT DATE April 1985
		6. PERFORMING ORGANIZATION CODE
7. AUTHOR(S) G. Z. Whitten, J. P. Killus, and R. G. Johnson		8. PERFORMING ORGANIZATION REPORT NO.
9. PERFORMING ORGANIZATION NAME AND ADDRESS Systems Applications, Inc. 101 Lucas Valley Road SanRafael, CA 94903		10. PROGRAM ELEMENT NO. CDWA1A/01-1130 (FY-85)
		11. CONTRACT/GRANT NO. Contract 68-02-3735
12. SPONSORING AGENCY NAME AND ADDRESS Atmospheric Sciences Research Laboratory-RTP,NC Office of Research and Development U.S. Environmental Protection Agency Research Triangle Park, North Carolina 27711		13. TYPE OF REPORT AND PERIOD COVERED Final (8/82-7/84)
		14. SPONSORING AGENCY CODE EPA/600/09

15. SUPPLEMENTARY NOTES

16. ABSTRACT

A new generalized mechanism for photochemical smog has been developed. The mechanism is suitable for use in the Empirical Kinetics Modeling Approach (EKMA) to estimate the control of volatile organic compounds that is needed to achieve the National Ambient Air Quality Standard for ozone. The mechanism developed is called the CBM-X, and it is the fourth lumped-parameter mechanism to be designed in accordance with the carbon-bond reaction concept. The principal features that distinguish the CBM-X from previous carbon-bond mechanisms include separating formaldehyde from the other oxygenates, treating toluene separately from the other aromatics and including a more detailed, up-to-date representation of aromatic hydrocarbons chemistry. The CBM-X was tested by comparing the predictions obtained with the mechanism against smog chamber data of dilute auto exhaust/oxides of nitrogen mixtures obtained in the outdoor smog chamber facility operated by the University of North Carolina.

17. KEY WORDS AND DOCUMENT ANALYSIS

a. DESCRIPTORS	b. IDENTIFIERS/OPEN ENDED TERMS	c. COSATI Field/Group

18. DISTRIBUTION STATEMENT RELEASE TO PUBLIC	19. SECURITY CLASS (This Report) UNCLASSIFIED	21. NO. OF PAGES 369
	20. SECURITY CLASS (This page) UNCLASSIFIED	22. PRICE

EPA Form 2220-1 (Rev. 4-77) PREVIOUS EDITION IS OBSOLETE

NOTICE

The information in this document has been funded by the United States Environmental Protection Agency under Contract No. 68-02-3735 to Systems Applications, Inc. It has been subject to the Agency's peer and administrative review, and it has been approved for publication as an EPA document. Mention of trade names or commercial products does not constitute endorsement or recommendation for use.

ABSTRACT

A new chemical kinetics mechanism for modeling photochemical smog has been developed and tested against an extensive smog chamber data base. The mechanism, called the expanded Carbon-Bond Mechanism (CBM-X), is suitable for use in the Empirical Kinetics Modeling Approach (EKMA) to estimate the amount of control of organic compounds needed to achieve the air quality standard for ozone. The CBM-X contains 146 reactions and 65 species and is a hybrid of explicit chemistry, lumped generalized chemistry, and surrogate approximations. Explicit chemistry is used to describe the reactions of the inorganic species, the carbonyls, ethene, toluene and m-xylene. The carbon-bond lumped structure approach is used to treat the reactions of paraffin groups and the carbon double bonds of 1-olefins. Surrogate approximations are used to describe (1) the behavior of internal olefins, which are simulated as a mixture of aldehydes and ketones, (2) mono-alkylated aromatics, which are assumed to react like toluene, (3) highly substituted aromatics, which are assumed to react like m-xylene, and (4) the higher aldehydes, which are assumed to react like acetaldehyde. The individual components of the CBM-X, such as formaldehyde, methylglyoxal, ethene, etc., were independently tested against an extensive smog chamber data base. The complete CBM-X was tested against smog chamber data of dilute auto exhaust/oxides of nitrogen mixtures that were obtained in the modern outdoor chamber facility operated by the University of North Carolina.

CONTENTS

Abstract iii

Figures vii

Tables ix

1 INTRODUCTION 1

- Background 1
- Carbon-Bond Approach 2
- Report Structure 5

2 THE EXPANDED CARBON-BOND MECHANISM 6

- Introduction 6
- The Hierarchical Concept 6
- Specific Features of CBM-X 14
- Summary 16

3 THE INORGANIC AND CARBONYL REACTION SET 17

- Introduction 17
- Photolytic Reactions 21
- Inorganic Chemistry 21
- Carbonyl Chemistry 26
  - Formaldehyde 26
  - Acetaldehyde 31
  - Acetone 35
- Dicarbonyl Chemistry 35
  - Methyl Glyoxal 36
  - Glyoxal 42

Preceding page blank

4 EXPLICIT HYDROCARBONS AND SURROGATE APPROXIMATIONS 43

Introduction 43
Individual Compounds of Importance in Urban Air 43
Ethene Chemistry 53
Aromatics Chemistry 55
Surrogate Approximations 60

5 THE LUMPED STRUCTURE MECHANISM 64

Alkane Chemistry 67
Olefin Chemistry 69
Ketone Chemistry 69
Validation of the Lumped Mechanism 69

6 VALIDATION OF THE EXPANDED CARBON-BOND MECHANISM 71

Introduction 71
UNC Auto Exhaust Data 71
Results 78

7 SUMMARY AND RECOMMENDATIONS 173

References 176

Appendixes

A Simulation Results for UNC Formaldehyde Experiments 183
B Simulation Results for UNC Acetaldehyde Experiments 234
C Simulation Results for UNC Ethene Experiments 274
D Simulation Results for UNC Toluene and M-Xylene Experiments..333

FIGURES

Number		Page
1	Schematic diagram of hierarchical levels of species in photochemical smog	13
2	Plot of Actaldehyde $I \sigma\phi$ products using fluxes and cross sections recommended by Demerjian, Schere, and Peterson (1981) on the quantum yields of Horowitz and Calvert (1982).	32
3	Simulation results for UNCB 70980 assuming formation of peroxyptruvic radical	38
4	Simulation results for UNCB 70980 assuming pyruvyl radical decomposition	40
5	Simulation results for UNCB 100181 assuming formation of peroxypyruvyl	41
6	Simulation results for UNCB 100181 assuming pyruvyl radical decomposition	42
7	Nitrogen and ozone data, both chamber sides	66
8	Simulation results for UNCB 62582	83
9	Simulation results for UNCR 62582	87
10	Simulation results for UNCB 62982	91
11	Simulation results for UNCR 69282	95
12	Simulation results for UNCB 63082	98
13	Simulation results for UNCR 63082	101
14	Simulation results for UNCB 70182	104

Number Page

15 Simulation results for UNCR 70182 107

16 Simulation results for UNCB 71582 110

17 Simulation results for UNCR 71582 113

18 Simulation results for UNCB 80382 116

19 Simulation results for UNCR 80382 120

20 Simulation results for UNCB 91782 123

21 Simulation results for UNCR 91782 127

22 Simulation results for UNCB 92982 130

23 Simulation results for UNCR 92982 133

24 Simulation results for UNCR 100682 136

25 Simulation results for UNCB 700682 139

26 Simulation results for UNCB 70283 143

27 Simulation results for UNCR 70283 146

28 Simulation results for UNCB 71583 149

29 Simulation results for UNCR 71583 152

30 Simulation results for UNCB 81183 155

31 Simulation results for UNCR 81183 158

32 Simulation results for UNCB 100483 161

33 Simulation results for UNCR 100483 164

34 Simulation results for UNCB 100783 167

35 Simulation results for UNCR 100783 170

TABLES

Number		Page
1	The expanded Carbon-Bond Mechanism (CBM-X)	7
2	Species in the ICRS Carbon-Bond Mechanism	18
3	Photolysis reaction rates used in the ICRS relative to NO_2 photolysis	22
4	Ozone photolysis constants of O^{1D} relative to NO_2 photolysis	24
5	Effect of excluding the $O_3 + h\nu \rightarrow O^{1D}$ reaction on calculated EKMA control requirements	25
6	Formaldehyde photolysis ratios to NO_2 as a function of solar zenith angle	27
7	Formaldehyde experiments	29
8	Acetaldehyde experiments	33
9	Compounds for which explicit mechanisms exist	44
10	Ambient hydrocarbon concentrations measured in Los Angeles in 1969	45
11	Ambient hydrocarbons measured in Los Angeles in 1974	46
12	Example of light- and heavier-molecular-weight HC composition in ambient Los Angeles air	48
13	Compound rankings by mass	49
14	Compound rankings by relative OH reaction	50
15	Compound rankings by 12-hour reaction mass	52

Number		Page
16	Species contained in the ethene mechanism	54
17	Ethene experiments	56
18	Species contained in toluene and m-xylene mechanism	58
19	Toluene and m-xylene experiments	61
20	Species involved in the oxidation of paraffin	68
21	Species involved in the oxidation of olefin	70
22	Auto exhaust data for 1982 and 1983 smog chamber experiments	74

SECTION 1

INTRODUCTION

BACKGROUND

For several years, the U.S. Environmental Protection Agency (EPA) has sponsored a coordinated research program consisting of chemical kinetic studies, smog chamber experiments, and kinetic model development. The ultimate goal of this program is to develop air quality simulation models capable of describing the gaseous photochemical reactions that take place in the lower troposphere. As a result of this program, considerable effort has been devoted to the development of reaction mechanisms that describe photochemical air pollution, either through the numerous direct contributions of the EPA program or through the stimulus the program has provided others in this field. Part of this effort has involved the development of chemical kinetics mechanisms for use in the Empirical Kinetic Modeling Approach (EKMA).

The mechanisms currently available for use in EKMA suffer from a number of deficiencies. Some are out of date. One example is the Dodge/EKMA mechanism, which was developed prior to the development of our understanding of the chemistry of aromatics. The Dodge/EKMA mechanism is a detailed or explicit photochemical smog mechanism for the chemistry of propene and butane (Dodge, 1977a), which serve as surrogates for the actual urban mixture. In this mechanism, reactivity was empirically adjusted by arranging the propene/butane ratio so that a series of indoor smog chamber experiments performed in 1968 with auto exhaust emissions could be best simulated (Dodge, 1977b). The original surrogate mechanism and the original empirical propene-to-butane ratio of 1:3 are still in use today. Other available mechanisms were designed for use in sophisticated AQSMs but they are more compact than is needed for use in EKMA. Expansion of these mechanisms for use in EKMA would make it possible to achieve greater realism in the modeling of atmospheric chemistry.

Another shortcoming of existing mechanisms is that none has been validated with a data base representative of the actual urban environment. Most mechanisms have been tested against data collected in indoor smog chambers or in chamber studies that involved the use of surrogate atmospheric mixtures. However, a new data base is now available from experiments in which real auto exhaust was irradiated in an outdoor chamber under realistic conditions. Thirty dual smog chamber experiments were performed in which the hydrocarbon-to-NO_x ratio, concentration, automobile, gasoline fuel, and sample collection method were varied (Jeffries, et al., 1984). The purpose of the study reported here was to utilize these auto exhaust data to develop an improved EKMA mechanism. The design of the mechanism is based, in part, on the carbon-bond condensed reaction concept (Whitten, Hogo, and Killus, 1980). A discussion of this concept and how it differs from other techniques used to condense mechanisms is presented next.

CARBON-BOND APPROACH

Comparison of Available Kinetic Mechanisms

Several hundred organic compounds have been identified in the urban atmosphere (Altshuller and McPherson, 1963; Mayrsohn and Crabtree, 1976). Even if relevant chemical data for each compound were available, the computational requirements of using a detailed kinetic mechanism for each atmospheric species would be prohibitive. Thus, a variety of simplifying assumptions have been used to reduce chemical mechanisms to manageable proportions. Photochemical kinetic mechanisms intended for atmospheric applications can be classified into three types: surrogate mechanisms, lumped molecule mechanisms, and lumped structure mechanisms. Each type of mechanism differs in the nature of the simplifications used to make the complex reaction sequences and multitude of organic compounds involved in urban smog tractable; however, all mechanisms tend to be the same in their explicit treatment of basic inorganic chemistry as derived from review and evaluation studies (Baulch et al, 1982; NASA, 1983; Atkinson and Lloyd, 1984).

Surrogate mechanisms are perhaps the easiest to understand. Mechanisms that explicitly treat every intermediate compound involved in the photochemical smog formation process have been developed from laboratory smog chamber experiments involving individual primary hydrocarbon species. In the surrogate mechanism approach, the explicit mechanisms for one or more hydrocarbons are combined. The complex urban mix is then assumed to be represented by some blend of the hydrocarbons treated by the explicit chemistry. Difficulties with this approach involve the validity of the surrogate blend. The Dodge mechanism used in the present form of EKMA is such a surrogate mechanism and a 25 percent propene/75 percent butane mix is used to simulate automobile exhaust (Dodge, 1977a). (Appropriate mixes for nonautomotive emissions have not been established.)

The lumped molecule approach to kinetic modeling was one of the first methods developed to simplify smog chemistry. Such mechanisms use the approach of Hecht et al. (1974) wherein specific molecular species are averaged into general species such as olefins, paraffins, aldehydes and, usually, aromatics. Rate constants for each generalized hydrocarbon class should, in theory, be some appropriate average rate of the individual compounds contained in each class. However, in practice, these mechanisms usually specify some default value that may or may not approximate the ensemble average. When a default value is used, such mechanisms actually become condensed versions of the surrogate approach.

In general, lumped molecule mechanisms require noninteger stoichiometric parameters to describe reaction pathways for the lumped molecular species and the lumped intermediates generated by the chemistry (Falls and Seinfeld, 1978; Atkinson et al., 1982). The choice of the proper value for the stoichiometric parameters poses a problem that is related to the averaging of rate constants just described. However the stoichiometric parameters that describe the average size and distribution of the lumped species can also affect both reactivity and carbon balance; specification of these parameters to simultaneously satisfy all of these constraints can be difficult, and some lumped mechanisms have been shown to violate the reactive carbon conservation requirement (Whitten, 1982).

The lumped structure approach is an attempt to decouple reactivity and carbon conservation. The concept derives from the work of Benson (1976) in which molecular reactivity is calculated from submolecular components. Thus, in the lumped structure appproach, the carbon structures within the hydrocarbon molecules are the lumping category. For example, one lumped species might be used to represent all the single-bonded carbon atoms that occur in alkanes and other organics such as olefins and substituted aromatics. Another lumped species might be used to represent the carbon-carbon double bond groups that are found in olefins. The lumped structure approach offers several advantages over the lumped molecular approach. Because similar structures have similar reaction rate constants, the averaging problem is minimized. Carbon conservation can be expressly maintained, and carbon balance during the simulation can be monitored. The principal disadvantage is that intramolecular processes such as decomposition can be difficult to treat. Also, because the lumped structure approach is less intuitive than is the lumped molecule approach, extensive documentation is required to enable others to use mechanisms based on lumped structure approach.

Description of the Carbon-Bond Formulation

Chemists and physicists have known for some time that most properties of larger molecules can be roughly considered to be made up of additive contributions from the individual atoms or bonds in the molecule. The physical basis of such an empirical finding appears to be that the forces between atoms in the same or different molecules are very "short range"; that is, they are appreciable only over distances of the order of 0.1 to 0.3 nm (Benson, 1976; Benson and Bass, 1958). Benson and Bass (1958) have shown that it is possible to describe many molecular properties using a hierarchical system of additivity laws in which the simplest- or "zeroth-order" law would be the law of additivity of atom properties. In an atom-additivity scheme, one assigns partial values for the property in question to each atom in the molecule. The molecular property is thereby the sum of all the atom contributions.

For a property such as molecular weight, the "zeroth-order" law is precise, and the carbon-conservative nature of the Carbon-Bond formulation is thereby intrinsically guaranteed. However, molecular reactivity is a higher-order approximation and can best be described at the level of molecular bonds or groups. It is this level of approximation that forms the kinetic basis of the Carbon-Bond approach. Consider, for example, the reactivity of alkanes. Greiner (1970) has shown that the overall reaction rate of alkanes with OH can be calculated by summing the individual reactivities of primary, secondary, and tertiary carbon-hydrogen bonds. Thus, one possible formulation using the Carbon-Bond approximation would be to treat primary, secondary, and tertiary bond structures individually in the mechanism.

The Carbon-Bond approach has several important advantages over the lumped molecule approach. It is expressly conservative of reactive carbon, and does not require the cumbersome notion of "average molecular weight" that has caused difficulty in the application of lumped molecular mechanisms (Atkinson and Lloyd, 1984). Furthermore, use of the Carbon-Bond approach permits easy calculation of carbon mass balance during simulations (Killus and Whitten, 1984), whereas such calculations can only be approximated using some other mechanisms.

The second important advantage afforded by the Carbon-Bond approach is a considerable reduction in the range of reaction-rate constants that must be covered for each of the lumped hydrocarbon species that use an appropriate average rate constant. This is true for paraffins, in which isobutane has a molecular reaction-rate constant with OH of 5000 $\text{ppm}^{-1}\,\text{min}^{-1}$, and isooctane has a reaction rate of 11,500 $\text{ppm}^{-1}\text{min}^{-1}$. These reactivity rates, normalized to the number of carbon atoms per molecule, are 1250 $ppm^{-1}min^{-1}$ and 1440 $ppm^{-1}min^{-1}$, respectively. The relative difference between these two numbers is thus much smaller than the relative difference in the molecular reaction rates. The Carbon-Bond approach also offers a practical means of accounting for the atmospheric chemistry of many complex or unusual molecules such as styrene (an olefin plus an aromatic) or 1-octene (an olefin plus an alkane).

Carbon-Bond Mechanism Development

Three versions of the Carbon-Bond Mechanism (CBM-I, Whitten et al., 1980; CBM-II, Stewart and Liu, 1981; and CBM-III, Killus and Whitten, 1984) deriving from the Carbon-Bond approach have been developed by the EPA for use in sophisticated Air Quality Simulation Models (AQSM). However, as noted, the chemical reactions in these versions are very condensed. A mechanism designed for use in EKMA applications does not need to be this condensed. Consequently, the goal of the work reported here was to develop an expanded Carbon-Bond Mechanism (CBM-X) for use in EKMA and to validate this expanded mechanism with newly available auto exhaust smog chamber data.

REPORT STRUCTURE

In Section 2, we describe the expanded Carbon-Bond Mechanism (CBM-X) developed in this study and discuss its general features. The remaining sections discuss the individual components of the mechanism and present the experimental studies used to validate these components. In particular, Section 3 discusses the inorganic and carbonyl portions of the mechanism and the simulations conducted to validate the individual mechanisms for formaldehyde, acetaldehyde, glyoxal, and methylglyoxal. Section 4 discusses hydrocarbons that are treated explicitly in the mechanism, namely, ethene, toluene, and m-xylene; Section 4 also includes a discussion of hydrocarbons in the CBM-X that are treated by surrogate approximations. Section 5 describes the development of the generalized lumped structure mechanism for treating the remainder of urban and auto exhaust organics. Section 6 discusses the validation studies conducted to test the full CBM-X mechanism. Our summary and conclusions are presented in Section 7. Appendixes A through D, respectively, present results for simulation of smog chamber experiments for formaldehyde, acetaldehyde, ethene, and m-xylene and toluene.

2 THE EXPANDED CARBON-BOND MECHANISM

INTRODUCTION

The expanded Carbon-Bond Mechanism (CBM-X) developed in this study has a hierarchical structure. Its central "core," i.e, the basis of the hierarchy, consists of a set of inorganic reactions plus the reactions of the carbonyl species that are central to most photooxidation systems. This "core" reaction set is called the Inorganic and Carbonyl Reaction Set (ICRS) and is the basis of all of our mechanism development studies (Whitten, 1983). The details of the ICRS are described in Section 3; reactions in this core set are the first 79 reactions in Table 1. The remainer of the CBM-X is made up of various organic reaction subsets that either (1) describe specific hydrocarbons (namely ethene, toluene, and m-xylene) important in urban atmospheres, or (2) describe in condensed form the chemistry of other hydrocarbons (or hydrocarbon structures) also considered important in urban atmospheres. The hydrocarbon components of the CBM-X are described in Sections 4 and 5; their chemistry is represented by Reactions 80-146 of Table 1.

THE HIERARCHICAL CONCEPT

The hierarchical approach to mechanism development was first outlined for a series of mechanisms in Whitten et al. (1979); a more recent description is contained in Whitten (1983). The most important objective of this approach is the minimization of compensating errors in the final overall smog mechanism. Also, the approach allows each of the organic components of the mechanism to be developed and validated independently. Figure 1 is a schematic illustration of the hierarchical structure of the CBM-X.

A reactions set such as the ICRS, which includes both carbonyl and inorganic smog reactions, is in itself a complete reaction scheme that can be independently tested against smog chamber data. As discussed by Whitten (1983), such a reaction scheme contains all the essential components required to generate photochemical ozone in the lower troposphere. These essential components include nitrogen oxides, a hydrogen-containing radical source, and a means of converting OH radicals to HO_2,

Table 1. The expanded Carbon Bond Mechanism (CBM-X).

	REACTIONS[a]		RATE CONSTANTS[b]	ACTIVATE ENERGY (K)[c]
1	NO_2	$= NO + 0$	vary	
2	$0 + 0_2 + M$	$= 0_3 + M$	2.22×10^{-5}	-690.
3	$0_3 + NO$	$= NO_2$	26.6	1430.
4	$0 + NO_2$	$= NO$	13800.0	
5	$0 + NO_2 + M$	$= NO_3 + M$	0.00232	-600.
6	$0 + NO + M$	$= NO_2 + M$	0.00312	-411.
7	$NO_2 + 0_3$	$= NO_3$	0.0474	2450.
8	0_3	= 01D	vary	
9	0_3	= 0	$0.042 \times k_1$	
10	01D + M	= 0 + M	42900.0	-100.
11	01D + H_20	= OH + OH	326000.0	
12	$0_3 + OH$	$= HO_2$	100.0	940.
13	$0_3 + HO_2$	= OH	3.0	580.
14	$NO_3 + NO$	$= NO_2 + NO_2$	28100.0	-250.
15	$NO_3 + NO_2$	$= NO + NO_2$	0.59	1230.
16	$NO_3 + NO_2 + M$	$= N_20_5 + M$	0.00178	60.
17	$N_20_5 + H_20$	$= HNO_3 + HNO_3$	1.9×10^{-6}	
18	$N_20_5 + M$	$= NO_3 + NO_2 + M$	3.12×10^{-6}	10840.
19	$NO + NO_2 + H_20$	$= HNO_2 + HNO_2$	1.6×10^{-11}	
20	$HNO_2 + HNO_2$	$= NO + NO_2 + H_20$	1.5×10^{-5}	
21	HNO_2	= NO + OH	$0.18 \times k_1$	
22	$NO_2 + OH + M$	$= HNO_3 + M$	0.0163	-560.
23	$NO + OH + M$	$= HNO_2 + M$	0.00977	-427.
24	$HO_2 + NO$	$= OH + NO_2$	12300.0	-240.
25	$NO + NO + 0_2$	$= NO_2 + NO_2$	7.28×10^{-10}	-530.
26	H_20_2	= OH + OH	0.0014	
27	$OH + H_20_2$	$= HO_2$	2520.0	187.
28	$OH + HNO_2$	$= NO_2$	9770.0	
29	$OH + HNO_3$	$= NO_3$	192.0	-778.

Table 1 (continued)

			ACTIVATE	
	REACTIONS[a]		RATE CONSTANTS[b]	ENERGY (K)[c]
30	NO_3	$= NO_2 + O$	$26.0 \times k_1$	
31	NO_3	$= NO$	$4.6 \times k_1$	
32	$HO_2 + HO_2$	$= H_2O_2$	4144.0	-1150.
33	$HO_2 + HO_2 + H_2O$	$= H_2O_2 + H_2O$	0.218	-5800.
34	$HO_2 + NO_2 + M$	= PNA + M	0.00163	-617.
35	PNA + M	$= HO_2 + NO_2 + M$	5.12×10^{-6}	10420.
36	OH + CO + M	$= HO_2 + M$	0.0004	
37	$FORM + HO_2$	= FROX	14.8	
38	FORM + OH	$= HO_2 + CO$	15000.0	
39	FORM	$= HO_2 + HO_2 + CO$	vary	
40	FORM	= CO	vary	
41	FORM + O	$= OH + HO_2 + CO$	237.0	1550.
42	$FORM + NO_3$	$= HNO_3 + HO_2 + CO$	0.93	
43	FROX + NO	$= FACD + NO_2 + HO_2$	10400.0	
44	FROX	$= HO_2 + FORM$	90.0	
45	ALD2 + O	$= C_2O_3 + OH$	636.0	986.
46	ALD2 + OH	$= C_2O_3$	24000.0	-250.
47	$ALD2 + NO_3$	$= C_2O_3 + HNO_3$	3.7	
48	ALD2	$= MEO_2 + HO_2 + CO$	vary	
49	$ALD2 + HO_2$	$= MEO_2 + FORM$	5.0	
50	$C_2O_3 + NO$	$= MEO_2 + NO_2$	16500.0	-250.
51	$C_2O_3 + NO_2$	= PAN	9000.0	-250.
52	PAN	$= C_2O_3 + NO_2$	0.0222	14000.
53	$MEO_2 + NO_2 + M$	= MPNA + M	0.006	-735.
54	MPNA + M	$= MEO_2 + NO_2 + M$	9.2×10^{-5}	10400.
55	$MEO_2 + NO$	$= MEO + NO_2$	11000.0	-180.
56	MEO + NO	= MNIT	44400.0	-200.
57	MEO + NO	$= FORM + HO_2 + NO$	1920.0	
58	$MEO + NO_2$	= MEN3	22200.0	
59	$MEO + O_2$	$= FORM + HO_2$	1.88	1313.

Table 1 (continued)

			ACTIVATE	
	REACTIONS^a		RATE CONSTANTS^b	ENERGY (K)^c
60	MEN3 + OH	= FORM + NO_2	2220.0	360.
61	MNIT + OH	= FORM + NO	2370.0	340.
62	MNIT	= MEO + NO	$0.3 \times k_1$	
63	MEO_2 + MEO_2	= MEO + MEO	175.0	-220.
64	MEO_2 + MEO_2	= FORM + MEOH	328.0	-220.
65	MEO_2 + C_2O_3	= MEO + MEO_2	4400.0	
66	C_2O_3 + C_2O_3	= MEO_2 + MEO_2	3700.0	
67	MEO_2 + HO_2	= PROX	8900.0	-1300.
68	C_2O_3 + HO_2	= PROX	9600.0	
69	AONE	= MEO_2 + C_2O_3	$0.00004 \times k_1$	
70	AONE + OH	= ANO_2	580.0	
71	ANO_2 + NO	= NO_2 + FORM + C_2O_3	12000.0	
72	GLY	= CO + CO	$0.0052 \times k_1$	
73	GLY	= CO + FORM	$0.0016 \times k_1$	
74	GLY	= HO_2 + HO_2 + CO + CO	0.0007	
75	GLY + OH	= HO_2 + CO + CO	15000.0	
76	MGLY	= C_2O_3 + HO_2 + CO	$0.02 \times k_1$	
77	MGLY + OH	= MGPX	26000.0	
78	MGPX + NO	= C_2O_3 + NO_2	12000.0	
79	OH + M	= MEO_2	2.1×10^{-5}	
80	PAR + OH	= RO_2	150.0	
81	PAR + OH	= RO_2R	1000.0	
82	RO_2 + NO	= NO_2 + HO_2 + ALD2 + X	12000.0	
83	RO_2R + NO	= NO_2 + ROR	12000.0	
84	RO_2R + NO	= NTR	1000.0	
85	ROR + NO_2	= NTR	22000.0	
86	ROR	= KET + HO_2	150000.0	
87	ROR	= ALD2 + D + X	90000.0	7000.
88	ROR	= AONE + D + X + X	240000.0	
89	X + PAR	=	10000.0	

Table 1 (continued)

	REACTIONS[a]		RATE CONSTANTS[b]	ACTIVATE ENERGY (K)[c]
90	D + PAR	= RO_2	3000.0	
91	D + PAR	= AO_2 + X + X	7000.0	
92	D + KET	= C_2O_3 + X	10000.0	
93	AO_2 + NO	= NO_2+ HO_2 + AONE	12000.0	
94	KET	= C_2O_3 + RO_2 + X + X	0.0003 x k_1	
95	O + OLE	= MEO_2 + C_2O_3 + X	300.0	324.
96	O + OLE	= RO_2 + HO_2 + CO + X	880.0	324.
97	O + OLE	= ALD2	4740.0	324.
98	OH + OLE	= MEO_2 + ALD2 + X	42000.0	-537.
99	O_3 + OLE	= ALD2 + CRIG + X	0.0054	1897.
100	O_3 + OLE	= FORM + MCRG + X	0.0054	1897.
101	O_3 + OLE	= ALD2 + HOTA + X	0.0036	1897.
102	O_3 + OLE	= FORM + HTMA + X	0.0036	1897.
103	NO_3 + OLE	= PNO_2	11.4	
104	O + ETH	= MEO_2 + HO_2 + CO	1080.0	800.
105	OH + ETH	= MEO_2 + FORM	12000.0	-382.
106	O_3 + ETH	= FORM + CRIG	0.001	2840.
107	O_3 + ETH	= FORM + HOTA	0.0017	2840.
108	HOTA		25.0	
109	HOTA	= CO	58.0	
110	HOTA	= HO_2 + HO_2	10.0	
111	HOTA	= FACD	7.0	
112	HTMA		200.0	
113	HTMA	= MEO_2 + CO + OH	400.0	
114	HTMA	= MEO_2 + HO_2	320.0	
115	HTMA	= HO_2 + CO + FORM + HO_2	80.0	
116	CRIG + NO	= FORM + NO_2	10000.0	
117	CRIG + NO_2	= FORM + NO_3	1000.0	
118	CRIG + H_2O	= FACD	0.006	
119	CRIG + FORM	= OZD	30.0	

Table 1 (continued)

	REACTIONS[a]		RATE CONSTANTS[b]	ACTIVATE ENERGY (K)[c]
120	CRIG + ALD2	= OZD	30.0	
121	MCRG + NO	= ALD2 + NO_2	10000.0	
122	MCRG + NO_2	= ALD2 + NO_3	1000.0	
123	MCRG + H_2O	= ACAC	0.006	
124	MCRG + FORM	= OZD	30.0	
125	MCRG + ALD2	= OZD	30.0	
126	PNO_2 + NO	= DNIT	1000.0	
127	PNO_2 + NO	= NTR + HO_2 + NO_2	10000.0	
128	TOL + OH	= OPEN + GLY	5500.0	
129	TOL + OH	= PHEN + HO_2 + PAR	3500.0	
130	TOL + OH	= BO_2	750.0	
131	OPEN + NO	= NO_2 + HO_2 + MGLY + GLY	10000.0	
132	PHEN + NO_3	= PHO + HNO_3	14000.0	
133	BZA + OH	= BZO_2	20000.0	
134	BZO_2 + NO_2	= PBZN	2500.0	
135	BZO_2 +NO	= NO_2 + PHO_2 + CO	3700.0	
136	BO_2 + NO	= NO_2 + BZA + HO_2	12000.0	
137	PBZN	= BZO_2 + O_2	0.022	14000.
138	BZA	= PROD	0.004 x k_1	
139	PHO + NO_2	= NPHN	20000.0	
140	PHO_2 + NO	= NO_2 + PHO	12000.0	
141	XYL + OH	= XYLO	2000.0	
142	XYLO + NO	= NO_2 + HO_2 + TLA	12000.0	
143	TLA + OH	= TLO_2	20000.0	
144	TLO_2 + NO	= NO_2 + PHO + PAR + PAR	4000.0	
145	XYL + OH	= HO_2 + PHEN + PAR + PAR	10000.0	
146	XYL+ OH	= OPEN + MGLY	24000.0	

Table 1 (concluded)

[a] The species used are listed separately in Tables 2, 16, 18, 20, and 21.

[b] All rate constants are in appropriate ppm and min units at 298K and one atmosphere of air. That is, all unimolecular and photolysis reactions (+ hν) are in units of min^{-1}, all bimolecular reactions are in units of ppm^{-1} min^{-1}, and all ter-molecular reactions are in units of ppm^{-2} min^{-1}. Rate constants designated by the term "vary" are defined in Table 3.

[c] The numbers listed are Arrhenious temperature coefficients in degrees Kelvin for B in the expression $k_T = k_{298} \exp(B \times \frac{1}{298} - \frac{1}{T})$

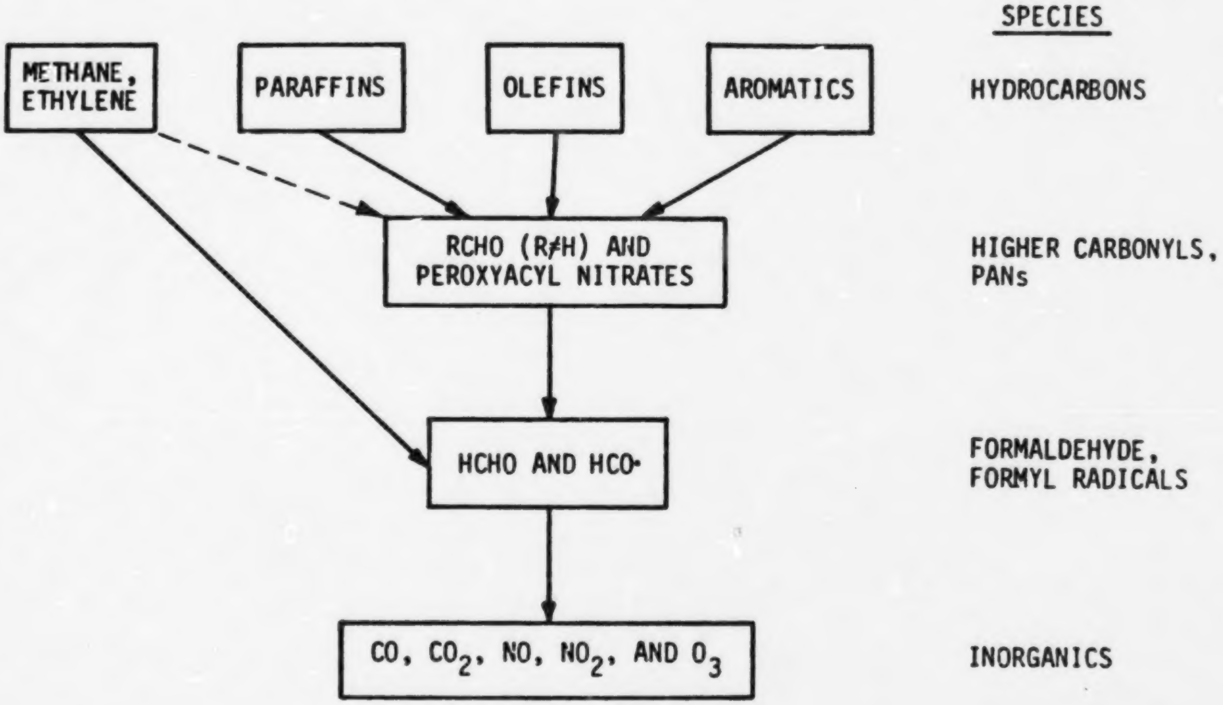
SPECIES
METHANE, ETHYLENE
PARAFFINS
OLEFINS
AROMATICS
HYDROCARBONS
RCHO (R≠H) AND PEROXYACYL NITRATES
HIGHER CARBONYLS, PANs
HCHO AND HCO·
FORMALDEHYDE, FORMYL RADICALS
CO, CO2, NO, NO2, AND O3
INORGANICS

Figure 1. Schematic diagram of hierarchical levels of species in photochemical smog

which, in turn, converts NO to NO_2 and OH, completing a chain process. Hence, smog chamber experiments containing only a nitrogen oxide and one or more of the five carbonyls included in the ICRS (formaldehyde, acetaldehyde, acetone, glyoxal, and methylglyoxal) will generate photochemical ozone at rates sufficiently above background levels to test this ICRS or any other inorganic-plus-carbonyl scheme.

The use of smog chamber data to test only an overall mechanism such as the complete CBM-X of this particular study leaves open the question of compensating errors. For example, an incorrect treatment of aromatics chemistry might be compensated for by incorrect treatment of the dicarbonyl products formed from aromatics (Tuazon et al., 1984). However, independent smog chamber experiments containing a dicarbonyl as the only organic have been performed and successfully simulated using the ICRS of Table 1. Thus, the chemical scheme for the dicarbonyls must be close to "reality," at least as a package. Of course, errors can still exist in the yield of these highly reactive dicarbonyls from aromatics. However, we now know that any other products that might be formed appear to have a similar reactivity to the dicarbonyls. Therefore, the excess dicarbonyls (if any) can, for the time being, serve as a surrogate for other compounds that might be forming from the aromatics chemistry.

The hierarchical approach is also helpful in explicit mechanism development for specific organic species. For example, in the development of an explicit scheme for isoprene, the chemistry of intermediate compounds such as methacrolein and methyl vinyl ketone were identified (Killus and Whitten, 1984). As a result, smog chamber experiments using methyl vinyl ketone or methacrolein as the only organic were requested by Killus and Whitten (1984b) and were subsequently performed at the University of North Carolina (UNC) smog chamber and simulated using the ICRS and reactions specific to these organics. Hence, intermediate levels in the hierarchy are associated with the chemistry of intermediate organic products, and these subsets of the overall chemistry can be independently tested.

SPECIFIC FEATURES OF THE CBM-X

In keeping with the hierarchical approach just outlined, the overall CBM-X mechanism assembled in Table 1 is organized into the following subsets:

Inorganic Chemistry

Reactions 1 through 36 have been selected to describe the atmospheric chemistry of species that contain only oxygen, nitrogen, and hydrogen atoms, plus one reaction involving CO.

Common Carbonyl Chemistry

Reactions 37 through 78 describe the detailed chemistry for the common carbonyl compounds of formaldehyde, acetaldehyde, acetone, glyoxal, and methylglyoxal. Reaction 79 describes the chemistry of methane. Since methane in the atmosphere does not decay from a constant level of 1.6 ppm, the concentration of methane has been lumped into the rate constant. These 79 reactions provide enough overall chemistry to generate photohemical ozone and PAN; therefore, this set can be independently tested against smog chamber experiments. Section 3 describes the development of this reaction set and describes some of these tests.

Paraffinic or Single-Bonded Carbon Chemistry

Reactions 80 through 94 are intended to describe a typical mixture of paraffins from butane to decane. The single-bonded constituents of other types of molecules, such as olefins and aromatics, are also treated as the one-carbon PAR species.

Olefin Chemistry

Reactions 95 through 127 constitute the subset of reactions specific to molecules containing double bonds. Since such molecules can have a wide range of reactivity, the atmospheric mix of olefins in the CBM-X is treated in three different ways. Ethene, which is the least reactive of the olefins, is treated explicitly. The ethene mechanism has no significant condensation except for the elimination of the pathway to glycolaldehyde and its subsequent chemistry. The glycolaldehyde yield from the OH attack on ethene appears to be about 22 percent (Niki et al., 1981). Elimination of this pathway is equivalent to assuming the alternative products to be equal in reactivity to glycolaldehyde. The accuracy of this assumption is not clear at this time since smog chamber data for glycolaldehyde are not yet available.

Terminal olefins such as propene are of intermediate reactivity and are handled in condensed form via the species OLE. OLE is a two-carbon lumped structure species that represents the carbon bond found in 1-olefins.

Highly reactive olefins such as those with internal double bonds (e.g., cis-2-butene) are treated by assuming that they have already reacted in the atmosphere to two higher aldehydes (i.e., 2 ALD2). This condensation has been successfully demonstrated in Whitten et al. (1979) and was recommended for use with the first version of the Carbon-Bond Mechanism (Whitten et al., 1980).

Aromatics Chemistry

Reactions 128 through 146 provide a moderately condensed treatment of aromatic hydrocarbons. As recommended by Whitten et al. (1985), two levels of reactivity based on toluene chemistry (Killus and Whitten, 1982) and m-xylene chemistry (Killus and Whitten, 1983) are used. The toluene chemistry is used to represent the mono-substituted benzenes (toluene, ethylbenzene, propyl-benzenes, etc.), whereas the m-xylene chemistry is used to represent the highly reactive multiple-substituted benzenes (xylenes, ethyltoluenes, trimethylbenzenes, etc.).

SUMMARY

The mechanism shown in Table 1 can be used to model the entire atmospheric mix of organics. Also, because the mechanism is grouped into components, it is fairly adaptable to substitution, updates, and additions. That is, the chemistry of natural hydrocarbons such as α-pinene or isoprene (Killus and Whitten, 1984) might be added to the CBM-X. Similarly, a newer version of aromatics chemistry might be substituted for this subset. However, any updates and substitutions should be accompanied by a revalidation procedure to ensure the fidelity of the precautions taken in the development of the present CBM-X to minimize compensating errors between the various subsets and between each subset and the basic ICRS set.

SECTION 3

THE INORGANIC AND CARBONYL REACTION SET

INTRODUCTION

The Inorganic and Carbonyl Reaction Set (ICRS) used in this study is composed of the first 79 reactions presented in Table 1. These 79 reactions describe the inorganic and carbonyl chemistry common to virtually all urban conditions leading to the generation of photochemical smog. The species contained in the ICRS are given in Table 2. The ICRS reactions are based on and are consistent with all reactions recommended for consideration in reviews of atmospheric models (e.g., Atkinson and Lloyd, 1984). No condensation techniques have been employed in this set of reactions other than the commonly used technique of eliminating the rapid, noncompetitive addition and displacement reactions of molecular oxygen with such radical species as hydrogen atoms or formyl radicals. Detailed explicit inorganic and carbonyl chemistry is also used in other complete mechanisms such as that of Atkinson et al. (1982).

Conceivably, the ICRS presented here might be exchanged, modified, or updated independently from the overall CBM-X Mechanism. Each ICRS reaction given in Table 1 has been carefully reviewed and independently studied under laboratory conditions using a variety of techniques. Many of these laboratory conditions were far removed from those typical of the atmosphere, but usually included conditions as close as possible to the pressure, light flux, and oxygen content of the lower troposphere. Such a wide range of conditions and experimental techniques helps to verify the chemical reaction rate constant and reaction product yields recommended by reviewers because data taken from diverse conditions can be compared and evaluated using thermodynamic and kinetic theories.

Because the ICRS contains all the components necessary to generate photochemical smog, as described in Section 2 and in Whitten (1983), this overall set of reactions has itself been subjected to an extensive validation procedure involving the successful computer modeling of a large number of smog chamber experiments using both simulated and natural sunlight. This part of the validation process insures that any inadequacies in the estimation, laboratory measurement, and review evaluations of its

TABLE 2. Species in the ICRS Carbon-Bond Mechanism.

Symbol	Definition
NO_2	--
NO	--
NO_3	--
N_2O_5	--
HNO_2	--
HNO_3	--
PNA	HO_2NO_2
O	O(3P)
O^{1D}	--
O_2	--
O_3	--
M	$O_2 + N_2$
MNIT	CH_3ONO
MEN3	CH_3ONO_2
MPNA	CH_3OONO_2
PAN	$CH_3CO_3NO_2$
OH	--
HO_2	--
H2O2	--
H_2O	--
FORM	HCHO
MEO2	CH_3O_2
MEO	CH_3O
MEOH	CH_3OH
CO	--
FROX	HO_2CH_2O
ALD2	CH_3CHO
C2O3	CH_3CO_3
PROX	CH_3CO_3H
FACD	Formic acid
AONE	Acetone
ANO_2	$CH_3C(O)CH_2O_2$
GLY	Glyoxal
MGLY	Methylglyoxal
MGPX	$CH_3(CO)CO_3$

individual reactions (1) are likely to be of negligible importance and (2) are not cumulative under conditions close to those for which the chemical reaction mechanism is to be utilized. Thus, extrapolations necessary for atmospheric studies are founded on as firm a basis as is technically possible.

Such a firm foundation for the ICRS is essential because it is the basis for our hierarchical approach to mechanism development. The ICRS is stored on our computer system in a special file used for all simulations involving explicit chemistry, the CBM-X, or subsets of the CBM-X such as an olefin-only simulation. For example, if we were evaluating the condensed subset for ethene in the CBM-X, we would compare the performance of this subset with an even more expanded explicit subset containing all reactions considered relevant to ethene chemistry. Both sets of simulations would use the same ICRS file to treat the inorganic and common carbonyl parts of the overall chemistry required to describe ethene/NO_x smog chamber experiments.

The ICRS is also used to assess chamber effects. Such effects must be considered when attempting to model data from any chamber facility. Although the magnitude of chamber artifact effects is a controversial topic (Killus and Whitten, 1981; Carter et al., 1982), a series of smog chamber experiments have been designed to test various aspects of these effects using the ICRS. These include

> Nitrogen Oxide Offgassing: Acetaldehyde by itself (usually at a concentration of 1 ppmC) is injected into the chamber. The production of PAN observed in this supposedly NO_x-free system can usually be simulated with the ICRS, using a small zero-order reaction to describe the release from the walls of NO, NO_2, or a nitrogen oxide precursor such as HNO_2.
>
> Organic Reactivity: A nitrogen oxide (preferably NO at a concentration of 0.5 ppm) is injected into the chamber. Observations of the conversion of NO to NO_2 indicate the presence of peroxy radicals and/or hydroxy radicals. The peroxy radicals can arise from organics that are present in the pure air system used to fill the chamber or they can arise from the offgassing of organics from the chamber walls. In most cases, the background organic reactivity can be simulated using the ICRS and a zero or first-order reaction that "bleeds in" formaldehyde. The experiment might often include trace organics such as propane and propene to monitor OH levels (Carter et al., 1982). As a result of this additional information on OH levels, the use of formaldehyde as the only surrogate for organic reactivity may not be justified; however, usually some additional organic such as acetaldehyde (ALD_2) can adequately simulate the observed data.

These data often include PAN observations, in which case acetaldehyde can be even more useful to supplement the formaldehyde surrogate.

Radical Sources: The nitrogen-only experiments for organic reactivity are supplemented by similar experiments in which 50 to 100 ppm CO is added. Organic reactivity stems from a combination of peroxy radical generation (usually from OH attack) and a means of producing hydrogen-containing radicals (usually from photolysis of secondary carbonyl products). The addition of CO to the organic background test supplants the peroxy radical generation component and enhances our ability to model chamber effects. In the presence of NO in air, essentially any hydrogen-containing radical will eventually lead to the production of a hydroxyl radical through a series of radical transfer reactions. A moderately high CO level ensures that (1) the termination reaction of OH with NO_2 is suppressed and (2) a chain reaction sequence is repeated between OH + CO and HO_2 + NO, giving rise to several conversions of NO to NO_2. Hence, the CO acts like an amplifier to enhance the detection of any chamber-derived radicals. Again, radical sources in these runs can be simulated assuming the presence of an organic source such as HCHO and an NO_x source such as HNO_2. This combination, with an occasional use of some extra acetaldehyde, has proved quite successful in simulating the chamber effects of several smog chambers.

The chamber effects (added HNO_2, formaldehyde, and, occasionally, acetaldehyde) are used in conjunction with smog chamber data to validate the various components of the CBM-X. In most cases, the simulated chamber effects play a minor role in the overall computer model tests. The main problem in dealing with chamber effects occurs when they are not constant from experiment to experiment.

A final note regarding the general features of the ICRS and its use in mechanism development concerns updates or adjustments. The ICRS has been used to simulate a wide range of experiments in several chambers involving "clean air," carbon monoxide, nitrogen oxides, formaldehyde, acetaldehyde, methylglyoxal, acetone, and all available combinations of these species. The validation set also encompasses several years of experiments over wide ranges of seasons, temperatures, sky conditions, humidity, and precursor concentrations. Therefore, one of the reactions in the ICRS cannot be altered to improve the agreement between a simulation and some particular experiment without a serious consideration of the effect of such a change in the ICRS on the overall validation system of which it is the core.

The remainder of this section will be devoted to a detailed discussion of the characteristics of the ICRS. Because photolytic reactions play an essential role in this core mechanism, they will be discussed first.

PHOTOLYTIC REACTIONS

Photolytic reactions require special treatment; their reaction rates differ from chamber to chamber. In outdoor chambers or in the atmosphere, their reaction rates also vary as a function of zenith angle. Photolytic reactions in the ICRS are treated in two ways:

> Some photolysis reactions are known to vary with zenith angle in a fashion similar to that of NO_2. For these reactions, the photolytic rate constants can be expressed as some multiple of the rate constant for NO_2 photolysis (Reaction 1). The species in the ICRS that are assumed to photolyze in a manner similar to NO_2 are HNO_2, H_2O_2, NO_3, MNIT, AONE, GLY, and MGLY (Reactions 21, 26, 30, 31, 62, 69, 72, 73, and 76). In addition, the photolysis of O_3 to $O(^3P)$ atoms (Reaction 9) is also expressed as a multiple of the photolytic constant for NO_2.
>
> The rates of some photolytic reactions, however, are known to vary with zenith angle in a fashion that is not similar to NO_2. Significant errors would be introduced into the mechanism if a constant ratio to k_1 were used to describe these photolytic processes. The species in the ICRS whose photolysis ratios relative to NO_2 are assumed to vary with zenith angle are formaldehyde, acetaldehyde, and O_3 photolysis to O^{1D}--Reactions 8, 39, 40, and 48. The photolysis ratios relative to NO_2 that should be used for these reactions as a function of zenith angle are given in Table 3.

Some of the more interesting of the photolytic processes will be discussed in greater detail in subsequent portions of this section.

INORGANIC CHEMISTRY

Reactions 1 through 36 in Table 1 constitute the inorganic chemistry subset; the reactions and the rate constants given in Table 3 are taken from the work of Atkinson and Lloyd (1984), the only exceptions occurring in the presentation of photolysis rate constants and in NO_3 chemistry. Kerr and Calvert (1985) have recently reevaluated a series of NO_3 reactions, and their recommended values are used. Atkinson and Lloyd (1984) provide evaluated cross-section and quantum yield information for the various species that photolyze in sunlight. In many cases their recommendations are also used in the ICRS. One of the exceptions to the

TABLE 3. Photolysis reaction rates used in the ICRS relative to NO_2 photolysis.

Zenith Angle	ALD2 + hν → MEO2 + HO2 + CO	FORM + hν → CO	FORM + hν → HO2 + CO	O_3 + hν → O^{1D}
0	6.44E-4	2.71E-3	3.76E-3	4.66E-3
10	6.24E-4	2.70E-3	3.75E-3	4.55E-3
20	6.05E-4	2.61E-3	3.70F-3	4.16E-3
30	5.40E-4	2.48E-3	3.60E-3	3.53E-3
40	4.73E-4	2.28E-3	3.46E-3	2.77E-3
50	3.74E-4	2.01E-3	3.26E-3	1.92E-3
60	2.74E-4	1.64E-3	2.99E-3	1.11E-3
70	1.91E-4	1.25E-3	2.59E-3	4.76E-4
78	1.08E-4	9.15E-4	2.29E-3	2.10E-4
86	5.40E-5	6.90E-4	2.18E-3	1.12E-4

Atkinson and Lloyd (1984) review, however, is the photolysis of ozone to the excited oxygen atom species O^{1D}. We discuss that photolysis reaction next.

O_3 Photolysis

In Table 4 we present some O^{1D} formation photolysis rate constants for ozone photolysis relative to NO_2 photolysis as a function of zenith angle. The values listed in this table have been used by various modelers to describe O^{1D} formation in the atmosphere. The considerable spread in the rate constant listed here reflects the current uncertainty regarding the rate of O^{1D} production. The values shown for Atkinson et al. (1982) were derived from information contained in McRae et al. (1983) by assuming that the reaction of O^{1D} with air is much faster than the O^{1D} reaction with H_2O; the appropriate rate constant ratio between these reactions is that given by NASA (1983). The Killus and Whitten (1984) values are actually 0.53 times those given by Schere and Demerjian (1977). The values shown for this work in Table 4 were calculated as follows:

> Actinic fluxes were taken from Peterson (1976) for the "best estimate of surface albedo."
>
> Quantum yields and absorption cross sections of O^{1D} formation were those recommended by NASA (1983).
>
> Quantum yields and absorption cross sections of NO_2 photolysis were also those recommended by NASA (1983).
>
> The resulting integrated photolysis constant ratios were then multiplied by a factor of 1.4 to bring the numbers up to the measured values of Bahe et al. (1979).

However, the measurements of Bahe et al. (1979a) were absolute photolysis constants for O^{1D} only. Unfortunately, Bahe et al. published neither the overall corrected photon fluxes (which they measured) nor the simultaneous NO_2 photolysis constants.

In our previous work, we found O^{1D} formation and subsequent OH generation to be relatively unimportant to chemical mechanism results. However, during this project we have been testing the effects of various mechanism subprocesses on control strategy results. Our findings have been surprising: small mechanistic differences can often have significant effects on control predictions. Table 5 demonstrates the sensitivity of three different mechanisms to O^{1D}--the Dodge/EKMA mechanism and two versions of the CBM-III.

TABLE 4. OZONE PHOTOLYSIS CONSTANTS TO O^{1D} RELATIVE TO NO_2 PHOTOLYSIS.*

Zenith Angle (degrees)	This Work	Killus and Whitten (1984)	Penner and Walton (1982)	Atkinson Lloyd and Winges (1982)	Demerjian et al. (1980)	Schere and Demerjian (1977)
0	4.66	3.86	5.29	5.47	5.14	7.28
10	4.55	3.79	5.15	5.33	5.03	7.16
20	4.16	3.54	3.80	4.95	4.62	6.67
30	3.53	3.13	4.03	4.30	4.03	5.91
40	2.77	2.59	3.17	3.39	3.25	4.89
50	1.92	1.96	2.21	2.47	2.35	3.69
60	1.11	1.26	1.25	1.56	1.46	2.38
70	0.48	0.66	0.47	0.81	0.73	1.25
78	0.21	0.31	0.17	0.39	0.34	0.58
86	0.11	0.15	0.10	0.17**	0.26	0.28

* All values multiplied by 1000

** Listed for 84 degrees instead of 86 degrees

TABLE 5. Effect of excluding the $O_3 + h\nu \rightarrow O^{1D}$ reaction on calculated EKMA control requirements

Case	Predicted NMOC Control Needed (%)
Dodge Chemistry	
With O^{1D}	45.4
Without O^{1D}	36.2
CBM-III (1982)*	
With O^{1D} at full Schere and Demerjian (1977)	54.8
Without O^{1D}	34.7
CBM-III/EKMA (1984)*	
With O^{1D}	38.0
Without O^{1D}	23.7

---

* The CBM-III/EKMA (1984) is the current and updated version of condensed Carbon-Bond chemistry used in EKMA and is nearly half the size of the CBM-X (Killus and Whitten, 1984). The CBM-III (1982) is an earlier version (Killus and Whitten, 1982).

In the simulations presented here, the EKMA procedure was used for a hypothetical case to estimate the percent reduction in NMOC that would be needed to reduce O_3 from a level of 0.17 ppm to the air quality standard of 0.12 ppm. With each mechanism the simulation was first run assuming that O_3 does photodissociate to O^{1D}. This photolysis pathway was then removed and the simulation was repeated. As shown in Table 5, all three mechanisms show strong sensitivity to the radical source derived from O^{1D} and H_2O.

CARBONYL CHEMISTRY

Formaldehyde

Formaldehyde represents the simplest precursor of photochemical smog. It also is an intermediate product in the oxidation of almost all organics. Our ICRS contains eight reactions (Reactions 37-44) involving formaldehyde: reaction with hydroxyl, oxygen atoms, NO_3, and HO_2, two photolysis reactions, and two reactions of an intermediate species. The main decay pathway for formaldehyde in typical urban atmospheres is the reaction with hydroxyl. However, the photolysis of formaldehyde is much more important to overall smog chemistry because one of the photolysis pathways involves the generation of radicals. These radicals can drive the overall oxidation of all organics. The NO_3 reaction may be most important during nighttime simulations.

Table 6 presents the formaldehyde photolysis constants now in use for atmospheric modeling. Note that the current photolysis values are roughly two-thirds of those recommended by Demerjian et al. (1980). However, the recent study by Bass et al. (1980) indicates that the cross sections for formaldehyde used by Demerjian et al. (1980) should be multiplied by two-thirds. The previous cross sections used by Demerjian et al., as well as many others, were measured by Calvert et al. (1972) at 353 K. The new values by Bass et al. (1980) were measured at 223 K and 296 K and show a pronounced temperature effect. A previous study of important wavelengths (Whitten et al., 1979) showed that formaldehyde photolysis peaks at about 320 nm when the product of the cross section, quantum yield, and solar flux is considered. Hence the new cross-section data at 320 nm suggest that the Demerjian et al. (1980) rate constants for formaldehyde should be multiplied by two-thirds. Furthermore, the resultant photolysis rate

TABLE 6 . FORMALDEHYDE PHOTOLYSIS RATIOS TO NO_2 AS A FUNCTION OF SOLAR ZENITH ANGLE. *

Solar Zenith Angle (deg.)	$HCHO + h\nu \rightarrow H_2 + CO$ Ratio to $NO_2 + h\nu$		$HCHO + h\nu \rightarrow H\cdot + HCO\cdot$ Ratio to $NO_2 + h\nu$	
	This Work	Demerjian et al.	This Work	Demerjian et al.
0	3.76	5.55	2.71	4.20
10	3.75	5.53	2.70	4.17
20	3.70	5.45	2.61	4.05
30	3.60	5.31	2.48	3.85
40	3.46	5.09	2.28	3.56
50	3.26	4.78	2.01	3.15
60	2.99	4.29	1.64	2.61
70	2.59	3.74	1.25	2.03
78	2.29	3.28	0.91	1.53
86	2.18	2.96	0.69	1.16

* All values multiplied by 1000.

constants in the simulations of the formaldehyde experiments reported here provide the best agreement with UNC data.

The set of formaldehyde photolysis rate constants used are important because they represent a key link between smog chamber modeling and atmospheric modeling, i.e., the photolysis constants that best represent outdoor chambers can be used in atmospheric models. This link is made possible by a successful modeling of outdoor formaldehyde chamber runs and the fact that NO_2 photolysis constants are available for both the smog chamber and the atmosphere.

Our recent upward adjustment in the formaldehyde photolysis constants has two main implications: (1) the new numbers are in excellent agreement with the adjusted values of Demerjian et al. (1980), based on the new cross sections of Bass et al. (1980), and (2) the new numbers imply fewer chamber-dependent radical sources. In previous simulations of the formaldehyde set of experiments for this project, higher levels of chamber-dependent radicals were assumed via some extra amount of formaldehyde presumed to desorb from the walls and then photolyze.

Initial conditions for the UNC formaldehyde experiments modeled in this study are shown in Table 7a. Our simulations of these experiments are presented in Appendix A. It was possible to simulate all these experiments with the ICRS component of the CBM-X. However, some of the simulations required steps for simulating the loss and reappearance of formaldehyde to and from the condensed water on the chamber walls.

Performance data for these experiments are shown in Table 7b. The overall average difference between simulated and observed ozone maxima is +40 ppb ozone. However, most of this positive bias is due to two high-formaldehyde experiments performed in September of 1978. Without these two experiments, the overall bias is only +14 ppb. Since the average observed ozone maximum for this series of experiments was 580 ppb, the 40 and 14 ppb absolute bias actually imply about 7 percent and 2.5 percent relative bias, respectively. There was no significant bias in the time to ozone maxima on the overall average. The standard deviation between observed and simulated time to ozone maxima was about 22 minutes.

The successful modeling of the UNC formaldehyde experiments was an important step in the validation of the ICRS because it is composed of reactions measured and evaluated independently elsewhere. This ICRS mechanism (inorganic reactions plus the formaldehyde reactions) forms the basic set of reactions central to smog chemistry. Virtually all other mechanisms that characterize the atmospheric photochemistry of organics involve this mechanism.

TABLE 7. Formaldehyde experiments.

(a) Initial Conditions

Date/Side	Formaldehyde	ALD2	Wall* Formaldehyde	Wall ALD2	O_3	NO	NO_2	HONO*	H_2O	CO	NX*
81178R	0.00		0.052		0.0065	0.0	0.014	0.0	20K	0.3	0.01
81178B	0.00		0.06		0.007	0.0	0.016	0.0	20K	0.3	0.015
81478R	0.07		0.07		0.0	0.512	0.02	0.002	20K	0.3	0.0
81478B	0.07		0.07		0.0	0.52	0.01	0.002	20K	49.4	0.0
51877B	0.35	0.02	0.9	0.15	0.0	0.285	0.080	0.004	20K	0.3	
71877R	1.18		0.0		0.0	0.38	0.141	0.02	8.2K	0.3	
72777R	0.60	0.02	0.6			0.388	0.164	0.0005	20K	0.3	
72877R	1.05		0.2			0.37	0.163	0.001	18K	0.3	
72877B	2.25		0.1			0.37	0.171	0.001	10K	0.3	
91477R	0.90		0.3			0.293	0.103	0.006	20K	0.2	
91477B	1.15		0.1		0.027	0.0	0.001	0.0	20K	0.2	0.015
91977R	0.50		0.9			0.3	0.084	0.01	20K	0.27	
91977B	0.40		0.65			0.3	0.086	0.008	20K	0.3	
90878R	0.10		3.2			0.817	0.151	0.004	21.2K	0.4	
90878B	0.10		1.0			0.761	0.155	0.010	20.2K	0.42	
91978B	2.08		0.10			0.570	0.118	0.0	10.8K	0.3	
91578B	1.40		0.7	0.011		0.211	0.057	0.0005	8.2K	0.45	
92178B	2.02		0.0			0.19	0.067	0.0	14K	0.45	
73079R	1.45		0.05			0.218	0.067	0.0	20K	15.75	
73079B	1.55		0.05			0.219	0.067	0.0	20K	0.3	
73179R	0.40		1.03	0.05		0.407	0.106	0.008	20K	0.35	
80179B	1.01		0.05	0.10		0.279	0.076	0.0	10K	0.32	
80274B	1.00		0.04	0.05		0.157	0.058	0.0	21K	0.4	
80479B	0.48		0.14			0.17	0.063	0.0	10K	0.41	
80579B	0.60		0.6			0.407	0.014	0.001	15K	0.34	
81280R	0.80	0.05	0.07	0.07		0.371	0.106	0.011	20K	0.09	

continued

84188r5

TABLE 7. (concluded)

(b) Comparisons of Simulations and Experiments

Date/Side	Initial NO_x (ppm)	Initial NO_2/NO_x Ratio	Initial HC/NO_x ppmC/ppm	Maximum O_3 (ppm)		Difference in O_3 Maxima	Time to Maximum O_3 (min)		Difference in Time to O_3 Maxima (min
				Simulated	Measured		Simulated	Measured	
81178R	0.014	1.000	0.00	0.65	0.58	0.07	> 420	> 420	-
81178B	0.016	1.000	0.00	0.79	0.72	0.07	> 560	> 560	-
81478R	0.532	0.038	0.13	0.004	0.001	0.003	-	-	-
81478B	0.530	0.019	0.13	0.04	0.02	0.02	500	500	0
51877B	0.365	0.219	0.96	0.84	0.74	0.10	535	535	0
71877R	0.521	0.271	2.26	0.47	0.65	-0.18	500	> 640	-
72777R	0.552	0.297	1.09	0.57	0.60	-0.03	620	580	40
72877R	0.533	0.306	1.97	0.57	0.59	-0.02	610	640	-30
72877B	0.541	0.316	4.19	> 1.25	1.05	-	400	360	40
91477R	0.396	0.260	2.27	0.59	0.62	-0.03	530	540	-10
91477B	0.001	1.000	1150.00	0.34	0.34	0.00	540	540	0
91977R	0.384	0.219	1.30	0.60	0.60	0.00	> 480	> 480	-
91977B	0.386	0.223	1.04	0.38	0.39	-0.01	> 480	> 480	-
90878R	0.968	0.156	0.10	1.35	1.28	0.07	510	450	60
90878B	0.916	0.169	0.11	0.04	0.02	0.02	490	510	-20
91978B	0.688	0.172	3.02	1.01	1.15	-0.14	450	390	60
91578B	0.268	0.213	5.22	0.95	0.47	0.48	465	465	0
92178B	0.257	0.261	7.86	1.02	0.74	0.28	420	420	0
73079R	0.275	0.244	5.27	> 1.00	0.72	-	-	460	-
73079B	0.276	0.243	5.62	0.88	0.67	0.21	400	440	-40
73179R	0.513	0.207	0.78	0.75	0.68	0.07	> 600	> 600	-
80179B	0.355	0.214	2.85	0.70	0.62	0.08	> 560	520	-
80279B	0.215	0.270	4.65	0.70	0.61	0.08	405	400	5
80479B	0.233	0.270	2.06	0.35	0.38	-0.03	> 640	> 640	-
80579B	0.421	0.033	1.43	0.49	0.51	-0.02	> 640	> 640	
81280R	0.477	0.222	1.68	0.38	0.40	-0.02	> 720	> 720	-

Acetaldehyde

Acetaldehyde and its associated species, PAN, methyl peroxy radicals, etc., is represented by Reactions 45 to 68 in the CBM-X mechanism. It includes reactions of acetaldehyde with OH, NO_3, O, and HO_2, as well as the photolysis of acetaldehyde to free radical species. The photolysis scheme we are using is based on recent results of Horowitz and Calvert (1982), who reported quantum yields for three primary processes:

$$CH_3CHO + h\nu \xrightarrow{O_2} CH_3O_2 + HO_2 + CO \qquad (I)$$

$$\rightarrow CH_4 + CO \qquad (II)$$

$$\xrightarrow{O_2} CH_3CO_3 + HO_2 \qquad (III)$$

Process I was found to be the predominant pathway. For example, at 313 nm, Horowitz and Calvert reported quantum yields for Processes I, II, and III, respectively, of 0.924, 0.018, and 0.055. Because Processes II and III were found to be of much less importance than Process I, only Process I was included in the ICRS.

On the basis of the quantum yields reported by Horowitz and Calvert, photolytic rate constants were calculated for Process I. Figure 2 shows the narrowness of the light spectra where the photolysis reaction occurs. Because of this narrowness, it is difficult to accurately derive photolytic rate constants based on reported quantum yield data at selected wavelengths. We found that it was necessary to include an additional factor of 1.8 over the calculated values of Horowitz and Calvert in order to generate sufficient radicals to simulate the UNC acetaldehyde experiments. This factor of 1.8 over the Horowitz and Calvert values is included in the photolysis values for acetaldehyde that are listed in Table 3.

The initial conditions used to simulate the UNC acetaldehyde runs are given in Table 8a. A representative set of simulations for this data set is shown in Appendix B. The need to use almost a factor of 2 over the recommendations of Horowitz and Calvert (1982) for acetaldehyde photolysis is most apparent in the dual smog chamber experiments performed on

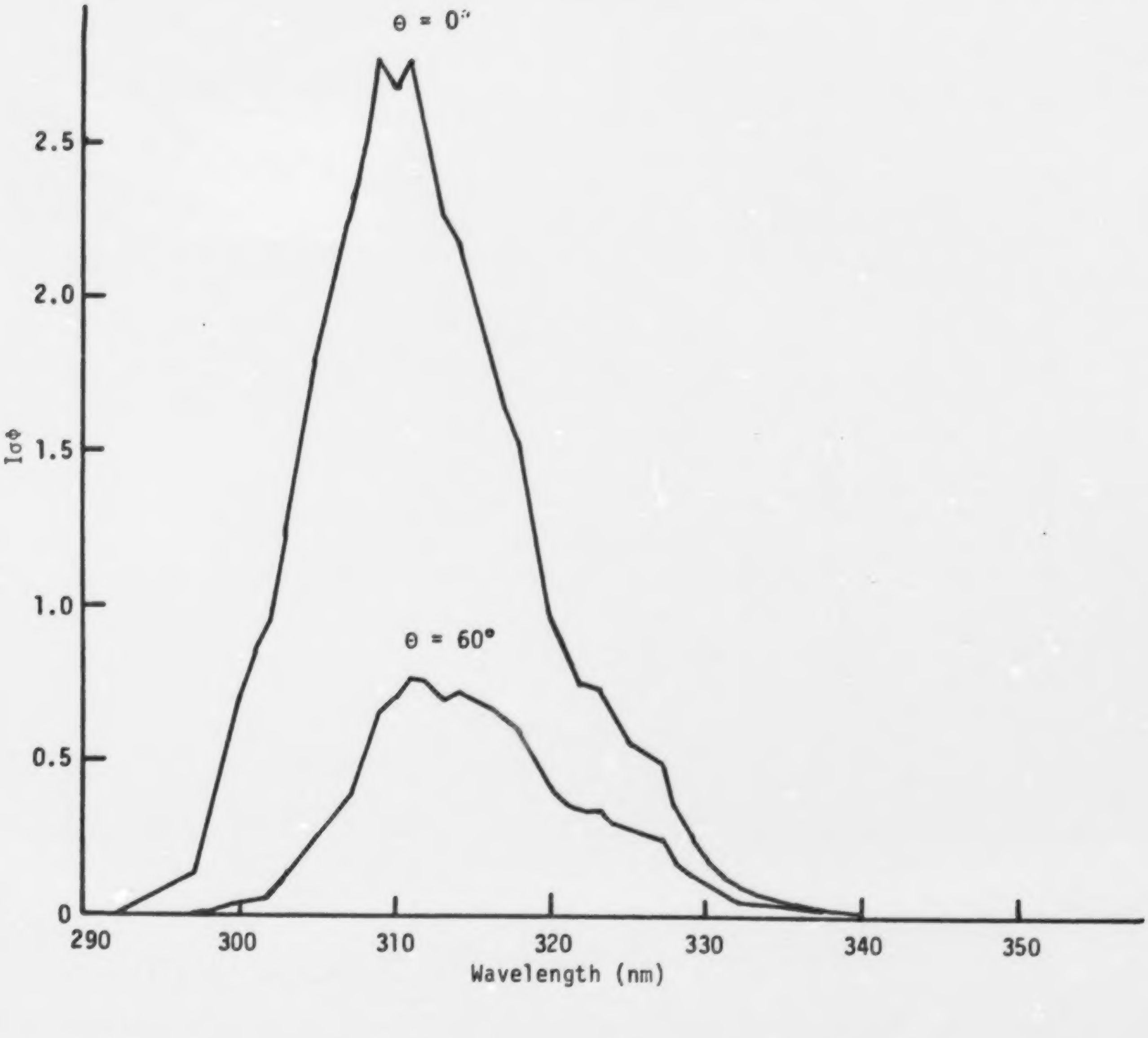

FIGURE 2. Plot of Acetaldehyde IσΦ products using fluxes and cross sections recommended by Demerjian, Schere, and Peterson (1980) on the quantum yields of Horowitz and Calvert (1982). I = light flux, σ = cross section, Φ = quantum yield, and Θ = zenith angle.

TABLE 8. Acetaldehyde experiments.

(a) Initial Conditions

Date	Beginning Temperature (K°)	Sky Conditions	Beginning Time	Acetal-dehyde	NO	NO_2	HONO*	H_2O	FORM*	CO	O_3	NX*	Ethene	Wall* Formal-dehyde
51877R	297	Clear	6:00	0.94	0.285	0.076	0.006	2.0×10^4	0.05	0.0	0.0017	0.00	0.00	0.01
71877B	303.5	Cloudy	6:08	0.50	0.385	0.152	0.015	2×10^4	0.10	0.45	0.0	0.00	0.00	0.15
111277B	269.4	Cloudy	7:44	0.86	0.340	0.122	0.001	3400	0.00	0.00	0.00	0.00	0.00	0.00
111977B	270.8	Cloudy	7:45	1.94	0.40	0.11	0.002	4400	0.15	0.25	0.0	0.0	0.0	0.10
112077B	272.3	Clear	7:30	1.96	0.775	0.170	0.002	5800	0.15	0.25	0.00	0.00	0.00	0.15
122677B	266.7	Cloudy	8:09	1.80	0.273	0.118	0.00	5700	0.0	0.25	0.0	0.0	0.0	0.0
22778B	264.6	Cloudy	8:00	0.960	0.268	0.087	0.00	1.2×10^4	0.0	0.22	0.00	0.00	0.00	0.0
30678B	270.6	Cloudy	7:36	0.900	0.291	0.0775	0.005	1.4×10^4	0.10	0.25	0.0	0.00	0.00	0.15
33178B	273.5	Overcast	6:48	1.000	0.338	0.0615	0.00	2×10^4	0.07	0.25	0.0	0.00	0.00	0.0
80878R	294.9	Cloudy	6:20	0.455	0.406	0.114	0.010	2×10^4	0.07	0.25	0.00	0.00	0.00	0.10
80878B	294.9	Cloudy	6:20	1.900	0.43	0.103	0.010	2×10^4	0.07	0.25	0.00	0.00	0.00	0.10
81778B	294.8	Cloudy	6:40	2.00	0.614	0.094	0.015	1.5×10^4	0.15	0.35	0.00	0.00	0.00	0.0
81778R	294.8	Cloudy	6:40	0.480	0.614	0.092	0.015	1.5×10^4	0.15	0.35	0.00	0.00	0.00	0.0
101378R	283.1	Cloudy	7:13	0.400	0.38	0.114	0.002	1.5×10^4	0.07	0.300	0.00	0.00	0.00	0.07
101378B	283.1	Cloudy	7:13	1.040	0.772	0.126	0.006	1.51×10^4	0.02	0.300	0.00	0.00	0.00	0.1
72179R	294.8	Cloudy	5:40	1.00	0.00	0.010	0.005	2.9×10^4	0.07	0.00	0.02	0.08	0.00	0.07
72179B	294.8	Cloudy	5:40	0.94	0.00	0.015	0.005	2.9×10^4	0.07	0.00	0.02	0.120	0.00	0.07
80179R	299.3	Clear	6:32	0.940	0.274	0.088	0.005	3.3×10^4	0.01	0.40	0.00	0.00	0.00	0.00
80880R	294.5	Clear	6:18	1.00	0.325	0.098	0.012	1×10^4	0.08	0.00	0.00	0.00	0.00	0.15
101278R	280.2	Clear	7:24	0.630	0.368	0.110	0.002	2×10^4	0.00	0.300	0.00	0.00	0.099	0.03
102578R	272.9	Clear	7:14	0.580	0.344	0.100	0.002	2×10^4	0.03	0.500	0.00	0.00	0.096	0.00
81679B	287.1	Overcast	6:40	0.600	0.302	0.136	0.002	1×10^4	0.03	0.270	0.00	0.00	0.082	0.03

* These chamber effects were used to optimize agreement between data and simulations; see text for further discussion. NX is amount of NO_x offgassing from chamber walls.

TABLE 8. (concluded)

(b) Comparisons of Simulations and Experiments

Date/Side	Initial NO_x (ppm)	Initial NO_2/NO_x Ratio	Initial HC/NO_x (ppmC/ppm)	Maximum O_3 (ppm)		Difference in O_3 Maxima (ppm)	Time to Maximum O_3 (min)		Difference in Time to O_3 Maxima (min)
				Simulated	Measured		Simulated	Measured	
51877R	0.361	0.211	5.21	0.92	0.92	0.00	650	650	0
71877B	0.537	0.283	1.86	0.66	0.72	-0.06	640	640	0
111277B	0.462	0.264	3.77	0.02	0.05	0.03	480	450	30
111977B	0.510	0.216	7.61	0.19	0.18	0.01	470	470	0
112077B	0.945	0.180	4.15	0.04	0.06	-0.02	480	480	0
122677B	0.391	0.302	9.21	0.07	0.04	0.03	490	470	20
22778B	0.355	0.245	5.41	0.15	0.15	0.00	540	540	0
30678B	0.368	0.211	4.89	0.26	0.26	0.00	560	590	-30
33178B	0.400	0.154	5.00	0.52	0.52	0.00	> 640	> 640	-
80878R	0.520	0.219	1.75	0.49	0.51	-0.02	> 640	> 640	-
80878B	0.533	0.193	7.13	1.05	1.06	-0.01	640	640	0
81778B	0.708	0.133	5.65	0.21	0.18	0.03	640	640	0
81778R	0.706	0.130	1.36	1.10	1.30	-0.20	560	560	0
101378R	0.394	0.298	2.03	0.08	0.08	0.00	540	470	70
101378B	0.898	0.140	2.32	0.10	0.14	-0.04	540	470	70
72179R	0.010	1.000	200.0	0.40	0.36	0.04	650	660	-10
72179B	0.015	1.000	125.0	0.48	0.46	0.02	650	650	0
80179R	0.362	0.314	5.19	1.05	0.90	0.15	> 560	> 560	-
80880R	0.423	0.227	4.73	0.87	1.04	-0.17	630	630	0
101278R	0.478	0.230	2.64	0.24	0.26	-0.02	560	540	20
102578R	0.444	0.225	2.61	0.13	0.14	-0.01	540	530	10
81679B	0.438	0.311	2.74	0.52	0.54	-0.02	670	675	-5

8 August 1978, 17 August 1978, and 13 October 1978 (80878-R; 80878-B; 81778-R; 81778-B; 101378-R; 101378-B). Each of these dual experiments compared high and low concentrations of acetaldehyde. Care was taken to use similar background assumptions for both sides of the chamber in these paired experiments. If the photolysis rates for acetaldehyde had been set lower than the 1.8 factor used, the high concentration side of these experiments would have been too unreactive. Then, if the assumed background levels had been raised to simulate the high concentration sides, the low concentration sides would have been too reactive. The factor of 1.8 can also be used with assumed background levels similar to those that were used to model the formaldehyde series of experiments.

The rapid decrease in acetaldehyde photolysis with increasing zenith angle allowed us to adequately simulate the temperature extremes seen in this data set. In this case, we can compare the "cold" experiments of 26 December 1977 and 27 February 1978 (122677-B; 22778-B) with the "warm" experiments of 8 August 1978 and 1 August 1979 in Appendix B. We note, however, that the winter/cold experiments are only marginally simulated using minimal or zero assumed background conditions (there are almost too many radicals), whereas the summer/warm experiments are marginally simulated using quite high levels of assumed background reactivity.

Performance data for the simulations presented in Appendix B are shown in Table 8b. The overall average difference is only -10 ppb, which indicates little bias. The standard deviation from an average observed ozone of 450 ppb is about 70 ppb, or about a 15 percent deviation. The timing of the ozone maximum is, on average, within 10 minutes of the observation.

Acetone

Acetone chemistry in the ICRS is described by Reactions 69-72. It includes photolysis, reaction with OH to form a peroxy-type radical (ANO_2), and reaction of the ANO_2 radical with NO to form FORM + C_2O_3.

DICARBONYL CHEMISTRY

The carbonyl species, HCHO and CH_3CHO, are produced during the photooxidation of all alkanes and olefins. For this reason, they are included in the ICRS. However, an additional set of carbonyl species is required for simulations involving aromatic compounds. Although many trace compounds have been identified in aromatic systems, two of the more important products of aromatic ring opening appear to be methylglyoxal and glyoxal. Smog chamber data are available for methylglyoxal, and we have validated a mechanism for this species, whereas our mechanism for glyoxal must be considered speculative since chamber data for this species are not available.

Dicarbonyl chemistry in the CBM-X is represented by Reactions 72-78. The first four reactions describe the chemistry of glyoxal (GLY). The next three reactions describe the chemistry of methyl glyoxal (MGLY). A detailed discussion of the mechanisms developed for these two dicarbonyls is presented next.

Methyl Glyoxal

The formation and photolysis of methyl glyoxal (also known as pyruvic aldehyde) is central to current mechanisms for the photooxidation of aromatic hydrocarbons such as toluene and xylene. Recently, Bessemer (1982) reported the results of several irradiation experiments, including an experiment in which methylgloxal ($\approx$ 5 ppmv) was irradiated (K_D for $NO_2 \approx 0.25\ min^{-1}$) with 0.25 ppm NO_x. Bessemer reported no formation of O_3 or PAN; on the basis of this observation, he appears to conclude that methylgloxal does not photolyze to radicals.

Our criticisms of the experimental conditions used by Bessemer (1982) have been noted elsewhere (Killus and Whitten, 1983). In our simulation of the UNC methylglyoxal runs, it became clear that the photolysis of methylgloxal (1 - 1.5 ppmC) under atmospheric conditions at moderate-to-high levels of NO_x (0.4 - 0.7 ppm) does produce large amounts of O_3 and PAN. The methylgloxal used in the UNC experiments was specifically tested for biacetyl contamination (Kamens 1983, private communication) and none was found. Other possible contaminants, e.g., methane, acetaldehyde, and acetone (Orchard, 1969), are not reactive enough to generate the large radical fluxes observed in the experimental systems. Moreover, the background reactivity of the UNC facility has been well characterized (Whitten, et al. 1983) and is far too low to explain the reactivity of methylgloxal. Thus, contaminant effects, as suggested by Bessemer and Nieboer (1983), do not explain the observed intense reactivity of methylglyoxal experiments.

The reaction included in the CBM-X mechanism to describe the photolysis of methylglyoxal is

$$CH_3(CO)HCO + h\nu \xrightarrow{2O_2} CH_3CO_3 + HO_2 + CO$$

We assume that this reaction proceeds at a rate equal to 0.02 times NO_2 photolysis. This is the rate reported by Plum et al. (1983). Only photolysis-to-radical products are included in the ICRS. The 20 percent yield of acetaldehyde noted by Bessemer (1982) may occur; however, its effect on the overall methylglyoxal photochemistry is negligible in much the same way that the photolysis of formaldehyde to stable products (H_2 and CO) is of minor importance in propene and butane chemistry (Carter et al., 1979).

We also use the published value of Plume et al. (1983) for the reaction of methylglyoxal with OH. This is 2.4 times greater than the previously reported value of Kleineinst et al. (1982) and 3.7 times greater than the value used in one of our previous mechanisms (Killus and Whitten, 1982). Prior mechanisms for methylglyoxal oxidation (Atkinson et al., 1980; Killus and Whitten, 1982) assumed the formation and decomposition of the pyruvyl radical,

$$CH_3(CO)HCO + OH \rightarrow CH_3(CO)CO\cdot \text{ (pyruvyl)},$$

$$CH_3(CO)CO\cdot \rightarrow CO + CH_3(CO)\cdot \text{ (acetyl)},$$

and the subsequent formation of peroxyacetyl. The scheme we chose to include in our mechanisms is

$$CH_3(CO)CO\cdot + O_2 \rightarrow CH_3(CO)CO_3 \text{ (peroxypyruvyl)}$$

$$CH_3(CO)CO_3 + NO \rightarrow NO_2 + CO_2 + CH_3CO.$$

The peroxypyruvyl radical is denoted as MGPX in the ICRS. The effect of the peroxypyruvyl radical is to produce an additional conversion of NO to NO_2 (thereby increasing the ozone yield) and to form CO_2 instead of CO. Both of these features are apparent in the UNC data. If the pyruvyl radical is assumed to decompose, CO formation from methylglyoxal is overpredicted; however, if the peroxypyruvyl radical is formed, CO production is more correctly predicted.

Representative simulations for two of the UNC methylglyoxal experiments are shown in Figures 3 and 5. Figures 4 and 6 show the effect of simulating these experiments if the products of the methylglyoxal + OH

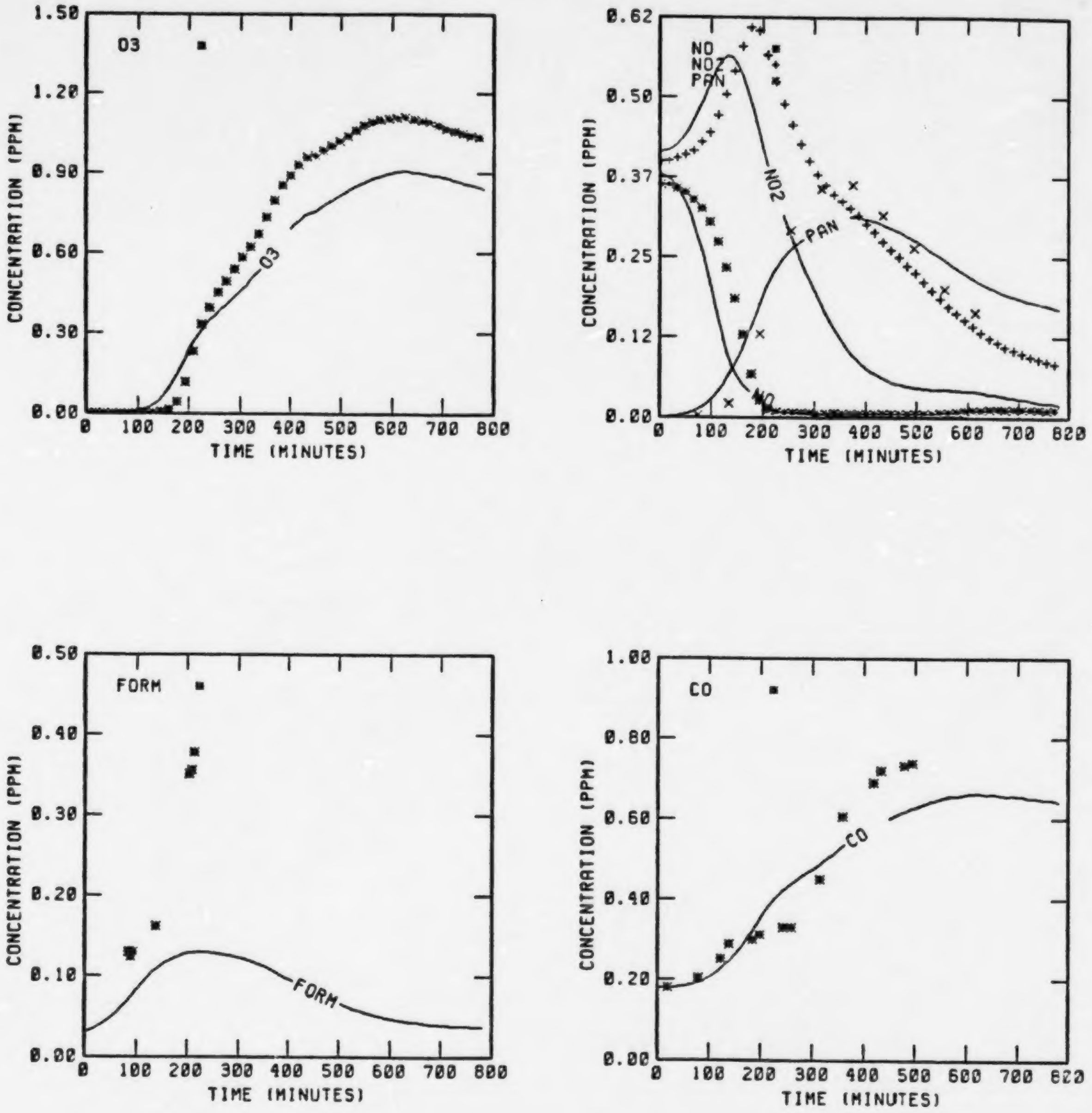

FIGURE 3. SIMULATION RESULTS FOR UNCB 70980 ASSUMING FORMATION OF PEROXYPYRUVIC RADICAL

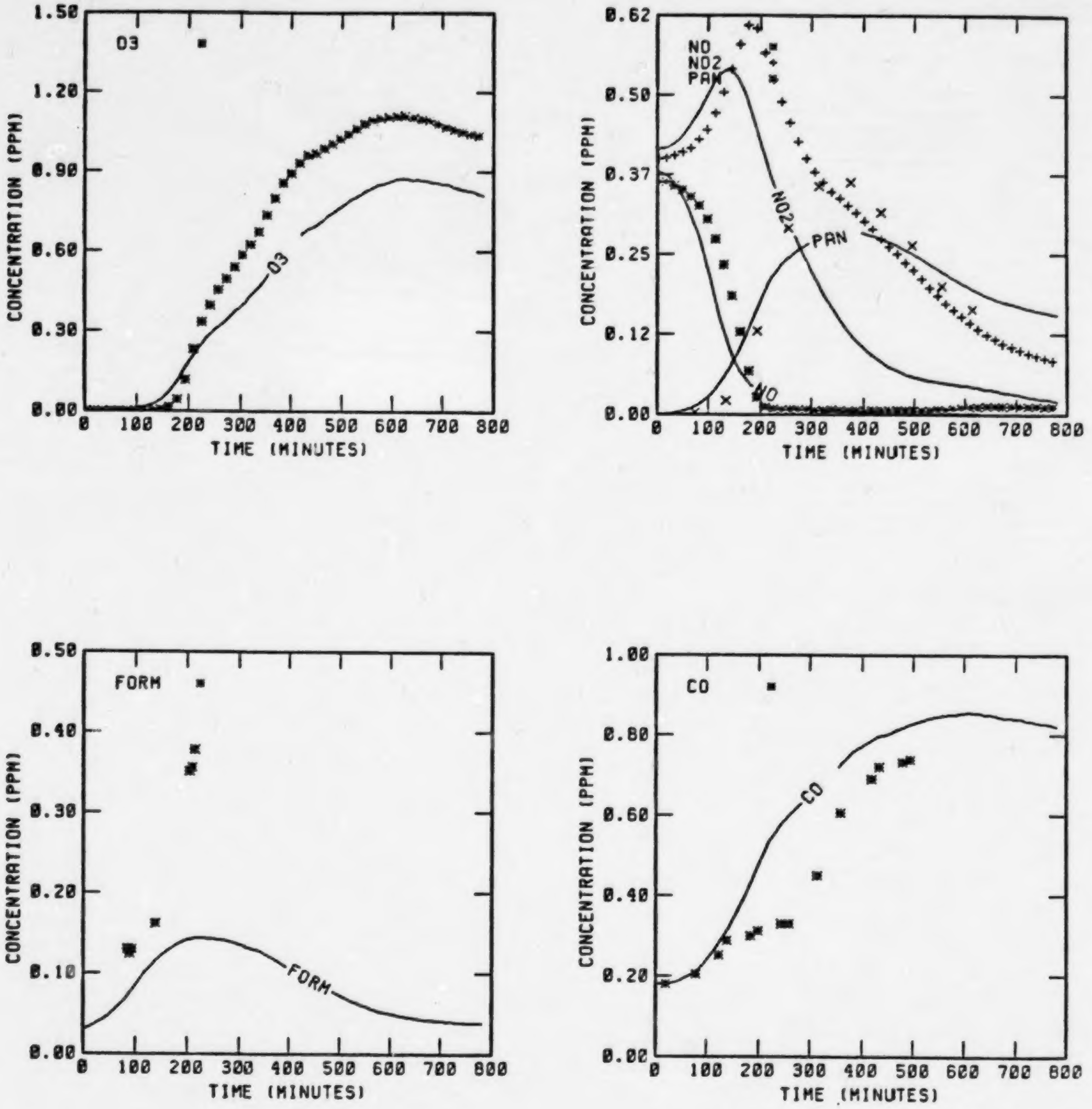

FIGURE 4. SIMULATION RESULTS FOR UNCB 70980 ASSUMING PYRUVYL RADICAL DECOMPOSITION

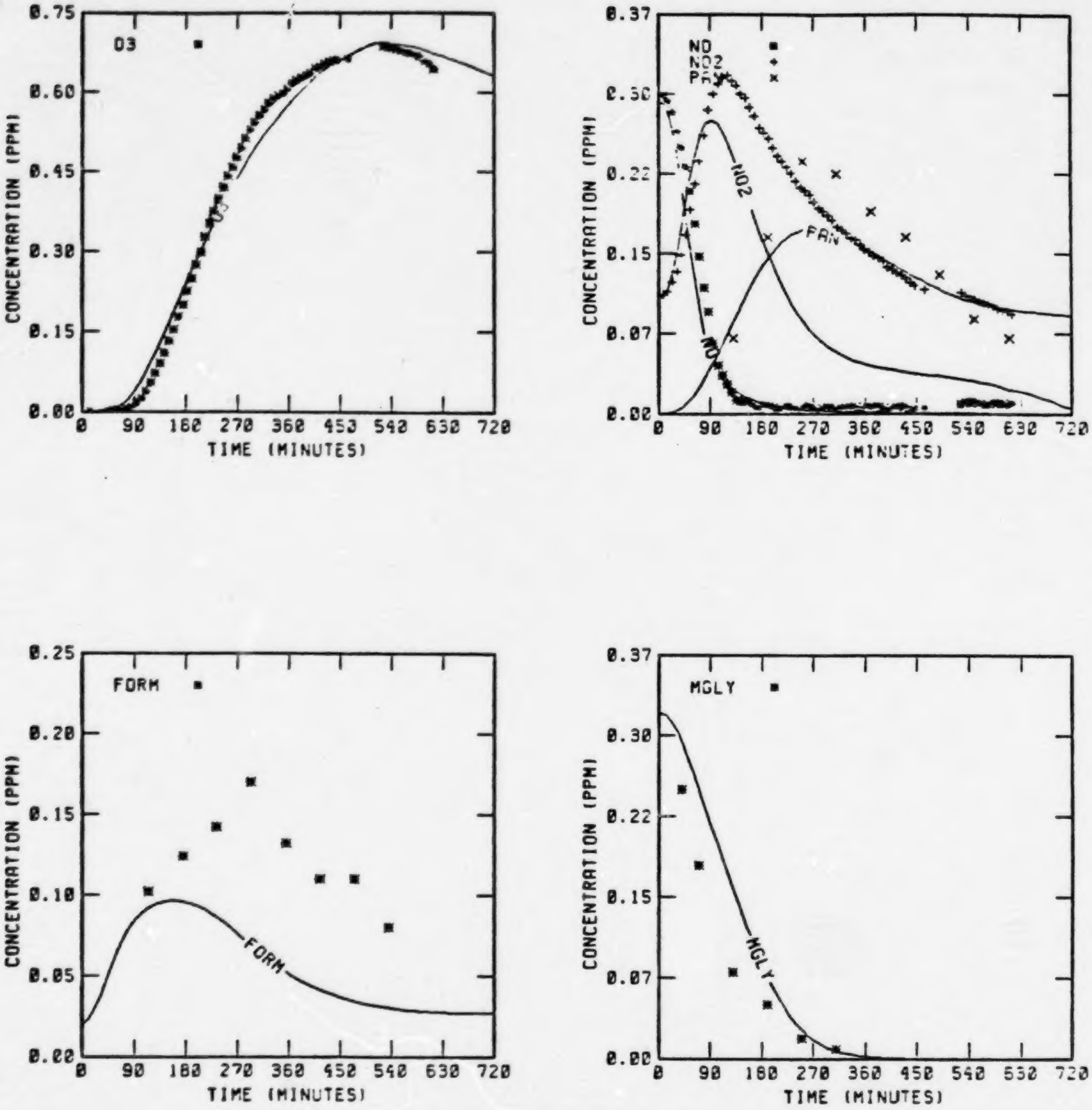

FIGURE 5. SIMULATION RESULTS FOR UNCB 100181 ASSUMING FORMATION OF PEROXYPYRUVYL

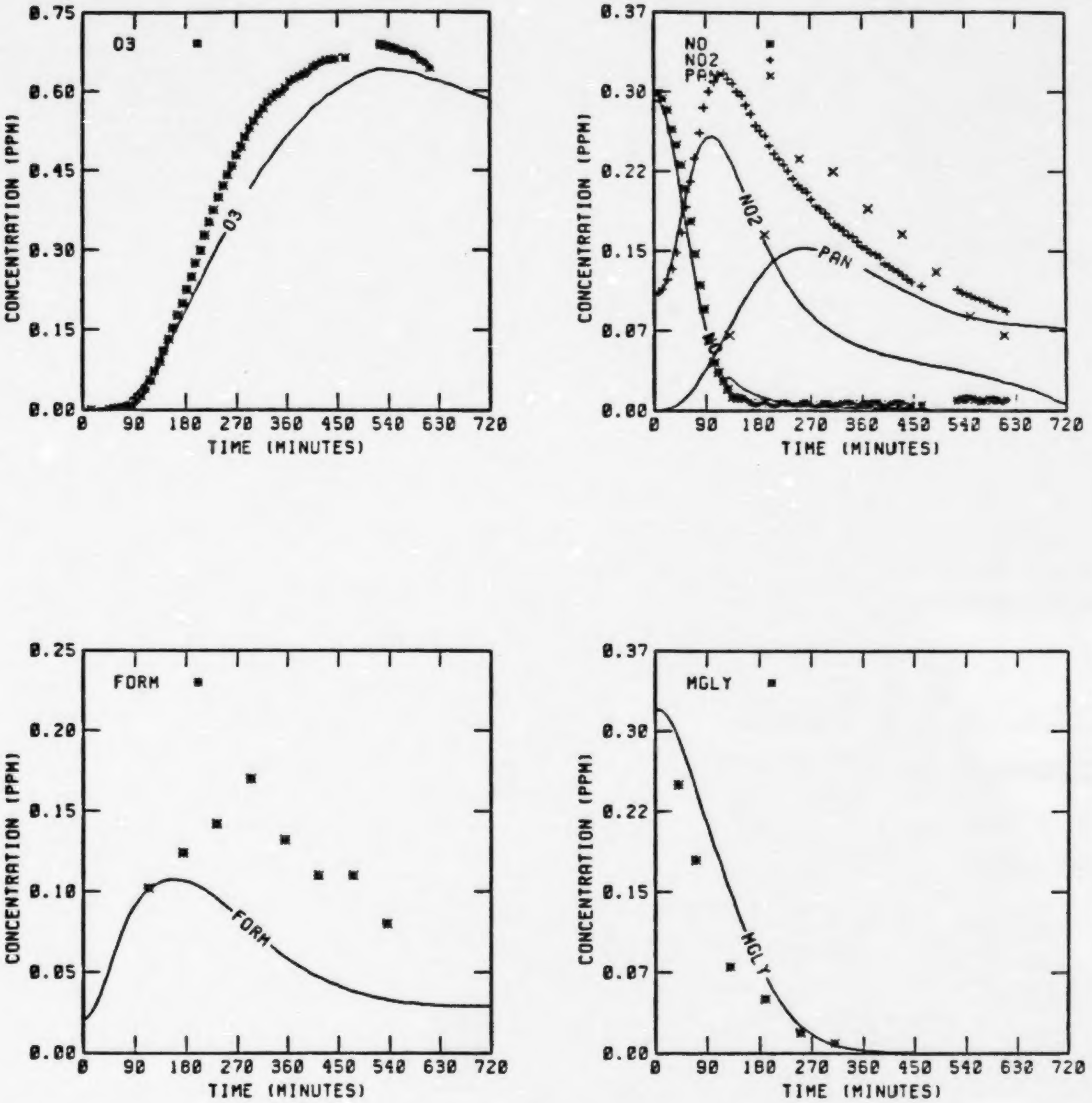

FIGURE 6. SIMULATION RESULTS FOR UNCB 100181 ASSUMING PYRUVYL RADICAL DECOMPOSITION

reaction are assumed to be pyruvyl radicals rather than peroxypyruvyl radicals. Figures 4 and 6 show that assuming the formation of pyruvyl radicals results in an underprediction of O_3. It should be noted that in all four figures, the formaldehyde data are significantly underpredicted. On the basis of mass balance calculations, it is our belief that the formaldehyde data are in error, probably due to interference from PAN or some other compound. That is, we believe that PAN is decomposing to formaldehye during the formaldehyde measurements.

Glyoxal

Our current mechanism for glyoxal is speculative, as must be the case for a compound that polymerizes easily, is difficult to measure, and presents practical obstacles to the introduction of the pure compound into the gas phase at atmospheric pressures. The CBM-X contains reactions for glyoxal photolysis and reaction with OH. The reaction of glyoxal with OH occurs at a rate similar to that of formaldehyde and its products are similar as well. The rate of glyoxal photolysis has been measured, but product yields, especially under atmospheric conditions, are still conjectural. In the CBM-X, we assume that photolysis to stable products ($2CO + H_2$) is the most significant of the three processes.

Three reactions are included to describe the photolysis of glyoxal.

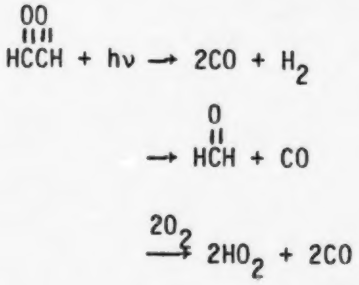

$$\mathrm{H\overset{O}{\overset{\|}{C}}\overset{O}{\overset{\|}{C}}H} + h\nu \rightarrow 2CO + H_2$$

$$\rightarrow \mathrm{H\overset{O}{\overset{\|}{C}}H} + CO$$

$$\xrightarrow{2O_2} 2HO_2 + 2CO$$

A reaction is also included to describe the reaction of glyoxal with OH.

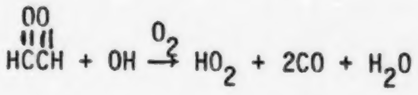

$$\mathrm{H\overset{O}{\overset{\|}{C}}\overset{O}{\overset{\|}{C}}H} + OH \xrightarrow{O_2} HO_2 + 2CO + H_2O$$

SECTION 4

HYDROCARBONS AND SURROGATE APPROXIMATIONS USED IN THE EXPANDED CARBON-BOND MECHANISM

INTRODUCTION

The expanded Carbon-Bond Mechanism (CBM-X) developed in this project uses a combination of explicit and condensed mechanisms for the treatment of both specific and generalized organic species. In developing the CBM-X, it was necessary to determine which compounds should be treated explicitly. The ICRS explicitly treats product species common to several hydrocarbon mechanisms: formaldehyde, acetaldehyde, PAN, acetone, methylglyoxal and glyoxal. Compounds for which explicit mechanisms have been developed are listed in Table 9. To determine which of these hydrocarbons warranted explicit treatment in the CBM-X, we drew upon three studies of the hydrocarbon speciation of Los Angeles smog: (1) Kopczynski et al. (1972), Table 10; (2) Calvert (1976), Table 11; and (3) Grosjean et al. (1981), Table 12. These studies represent a 10-year sampling period for Los Angeles. We also examined studies of other cities and found hydrocarbon speciation in most urban areas to be similar to that for Los Angeles (Killus and Whitten, 1982).

INDIVIDUAL COMPOUNDS OF IMPORTANCE IN URBAN AIR

To identify hydrocarbons warranting explicit treatment in the CBM-X we ranked the hydrocarbon species data presented in Tables 10 through 12 in three ways. These data were first ranked by concentration level in ppbC (Table 13). However, the drawback to such a mass ranking scheme is that it does not take reactivity into account. In such a ranking scheme methane, which has practically no effect on urban photochemistry, has the highest concentration level. The second ranking scheme, which employs the relative rate of reaction with hydroxyl (OH), attempts to address this problem (Table 14). Calvert (1976) used this technique to estimate the relative importance of various compounds in urban smog. In this scheme, the hydrocarbon concentration is multiplied by the compound's rate constant for reaction with the hydroxyl radical. This second ranking scheme also has certain imperfections:

TABLE 9. COMPOUNDS FOR WHICH EXPLICIT MECHANISMS EXIST.

Ethene
Propene
t-2-butene
isobutene
isoprene
methyl vinyl ketone
methacrolein
ethane[†]
propane[†]
MEK
butane
2,3, dimethyl butane
toluene
benzaldehyde
m-xylene
p-xylene[†]
o-xylene
methanol
ethanol[†]
propanol[†]
formic acid[†]
acetic acid
benzene[†]

[†] Not validated.

TABLE 10. AMBIENT HYDROCARBON CONCENTRATIONS MEASURED IN LOS ANGELES IN 1969

Measured Hydrocarbon Paraffins	ppbC	Measured Hydrocarbon Olefins	ppbC	Measured Hydrocarbon Aromatics	ppbC
Ethane	191	Ethylene	151	Toluene	271
Propane	140	Propylene	60	Ethylbenzene	67
Isobutane	65	1-Butene	47*	p-Xylene	100
n-Butane	286	Isobutene		m-Xylene	215
Isopentane	312	trans-2-Butene	12	o-Xylene	87
n-Pentane	171	Methylacetylene		n-Propylbenzene	21
Cyclopentane	138*	cis-2-Butene	8	m-Ethyltoluene	111*
2-Methylpentane		1,3-Butadiene	11	p-Ethyltoluene	
3-Methylpentane	68	1-Pentene	11	tert-Butylbenzene	23*
n-Hexane	82	2-Methyl-1-butene	15	o-Ethyltoluene	
2,4-Dimethylpentane	89	trans-2-Pentene	22	sec-Butylbenzene	137*
Cyclohexane	16	cis-2-Pentene	10	1,2,4-Trimethylbenzene	
3-Methylhexane	68	2-Methyl-2-butene	29	1,3,5-Trimethylbenzene	29
n-Heptane	40	1-Hexene	15	Isopropylbenzene	76*
Methylcyclohexane	49	Unknown 7[†]	6 } 9	Styrene	
Unknown 1	6	Unknown 8[†]	3		
Unknown 2	11				
Unknown 3	37				
Unknown 4	28				
Unknown 5	23				
Unknown 6	80				
(Acetylene)	160				

*Based on compound ratios in other studies, we estimate the following concentrations for overlapping compounds:

Cyclopentane	22	ppbC
2-Methylpentane	116	ppbC
1-butene	15.7	ppbC
Isobutene	31.3	ppbC
m-ethyltoluene	37.	ppbC
p-ethyltoluene	74	ppbC
sec-butylbenzene	47	ppbC
1,2,4 trimethylbenzene	90	ppbC

Source: Kopczynski et al. 1972.

TABLE 11. AMBIENT HYDROCARBONS MEASURED IN LOS ANGELES IN 1974.

Compound	Rel.rate, HO reaction
CH_4	2.01
C_2H_6	0.049
C_2H_4	0.043
C_2H_2	0.038
C_3H_8	0.037
C_3H_6	0.0087
iso-C_4H_{10}	0.012
n-C_4H_{10}	0.037
1-C_4H_8	0.0015
iso-C_4H_8	0.0030
iso-C_5H_{12}	0.0443
n-C_5H_{12}	0.0162
Cyclo-C_5H_{10}	0.0026
1-C_5H_{10}	0.004
2-Methylbutene	0.0008
2,2 Dimethylbutane[1]	0.0008
2-Methylpentane	0.0110
3-Methylpentane	0.0100
1-Hexene	0.0017
n-Hexane	0.0100
Cychohexane[2]	0.0107
2,2,3-Trimethylbutane	0.0077
C_6H_6	0.0082
2-Methylhexane	0.0069
3-Methylhexane	0.0063

TABLE 11 (CONCLUDED).

Compound	Rel.rate, HO reaction
1-Heptene	0.0044
n-C_7H_{16}	0.0043
Methylcyclohexane	0.0037
2,2,3-and 2,3,3-Trimethylpentane	0.0019
2,2,4-Trimethylpentane	0.0025
Toluene	0.020
1-Methylcyclohexene	0.0047
2,2,5-Trimethylhexane	0.0010
n-C_8H_{18}	0.0021
EtC_6H_5	0.0041
p,m-Xylenes*	0.014
o-Xylene	0.0060
n-C_9H_{20}	0.0013
n-PrC_6H_5	0.0010
sec-BuC_6H_5	0.0050
n-$C_{10}H_{22}$	0.0011
n-$C_{11}H_{24}$	0.0010
n-$C_{12}H_{26}$	0.0003

*2:1 m-xylene to p-xylene

[1] misreported in Calvert (1976) as 2,2,-dimethylbutene

[2] misreported in Calvert (1976) as cyclohexene

Source: Calvert, 1976.

TABLE 12. EXAMPLE OF LIGHT- AND HEAVIER-MOLECULAR-WEIGHT HC COMPOSITION IN AMBIENT LOS ANGELES AIR

HC	Amount ($\mu g/m^3$)	HC	Amount ($\mu g/m^3$)
Ethane	13.5	3-methylhexane	7.3
Ethylene	21.8	Dimethylcyclopentanes	5.0
Acetylene	11.1	2,2,4-trimethylpentane	5.6
Propane	17.3	Heptane	5.0
Propene	10.3	Methylcyclohexane	5.4
Propyne	-	Ethylcyclopentane	-
Propadiene	-	2,5-dimethylhexane	-
Isobutane	24.2	2,4-dimethylhexane	3.1
Butane	53.2	2,3,4-trimethylpentane	2.0
1-butene	2.2	Toluene	130.7
Isobutene	6.6	2,3-dimethylhexane	0.9
trans-2-butene	5.9	2-methylheptane	4.8
cis-2-butene	-	3-methylheptane	2.7
Isopentane	48.4	2,2,5-trimethylhexane	-
Pentane	32.1	Dimethylcyclohexane	-
3-methyl-1-butene	1.8	Octane	2.7
1,3-butadiene	-	Ethylcyclohexane	1.0
1-pentene	0.9	Ethylbenzene	24.9
Isoprene	-	p- and m-xylene	109.1 *
trans-2-pentene	-	Styrene	1.7
cis-2-pentene	-	o-xylene	28.3
2-methyl-2-butene	-	Nonane	1.7
2,2-dimethylbutane	-	Isopropylbenzene	-
Cyclopentene	-	Propylbenzene	3.7
Cyclopentane	3.0	p-ethyltoluene	5.8
2,3-dimethylbutane	3.9	m-ethyltoluene	2.4
2-methylpentane	14.1	1,3,5-trimethylbenzene	2.7
cis-4-methyl-2-pentene	-	o-ethyltoluene	3.1
3-methylpentane	11.9	tert-butylbenzene	-
2-methyl-1-pentene	4.2	1,2,4-trimethylbenzene	9.9
Hexane	9.3	secbutylbenzene	2.2
trans-2-hexene	-	1,2,3-trimethylbenzene	1.8
2-methyl-2-pentene	-	Decane	1.6
cis-2-hexene	-	Methylstyrene	0.8
Methylcyclopentane	10.6	1,3-diethylbenzene	2.7
2,2,3-trimethylbutane	-	1,4-diethylbenzene	2.6
2,4-dimethylpentane	2.7	1,2-diethylbenzene	-
1-methylcyclopentene	-	Undecane	-
Benzene	10.4	Dodecane	-
Cyclohexane	4.6	α-pinene	-
2-methylhexane	4.7	β-pinene	-
2,3-dimethylpentane	7.3	Limonene	-
		Myrcene	-

Source: Grosjean et al., 1981.

*Assumed split: p-xylene - 36 ppb; m-xylene 73 ppb

TABLE 13. COMPOUND RANKINGS BY MASS

Calvert (1976)	Kopczynski et. al. (1972)	Grosjean et. al. (1981)
Methane	Methane	(Methane)
Isopentane	Isopentane	Toluene
N-Butane	N-Butane	m-Xylene
Toluene	Toluene	n-Butane
Propane	m-Xylene	Isopentane
Ethane	Ethane	p-Xylene
Ethene	Acetylene	n-Pentane
Acetylene	n-Pentane	o-Xylene
m-Xylene	Ethane	Ethylbenzene
Cyclohexane	Propane	Isobutane
2-Methylpentane	2-Methylpentane	Ethene
3-Methylpentane	p-Xylene	Propane
2,2,3-Trimethylbutane	1,2,4,-Trimethylbenzene	2-Methylpentane
Sec-Butylbenzene	2,4,-Dimethylpentane	3-Methylpentane
Benzene	o-Xylene	Acetylene

TABLE 14. COMPOUND RANKINGS BY RELATIVE OH REACTION

Calvert (1976)	Kopczynski et. al. (1972)	Grosjean et.al. (1981)
Ethene	Ethene	M-xylene
m-Xylene	m-Xylene	Toluene
Propene	2-Methyl-2-butene	Isobutene
Isopentane	Propene	Ethene
(Isobutene + t-2 butene)	Isobutene	Propene
1-Heptene	1,2,4-Trimethylbenzene	t-2-Butene
Toluene	Trans-2-pentene	p-Xylene
1-Pentene	Toluene	1,2,4 Trimethylbenzene
n-Butane	Isopentane	o-Xylene
o-Xylene	1,3-Butadiene	Ethylbenzene
Cyclohexane	n-Butane	Isopentane
3-Methylpentane	P-Xylene	n-Butane
n-Hexane	2-Methyl-1-butene	2-Methyl-1-Pentene
2-Methylpentane	1,3,5-Trimethylbenzene	n-Pentane
1-Hexene	o-Xylene	Isobutane

(1) It does not account for the reactivity and mass of the reaction products; and

(2) Trace compounds with very high reactivity (e.g., internal olefins) are overemphasized.

In attempting to solve these problems, we devised a third ranking scheme using the quantity of reacted hydrocarbon over a 12-hour period (Table 15). Assuming a 12-hour average OH concentration of 1.5×10^{-7} ppm, we calculated the fraction of hydrocarbon reacting during the day. In compounds more reactive than ethene, essentially all of the initial concentration reacts; thus, for hydrocarbons of high reactivity, this scale is essentially a concentration ranking, while for hydrocarbons of low reactivity, the scale is similar to the relative rate of reaction scale.

The results of these three ranking procedures indicate several gaps in our current set of explicit hydrocarbon mechanisms. First, and most apparent, isopentane is easily the most important alkane in the urban atmosphere, yet no explicit mechanism for this compound exists, nor is there a data base for deriving such a mechanism. Therefore, we recommend that smog chamber experiments be performed for this compound. Second, ethene is easily the most important olefin. Isoprene and terpenes were not observed at significant levels in these studies; however, their involvement in rural emissions and background reactivity justifies current mechanism development efforts.

A third finding concerns the importance of aromatic hydrocarbons. The high aromatic content of unleaded gasoline may be responsible for the large increase in the importance of aromatic compounds in atmospheric chemistry from 1970 to 1980. Although we were aware of this phenomenon, we were surprised by the total dominance of two compounds, toluene and m-xylene, in the data of Grosjean and Fung (1984). Fortunately, explicit mechanisms for these compounds already exist. Additional aromatic hydrocarbons of importance in urban air are o-, and p-xylene, ethylbenzene, and 1,2,4 trimethylbenzene.

On the basis of these three hydrocarbon rankings, we included explicit mechanisms for three precursor compounds in the CBM-X: ethene, toluene, and m-xylene. A discussion of the mechanisms developed for these three species and the smog chamber data used to validate them is provided in the following sections.

TABLE 15. COMPOUND RANKINGS BY 12-HOUR REACTION MASS

Calvert (1976)		Kopczynski et. al. (1972)		Grosjean et.al. (1981)	
Compound	MASS reacted (ppbc)	Compound	MASS reacted (ppbc)	Compound	MASS reacte (ppbc)
Isopentane	93	m-Xylene	207	Toluene	84.6
Toluene	90	Toluene	153	m-Xylene	72.
m-Xylene	71	Isopentane	127.	p-Xylene	33.5
Ethene	62.5	Ethene	108	o-Xylene	26.0
n-Butane	52.	1,2,4, Tmbenzene	90	Isopentane	22.3
o-Xylene	43.	n-Butane	90	Ethylbenzene	20.9
Cyclohexane	42.	p-Xylene	87	n-Butane	18.62
3-Methylpentane	40.	o-Xylene	76	Ethene	15.9
n-Hexane	36.	2-Methypentane	76.	n-Pentane	15.4
p-Xylene	35.	n-Pentane	70	Propene	10.9
1-Heptene	30.	Propene	58	1,2,4-Trimethyl-benzene	9.5
Propene	25.	n-Hexane	40	Isobutane	8.8

ETHENE CHEMISTRY

The specific chemistry of ethene is represented by Reactions 104 through 111 and 116 through 120 in the CBM-X (Table 1). Species contained in the mechanism are shown in Table 16. The mechanism used in the CBM-X is virtually an explicit mechanism except for the features noted in Section 2: the oxygen atom chemistry has been simplified and the formation of glycolaldehyde has been ignored. The key features of ethene that necessitate its treatment separate from that of other olefins are as follows:

Ethene is the most abundant olefin.

Ethene reacts more slowly via all pathways than does the next most abundant olefin, propene.

Ethene does not lead to PAN, whereas other olefins do.

The ethene + OH reaction (Reaction 105) has been simplified in the CBM-X to eliminate the intermediate peroxy-type radical that is actually produced. The ethene + OH reaction proceeds according to the following mechanism:

$$CH_2 = CH_2 + OH \xrightarrow{O_2} OHCH_2 = CH_2O_2$$

$$OHCH_2 = CH_2O_2 + NO \rightarrow NO_2 + OHCH_2CH_2O$$

$$OHCH_2CH_2O \xrightarrow{O_2} 2HCHO + HO_2$$

To avoid introducing the species $OHCH_2CH_2O_2$, we assume the following products for the ethene + OH reaction:

$$CH_2 = CH_2 + OH \rightarrow CH_3O_2 + HCHO$$

The predominant fate of CH_3O_2 in the CBM-X is

$$CH_3O_2 + NO \rightarrow CH_3O + NO_2$$

$$CH_3O + O_2 \rightarrow HCHO + HO_2$$

TABLE 16. Species contained in the ethene mechanism.

Symbol	Definition
ETH	Ethene
CRIG	Crigee intermediate
HOTA	Energy-rich "hot" formic acid
FACD	Formic acid
OZD	Ozonide

Thus, in our simplified mechanism we oxidize one NO molecule and form $2HCHO + 1\ HO_2$, the same products that are formed in an "accurate" representation of ethene chemistry. The use of the HCHO and MEO_2 products instead of the peroxy radical only causes differences in computer simulations for time scales near one second with NO concentrations below 0.01 ppm. Because little error is introduced, similar approximations are used to eliminate peroxy-type radicals that are produced during the reactions of other organics with OH. Namely, such approximations are used for the reaction of OH with OLE, TOL, and XYL in Reactions 98, 128, and 146.

The simulations performed with the UNC data to validate ethene chemistry are presented in Appendix C. Initial conditions and performance data for these simulations are given in Tables 17a and b. Although these results show a general overprediction due to the ethene mechanism, this is often a measurement problem. The series of experiments produces an average ozone level of 730 ppb; many of the ozone levels generated are over 1 ppm where saturation of the UNC ozone meter often occurred. Hence, the calculated average bias of + 100 ppb is only 14 percent. The timing of the ozone peaks is well simulated without significant bias.

AROMATICS CHEMISTRY

Both toluene and m-xylene are treated explicitly in the CBM-X. Toluene chemistry is represented by Reactions 128 through 140; m-Xylene chemistry is represented by Reactions 141 through 146. The species contained in these mechanisms are shown in Table 18. Although our present knowledge of aromatics is incomplete, the initial decay reactions and the overall reactivity of some aromatic species are fairly well characterized. Atkinson and Lloyd (1984) show that aromatics react with only one species of importance under atmospheric conditions: the hydroxyl radical. Olefins, on the other hand, react with O and O_3 as well as OH.

Toluene and m-xylene differ considerably in their overall reactivity and can presumably be used to represent the range of aromatics seen in the atmosphere. Similar to ethene in relation to other olefins, toluene is the most abundant but least reactive of the substituted aromatics, whereas m-xylene is the most abundant species of the highly reactive multiple-substituted aromatics in the atmosphere. As noted in Killus and Whitten (1983), toluene also has a special NO_x loss mechanism, which is apparently not as important for the more highly reactive aromatics. The special NO_x loss feature of toluene chemistry leads to ozone suppression at high $NMOC/NO_x$ ratios via reaction of the nitrate radical (NO_3) with phenol-type

TABLE 17. Ethene experiments.

(a) Initial Conditions

Date/Side	Beginning Temperature (°K)	Beginning Time	Ethene (ppm)	NO (ppm)	NO_2 (ppm)	HONO* (ppm)	H_2O (ppm)	FORM* (ppm)	CO (ppm)	Wall* Formal-dehyde (ppm)
101877R	271.2	7:26	1.900	0.375	0.112	0.003	20K	0.010	0.300	0.000
101877B	271.2	7:26	0.938	0.380	0.108	0.003	20K	0.060	0.300	0.000
111277R	269.4	7:46	1.000	0.375	0.116	0.003	20K	0.000	0.300	0.000
111977R	272.9	7:46	1.890	0.390	0.112	0.003	5K	0.070	0.300	0.050
112077R	270.6	7:32	2.185	0.400	0.116	0.004	15K	0.050	0.300	0.050
11078B	260.0	8:17	2.150	0.344	0.138	0.001	1.3K	0.000	0.200	0.000
61678R	286.7	6:17	2.000	0.430	0.185	0.004	16K	0.030	0.300	0.000
63078B	292.6	6:12	0.765	0.384	0.097	0.020	15K	0.060	0.300	0.100
71078R	293.7	5:54	0.720	0.680	0.209	0.020	20K	0.100	0.330	0.000
73078R	291.8	6:30	0.660	0.395	0.080	0.010	28K	0.050	0.440	0.000
80678B	295.8	6:31	1.249	0.418	0.156	0.020	26K	0.200	0.300	0.350
81078R	293.8	6:36	0.520	0.415	0.113	0.010	21K	0.100	0.300	0.000
81078B	293.8	6:36	1.505	0.408	0.114	0.008	21K	0.070	0.300	0.000
81578B	294.3	6:24	0.790	0.430	0.136	0.020	22K	0.150	0.280	0.150
82378R	287.2	6:58	1.470	0.410	0.110	0.001	15K	0.030	0.350	0.050
82378B	287.2	6:58	1.460	0.420	0.100	0.001	14K	0.030	0.350	0.050
91478B	289.0	6:57	0.440	0.232	0.062	0.004	13.8K	0.070	0.200	0.100
91578R	289.0	6:54	1.520	0.407	0.119	0.004	9.8K	0.020	0.400	0.000
91878R	292.9	7:05	1.488	0.403	0.104	0.020	20K	0.200	0.300	0.250
91978R	292.9	7:05	0.910	0.570	0.123	0.012	13.2K	0.150	0.260	0.100
92178R	291.0	7:07	0.966	0.193	0.068	0.007	17.6K	0.050	0.410	0.100
100278B	286.5	7:12	1.491	0.383	0.100	0.004	18K	0.000	0.360	0.050
100378R	282.1	7:17	0.489	0.359	0.135	0.004	15K	0.030	0.430	0.020
80479R	295.9	6:22	0.438	0.163	0.060	0.006	34K	0.030	0.340	0.250
80579R	296.4	6:14	2.057	0.503	0.140	0.006	29K	0.000	0.340	0.100
103179R	283.0	7:31	1.880	0.401	0.100	0.001	14K	0.000	0.340	0.000
103179B	283.0	7.31	1.860	0.403	0.097	0.000	5.6K	0.0000	0.340	0.000
70880R	291.6	5.53	1.020	0.370	0.370	0.008	10K	0.020	0.350	0.080

* These chamber effects were used to optimize agreement between data and simulations; see text for further discussion.

TABLE 17. (concluded)

(b) Comparison of Simulations and Experiments

Date/Side	Initial NO_x (ppm)	Initial NO_2/NO_x Ratio	Initial HC/NO_x (ppmC/ppm)	Maximum O_3 (ppm)		Difference in O_3 Maxima (ppm)	Time to Maximum O_3 (min)		Difference in Time to O_3 Maxima (min)
				Simulated	Measured		Simulated	Measured	
101877R	0.487	0.230	7.80	1.20	0.90	0.30	435	425	10
101877B	0.488	0.221	3.84	0.42	0.46	-0.06	> 560	> 560	-
111277R	0.491	0.236	4.07	0.10	0.06	0.04	430	420	10
111977R	0.502	0.223	7.53	0.82	0.80	0.02	470	410	60
112077R	0.516	0.225	8.47	0.81	0.76	0.05	480	410	70
11078B	0.482	0.286	8.92	> 0.15	0.04	-	-	460	-
61678R	0.615	0.301	6.50	> 1.50	1.10	0	0	440	-
63078B	0.481	0.202	3.18	1.12	0.98	0.14	550	520	30
70178R	0.889	0.235	1.62	0.11	0.26	-0.15	650	730	-80
73078R	0.475	0.168	2.78	0.91	0.80	0.11	610	675	-65
80678B	0.574	0.272	4.35	1.45	1.10	0.35	360	340	20
81078R	0.528	0.214	1.97	> 0.20	0.180	-	> 560	> 560	-
81078B	0.522	0.218	3.85	1.32	1.11	0.21	420	420	0
81578B	0.566	0.240	1.73	> 1.00	0.92	-	-	410	-
82378R	0.520	0.212	5.65	1.60	1.10	0.50	440	400	40
82378B	0.520	0.192	5.62	> 1.25	1.10	0	0	420	-
91478B	0.294	0.211	2.39	> 0.70	0.61	-	-	600	-
91578R	0.526	0.226	5.78	> 1.00	0.73	-	-	530	-
91878R	0.507	0.205	5.87	> 1.25	1.05	-	-	340	-
91978R	0.693	0.177	2.63	1.00	1.05	-0.05	> 560	530	-
92178R	0.261	0.261	7.40	1.10	0.82	0.28	460	450	10
100278B	0.483	0.207	6.17	> 1.25	0.88	-	> 520	> 520	-
100378R	0.494	0.273	1.98	> 0.03	0.025	-	-	490	-
80478R	0.228	0.263	3.84	0.86	0.071	0.15	470	550	-70
80579R	0.643	0.218	6.40	1.60	1.25	0.35	420	410	10
10379R	0.500	0.194	7.49	1.20	0.83	0.37	470	450	20
103179B	0.500	0.194	7.44	1.24	0.88	0.36	500	470	30
70880R	0.740	0.500	2.76	> 0.75	0.63	-	-	730	-

TABLE 18. Species contained in toluene and m-xylene mechanism.

Symbol	Definition
TOL	Toluene
OPEN	Peroxy radical ring-opening precursor
PHEN	Phenyl-type product (cresol for toluene)
BO2	OH abstraction peroxy precursor to benzaldehyde
PHO	Phenoxy radical
BZA	Benzaldehyde
BZO2	Peroxy benzoyl radical
PBZN	Peroxy benzoyl nitrate
PHO2	Peroxy phenyl radical
NPHN	Nitrophenol
XYL	Xylene
XYLO	OH abstraction peroxy precursor to tolualdehyde
TLA	Tolualdehyde
TLO2	Methyl-peroxybenzoyl radical

intermediates in aromatics photooxidation. The more reactive aromatics also produce phenol-type intermediates, but apparently with less net yield than that of toluene.

The aromatic chemistry used in the CBM-X differs from the aromatics chemistry featured in the mechanism of Atkinson et al. (1982). For example, in the CBM-X the oxygenation of the aromatic ring is taken to proceed to completion as part of the initial ring opening, yielding the prompt formation of HO_2, and three dicarbonyl molecules. For example, in the case of toluene (Reaction 128) we assume that initial ring opening leads to the formation of glyoxal and a five-carbon peroxy-type radical (OPEN):

$$\mathrm{TOL + OH \rightarrow GLY + OPEN}$$

The radical OPEN then reacts with NO to yield two additional dicarbonyl species:

$$\mathrm{OPEN + NO \rightarrow NO_2 + HO_2 + MGLY + GLY}$$

A similar mechanism is written to describe ring opening for m-xylene.

In the Atkinson et al. (1982) mechanism, the initial products of ring opening are assumed to be a dicarbonyl and a stable olefinic dial compound. Such dial compounds are not included in the CBM-X. Although Tuazon et al. (1984) argue that, in reality, the yields of methylglyoxal and glyoxal are lower than those used in the CBM-X, the high yields can be considered surrogates for the actual compounds formed. The evidence supporting the use of high yields of these highly reactive products is the need for reactivity in the secondary products demonstrated in the smog chamber experiments reported here. Hence, the subset for aromatics chemistry may require updating in the future to account for the chemistry that may actually be occurring, but the quality of performance of the present CBM-X in simulating the smog chamber experiments suggests that future changes would not seriously improve CBM-X performance.

The chemistries for the other two toluene + OH reactions (Reactions 129 and 130) are treated similary in the CBM-X and Atkinson et al. (1982) mechanisms. The abstraction reaction,

$$\mathrm{TOL + OH \rightarrow BO_2},$$

yields a peroxy radical that can further react to form benzaldehyde and peroxybenzoyl nitrate. The addition reaction,

$$TOL + OH \rightarrow PHEN + HO_2,$$

yields cresol, represented as PHEN in the CBM-X.

Initial conditions and performance data for the m-xylene and toluene experiments are presented in Tables 19a and b. Selected simulations performed with smog chamber data to validate the chemistries of m-xylene and toluene are contained in Appendix D. For the toluene experiments, there appears to be an overprediction bias of about 100 ppb for the three experiments where an ozone peak was apparent. However, the other three toluene experiments accurately simulate observed ozone. The nitrogen oxide chemistry, which involves conversion of NO to NO_2, is fairly well simulated in all the toluene experiments. Possible improvements to toluene chemistry in future studies may involve even more of an NO_x sink than that used in the present CBM-X chemistry. Additional NO_x loss would lower the ozone peak concentrations. For the m-xylene experiments, an apparent underprediction bias of -110 ppb was observed, with consistent early prediction of the ozone peak of about 45 minutes, on the average.

SURROGATE APPROXIMATIONS

Regardless of the nature of the organic kinetic mechanism (explicit, lumped molecular, lumped structure), it is often both possible and desirable to use a surrogate approximation for a given hydrocarbon species. A surrogate approximation can be used when a compound is sufficiently similar in its photooxidation behavior to an already existing class that it can be included in that class without modifications to the chemical parameters of the mechanism. As a practical matter, however, the surrogate approximation is often justified for compounds whose behavior is not known in detail; the behavior of such compounds must be estimated by analogy with other known compounds.

The CBM-X uses surrogate approximations to describe a number of compounds. The behavior of olefins with two or more alkyl groups (e.g., isobutene, internal olefins) is simulated as a mixture of the aldehyde and ketone products. In this case, the surrogate approximation is justified because such very reactive olefins oxidize to their products so rapidly that product behavior dominates. The second major surrogate approximation in the CBM-X involves monoalkylated aromatics (e.g., ethylbenzene). These compounds are considered to be similar to toluene, for which a condensed explicit mechanism is used. In keeping with the carbon balance considerations of the Carbon-Bond approach, the excess alkyl carbon in these molecules is treated in the alkyl carbon portion of the CBM-X. Multiple-substituted aromatics are considered to be similar to x-xylene. Another

TABLE 19. Toluene and m-xylene experiments.

(a) Initial Conditions

Date/Side	Beginning Temperature (°K)	Beginning Time	Xylene (ppm)	Toluene (ppm)	NO	NO_2	HONO*	H_2O	Wall* Formaldehyde	Form*	CO	NX*
81678B	294.0	6:33	-	0.560	0.604	0.088	0.010	10K	0.000	0.050	0.293	0.016
62779B	286.8	6:02	-	2.210	0.263	0.069	0.0001	10K	0.000	0.000	0.323	0.00
81579B	290.0	6:42	-	0.740	0.276	0.086	0.002	10K	0.000	0.020	0.338	0.01
81180R	295.4	6:23	-	0.460	0.225	0.090	0.008	10K	0.000	0.100	0.000	0.08
91478R	289.0	6:57	-	0.320	0.230	0.060	0.001	10K	0.000	0.020	0.200	0.016
73080R	292.5	6:03	-	0.550	0.156	0.026	0.004	10K	0.000	0.000	0.000	0.013
AVOC8	303.2	-	0.960	-	0.225	0.215	0.001	20K	0.001	0.005	0.660	0.01
AVOC21	303.2	-	1.110	-	0.244	0.252	0.001	20K	0.003	0.005	0.120	0.01
AVOC22	303.2	-	0.560	-	0.244	0.252	0.001	20K	0.003	0.005	0.100	0.01
AVOC24	303.2	-	0.285	-	0.122	0.122	0.003	20K	0.003	0.005	0.280	0.01
AVOC26	303.2	-	0.264	-	0.480	0.480	0.006	20K	0.003	0.005	0.185	0.06

* These chamber effects were used to optimize agreement between data and simulations; see text for further discussion. NX is amount of NO_x offgassing from chamber walls.

TABLE 19. (concluded)

(b) Comparison of Simulations and Experiments

Date/Side	Initial NO_x (ppm)	Initial NO_2/NO_x Ratio	Initial HC/NO_x (ppmC/ppm)	Maximum O_3 (ppm)		Difference in O_3 Maxima (ppm)	Time to Maximum O_3		Difference in Time to O_3 Maxima (min)
				Simulated	Measured		Simulated	Measured	
816788	0.692	0.127	5.66	> 0.30	> 0.26	-	> 640	> 640	-
627798	0.332	0.208	46.60	0.58	0.41	0.17	270	260	10
815798	0.362	0.238	14.31	0.47	0.41	0.06	600	410	190
81180R	0.315	0.286	10.22	> 0.52	0.40	-	> 560	450	-
91478R	0.290	0.207	7.72	> 0.32	> 0.32	-	> 640	> 640	-
73080R	0.182	0.143	21.15	0.38	0.27	0.11	580	430	150
AVOC8	0.440	0.489	17.45	0.45	0.66	-0.21	100	115	-15
AVOC21	0.496	0.508	17.96	0.47	0.54	-0.07	100	120	-20
AVOC22	0.496	0.508	9.03	0.44	0.53	-0.09	170	230	-60
AVOC24	0.244	0.500	9.34	0.29	0.42	-0.13	150	170	-20
AVOC26	0.960	0.500	2.20	0.41	0.47	-0.06	850	950	-100

84188r5

surrogate approximation involves chlorinated ethenes, which are considered to be similar to ethene itself. The atmospheric concentration of these compounds is small; C_3 and higher aldehydes are treated as acetaldehyde.

SECTION 5

THE LUMPED STRUCTURE MECHANISM USED IN THE CBM-X

The number of hydrocarbons involved in urban photochemistry precludes a fully detailed treatment of the photochemistry of each individual compound in a chemical kinetic mechanism. The problem in kinetic mechanism development, therefore, becomes one of generalization and categorization of compounds. The surrogate mechanism approach discussed in Section 1 offers a set of natural categories for hydrocarbon classification. However, a surrogate approximation inevitably involves departures from the true chemistry of the compound to be classified. If the classification error becomes too great, then another category must be added to the mechanism, and the simulation process becomes more cumbersome and expensive and less compact and analytically tractable.

Several techniques have been devised to improve the generalization/classification process. The most common involves molecular lumping. In this procedure, a general hydrocarbon category is developed from the average behavior of a number of different compounds. The principal requirement of a molecular lumping scheme is that the behavior of the individual compounds do not depart too greatly from the average behavior of the category.

Another technique that has been used to reduce the difficulty of compound generalization is known as structural reactivity classification. In structural reactivity classification, lumped molecular substructures are placed in separate categories. These structural reactivity groups are then put into the reaction categories of the mechanism. We favor the structural reactivity generalization technique for mechanism design because it eliminates many of the troublesome features of molecular lumping. The structural reactivity classification concept has been the basis of different versions of the Carbon-Bond Mechanism.

Although the Carbon-Bond Mechanism is perhaps the best known of the mechanisms that use structural reactivity classification, several other mechanisms use variations of this technique. For example, the Penner and Walton (PW) mechanism (Penner and Walton, 1982) uses what is termed "emissions reactivity weighting" within the context of a surrogate mechanism for butane, propene, and toluene. Basically, the PW mechanism assesses alkane reactivity, for example, in terms of "butane equivalents"; that is, one molecule of octane, which has approximately twice the reactivity to hydroxyl radicals as butane, is treated as two butane molecules. The close equivalence of alkane reactivity when normalized to carbon number has been discussed in Whitten et al. (1980). Thus, the treatment of alkanes in the PW mechanism is very similar in its underlying concept to that of the Carbon-Bond Mechanism.

Worth mentioning in this context is the Dodge mechanism used in the original EPA-EKMA. The empirical analysis of auto exhaust reactivity into propene-butane equivalents employed by this mechanism also avoids the molecular classification problem. This approach could have been extended to other emission categories (e.g., "auto exhaust equivalents" or differing mixtures of propene and butane), however the validation process required has made such a purely empirical approach unattractive for application to multiple source types.

A good example of the superiority of structural reactivity classification schemes over molecular averaging schemes is found in Figure 7. In this experiment, both butane and n-pentane were loaded into opposite sides of the UNC two-sided outdoor smog chamber along with equal amounts of NO_x. The hydrocarbon values were equivalent on a ppmC basis (Jeffries et al., 1979) and equal amounts of ozone were found.

Structural reactivity generalization schemes such as the CBM and the Penner and Walton mechanism can easily accommodate the results shown in Figure 7. In fact, for this experiment, the initial conditions for both bond groups and "butane equivalents" would be the same for both sides of the chamber. A molecular lumping scheme, however, cannot accommodate the result shown in Figure 7 without modifying basic parameters in the mechanism for each hydrocarbon (e.g., OH reaction rate constant; average molecular weight). Such ad hoc mechanism adjustments are impractical in actual applications, yet without such adjustments the molecular lumping approach would seem to require different molecular groups for C_4 and C_5 alkanes, which is also impractical. The CBM-X mechanism avoids this difficulty.

We next describe the chemistries of the structural lumping groups in the CBM-X. Since most molecules contain a paraffinic carbon group, it is appropriate to discuss alkyl chemistry first.

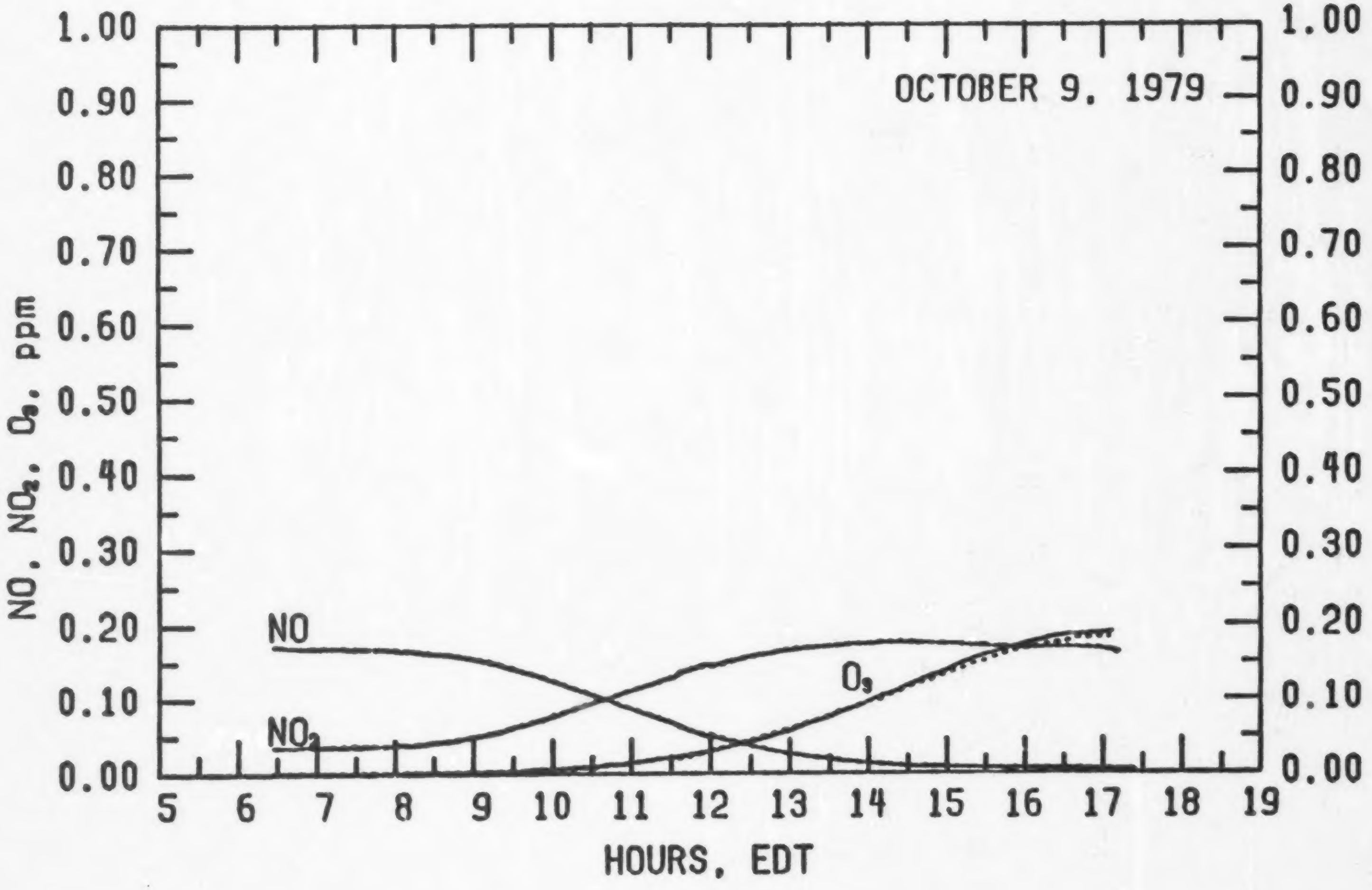

FIGURE 7. Nitrogen and Ozone Data, both chamber sides. Dashed line (······) is n-pentane and solid line (———) is n-butane. Both sides 14.2 ppmC.

ALKANE CHEMISTRY

The paraffinic carbon of molecules that are treated in the lumped structure approach are represented as PAR. The PAR chemistry is described by Reactions 80-94 in Table 1. The species involved in PAR oxidation are defined in Table 20. The alkyl groups represented by PAR can enter the photooxidation scheme either by direct reaction with OH or indirectly, when the bond adjacent to the alkyl group is broken. The former entry path is the same as for paraffin chemistry, with the added advantage in the structure approach that all alkyl groups are treated by only 2 OH reactions even though the alkyl group might actually be attached to some other molecule. For example, in 1-octene, an alkyl group of 6 carbons is attached to the second double-bonded carbon atom. In an explicit scheme, separate OH reactions for each of these six carbon atoms would be needed.

Indirect entry into the chemical scheme is more difficult to explain in the structural approach, but the approach still offers advantages over the use of explicit chemistry. Two species (X and D) are used in the CBM-X to treat indirect entry of alkyl carbon atoms. Species X is used to maintain carbon balance during the photooxidation of straight-chained paraffins. These alkanes react with OH to form peroxy radicals. The peroxy radicals then react with NO to form acetaldehyde and higher aldehydes. To represent this in the CBM-X, we use the following reactions:

$$\mathrm{PAR} + \mathrm{OH} \rightarrow \mathrm{RO_2}$$

$$\mathrm{RO_2} + \mathrm{NO} \rightarrow \mathrm{NO_2} + \mathrm{HO_2} + \mathrm{ALD2} + \mathrm{X}$$

In this example, the one-carbon PAR molecule reacts with OH to generate a one-carbon RO_2 radical. This RO_2 radical then reacts with NO to generate a two-carbon molecule product (ALD2). To restore the carbon balance, the fictitious species X has been introduced. Species X immediately reacts with PAR to remove a carbon atom from the system:

$$\mathrm{X} + \mathrm{PAR} \rightarrow$$

The species D accounts for the decomposition and isomerization pathways of alkyl groups containing 4 or more carbon atoms. Rather than acting as a carbon conservation measure as does X, species D accounts for the competitive splits between alternate pathways for alkoxyl radicals. In essence, D is a zero-carbon fictitious species that controls the amount of peroxy radicals that will undergo isomerization and the amount that will undergo decomposition to yield aldehydes and ketones. To be sure, the character of the alkyl group is the real governing factor for the split between such paths as decomposition or intra-molecular H atom transfer (isomerization). Therefore, the numbers chosen to accomplish the

TABLE 20. Species involved in the oxidation of paraffin.

Symbol	Definition
PAR	1-Carbon paraffin group
RO_2	Primary alkyl peroxy radical with C<4
RO_2R	See text--alkyl peroxy and long-chain radicals
ROR	Alkoxyl radicals
KET	Ketones other than acetone
AONE	Acetone
D	Fictitious species to account for alkoxyl radical decomposition and isomerization
AO2	Peroxy isopropyl radical
X	Fictitious steady-state species to maintain carbon balance
NTR	Organic nitrate

splits between such pathways are tied to an assumed mixture of alkyl groups. The sensitivity of CBM-X performance to the range of reasonable assumptions might be the subject of a follow-on study.

It should also be noted that fewer assumptions would be needed if three or more paraffinic species were used in the CBM-X. For example, during development of the CBM-X, the possibility of treating primary, secondary, and tertiary carbon atoms separately was considered. However, the sensitivity of the overall simulation results using typical urban or auto-exhaust mixtures to this extra degree of expansion did not appear to be warranted. The extra degree of expansion would increase the computer cost, the man-hours required to prepare input data, and the costs of analytical field data. Hence, the present CBM-X uses a single PAR species plus typical parameterized splits for the akyoxl radicals via the species D.

OLEFIN CHEMISTRY

The lumped structure approach for olefin chemistry is actually a surrogate that uses propene for all terminal olefins. Hence, the species OLE is treated like propene in Reactions 95-103 plus 108-127. The propene chemistry is based on the recommendations of Atkinson and Lloyd (1984). Species involved in the oxidation of olefins are given in Table 21.

KETONE CHEMISTRY

Ketones appear as products of alkane reactions. They undergo photolysis to yield peroxy and acylperoxy radicals as shown in Reaction 94. Because KET is a one-carbon entity in the CBM-X, two species X are added to the products of Reaction 94 to restore carbon balance.

VALIDATION OF THE LUMPED MECHANISM

The lumped structure portion of the mechanism was validated by comparing the predictions obtained with this mechanism against those obtained using explicit chemical mechanisms for propene, n-butane, and 2,3-dimethylbutane.

TABLE 21. Species involved in the oxidation of olefin.

Symbol	Definition
OLE	2-carbon double-bond group
CRIG	Crigee intermediate (dioxirane)
MCRG	Methyl Crigee
PNO_2	Peroxy isoproyl nitrate radical
HOTA	Energy-rich formic acid
HTMA	Energy-rich acetic acid
DNIT	Organic dinitrate
NTR	Organic nitrate
FACD	Formic acid
OZD	Ozonide
ACAC	Acetic acid

SECTION 6

VALIDATION OF THE EXPANDED CARBON-BOND MECHANISM

INTRODUCTION

Validation of several components of the CBM-X has already been accomplished on an independent basis. The inorganic and carbonyl reaction set (ICRS), which includes the chemistry of formaldehyde, acetaldehyde, PAN, and methyl glyoxal, has been validated with numerous experiments involving those compounds. Our explicit mechanisms for ethene, toluene, and m-xylene have also been independently validated against chamber data. The carbon-bond formulation for 1-olefins was compared to an explicit, validated mechanism for propene, and so can also be considered to be validated as a subcomponent of the full mechanism. The carbon-bond formulation for PAR was compared to explicit, validated mechanisms for n-butane and 2,3-dimethylbutane.

The final step involved validation of the entire CBM-X mechanism. To accomplish this it was necessary to use smog chamber data from a study in which the initial reactants and chamber operating conditions were representative of the actual emissions and conditions that prevail in the urban environment. Such a study using dilute auto exhaust and NO_x mixtures has recently been completed by the University of North Carolina (UNC) (Jeffries et al., 1985).

UNC AUTO EXHAUST DATA

The outdoor smog chamber at the University of North Carolina has been in operation for 10 years. The special features of the facility are its large size, Teflon-film walls, and two-sided chamber. The chamber consists of an external wooden A-frame, which supports a covering of 5-mil (FEP) Teflon film. A center panel divides the overall chamber into two equal chambers of 148 m^3 (5230 ft^3). The size of the chamber would require a massive and costly air purification system unless the ambient air were sufficiently clean. Hence, the facility is located in a rural area 17 miles southwest of Chapel Hill, North Carolina. The air around the chamber typically contains less than 0.015 ppm NO_x and the nonmethane concentration of organics is usually less than 0.20 ppmC. A recent study indicates that background reactivity during recent years has been low enough to conduct meaningful experiments as long as (1) the air has been dried to prevent condensation and (2) the added precursors are significantly above the typical background levels, or the ambient air is allowed to react for one day prior to injection of the precursors (Whitten and Killus, 1985).

The UNC facility has built up an experienced staff and analytical capabilities during the 10 years it has been in operation. Because of this, it was possible for them to gather a data base on the reactivity of auto exhaust (NO_x samples). The only other auto exhaust data base that has been widely used to test chemical mechanisms was generated in 1967-1968 at the Bureau of Mines Research Center at Bartlesville, Oklahoma, in an aluminum and glass chamber of only 100 ft^3 using artificial sunlight (Dimitriades, 1970). The limited analytical capabilities available in 1967 and the use of only one 1963 automobile restricted the continued use of the original data set. The UNC new data base has been generated in an established facility with well-characterized chamber effects, dual chambers with which to compare a variety of effects under actual variations in sunlight and temperature, and much improved analytical capabilities. Furthermore, the new data set provides a comparison of automobiles, fuels, and synthetic organic mixtures designed to duplicate auto exhaust reactivity. The new data base contains fairly reliable information on exhaust hydrocarbon speciation, total NMHC, detailed aldehyde and oxygenates, CO, PAN, HNO_3, organic nitrates, NO_x, and O_3.

In the UNC study, the chamber was injected with auto exhaust obtained from two automobiles: a 1979 Plymouth Volare with a 6-cylinder catalyst-equipped engine and a 1972 Dodge Charger with a V-8 noncatalytic engine. The Volare was driven under "normal" conditions when not supplying exhaust fumes to the smog chamber and its total mileage was about 37,000 to 54,000 miles during the period of the smog chamber tests (March 1982 to March 1984). The Charger, on the other hand, had already been driven 116,000 miles in March of 1982 and was not driven more than required by the smog chamber tests. Both premium and regular unleaded gasolines were used to fuel these cars.

The UNC auto exhaust experiments were conducted during the 1982 and 1983 smog seasons. In all, UNC conducted auto exhaust runs on 30 different days. Since the chamber is divided in half so that two runs are conducted simultaneously, 60 auto exhaust runs were completed under the UNC program. To date, only 32 of these 60 runs have been fully processed by UNC. Many of the runs have not been processed because they are not suitable for modeling. There are several reasons for this:

On some days the sunlight was poor (overcast conditions) or the weather was not conducive for photochemical reactivity, e.g., it rained.

On some days there were instrumental failures that prevented the collection of data for key species.

Occasionally the computer data acquisition system failed, resulting in a loss of data.

Twenty-eight of the 32 runs that have been fully processed by UNC were modeled in this study. The remaining 4 runs (6 and 7 August 1982) were not modeled because experimental difficulties were encountered during the loading of the chamber. The amount of auto exhaust sample that was injected into the chamber was so low that it was impossible for UNC to obtain speciated data for more than a few of the auto exhaust hydrocarbons.

Initial conditions for the 1982 and 1983 auto exhaust runs modeled in this study are given in Table 22. In order to simulate these runs, the NMHC data reported by UNC had to be partitioned among the seven reactive organic groupings used in the CBM-X (PAR, ETH, OLE, ALD2, FORM, TOL, XYL). This was accomplished easily for the 1983 runs since good speciated HC data were obtained during the 1983 chamber season. In the 1982 runs, however, as much as 40-60 percent of the reported NMHC was not speciated.

For these runs, similar unleaded fuel was used for both automobiles for several tests in both 1982 and 1983.* The amounts of ethene and propene tended to vary from run to run because of minor differences in warmup. Also, the 1982 data, except for the 15 July 1982 simulation, contain ethene, propene, and toulene information processed and reported by Jeffries et al. (1985). The 1983 data was processed and reported for these species as well as the higher olefins and the higher aromatics. The assumption was made that the ratios of propene to higher olefins and toluene to higher aromatics would be constant for each of the automobiles in 1982, and that these ratios would be the averages of the 1983 data for the same automobiles. Actually the ratios derived in this fashion turned out to be virtually identical for the two automobiles. The computed OLE/propene ratio for both automobiles was 1.6 to 1. The TOL/toluene ratio for the Volare was 1.3 to 1 while the ratio for the Charger was 1.4 to 1. Both sets of data gave XYL/TOL ratios of 0.68 to one. For 15 July 1982, an average of the 1983 Volare splits was used for the auto exhaust fraction.

---

* The methodology adopted was based on discussions with Jeffries and Sexton of UNC; privte communications 1985.

TABLE 22. Auto exhaust data for 1982 and 1983 smog chamber experiments.

(a) Initial Conditions

UNC Experiment No.	NO	NO_2	HNO_2*	Wall* Formal-dehyde	H_2O	CO	ETH	PAR	OLE	TOL	XYL	ALD	FORM	NMHC
62582B	0.608	0.044	0.002	0.007	17,000	7.60	0.052	0.158	0.033	0.018	0.012	0.005	0.015	0.550
62582R	0.618	0.045	0.000	0.007	17,000	7.60	0.056	0.141	0.030	0.019	0.013	0.005	0.030	0.550
62982B	0.233	0.027	0.000	0.010	20,000	56.50	0.150	1.440	0.081	0.046	0.032	0.025	0.027	2.480
62982R	0.219	0.025	0.000	0.003	24,500	63.00	0.150	1.380	0.083	0.049	0.034	0.025	0.027	2.460
63082B	0.284	0.035	0.000	0.010	20,000	68.60	0.226	1.440	0.102	0.064	0.043	0.027	0.029	2.840
63082R	0.290	0.032	0.000	0.005	20,000	68.00	0.234	1.690	0.099	0.062	0.042	0.020	0.020	3.130
70182B	0.330	0.030	0.001	0.000	20,000	79.00	0.330	1.810	0.122	0.070	0.047	0.020	0.020	3.600
70182R	0.340	0.029	0.001	0.000	20,000	76.00	0.323	1.830	0.100	0.069	0.047	0.020	0.020	3.600
71582B	0.555	0.043	0.003	0.000	21,000	8.80	0.100	0.540	0.006	0.123	0.026	0.010	0.010	1.881
71582R	0.540	0.030	0.0003	0.000	21,000	7.55	0.085	0.470	0.031	0.032	0.097	0.006	0.006	1.702
80382B	0.099	0.066	0.004	0.002	16,000	10.70	0.070	0.830	0.034	0.017	0.012	0.010	0.010	1.250
80382R	0.420	0.040	0.001	0.000	19,000	19.20	0.072	1.960	0.049	0.020	0.014	0.040	0.030	2.600
91782B	0.150	0.096	0.006	0.000	15,500	25.00	0.137	1.520	0.067	0.039	0.027	0.010	0.020	2.419
91782R	0.150	0.100	0.010	0.000	21,000	21.50	0.118	1.500	0.058	0.025	0.017	0.010	0.020	2.160
92982B	0.320	0.074	0.003	0.012	8,300	20.70	0.087	1.080	0.051	0.031	0.021	0.018	0.020	1.740
92982R	0.317	0.075	0.006	0.000	7,500	16.10	0.091	1.000	0.049	0.035	0.024	0.002	0.002	1.720
100682B	0.369	0.097	0.008	0.000	12,900	24.20	0.142	0.803	0.027	0.039	0.027	0.030	0.022	1.960
100682R	0.369	0.097	0.000	0.015	12,000	21.00	0.139	1.130	0.024	0.020	0.024	0.020	0.022	1.788
70283B	0.162	0.022	0.001	0.000	18,000	38.60	0.085	0.943	0.039	0.041	0.028	0.002	0.006	1.700
70283R	0.160	0.014	0.0005	0.000	18,000	11.30	0.046	0.947	0.021	0.045	0.031	0.000	0.020	1.644
71583B	0.307	0.045	0.003	0.000	15,500	12.70	0.100	1.190	0.057	0.060	0.041	0.030	0.030	2.250
71583R	0.314	0.045	0.008	0.000	20,000	3.00	0.057	1.210	0.046	0.061	0.044	0.000	0.014	2.190
81183B	0.185	0.043	0.000	0.008	18,000	17.70	0.066	0.180	0.027	0.026	0.018	0.002	0.020	0.678
81183R	0.185	0.038	0.0015	0.000	18,000	58.00	0.058	0.893	0.077	0.058	0.040	0.006	0.020	2.151
100483B	0.214	0.037	0.0005	0.000	17,000	20.34	0.225	0.579	0.044	0.073	0.052	0.019	0.043	2.190
100483R	0.216	0.038	0.003	0.000	10,000	15.84	0.101	1.640	0.041	0.041	0.053	0.020	0.020	2.600
100783B	0.300	0.036	0.000	0.000	14,000	0.15	0.311	0.694	0.057	0.073	0.066	0.039	0.020	2.685
100783R	0.293	0.041	0.0005	0.000	12,000	0.21	0.111	1.62	0.066	0.050	0.040	0.047	0.000	2.698

* These chamber effects were used to optimize agreement between data and simulations; see text for further discussion.

TABLE 22. (concluded)

(b) Comparison of Simulations and Experiments

UNC Experiment Number	Initial NO_x	Initial NO_2/NO_x	Initial HC/NO_x	Maximum O_3		Difference in O_3 Maxima (ppm)	Time to Maximum O_3 (min)		Difference in Time to O_3 Maxima (min)
				Simulated	Measured		Simulated	Measured	
62582B	0.652	0.067	0.84	0.003	0.003	0.000	600	600	0
62582R	0.653	0.069	0.84	0.003	0.003	0.000	650	600	50
62982B	0.260	0.104	9.54	1.00	0.77	0.23	520	480	40
62982R	0.244	0.102	10.08	0.91	0.70	0.21	520	470	50
63082B	0.319	0.110	8.90	1.08	0.85	0.23	520	540	-20
63082R	0.322	0.100	9.72	1.03	0.81	0.22	535	535	0
70182B	0.360	0.083	10.00	> 1.00	0.75	-	-	410	-
70182R	0.369	0.079	9.76	> 1.00	0.74	-	-	420	-
71582B	0.598	0.072	3.15	0.04	0.04	0.00	> 720	> 720	-
71582R	0.570	0.053	2.99	0.38	0.22	0.16	> 720	> 720	-
80382B	0.165	0.400	7.58	0.65	0.58	0.07	> 560	> 560	-
80282R	0.460	0.087	5.65	0.26	0.34	-0.08	> 560	> 560	-
91782B	0.246	0.390	9.83	0.85	0.64	0.21	590	525	65
91782R	0.250	0.400	8.64	0.73	0.52	0.21	590	520	70
92982B	0.394	0.188	4.42	0.24	0.20	0.04	> 600	> 600	-
92982R	0.392	0.191	4.39	0.12	0.07	0.05	> 560	> 560	-
100682B	0.466	0.208	4.4	0.41	0.45	-0.04	> 560	> 560	-
100682R	0.466	0.208	3.84	0.33	0.36	-0.03	> 600	> 600	-
70283B	0.184	0.120	9.24	0.87	0.69	0.18	605	500	105
70283R	0.174	0.080	9.45	0.72	0.59	0.13	630	560	70
71583B	0.352	0.125	6.39	0.95	0.92	0.03	> 640	560	-
71583R	0.359	0.125	6.10	0.81	0.85	-0.05	> 640	> 640	-
81183B	0.228	0.184	2.97	> 0.70	0.60	-	> 640	> 580	-
81183R	0.223	0.170	9.65	1.08	0.85	0.23	540	485	65
100483B	0.251	0.147	8.73	0.81	0.63	0.18	500	400	100
100483R	0.254	0.150	10.24	> 0.80	0.60	-	-	480	-
100783B	0.336	0.106	5.28	0.74	0.46	0.28	530	530	0
100783R	0.334	0.123	7.91	> 0.25	0.18	-	-	545	-

Due to the overall uncertainties of this approach, the unreactive hydrocarbons were not separated. The remaining carbon from the reported NMHC values minus ETH, OLE, TOL, and XYL were assumed to react as PAR. Aldehydes ALD2 and FORM were assumed to be near one percent of the NMHC each unless such assumed formaldehyde levels seemed unreasonably lower than the typical chamber effects used in the mechanism validation simulations. These experiments are briefly described next.

25 June 1982

Both sides of the chamber were loaded with direct injections of exhaust from the Plymouth Volare using premium unleaded gasoline. These NMHC and NO_x ratios were equal and both sides yielded similar results. The ratio of NMHC/NO_x was the lowest of all the experiments.

29 June 1982

In these experiments, both sides of the chamber were injected with exhaust obtained from the Plymouth Volare using premium unleaded gasoline. The same levels of NMHC and NO_x were injected into both sides of the chamber.

30 June 1982

These experiments were essentially a repetition of the 29 June 1982 runs except that the levels of auto exhaust and NO_x injected into the chamber were somewhat higher.

1 July 1982

These experiments were matched-injection experiments in which both sides of the chamber were loaded with exhaust from the Dodge Charger fueled with unleaded regular gasoline.

15 July 1982

Although both sides received matched injections from the Plymouth Volare in this experiment, toluene was added to one side and m-xylene was added to the other side. The side with m-xylene showed much more reactivity.

3 August 1982

On this day, each side of the chamber was loaded with different levels of NO_x and auto exhaust. The auto exhaust was obtained from the

Dodge Charger fueled with unleaded regular gasoline. The RHC/NO_x ratios on the two sides of the chamber differed by a factor of two.

17 September 1982

These experiments were supposed to be matched injections. However, the concentration of auto exhaust in the two chamber sides differed by about 10 percent, yielding a difference in peak O_3 of about 15 to 20 percent. For these experiments, auto exhaust from the Dodge Charger operated with unleaded regular gasoline was directly injected into one side of the chamber. At the same time, an identical exhaust sample was collected using UNC's cryocondenser. The cryocondenser sample was subsequently evaporated into the other side of the chamber.

29 September 1982 and 6 October 1982

These experiments compared matched direct injections from the Dodge Charger and the Plymouth Volare. Both cars were fueled with the same gasoline. There were a number of analytical difficulties encountered during these two days that made these data less than ideal for modeling purposes.

2 July 1983

Similar to the 29 September and 6 October 1982 experiments, the 2 July 1983 experiments compared direct injections from the Dodge Charger and Plymouth Volare fueled with the same gasoline.

15 July 1983

These experiments used matched injections with the same car but different fuels. The blue side of the chamber was injected with exhaust from the Dodge Charger fueled with unleaded regular gasoline. The red side of the chamber was injected with exhaust from the Dodge Charger fueled with premium unleaded gasoline.

11 August 1983

These experiments compared direct injections from the Plymouth Volare at different levels of NMHC. NO_x was matched in the two chamber sides, but NMHC differed by a factor of three.

4 October 1983

These experiments compared the effect of using a real auto exhaust sample with those obtained using a synthetic auto exhaust sample. On the basis of their gas chromatographic analyses of real exhaust samples, UNC constructed a synthetic exhaust mixture containing the 13 most prevalent organics in the real exhaust samples--ethene, propene, 1-butene, trans-2-butene, n-butane, isopentane, 2,2,4-trimethylpentane, benzene, toluene, m-xylene, o-xylene, 1,2,4-trimethylbenzene, and formaldehyde. The blue side of the chamber was injected with this synthetic mix. The red side of the chamber was injected with similar levels of real auto exhaust from the Dodge Charger, fueled with unleaded regular gasoline.

7 October 1983

In this comparison, the synthetic auto exhaust mixture was matched with a synthetic urban mixture. The overall NMHC and NO_x concentrations were well matched, but a considerable difference in ozone production was observed because the synthetic auto exhaust was much more reactive than the synthetic urban mixture.

RESULTS

Comparisons of results of the auto exhaust simulations with experimental data is presented in Figures 8-35, which are placed at the end of this section. A discussion of the results obtained for each experiment is presented in the following paragraphs.

25 June 1982

It was necessary to simulate the ozone loss due to reaction with NO in the sample line. This is typically not a serious problem when NO levels are less than 0.05 ppm, but in these runs the correction is rather substantial. The general reactivity of the auto exhaust data and the simulation are well matched at this low $NMHC/NO_x$ ratio. Such low ratios provide important tests of chemical models because NO and NO_2 behavior are sensitive to overall reactivity, and future control scenarios often aim in this direction. The results indicate that the simulations predict less reactivity (less conversion of NO to NO_2) near the end of the experiment on both sides of the chamber.

29 June 1982

On both sides of the chamber, ozone was overpredicted, but NO_2 peaks appear to be underpredicted. The overprediction is due partly to the treatment of unreactive hydrocarbons as PAR. Detailed speciation on these species was not available. The apparent underprediction of NO_2 peaks is explained by the response of the NO_2 detector to PAN. The use of NO_2 plus PAN or NO_2P as in the acetaldehyde experiments shown in Appendix B would eliminate this apparent discrepancy. Another instrument problem observed in the acetaldehyde experiments concerns formaldehyde where PAN apparently interferes as well. However, the PAN correction can account for only about half of the formaldehyde discrepancy between observations and the simulations.

30 June 1982

Since these runs were mainly a repetition of the previous day, the results were similar. Hence the previous discussion also applies. Note however that a PAN correction applied to the formaldehyde data would explain more than half of the discrepancy between observed and simulated formaldehyde.

1 July 1982

Ozone for this simulation was somewhat overpredicted and peak NO_2 was somewhat underpredicted. Simulated levels of both HCHO and PAN were lower than the experimental levels. Again, the previous discussion applies since the NO_x, NMHC, and ozone levels are similar even though a different automobile was used.

15 July 1982

Results for the side with added toluene agree well with the experiments but ozone is overpredicted on the side with m-xylene added (UNCR). However, if the reason for the overprediction in many of these experiments were known, the results for these runs may be an underprediction for the toluene side (UNCR).

3 August 1982

The HC/NO_x ratios in the two sides of the chamber on this day differed by a factor of two. A low prediction was obtained for the red side of the chamber, in which the RHC/NO_x ratio was only 3.4. The simulated reactivity of the system was less than the reactivity observed experimentally. Predictions obtained for the blue side of the chamber where the RHC/NO_x ratio was 6.2 were somewhat better although the simulated reactivity was greater than the observed reactivity. As mentioned earlier, very little of the hydrocarbon was speciated in the 1982 runs. On this particular day, 42 percent of the carbon on the high RHC/NO_x side of the chamber was not speciated and 59 percent of the carbon on the low RHC/NO_x side was not identified. The poor fits obtained could be a reflection of the uncertainty of the initial hydrocarbon species. There is a discrepancy in ratios of ethene, propene, and toluene between the sides and these are not similar to the ratio for NMHC even though the same exhaust was used on both sides.

17 September 1982

These runs compared results of direct injection of auto exhaust against those of auto exhaust obtained by evaporating a cryocondenser sample. In general, the fits obtained for both sides of the chamber were reasonably good although ozone was somewhat overpredicted.

29 September 1982 and 6 October 1982

These runs compared the effect of using different cars fueled with the same gasoline. The ozone predictions obtained for the 29 September run using the Plymouth Volare were quite good although somewhat high. The predictions obtained for the Dodge Charger runs on 6 October, were also in fair agreement, but low. The discrepancy in the fits obtained for these two runs may reflect the amount of hydrocarbon speciated data that were obtained in these runs. For the 29 September run, 44 percent of the NMHC data were unspeciated. All but 11 percent of the NMHC data were speciated in the 6 October run. However, the speciations are still being evaluated by Jeffries et al. (1985).

2 July 1983

These runs also compared the effect of using the same gasoline but different cars. In general, reasonable fits were obtained for both of these runs. Ozone was somewhat overpredicted, whereas PAN and formaldehyde were underpredicted.

15 July 1983

These runs compared the effects of using same car but different gasoline. In general, good agreement was obtained for all species in these two runs except PAN, which tended to be low, and ozone, which was predicted to be a little late in the simulations.

11 August 1983

These runs compared the effect of using the same car, gasoline, and NO_x level but different levels of NMHC. Both sides showed the ozone overprediction common to most simulations. However, PAN was somewhat overpredicted on the high NMHC side (UNCR) and underpredicted on the low NMHC side (UNCB).

4 October 1983

These runs compared real auto exhaust against a synthetic auto exhaust mixture. Respectable fits to the NO, NO_2, and O_3 data were obtained for both sides of the chamber. Formaldehyde predictions, however, were low by more than a factor of two for both experiments, which is only partially explained by corrections for PAN interference.

7 October 1983

These runs compared the synthetic auto exhaust mixture with a synthetic urban mixture of hydrocarbons. Unfortunately, overpredictions of ozone were large for both sides. The overprediction apparently indicates that the surrogate approximations need further study. For instance, the use of toluene chemistry for n-propyl benzene and sec-butyl benzene may be too reactive. However, the synthetic urban mix had a TOL/toluene ratio of 2 to 1, which is apparently greater than the auto exhaust measurements indicated (1.3 for the Volare and 1.4 for the Charger). The urban mixture OLE/propene ratio was 1.9, which was also larger than the auto exhaust ratio of 1.6.

OVERVIEW OF THE MODELING RESULTS

The general tendency in these tests has been an overprediction of ozone. Part of the overprediction can be explained by treating unreactive hydrocarbons as PAR, but some overprediction must apparently come from the mechanism itself and the use of unsubstantiated surrogate approximations. Experiments for some of the aromatics and olefins treated as toluene, m-xylene, propene, or carbonyls will need to be performed in the future to develop better surrogate approximations.

The overall average difference between observed and simulated ozone maxima indicates a positive bias of about 80 ppb. This is consistent with some of the validation tests of the mechanism such as formaldehyde and ethene. The standard deviation for the auto exhaust experiments is 130 ppb which implies about a 25 percent discrepancy from the average ozone observed of 530 ppb. Timing of the ozone maxima average about 23 minutes late.

In general, formaldehyde predictions are lower than observed values. Most of this discrepancy can be explained by a PAN interference in the UNC measurements. However, this discrepancy has not been confirmed by UNC. The acetaldehyde simulations which often involve high PAN concentrations show the apparent interference. Future tests with an alternate formaldehyde measurement technique in the presence of high PAN concentrations is recommended. Biacetyl may be a good PAN precursor for such experiments since formaldehyde to PAN ratios would apparently be low in such experiments.

The timing of the processed data from UNC, the final version of the Atkinson and Lloyd (1984) evaluation, and the end of this contract left little time to change the mechanism to obtain improved simulations of the auto exhaust data. However, the overall agreement for all of the validation sets testing components of the mechanism and the auto exhaust set testing the overall mechanism was fairly consistent. In spite of a general tendency towards overprediction, the mechanism performed well over a wide rang of concentrations and NMOC/NO_x ratios. Reliable simulation of wide ranges of conditions is necessary if a mechanism is to be used for control strategy predictions. Also, the result seen in this project both experimentally and in the simulations comparing synthetic auto exhaust with genuine auto exhaust is significant. This agreement between auto exhaust and synthetic exhaust indicates that there are no highly reactive or inhibiting organics missing from either the experiments or the chemistry. That is the unspeciated organics are not overly important in either a positive or negative manner. Hence, future refinements to the chemistry can be tested against synthetic auto exhaust which has the potential of more accurate data on initial conditions and is operationally less expensive to load the chamber and analyze data.

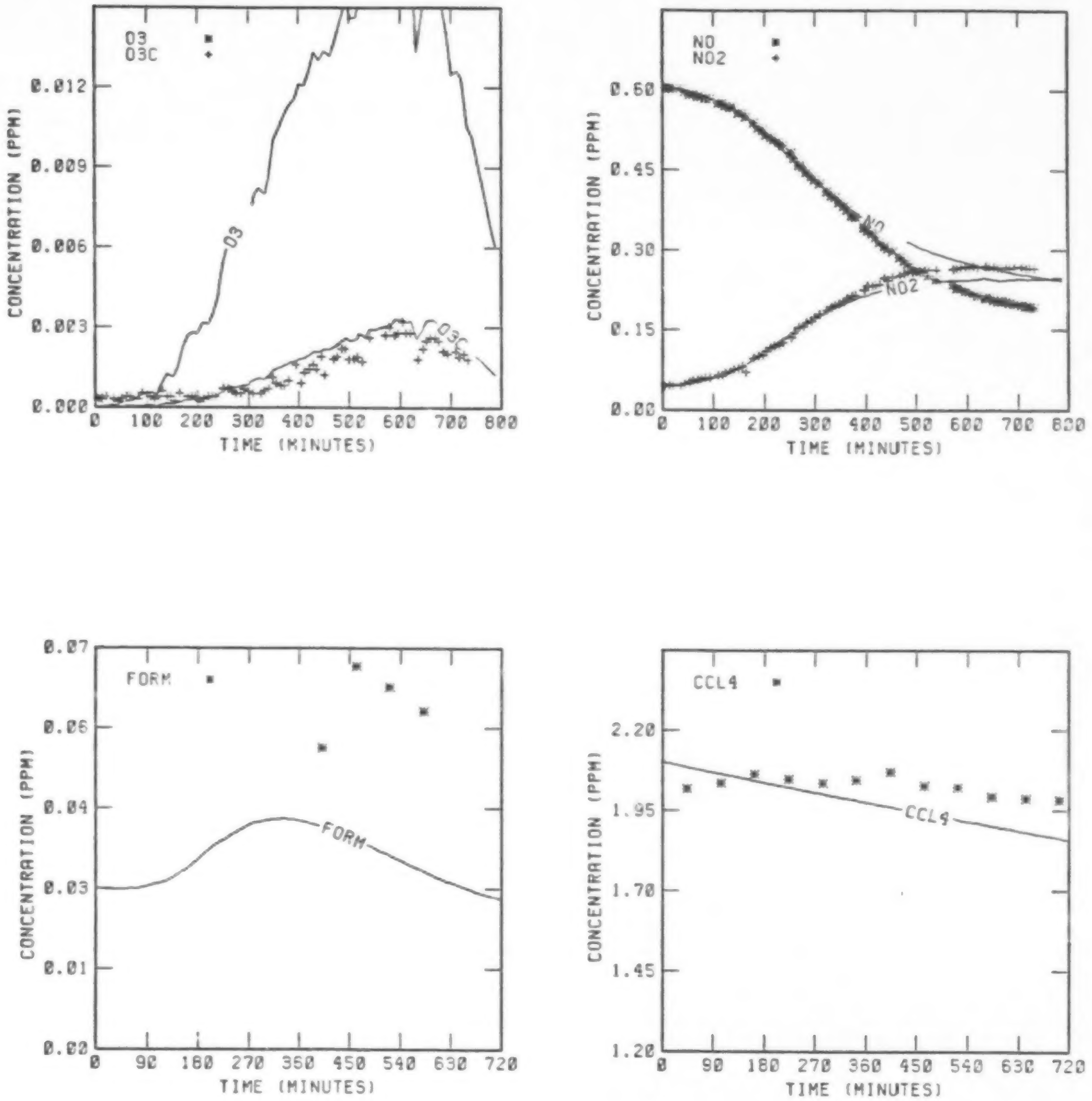

FIGURE 8 . SIMULATION RESULTS FOR
UNCB 62582

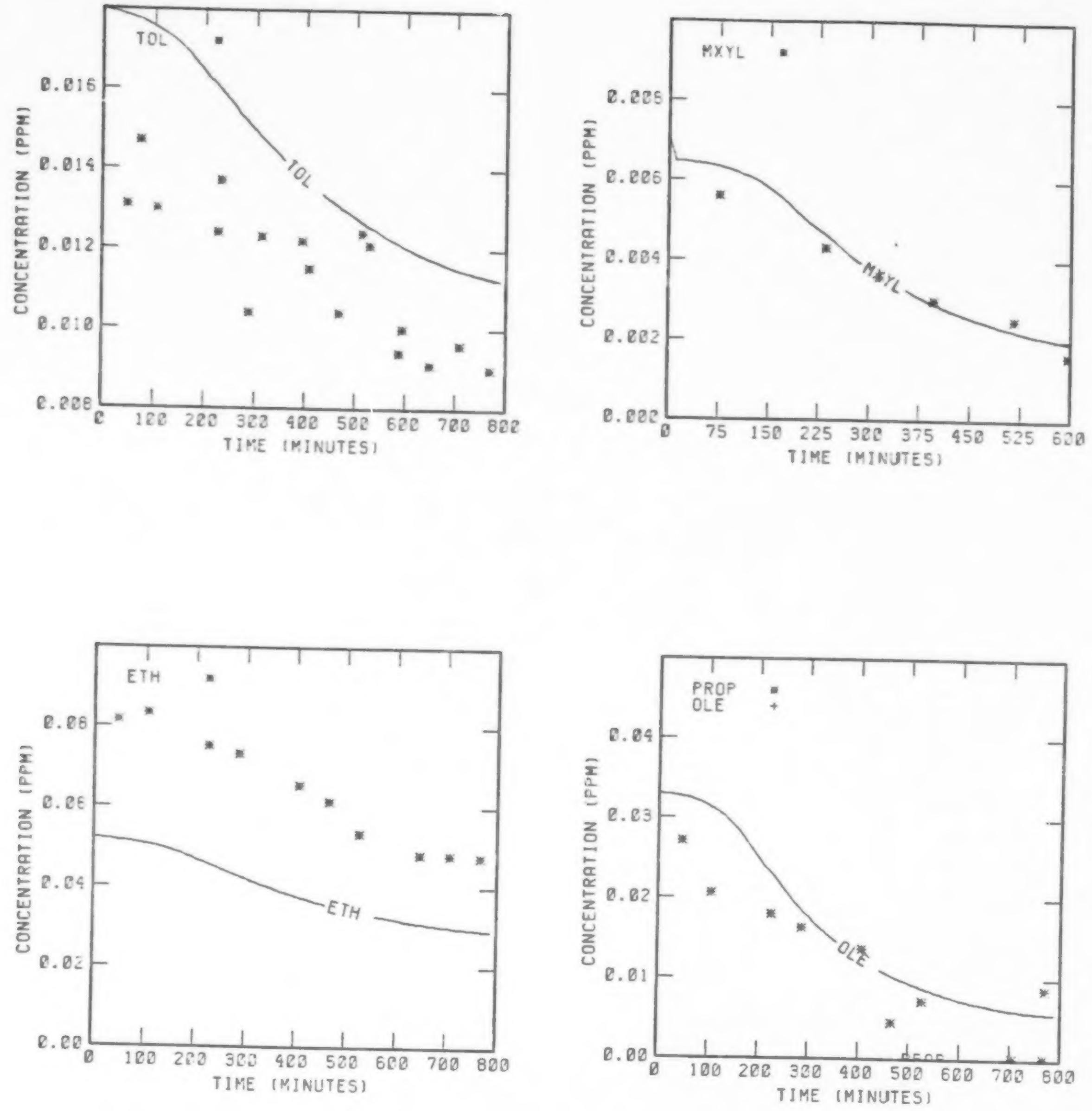

FIGURE 8 . SIMULATION RESULTS FOR
UNCB 62582
continued.

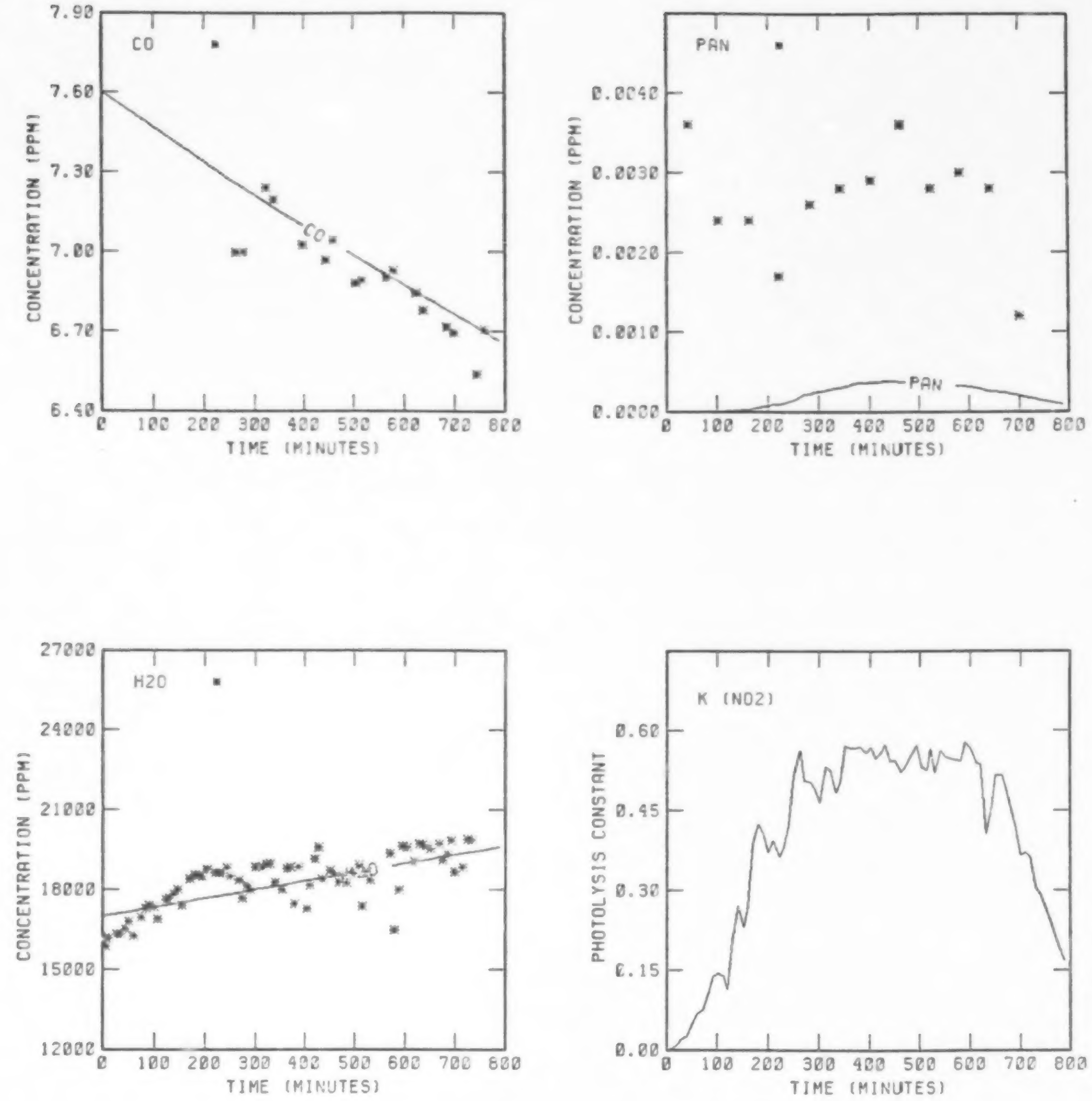

FIGURE 8 . SIMULATION RESULTS FOR
UNCB 62582

continued.

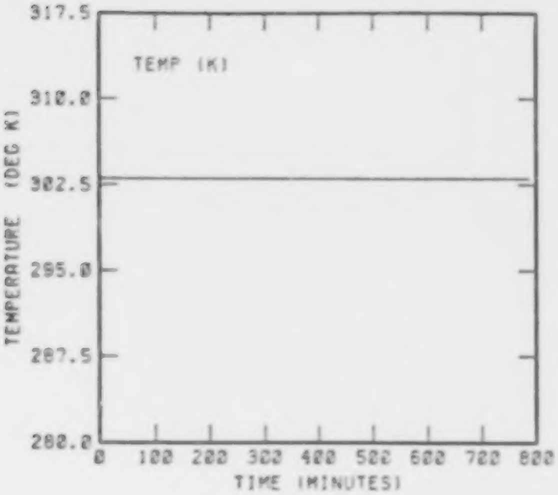

FIGURE 8 . SIMULATION RESULTS FOR
UNCB 62582
concluded.

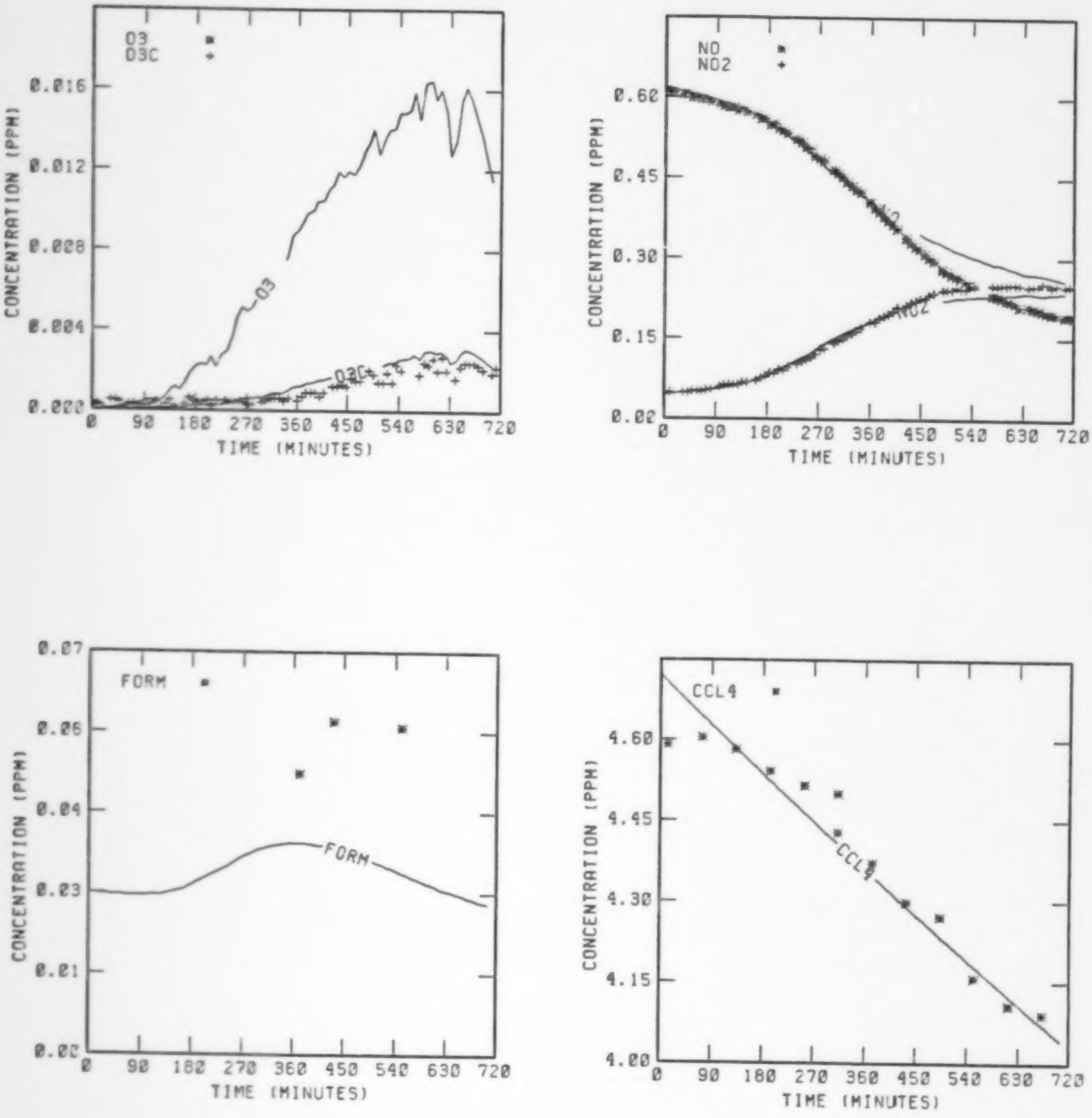

FIGURE 9 . SIMULATION RESULTS FOR
UNCR 62582

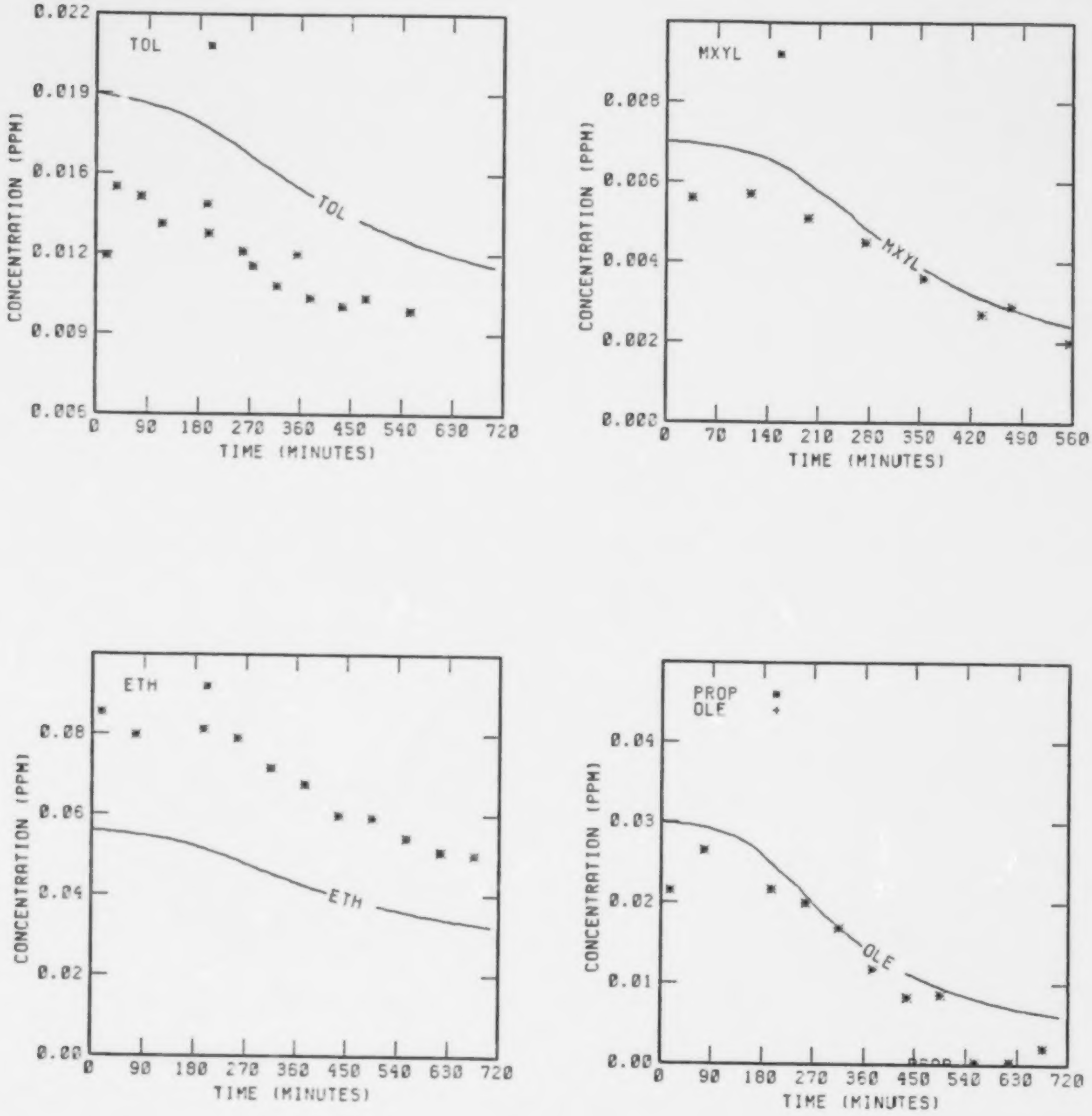

FIGURE 9 . SIMULATION RESULTS FOR
UNCR 62582
continued.

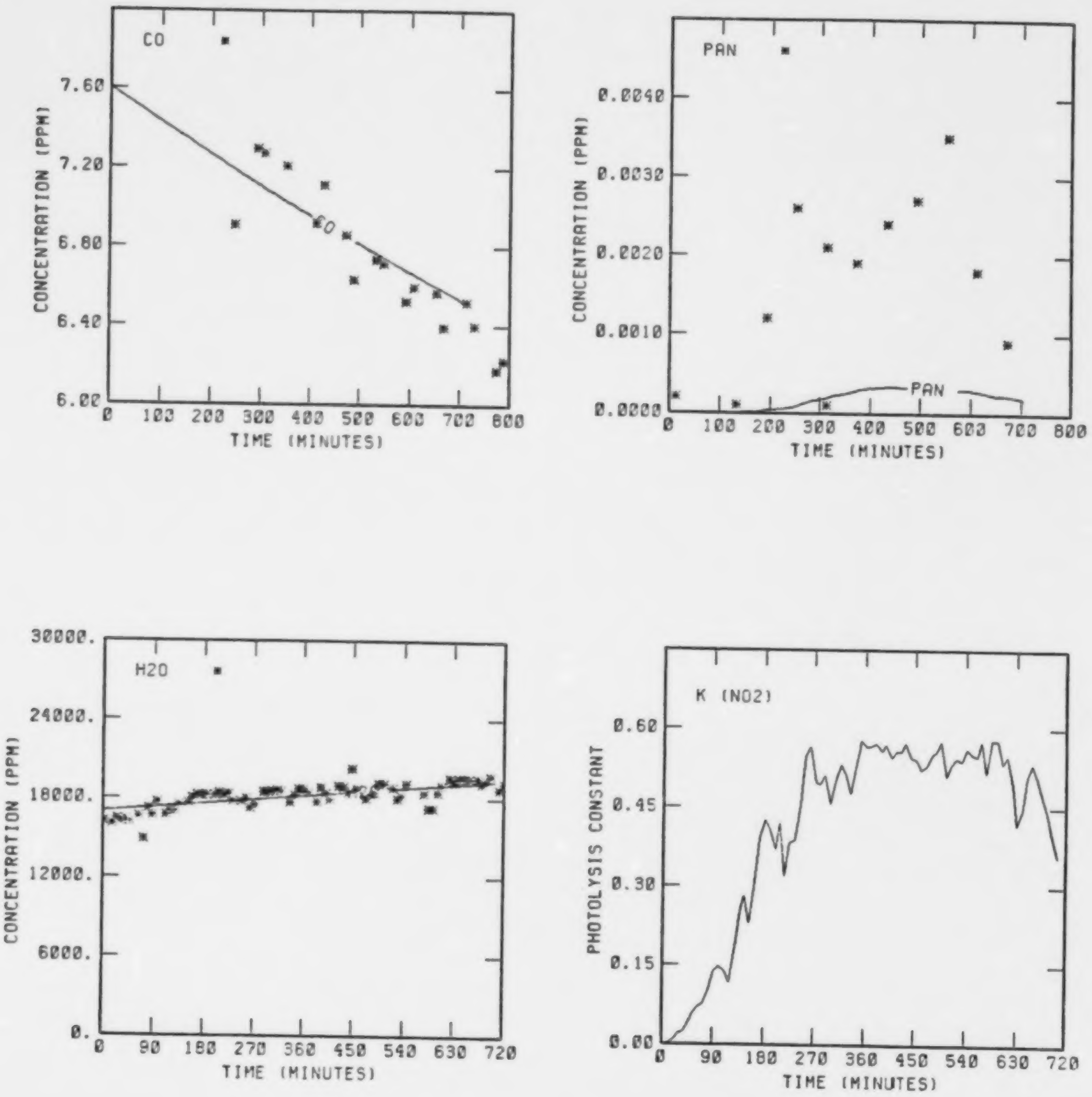

FIGURE 9 . SIMULATION RESULTS FOR
UNCR 62582

continued.

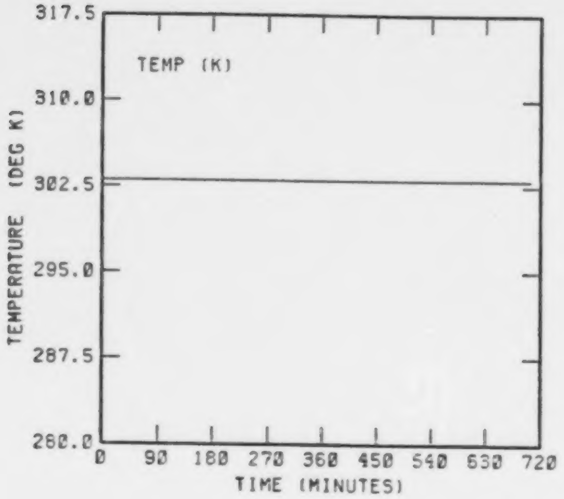

FIGURE 9 . SIMULATION RESULTS FOR UNCR 62582

concluded.

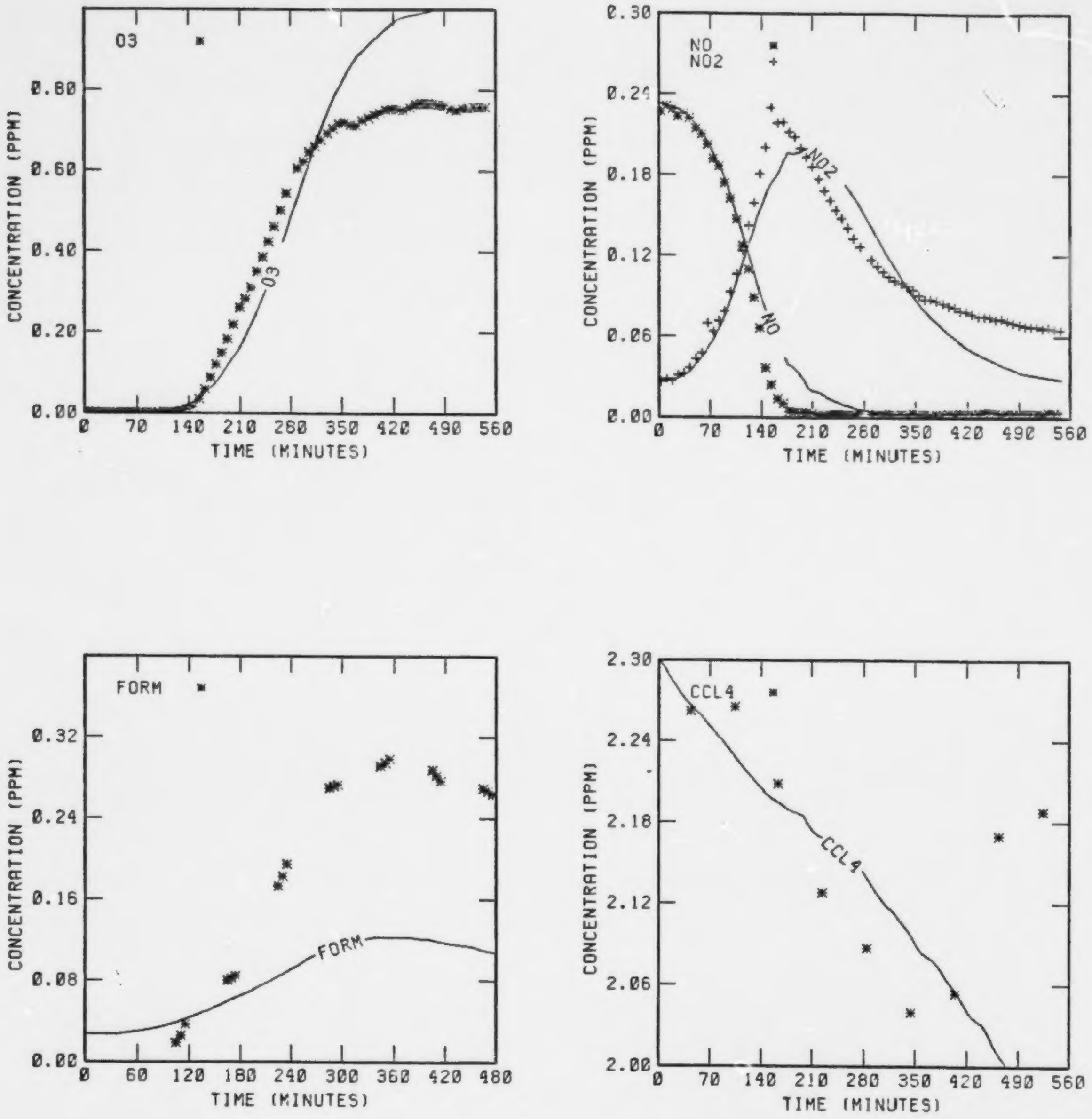

FIGURE 10. SIMULATION RESULTS FOR
UNCB 62982

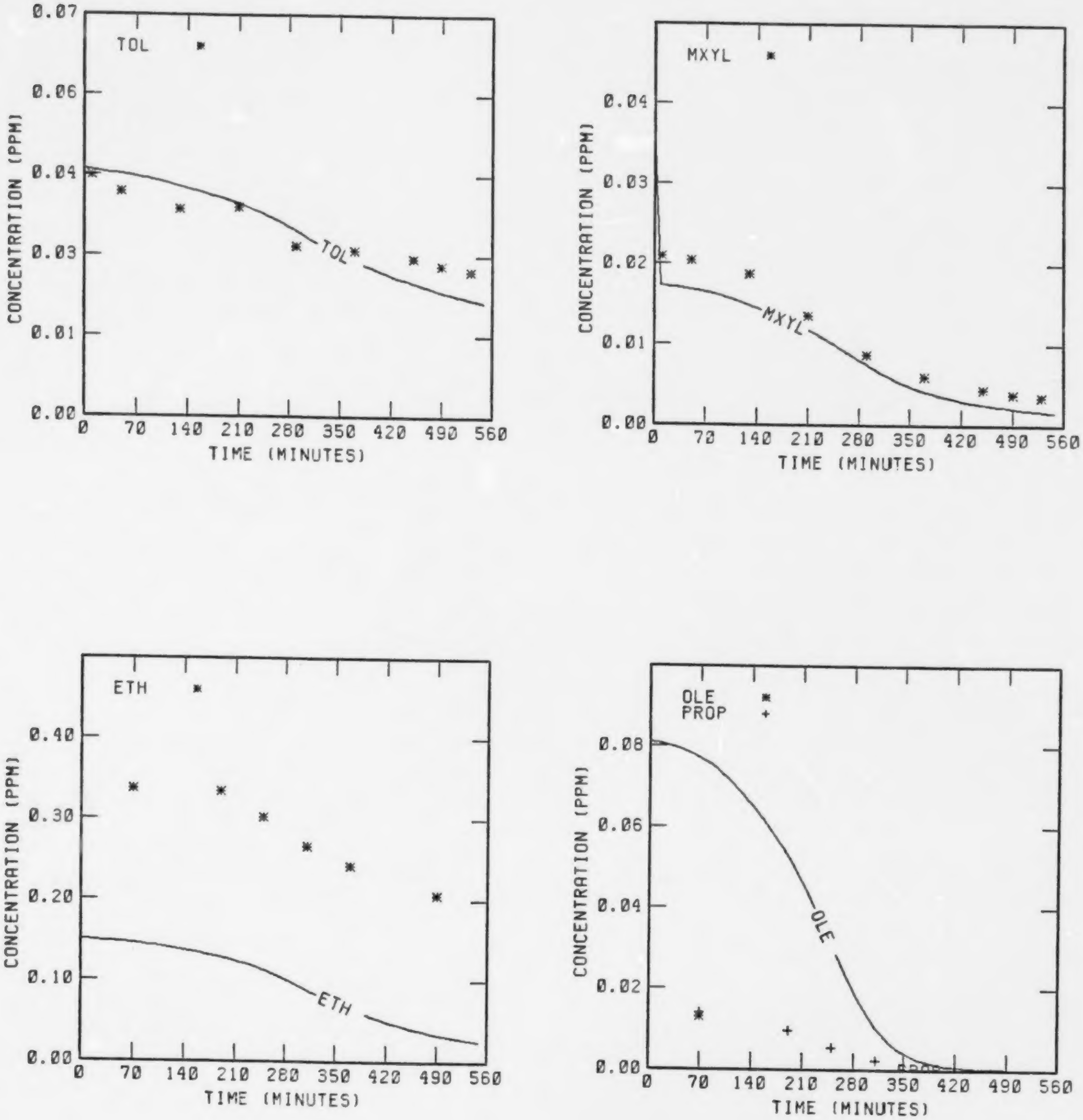

FIGURE 10. SIMULATION RESULTS FOR
UNCB 62982
continued.

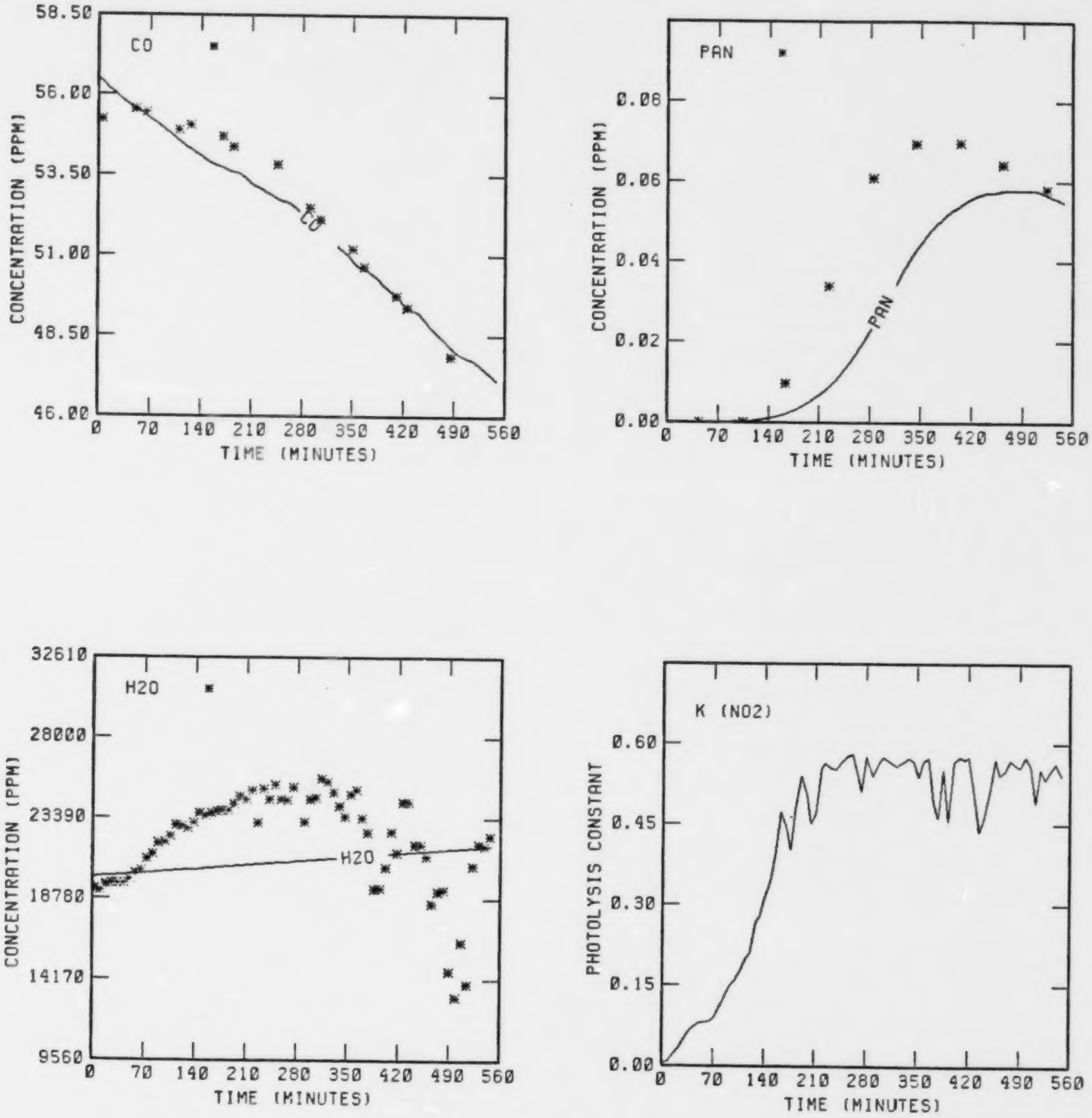

FIGURE **10.** SIMULATION RESULTS FOR UNCB 62982

continued.

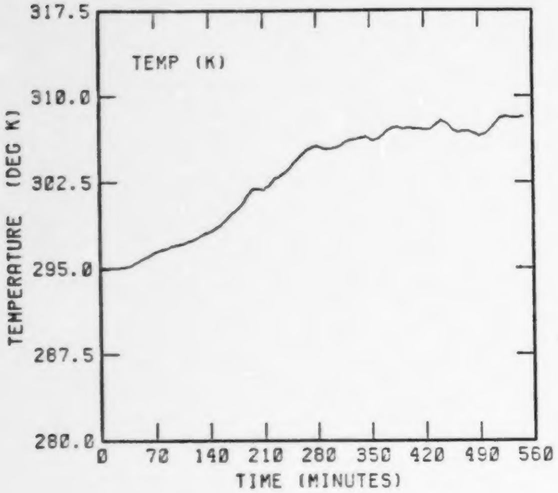

FIGURE 10. SIMULATION RESULTS FOR
UNCB 62982
concluded.

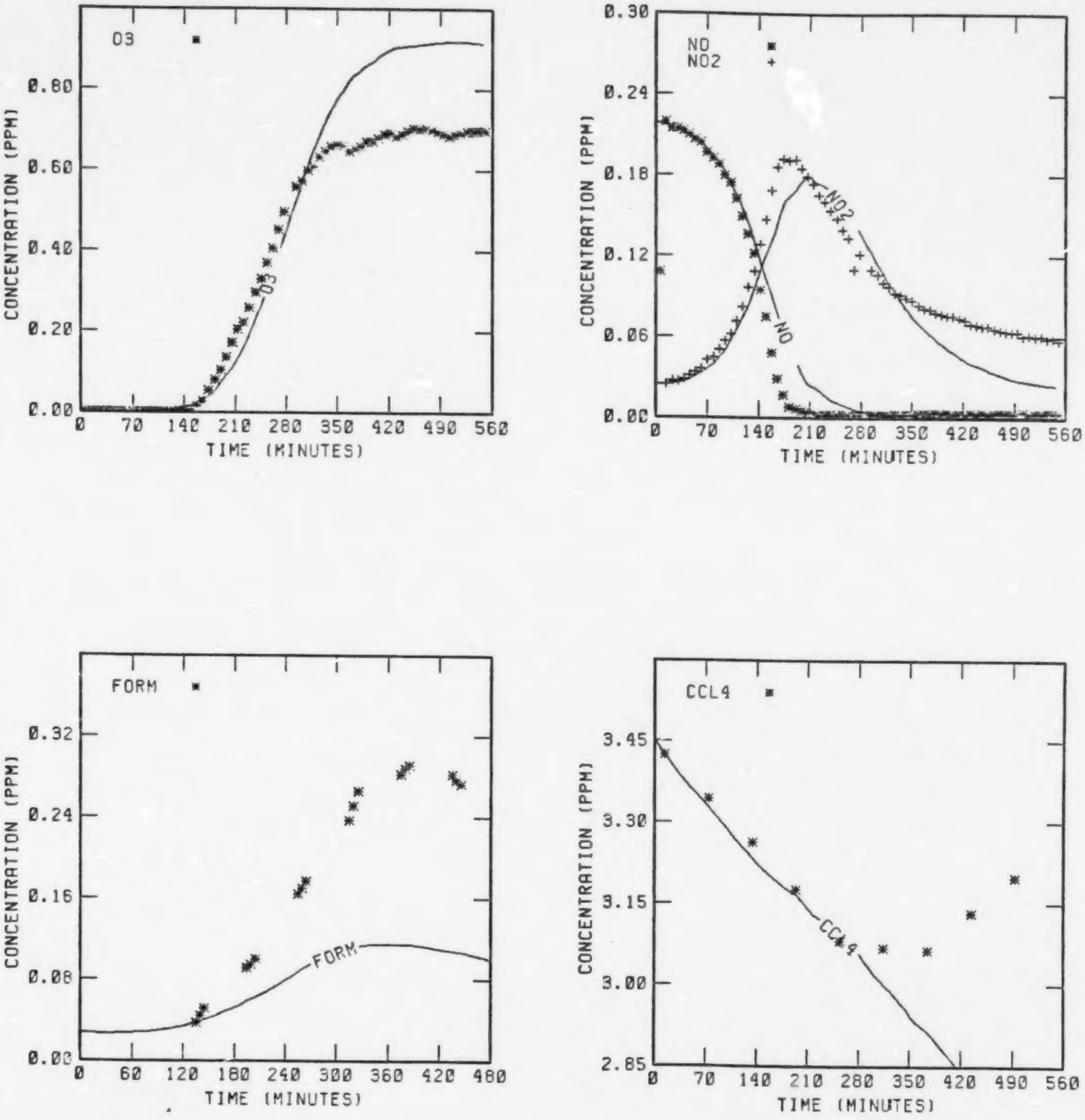

FIGURE 11 . SIMULATION RESULTS FOR
UNCR 62982

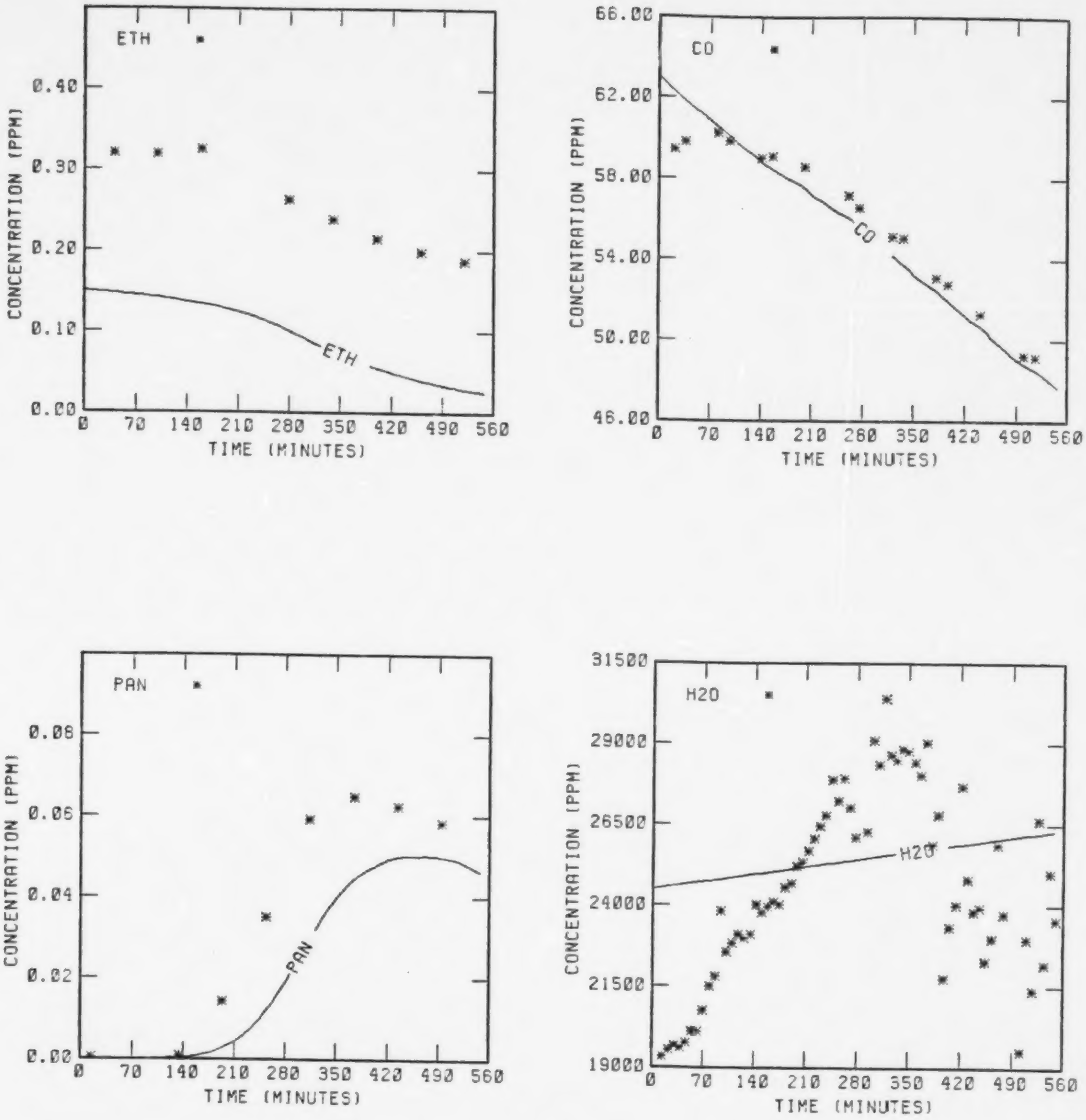

FIGURE 11. SIMULATION RESULTS FOR UNCR 62982

continued.

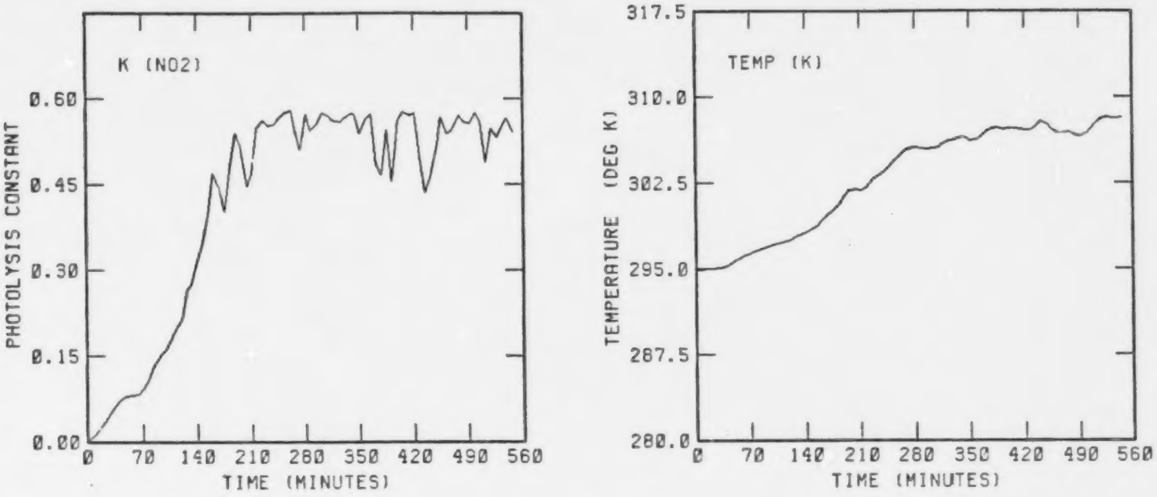

FIGURE **11**. SIMULATION RESULTS FOR
UNCR 62982
concluded.

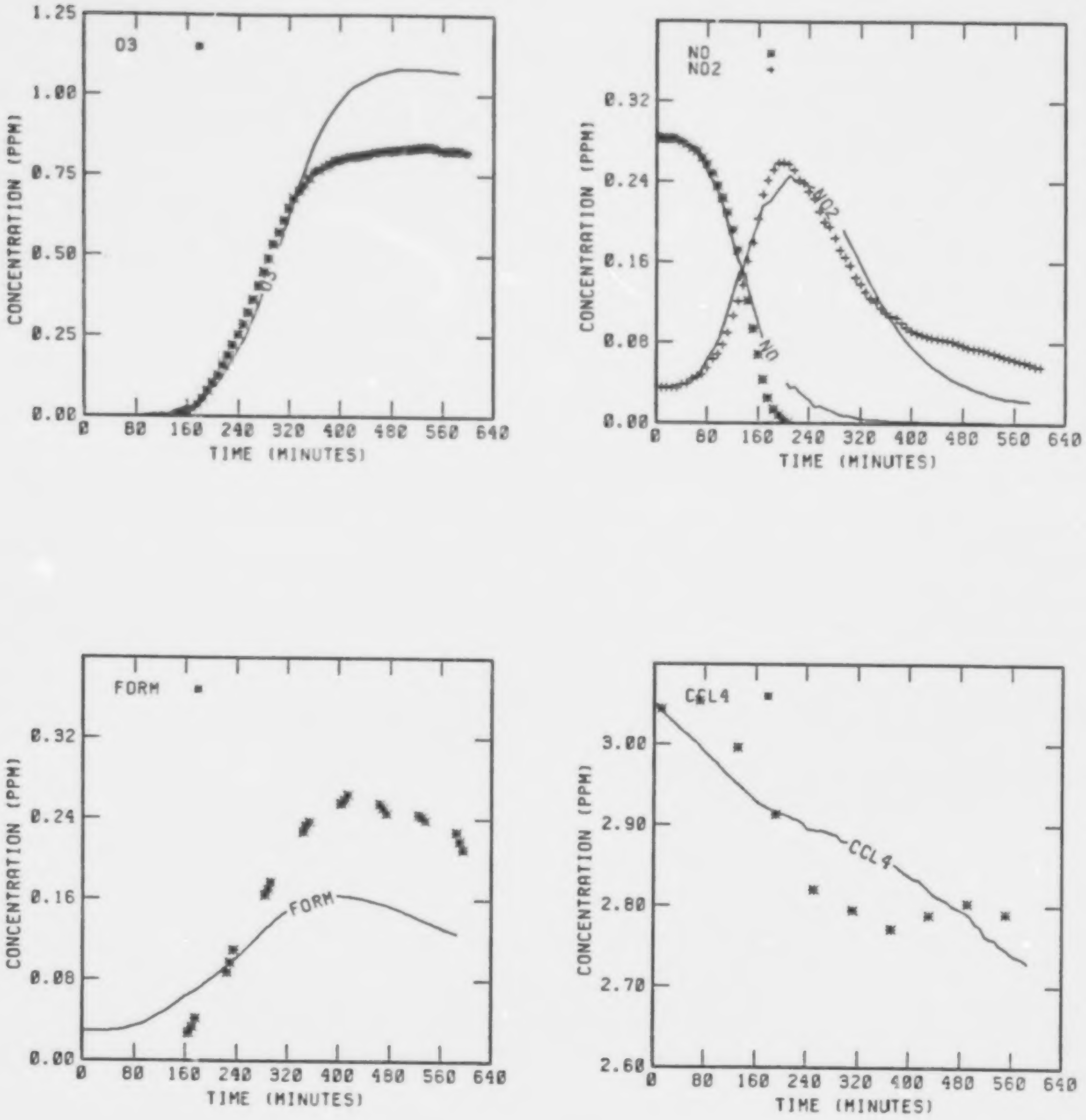

FIGURE 12. SIMULATION RESULTS FOR
UNCB 63082

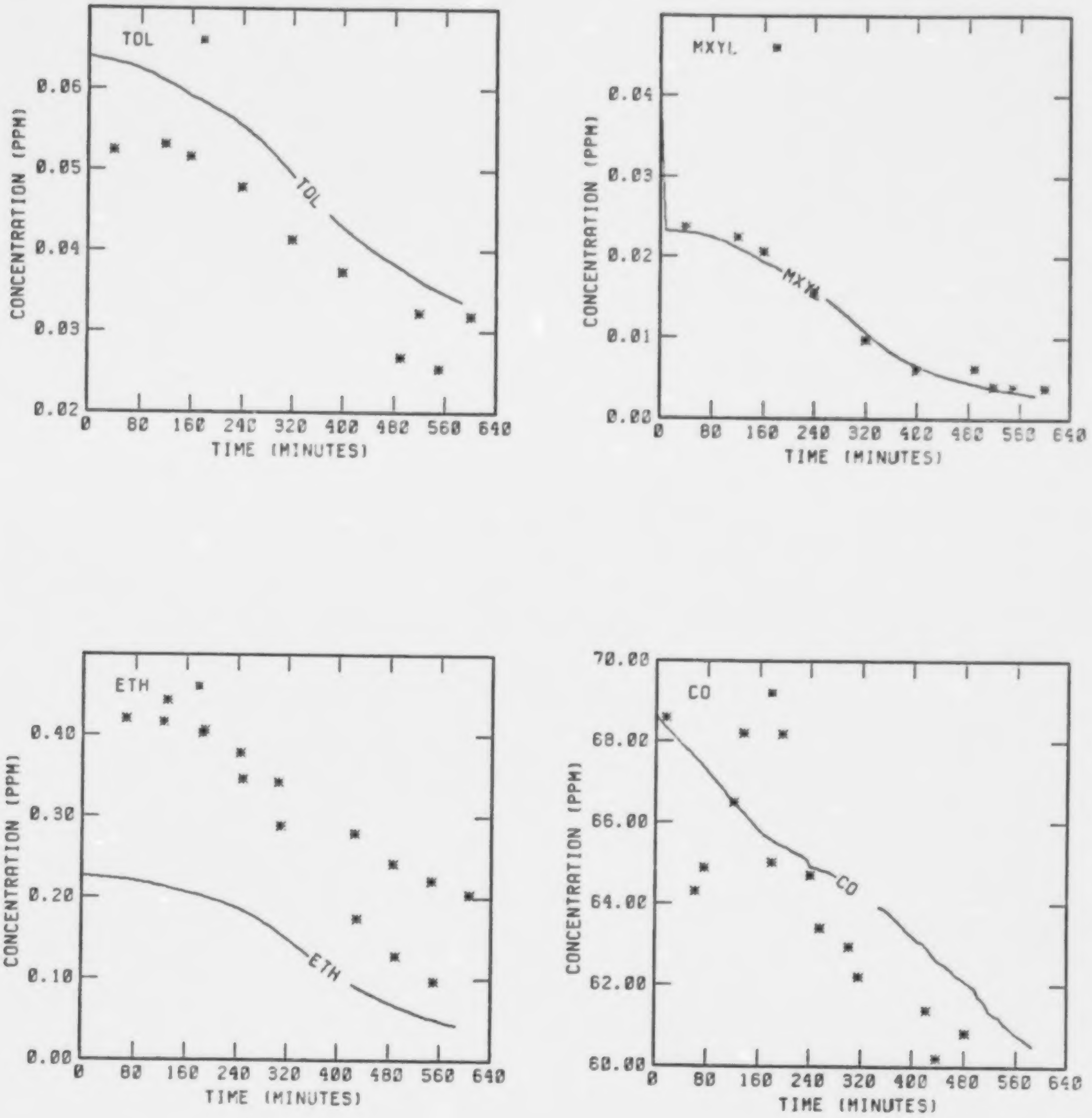

FIGURE 12 SIMULATION RESULTS FOR
UNCB 63082
continued.

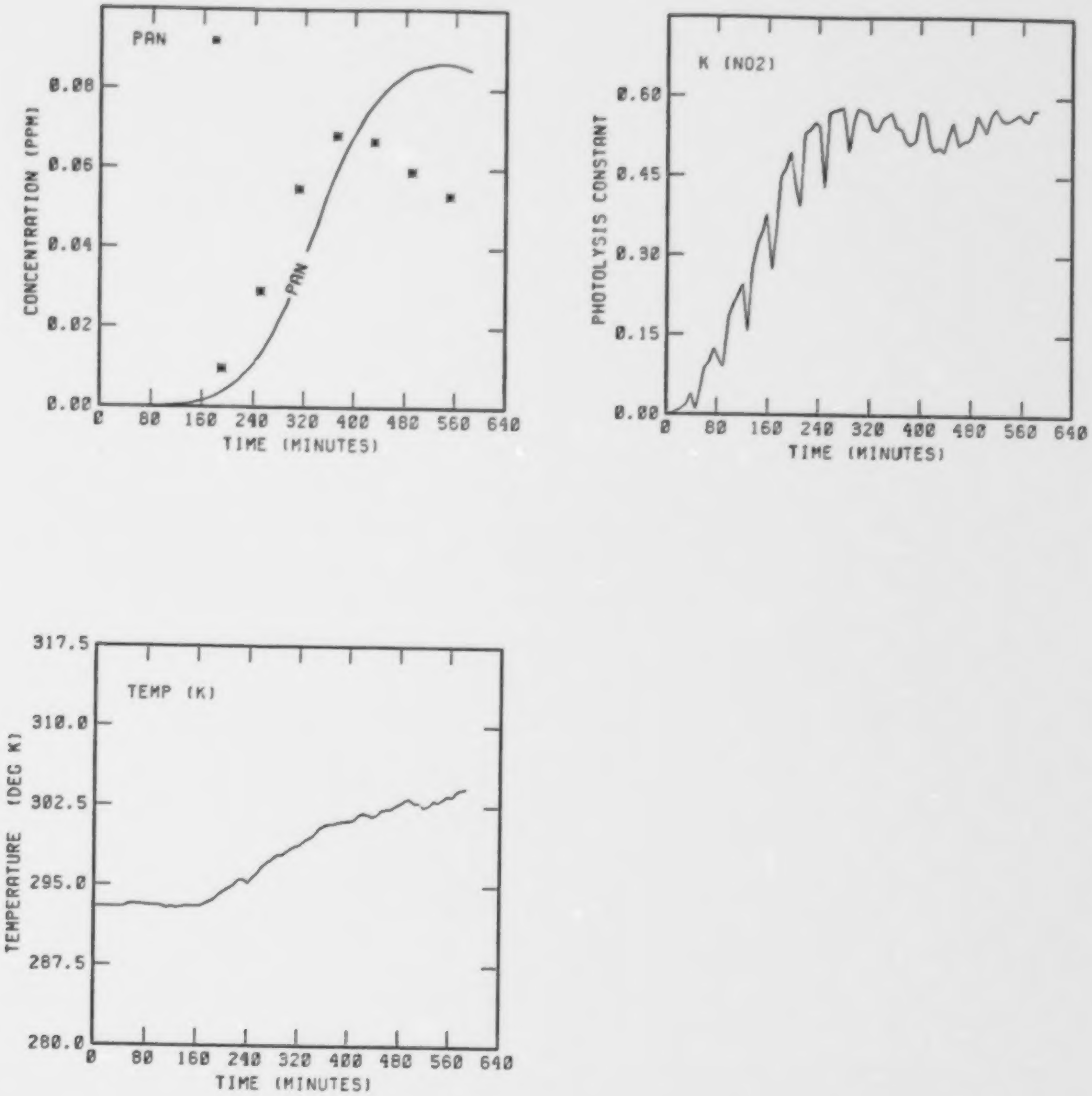

FIGURE 12 . SIMULATION RESULTS FOR
UNCB 63082

concluded.

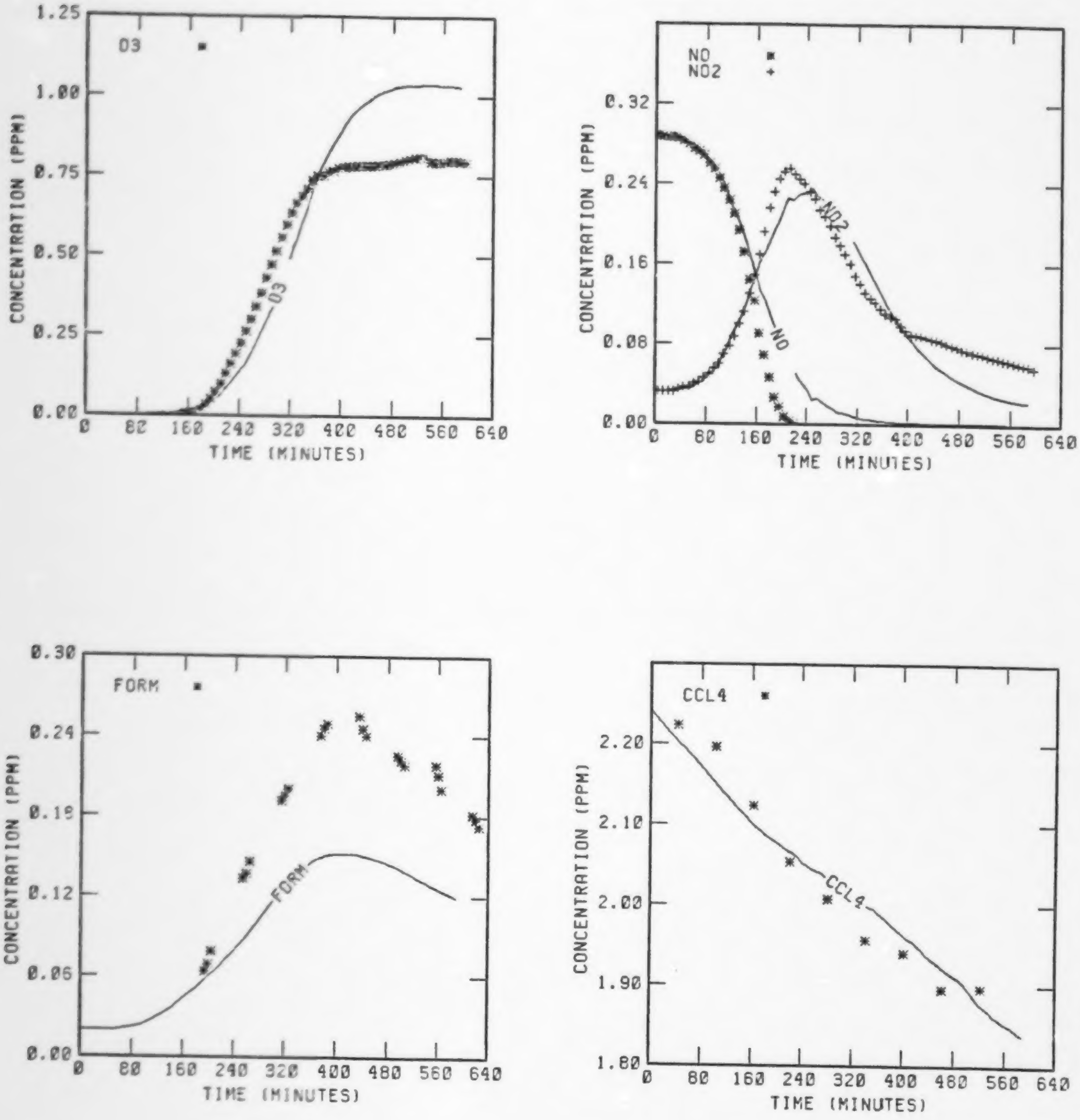

FIGURE 13. SIMULATION RESULTS FOR
UNCR 63082

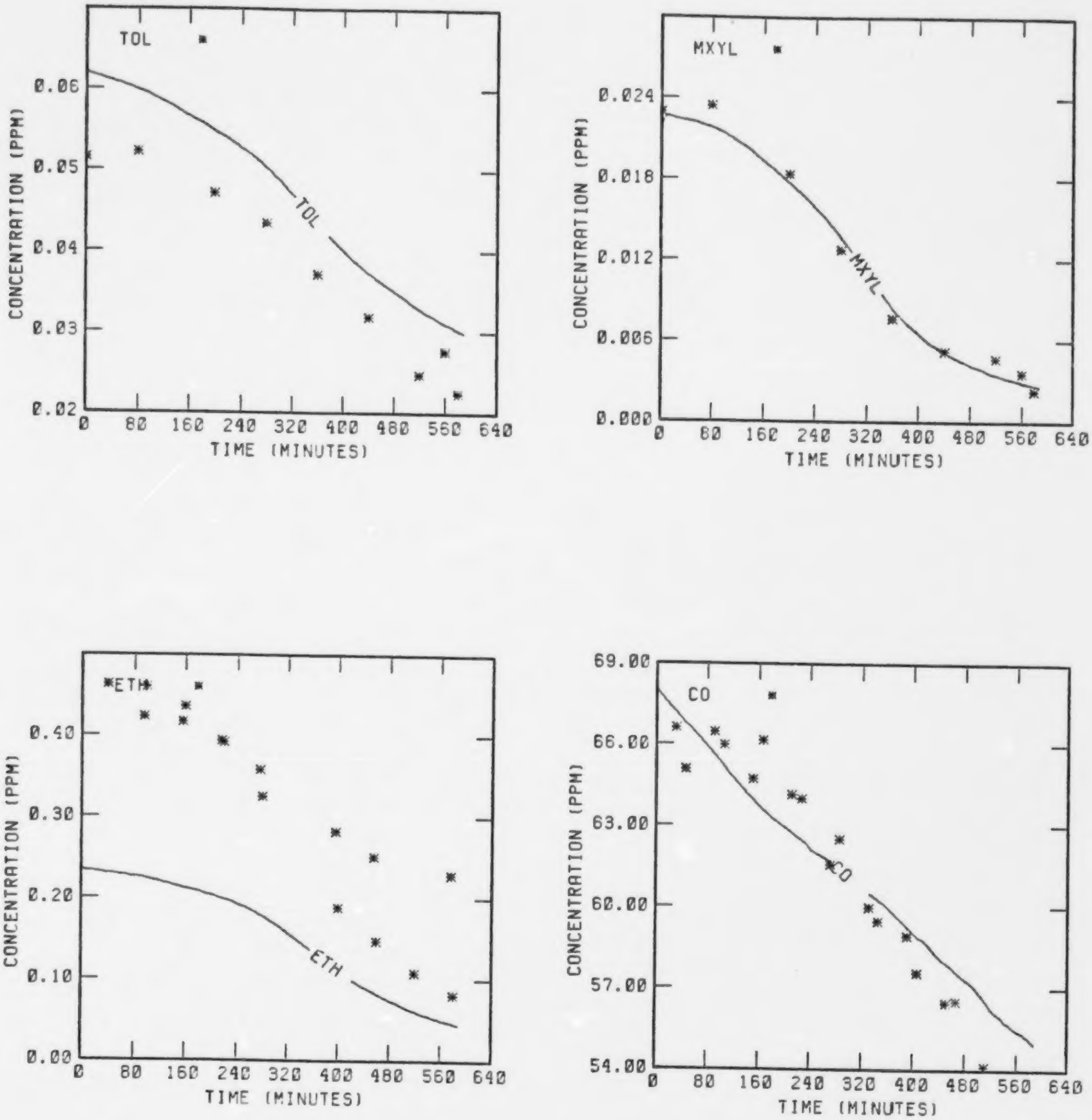

FIGURE 13. SIMULATION RESULTS FOR
UNCR 63082

continued.

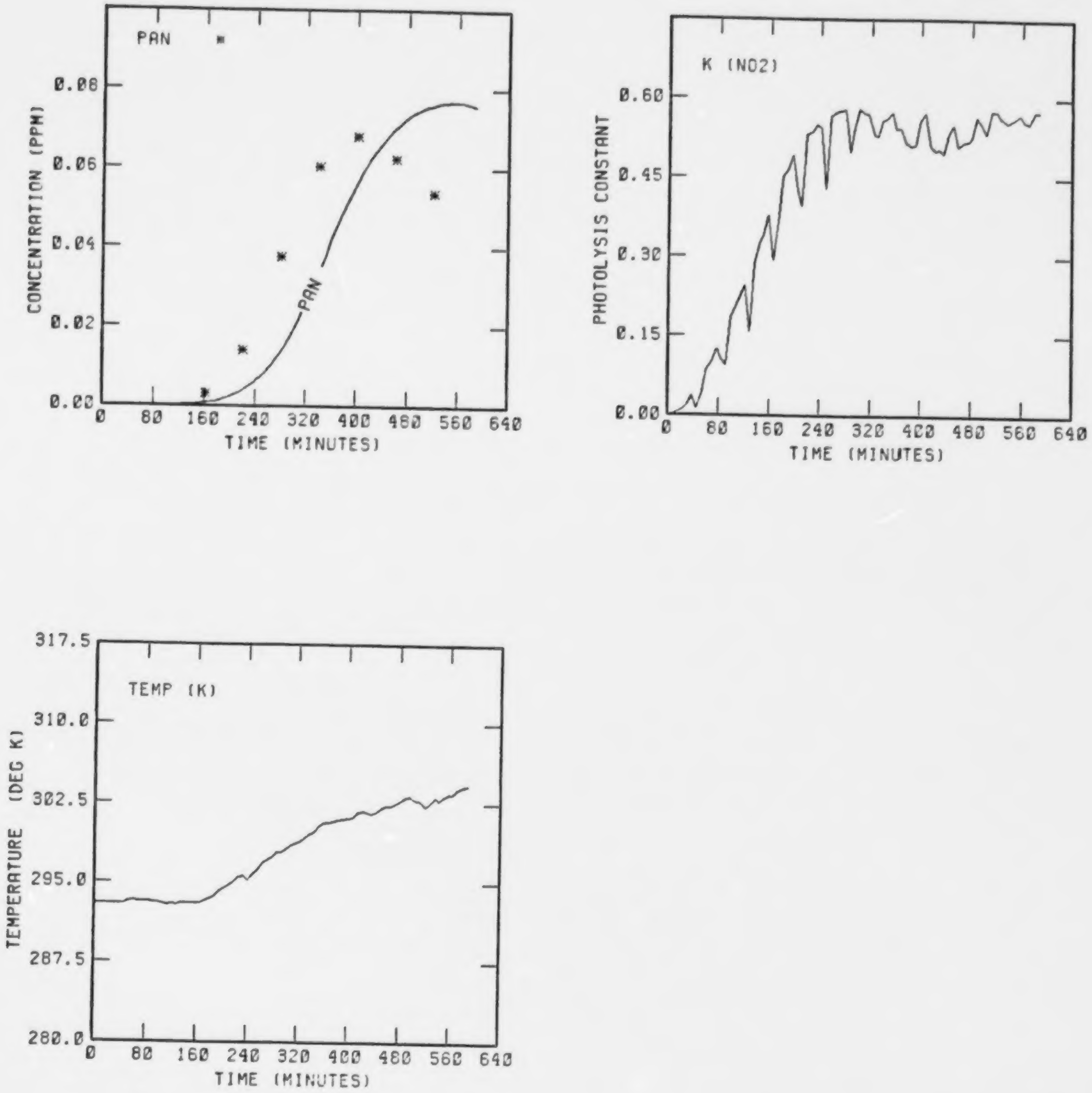

FIGURE 13. SIMULATION RESULTS FOR
UNCR 63082
concluded.

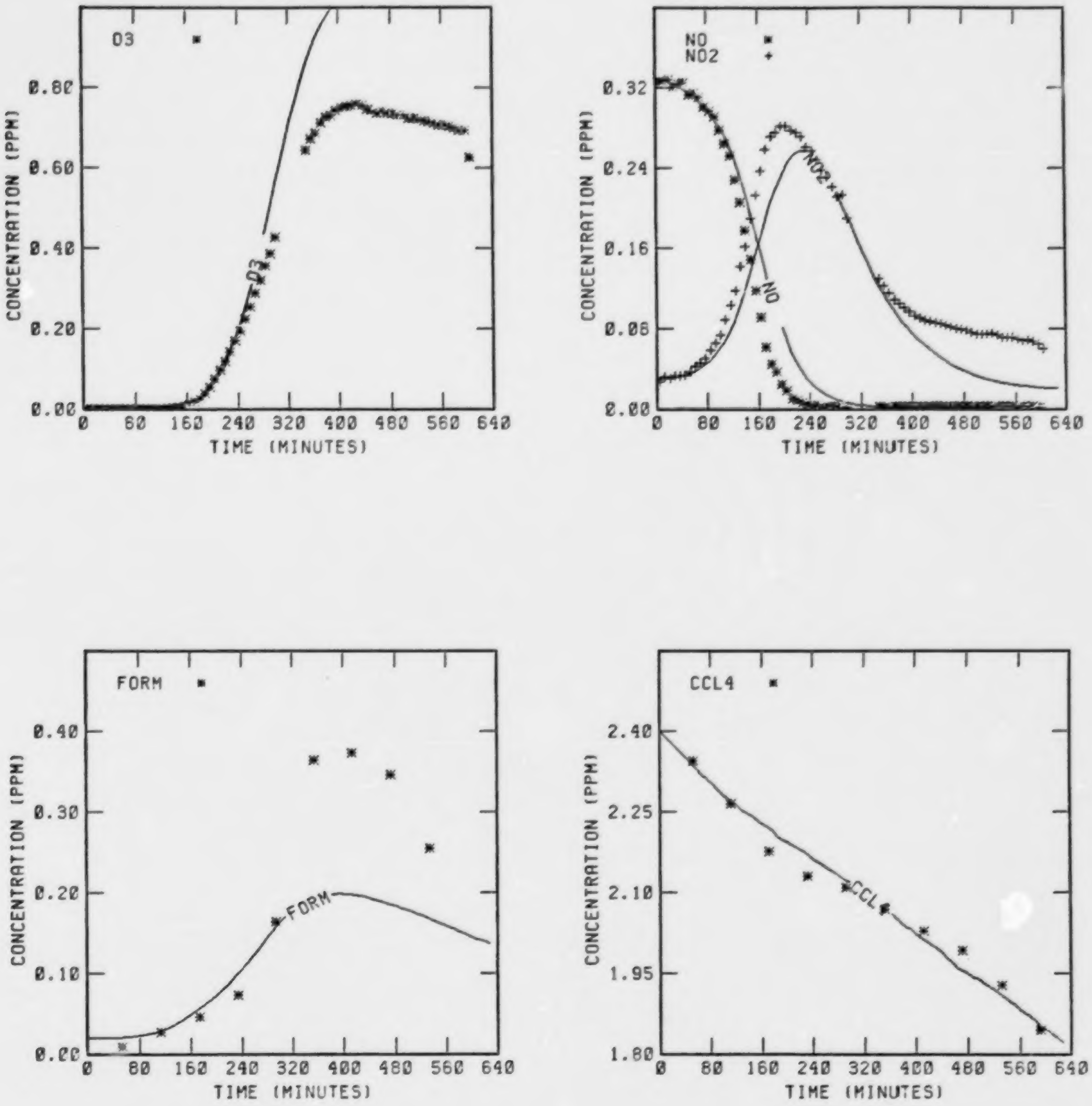

FIGURE 14. SIMULATION RESULTS FOR
UNCB 70182

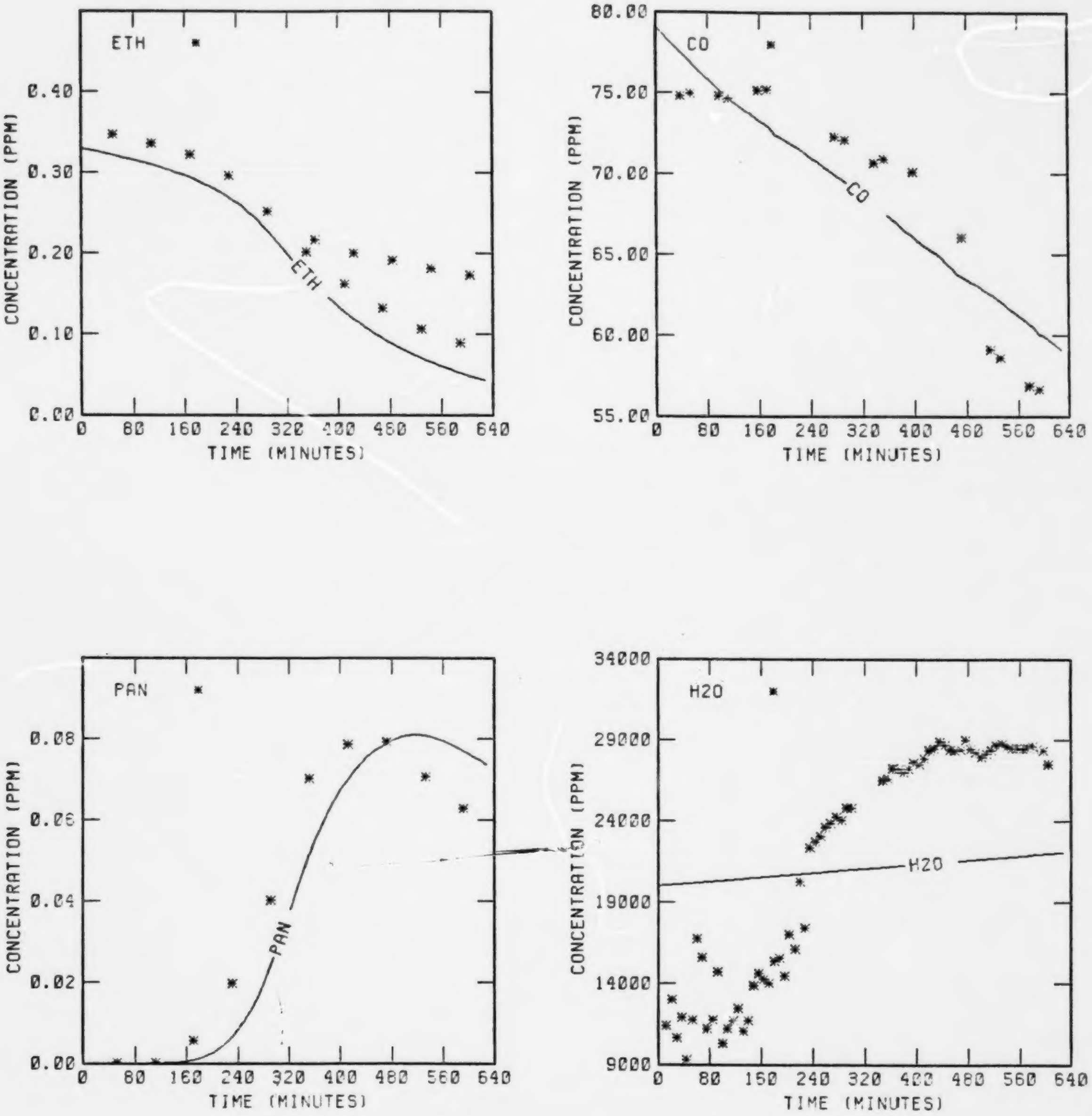

FIGURE **14**. SIMULATION RESULTS FOR
UNCB 70182
continued.

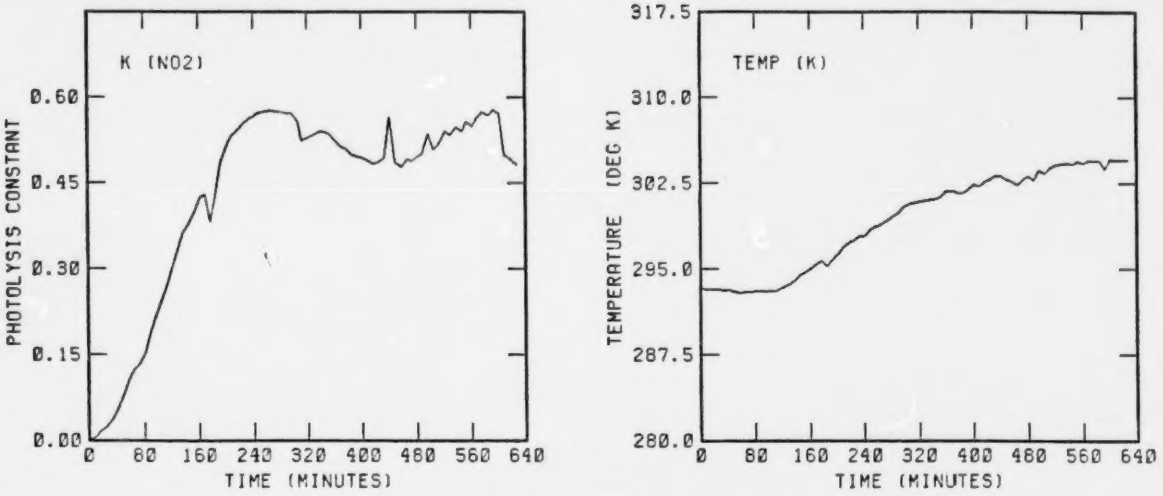

FIGURE 14 . SIMULATION RESULTS FOR
UNCB 70182
concluded.

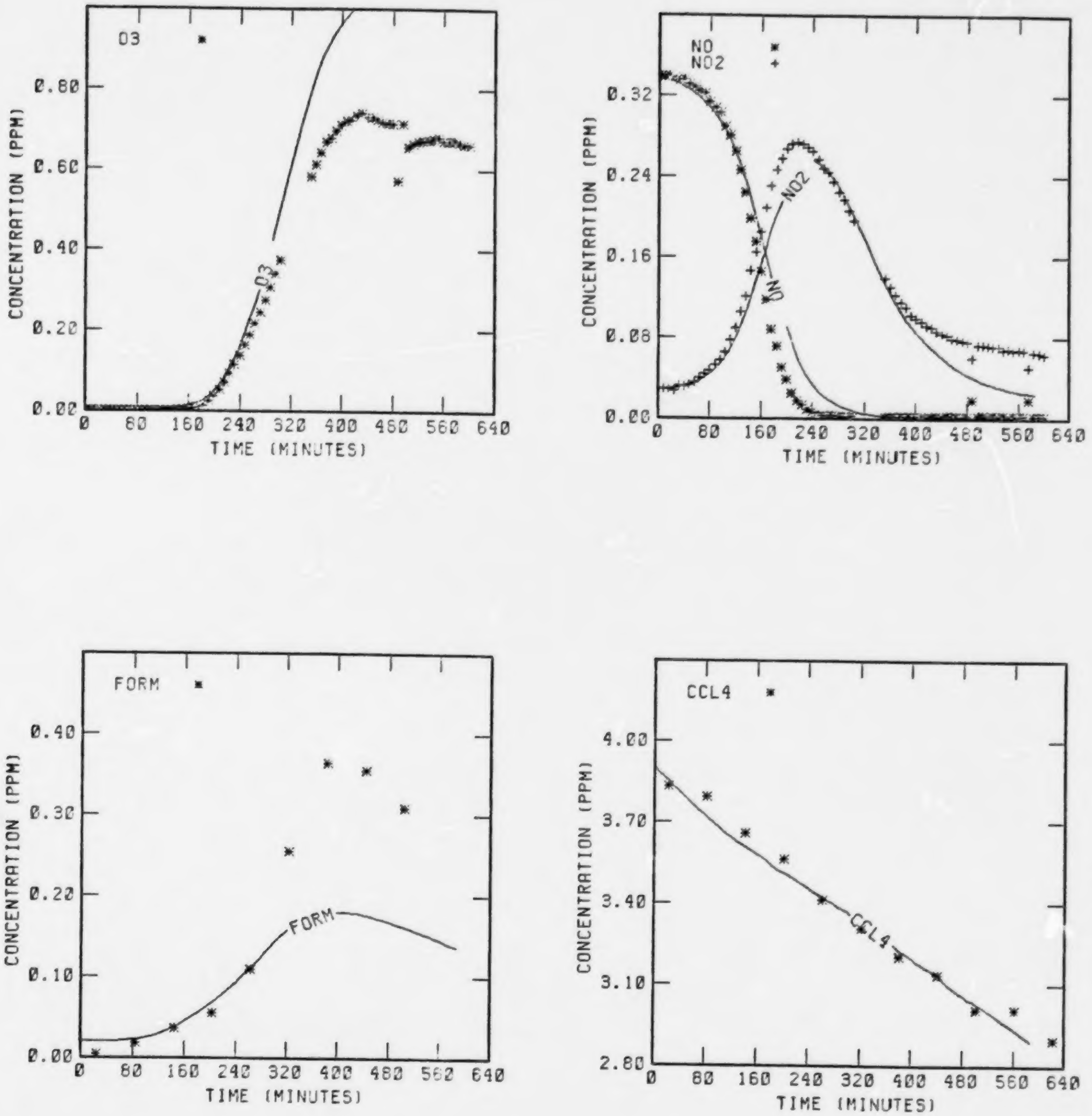

FIGURE 15 . SIMULATION RESULTS FOR
UNCR 70182

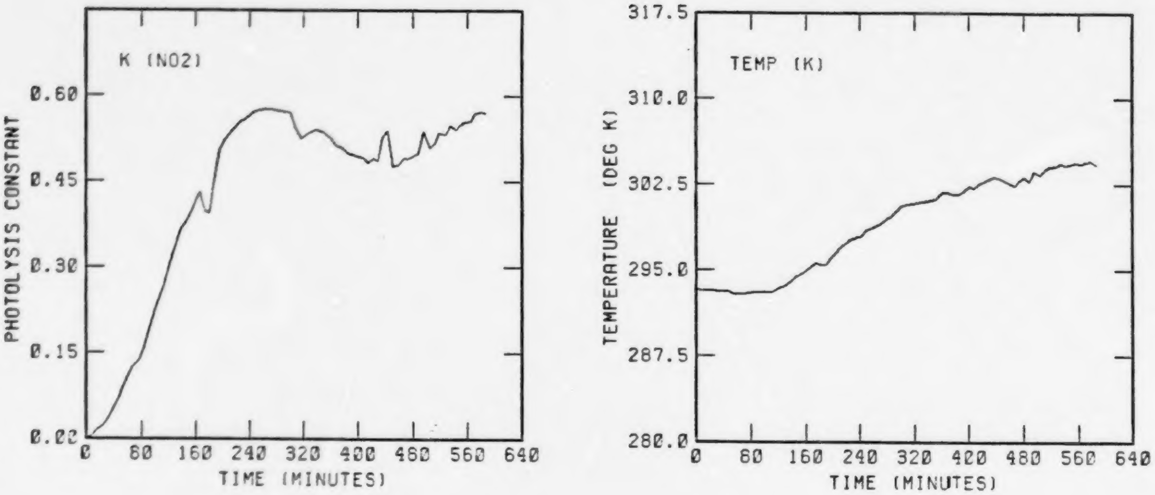

FIGURE **15** . SIMULATION RESULTS FOR
UNCR 70182
continued.

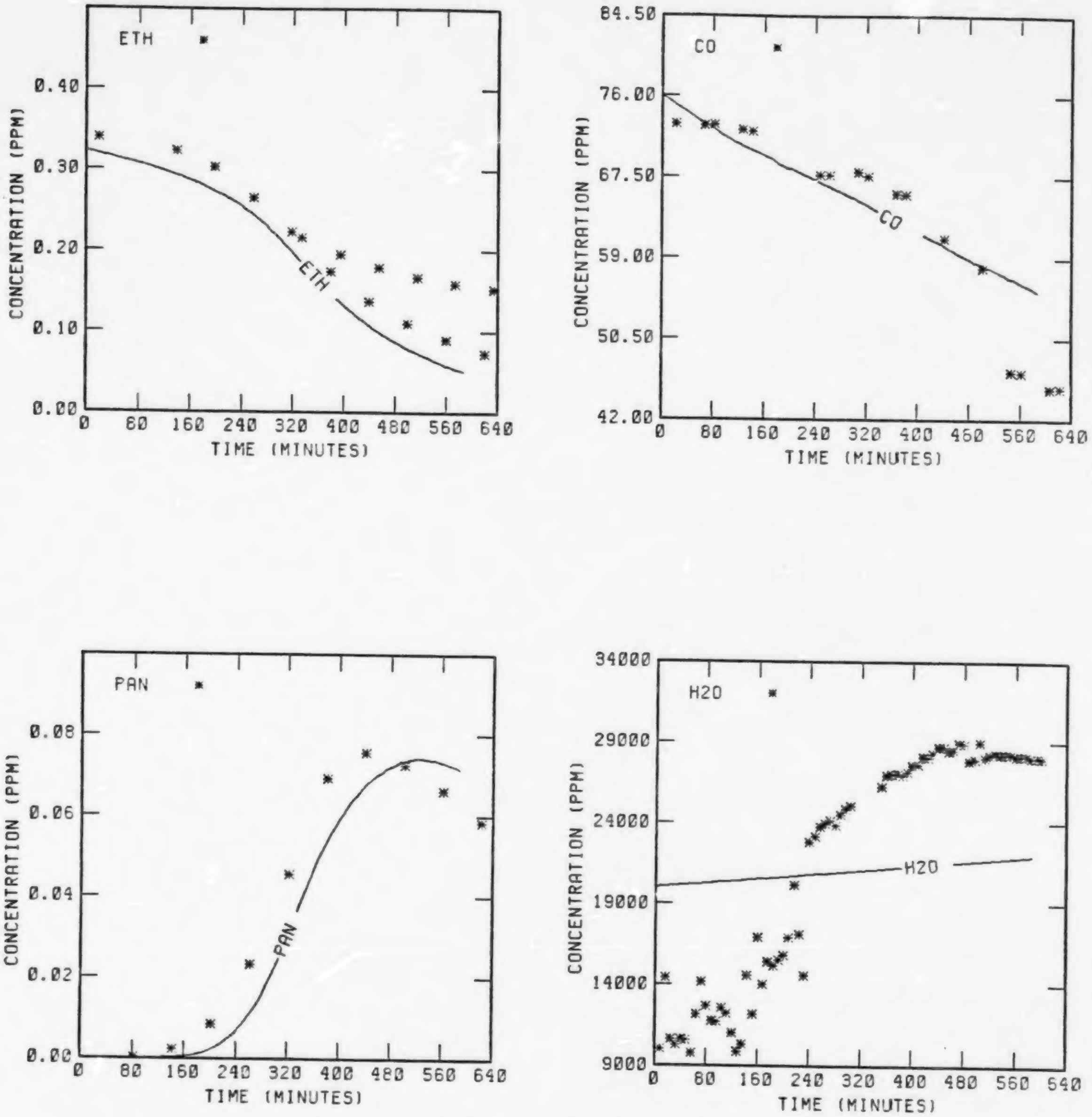

FIGURE **15** . SIMULATION RESULTS FOR
UNCR 70182
concluded.

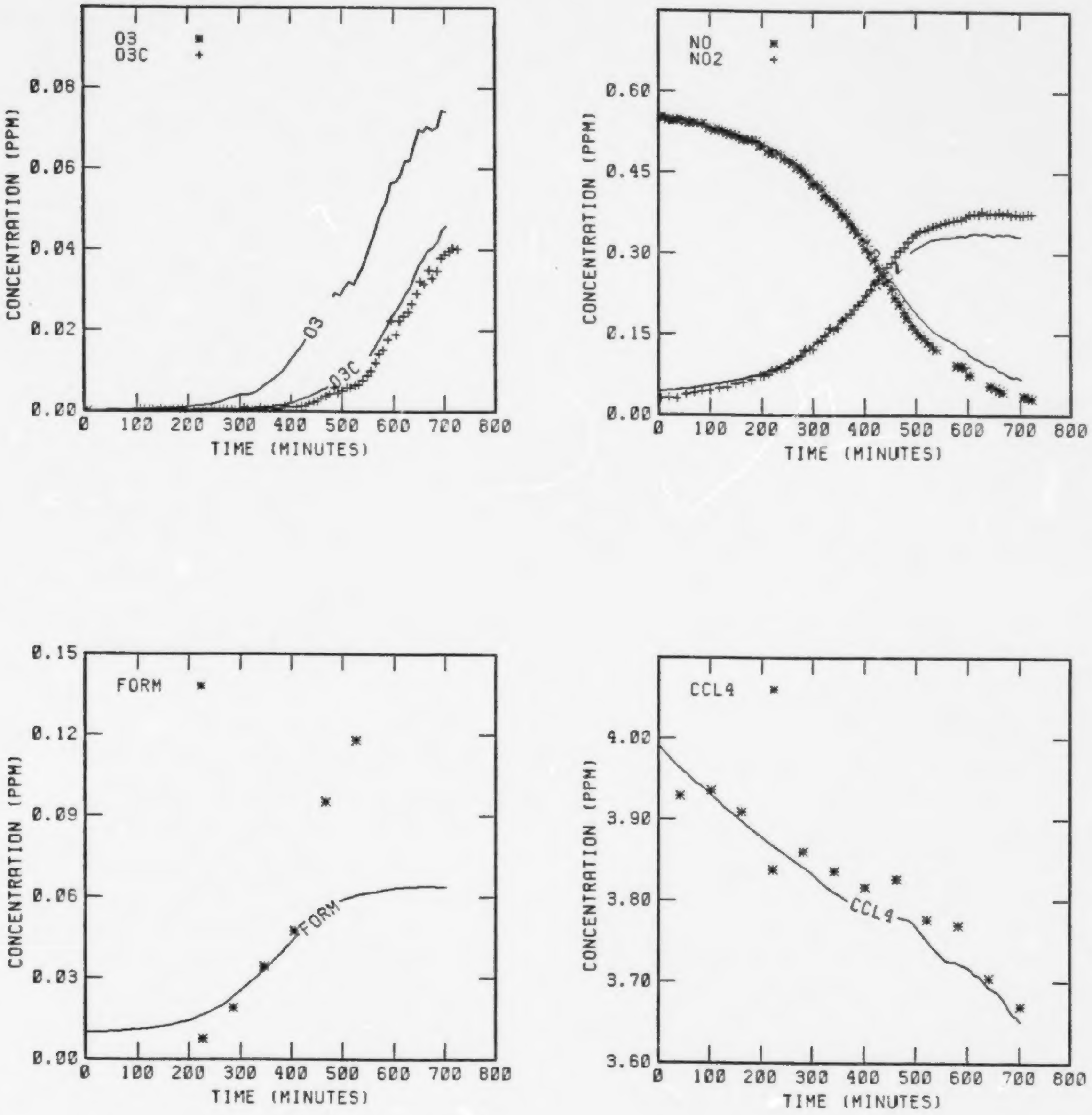

FIGURE 16 . SIMULATION RESULTS FOR
UNCB 71582

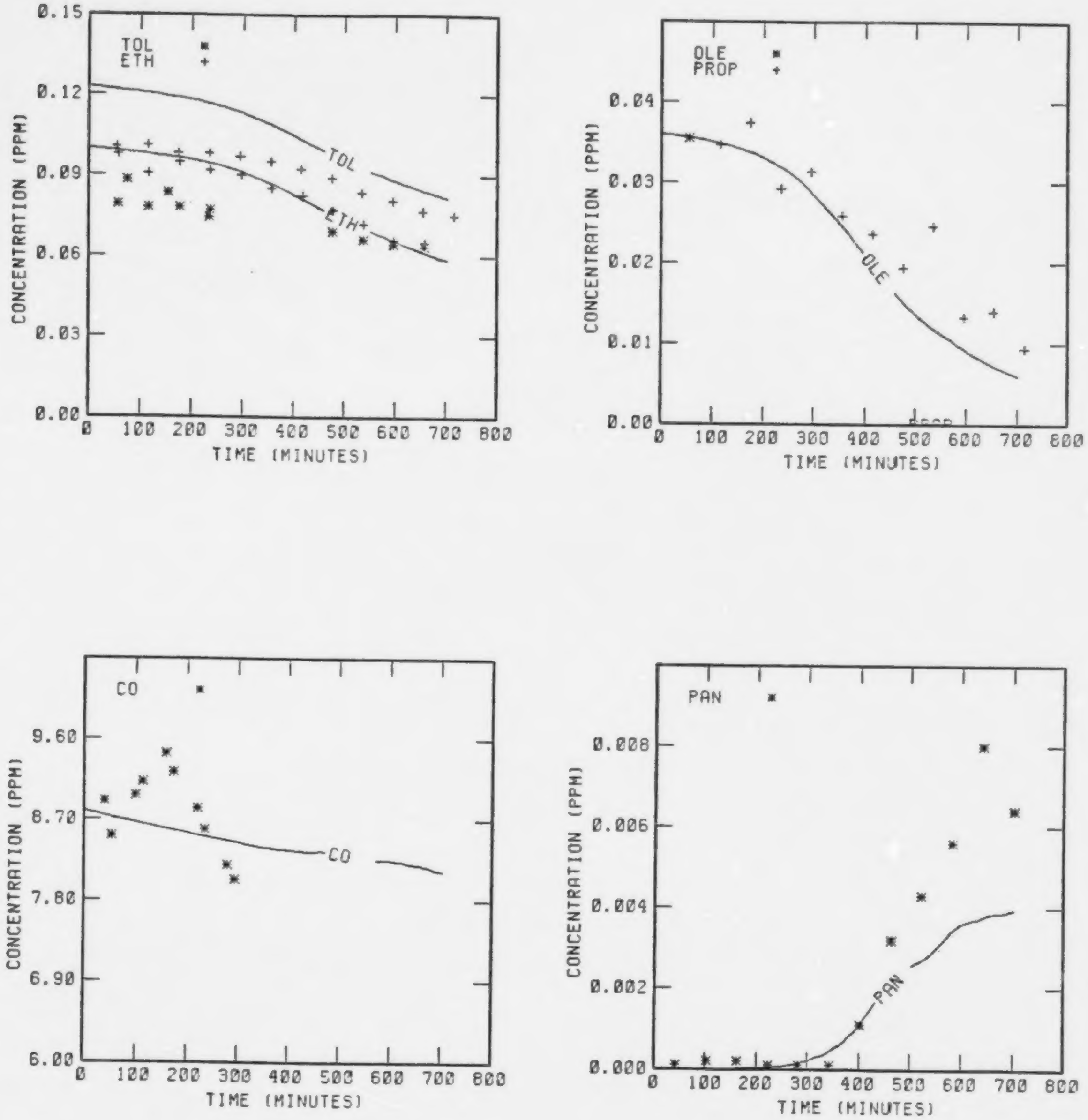

FIGURE 16 . SIMULATION RESULTS FOR
UNCB 71582
continued.

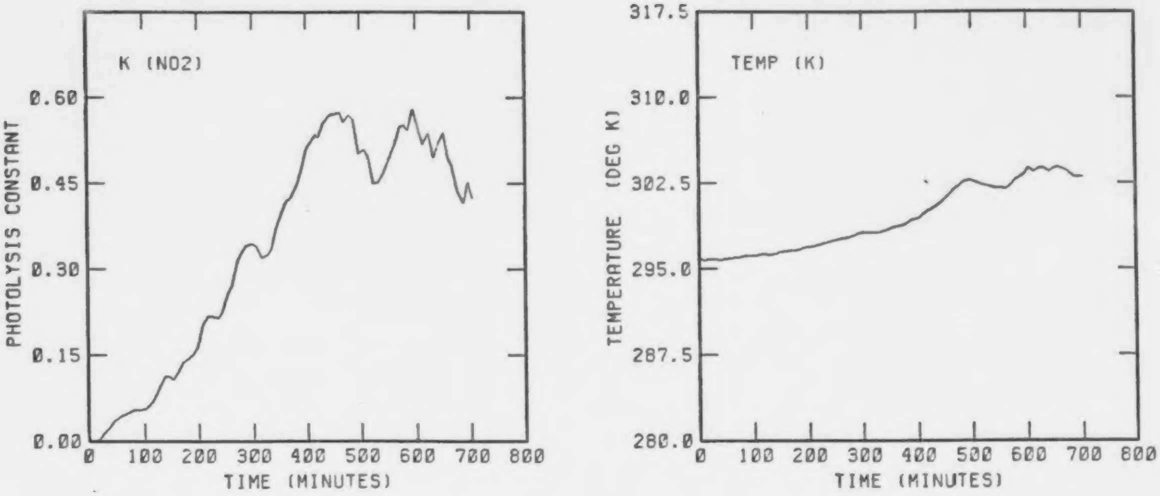

FIGURE 16 . SIMULATION RESULTS FOR
UNCB 71582
concluded.

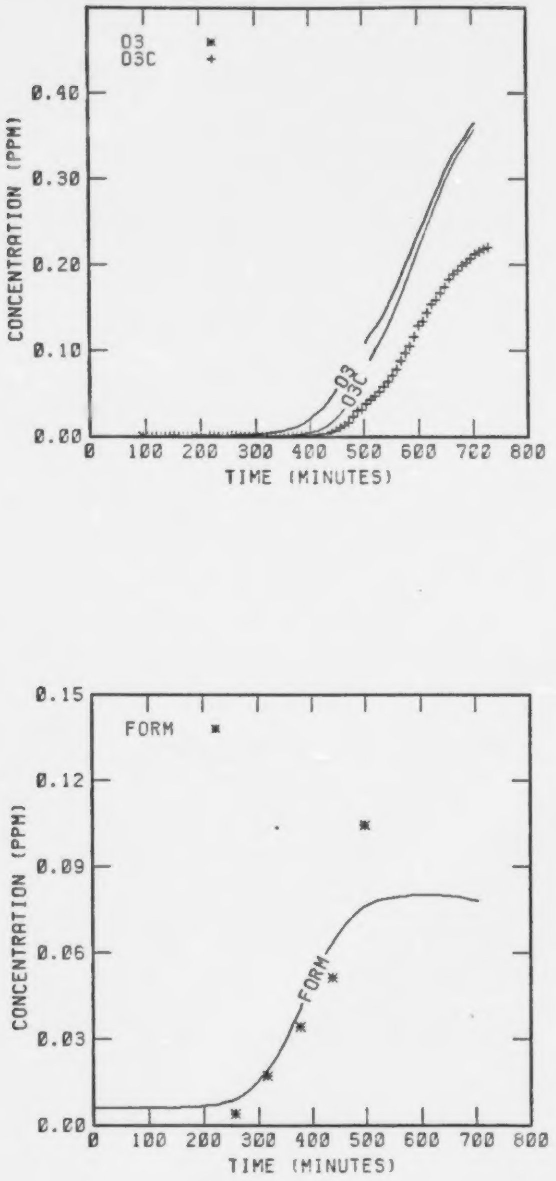

FIGURE 17 . SIMULATION RESULTS FOR
UNCR 71582

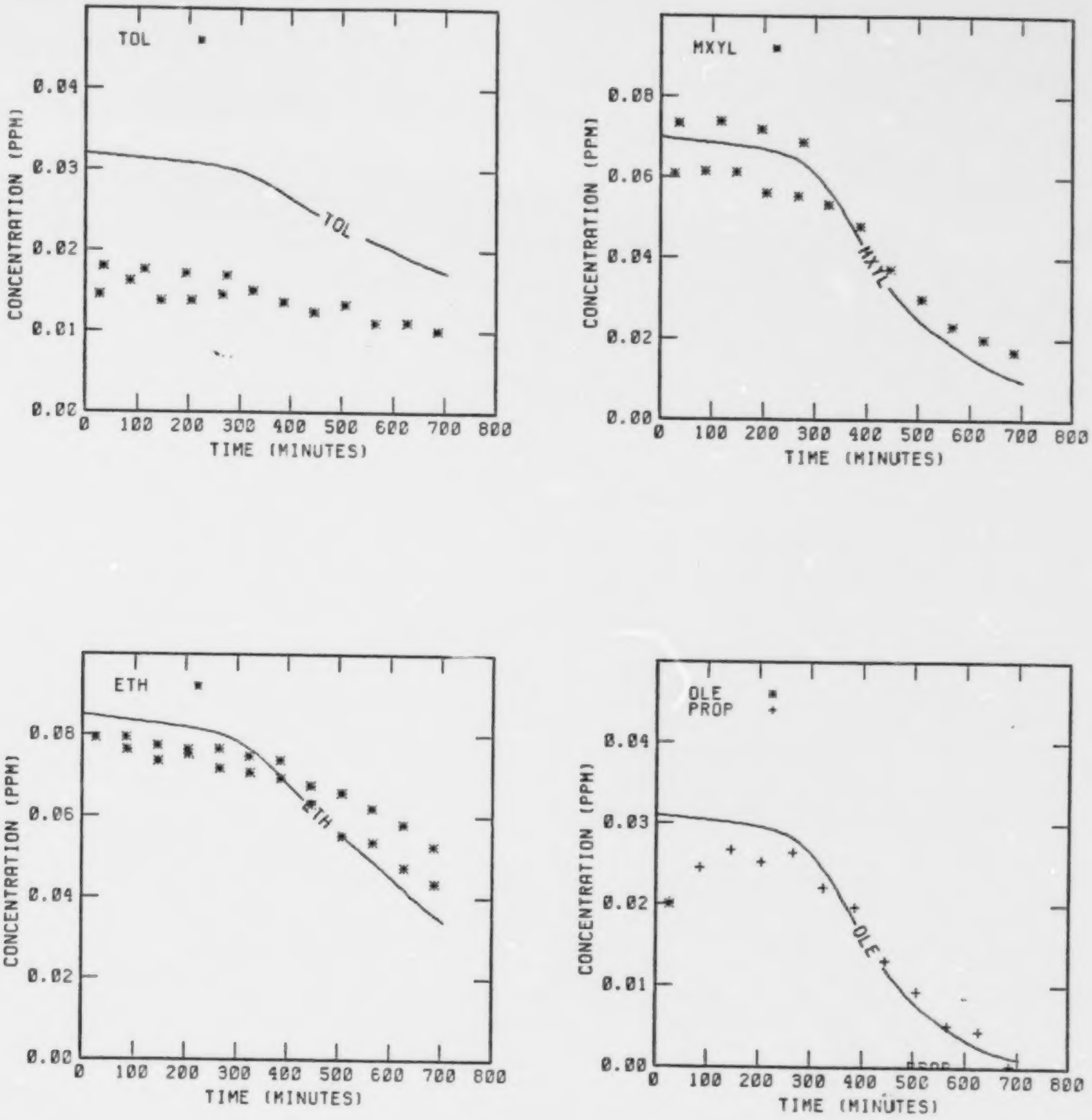

FIGURE 17 . SIMULATION RESULTS FOR
UNCR 71582

continued.

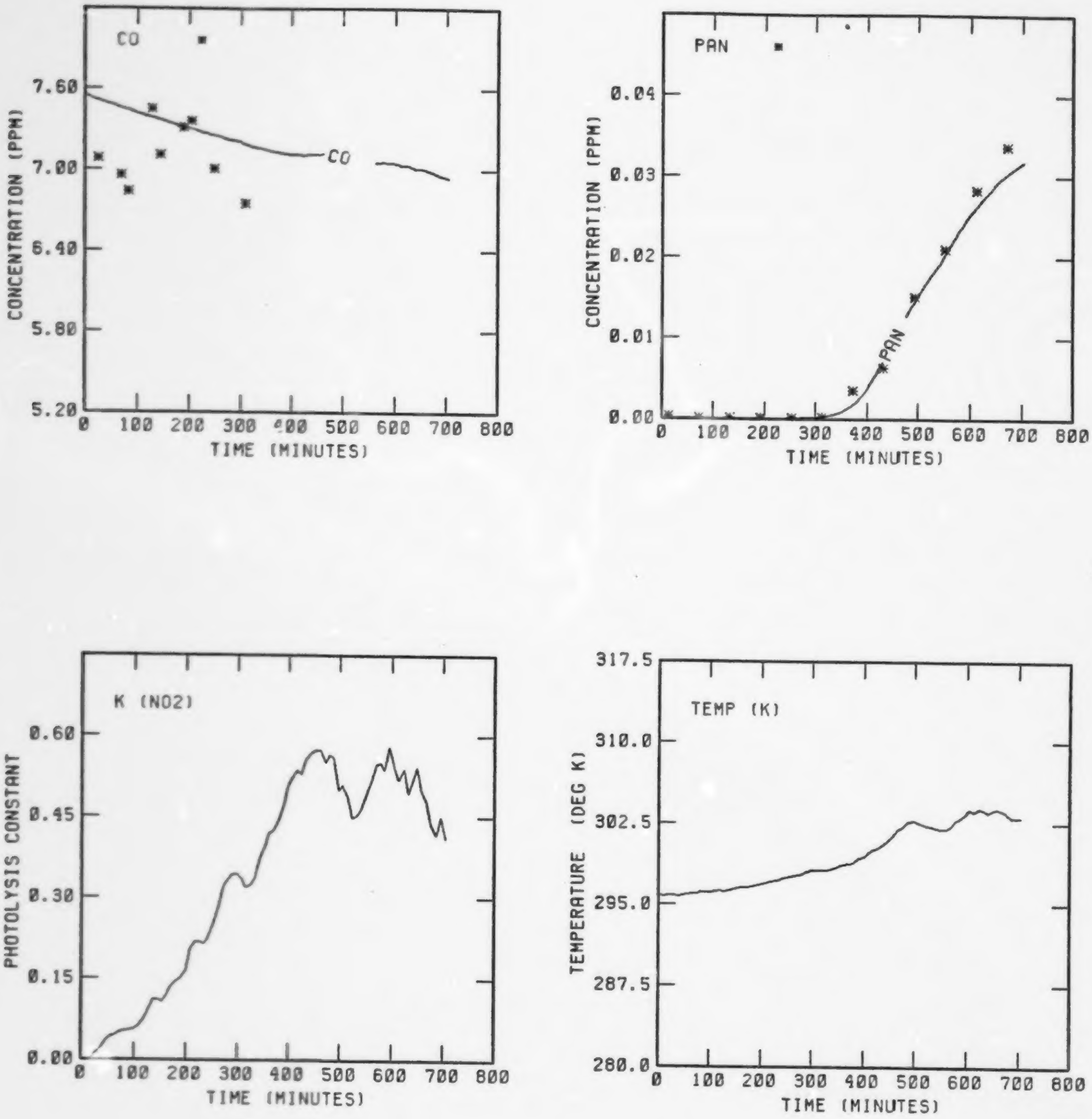

FIGURE 17 . SIMULATION RESULTS FOR
UNCR 71582
concluded.

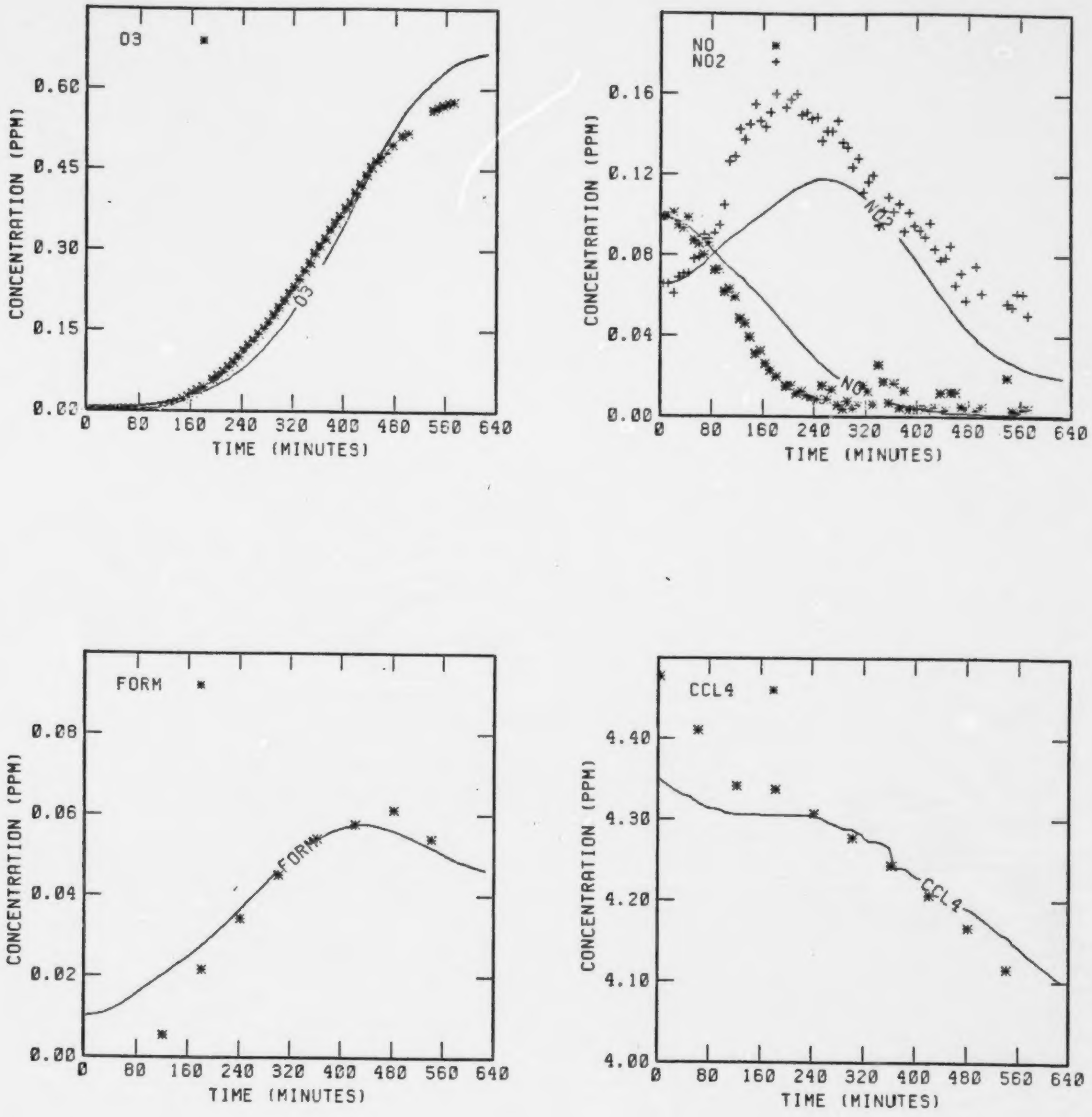

FIGURE 18 . SIMULATION RESULTS FOR UNCB 80382

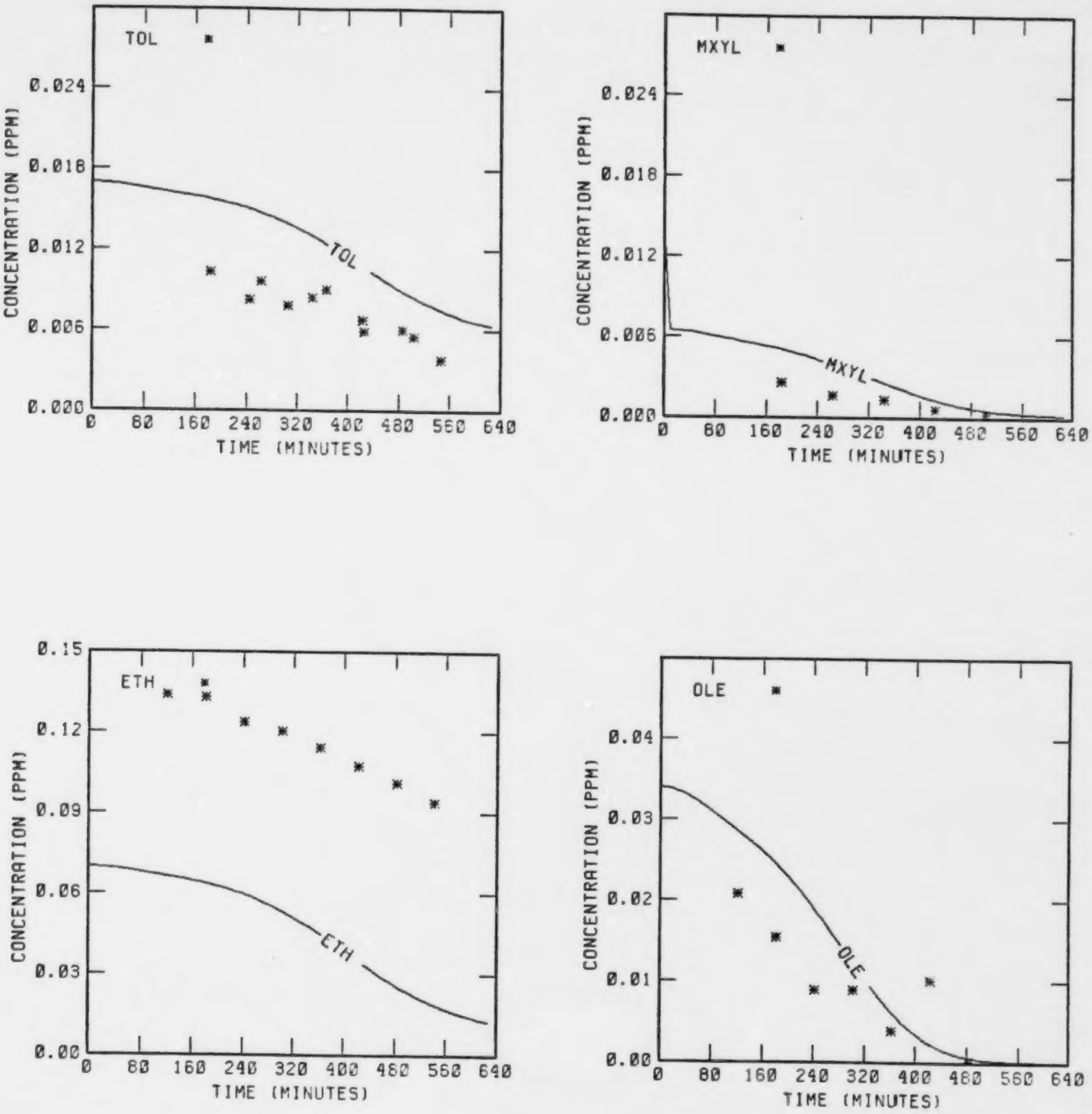

FIGURE 18 . SIMULATION RESULTS FOR
UNCB 80382
continued.

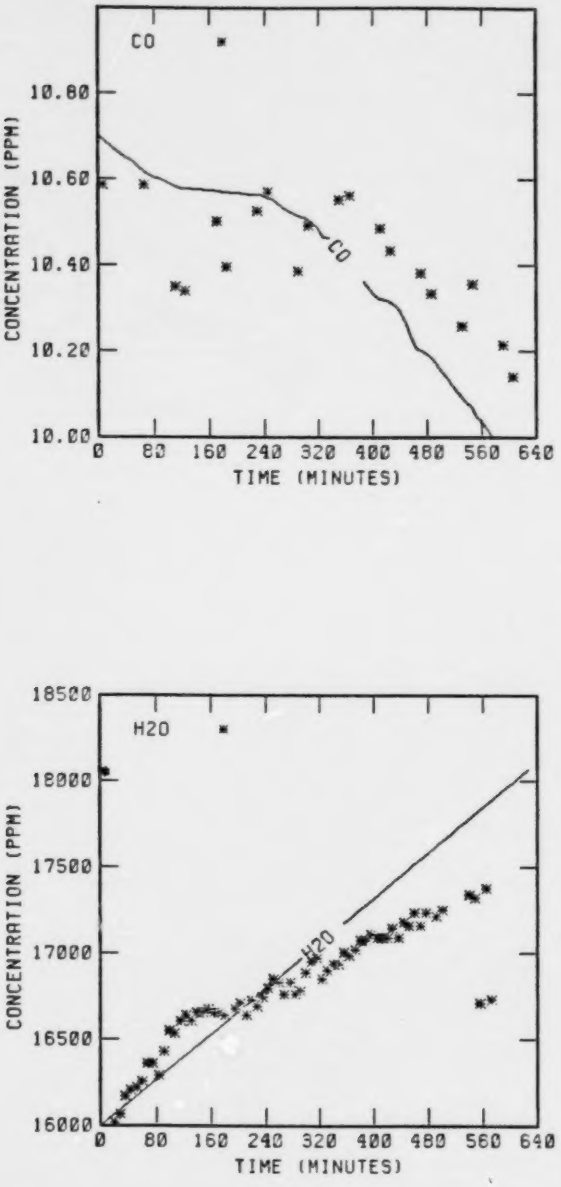

FIGURE 18 . SIMULATION RESULTS FOR
UNCB 80382

continued.

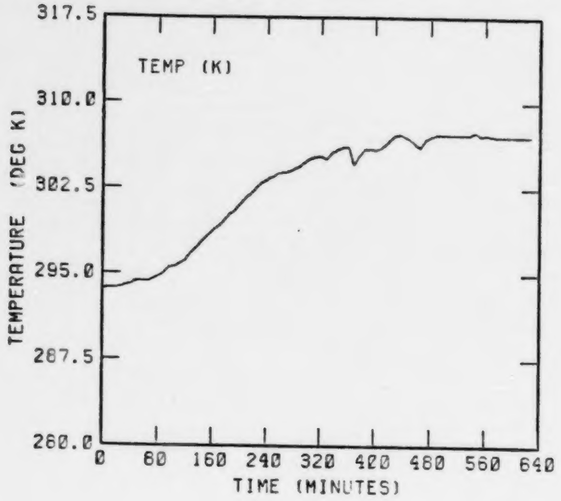

FIGURE 18. SIMULATION RESULTS FOR
UNCB 80382
concluded

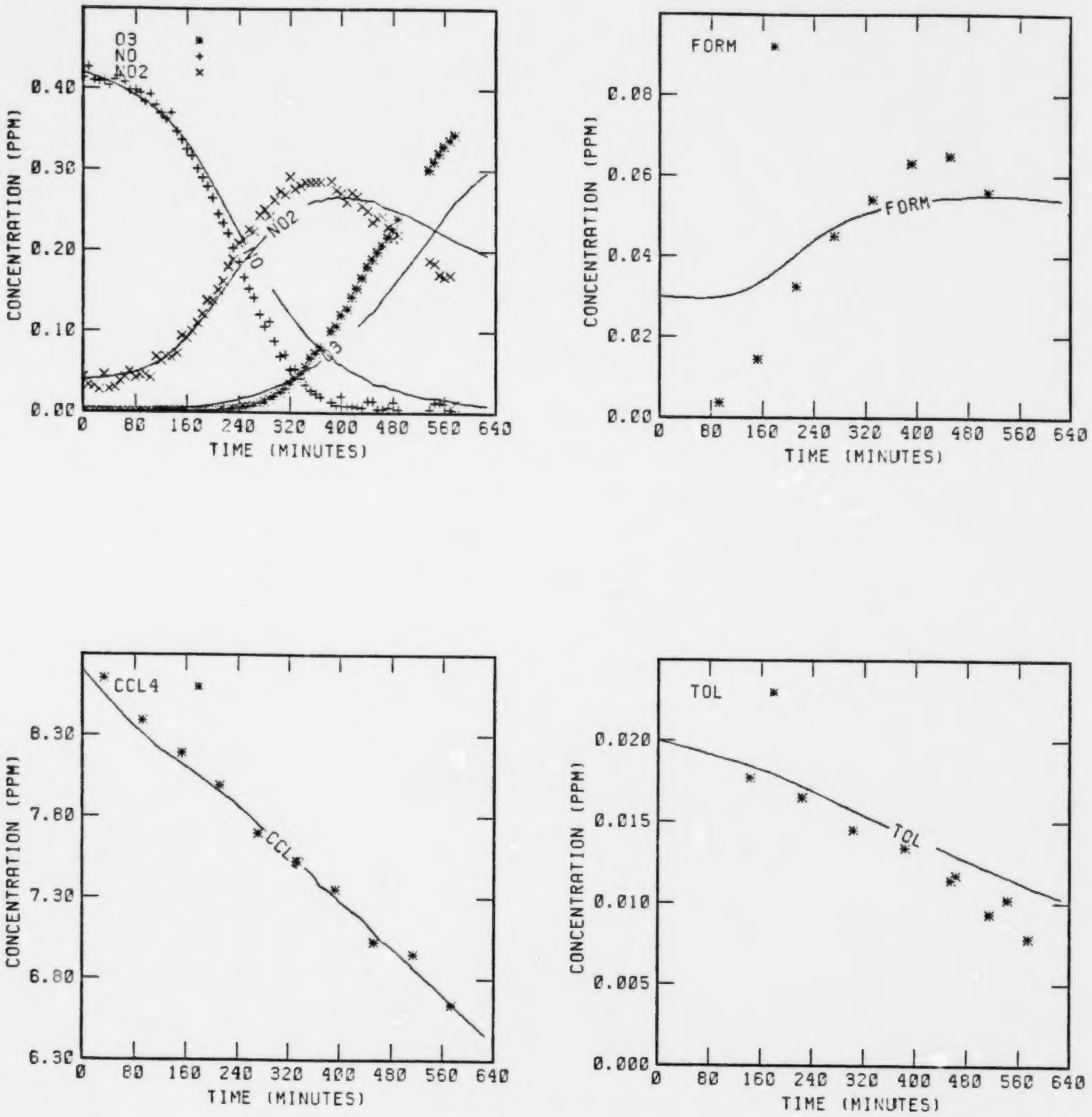

FIGURE 19 . SIMULATION RESULTS FOR UNCR 80382

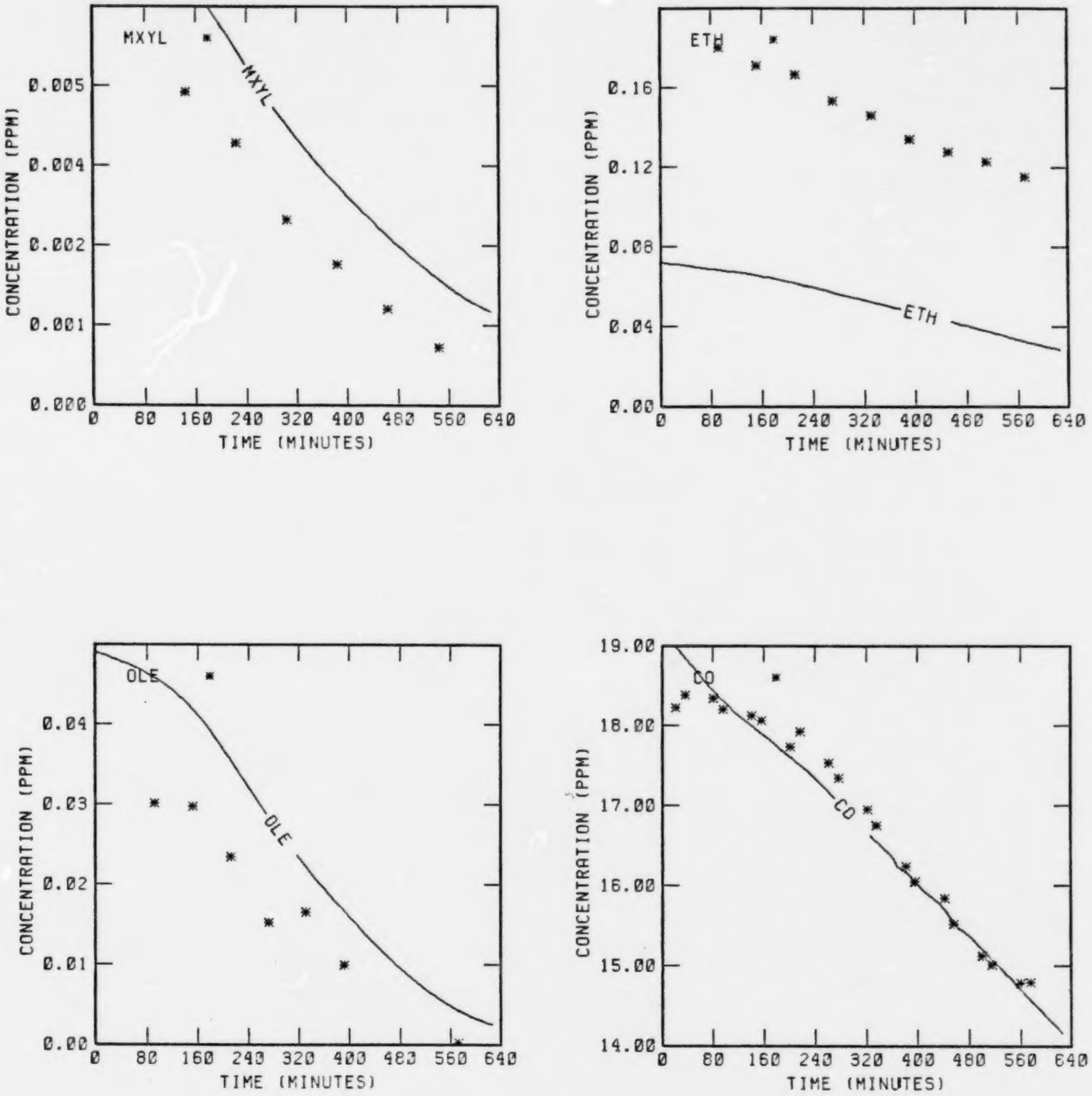

FIGURE **19** . SIMULATION RESULTS FOR
UNCR 80382

continued.

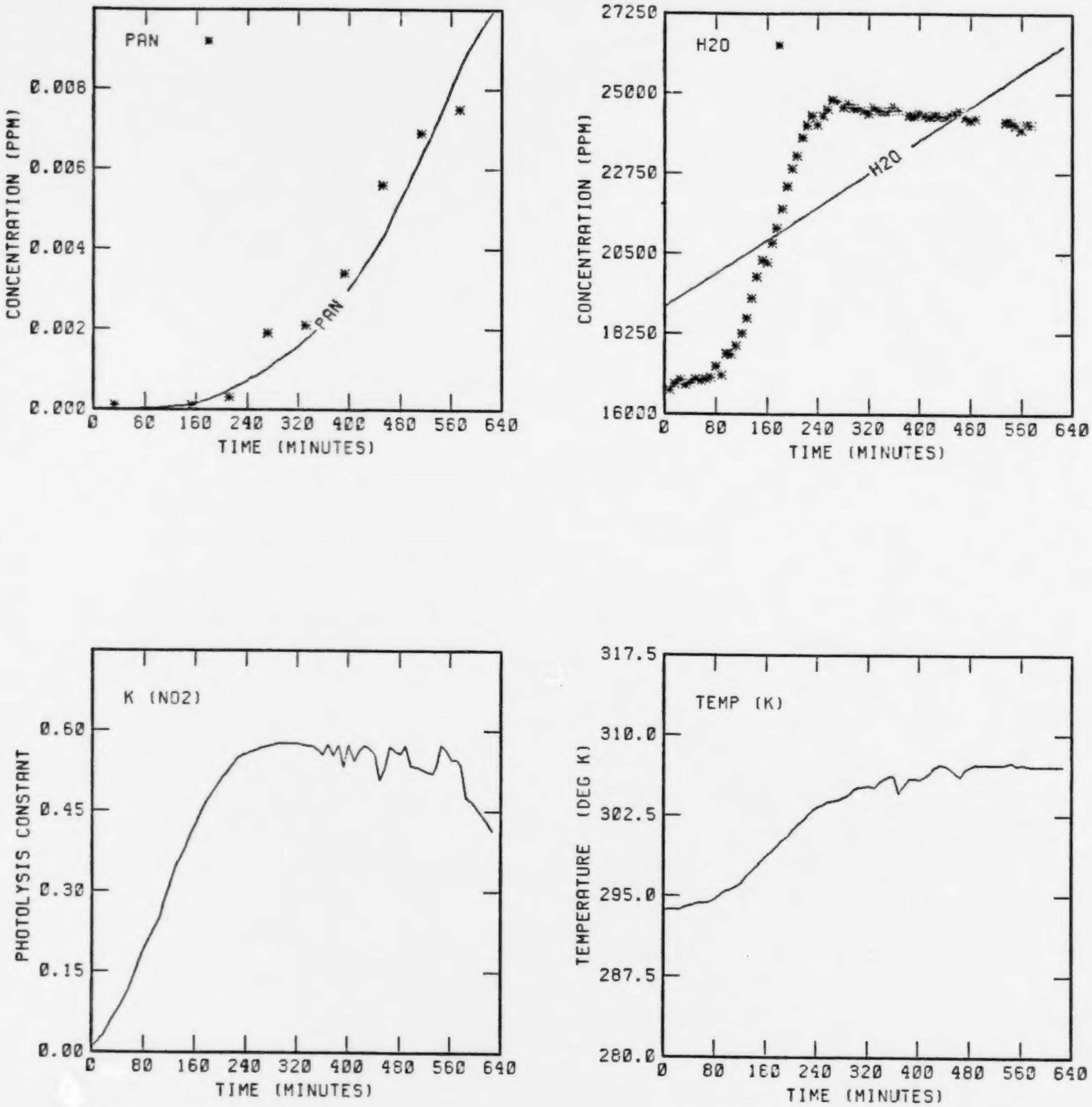

FIGURE 19. SIMULATION RESULTS FOR
UNCR 80382
concluded.

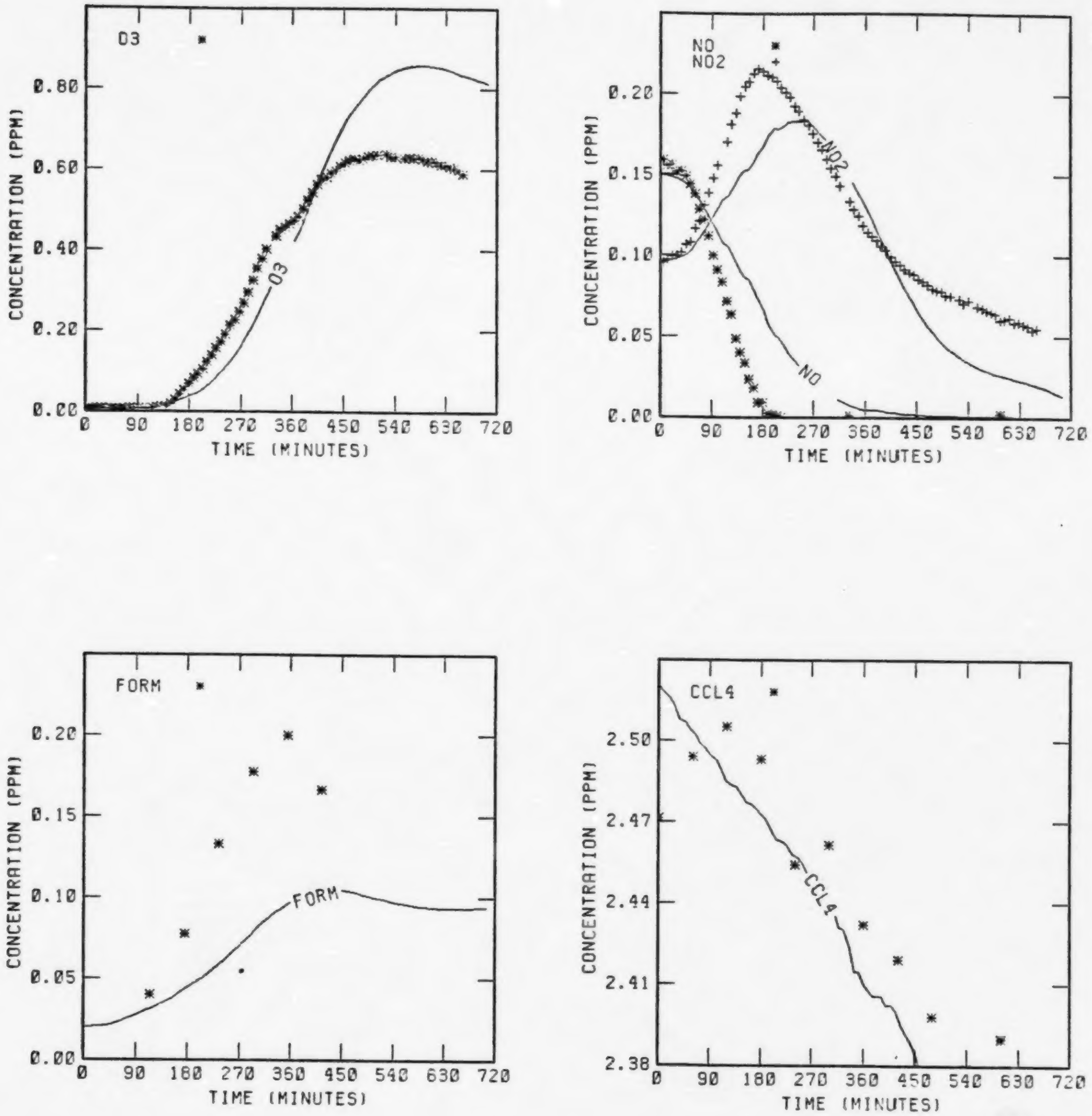

FIGURE 20 . SIMULATION RESULTS FOR UNCB 91782

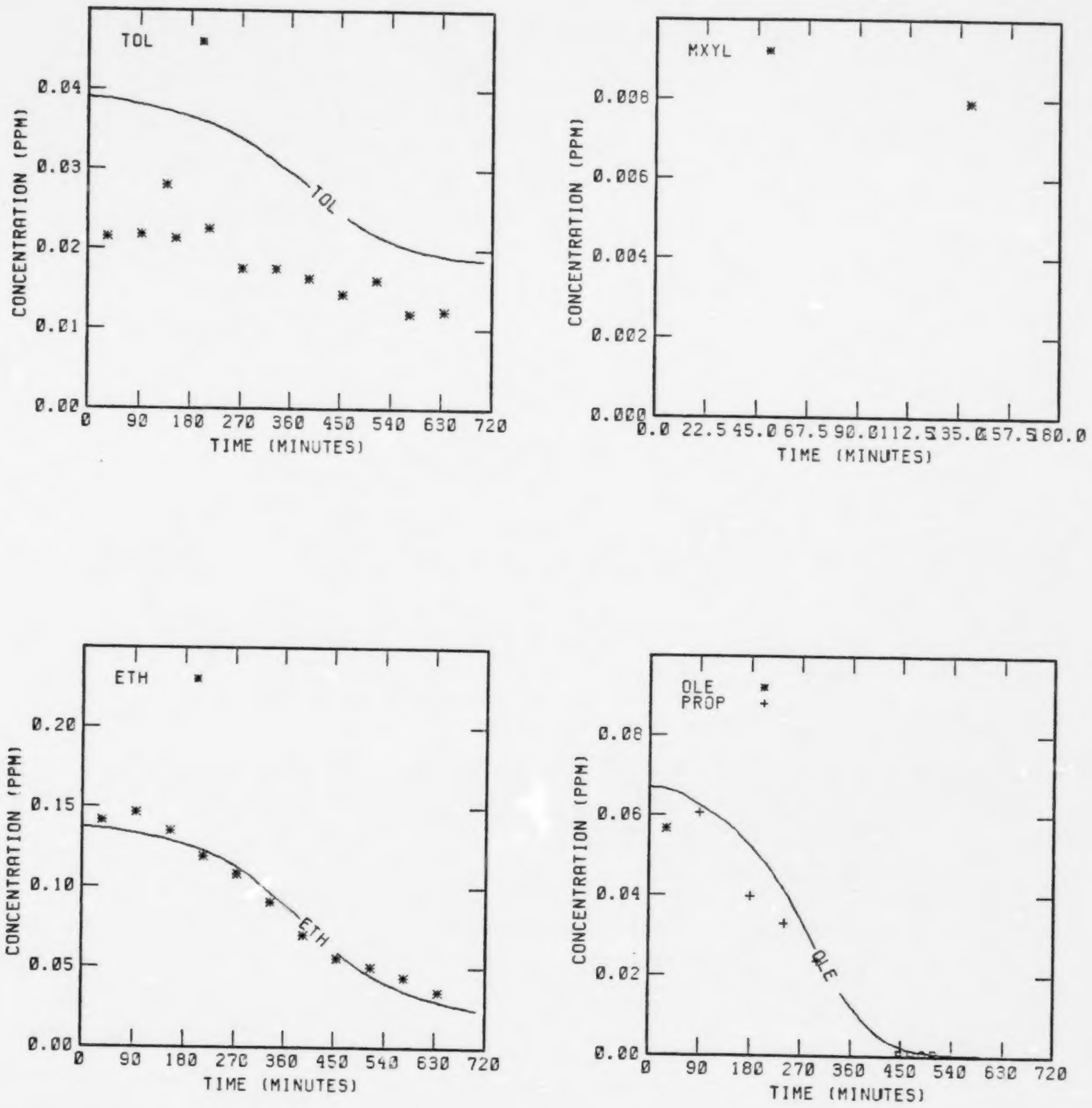

FIGURE 20 . SIMULATION RESULTS FOR
UNCB 91782
Continued.

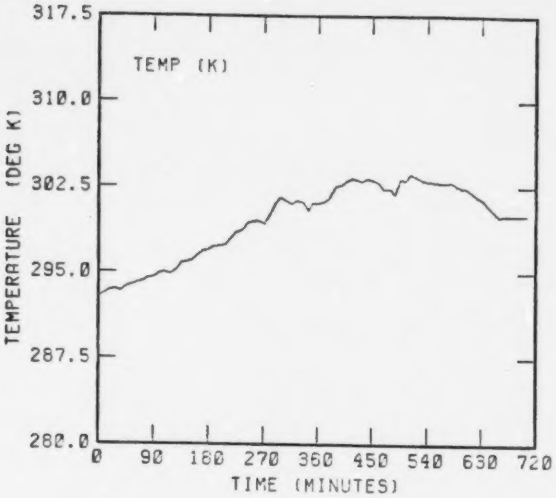

FIGURE 20 . SIMULATION RESULTS FOR
UNCB 91782
Concluded.

Preceding page blank

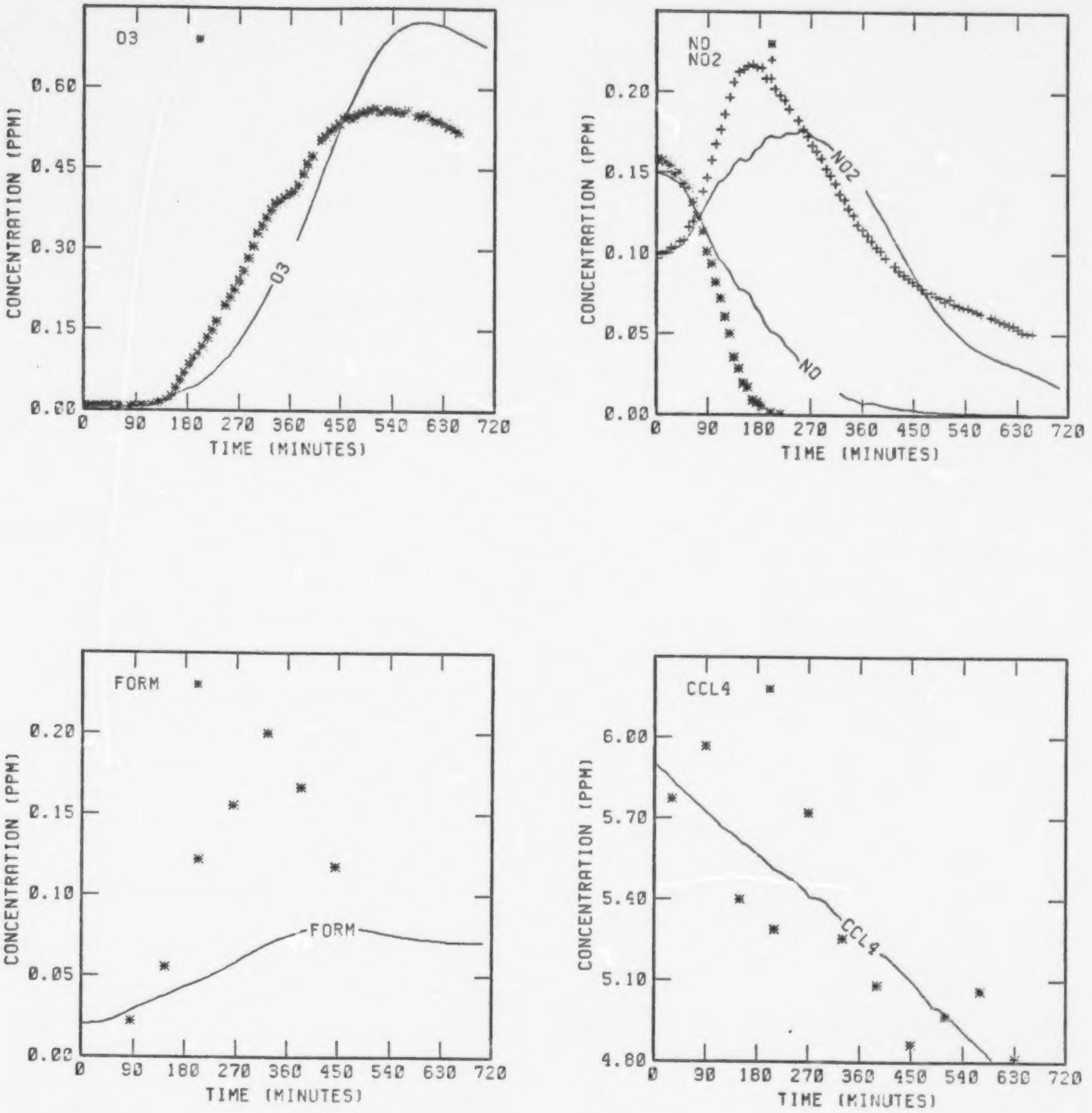

FIGURE 21. SIMULATION RESULTS FOR
UNCR 91782
Continued.

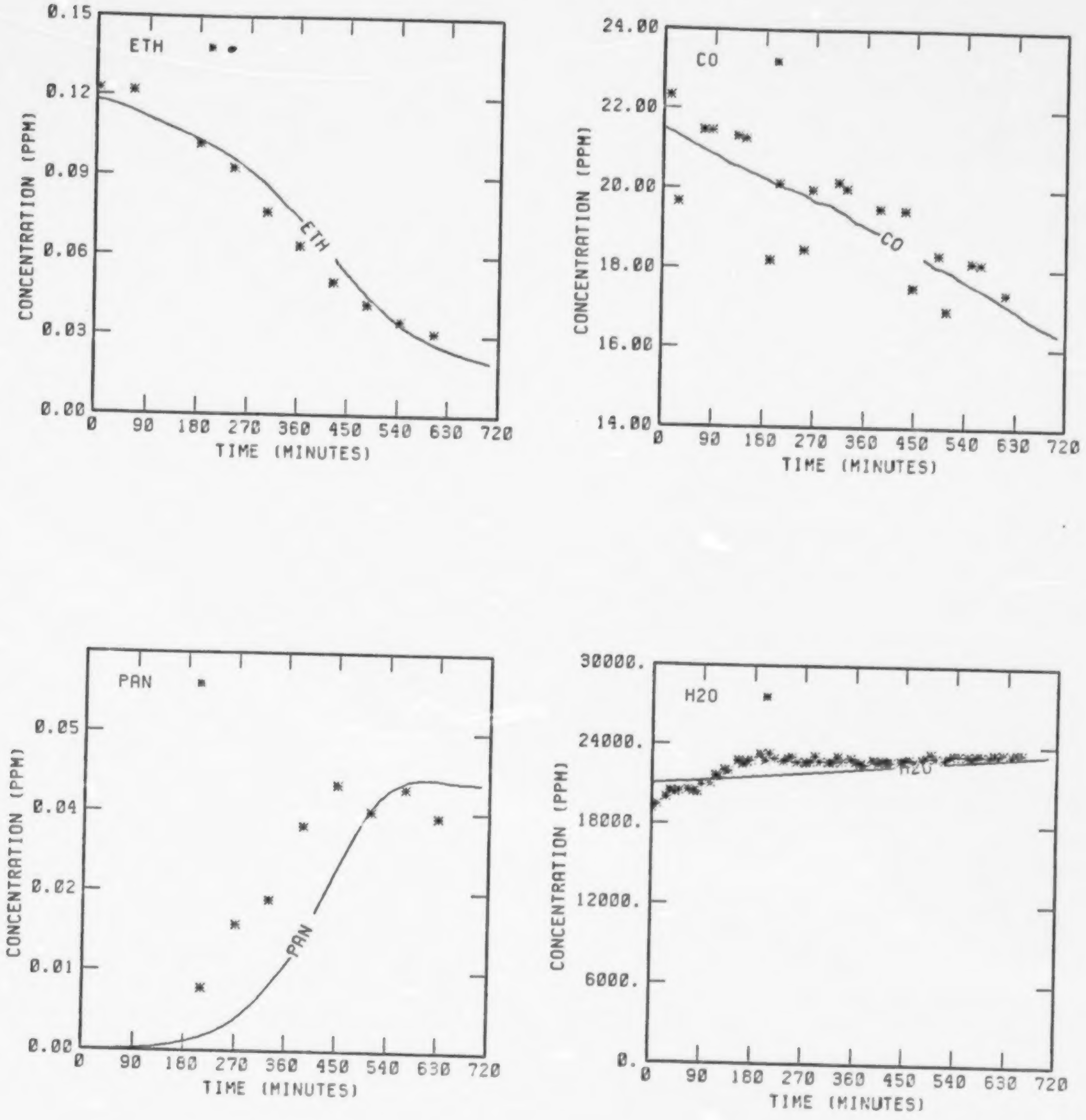

FIGURE 21. SIMULATION RESULTS FOR UNCR 91782 **Continued.**

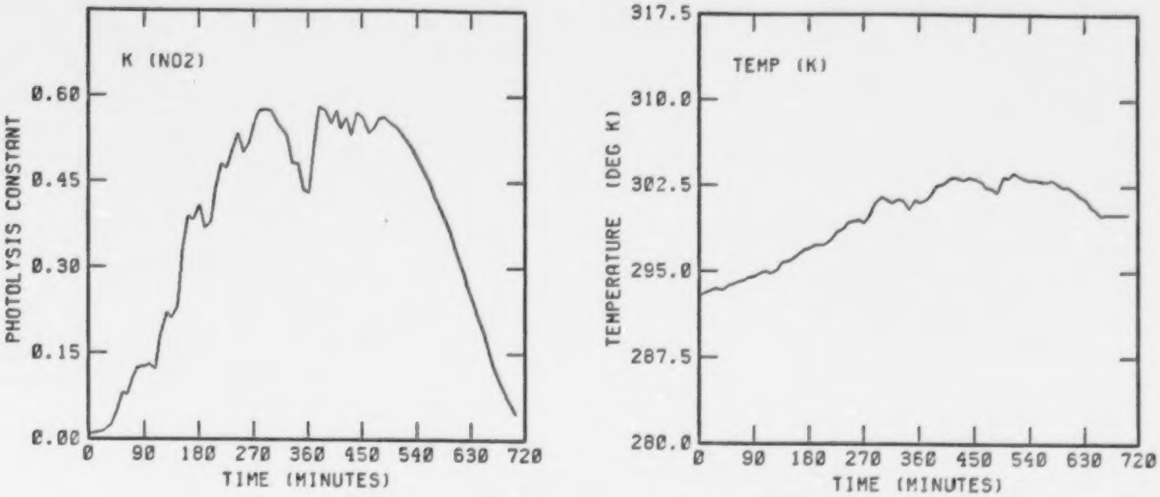

FIGURE 21 . SIMULATION RESULTS FOR
UNCR 91782
Concluded.

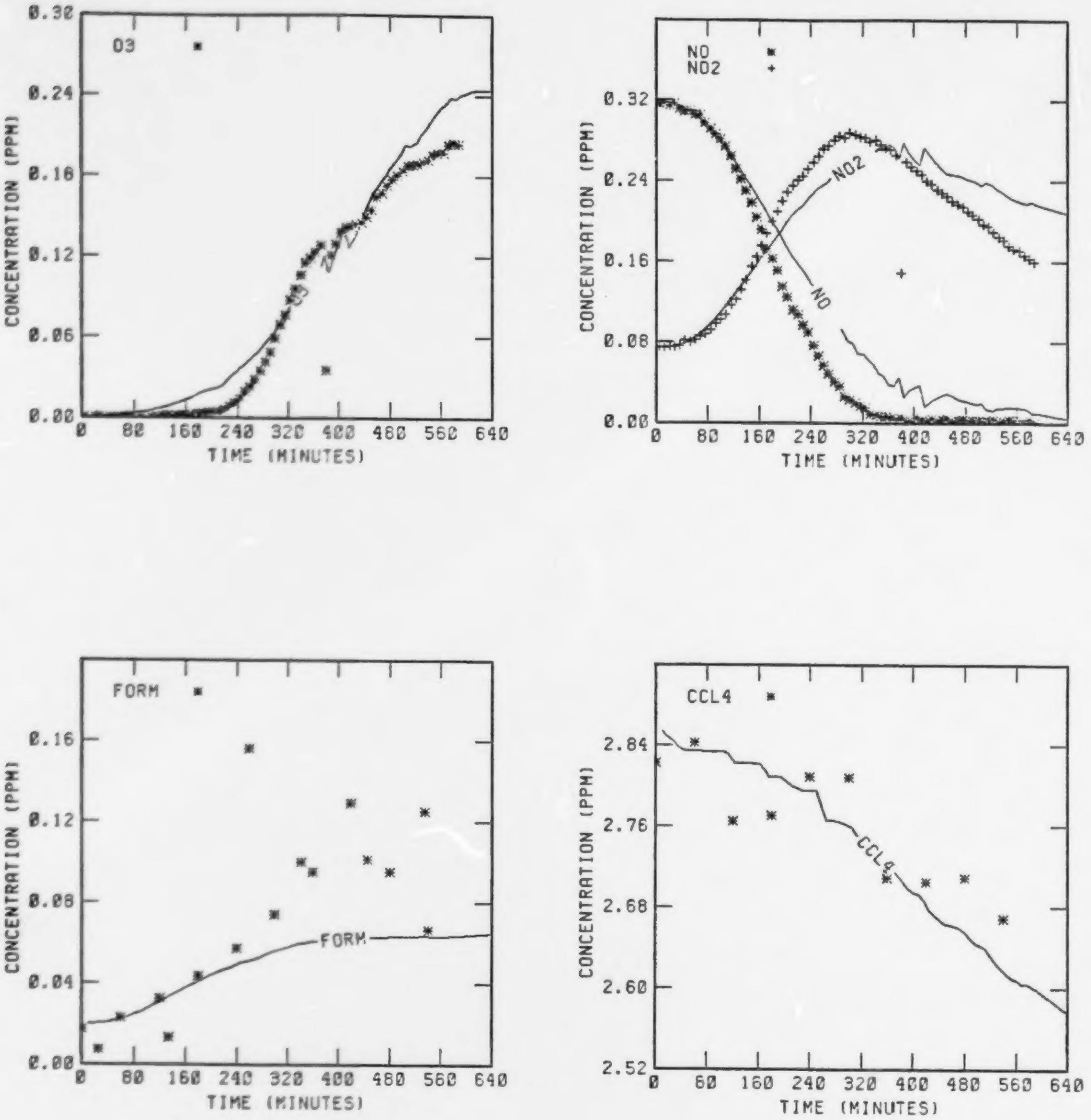

FIGURE 22 . SIMULATION RESULTS FOR
UNCB 92982

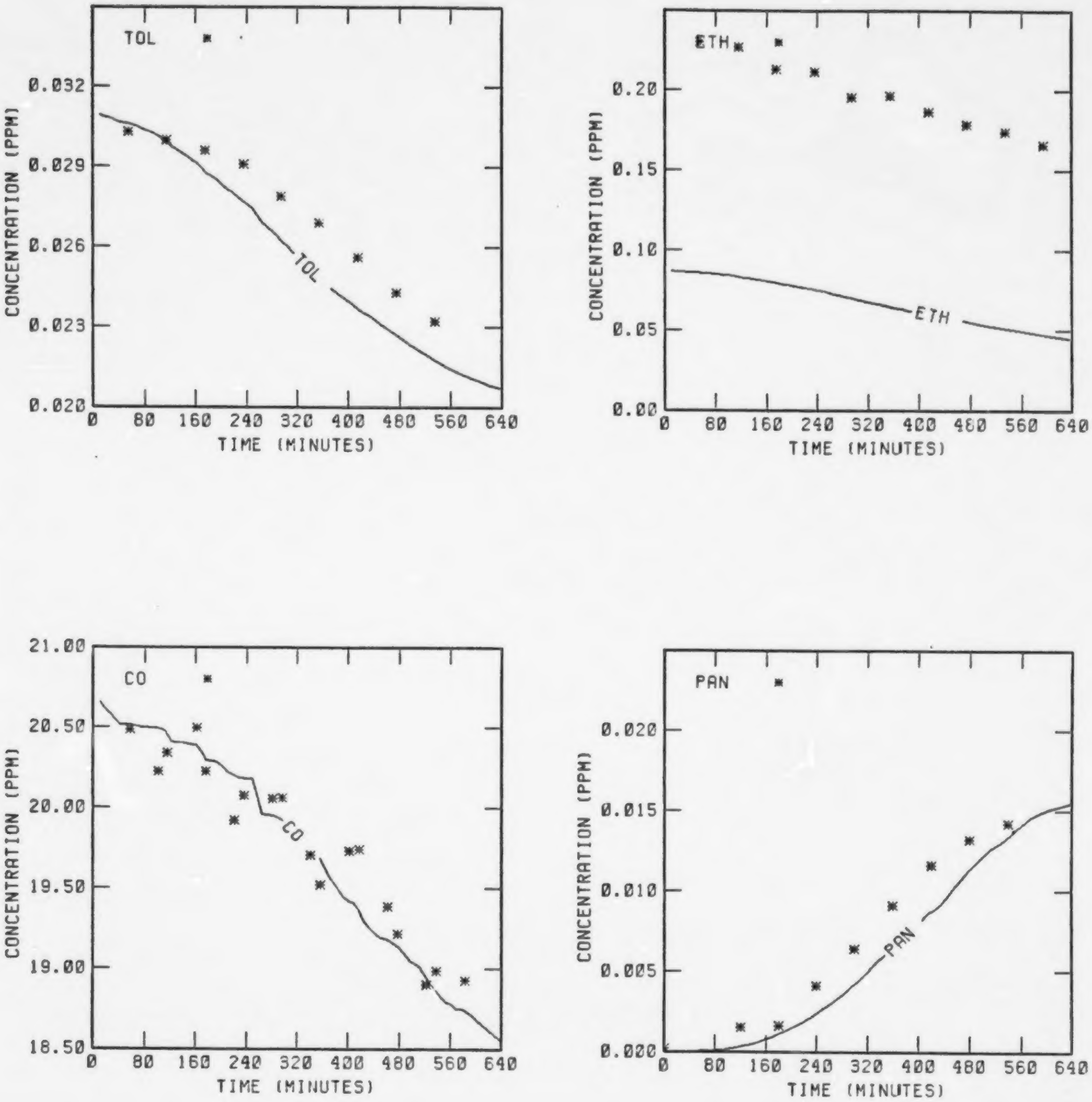

FIGURE 22 . SIMULATION RESULTS FOR
UNCB 92982
Continued.

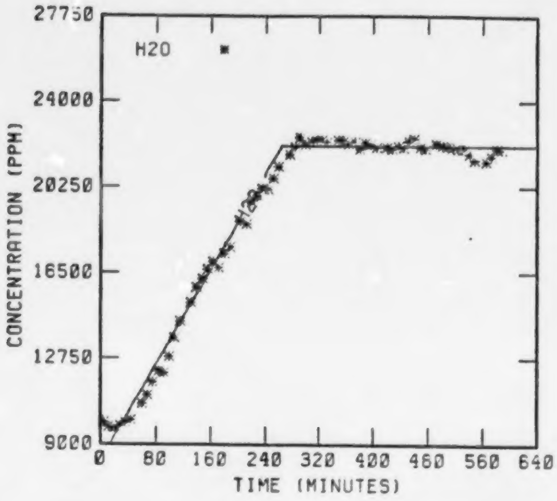

FIGURE 22 . SIMULATION RESULTS FOR
UNCB 92982
Concluded.

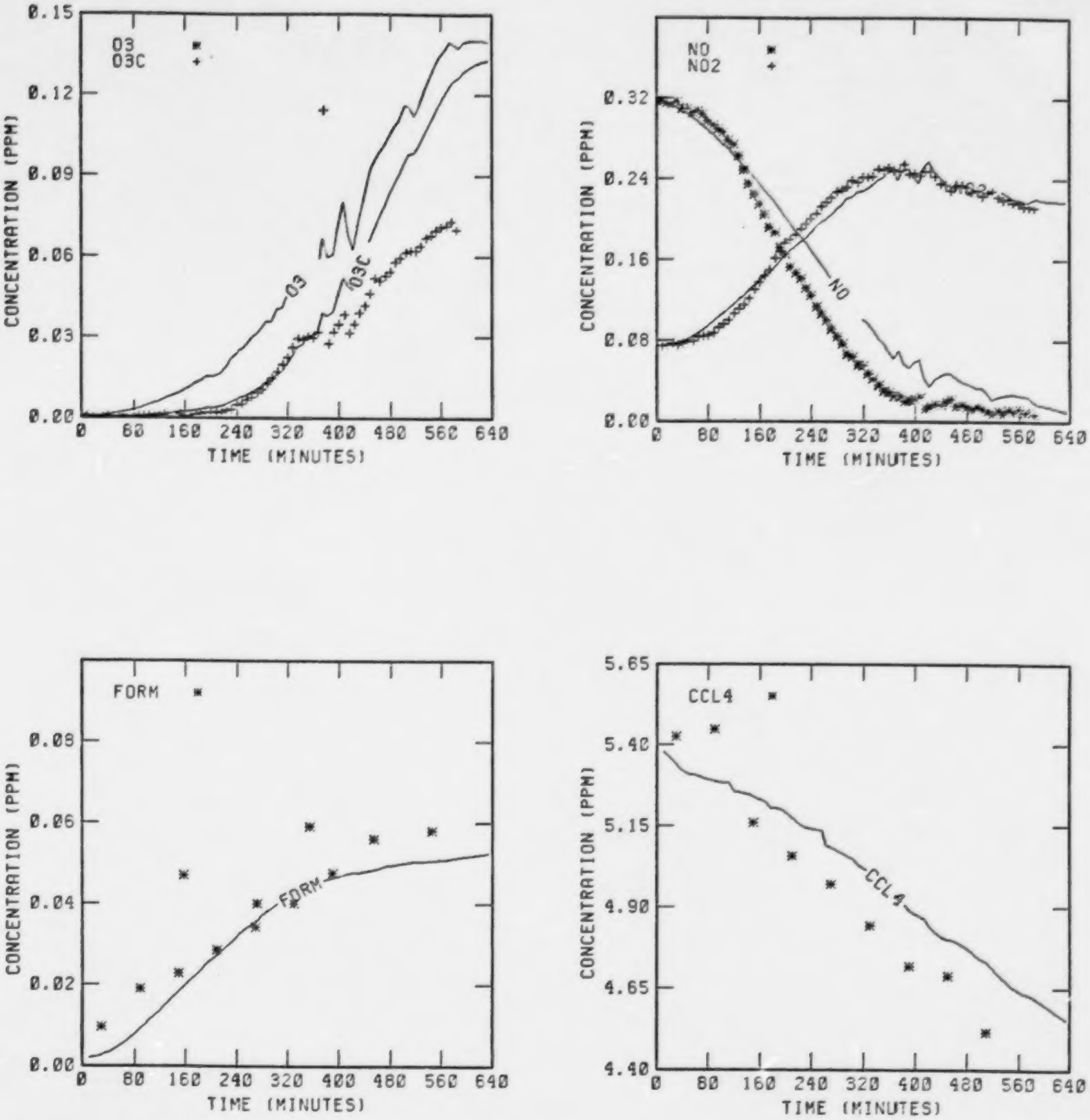

FIGURE 23 . SIMULATION RESULTS FOR UNCR 92982

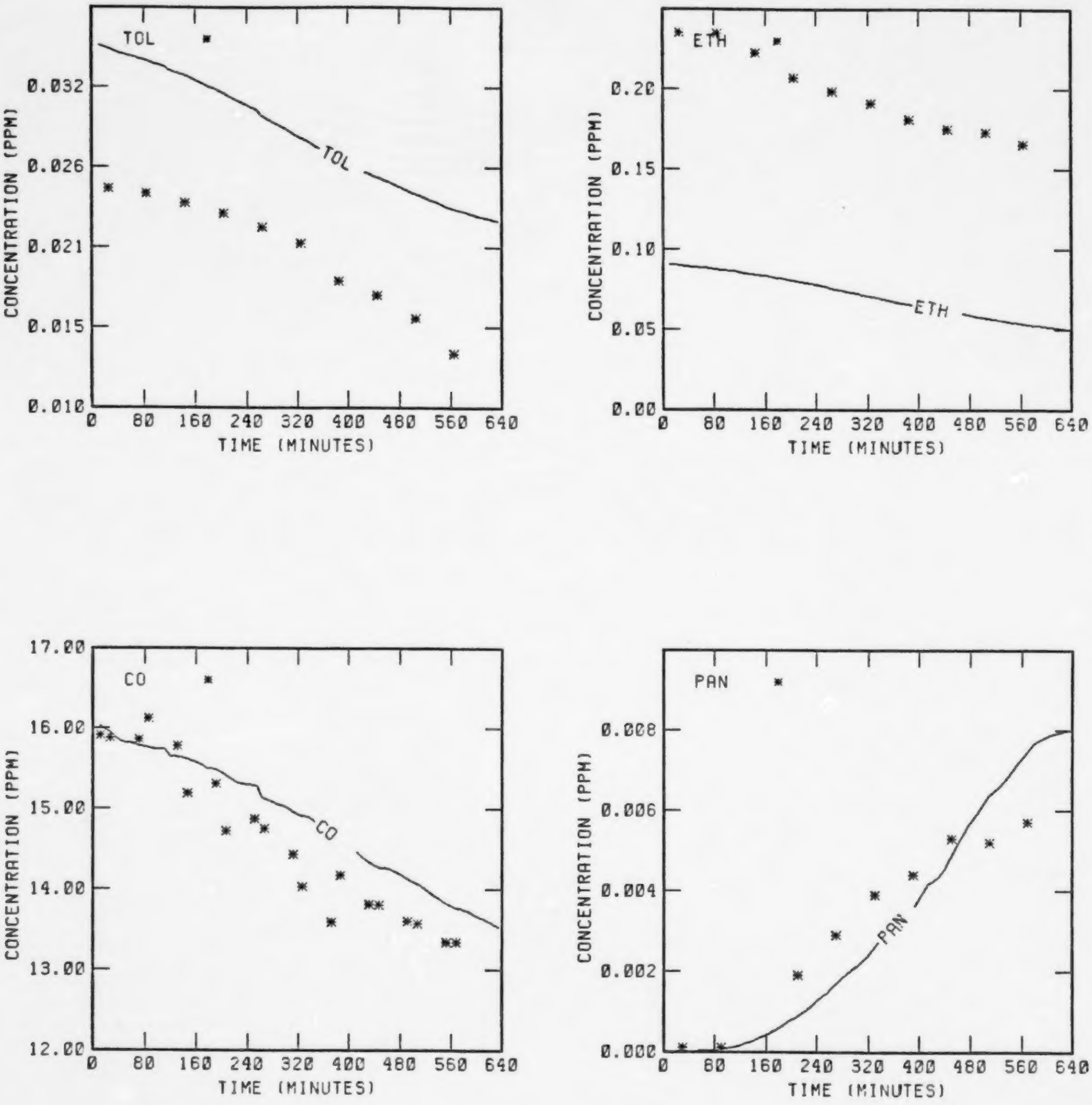

FIGURE **23** . SIMULATION RESULTS FOR
UNCR 92982
Continued.

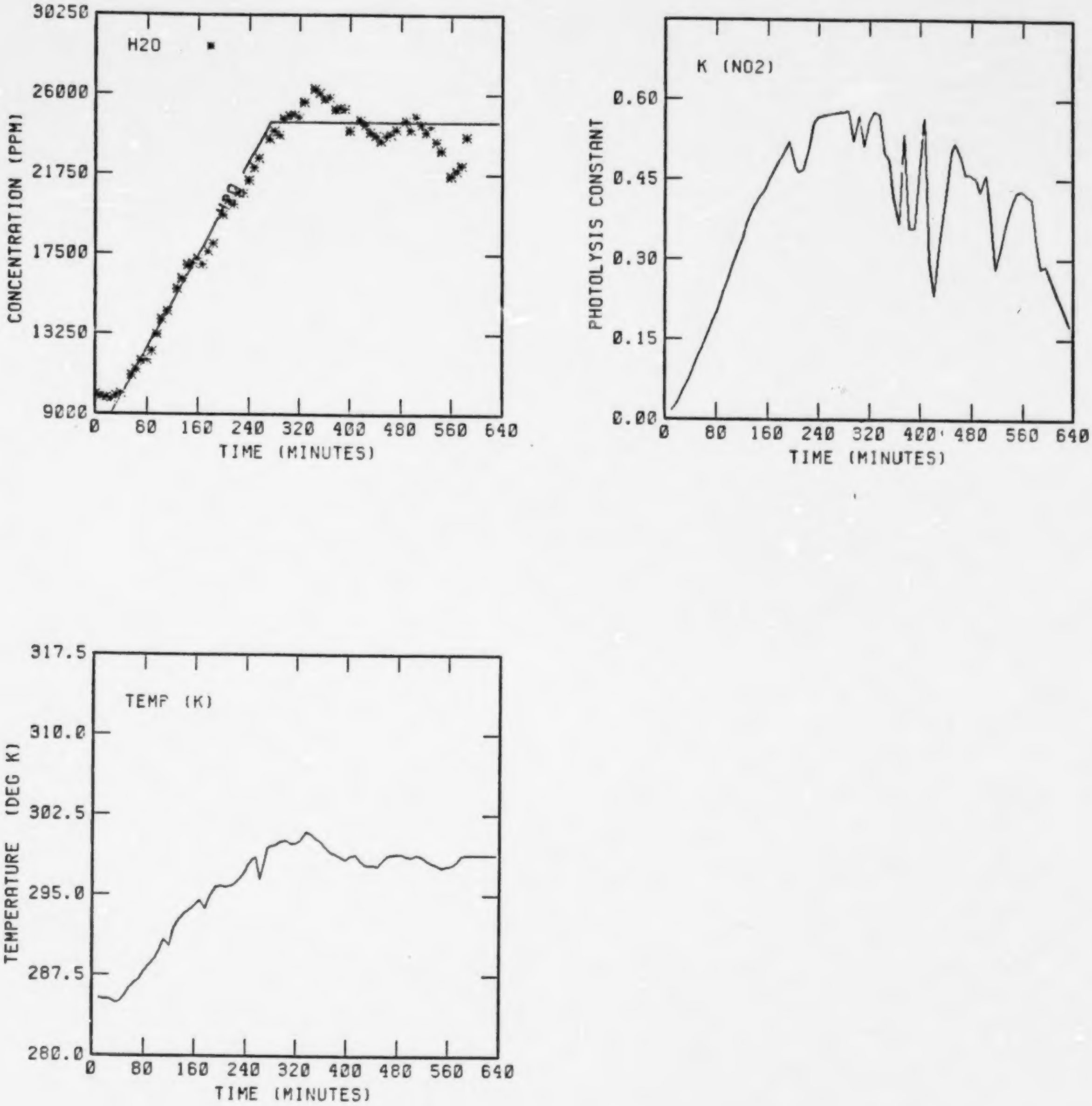

FIGURE 23 . SIMULATION RESULTS FOR
UNCR 92982
Concluded.

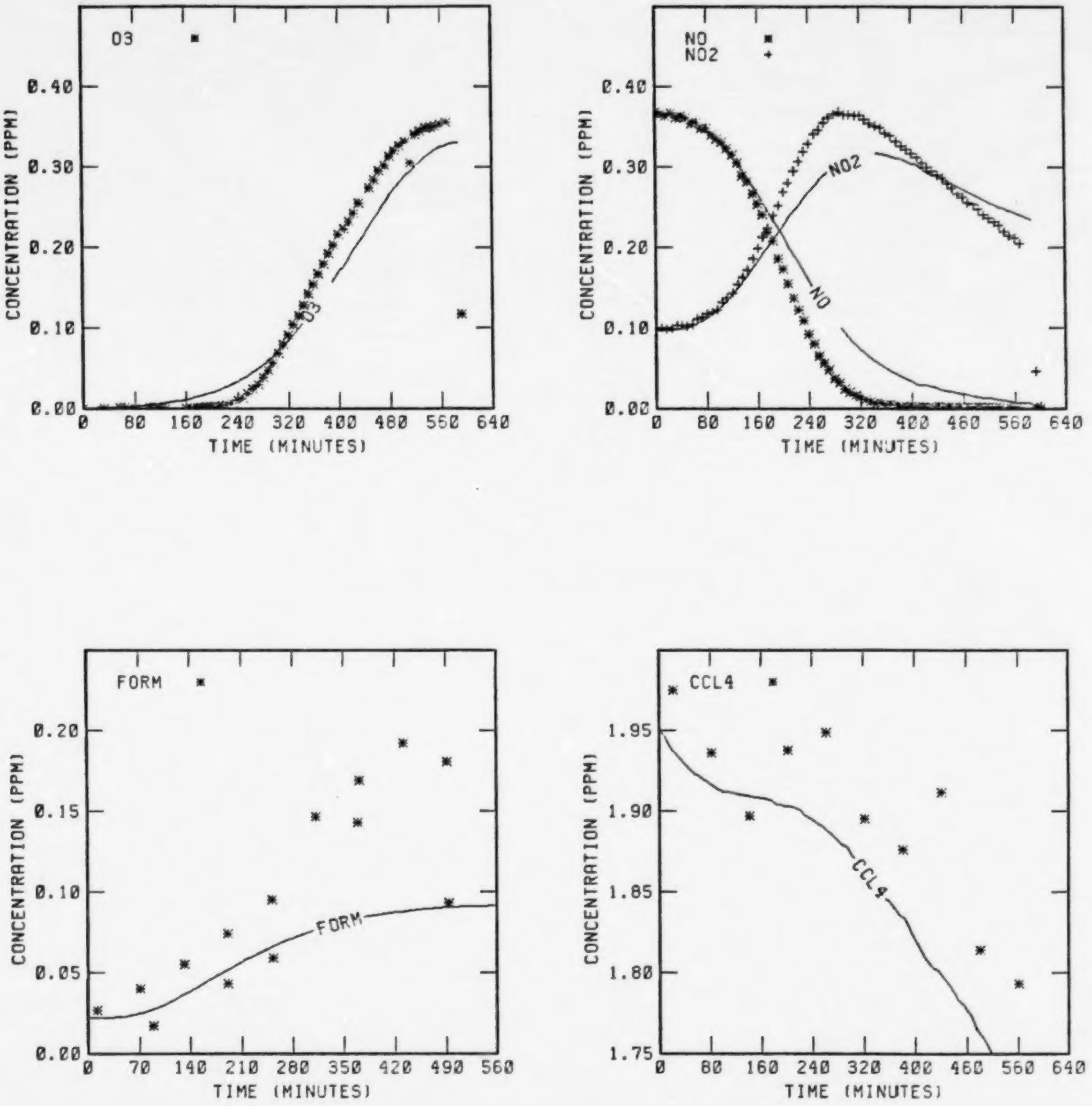

FIGURE 24 . SIMULATION RESULTS FOR UNCR 100682

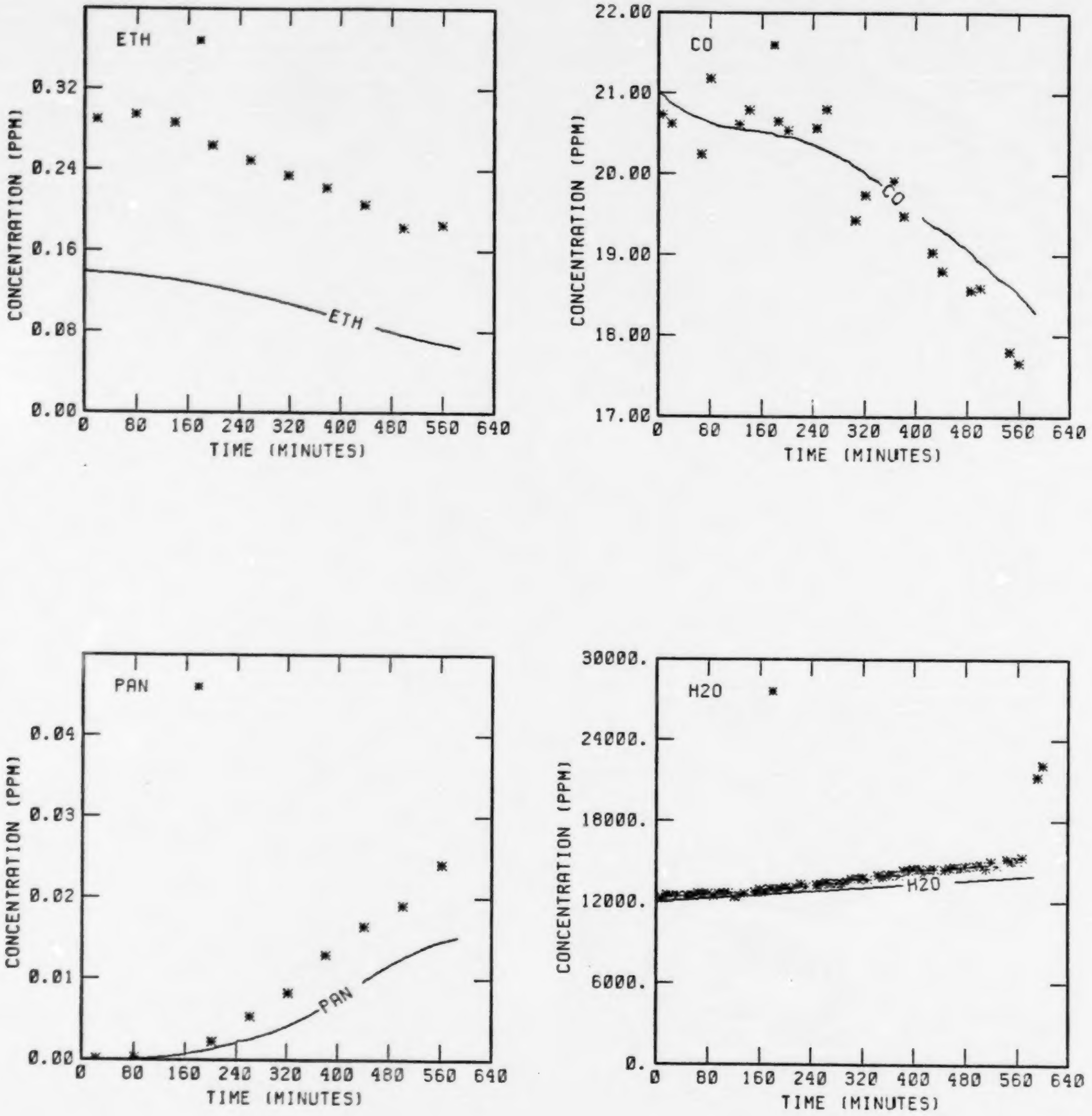

FIGURE 24. SIMULATION RESULTS FOR
UNCR 100682

Continued.

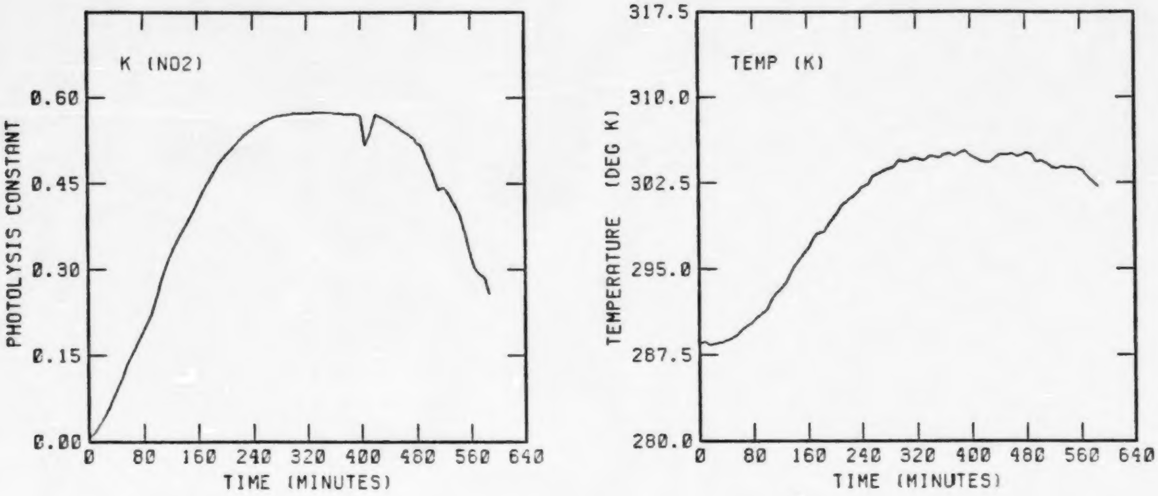

FIGURE 24 . SIMULATION RESULTS FOR
UNCR 100682
Concluded.

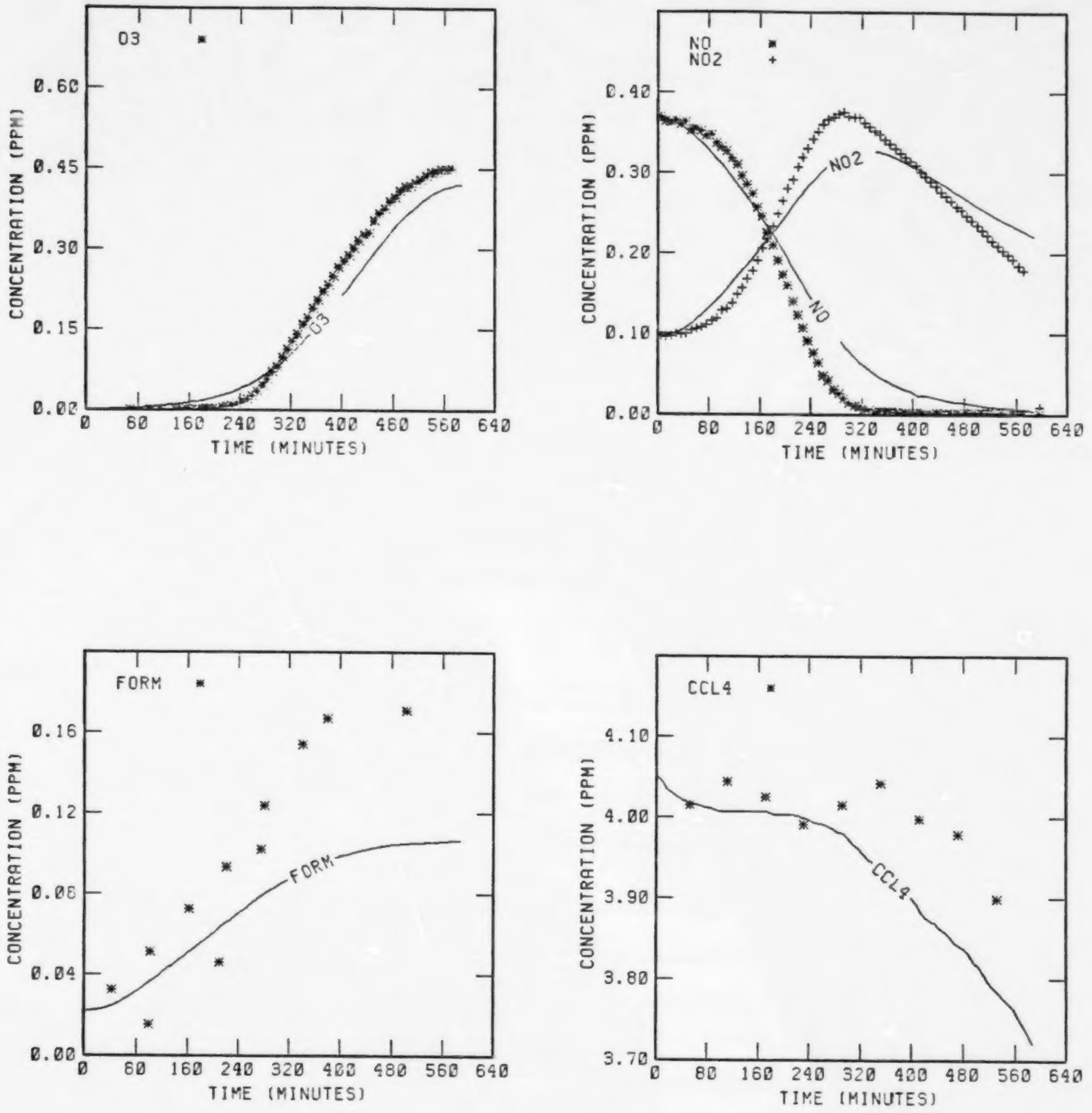

FIGURE 25 . SIMULATION RESULTS FOR
UNCB 100682

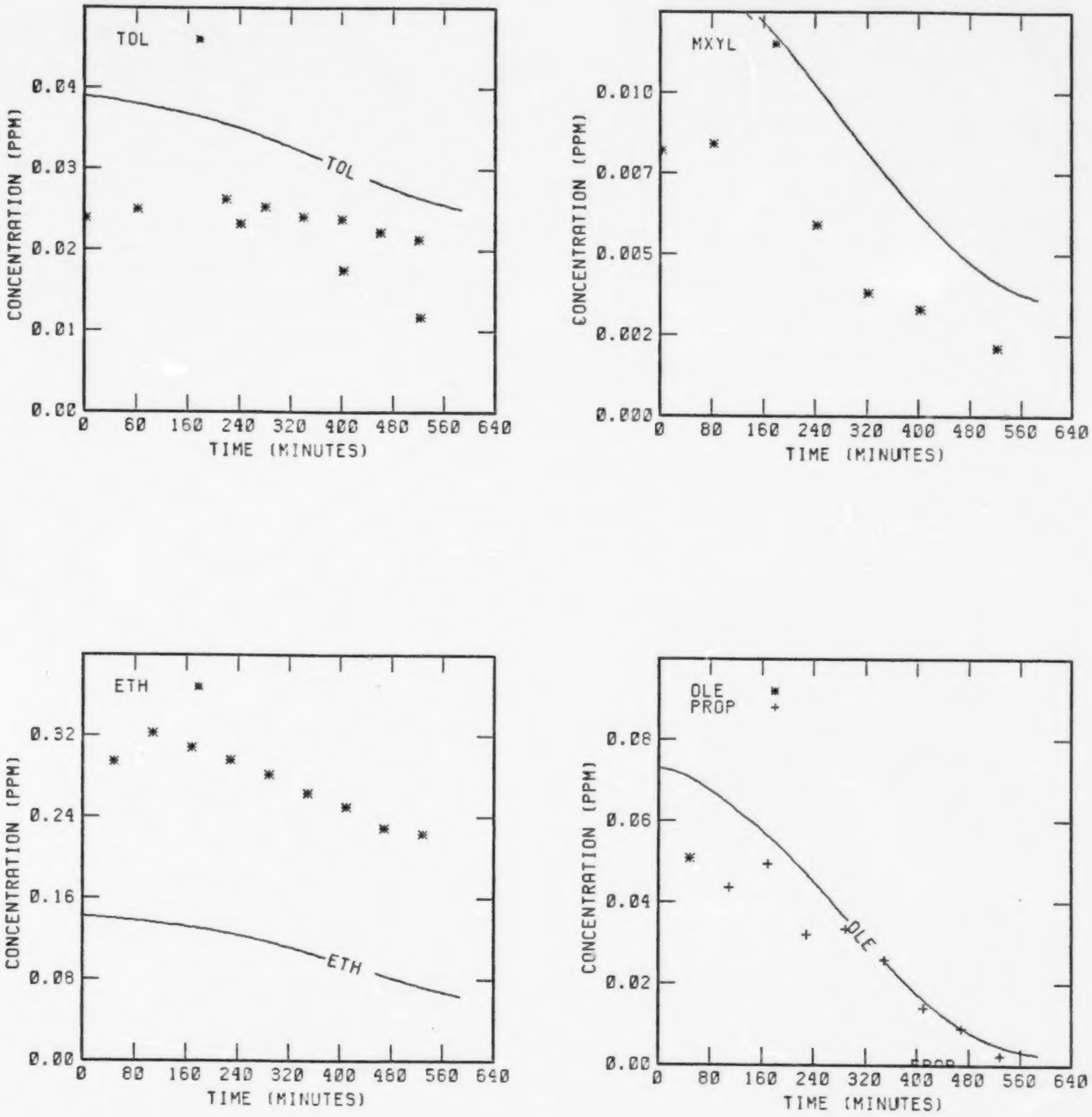

FIGURE 25. SIMULATION RESULTS FOR
UNCB 100682
Continued.

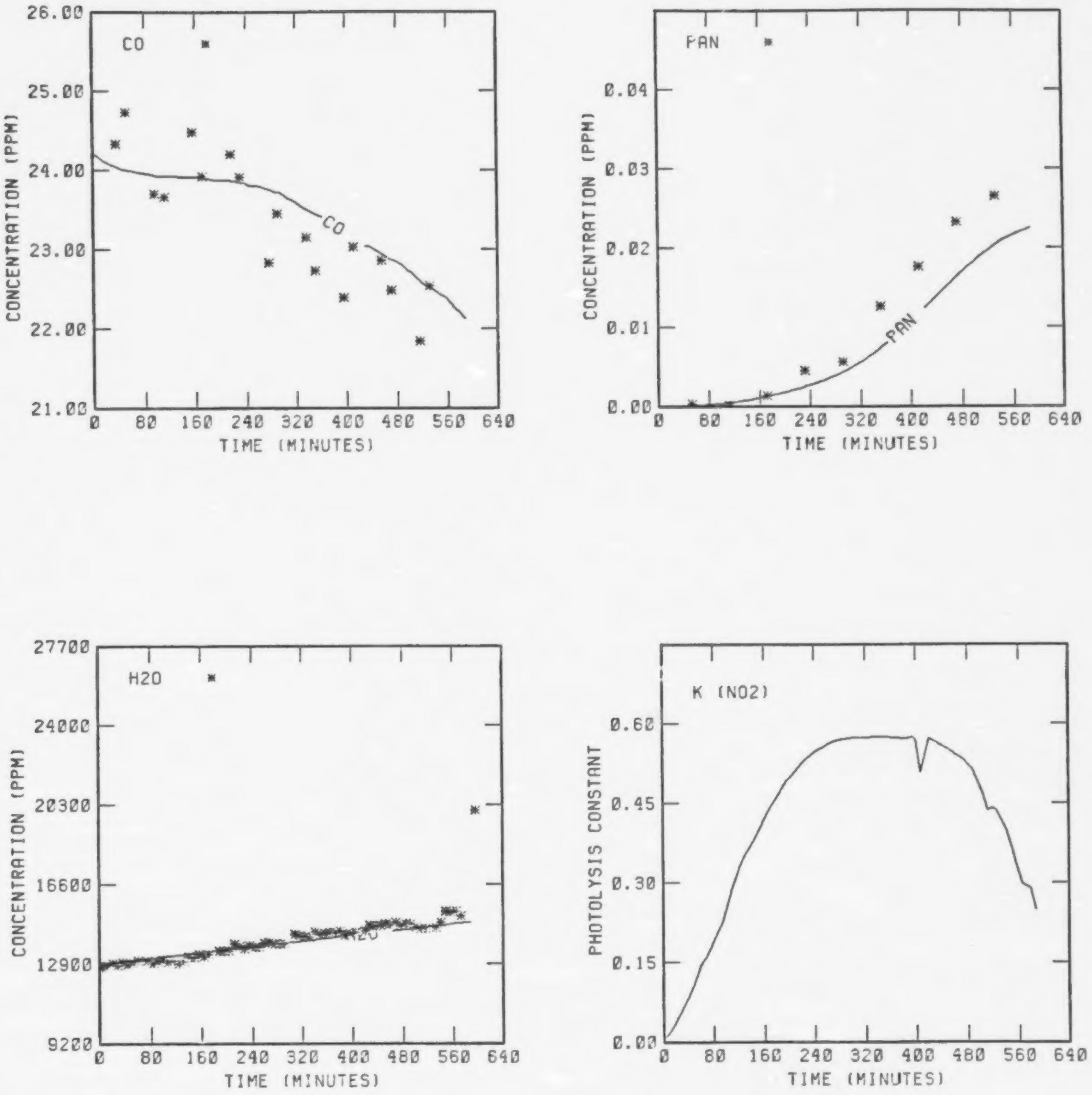

FIGURE 25. SIMULATION RESULTS FOR
UNCB 100682

Continued.

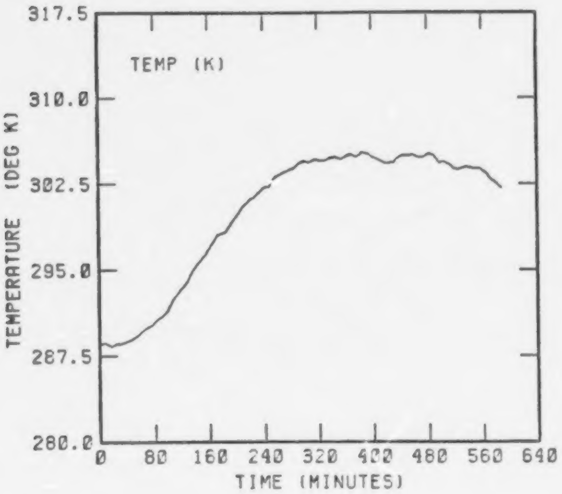

FIGURE 25. SIMULATION RESULTS FOR UNCB 100682

Concluded.

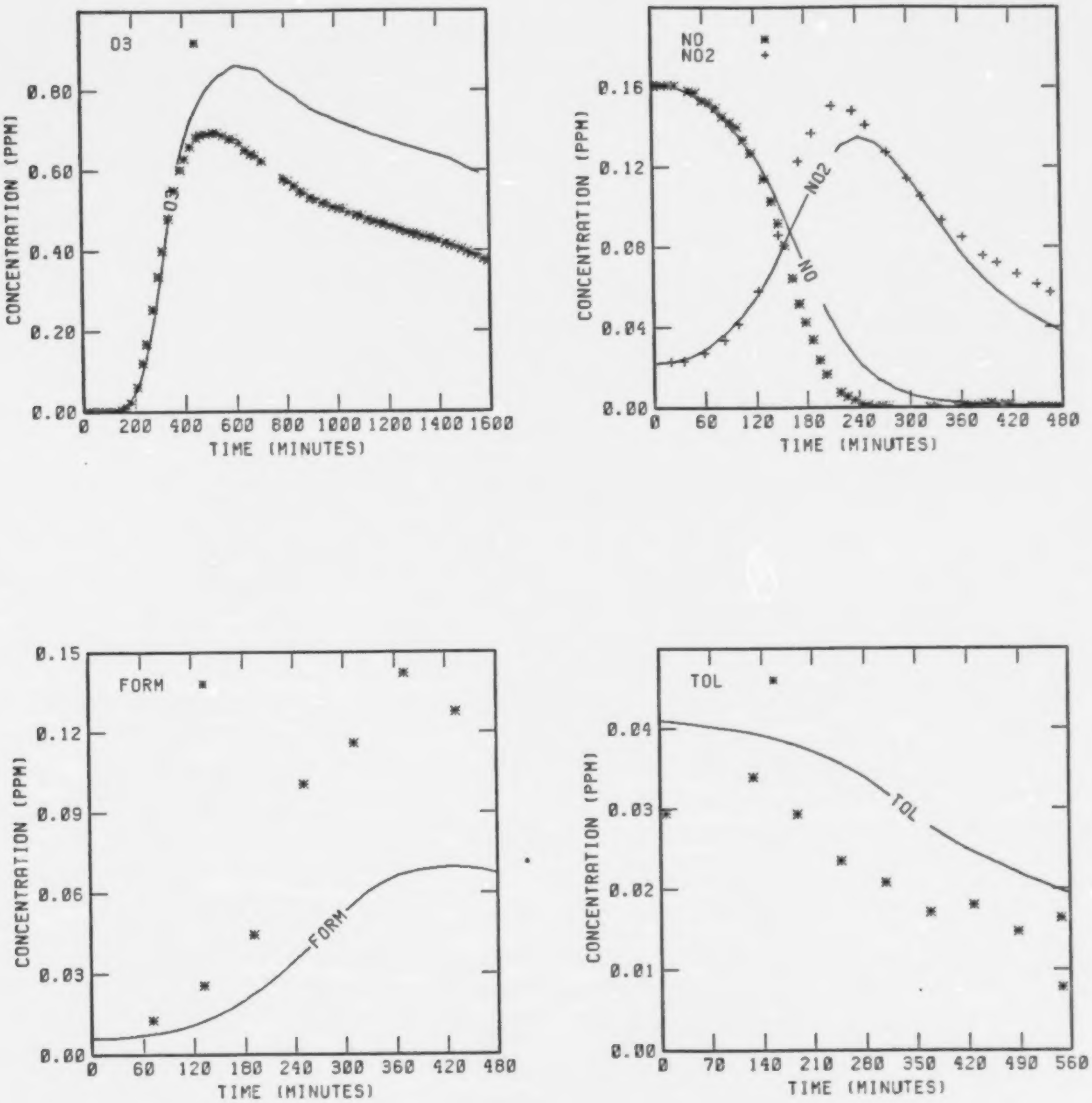

FIGURE 26. SIMULATION RESULTS FOR
UNCB 70283

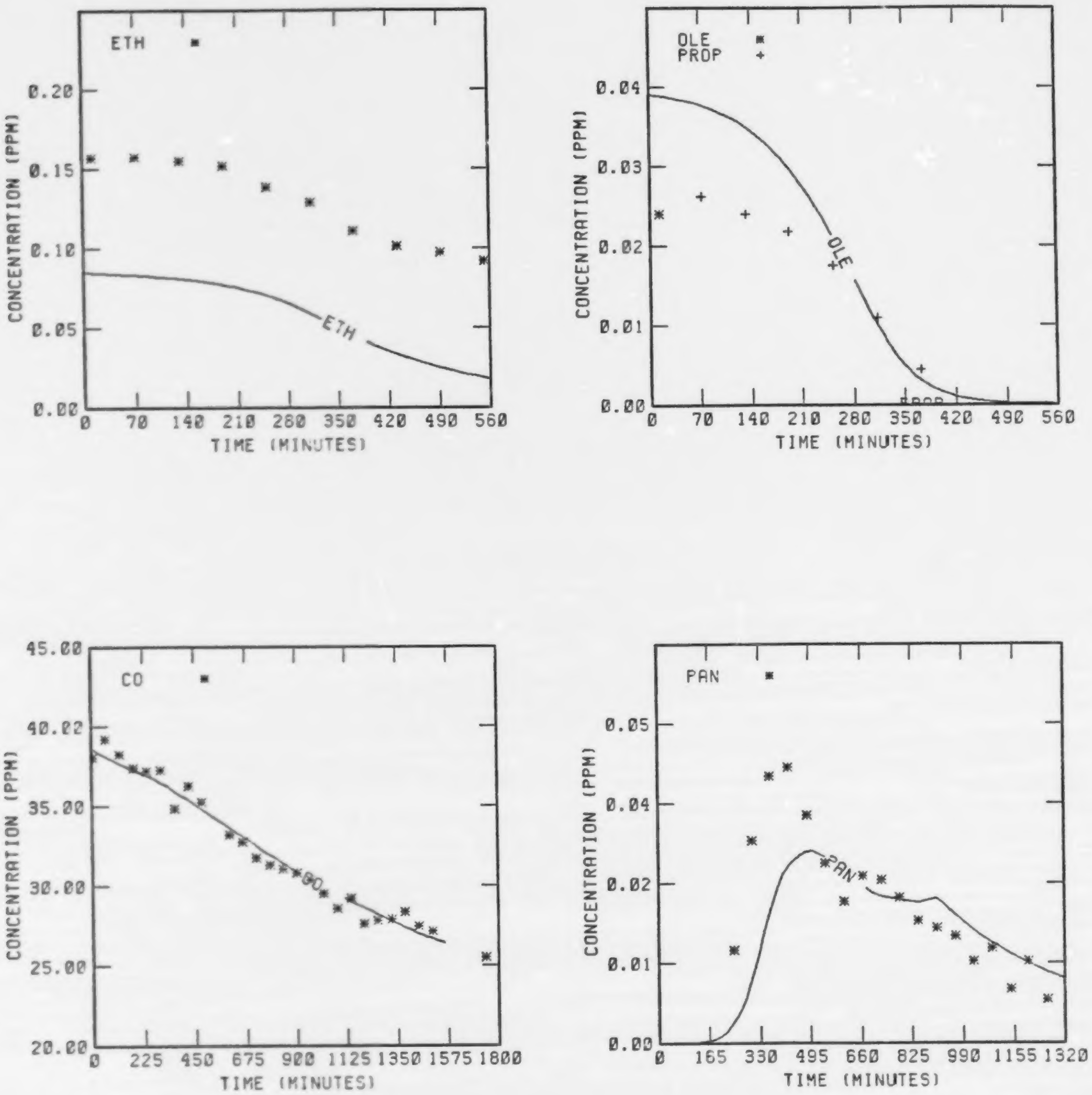

FIGURE 26 . SIMULATION RESULTS FOR
UNCB 70283
Continued.

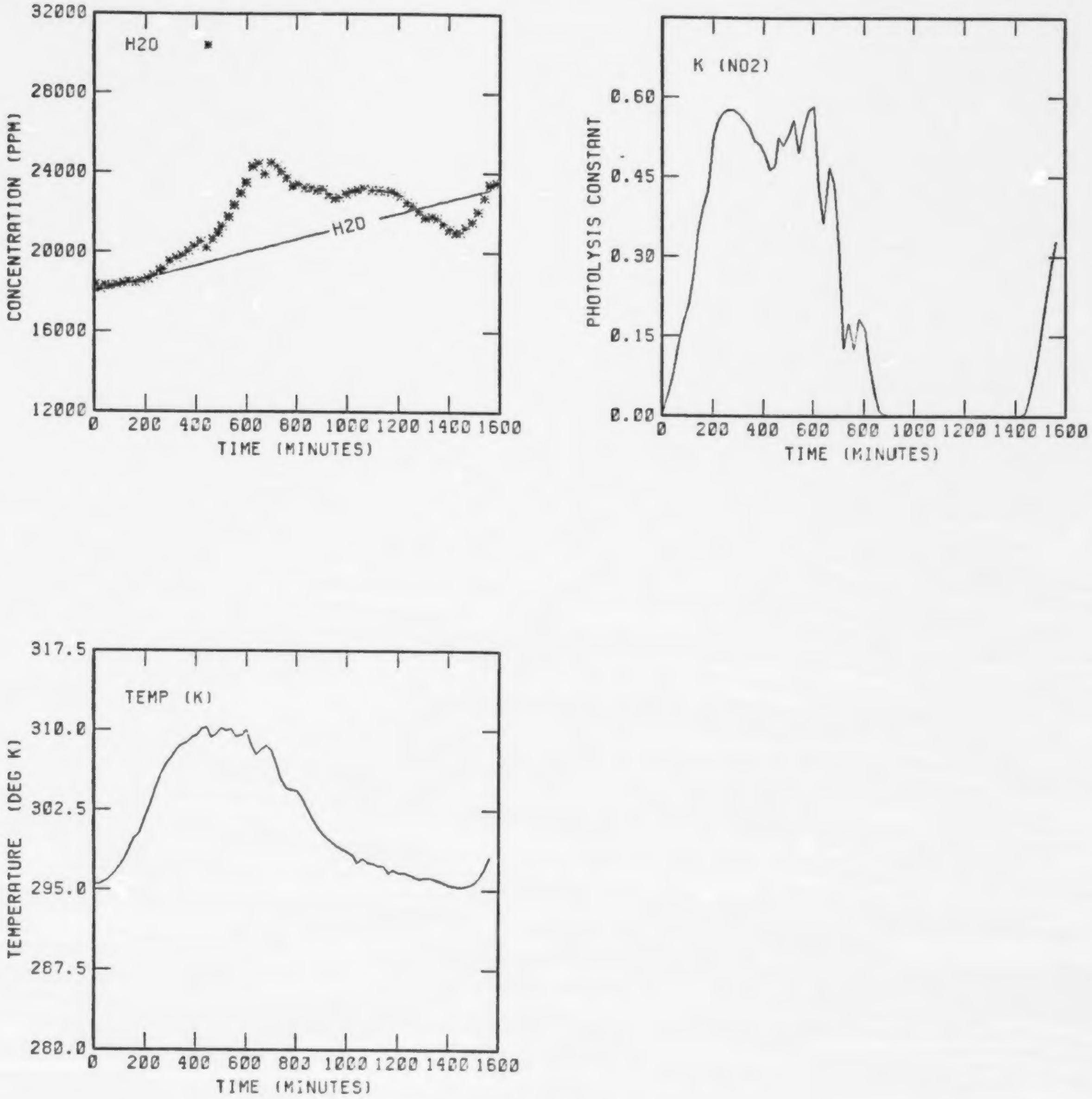

FIGURE 26. SIMULATION RESULTS FOR
UNCB 70283
Concluded.

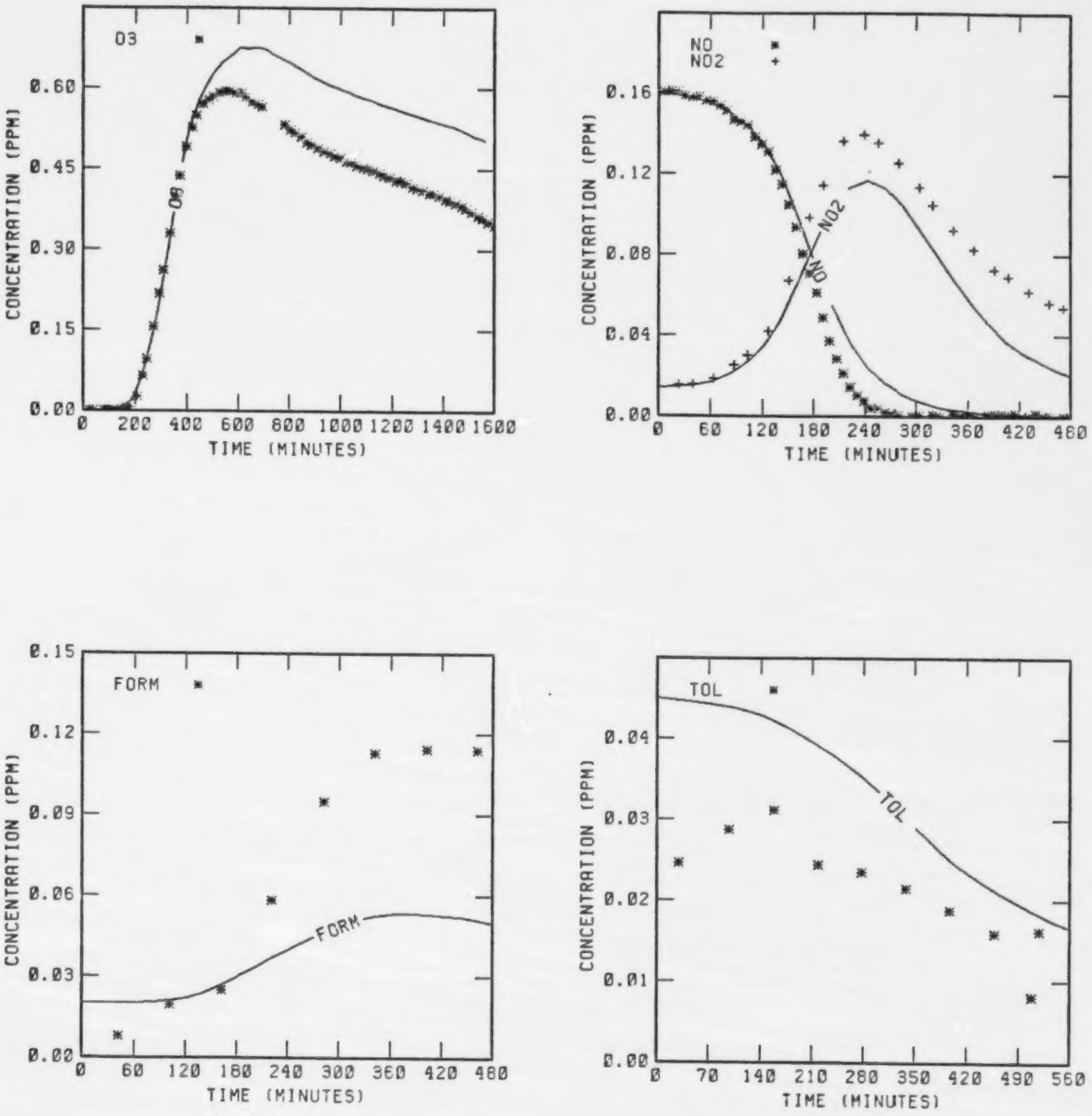

FIGURE 27. SIMULATION RESULTS FOR
UNCR 70283

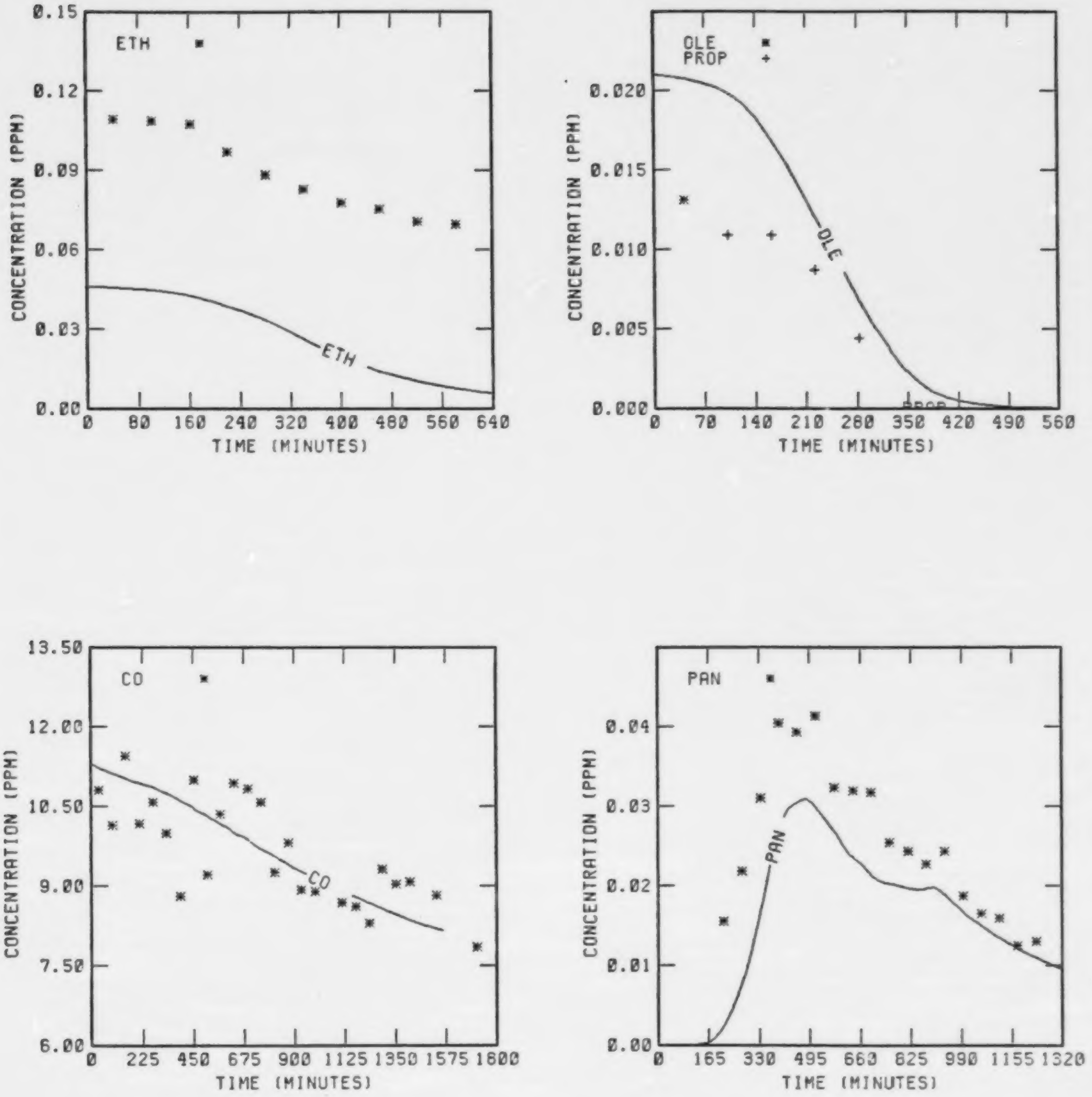

FIGURE 27. SIMULATION RESULTS FOR
UNCR 70283
Concluded.

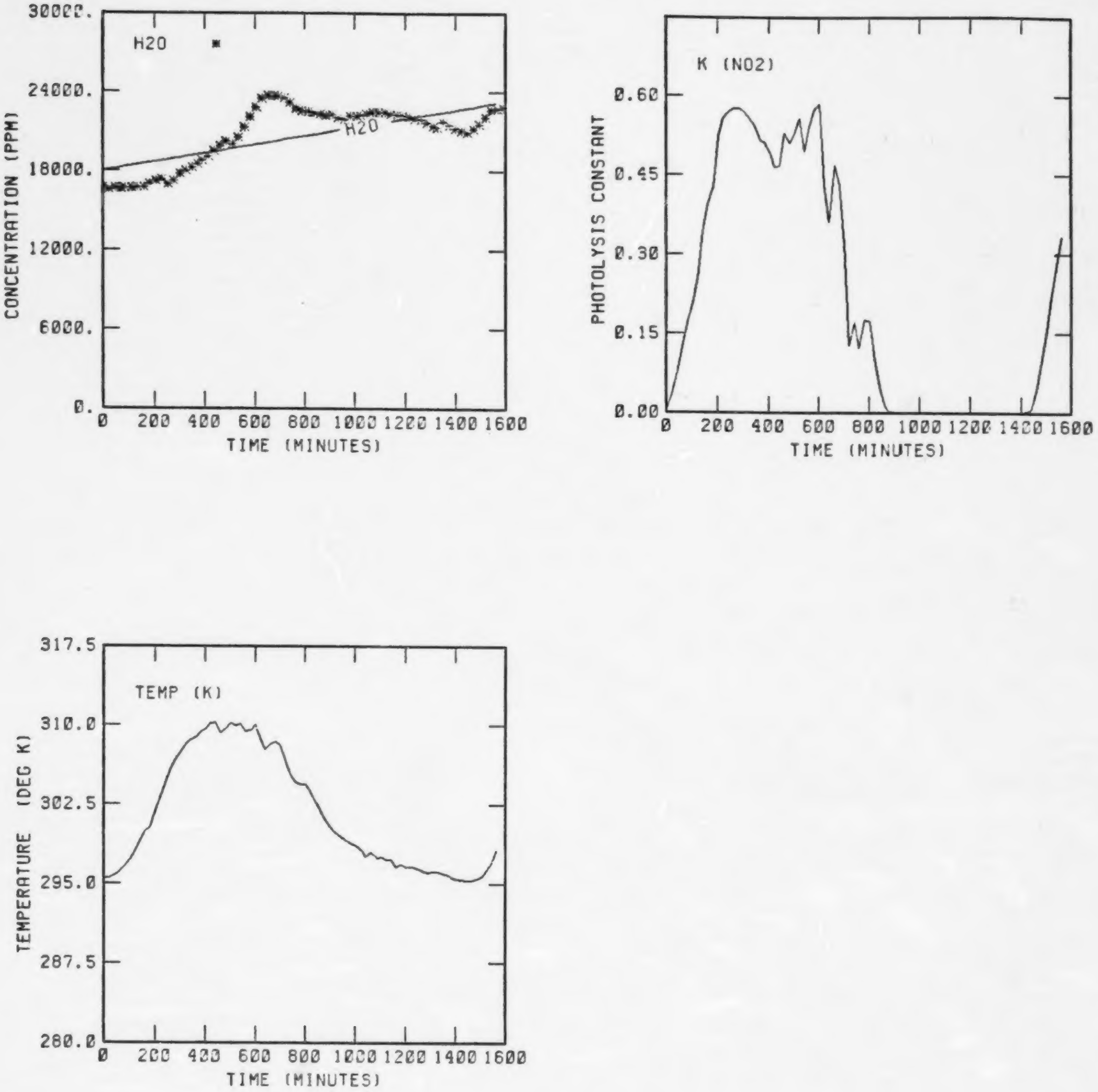

FIGURE 27. SIMULATION RESULTS FOR
UNCR 70283

Concluded.

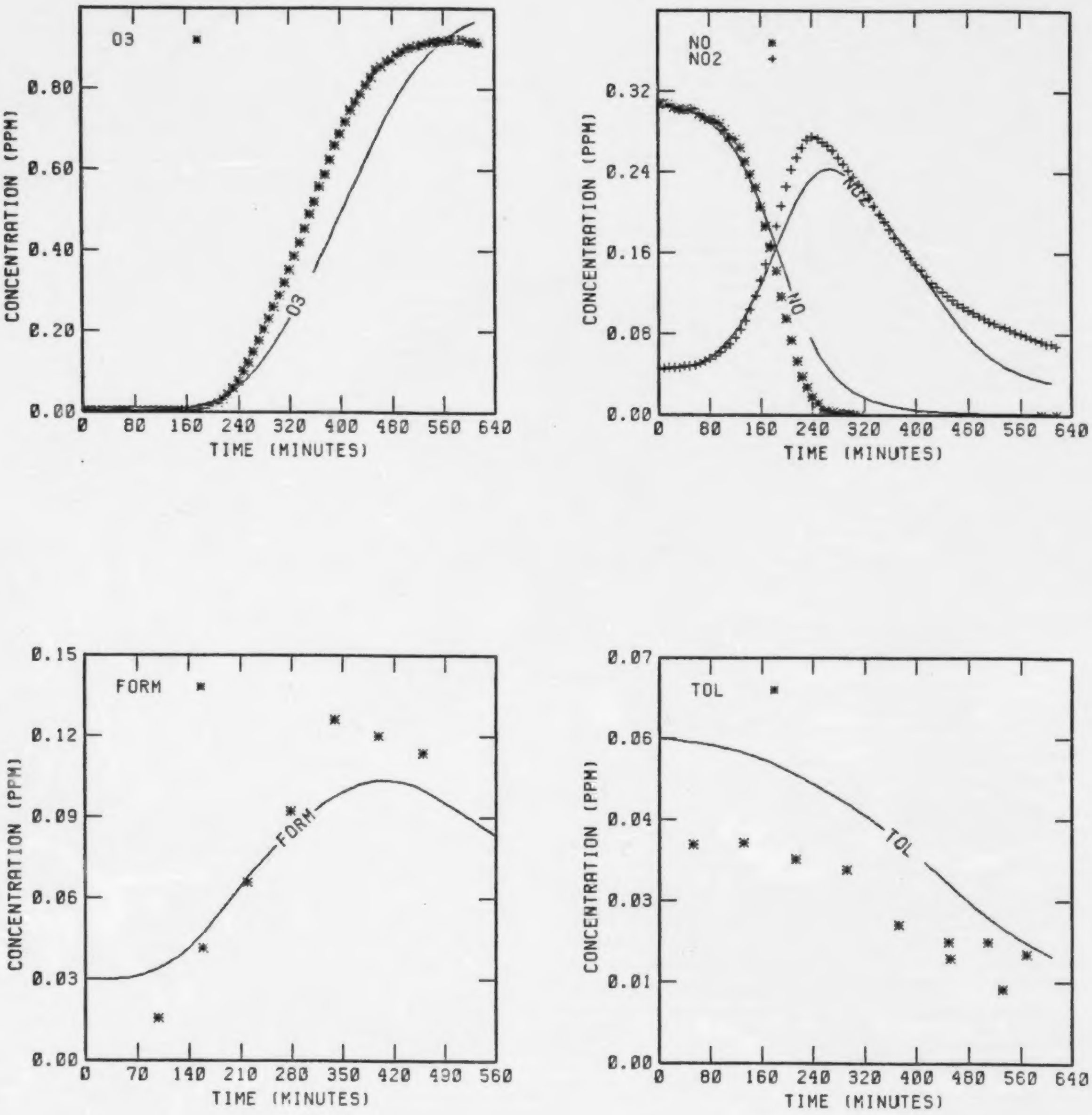

FIGURE 28. SIMULATION RESULTS FOR
UNCB 71583

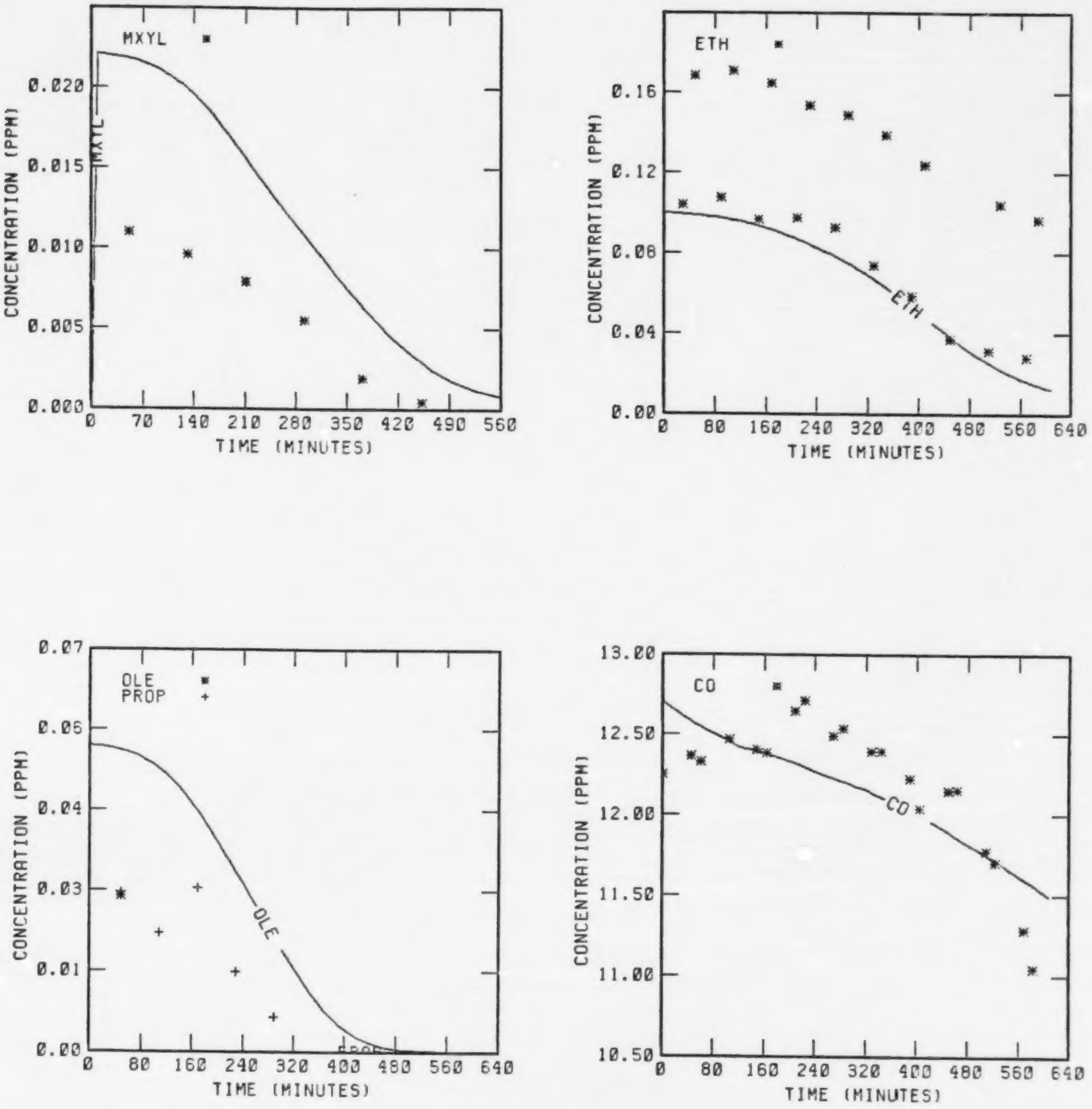

FIGURE 28. SIMULATION RESULTS FOR
UNCB 71583
Continued.

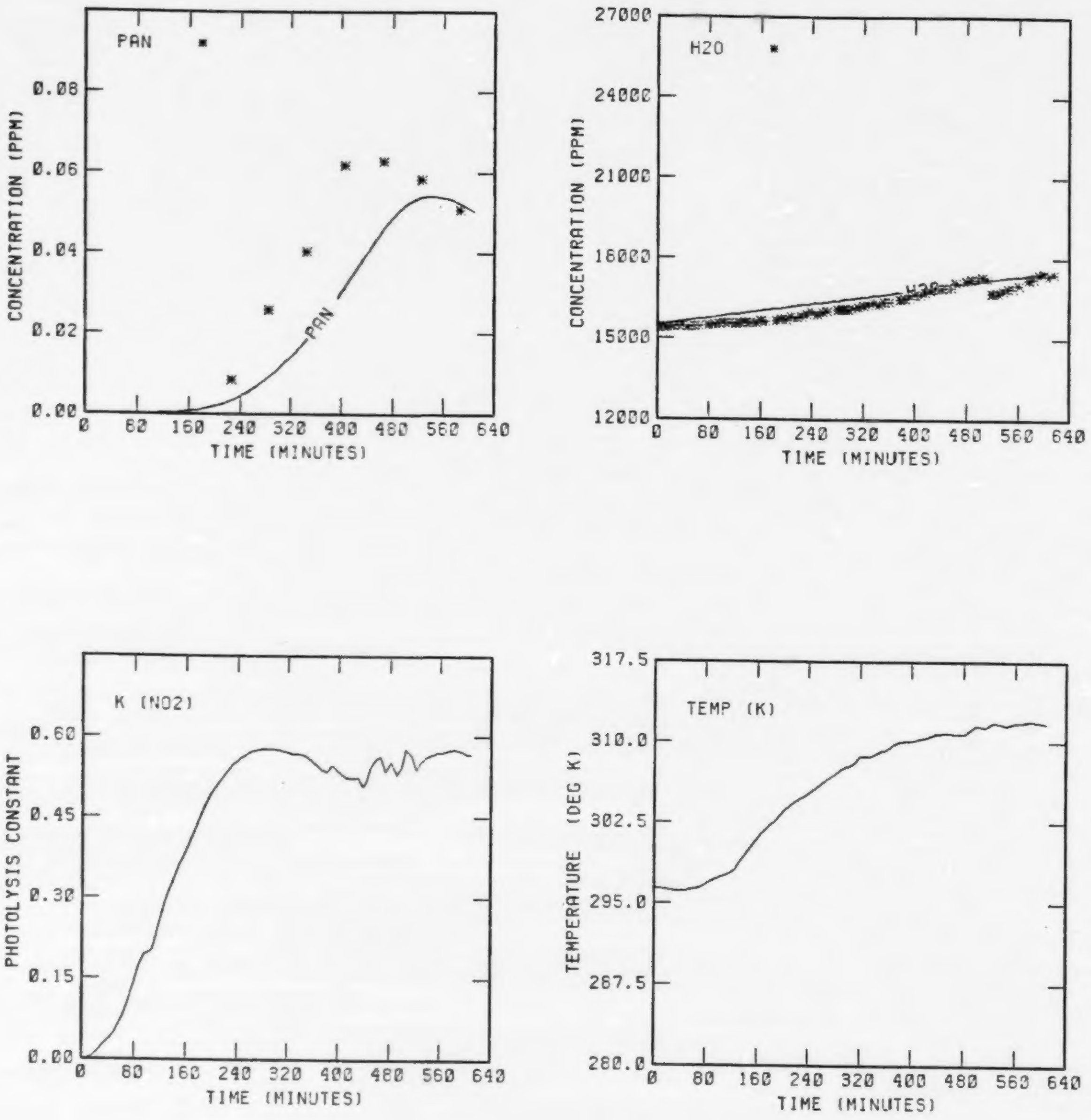

FIGURE 28 . SIMULATION RESULTS FOR
UNCB 71583
Concluded.

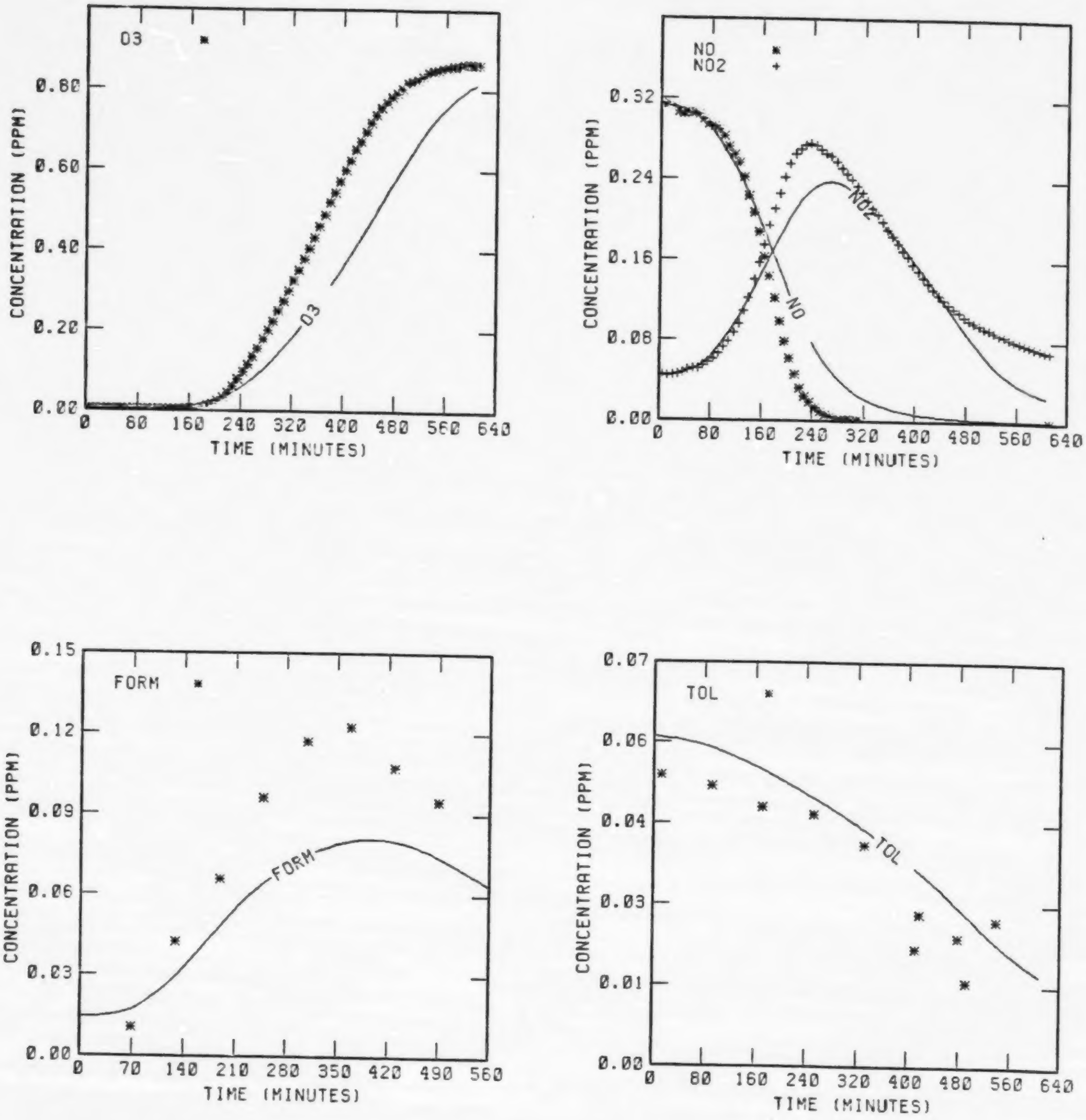

FIGURE 29. SIMULATION RESULTS FOR UNCR 71583

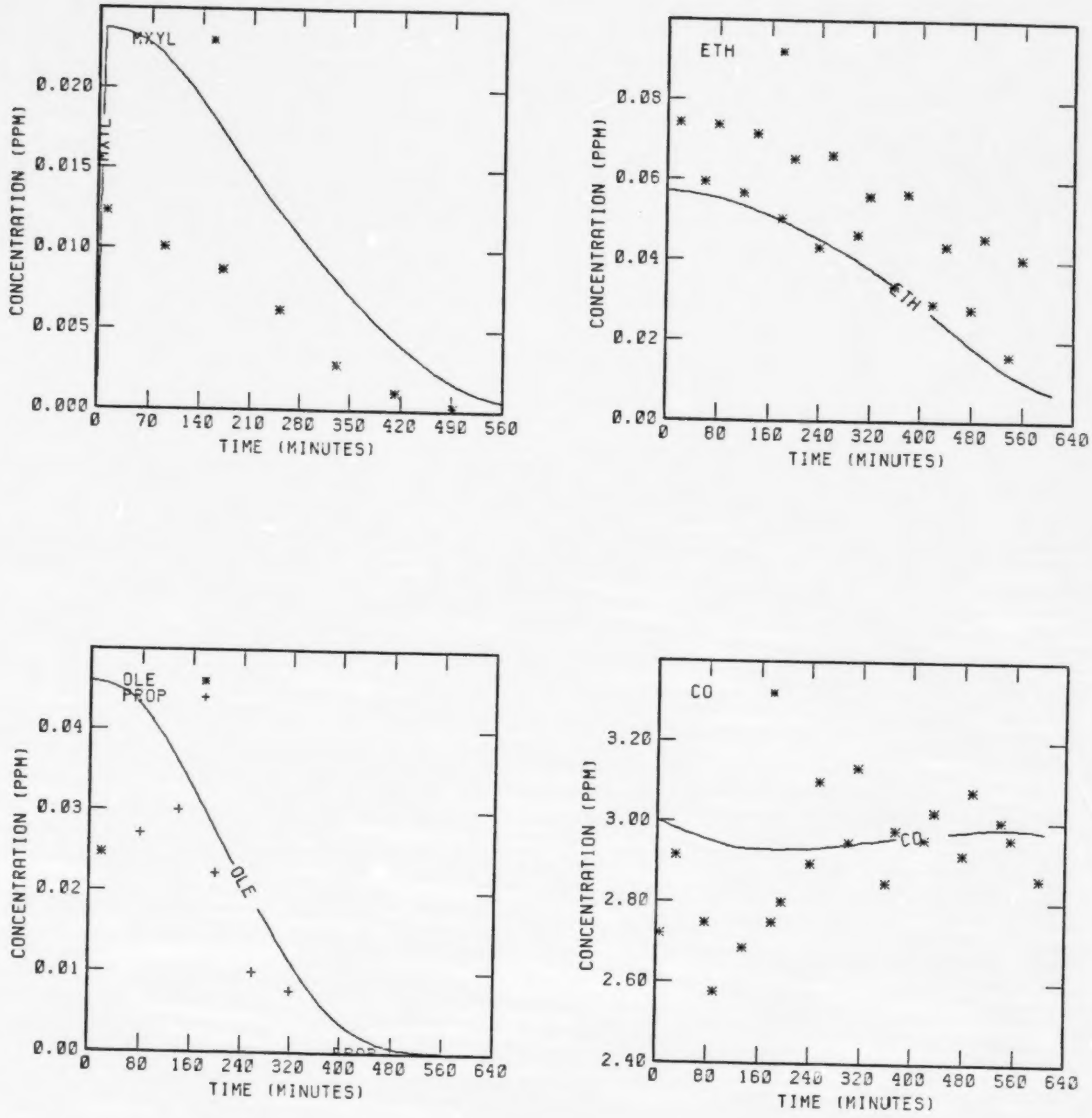

FIGURE **29.** SIMULATION RESULTS FOR
UNCR 71583
Continued.

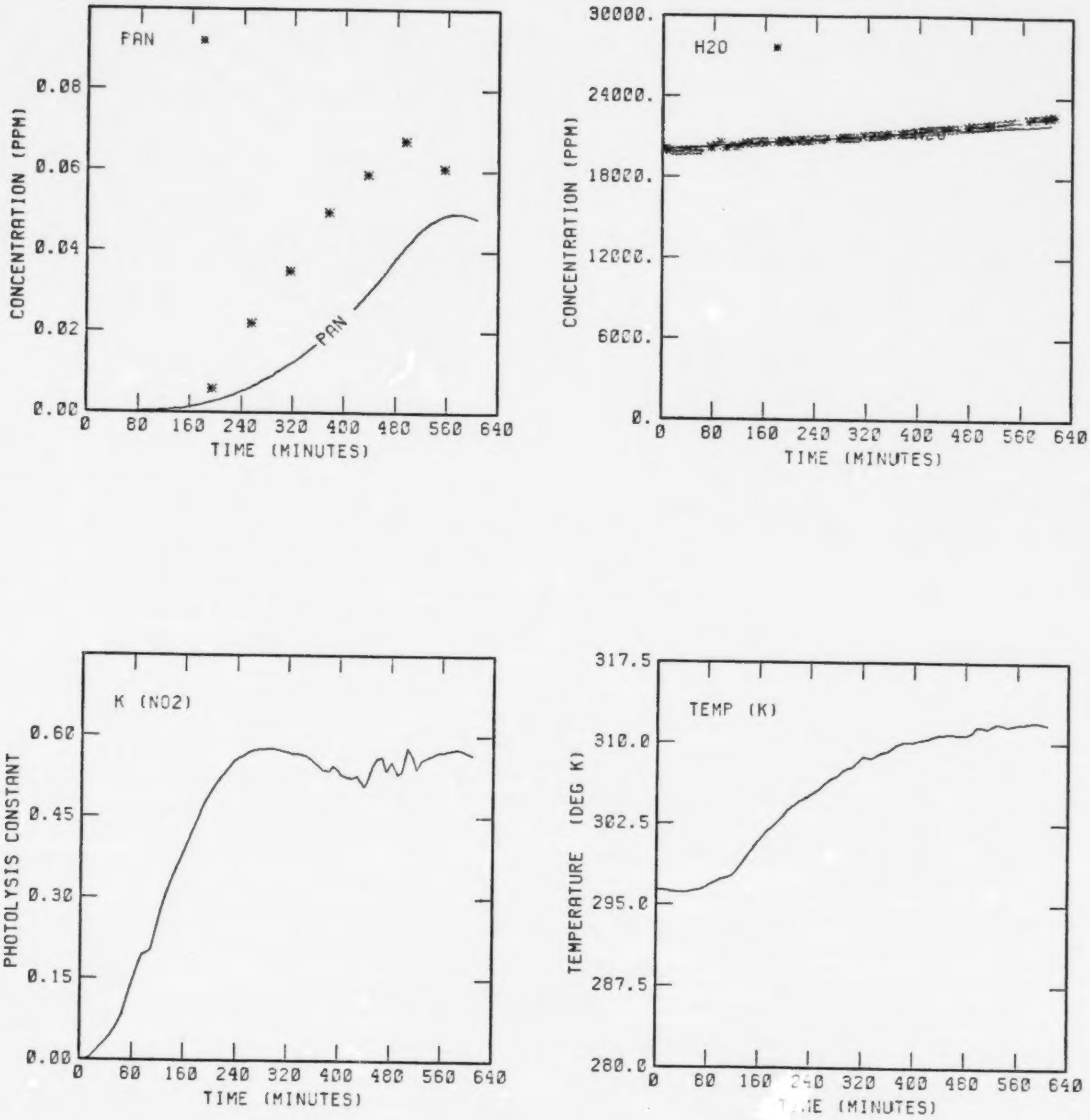

FIGURE 29. SIMULATION RESULTS FOR
UNCR 71583

Concluded.

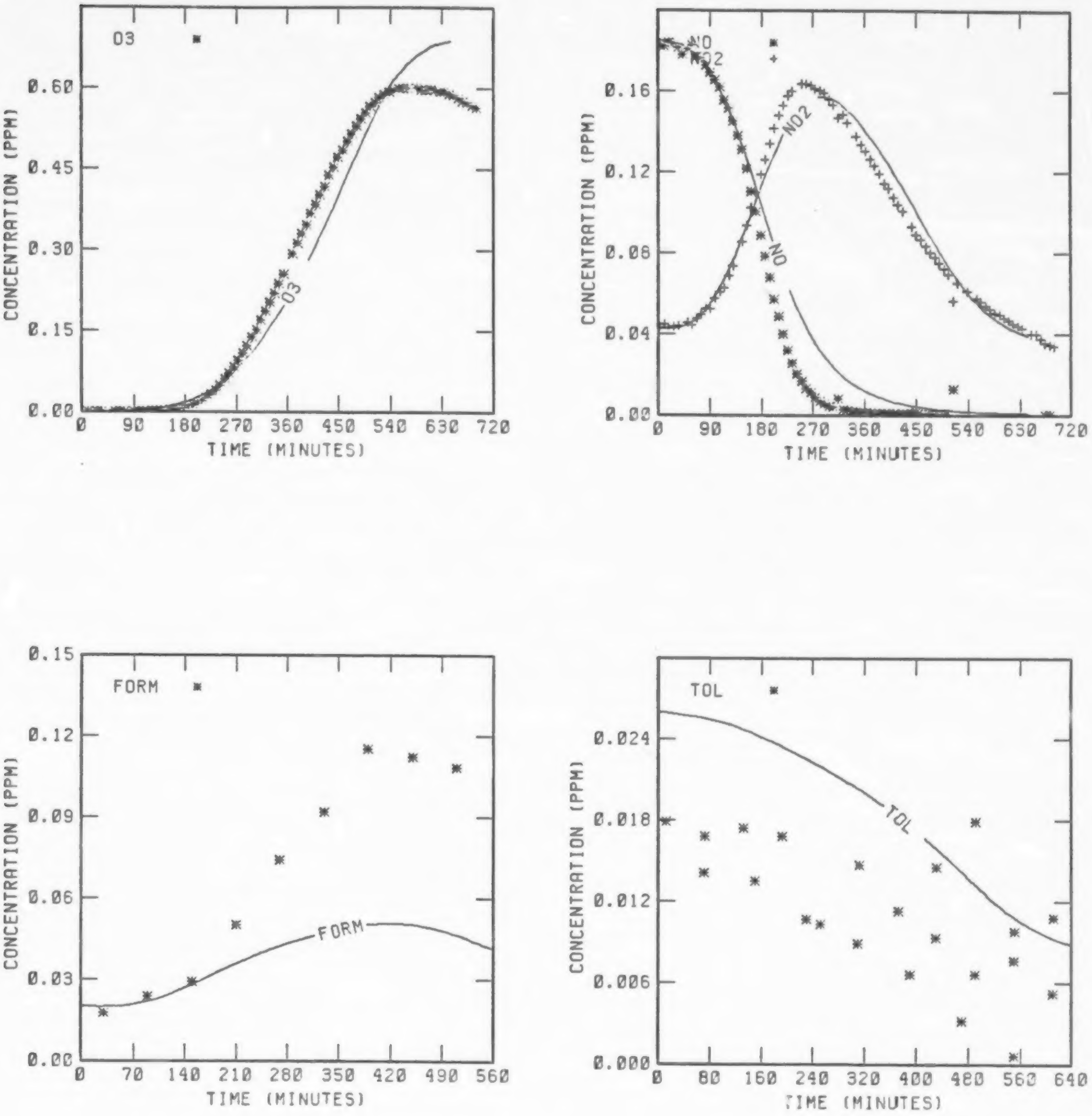

FIGURE 30. SIMULATION RESULTS FOR
UNCB 81183

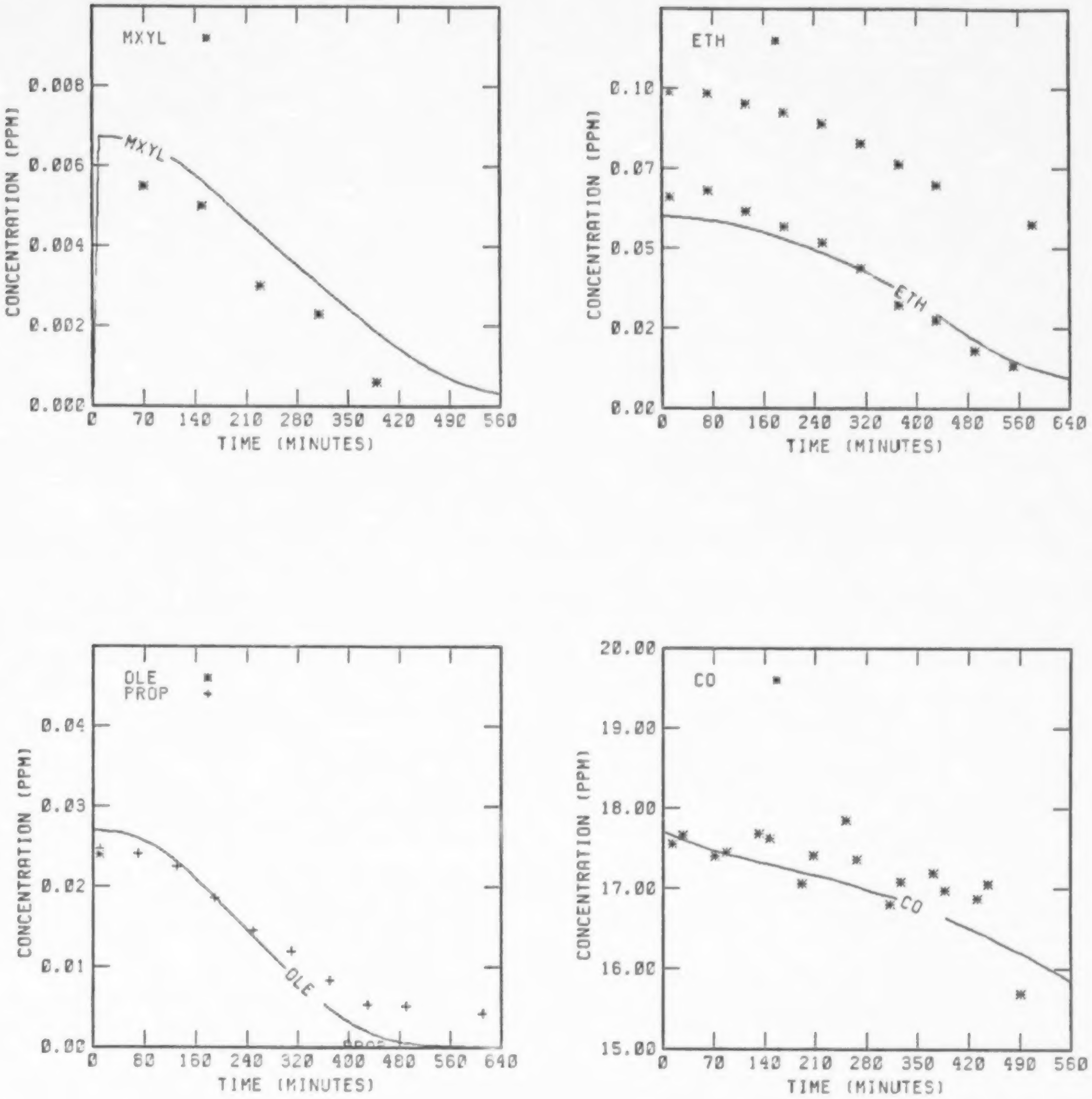

FIGURE 30. SIMULATION RESULTS FOR
UNCB 81183

Continued.

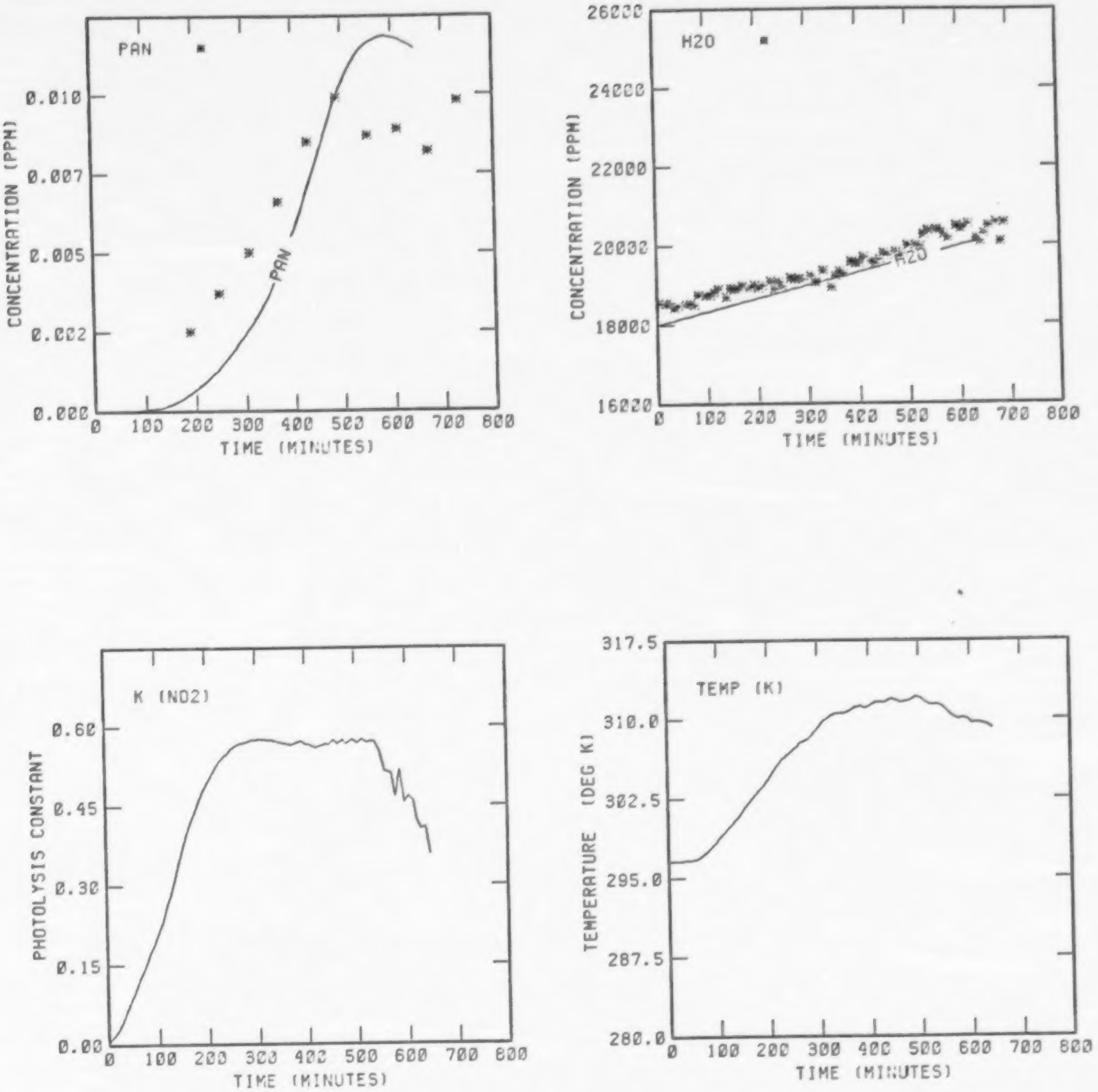

FIGURE 30. SIMULATION RESULTS FOR
UNCB 81183
Concluded.

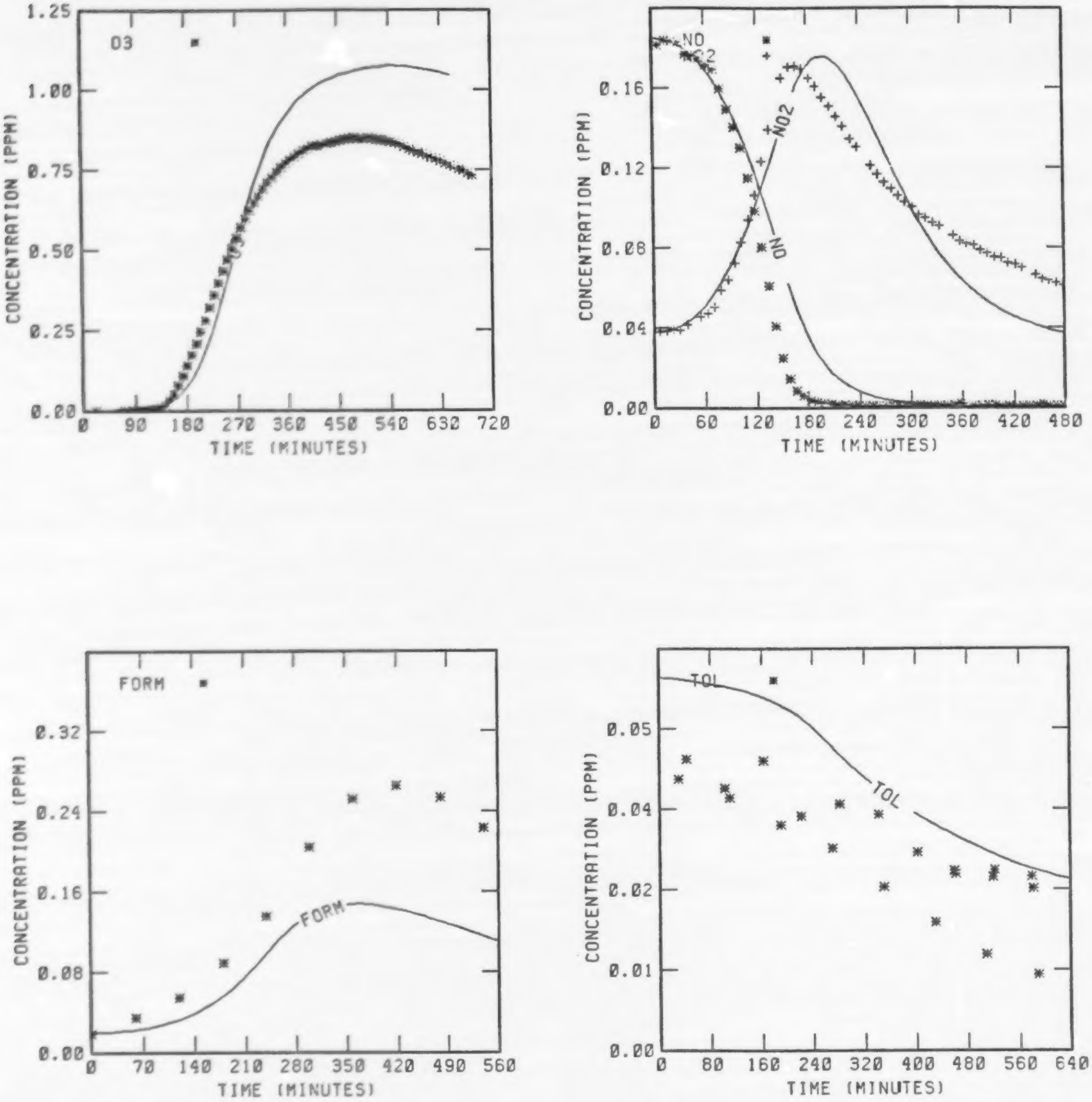

FIGURE 31. SIMULATION RESULTS FOR UNCR 81183

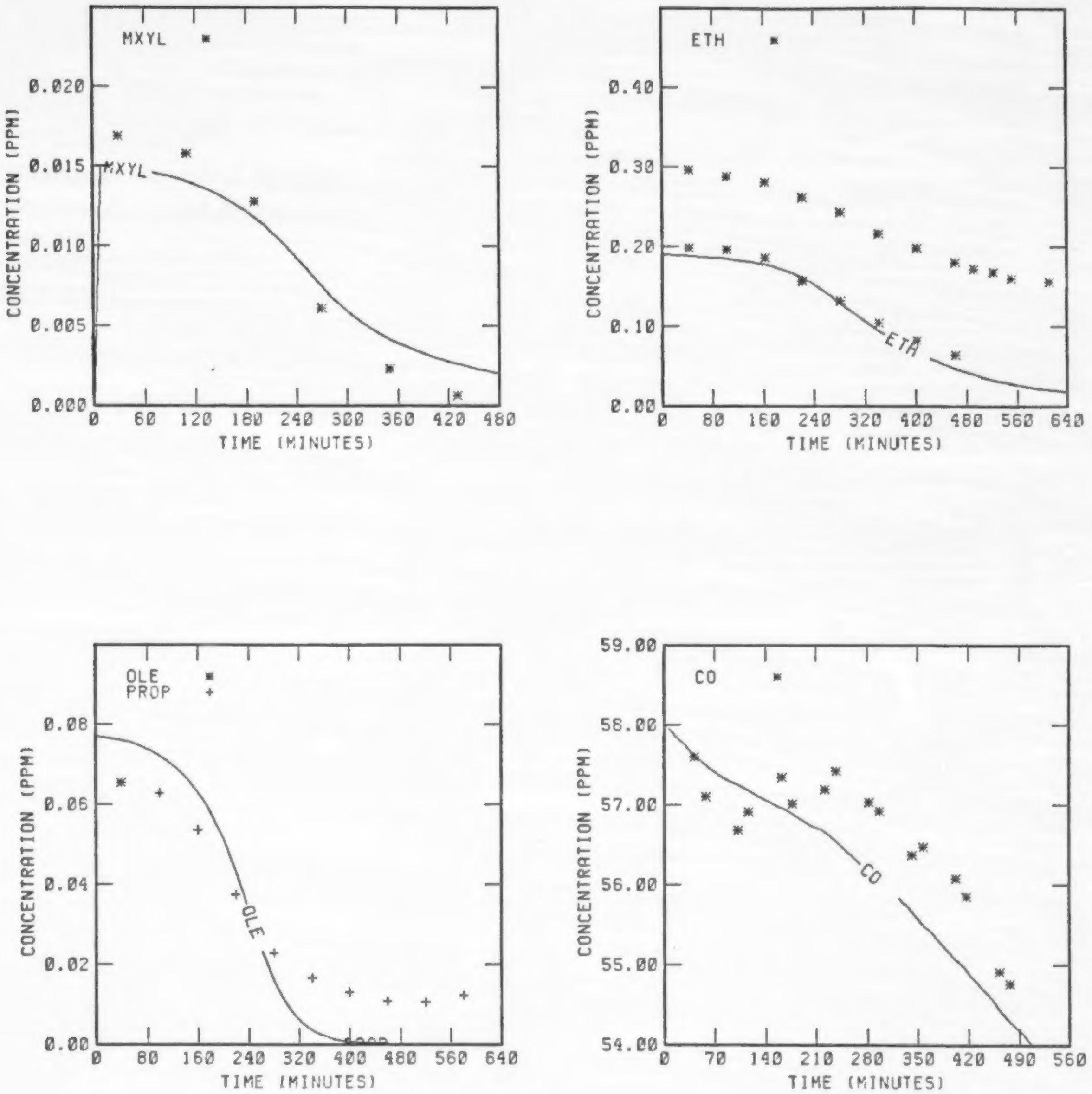

FIGURE 31. SIMULATION RESULTS FOR
UNCR 81183

Continued.

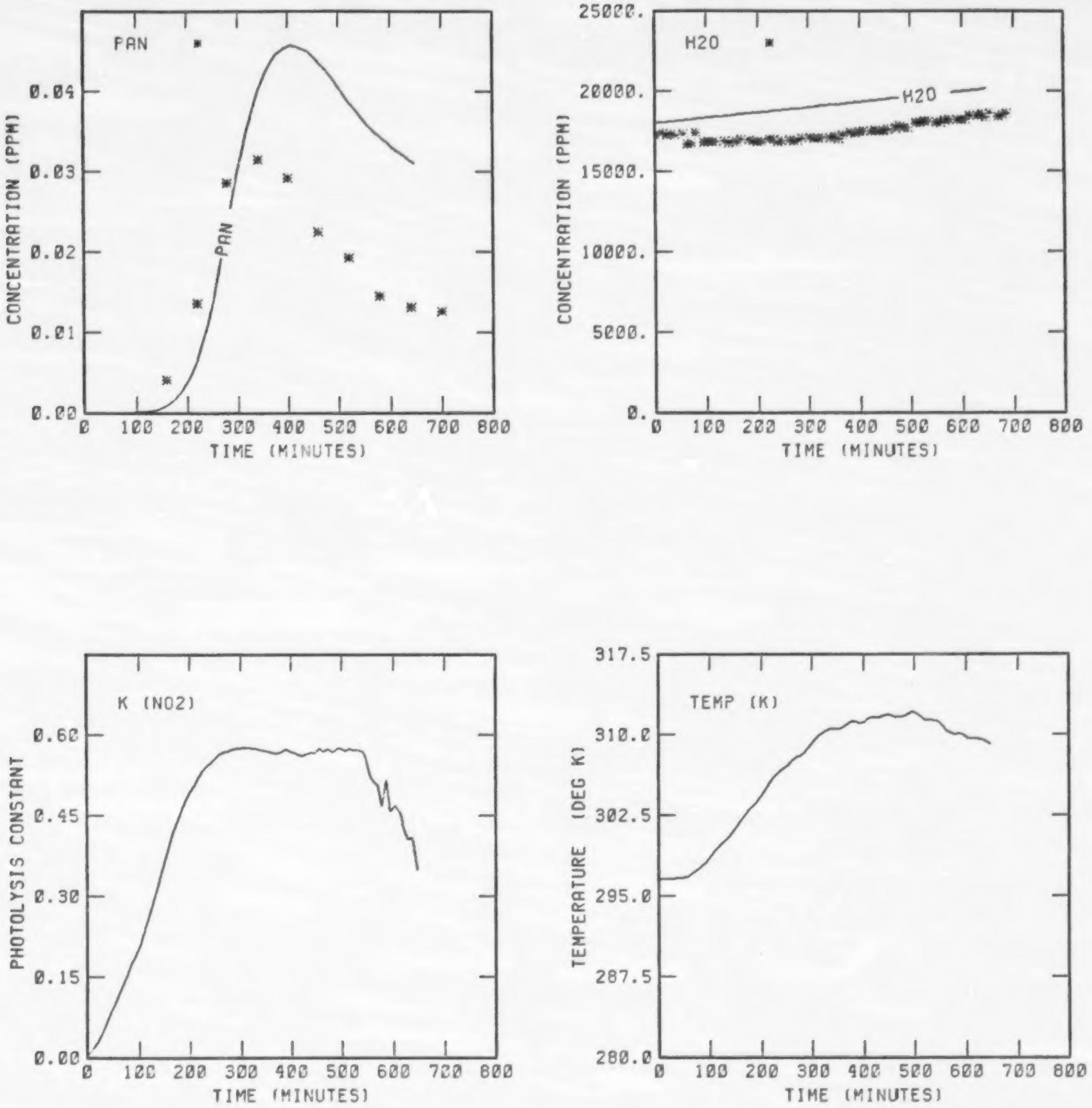

FIGURE 31. SIMULATION RESULTS FOR
UNCR 81183

Concluded.

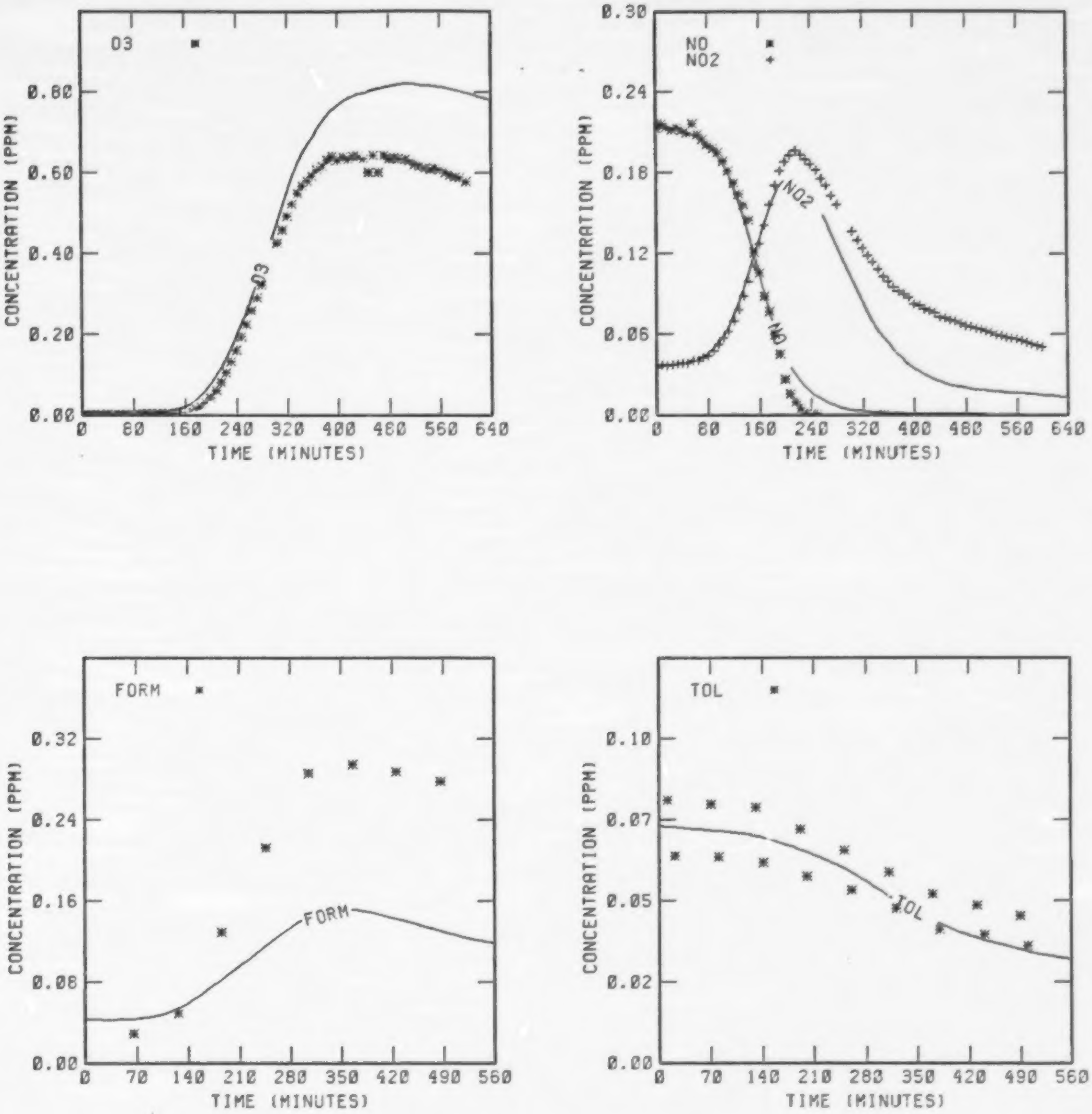

FIGURE 32. SIMULATION RESULTS FOR
UNCB 100483

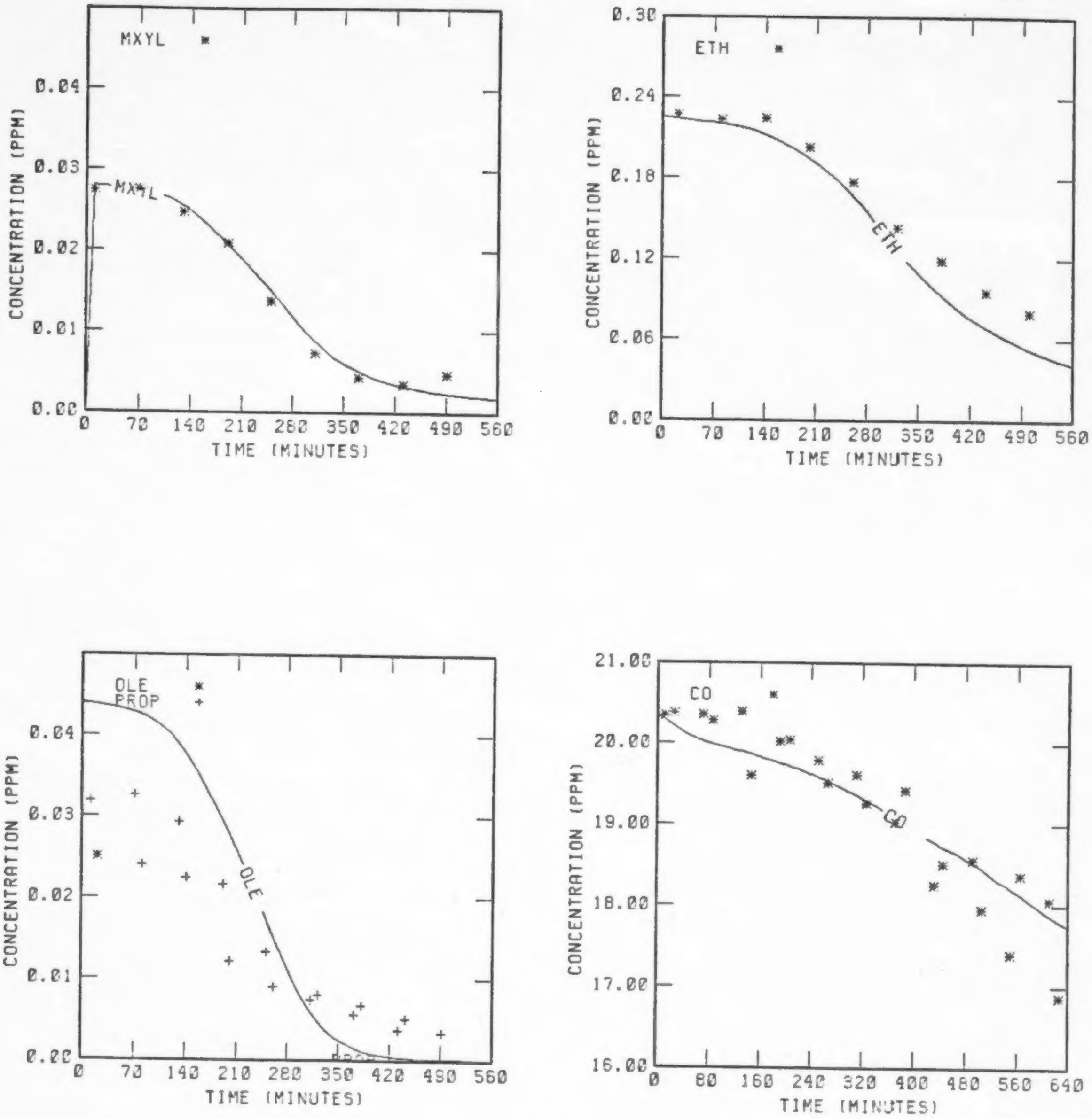

FIGURE 32. SIMULATION RESULTS FOR
UNCB 100483

Continued.

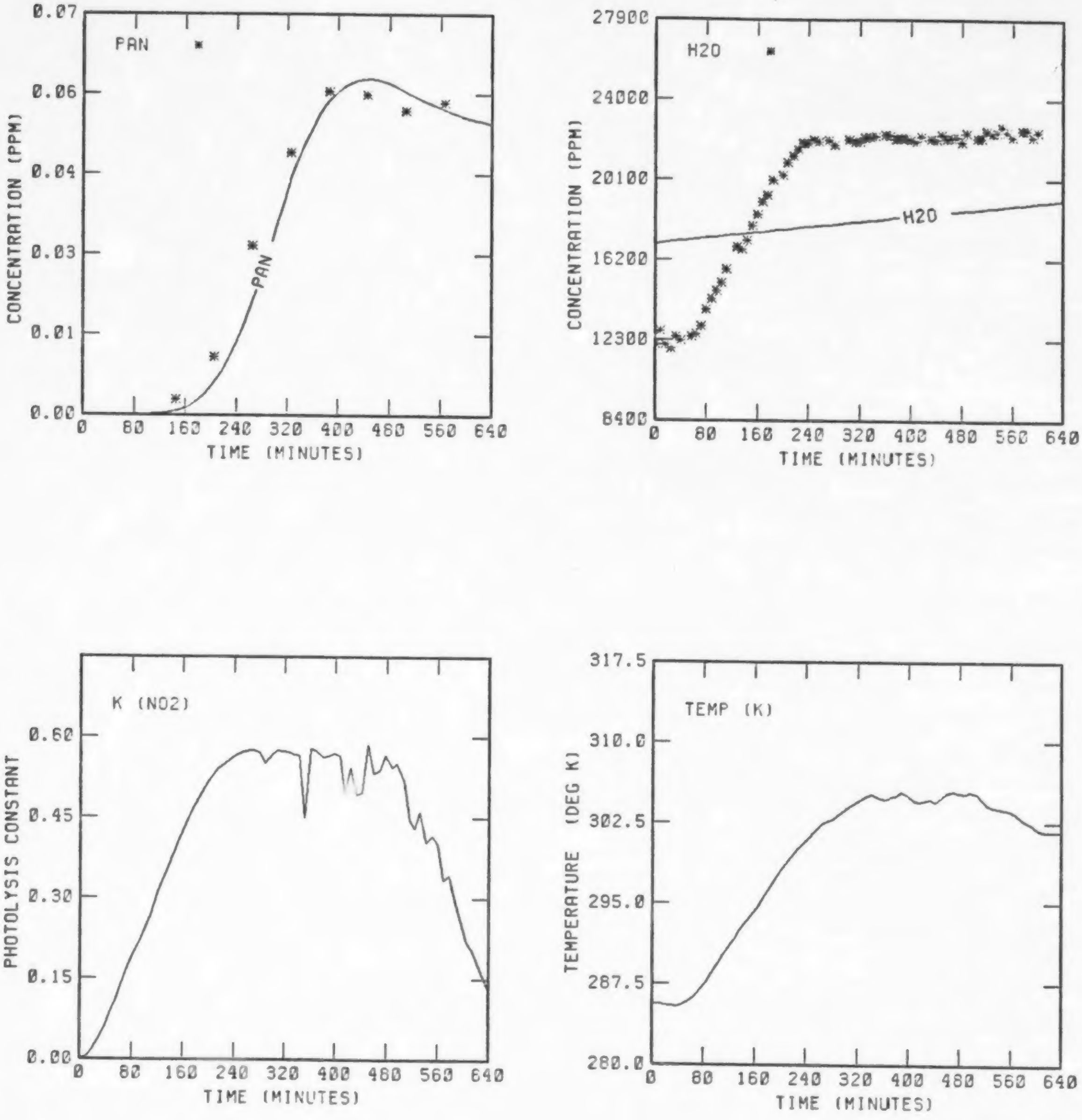

FIGURE 32. SIMULATION RESULTS FOR
UNCB 100483
Concluded.

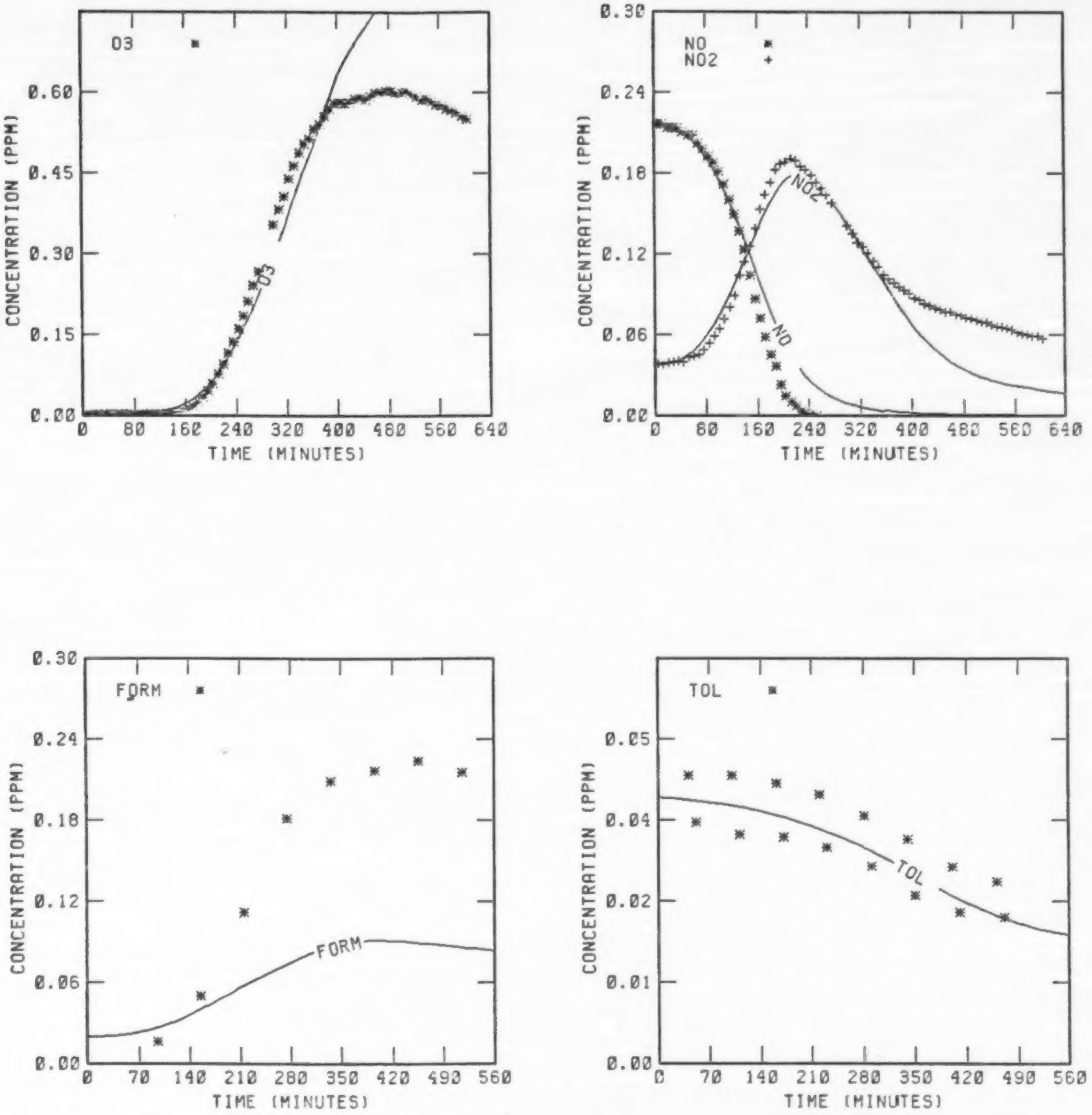

FIGURE 33. SIMULATION RESULTS FOR
UNCR 100483

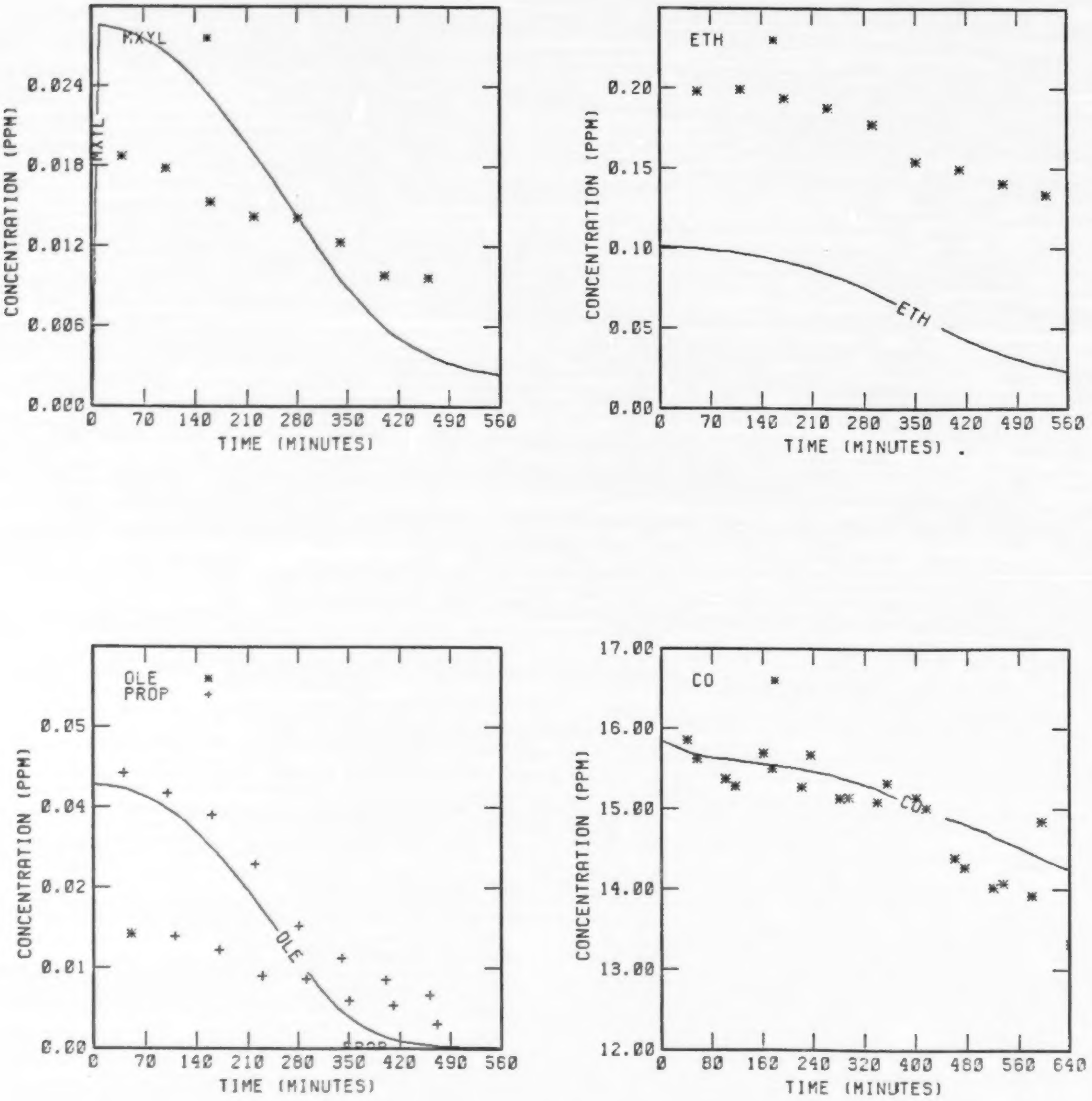

FIGURE 33. SIMULATION RESULTS FOR
UNCR 100483

Continued.

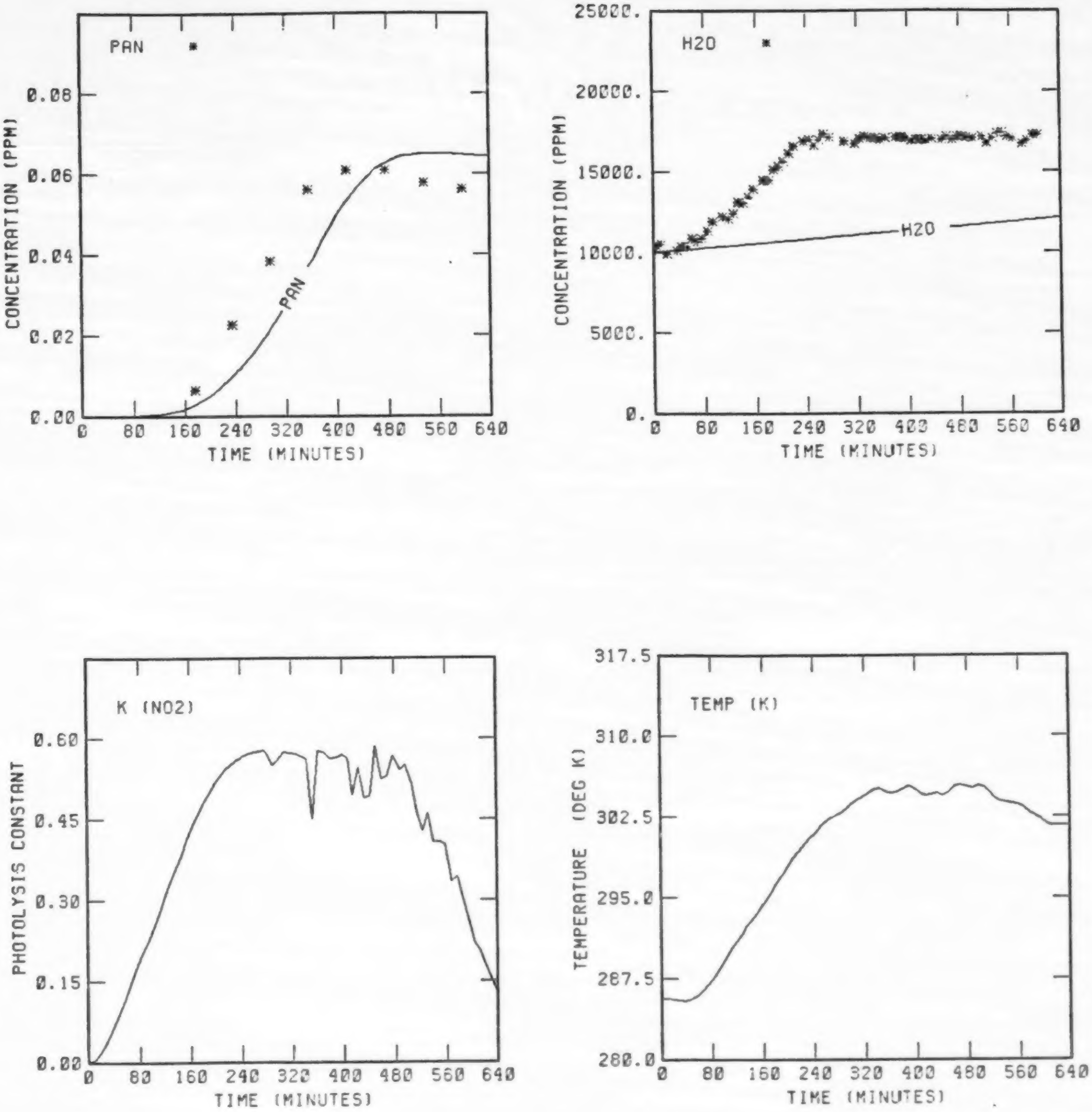

FIGURE 33. SIMULATION RESULTS FOR
UNCR 100483

Concluded.

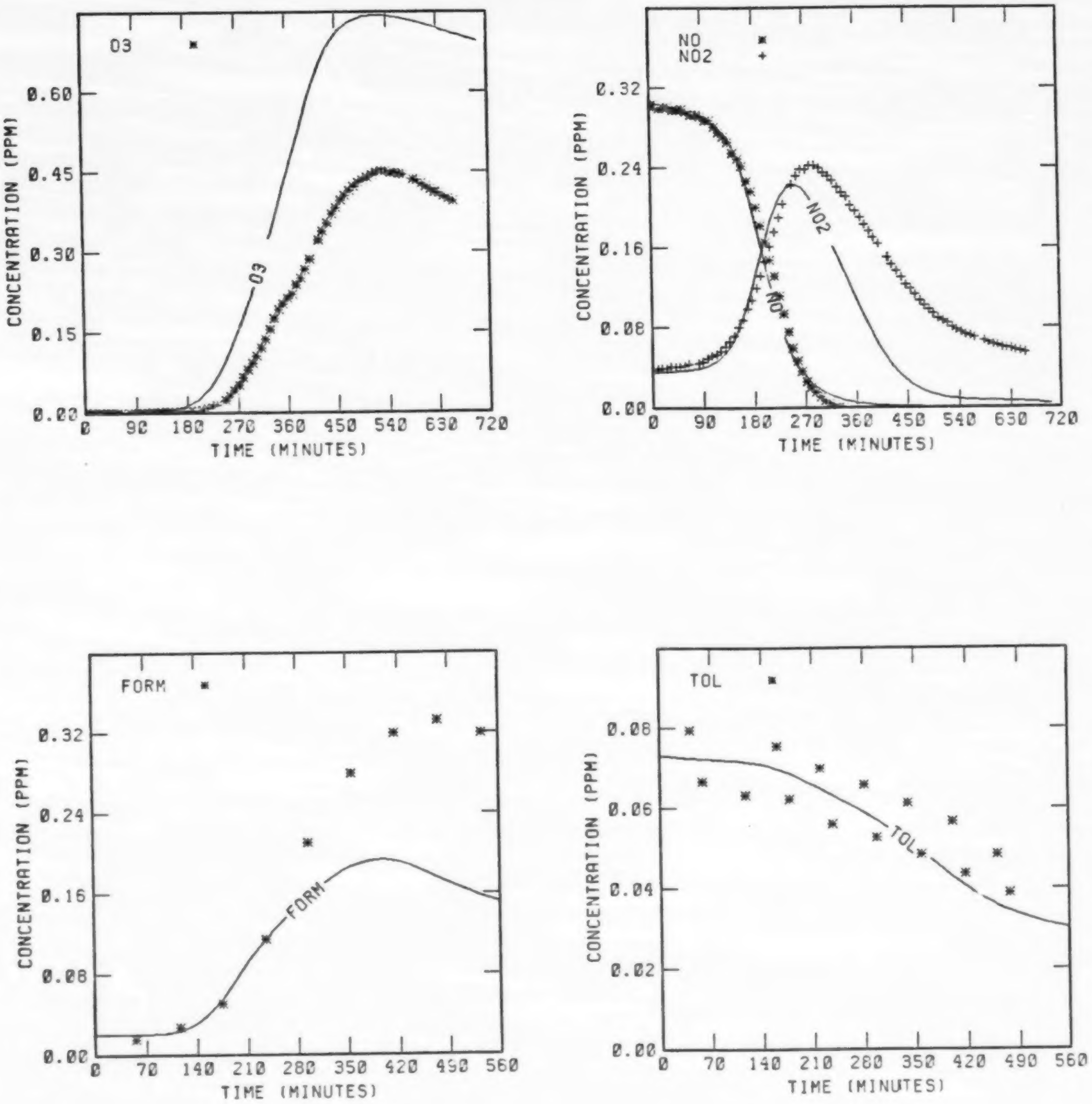

FIGURE 34. SIMULATION RESULTS FOR
UNCB 100783

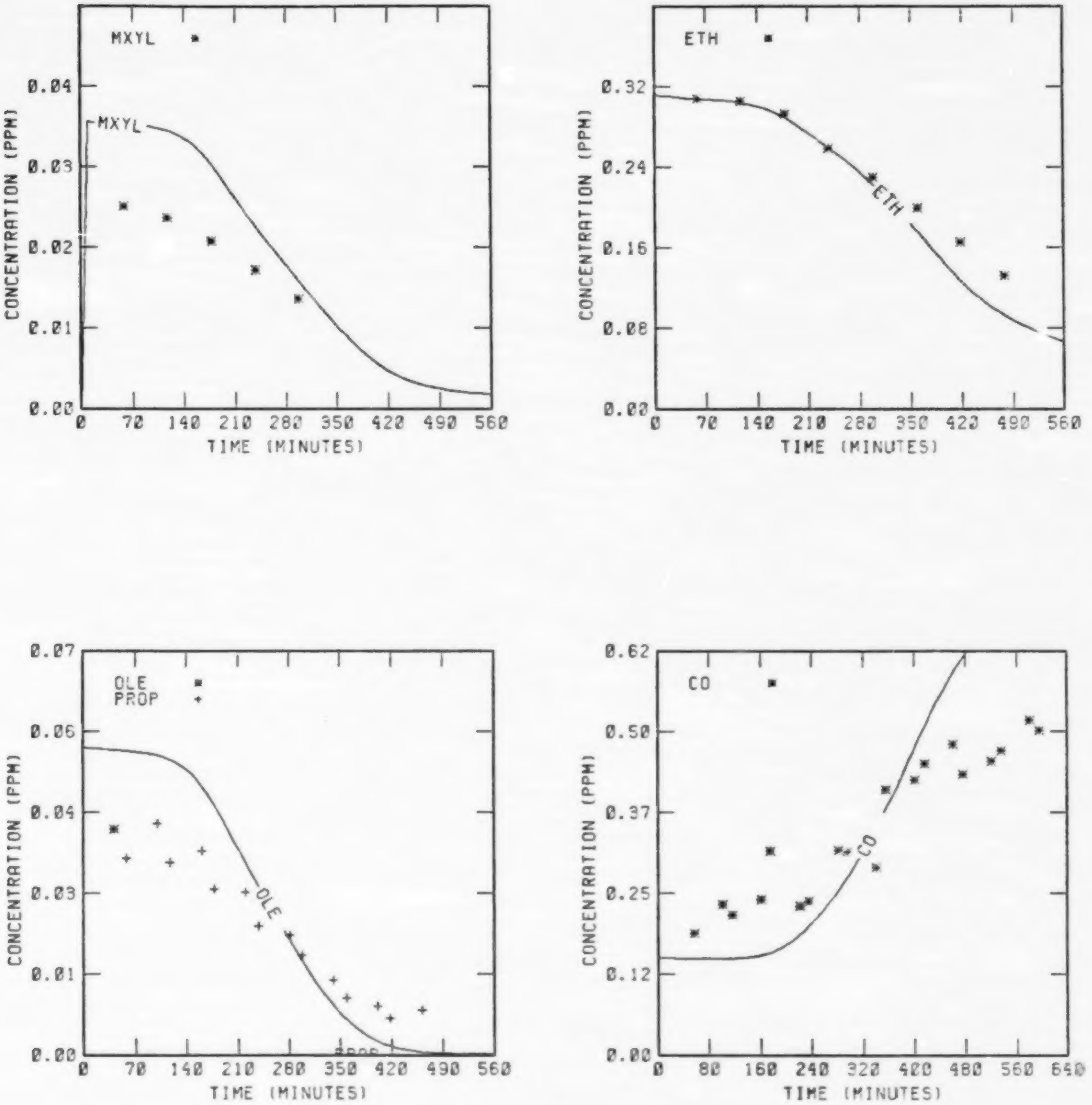

FIGURE 34 . SIMULATION RESULTS FOR
UNCB 100783

Continued.

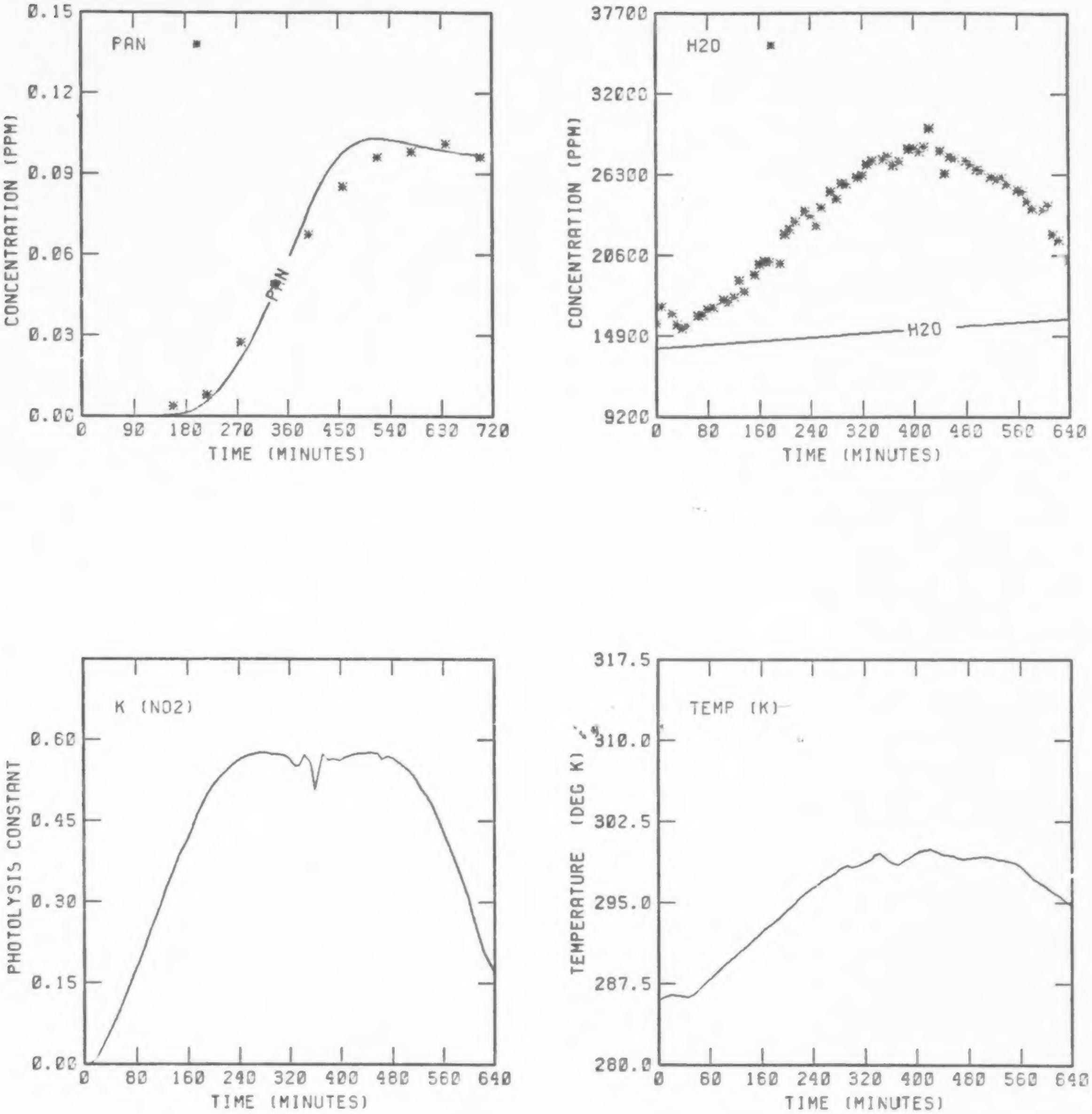

FIGURE 34. SIMULATION RESULTS FOR
UNCB 100783

Concluded.

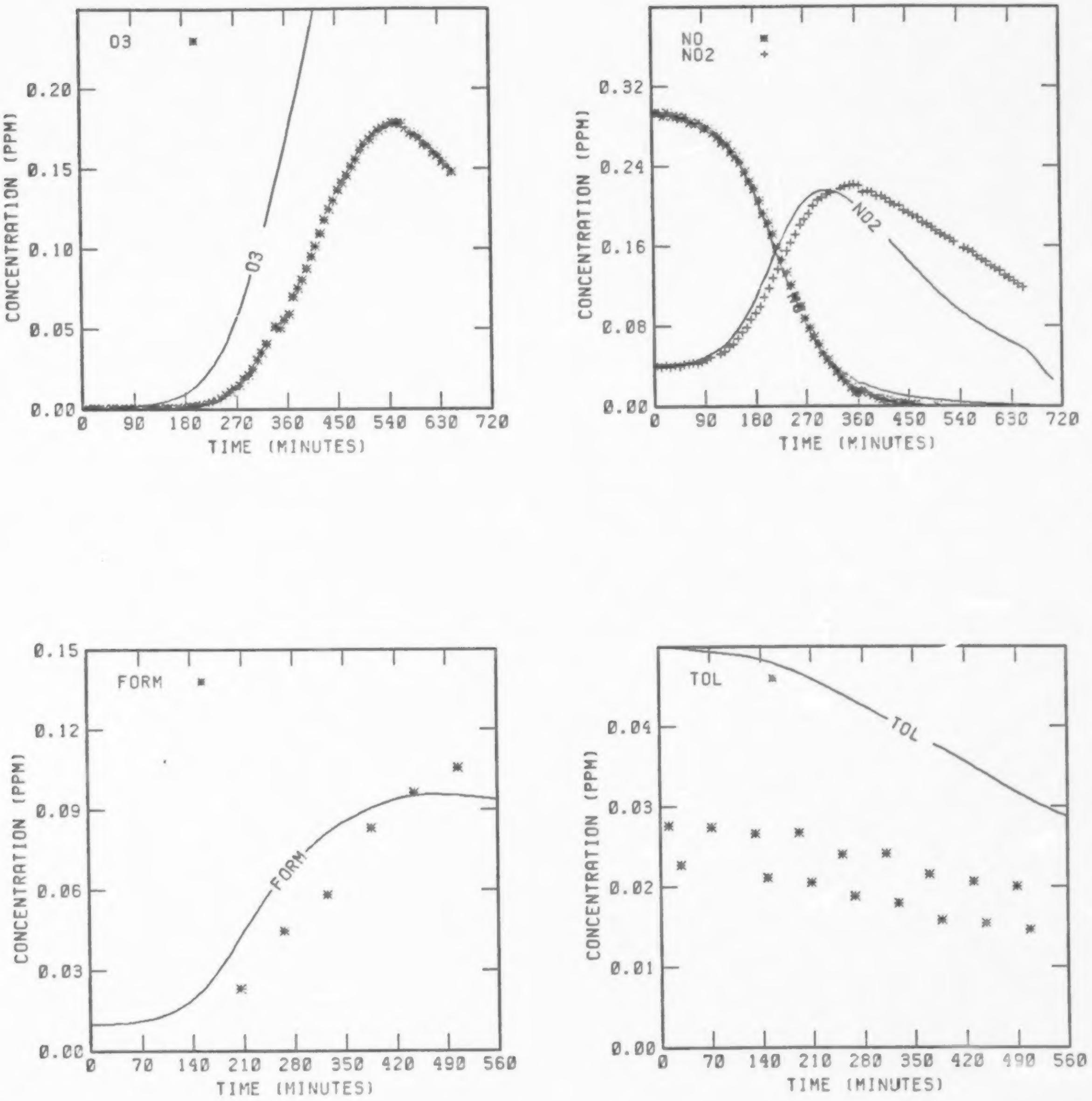

FIGURE 35 . SIMULATION RESULTS FOR
UNCR 100783

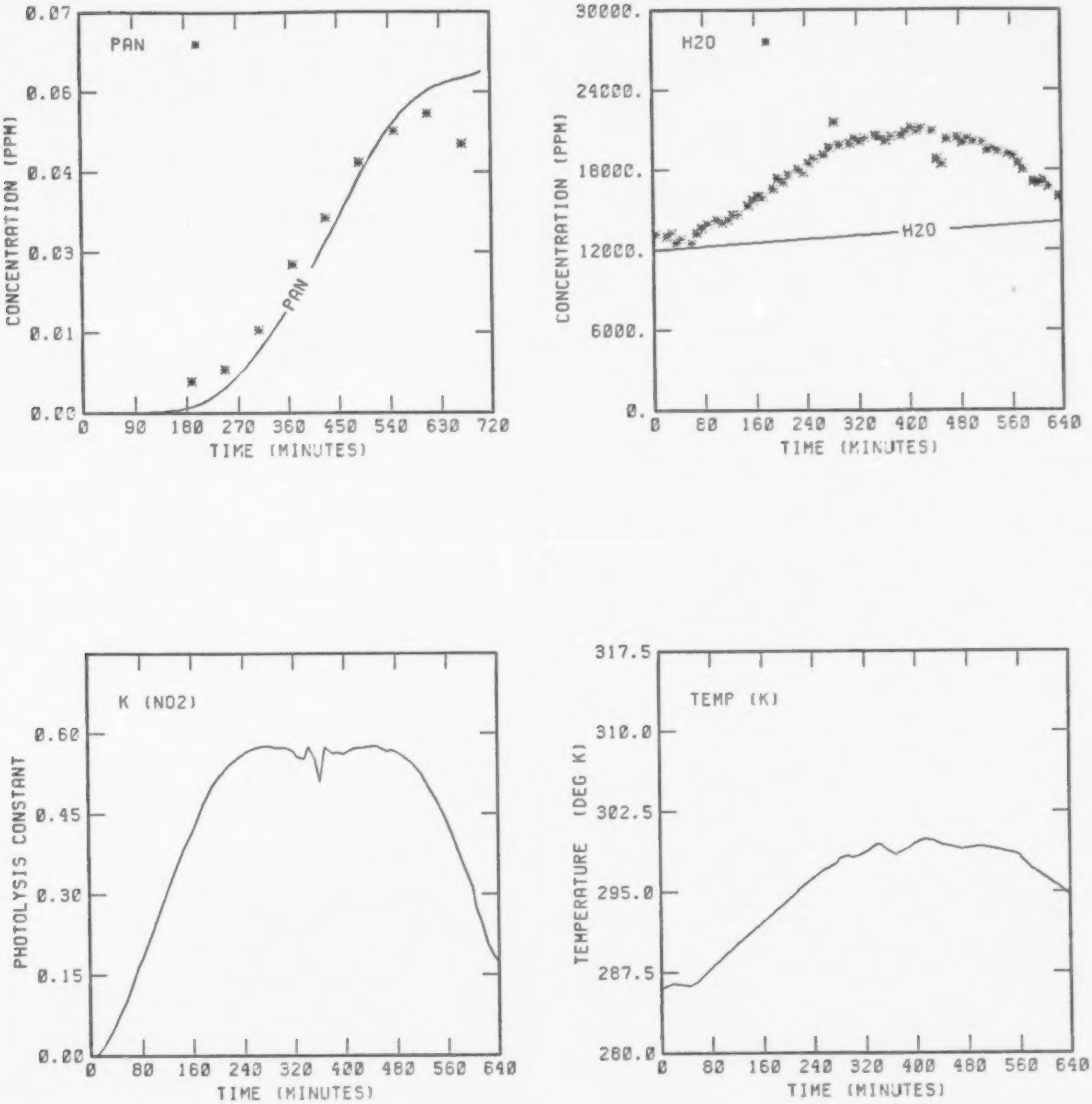

FIGURE 35. SIMULATION RESULTS FOR
UNCR 100783

Continued.

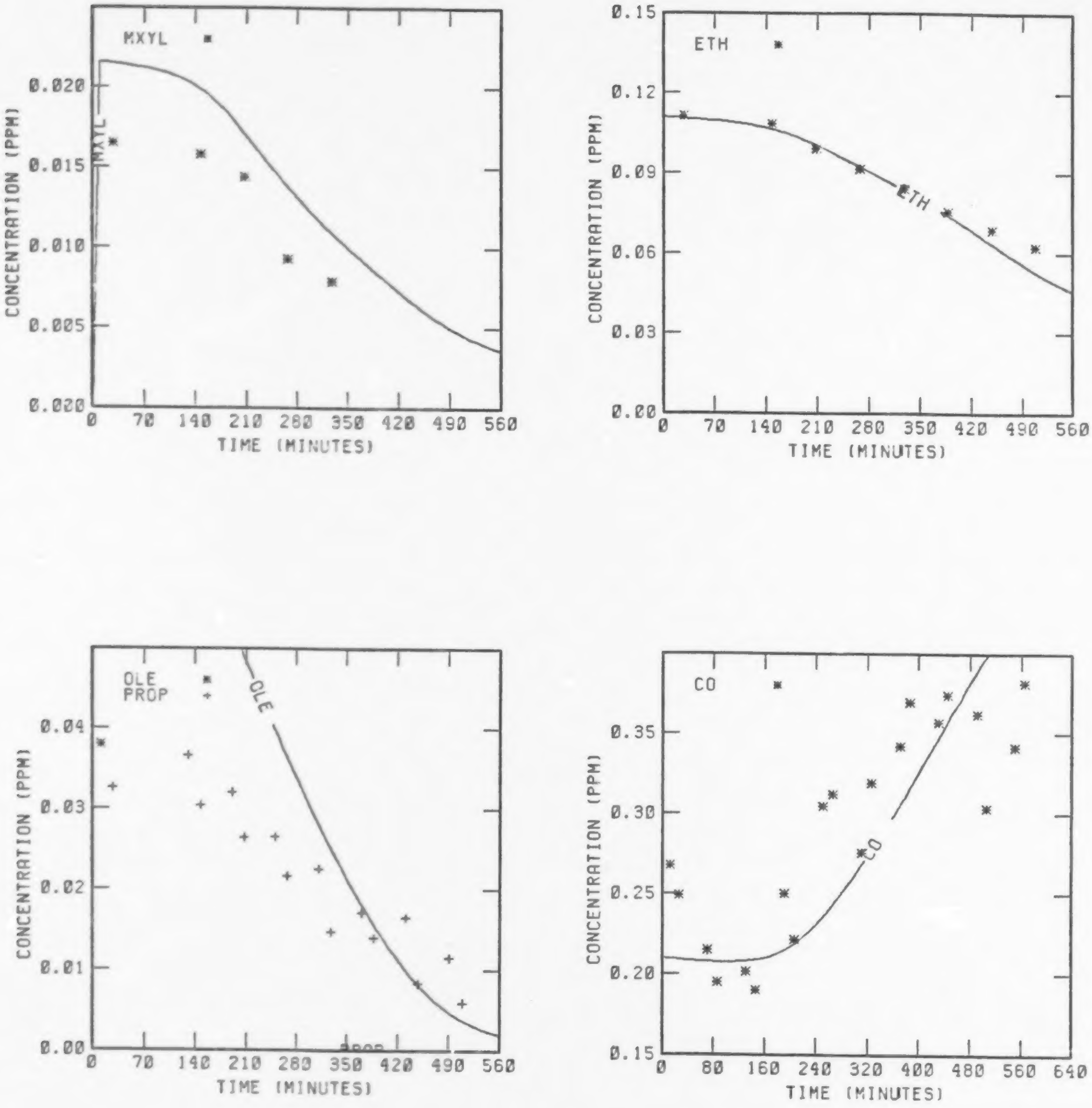

FIGURE 35. SIMULATION RESULTS FOR
UNCR 100783

Concluded.

SECTION 7

SUMMARY AND RECOMMENDATIONS

SUMMARY

General Description of CBM-X

The expanded Carbon-Bond Mechanism (CBM-X) described in this report is a hybrid of explicit chemistry, surrogate approximations, and lumped/generalized chemistry designed to simulate the broad features of urban smog chemistry. The explicit chemistry that forms the inorganic and carbonyl portion of the mechanism (ICRS) is the core of the CBM-X. The ICRS conforms to current literature review studies and has been extensively validated in simple organic/NO_x systems. The explicit and generalized chemical submodels of the CBM-X reflect our current understanding of the oxidation photochemistry of complex hydrocarbons. Each of the types of chemistry used has been carefully chosen to match the simulation sensitivity, analytical input needs, and state of knowledge requirements for an urban photochemical smog mechanism. Because the mechanism has been targeted for use in models utilizing simple dispersion algorithms (e.g., EKMA-type models), we have not focused on condensation techniques designed to reduce computer requirements. Where condensation techniques have been utilized, the main considerations have been to obtain a realistic balance between analytical inputs, the state-of-knowledge, typical concentrations of the species concerned, and the expected sensitivity of the overall computer simulations.

The CBM-X contains 146 reactions that treat the interactions of 65 species. However, only 10 primary precursors are required for most atmospheric applications: two NO_x species (NO and NO_2), two carbonyl species (formaldehyde and higher aldehydes), two olefinic species (ethylene and the 1-olefins or equivalents), two aromatic species (toluene and m-xylene or equivalents), alkyl carbon atoms (paraffins or paraffinic substituents), and carbon monoxide. Other primary precursors such as acetone, higher ketones, glyoxal, methylglyoxal, benzaldehyde, phenols, nitrous acid, hydrogen peroxide, dinitrogen pentoxide, and methyl nitrite, can also be used. This last group has been mentioned because these species, in addition to being intermediate products of photochemical smog systems, can on occasion also be emitted into the atmosphere.

The overall CBM-X mechanism has successfully simulated a new series of auto exhaust experiments that used a variety of conditions. These experiments were performed in the outdoor dual chamber facility of the University of North Carolina, which is a well-characterized chamber with extensive analytical capabilities. The conditions used for these experiments included various automobiles, fuels, driving cycles, and methods of sample preparation.

Updating and Reevaluation

Because of its modular hierarchical structure, the CBM-X can be easily updated and reevaluated as future needs require. For example, if new developments in NO_3 chemistry require modifications to the core set of inorganic and carbonyl reactions (ICRS), the data base for formaldehyde or other simple organic experiments could be rerun. It seems reasonable to assume that once the ICRS has been revalidated by accurately simulating such a data set, the new ICRS would perform as well as the present ICRS in the overall CBM-X simulations. A need for additional or updated organic subsets could be accommodated in a similar fashion using appropriate data subsets.

Current Uncertainties

Some uncertainties can currently be found in all the CBM-X subsets, but perhaps the most pressing uncertainties involve the ICRS and aromatics reaction sets. The inorganic reactions, especially, may require updating of the treatment of the nitrate radical (NO_3) and its effect on nighttime chemistry, due to some very recent reevaluations of this species by Kerr and Calvert (1984). The aromatics reactions may need to be updated to account for present discrepancies in dicarbonyl yields between observations and the mechanisms reported by Tuazon et al. (1984)

Work in Progress

This report is limited to a discussion of the development and testing of the CBM-X mechanism. It does not describe how this mechanism should be used for atmospheric modeling. That is the subject of a future report that is now in preparation. This latter report will provide detailed guidance on the use of CBM-X in the EKMA approach to oxidant control strategies. The report will be similar to the ones recently prepared by Killus and Whitten (1984) and Gipson (1984) describing the use of the CBM-III in EKMA. The report under preparation is titled "Guidelines for the

Use of the CBM-X Mechanism in EKMA," and it will be available for distribution in the Fall of 1985.

RECOMMENDATIONS FOR FUTURE STUDIES

(1) Future work to improve and refine the CBM-X should include more extensive sensitivity studies of the assumptions used in the present development work. Some of these assumptions involve the choice of primary species, the assumed distribution between primary, secondary, and tertiary alkyl carbon groups, the lengths of the carbon atom chains, the chemistry of glycolaldehyde, the completeness and product structure of radical-radical reactions, and the number of photolysis reactions requiring special zenith-angle treatment.

(2) Future work to test the CBM-X should include data sets that involve dilution and entrainment of reacting air, e.g., when the mixed layer entrains aged, polluted air aloft on episode days. Another area warranting future tests would involve a more diverse range in reactivity than that seen in typical auto exhaust or urban mixtures. For example, olefins might be used as the only organic initially present with aromatics bled in later or vice versa. Such tests might appear to be beyond the ranges typically encountered in atmospheric modeling; however, they could prove useful in highlighting mechanistic inadequacies. In addition, if successfully simulated by the CBM-X, such tests would enhance its expected accuracy and confidence in its use in novel reactivity-oriented control scenarios or atmospheric situations (e.g., cases in which kerosene emissions from airports, which are low in NO_x, mix with auto exhaust emissions rich in olefins, aromatics, and NO_x from major freeway complexes).

(3) Another area for future studies involves CBM-X adaptation for use in more complex atmospheric models. This would require more extensive condensation of the CBM-X, as well as use of steady-state approximations.

Finally, the experimental sets used to test and validate the CBM-X are probably the most extensive of their kind conducted to date. It is our hope that the CBM-X simulations of these experiments will set a standard for testing other mechanisms and that CBM-X usage in atmospheric models will serve as a guide for additional development and analysis in the modeling of atmospheric photochemistry.

REFERENCES

Addison, M. C., et al. 1980. Absorption spectrum and kinetics of the acetylperoxy radical. Chem. Phys. Lett., 73:283-287.

Altshuller, A. P., and S. P. McPherson. 1963. Spectrophotometric analysis of aldehydes in the Los Angeles atmosphere. J. Air Pollut. Control Assoc., 13(3).

Atkinson, R., A. C. Lloyd, and L. Winges. 1982. An updated chemical mechanism for hydrocarbon/NO_x/SO_2 photooxidations suitable for inclusion in atmospheric simulation models. Atmos. Environ., 16:1341-1352.

Atkinson, R., and A. C. Lloyd. 1984. Evaluation of kinetic and mechanistic data for modeling of photochemical smog. J. Phys. Chem. Ref. Data, 13:315.

Atkinson, R., W.P.L. Carter, K. R. Darnall, A. M. Winer, and J. N. Pitts, Jr. 1980. A smog chamber and modeling study of the gas-phase NO_x-air photooxidation of toluene and the cresols. Int. J. Chem. Kinet., 12:779-836.

Bahe, F. C., W. N. Marx, and U. Schurath. 1979a. Determination of the absolute photolysis rate of ozone by sunlight, $O_3 + h\nu \rightarrow O(^1D) + O_2(^1\Delta_g)$, at ground level. Atmos. Environ., 13:1515-1522.

Bahe, F. C., h. Illner, W. Marx, U. Schurath, and P. Roth. 1979b. "Messung der von Verandenengen der Ozonschicht stark abhangigen kurzwellijen Sonnenstrahlung." Gessellschaft fur Strahlen and Unweltforschung MBH, Munchen (NTIS:N81-24334).

Bass, A. M., L. C. Glasgow, C. Miller, J. P. Jenson, and D. L. Filkin. 1980. Temperature dependent absorption cross sections for formaldehyde (CH_2O): The effect of formaldehyde on stratospheric chlorine chemistry. Atmos. Environ., 28:675-679.

Baulch, D. L., R. A. Cox, R. F. Hampson Jr., J. A. Kerr, J. Troe, and R. T. Watson. 1980. Evaluated kinetic and photochemical data for atmospheric chemistry. Reprint No. 159 from Journal of Physical and Chemical Reference Data, 9(2):295-471.

Benson, S. W. and J. H. Bass. 1958. J. Chem Phys., 29:546.

Benson, S. W. 1976. Thermochemical Kinetics. John Wiley and Sons, New York, New York.

Bessemer, A. C. 1982. Formation of chemical compounds from irradiated mixtures of aromatic hydrocarbons and nitrogen oxides. Atmos. Environ., 16:1599-1602.

Calvert, J. G. 1976. Hydrocarbon involvement in photochemical smog formation in the Los Angeles atmosphere. Environ. Sci. Technol., 10(3):257.

Calvert, J. G., J. A. Kerr, K. L. Demerjian, and R. D. McQuigy. 1972. Photolysis for formaldehyde as a hydrogen atom source in the lower atmosphere. Science, 175:751-752.

Calvert, J. G., and J. N. Pitts, Jr. 1966. Photochemistry (John Wiley & Sons, New York, New York).

Carter, W.P.L., R. Atkinson, A. M. Winer, and J. N. Pitts, Jr. 1982. Experimental investigation of chamber-dependent radical sources. Int. J. Chem. Kinet., 14:1071-1103.

Carter, W.P.L., A. C. Lloyd, J. L. Sprung, and J. N. Pitts. 1979. Computer modeling of smog chamber data: Progress in validation of a detailed mechanism for the photooxidation of propene and n-butane in photochemical smog. Int. J. Chem. Kinet., 11:45-103.

Cox, R. A., K. F. Patrick, and S. A. Chant. 1981. Mechanisms of atmospheric photooxidation of organic compounds. Reactions of alkoxy radicals in oxidation of n-butane and simple ketones. Environ. Sci. Technol., 15:587.

Darnall, K. R., W.P.L. Carter, A. C. Lloyd, A. M. Winer, and J. N. Pitts, Jr. 1976. Importance of RO_2 + NO in alkyl nitrate formation from C_4-C_6 alkane photooxidation under simulated atmospheric conditions. J. Phys. Chem., 80:1948-1950.

Demerjian, K. L., K. L. Schere, and J. T. Peterson. 1980. Theoretical estimates of active (spherically integrated) flux and photolytic rate constants of atmospheric species in the lower troposphere. *Adv. Environ. Sci. Technol.*, 10:369-460.

Dodge, M. C. 1977a. "Effect of Selected Parameters on Predictions of a Photochemical Model." U.S. Environmental Protection Agency, Research Triangle Park, North Carolina (EPA-600/3-77-048).

Dodge, M. C. 1977b. "Combined Use of Modeling Techniques and Smog Chamber Data to Derive Ozone-Precursor Relationships." *Proc.: International Conference on Photochemical Oxidant Pollution and Its Control*, EPA-600/3-77-001b, Research Triangle Park, North Carolina.

EPA. 1984. "Guidelines for Using the Carbon-Bond Mechanism in City--Specific EKMA." Research Triangle Park, North Carolina (EPA-450/4-84-005).

Falls, A. H., and J. H. Seinfeld. 1978. Continued development of a kinetic mechanism for photochemical smog. *Environ. Sci. Technol*., 12(13):1398-1406.

Gibson, G. L. 1984. "Guideline for Using the Carbon-Bond Mechanism in City-Specific EKMA," EPA-450/4-84-005, Office of Air Quality Planning and Standards, U.S. Environmental Protection Agency, Research Triangle Park, North Carolina.

Greiner, N. R. 1970. Hydroxyl radical kinetics by kinetic spectroscopy: VI--reactions with alkanes in the range 300-500K. *J. Chem. Phys*., 53:1070-1076.

Greiner, N. R. 1970. Hydroxyl radical kinetics by kinetic spectroscopy: VI--Reactions with alkanes in the range 300 to 500K. *J. Chem. Phys.*, 53:1070-1076.

Grosjean et al. 1981. "ERT Outdoor Environmental Chamber and Dedicated Analytical Facilities," ERT Report No. A764-500, Westlake Village, California.

Grosjean, D., R. Countess, K. Fung, K. Ganesan, A. Lloyd, and F. Lurmann. 1981. "Deriving Empirical Kinetic Modeling Approach Isopleths from Experimental Data: The Los Angeles Captive-Air Study." Environmental Research and Technology, Inc., Westlake Village, California.

Hanst, P. L., N. W. Wong, and J. Bragin. 1982. A long-path infra-red study of Los Angeles smog. Atmos. Environ., 16(5):969-981.

Hecht, T. A., J. H. Seinfeld, and M. C. Dodge. 1974. Further development of a generalized kinetic mechanism for photochemical smog. Environ. Sci. Technol., 8(4):327-339.

Hendry, D. G., and R. A. Kenley. 1979. "Atmospheric Reaction Products of Organic Compounds." U.S. Environmental Protection Agency, Office of Toxic Substances, Washington, D.C. (EPA-560/12-79-001).

Horowitz, A., and J. G. Calvert. 1982. Wavelength dependence of the primary processes in acetaldehyde photolysis. J. Phys. Chem., 86:3105-3114.

Jeffries, H. E., R. M. Kamens, K. G. Sexton, and A. A. Gerhardt. 1982. "Outdoor Smog Chamber Experiments to Test Photochemical Models." U.S. Environmental Protection Agency, Office of Research and Development, Research Triangle Park, North Carolina, EPA-600/3-82-016.

Jeffries, H. E., K. G. Sexton, T. P. Morris, M. Jackson, R. G. Goodman, R. M. Kamens, and M. S. Holleman. 1984. "Outdoor Smog Chamber Experiments Using Automobile Exhaust." Draft report, U.S. Environmental Protection Agency, Research Triangle Park, North Carolina.

Jones, K. H., R. B. Ruch, Jr., J. B. Barone, J. F. Walsh, and R. A. Karpovich. 1983. "The Rationale and Need to Consider an Alternative to EKMA." Roy F. Weston, Inc., West Chester, Pennsylvania.

Kan, C. S., J. C. Calvert, and J. H. Shaw. 1980. "Reactive Channels of the CH_3O_2-CH_3O_2 Reaction." Department of Chemistry and Department of Physics, Ohio State University, Columbus, Ohio.

Kerr, J. A., and J. G. Calvert. 1985. "Chemical Transformation Modules for Eulerian Acid Deposition Models--Volume I: The Gas-Phase Chemistry." U.S. Environmental Protection Agency (available March 1985).

Killus, J. P., and G. Z. Whitten. 1981. Communications to the editor. Comments on "A Smog Chamber and Modeling Study of the Gas Phase NO_x-Air Photooxidation of Toluene and the Cresols. Int. J. Chem. Kinet., 13:1101-1103.

Killus, J. P., and G. Z. Whitten. 1984. "Technical Discussions Relating to the Use of the Carbon-Bond Mechanism in OZIPM/EKMA." U.S. Environmental Protection Agency, Research Triangle Park, North Carolina (EPA-450/4-84-009).

Killus, J. P., and G. Z. Whitten. 1982a. A mechanism describing the photochemical oxidation of toluene in smog. Atmos. Environ., 15(8):1973-1988.

Killus, J. P., and G. Z. Whitten. 1982b. "A New Carbon-Bond Mechanism for Air Quality Simulation Modeling." U.S. Environmental Protection Agency, Research Triangle Park, North Carolina (EPA 600/3-82-041).

Kleindlenst, T. E., G. W. Harris, and J. N. Pitts, Jr. 1982. Rates and temperature dependences of the reaction of OH with isoprene, its oxidation products, and selected terpenes. Environ. Sci. Technol., 16:844-846.

Kopczynski, S. L., W. A. Lonneman, F. D. Sutterfield, and P. E. Darley. 1972. Photochemistry of atmospheric samples in Los Angeles. Environ. Sci. Technol., 6(4):342.

Leighton, P. A., and F. E. Blacet. 1933. The photolysis of alipatic aldehydes II acetaldehyde. J. Am. Chem. Soc., 55:1766-1774.

Levy, A., D. F. Miller, and D. R. Hopper. 1975. "Motor-Fuel Composition and Photochemical Smog." Battelle, Columbus Laboratories, Columbus, Ohio.

Mayrsohn, H., and J. Crabtree. 1976. Source reconcilitation of atmospheric hydrocarbons." Atmos. Environ., 10:137-143.

McRae, G. J., J. A. Leone, and J. H. Seinfeld. 1983. "Evaluation of Chemical Reaction Mechanisms for Photochemical Smog Part I. Mechanism Description and Documentation." U.S. Environmental Protection Agency, (EPA-600/3-83-086).

Meyrahn, H., G. K. Moortgat, and P. Warneck. 1982. "The Photolysis of Acetaldehyde under Atmospheric Conditions." XVth Informal Conference on Photochemistry, Stanford, California, 1 July 1982.

[NASA]. National Aeronautics. 1983. "Chemical Kinetics and Photochemical Data for Use in Stratospheric Modeling: Evaluation Number 6." JPL Publication 83-62, Pasadena, California.

Niki, H., P. P. Maker, C. M. Savage, and L. P. Breitenbach. 1981a. An FTIR study of mechanisms for the HO radical initiated oxidation of C_2H_4 in the presence of NO: Detection of glycoladehyde. Chem. Phys. Lett., 80:499-503.

Niki, H., P. P. Maker, C. M. Savage, and L. P. Breitenbach. 1981b. An FTIR study of a transitory product in the gas-phase ozone-ethylene reaction. J. Phys. Chem., 85:1024-1027.

Niki, H., P. P. Maker, C. M. Savage, and L. P. Breitenbach. 1981c. "Fourier Transform Infrared Studies of the Self-Reaction of CO_3O_2 Radicals." Engineering and Research Staff, Ford Motor Company, Dearborn, Michigan.

O'Brien, B. J. Green, R. A. Doty, J. W. Vanderzanden, R. R. Easton, and R. P. Irwin. 1979. "Interaction of Oxides of Nitrogen and Aromatic Hydrocarbons under Simulated Atmospheric Conditions." In Nitrogenous Air Pollutants Chemical and Biological Implications. D. Grosjean ed., Ann Arbor Science Publishers, Inc., Ann Arbor, Michigan.

Orchard, S. W. 1969. "The Long Wavelength Photolysis of Methyl Glyoxal," M.S. thesis. Department of Chemistry, University of Natal, Pietermaritzburg, South Africa.

Penner, J. E., and J. J. Walton. 1982. Air Quality Model Update, Lawrence Livermore Laboratory Report UCID - 19300, Lawrence Livermore National Laboratory, University of California, Livermore, California.

Peterson, J. T. 1976. "Calculated Actinic Fluxes (290-700nm) for Air Pollution Photochemistry Applications." Environmental Science Research Laboratory, Environmental Protection Agency, Research Triangle Park, North Carolina (EPA-600/4-76-002).

Plum, C. N., E. Sanhueza, R. Atkinson, W.P.L. Carter, and J. N. Pitts. 1983. OH radical rate constants and photolysis rates of alpha-dicarbonyls. Environmental Science and Technology (in press).

Sander, S. P., and R. T. Watson. 1981. Temperature dependence of the self-reaction of CH_3O_2 radicals. J. Phys. Chem., 85:2960-2964.

Schere, K. L., and K. L. Demerjian. 1977. "Calculation of Selected Photolytic Rate Constants Over a Diurnal Range." U.S. Environmental Protection Agency, Research Triangle Park, North Carolina (EPA-600/4-77-015).

Shepson, P. B., and J. Heicklen. 1982. The wavelength and pressure dependence of the photolysis of proprionaldehyde in air. J. Photochem., 19:215-227.

Simonaitis, R., and J. Heicklen. 1983. A flash photolysis study of the photo-oxidation of acetaldehyde at room temperature. J. Photochem., 23:299-309.

Singh, H. B., W. Viezee, W. B. Johnson, and F. L. Ludwig. 1980. The impact of stratospheric ozone on tropospheric air quality." JAPCA, 30(9).

Stewart, D. A., and M. K. Liu. 1981. Development and application of a reactive plume model. Atmos. Environ., 15:2377-2393.

Whitten, G. Z. 1983. The chemistry of smog formation: A review of current knowledge. Environ. Int., 9:447-463.

Whitten, G. Z., H. Hogo, and J. P. Killus. 1980. The Carbon-Bond Mechanism: A condensed kinetic mechanism for photochemical smog. Environ. Sci. Technol., 14:690-700.

Whitten, G. Z., and J. P. Killus. 1981. "Description and Comparison of Available Kinetic Mechanisms." Invited Paper presented at Environmental Protection Agency Workshop on EKMA, 15-16 December 1981, Research Triangle Park, North Carolina.

Whitten, G. Z., J. P. Killus, and H. Hogo. 1979. "Modeling of Simulated Photochemical Smog with Kinetic Mechanisms." U.S. Environmental Protection Agency, Research Triangle Park, North Carolina (EPA-600/3-0012).

Whitten, G. Z., J. P. Killus, and H. Hogo. 1980. "Modeling of Simulated Photochemical Smog with Kinetic Mechanisms. Vol. 1--Final Report." U.S. Environmental Protection Agency, Office of Research and Development, Research Triangle Park, North Carolina (EPA-600/3-80-028a).

Whitten, G. Z., J. P. Killus, R. G. Johnson. 1982. "Modeling of Simulated Photochemical Smog with Kinetic Mechanisms." Final Report, U.S. Environmental Protection Agency, Research Triangle Park, North Carolina (EPA-600/3-83-043).

Appendix A

SIMULATION RESULTS FOR THE UNC FORMALDEHYDE EXPERIMENTS

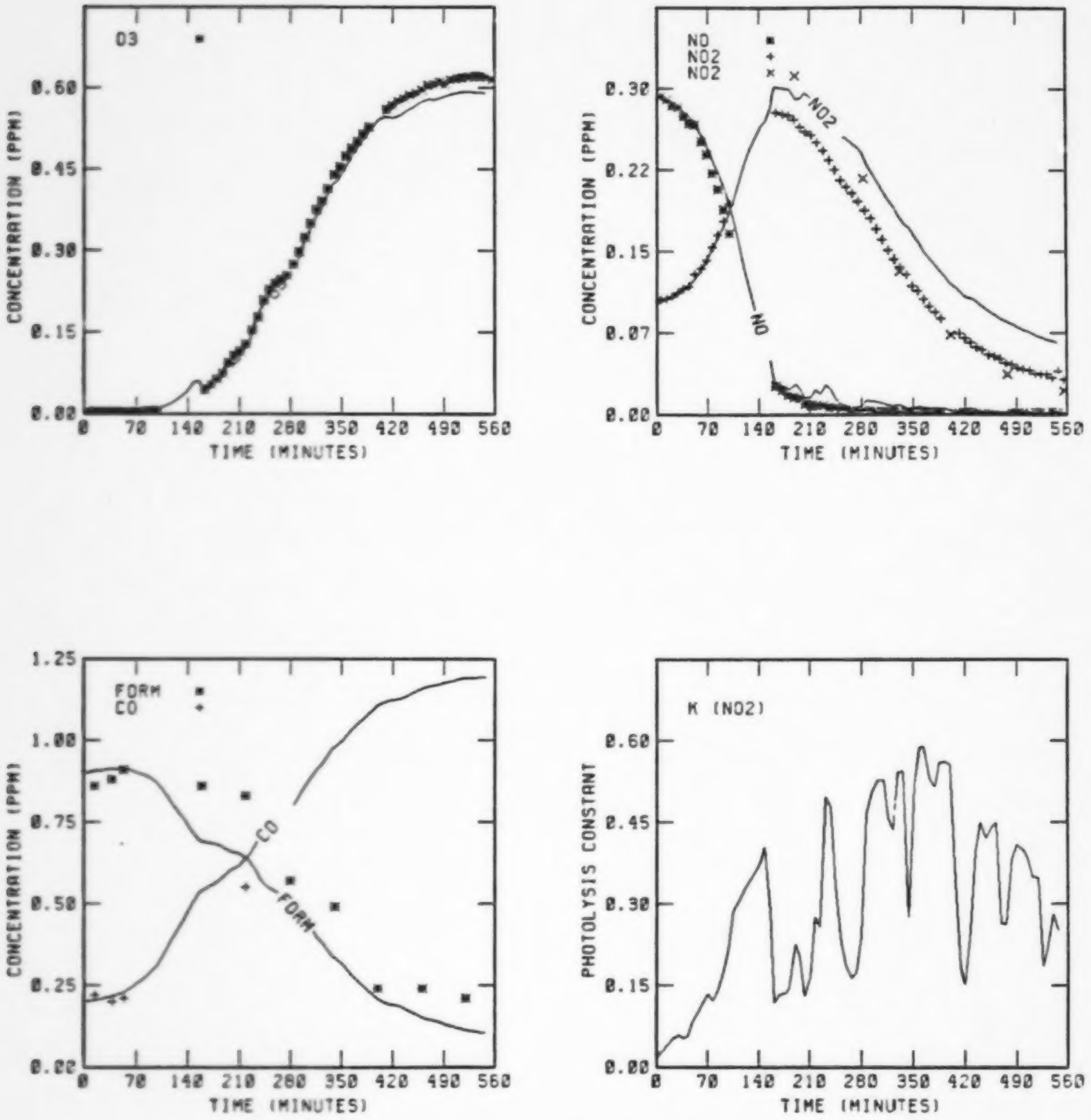

SIMULATION RESULTS FOR
UNCR 91477

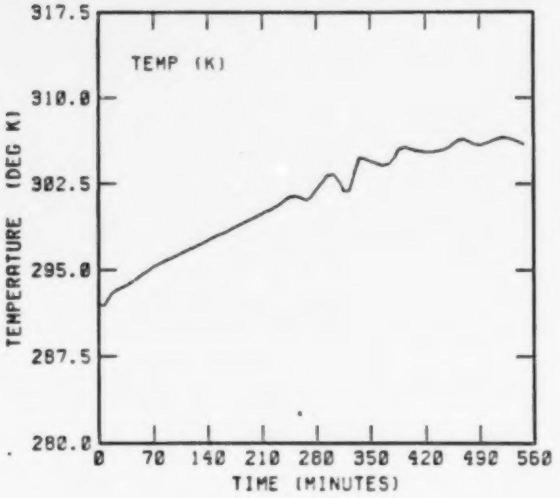

SIMULATION RESULTS FOR
UNCR 91477

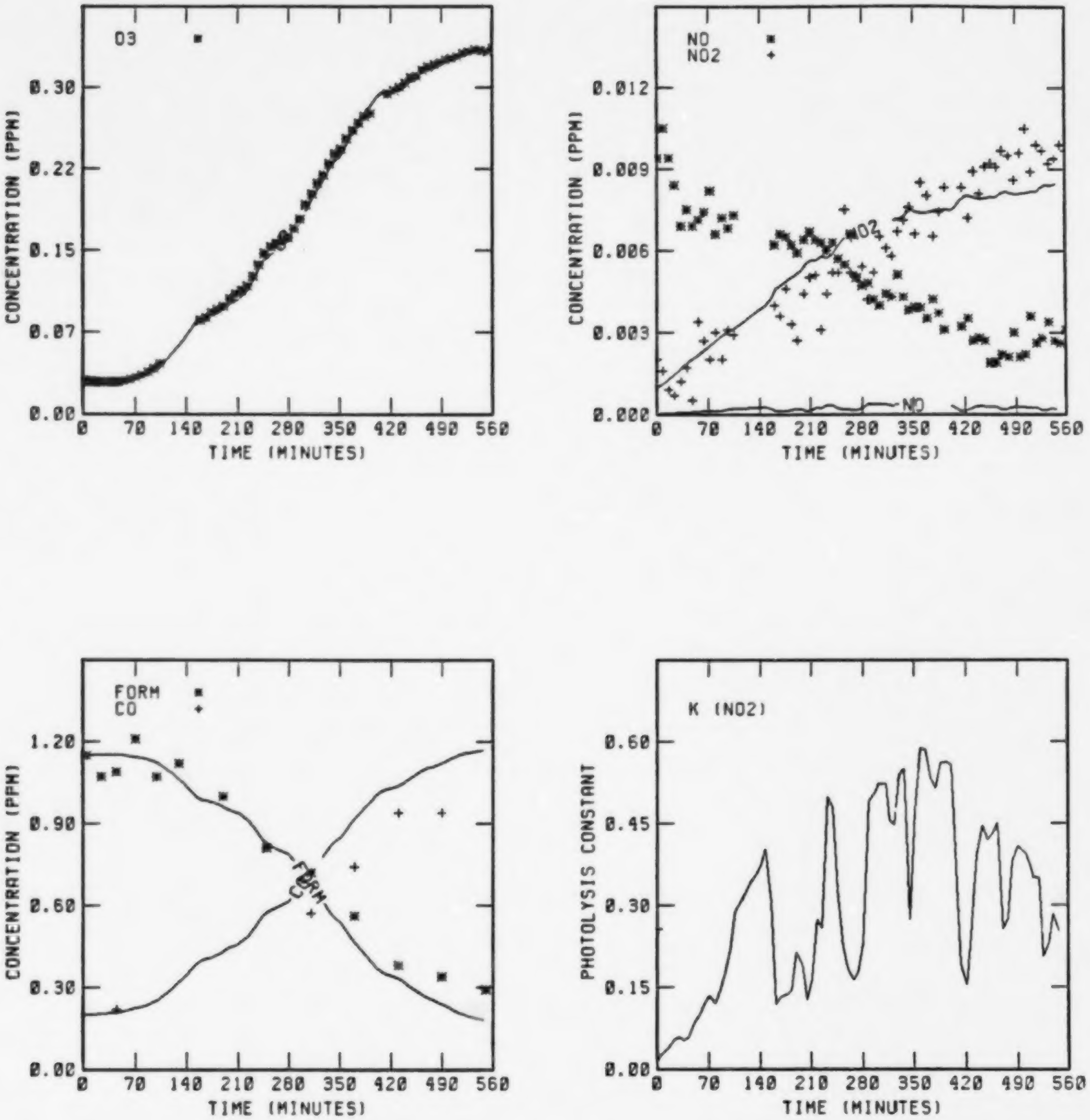

SIMULATION RESULTS FOR
UNCB 91477

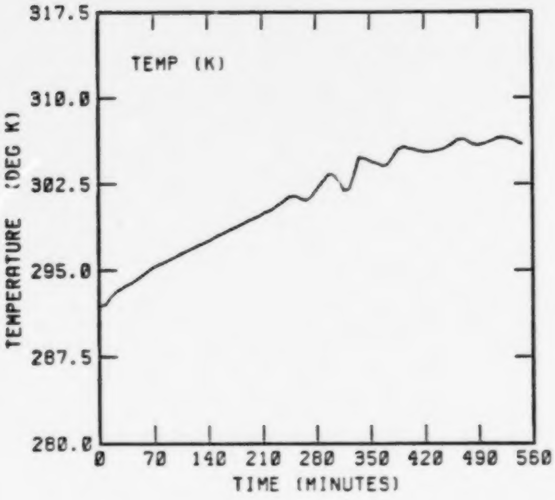

SIMULATION RESULTS FOR
UNCB 91477

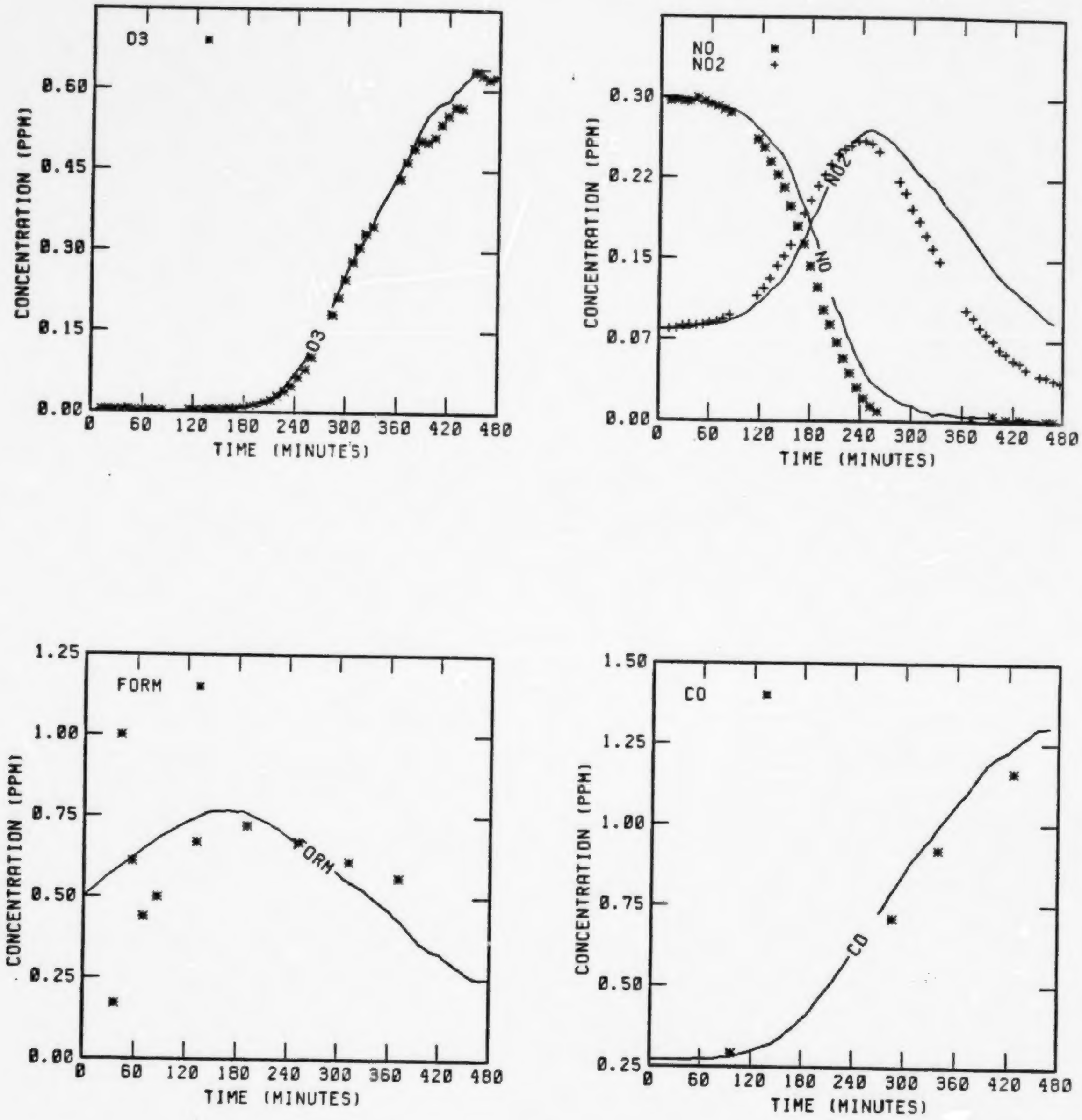

SIMULATION RESULTS FOR
UNCR 91977

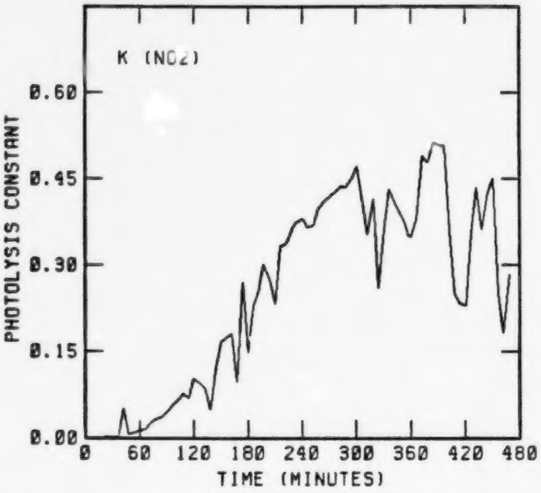

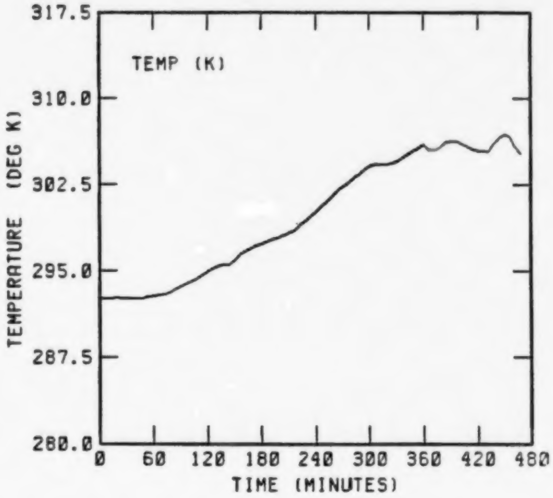

SIMULATION RESULTS FOR
UNCR 91977

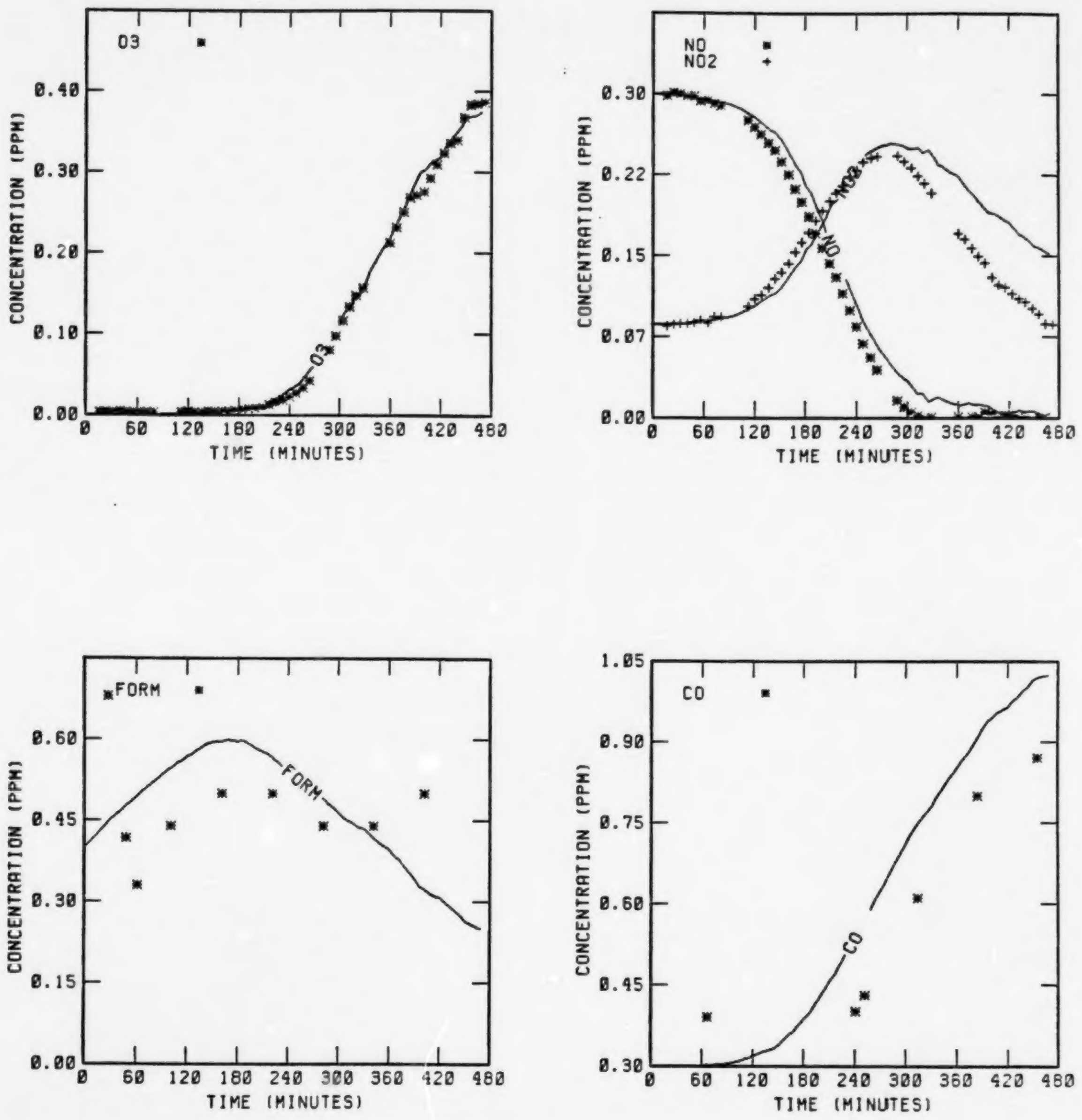

SIMULATION RESULTS FOR
UNCB 91977

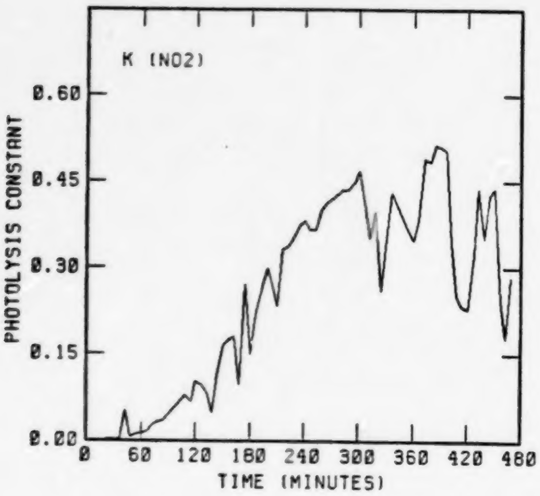

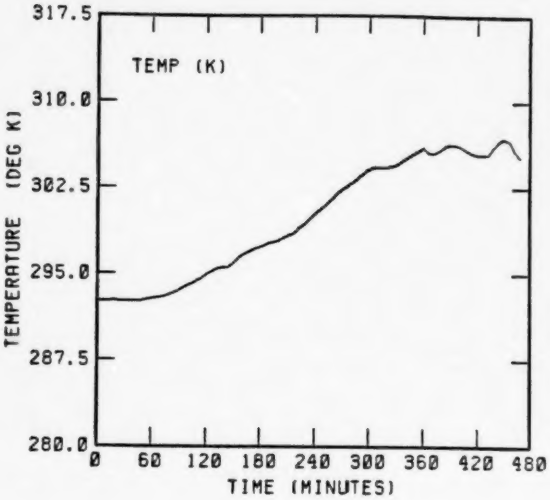

SIMULATION RESULTS FOR
UNCB 91977

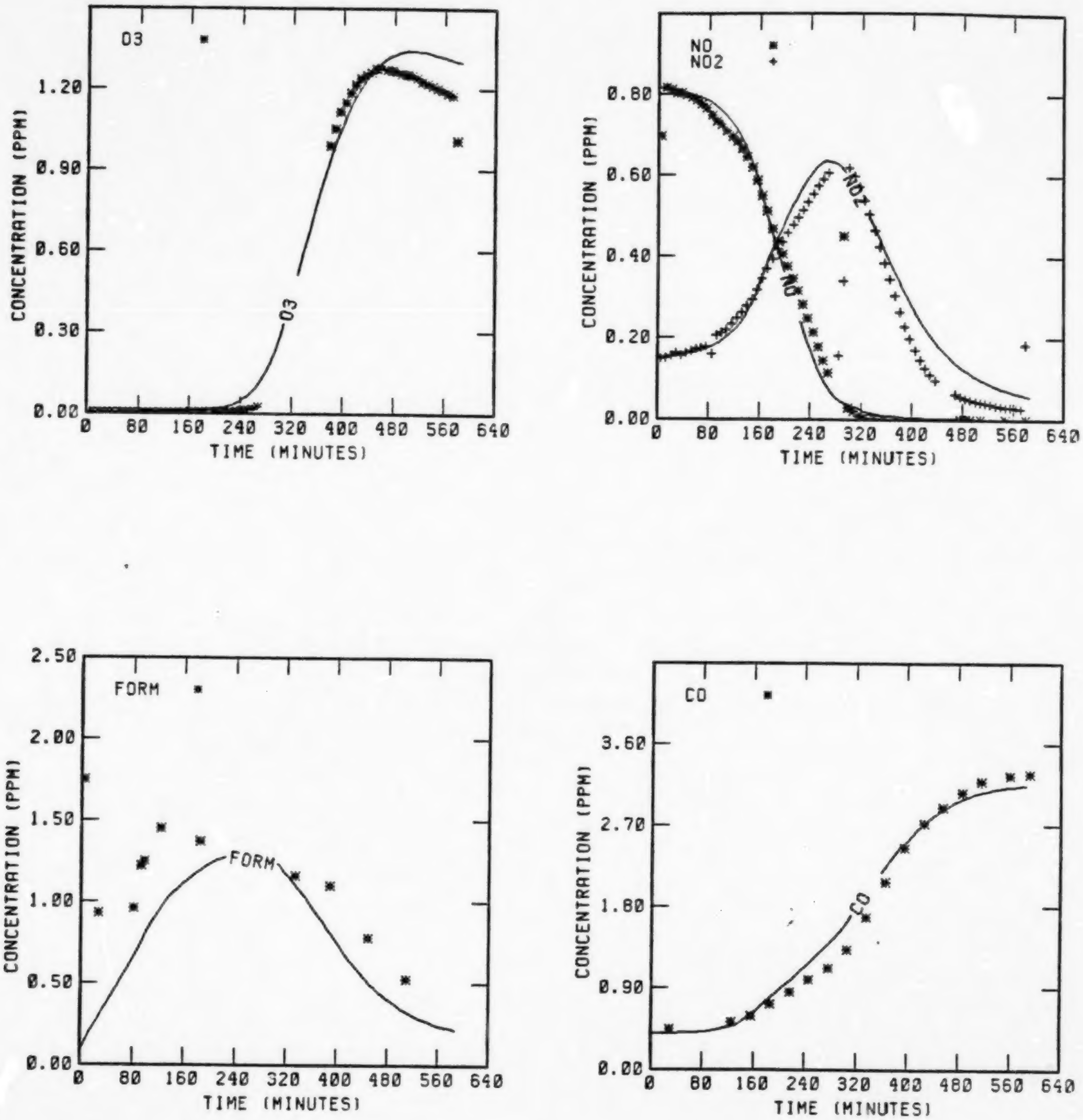

SIMULATION RESULTS FOR
UNCR 90878

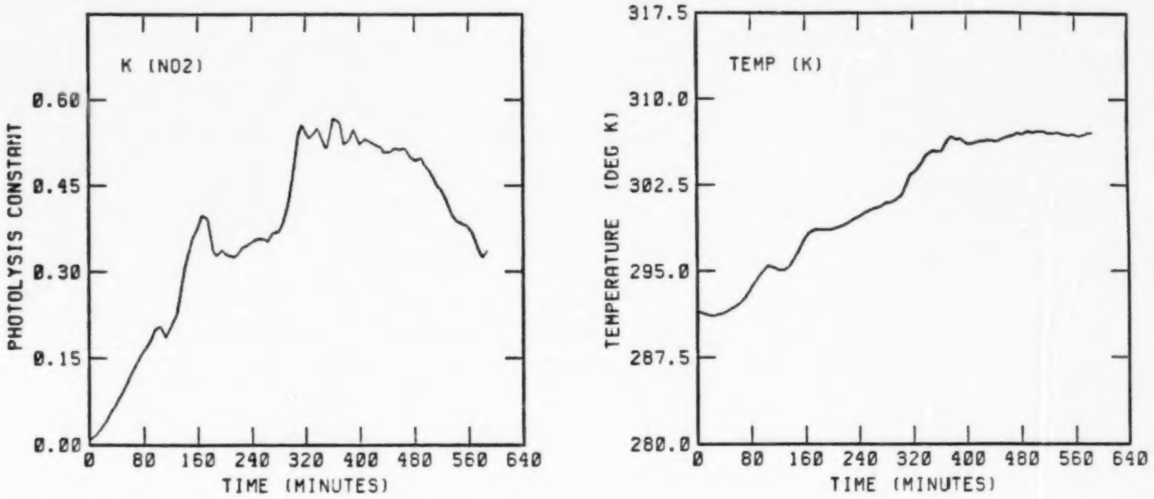

SIMULATION RESULTS FOR
UNCR 90878

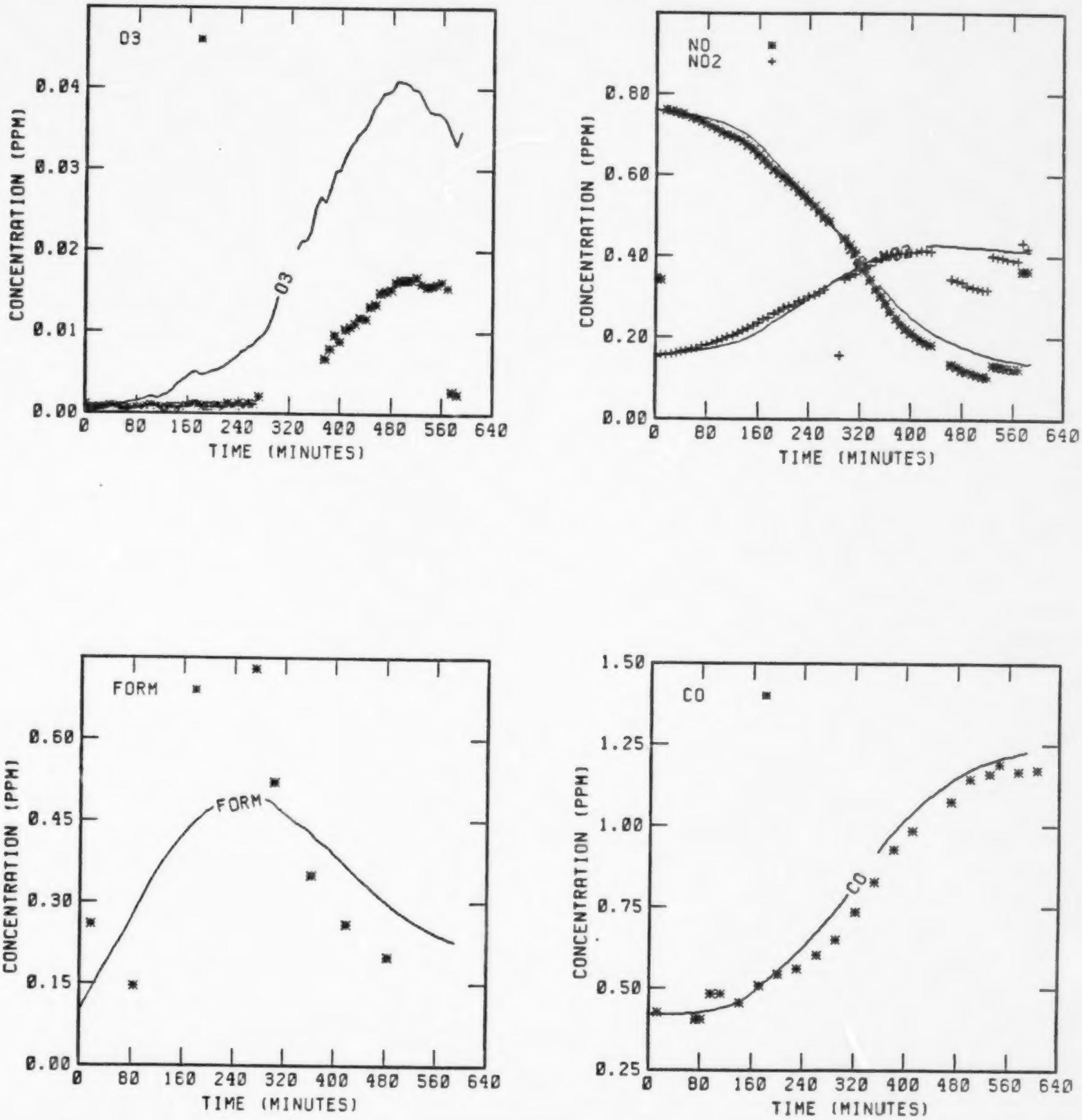

SIMULATION RESULTS FOR
UNCB 90878

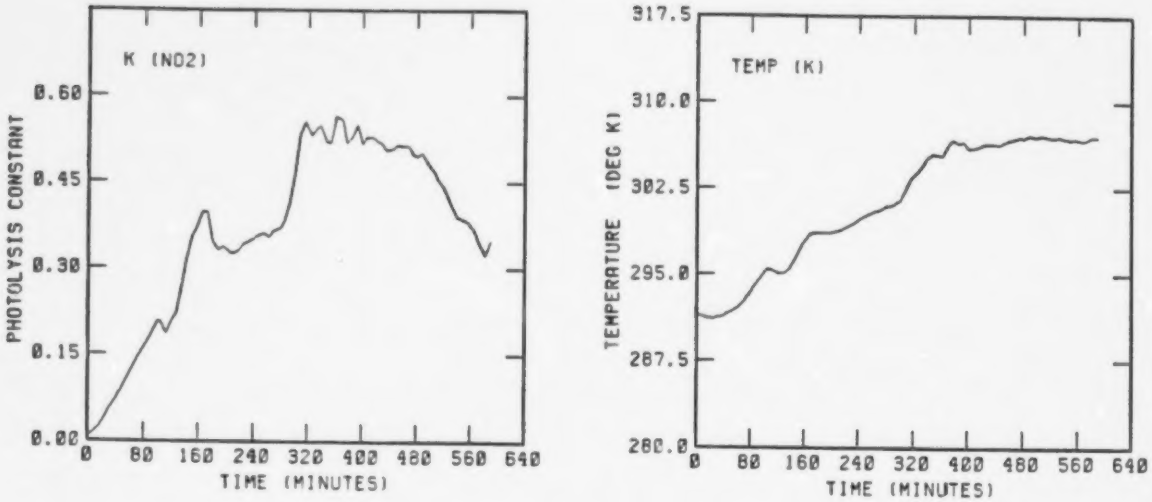

SIMULATION RESULTS FOR
UNCB 90878

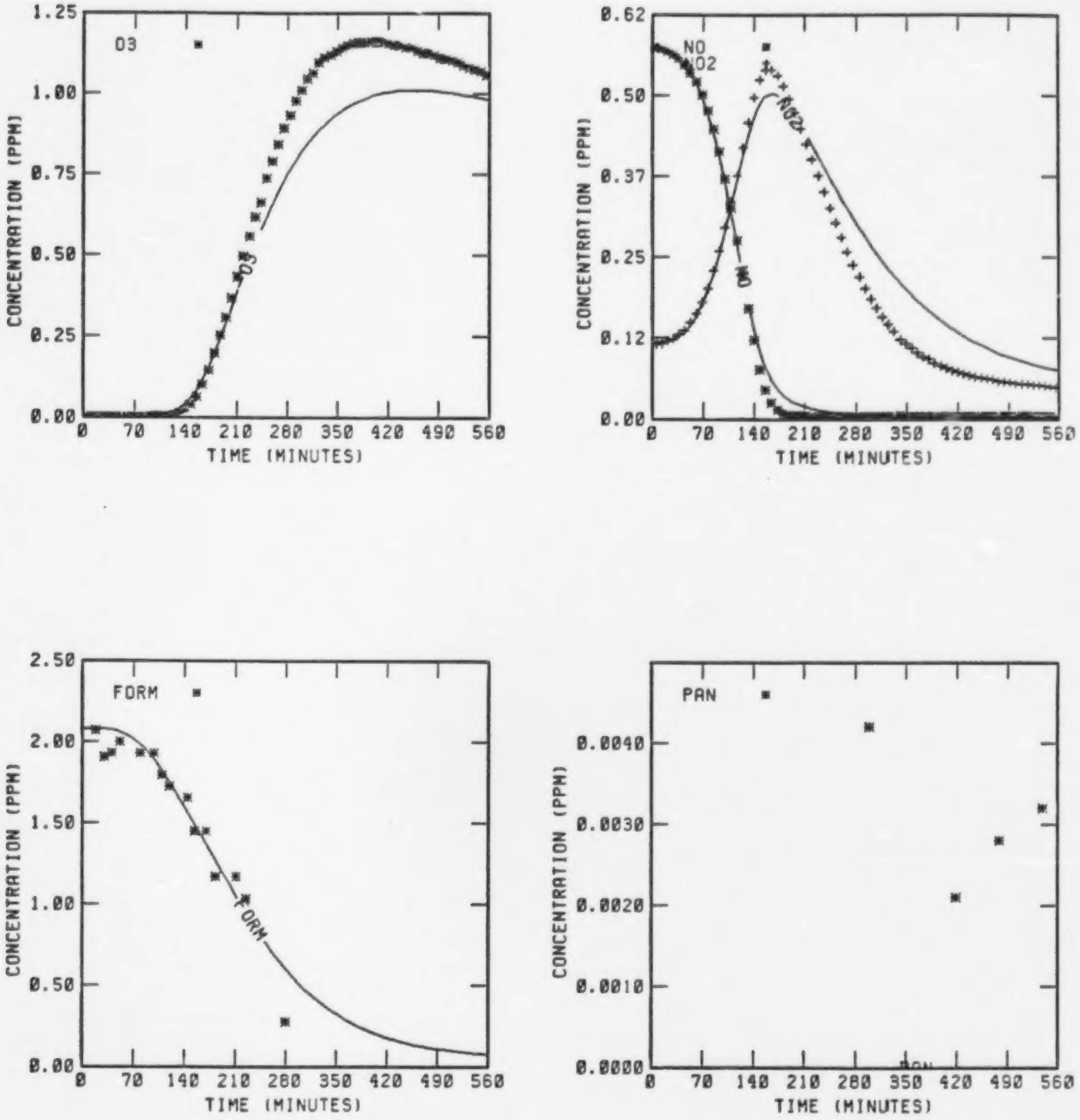

SIMULATION RESULTS FOR
UNCB 91978

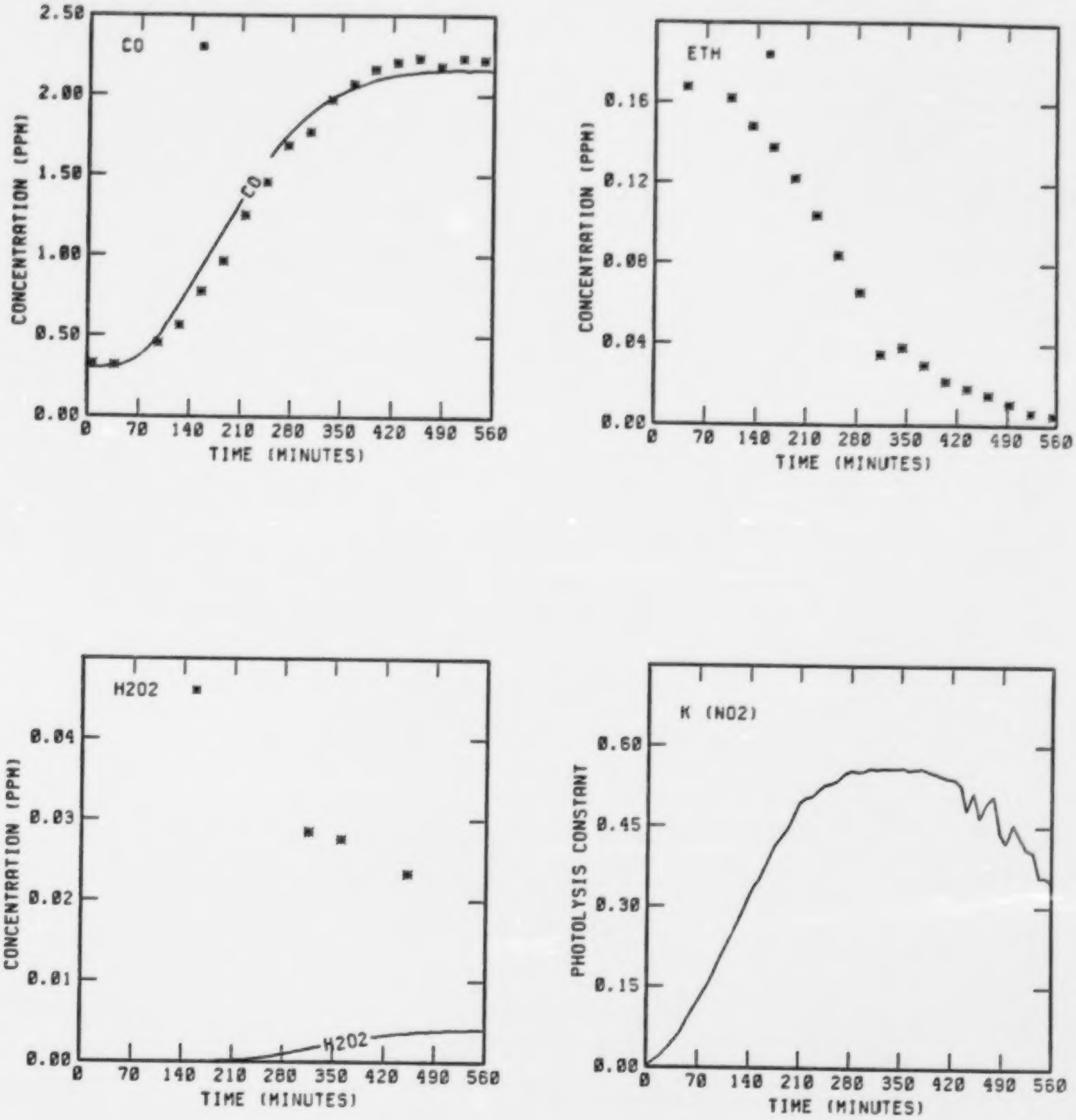

SIMULATION RESULTS FOR
UNCB 91978

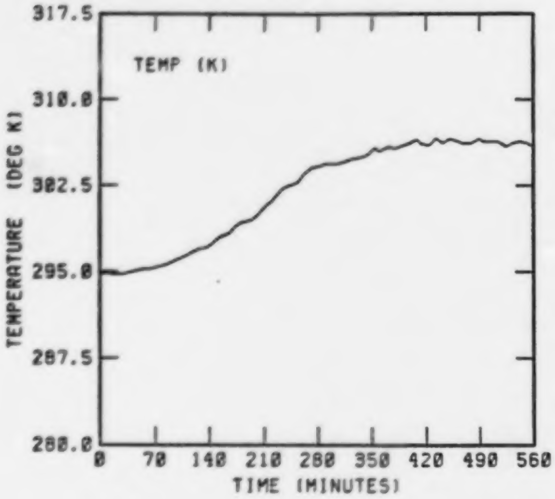

SIMULATION RESULTS FOR
UNCB 91978

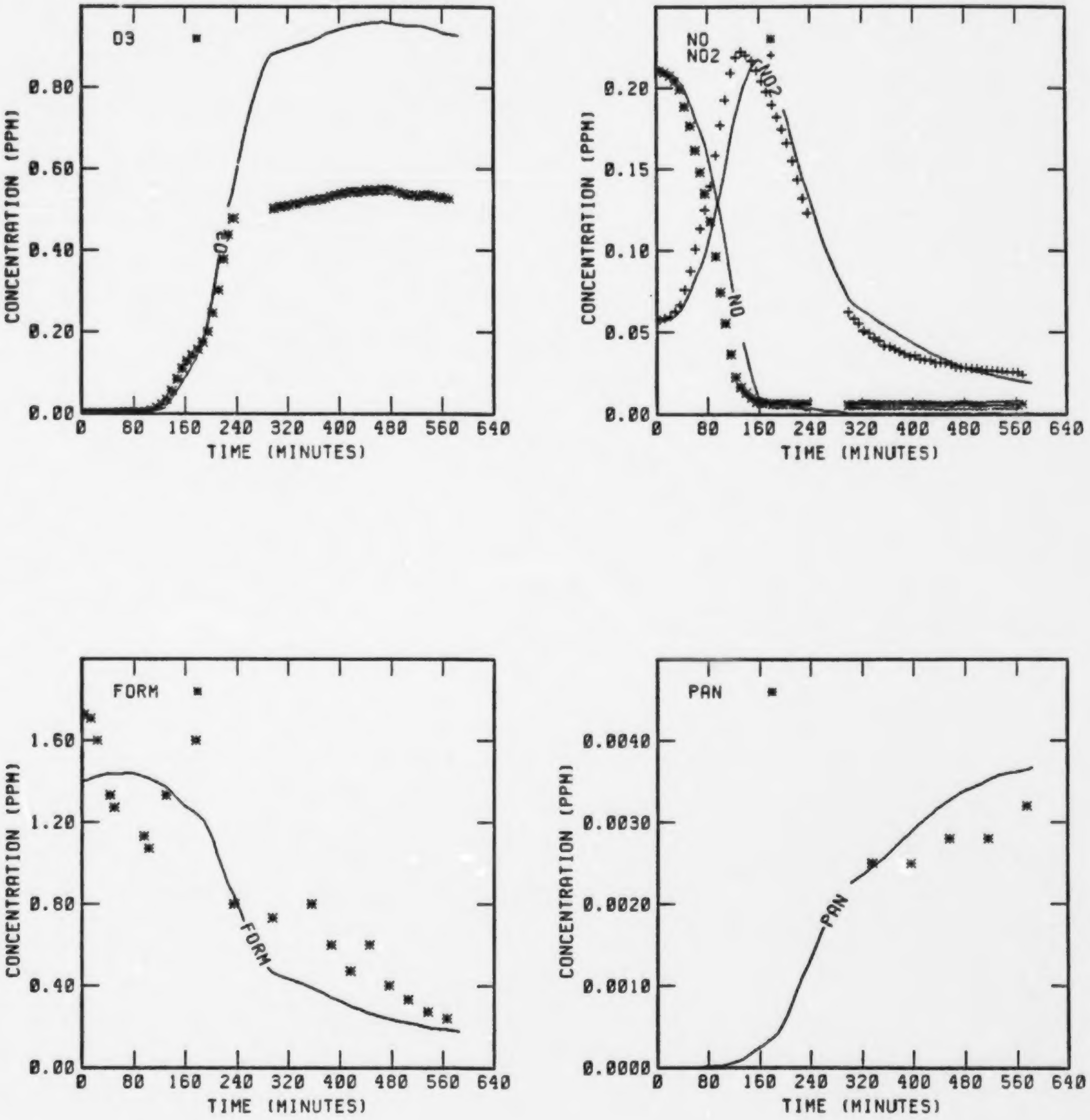

SIMULATION RESULTS FOR
UNCB 91578

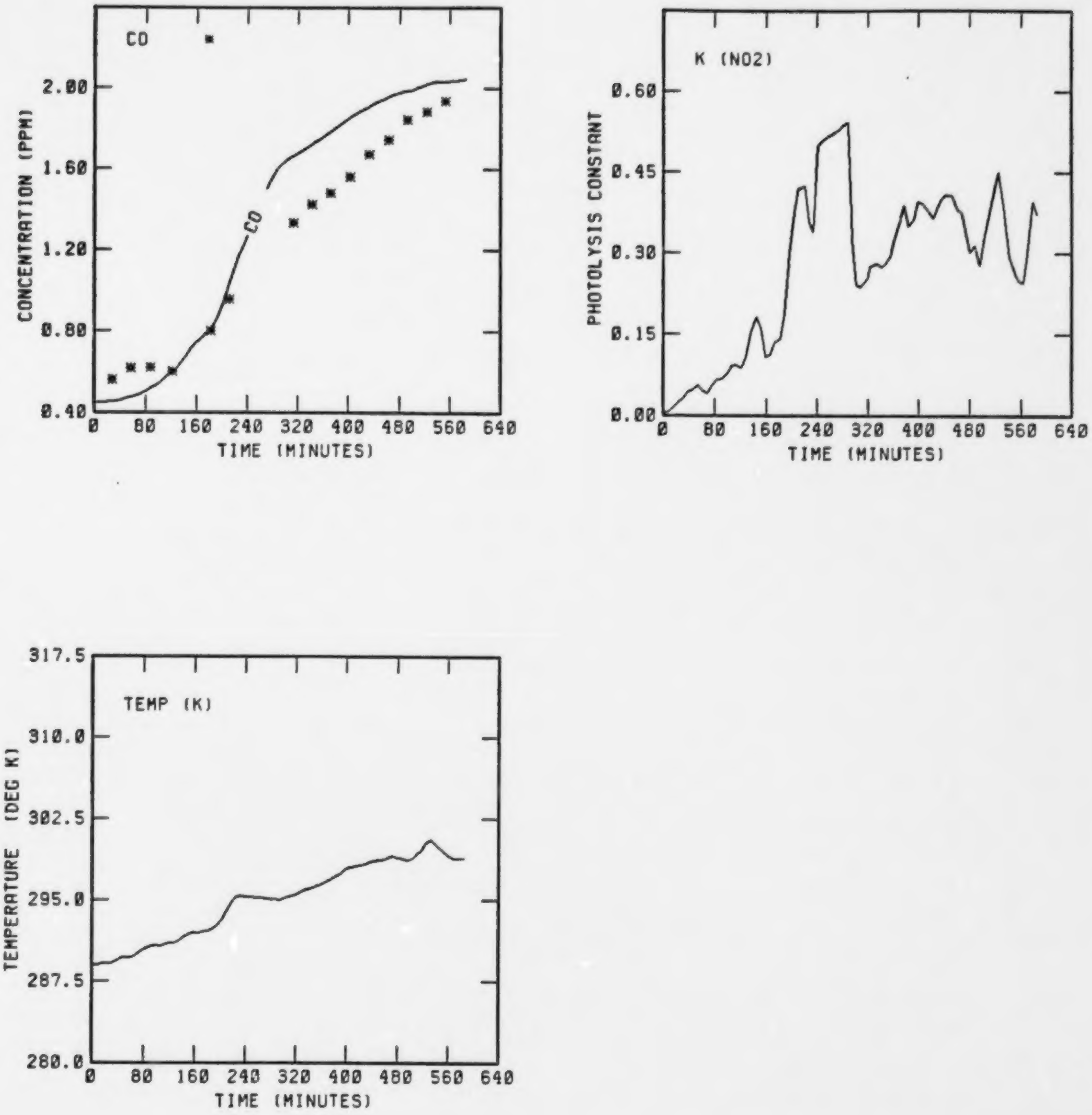

SIMULATION RESULTS FOR
UNCB 91578

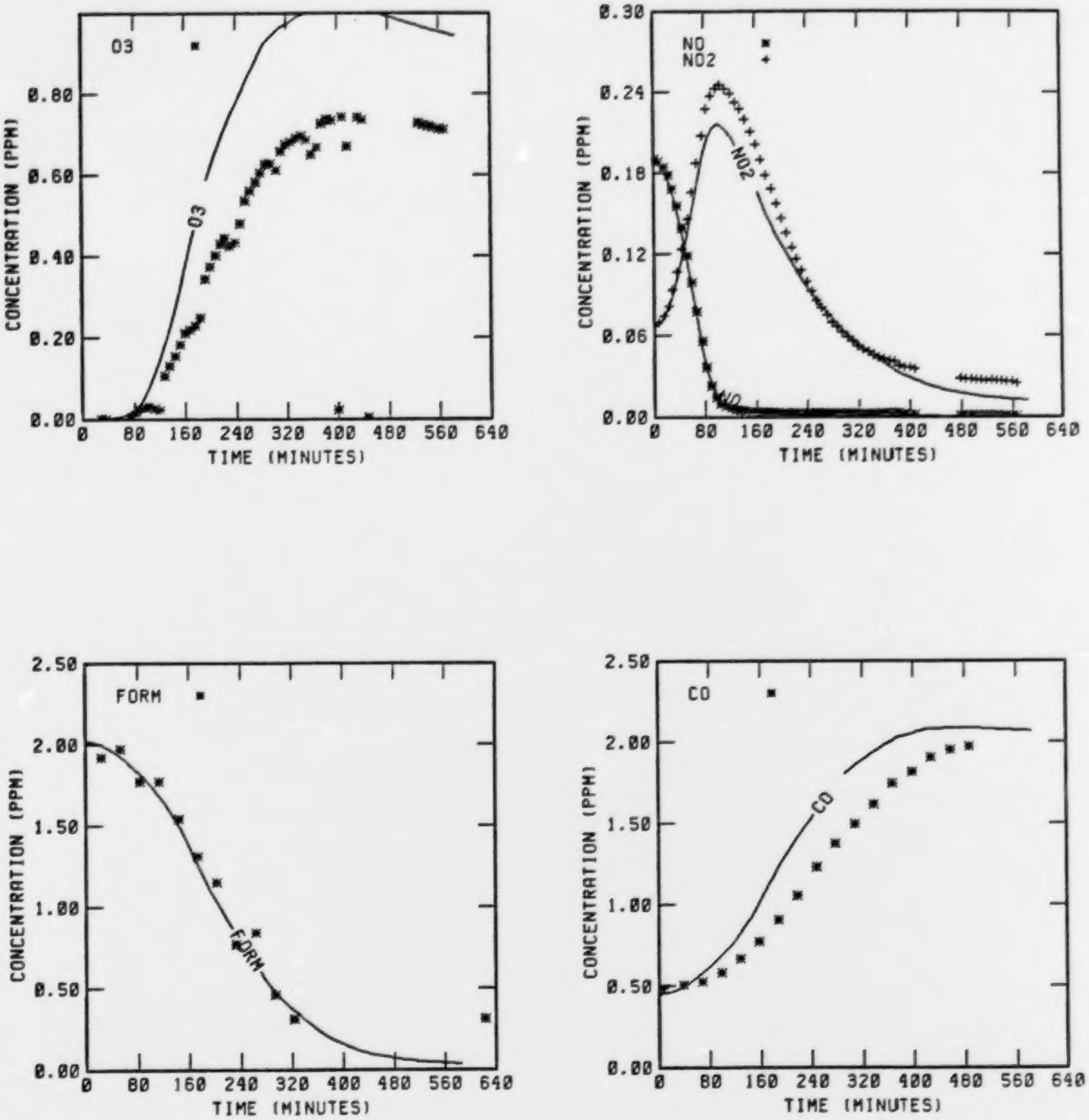

SIMULATION RESULTS FOR
UNCB 92178

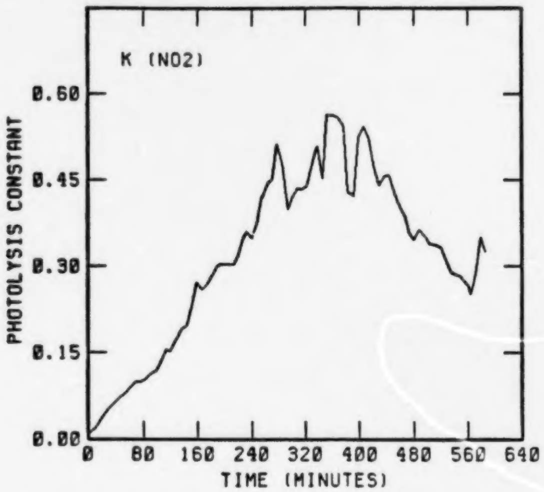

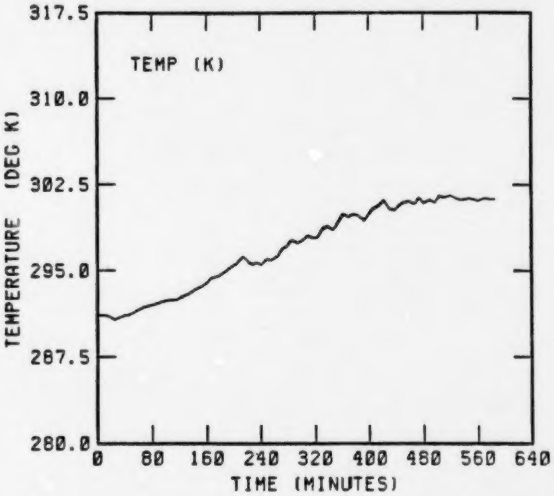

SIMULATION RESULTS FOR
UNCB 92178

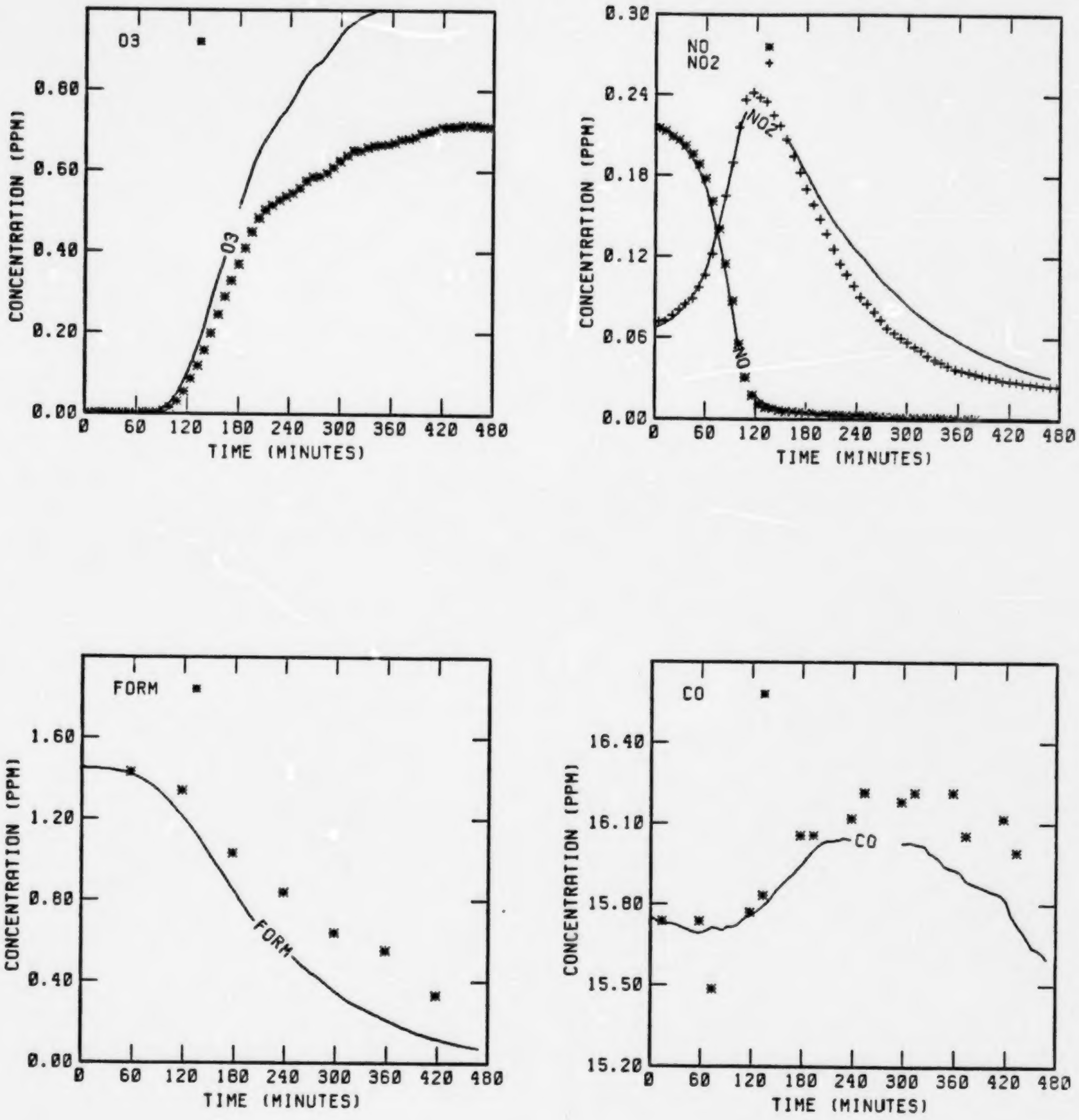

SIMULATION RESULTS FOR
UNCR 73079

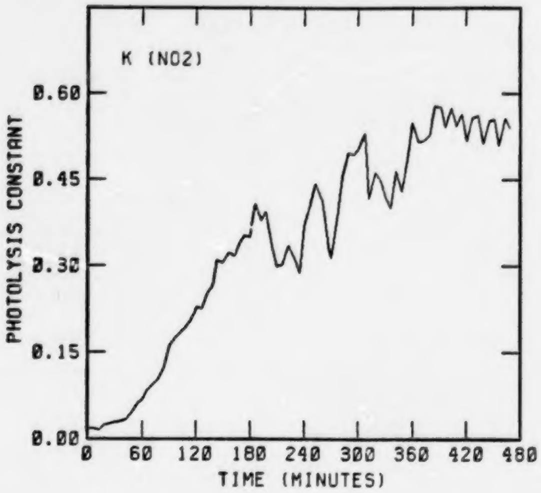

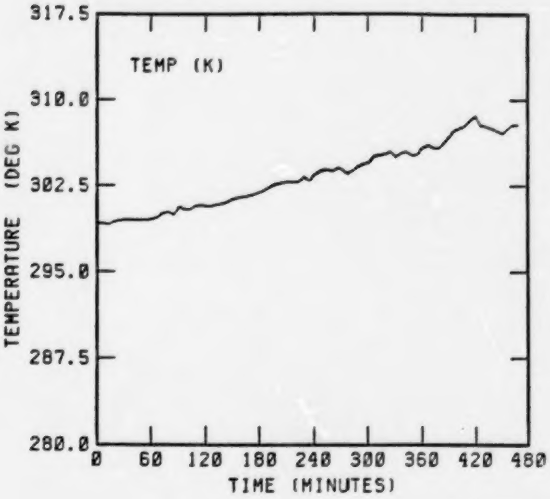

SIMULATION RESULTS FOR
UNCR 73079

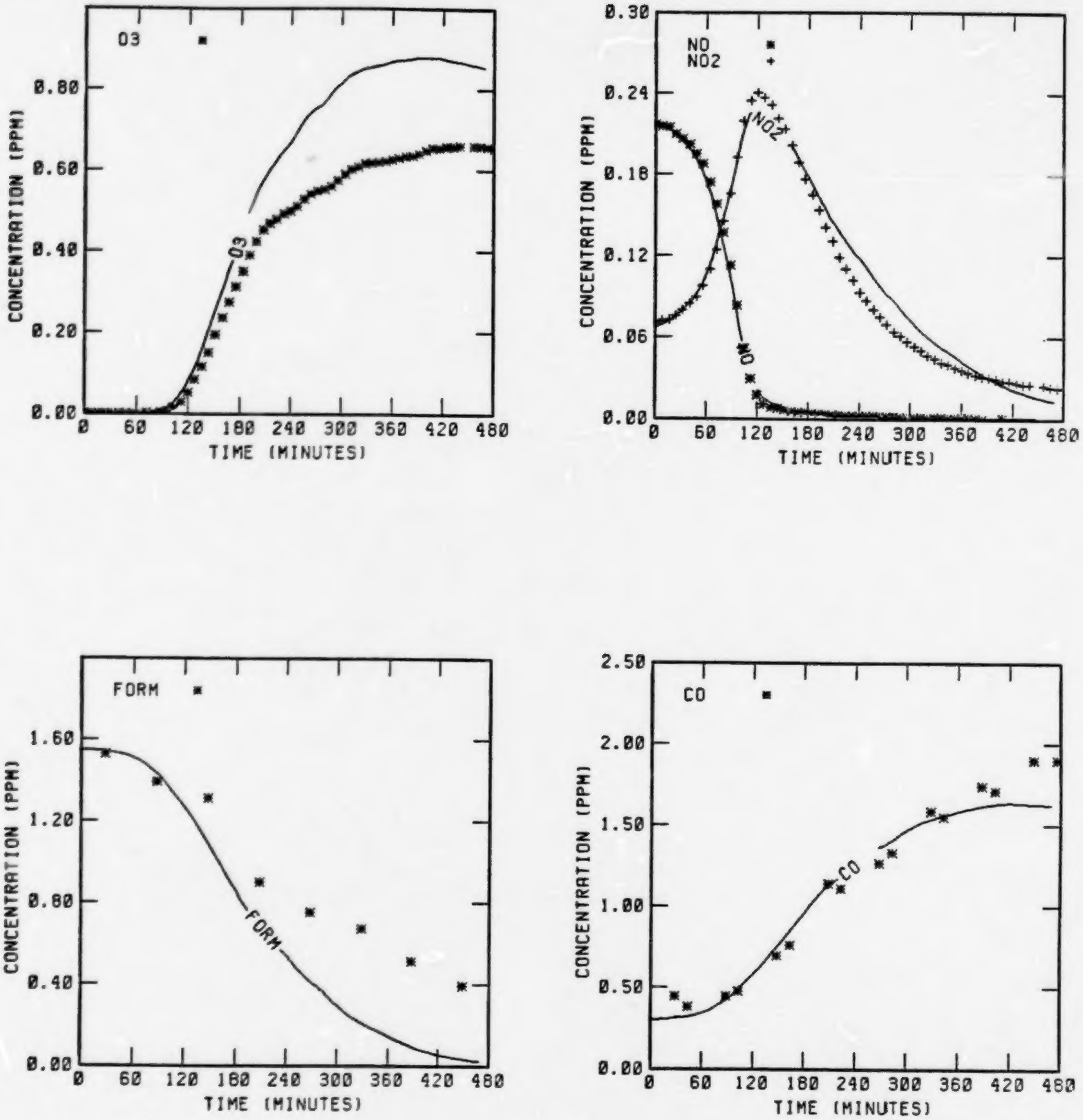

SIMULATION RESULTS FOR
UNCB 73079

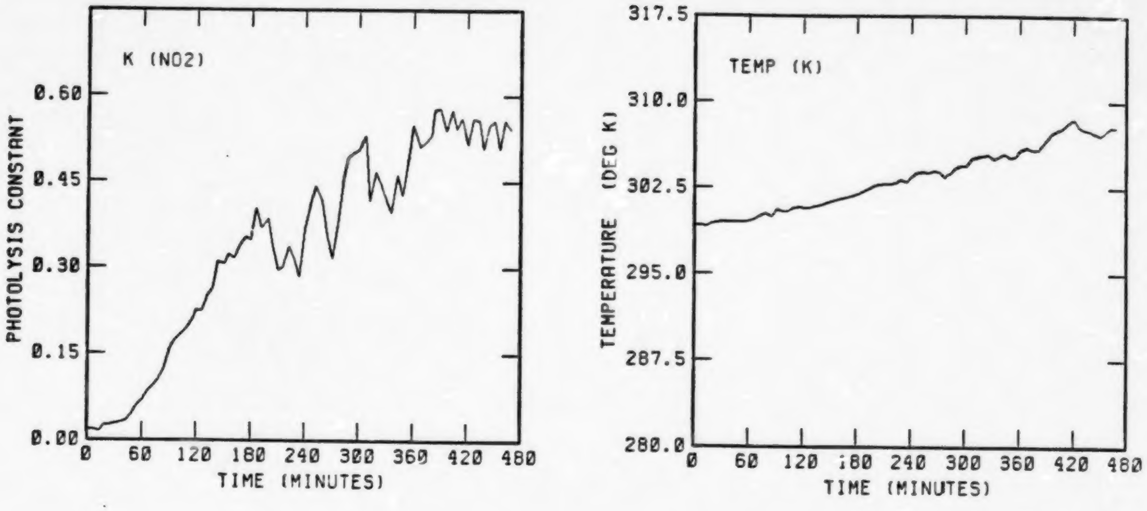

SIMULATION RESULTS FOR
UNCB 73079

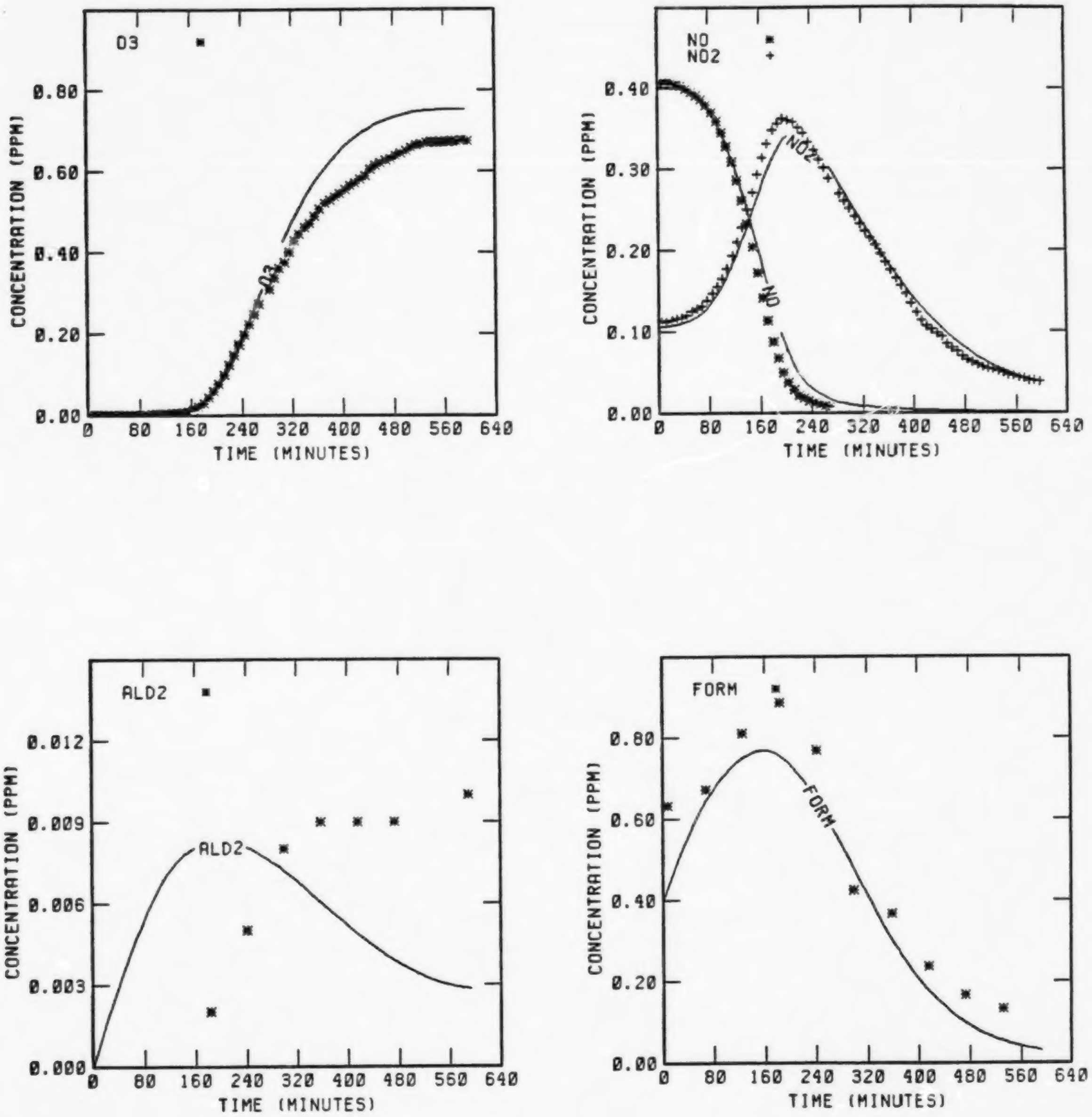

SIMULATION RESULTS FOR
UNCR 73179

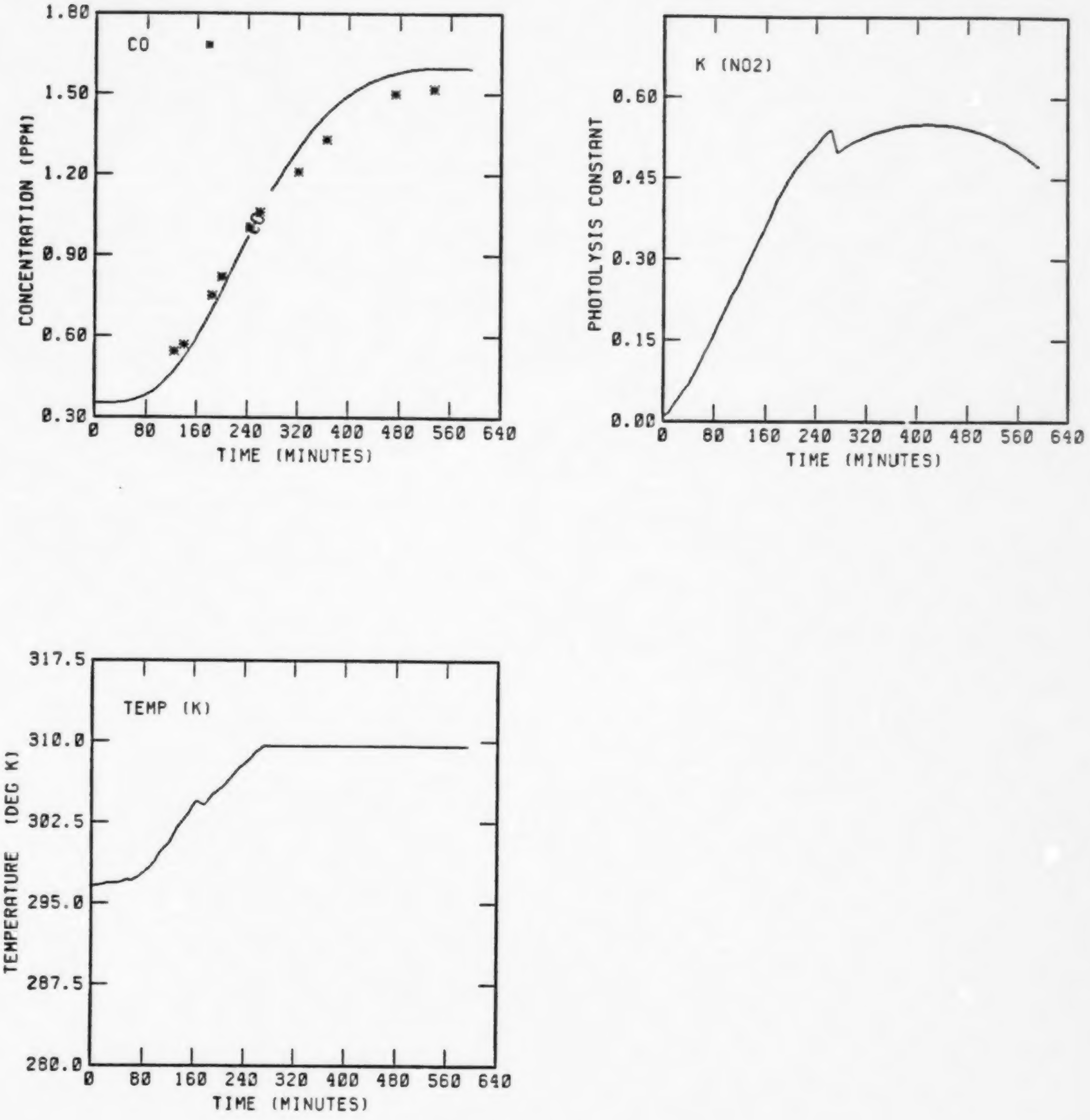

SIMULATION RESULTS FOR
UNCR 73179

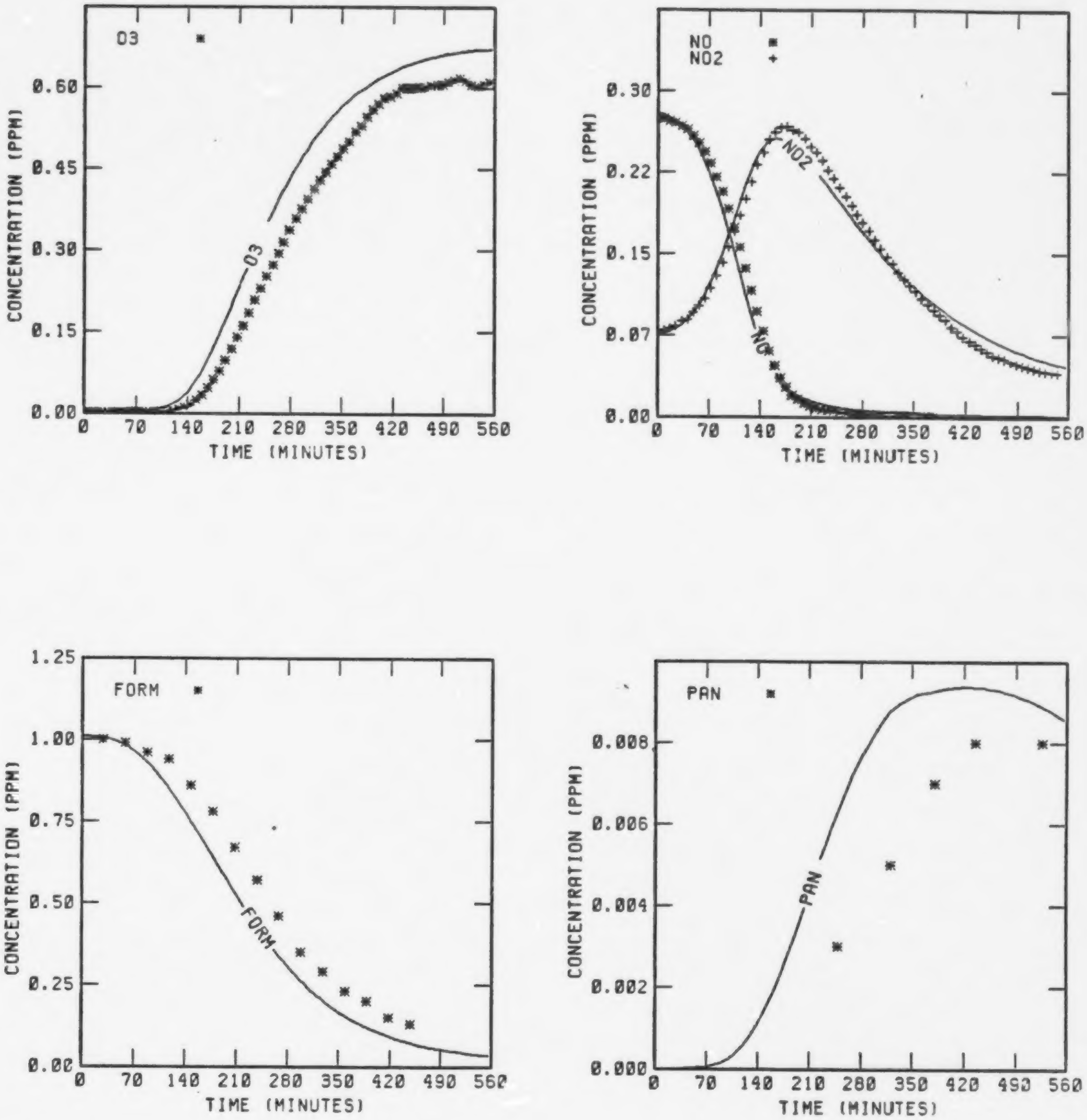

SIMULATION RESULTS FOR
UNCB 80179

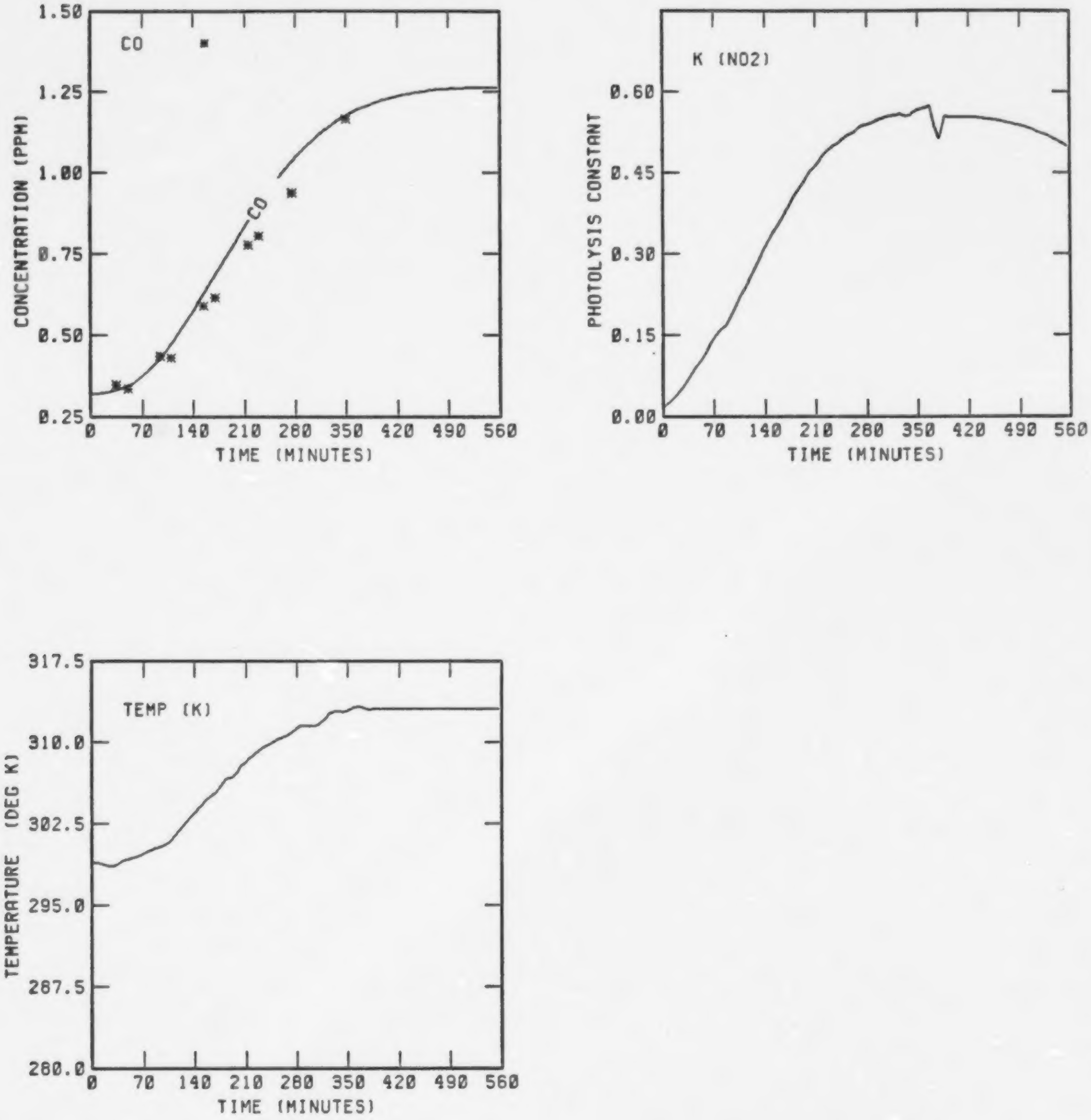

SIMULATION RESULTS FOR
UNCB 80179

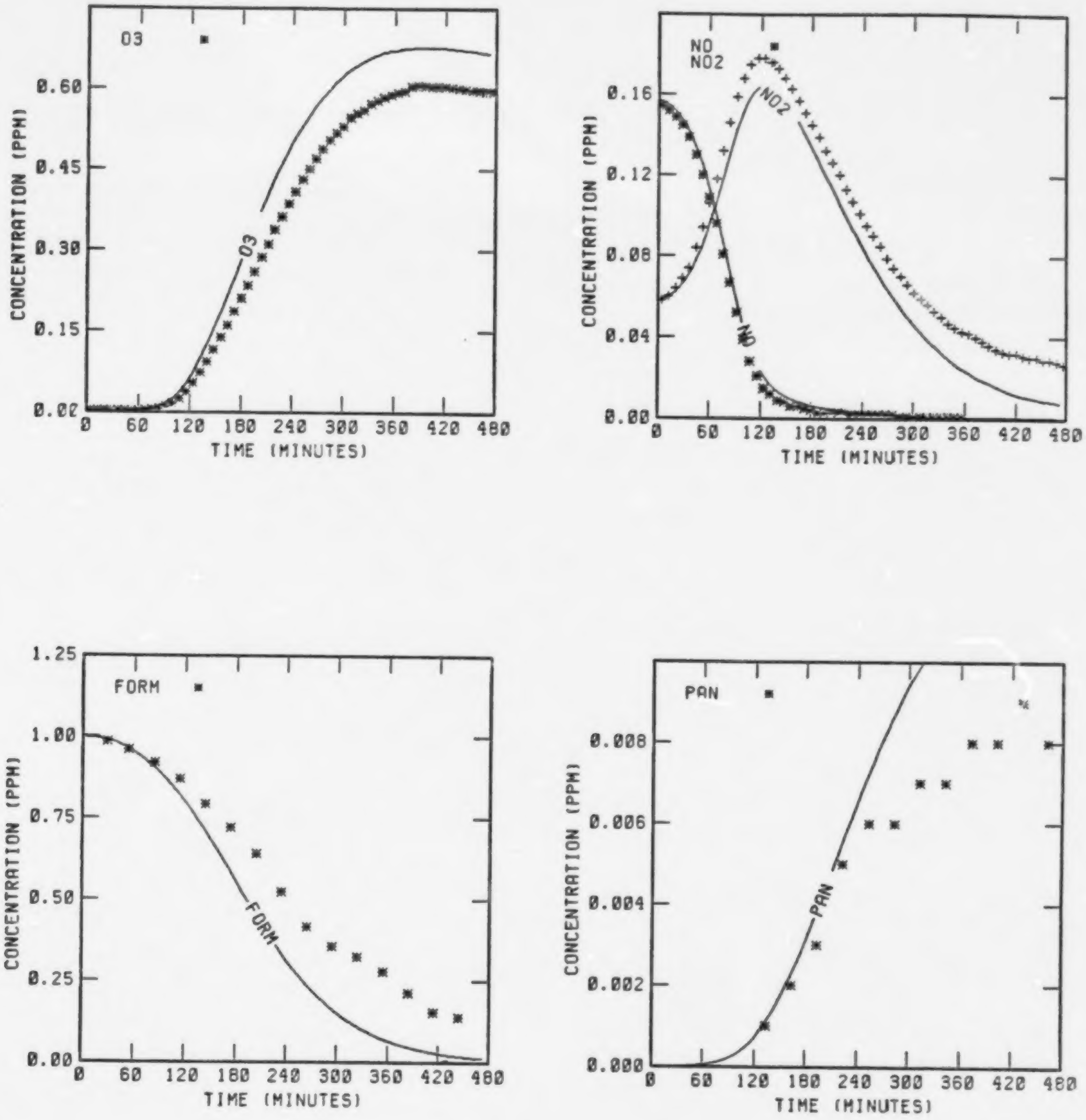

SIMULATION RESULTS FOR
UNCB 80279

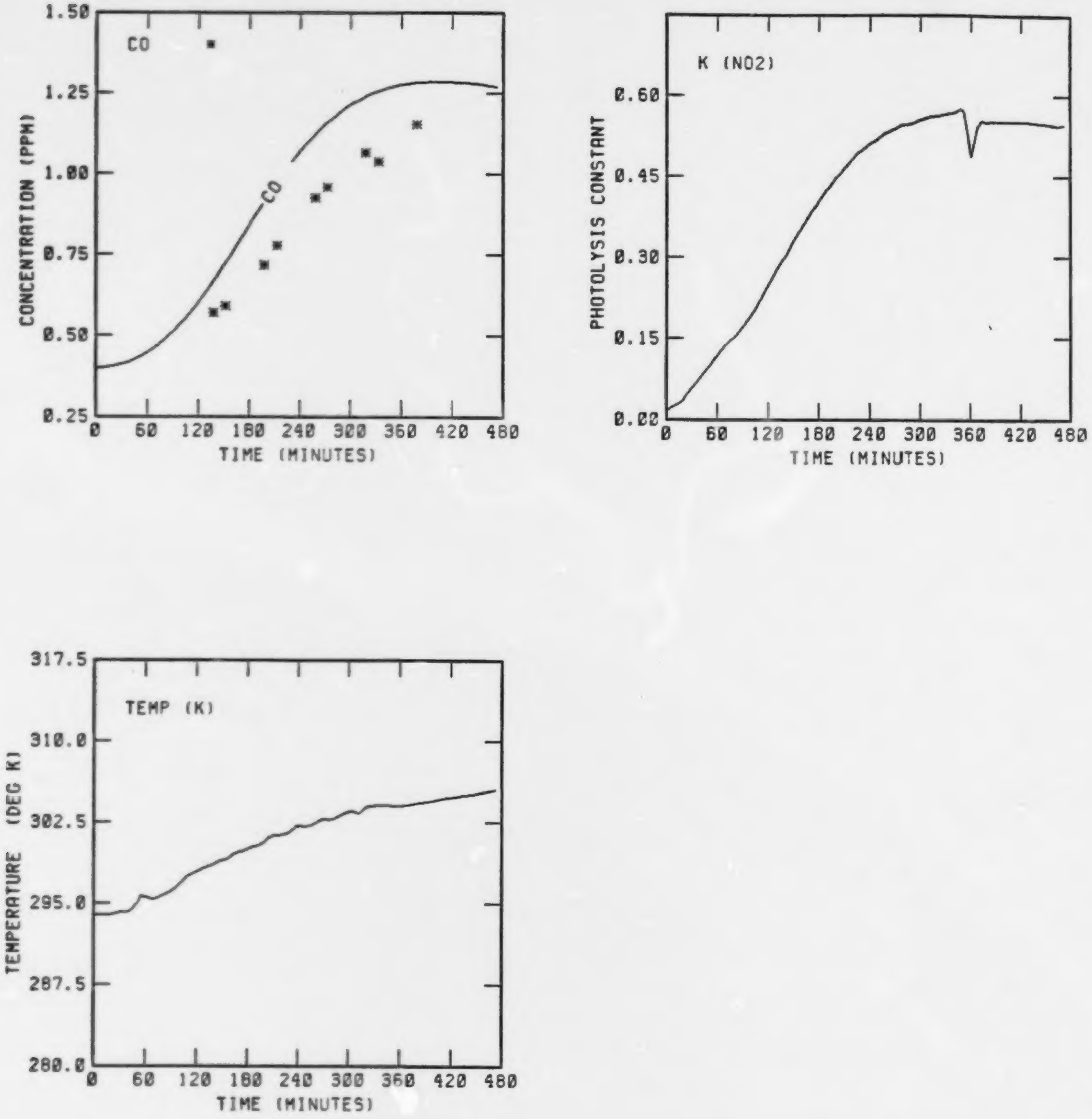

SIMULATION RESULTS FOR
UNCB 80279

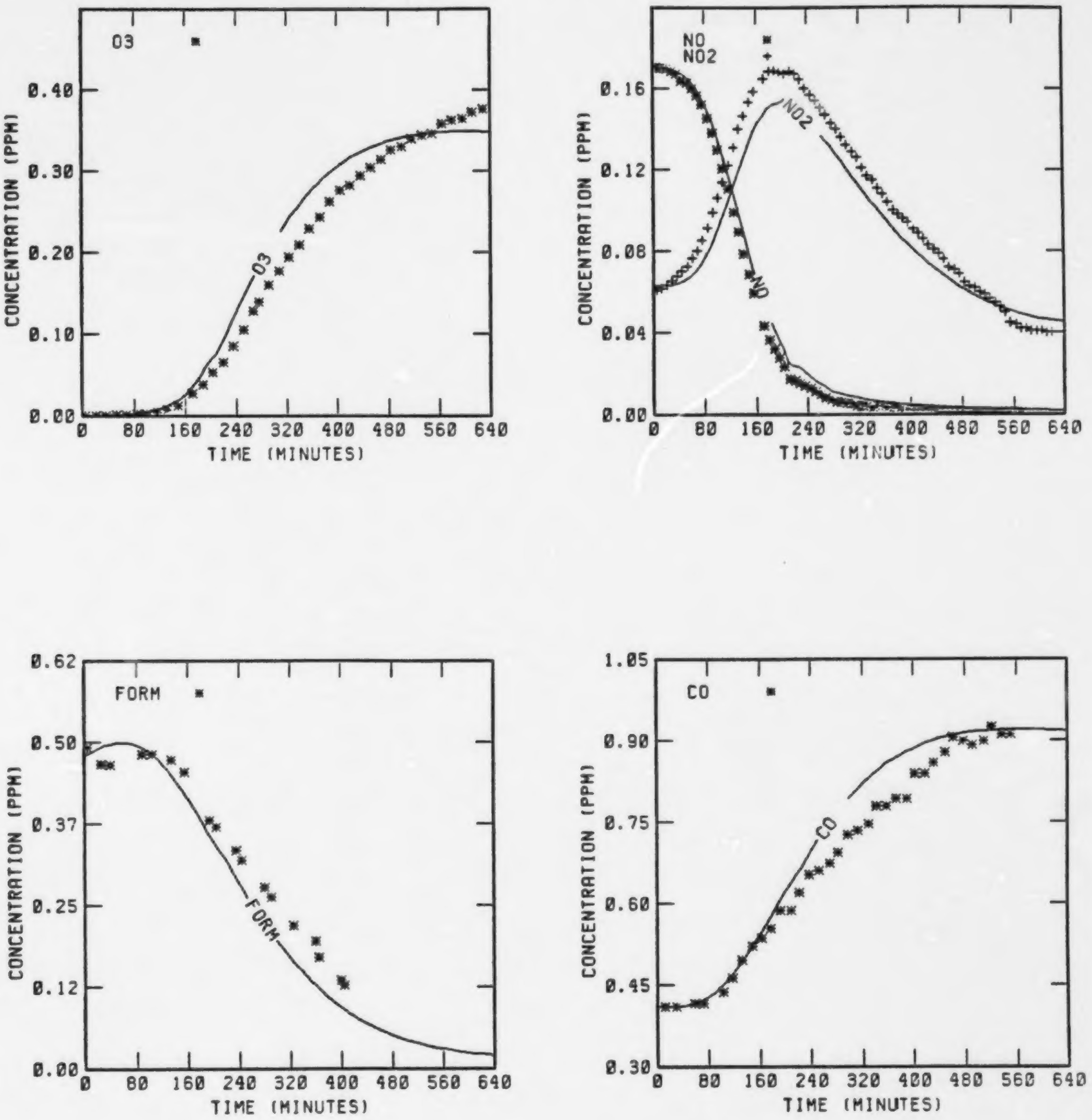

SIMULATION RESULTS FOR
UNCB 80479

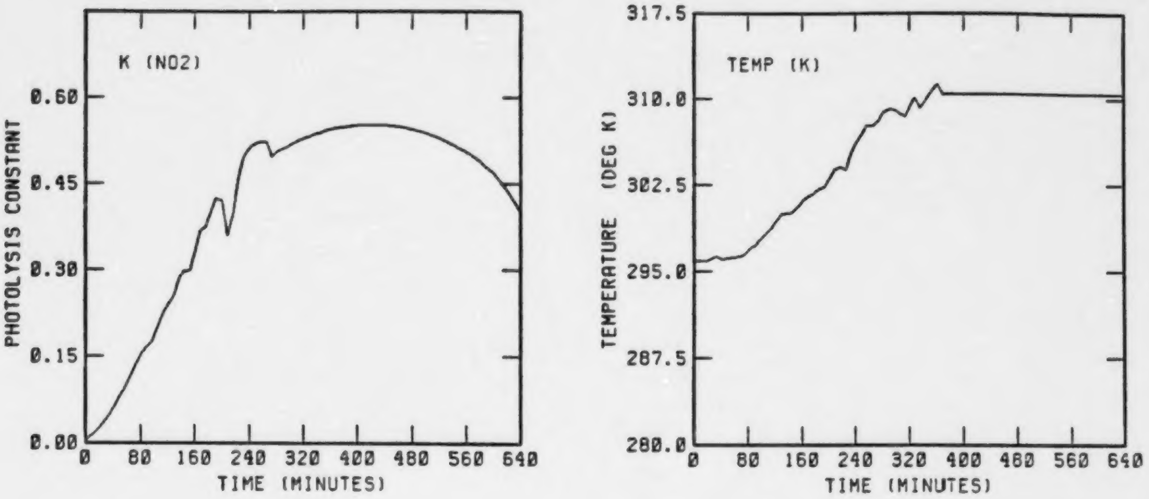

SIMULATION RESULTS FOR
UNCB 80479

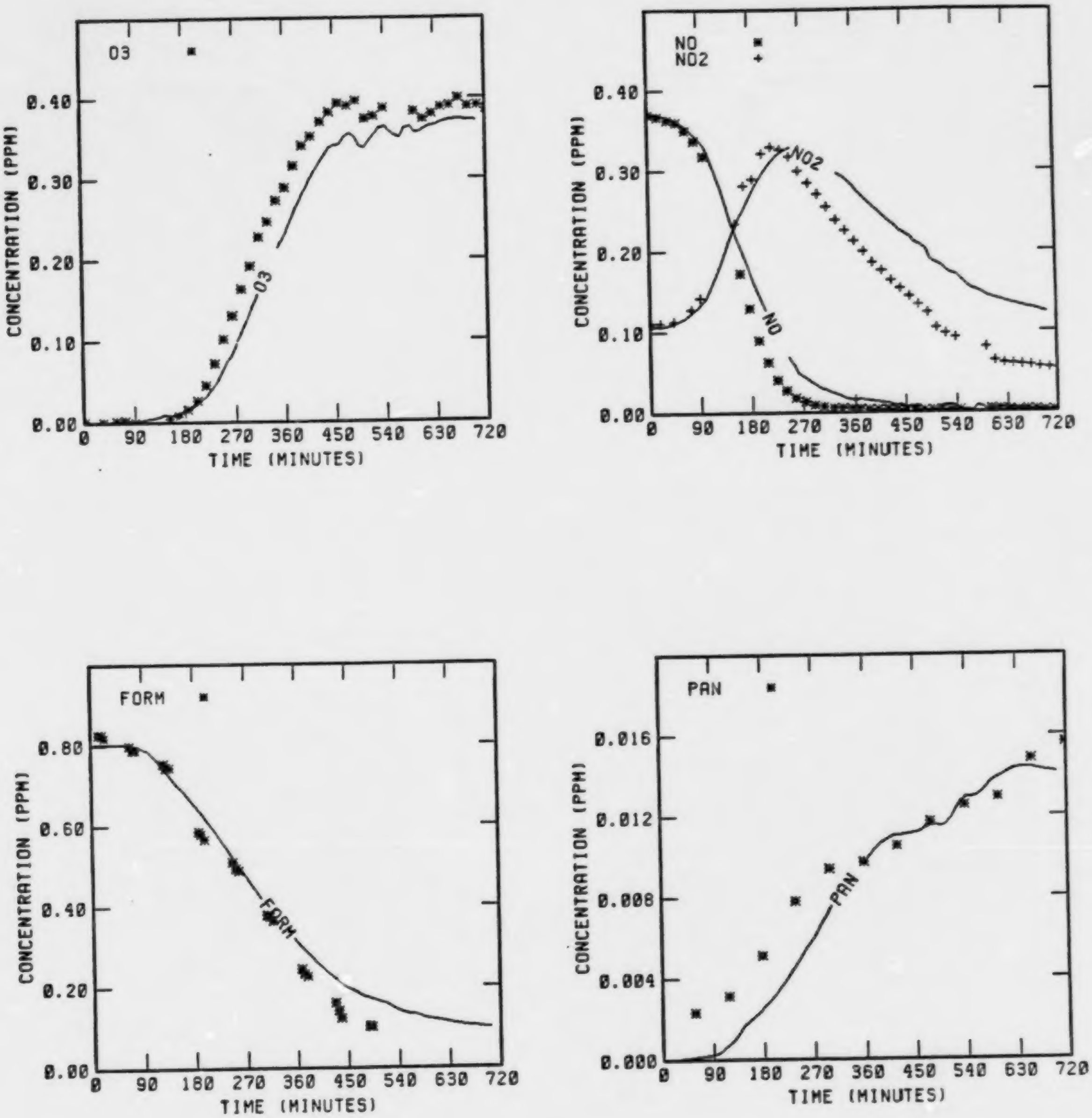

SIMULATION RESULTS FOR
UNCR 81280

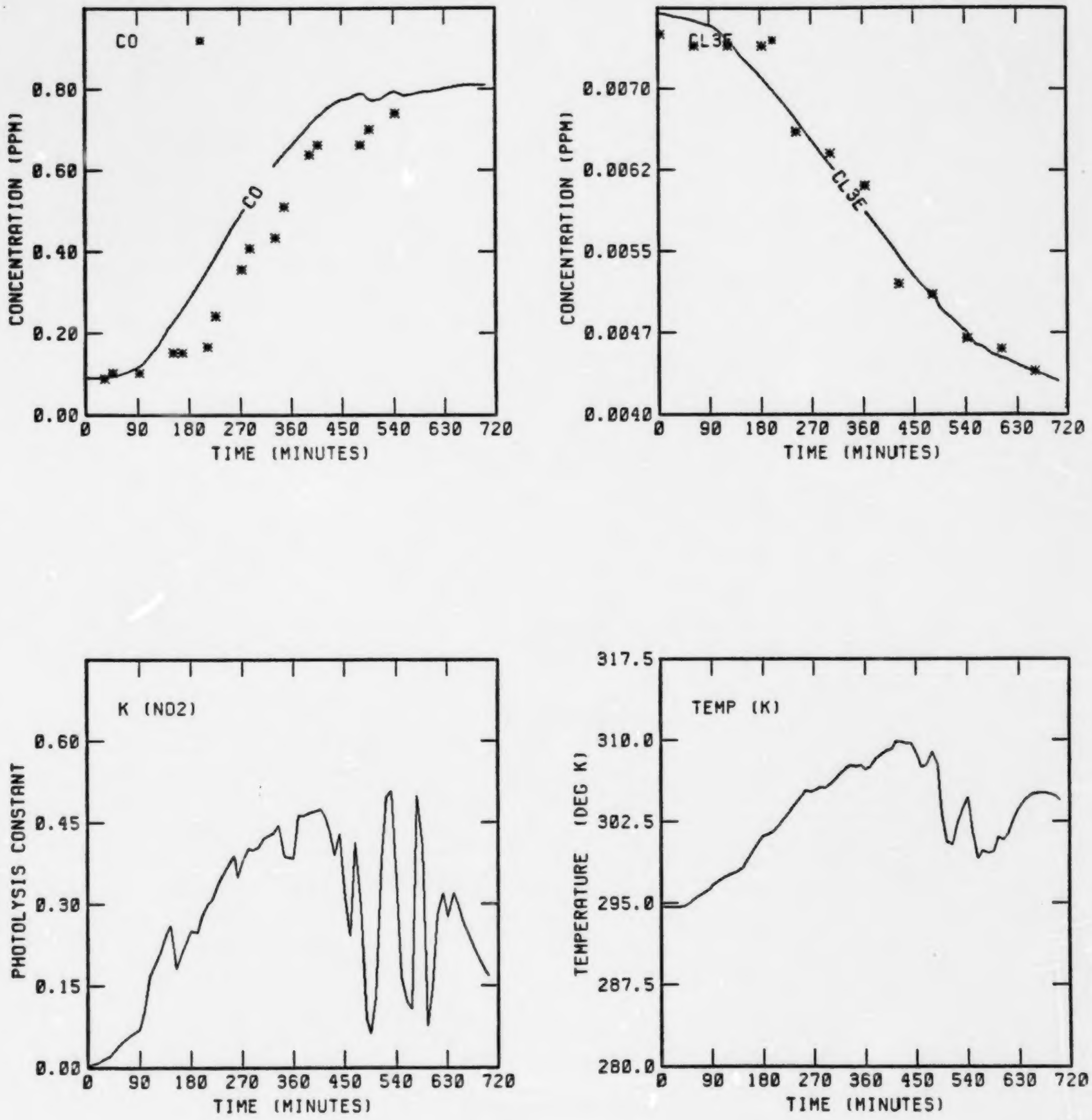

SIMULATION RESULTS FOR
UNCR 81280

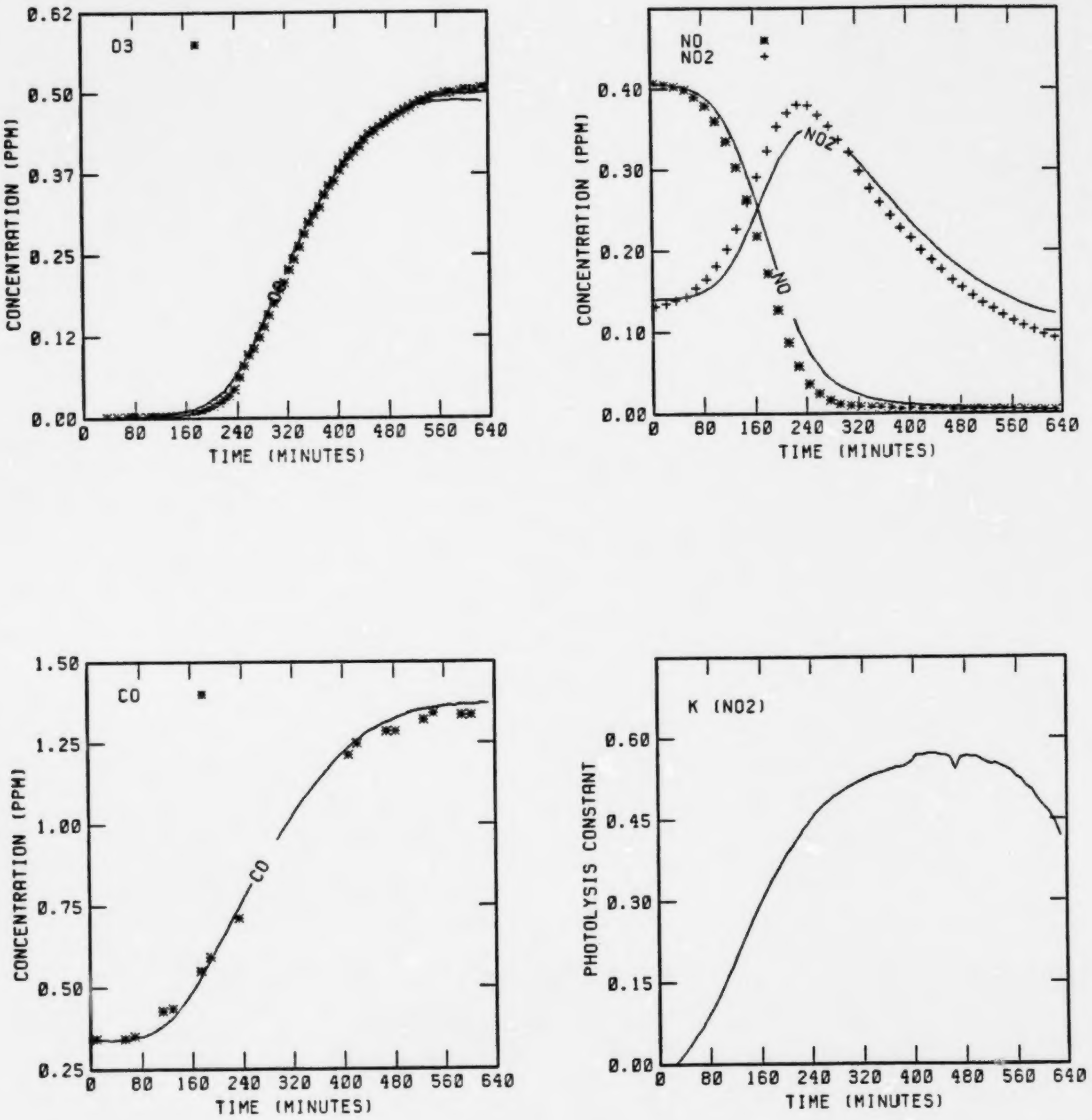

SIMULATION RESULTS FOR
UNCB 80579

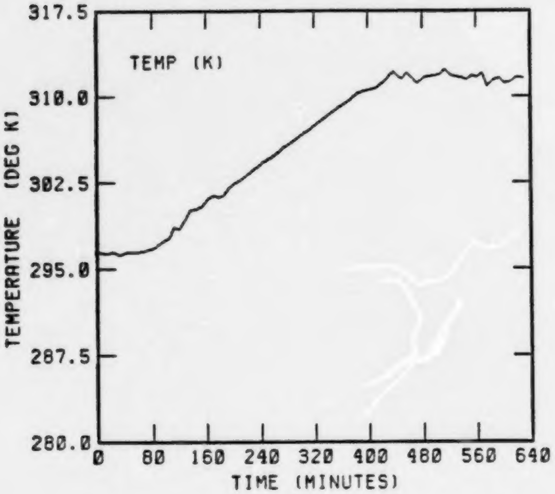

SIMULATION RESULTS FOR
UNCB 80579

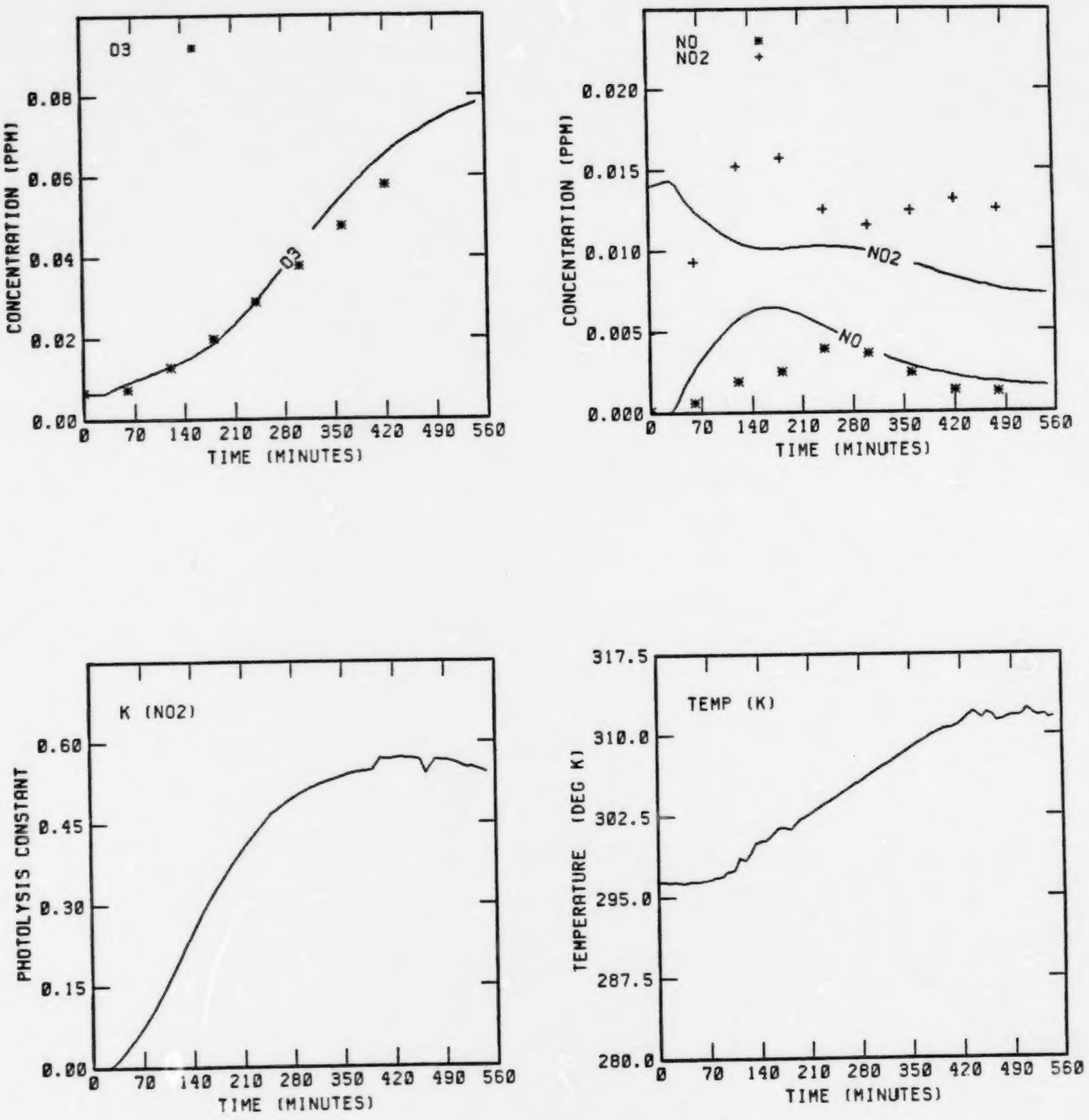

SIMULATION RESULTS FOR
UNCR 81178

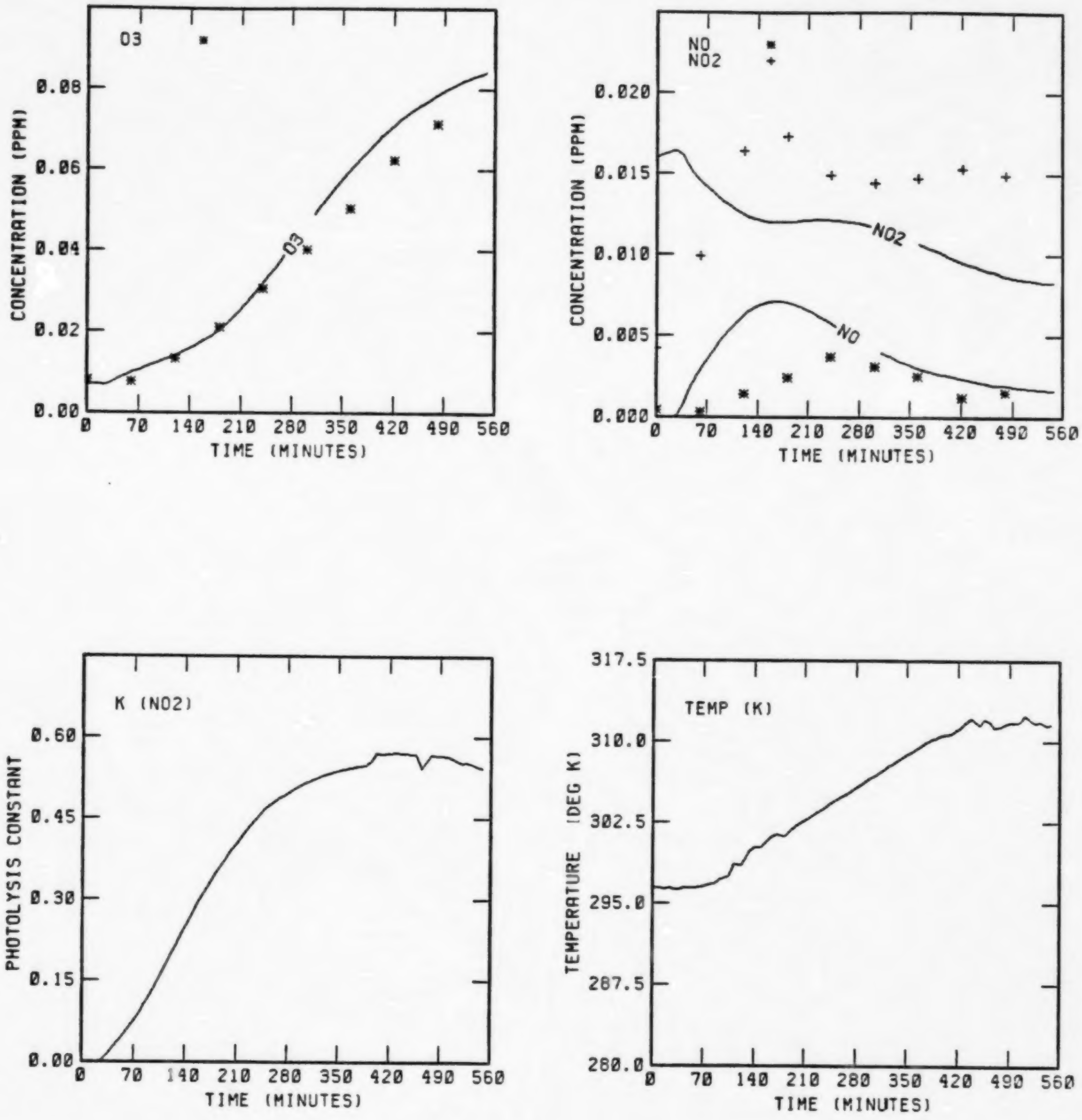

SIMULATION RESULTS FOR
UNCB 81178

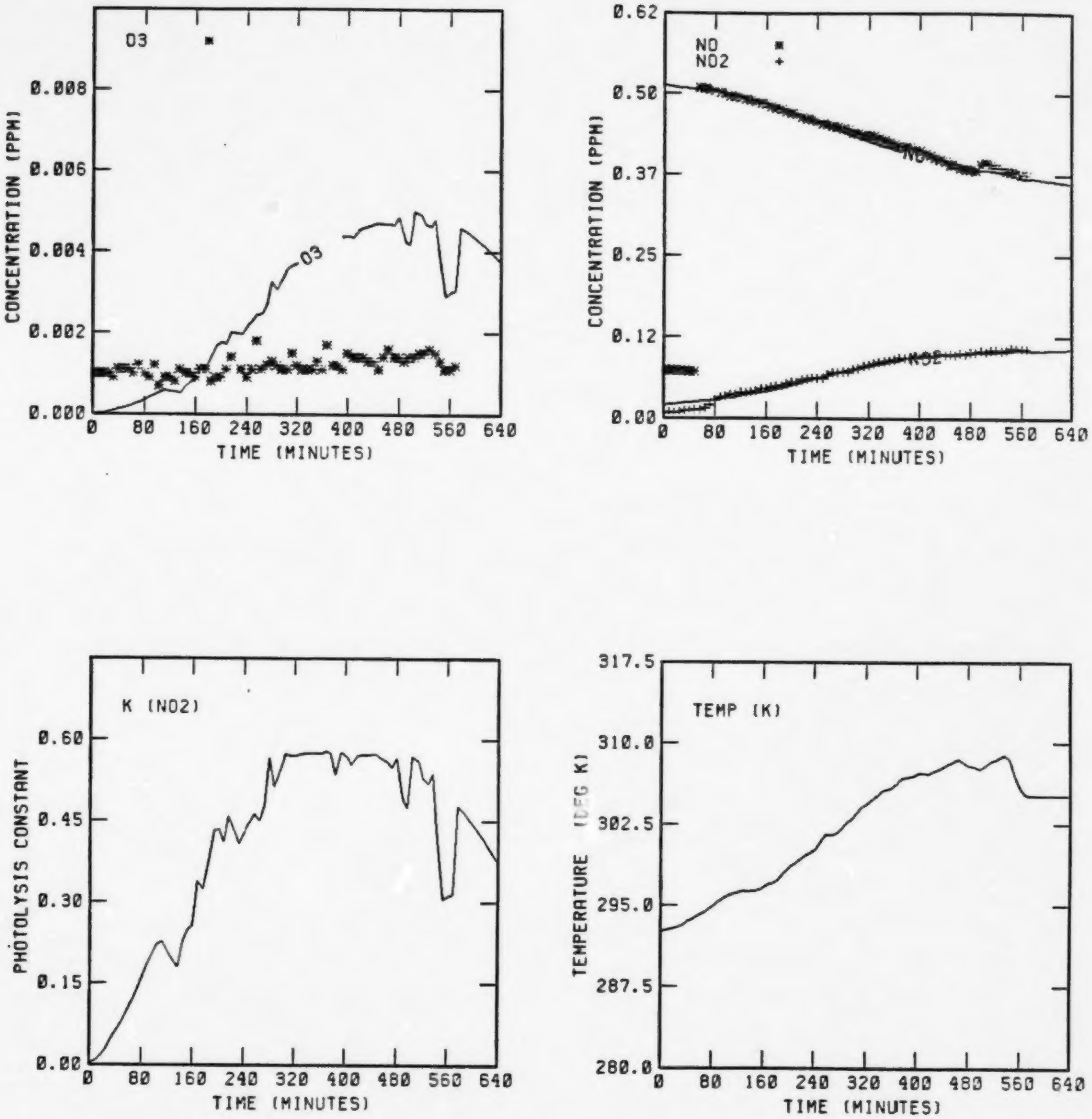

SIMULATION RESULTS FOR
UNCR 81478

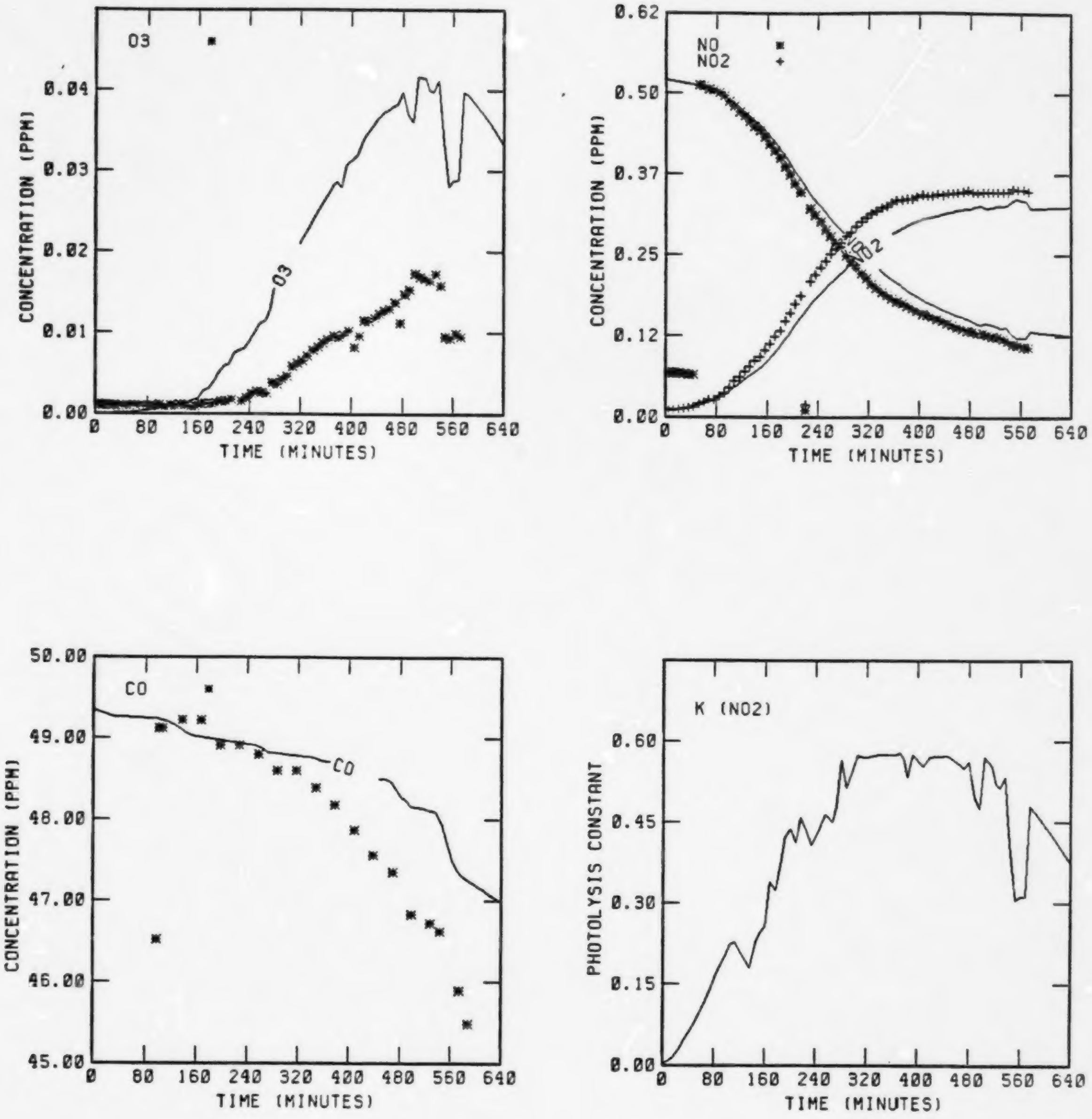

SIMULATION RESULTS FOR
UNCB 81478

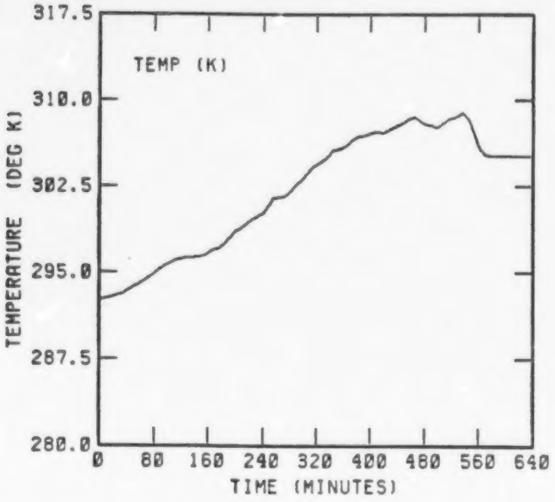

SIMULATION RESULTS FOR
UNCB 81478

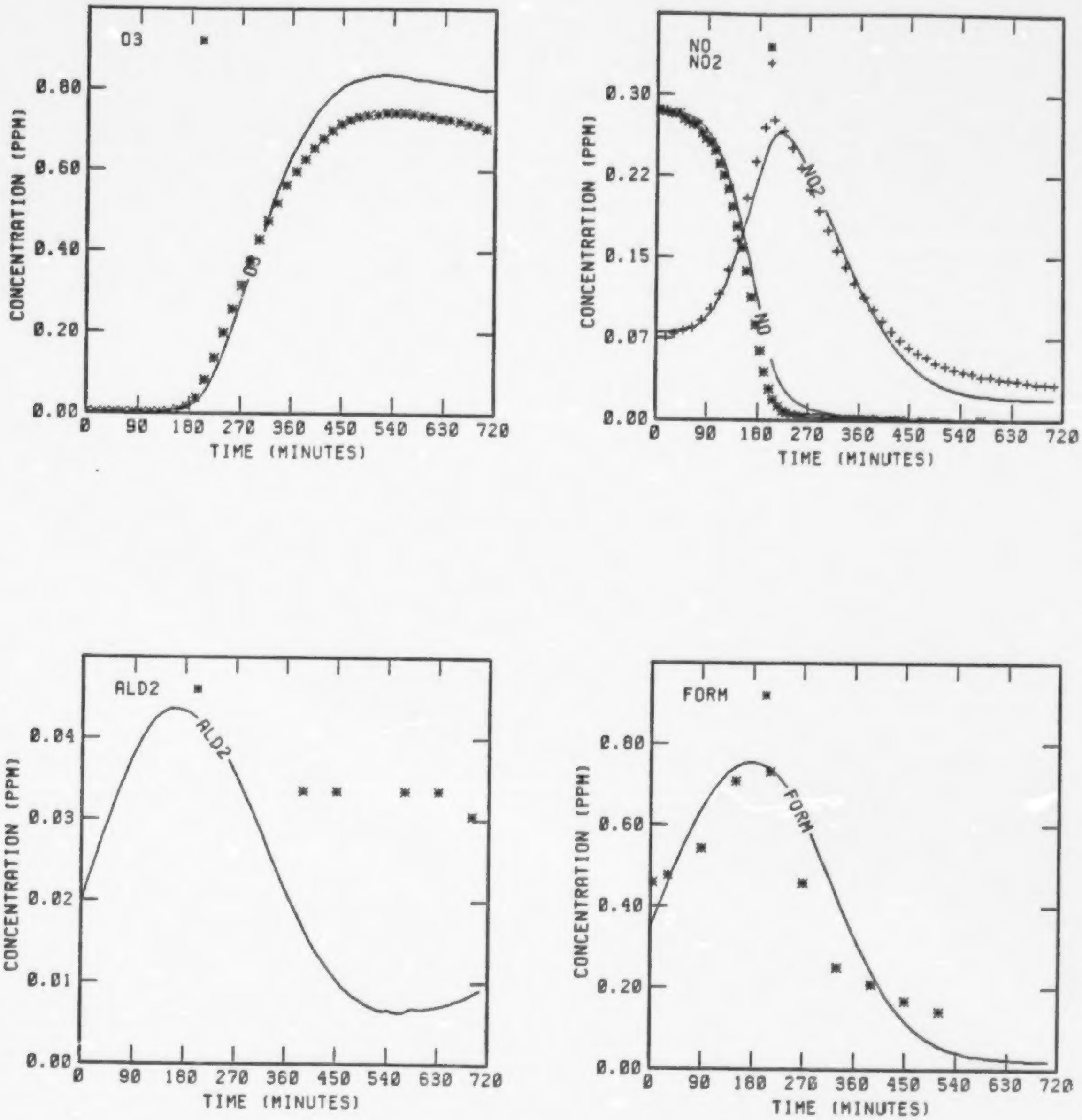

SIMULATION RESULTS FOR
UNCB 51877

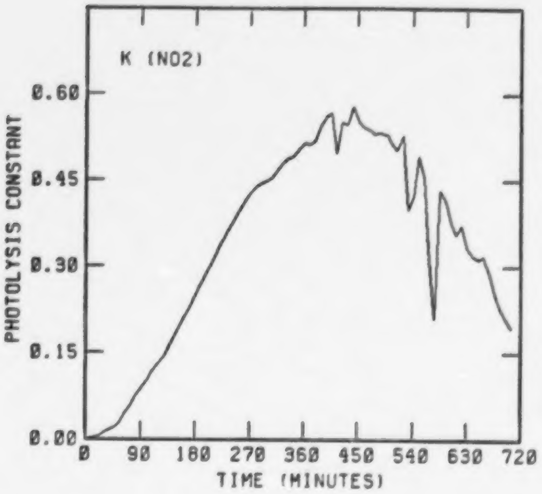

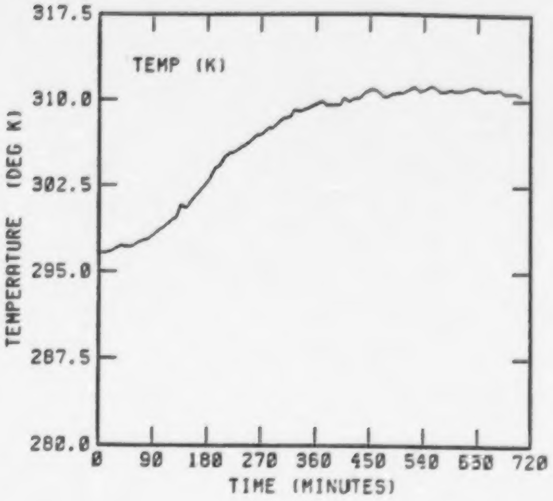

SIMULATION RESULTS FOR
UNCB 51877

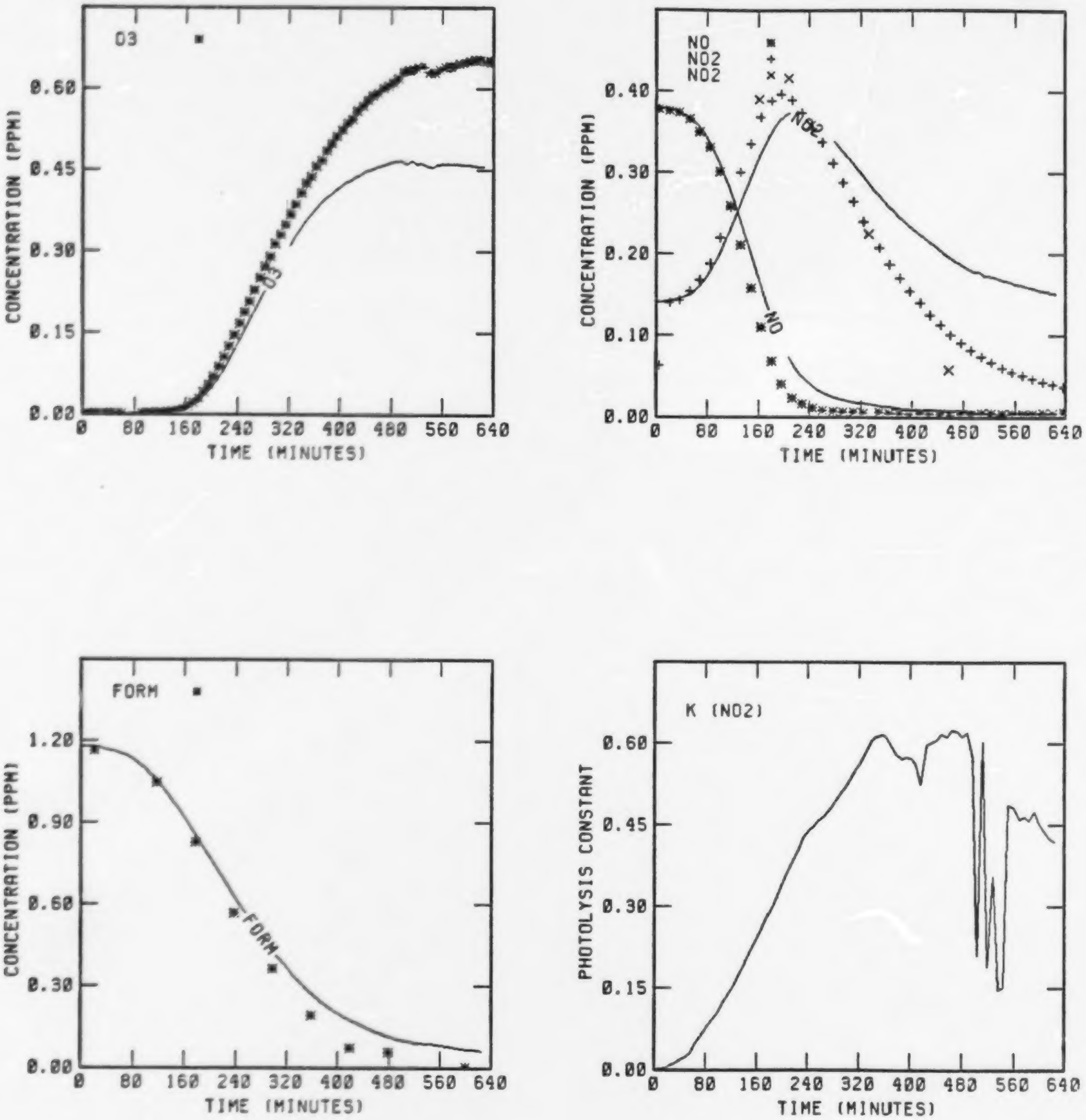

SIMULATION RESULTS FOR
UNCR 71877

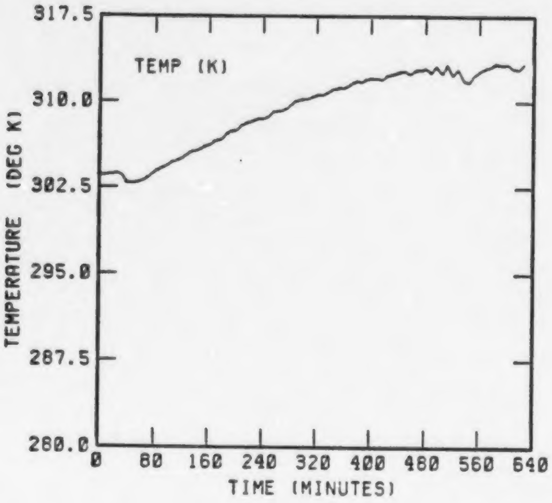

SIMULATION RESULTS FOR
UNCR 71877

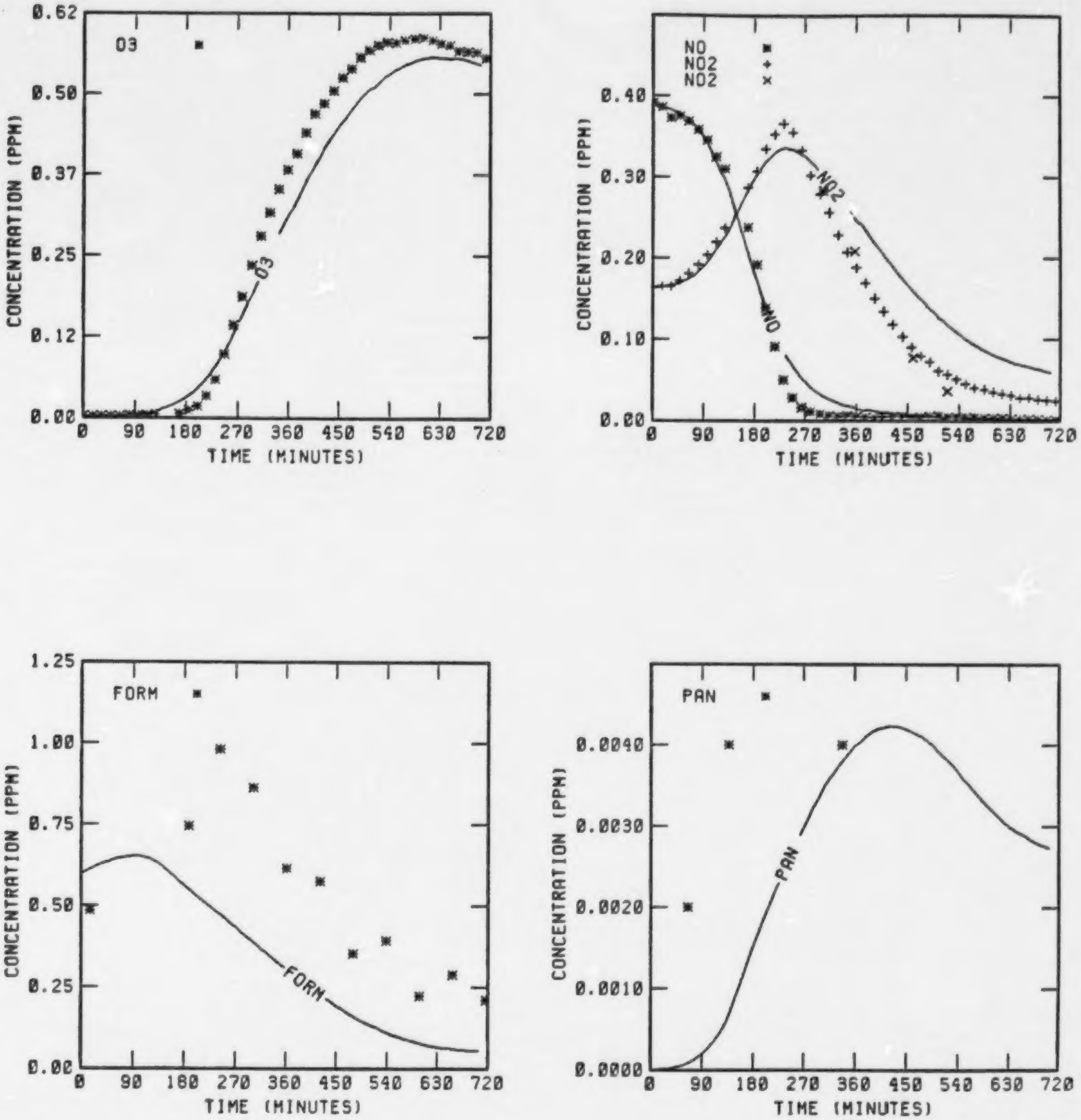

SIMULATION RESULTS FOR
UNCR 72777

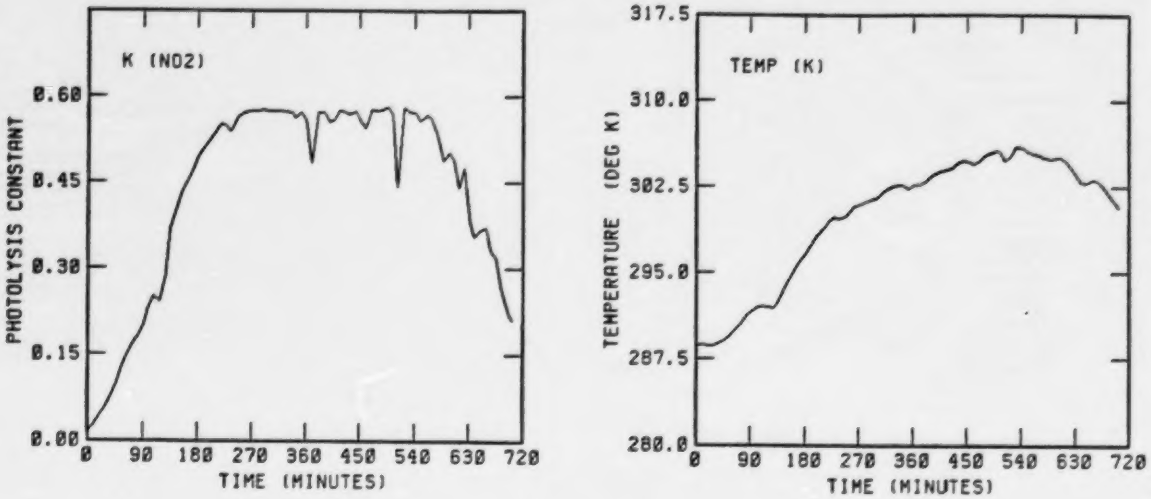

SIMULATION RESULTS FOR
UNCR 72777

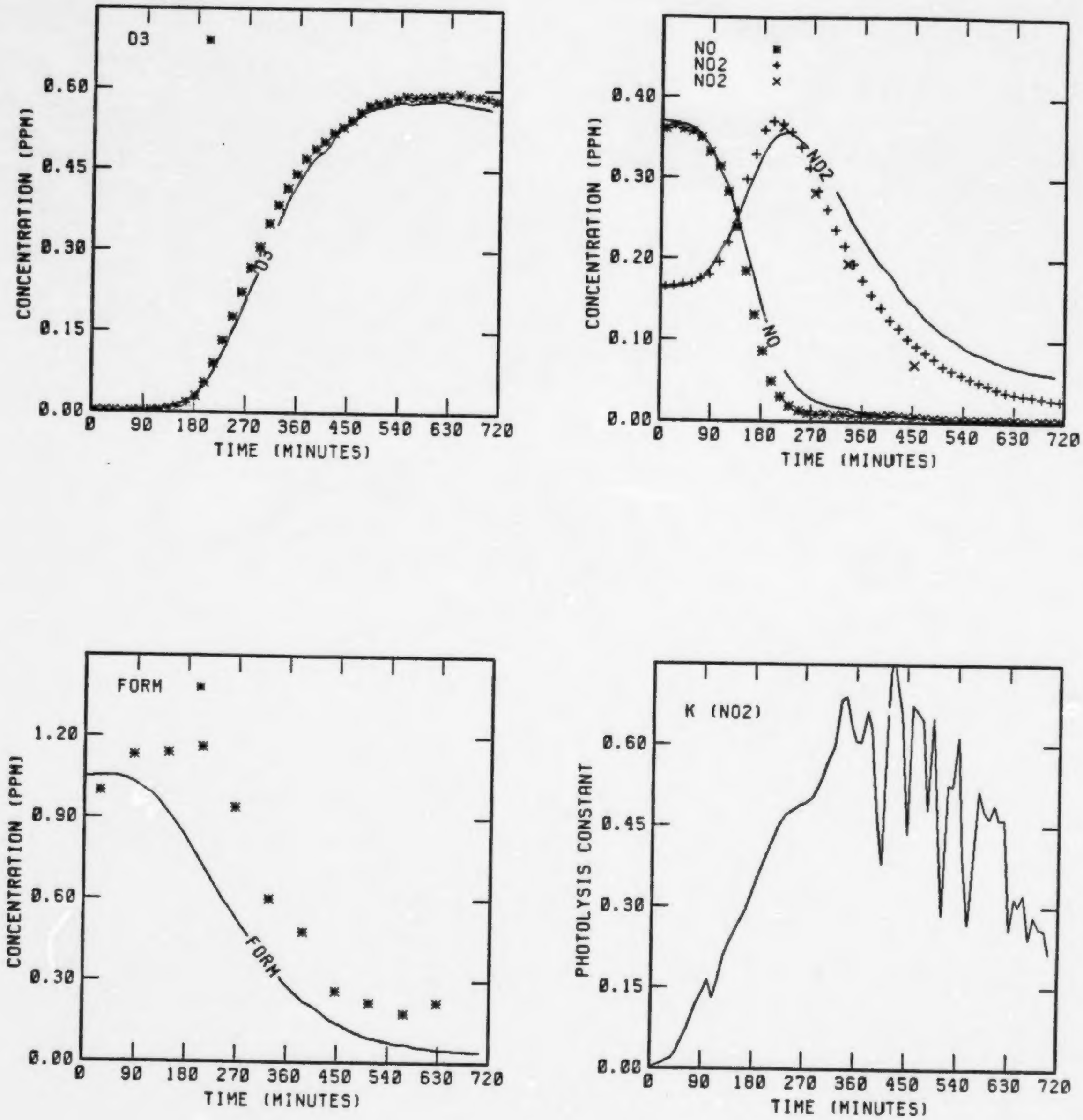

SIMULATION RESULTS FOR
UNCR 72877

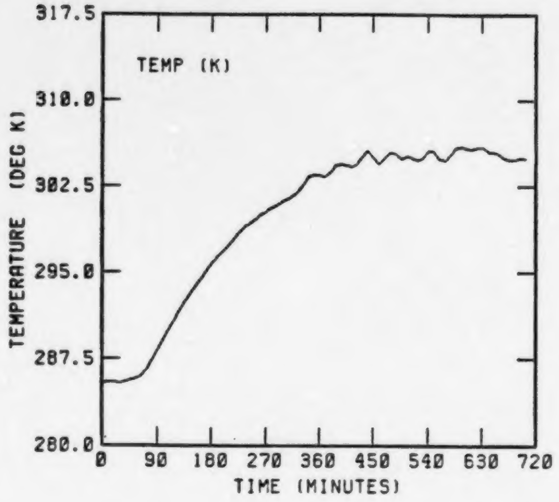

SIMULATION RESULTS FOR
UNCR 72877

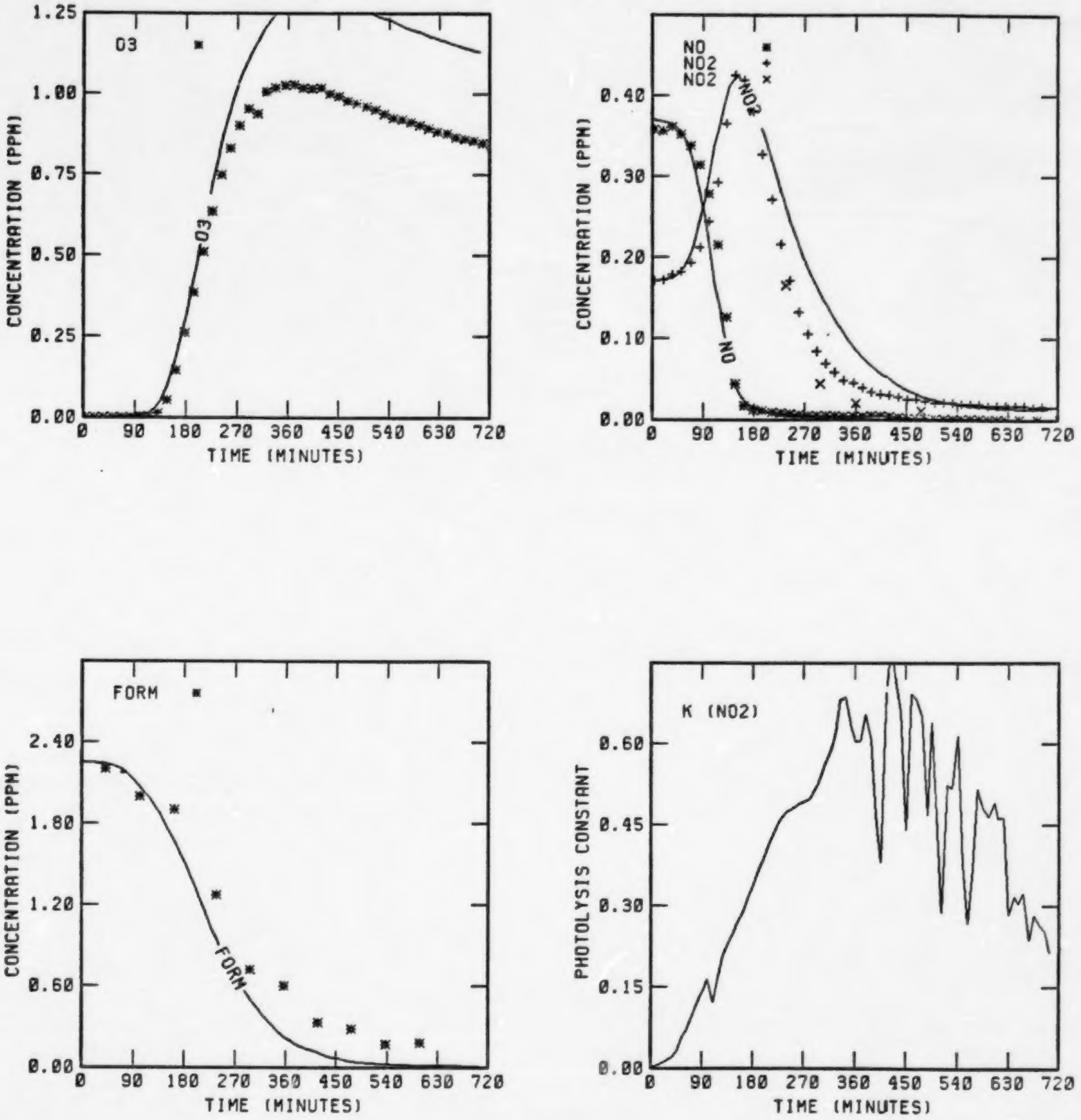

SIMULATION RESULTS FOR
UNCB 72877

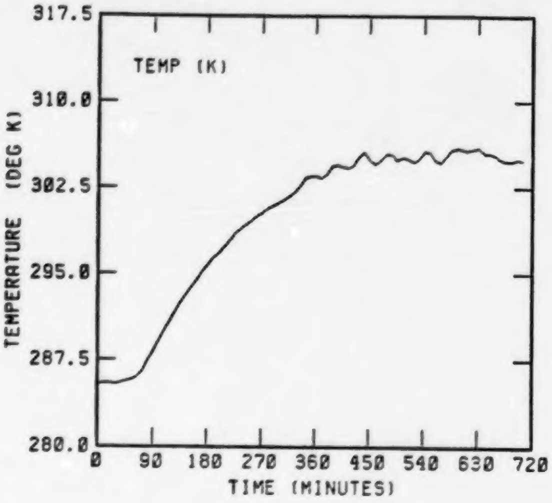

SIMULATION RESULTS FOR
UNCB 72877

Appendix B

SIMULATION RESULTS FOR THE UNC ACETALDEHYDE EXPERIMENTS

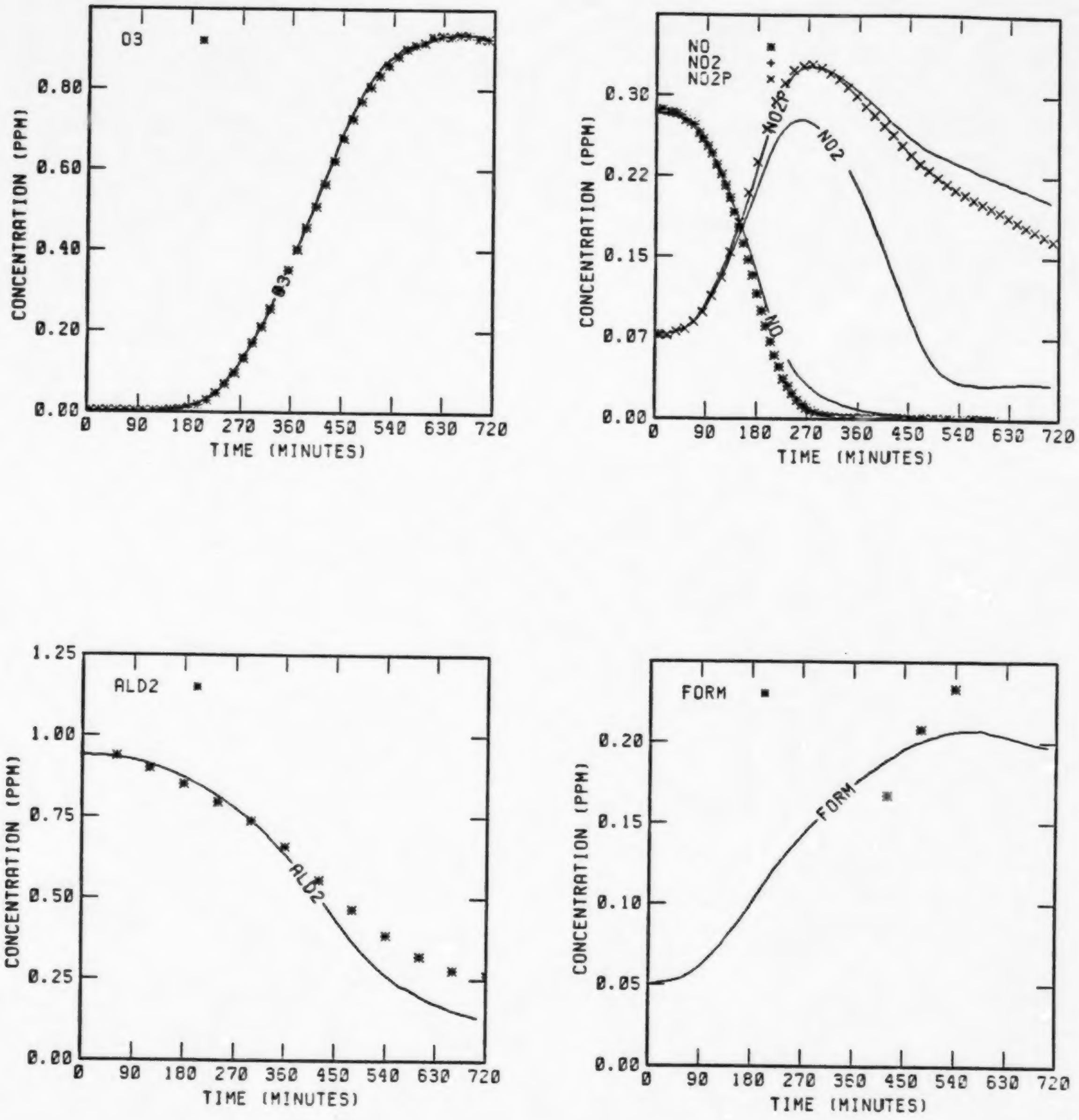

SIMULATION RESULTS FOR
UNCR 51877

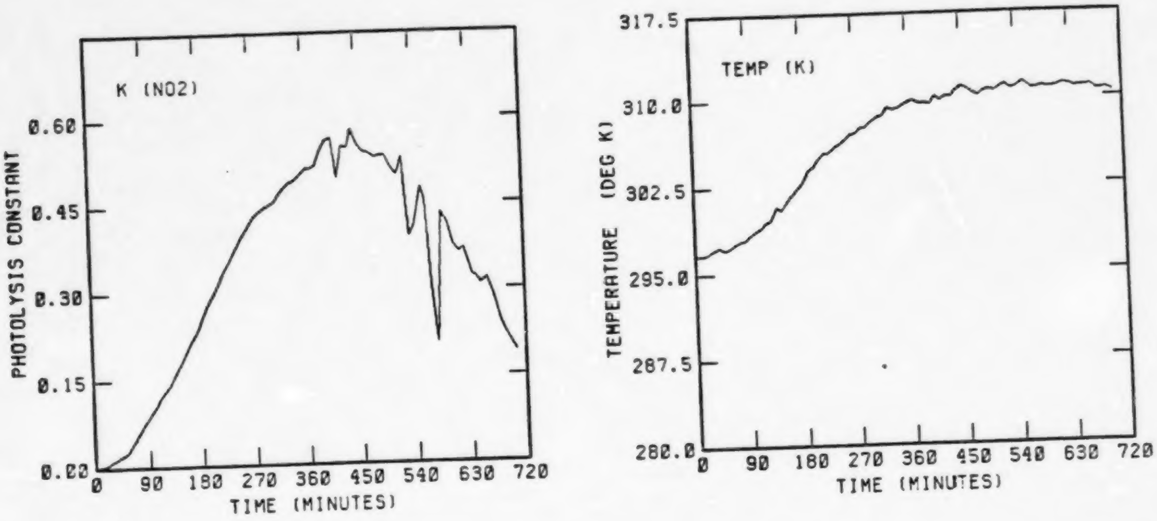

SIMULATION RESULTS FOR
UNCR 51877

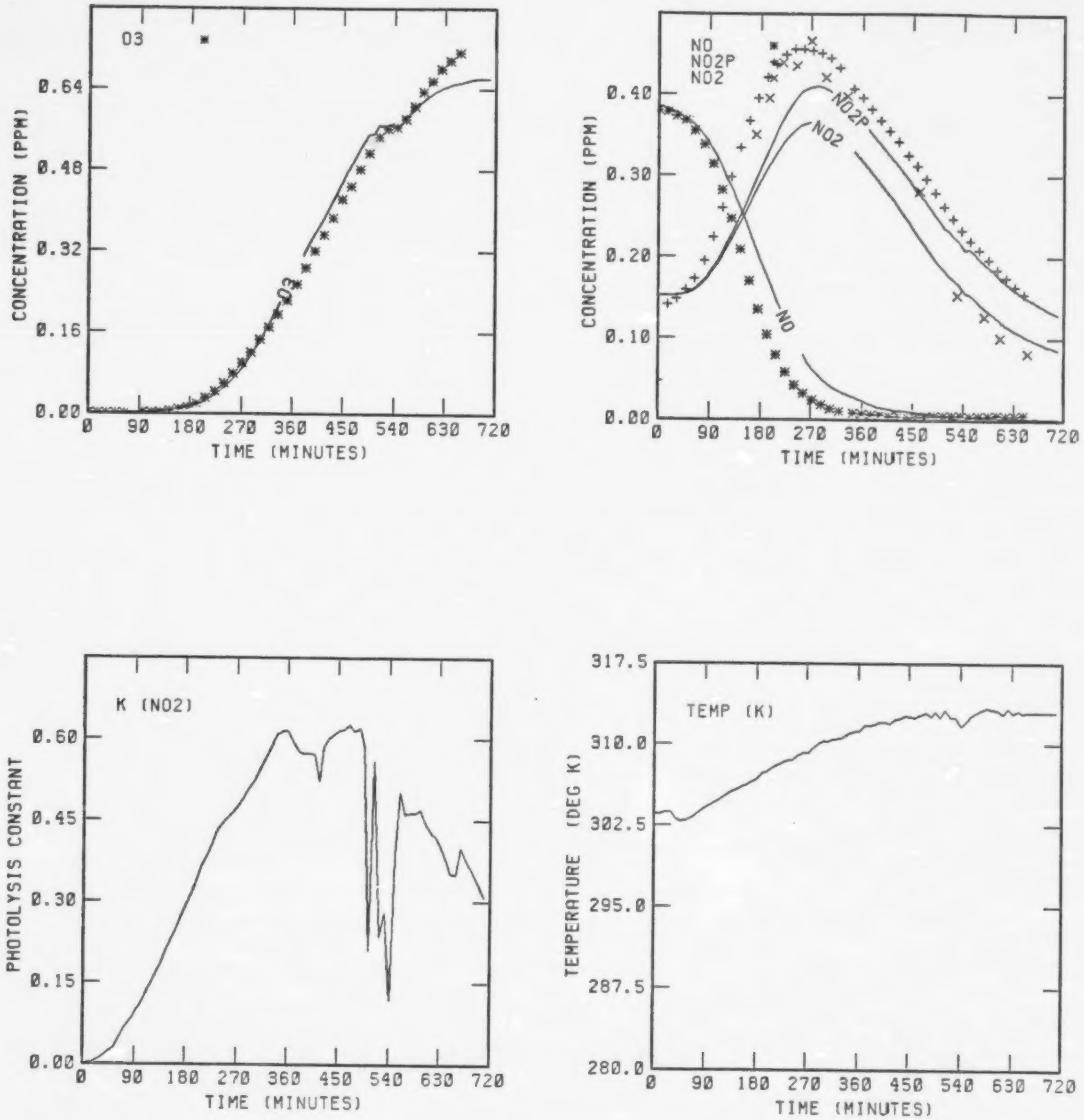

SIMULATION RESULTS FOR
UNCB 71877

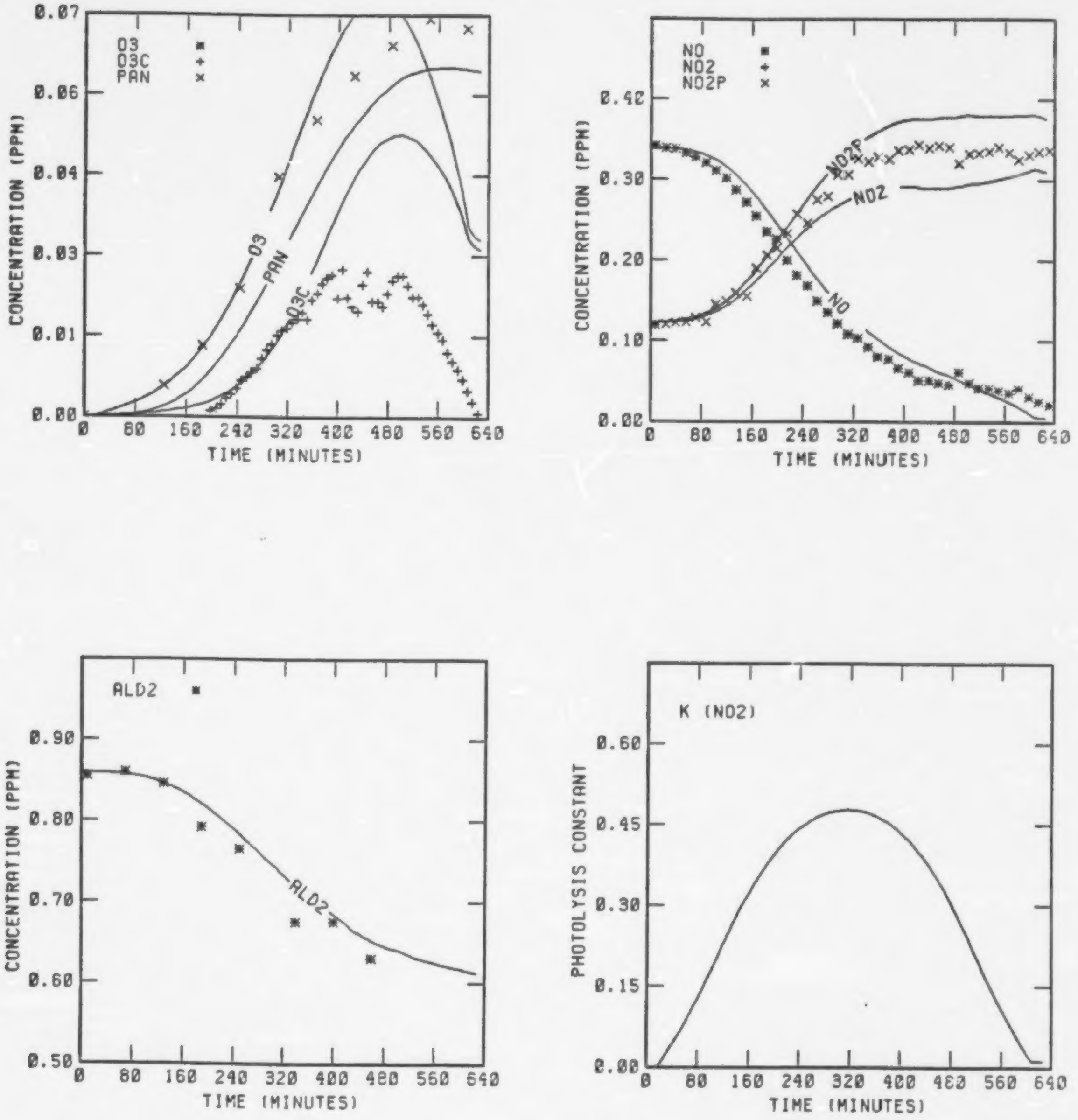

SIMULATION RESULTS FOR
UNCB 111277

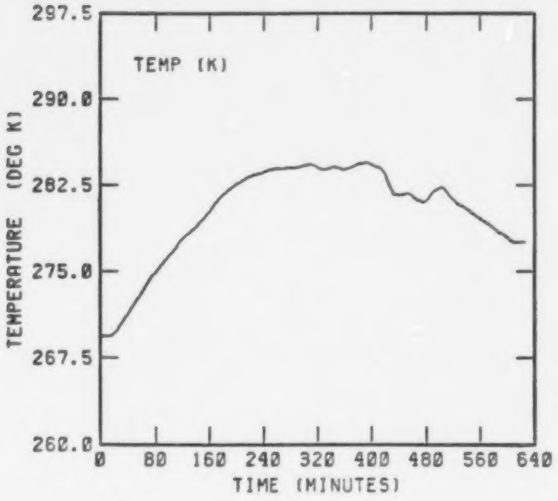

SIMULATION RESULTS FOR
UNCB 111277

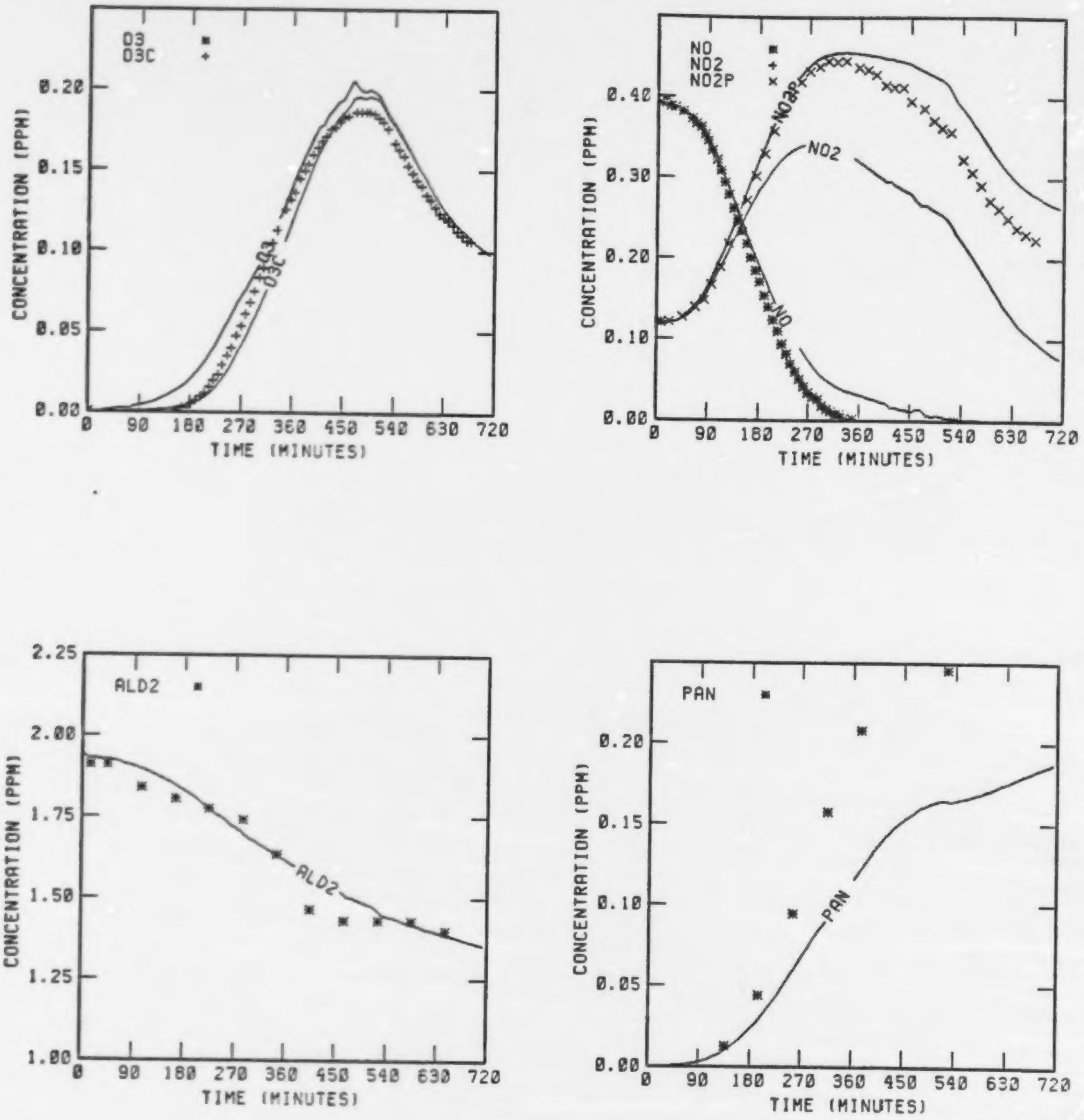

SIMULATION RESULTS FOR
UNCB 111977

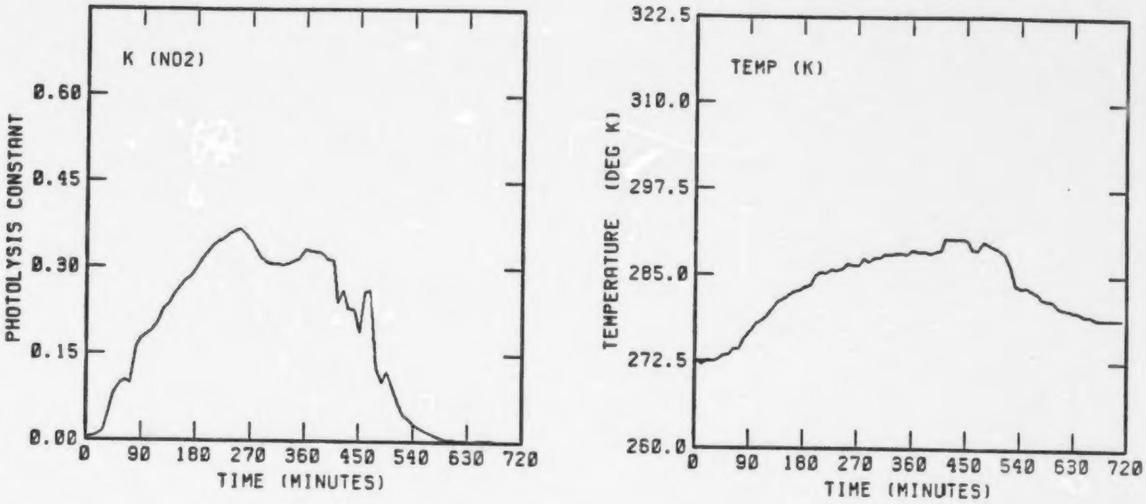

SIMULATION RESULTS FOR
UNCB 111977

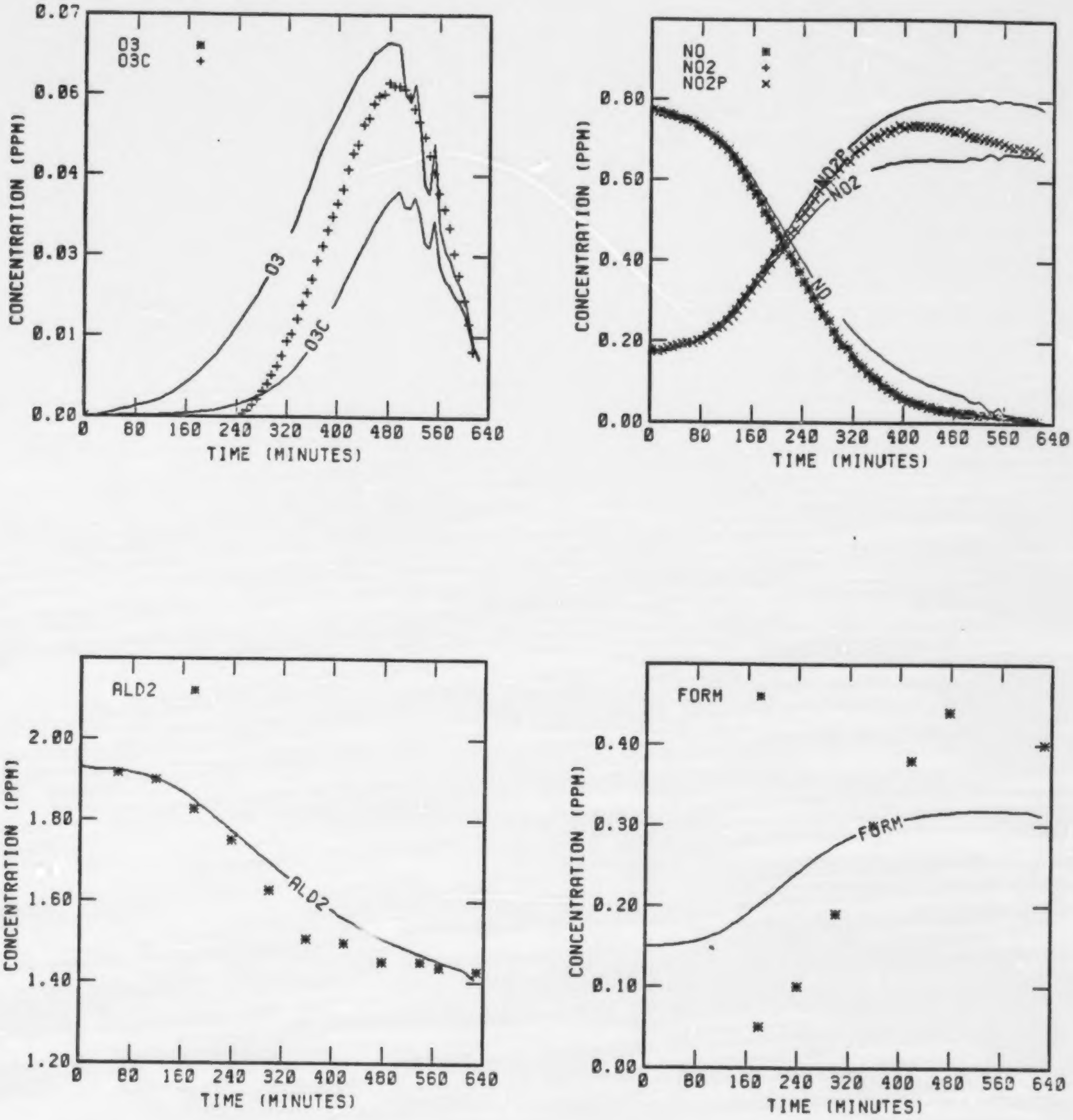

SIMULATION RESULTS FOR
UNCB 112077

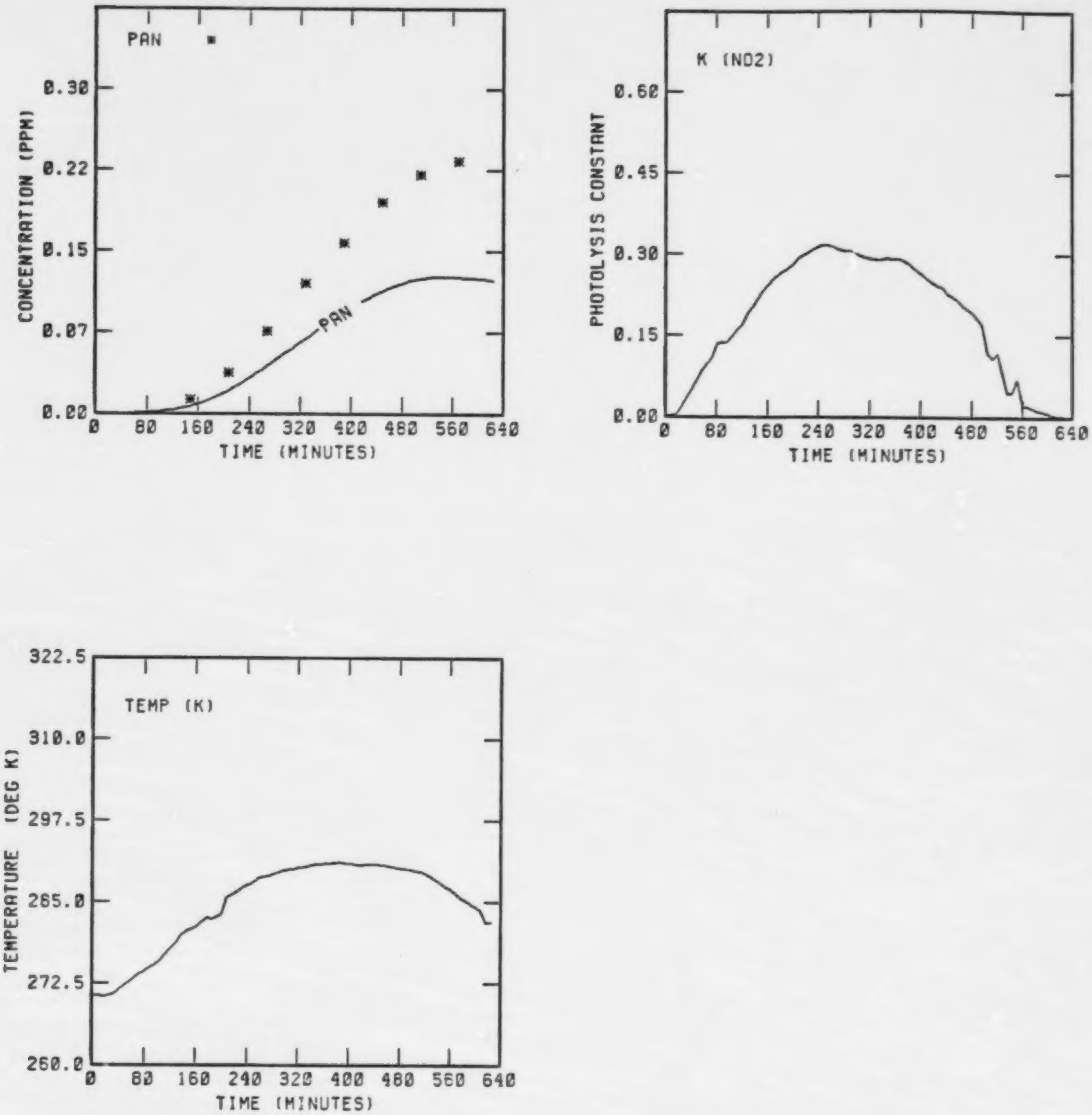

SIMULATION RESULTS FOR
UNCB 112077

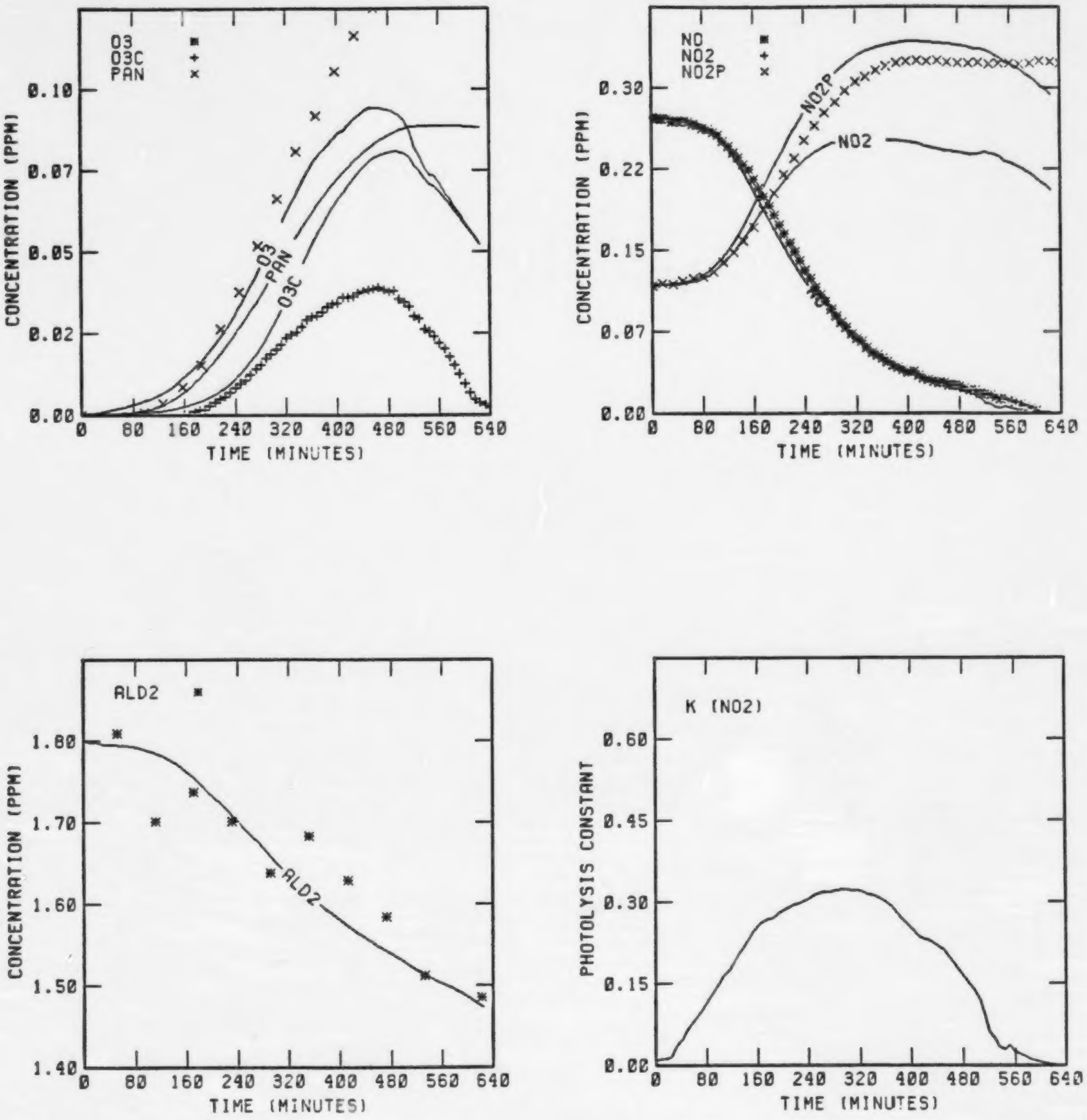

SIMULATION RESULTS FOR
UNCB 122677

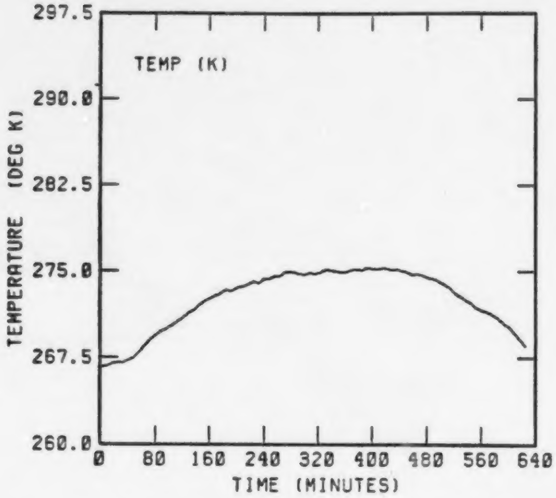

SIMULATION RESULTS FOR
UNCB 122677

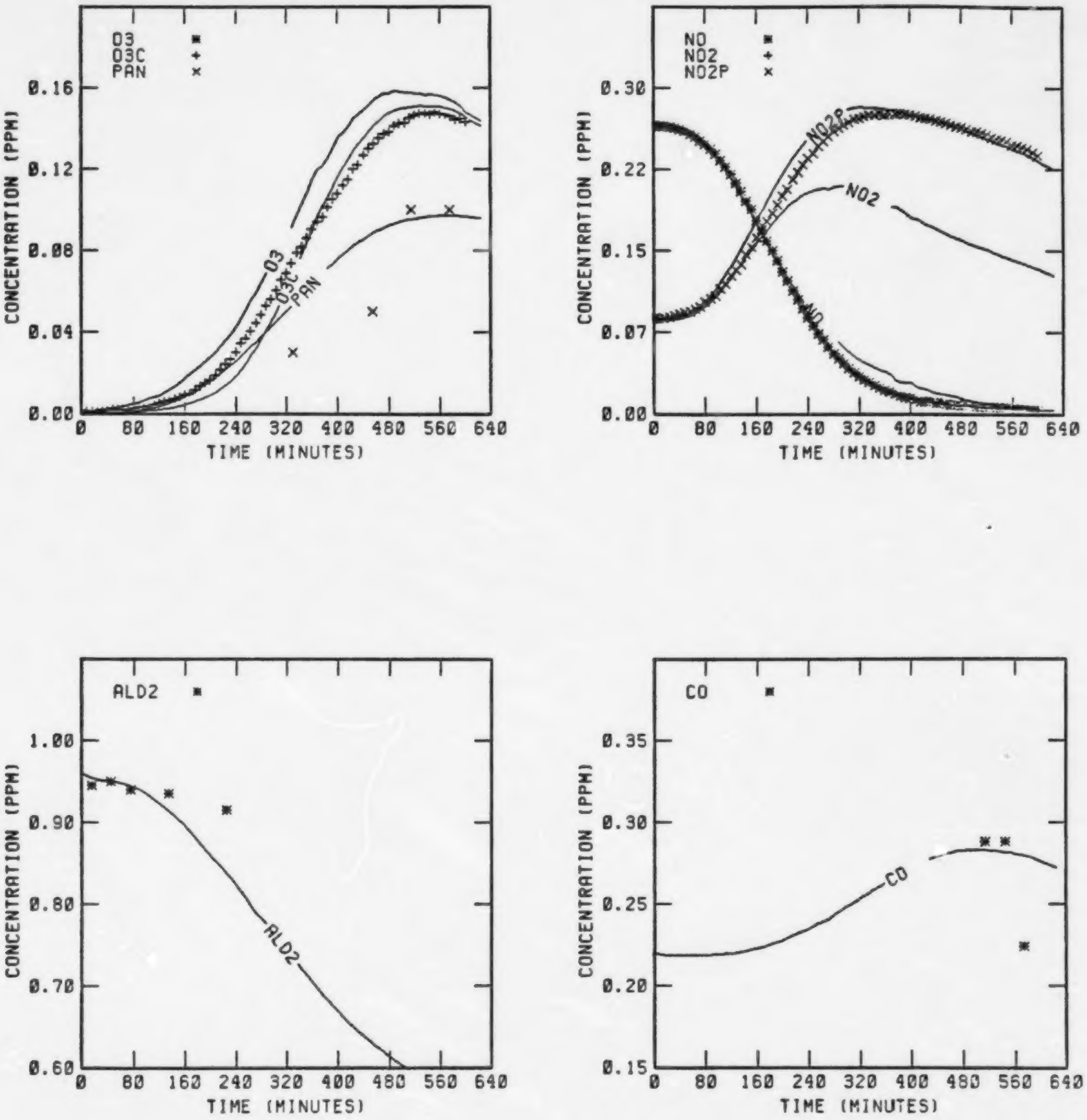

SIMULATION RESULTS FOR
UNCB 22778

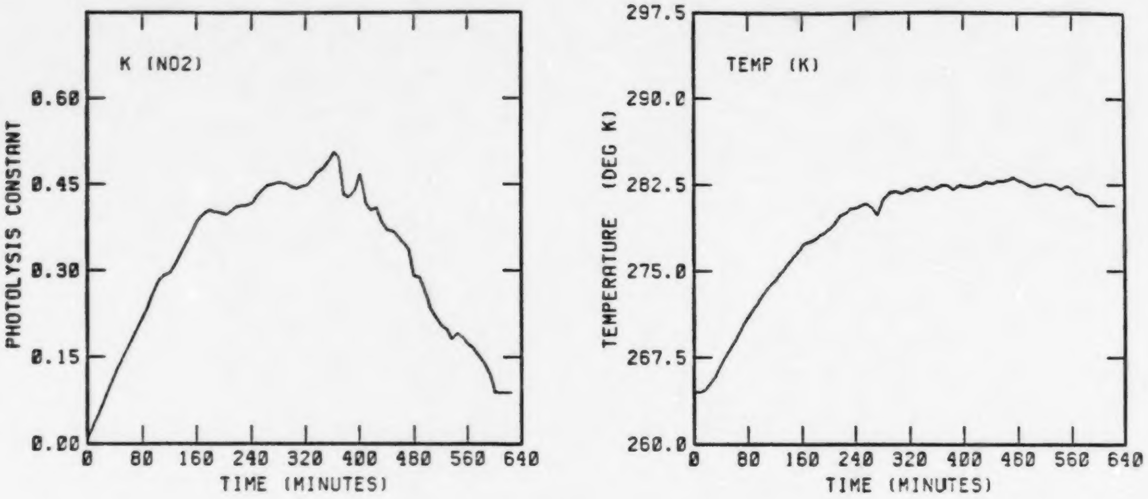

SIMULATION RESULTS FOR
UNCB 22778

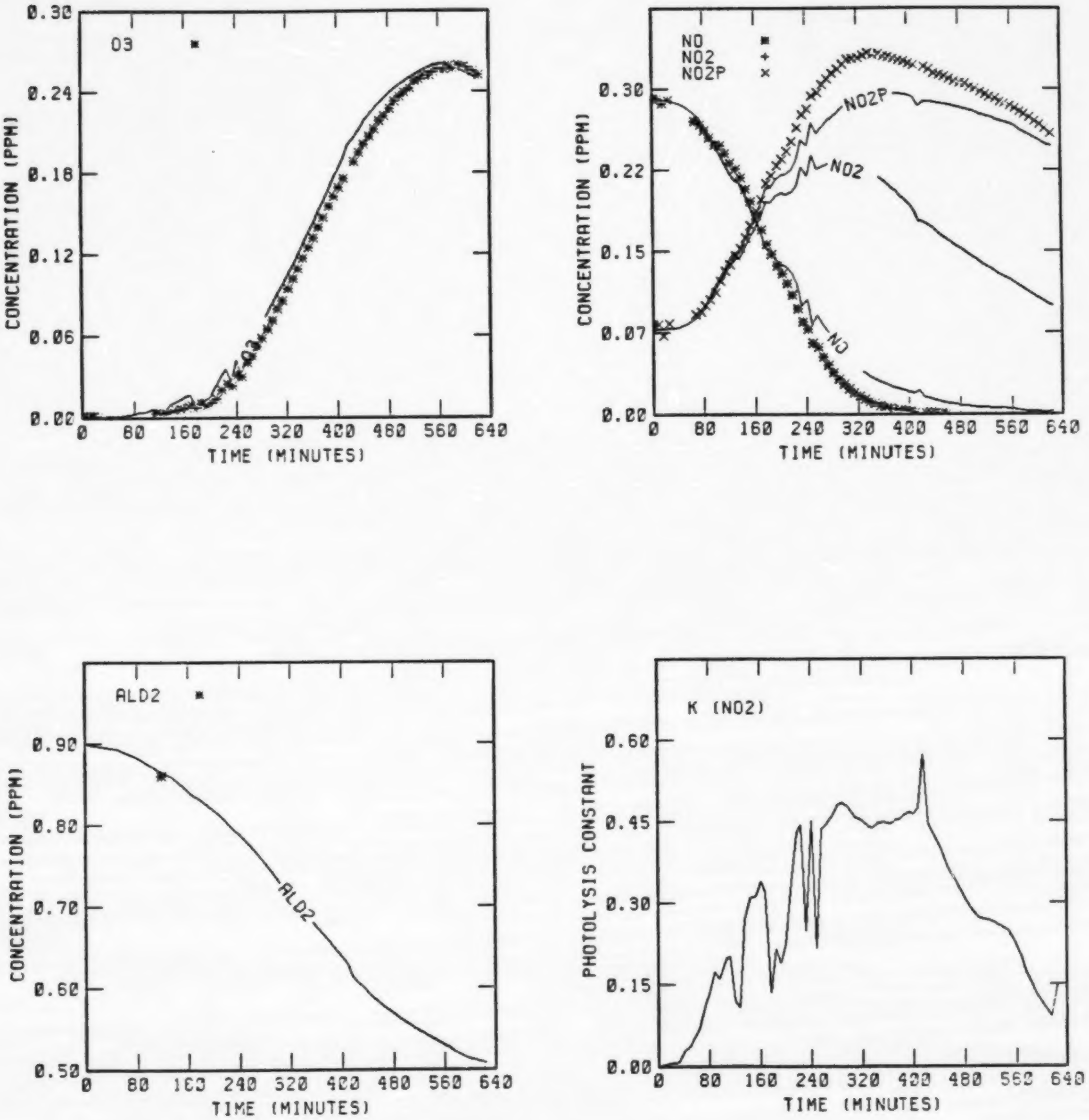

SIMULATION RESULTS FOR
UNCB 30678

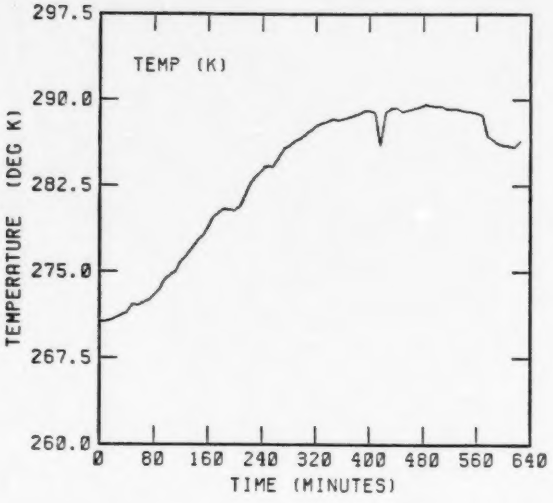

SIMULATION RESULTS FOR
UNCB 30678

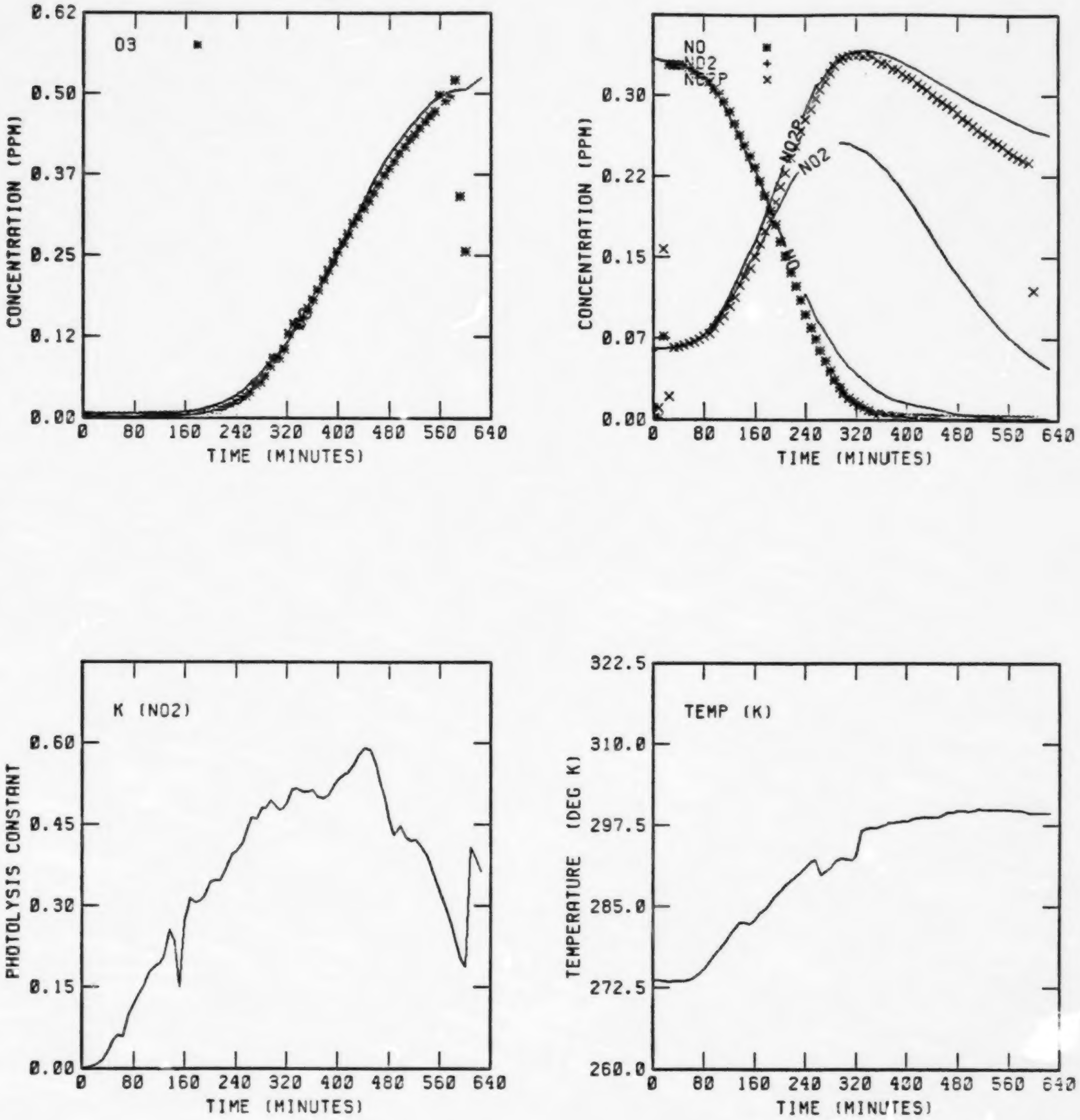

SIMULATION RESULTS FOR
UNCB 33178

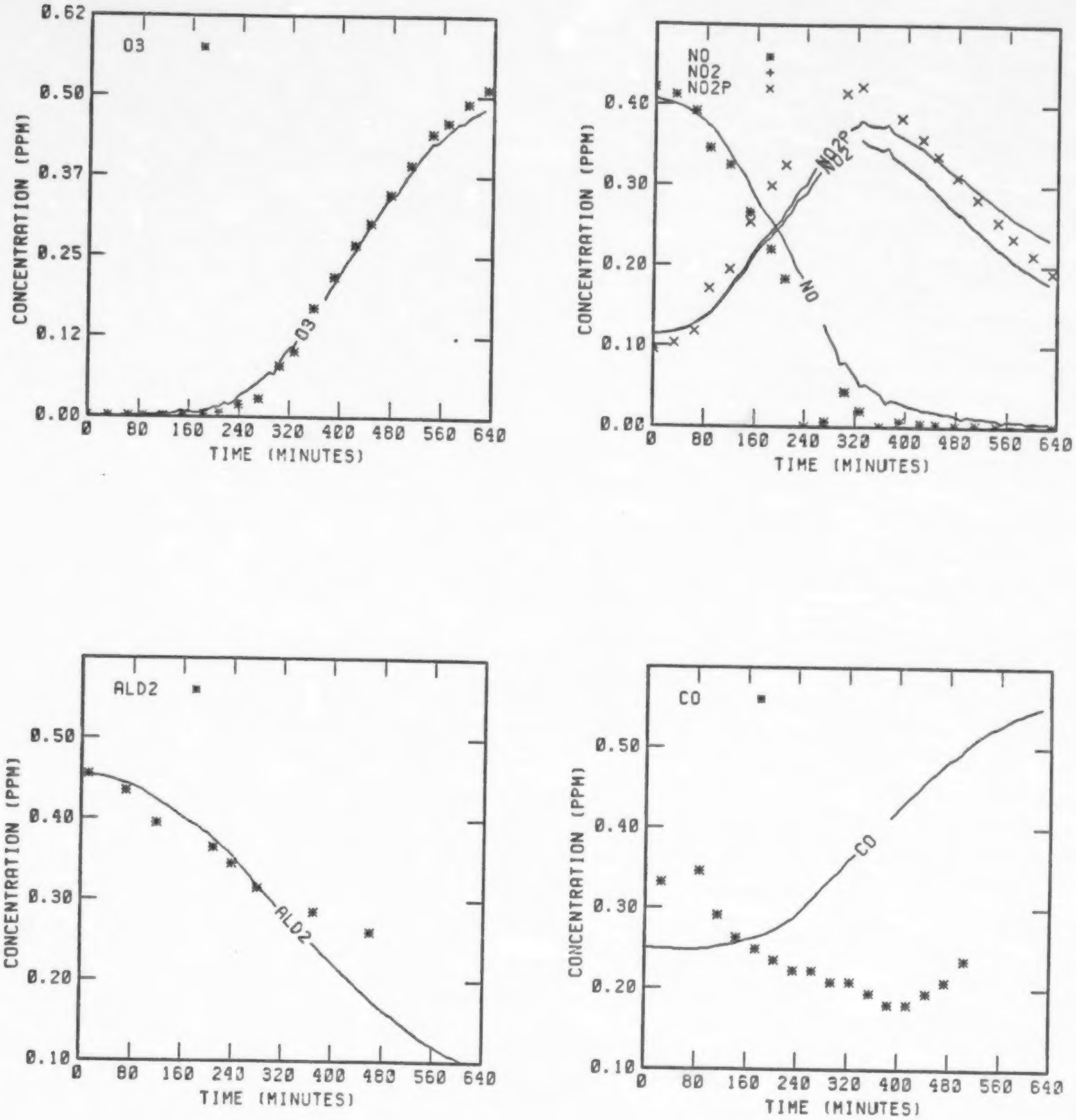

SIMULATION RESULTS FOR
UNCR 80878

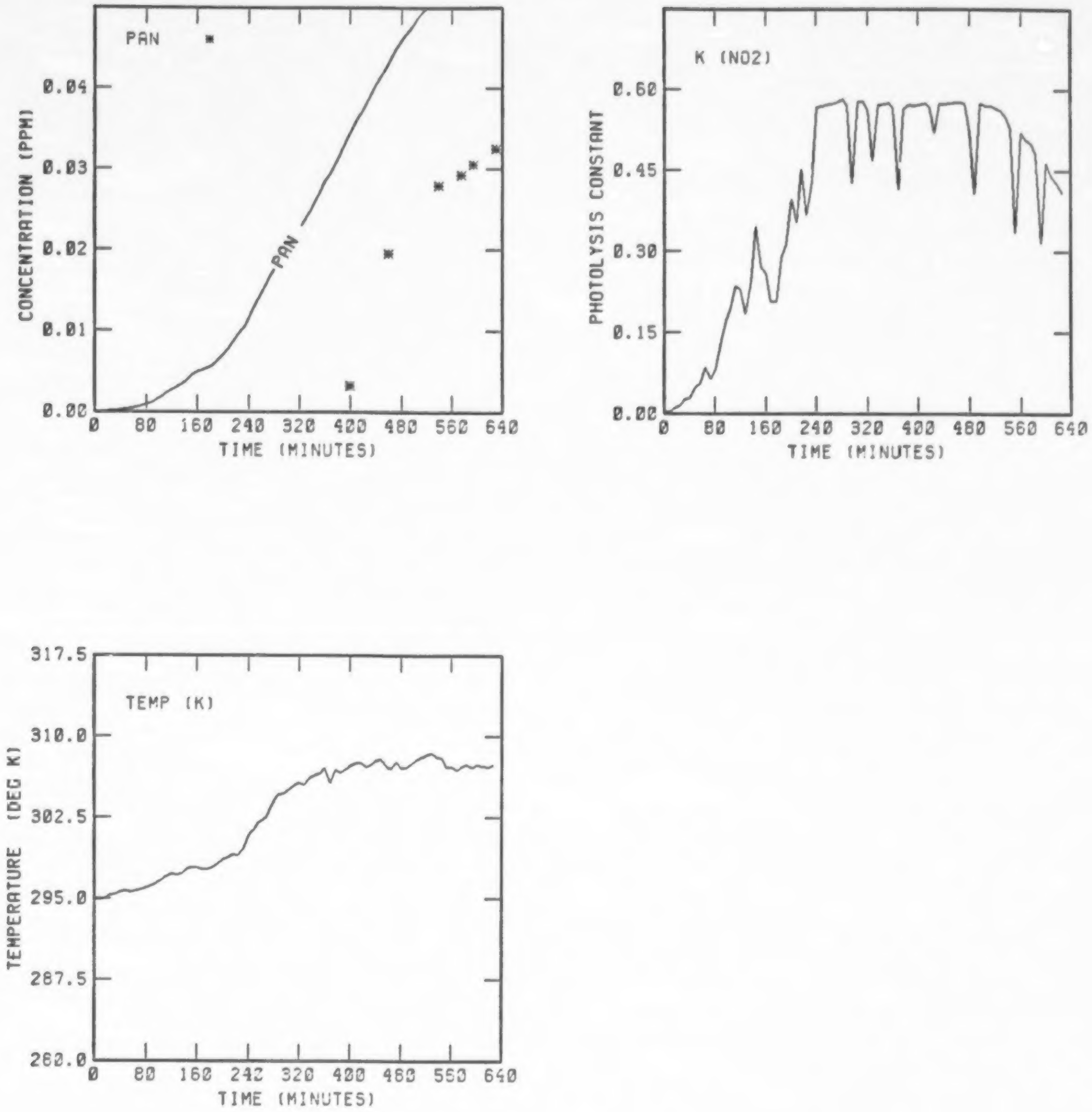

SIMULATION RESULTS FOR
UNCR 80878

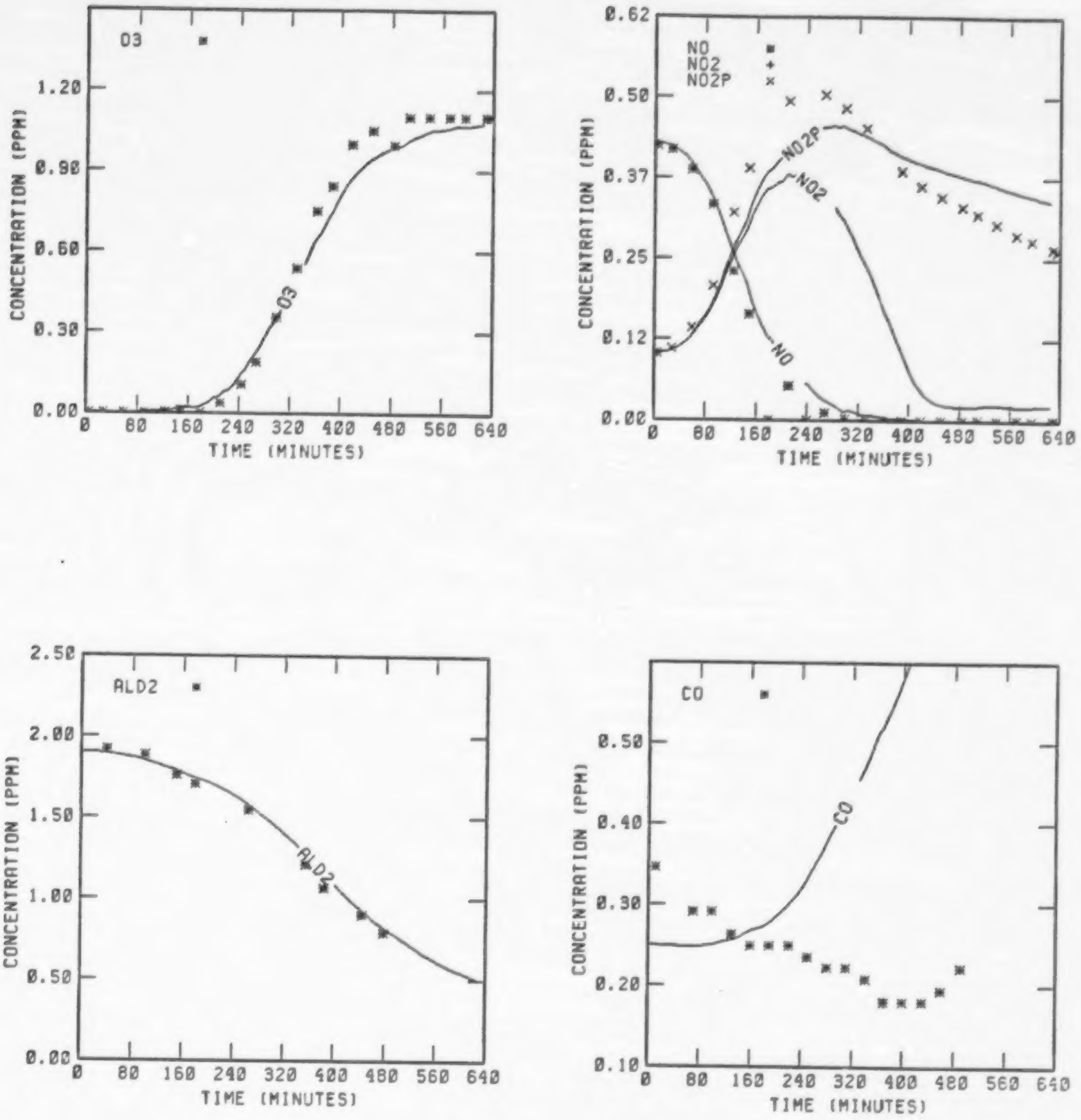

SIMULATION RESULTS FOR
UNCB 80878

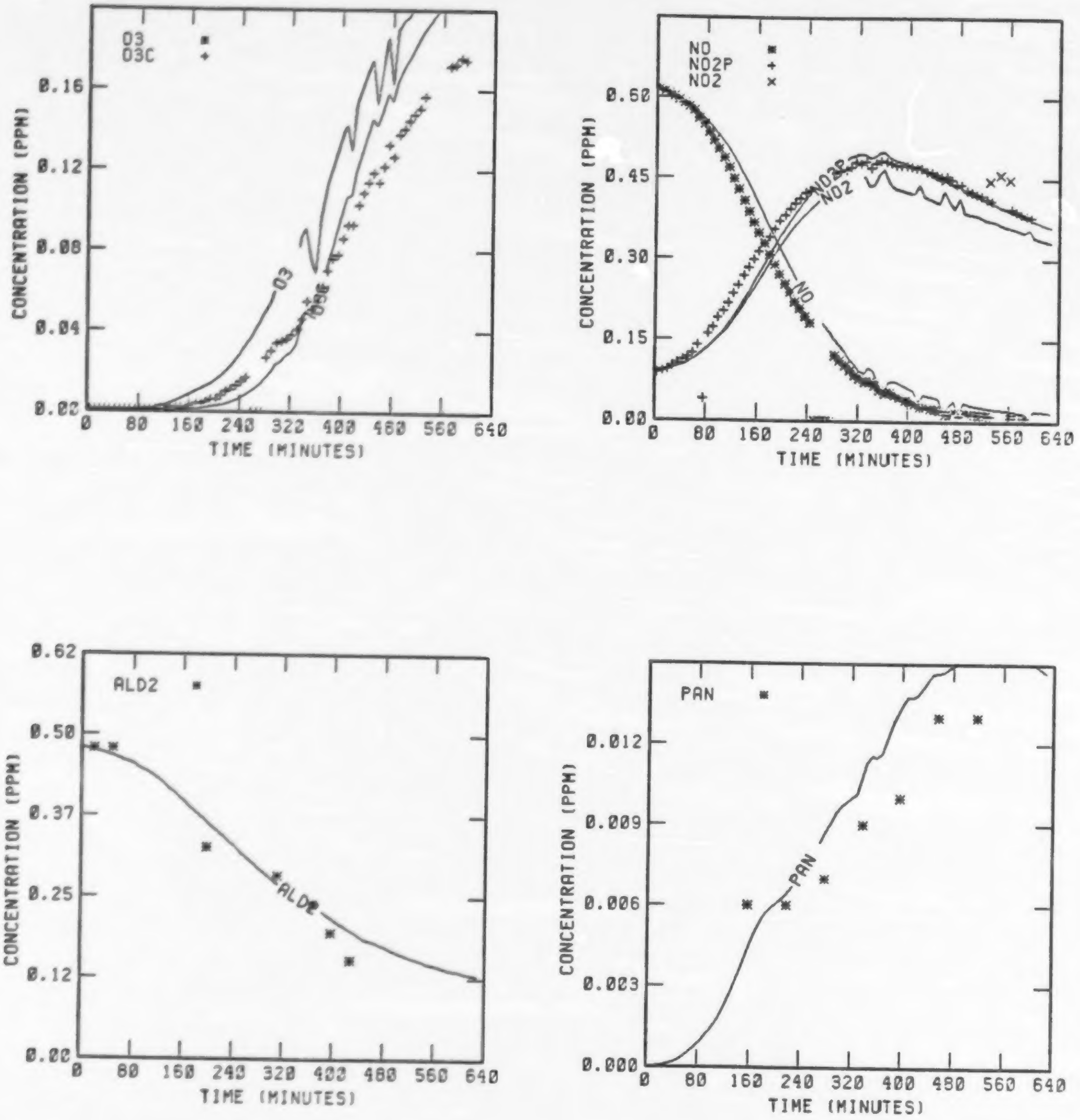

SIMULATION RESULTS FOR
UNCR 81778

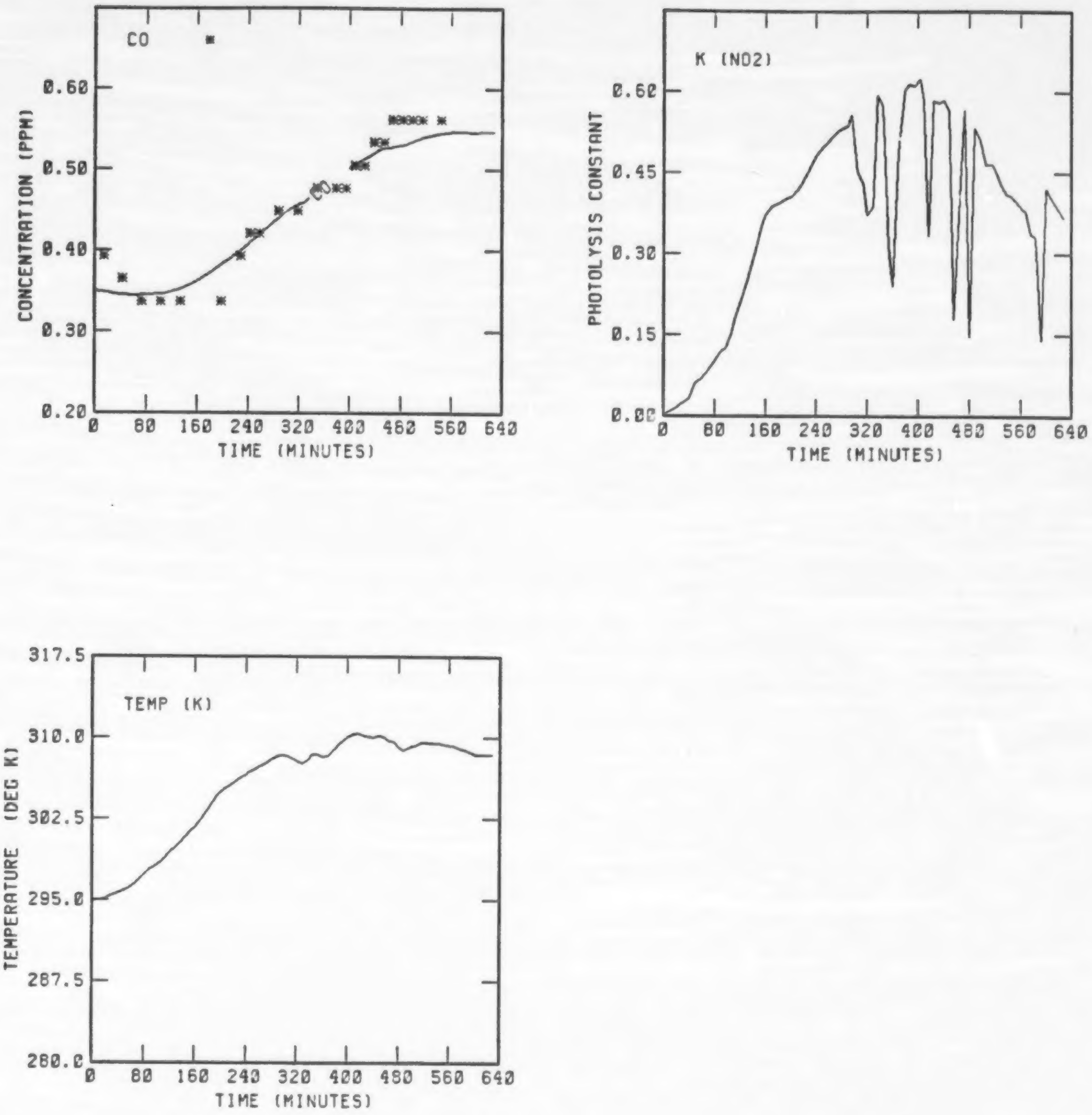

SIMULATION RESULTS FOR
UNCR 81778

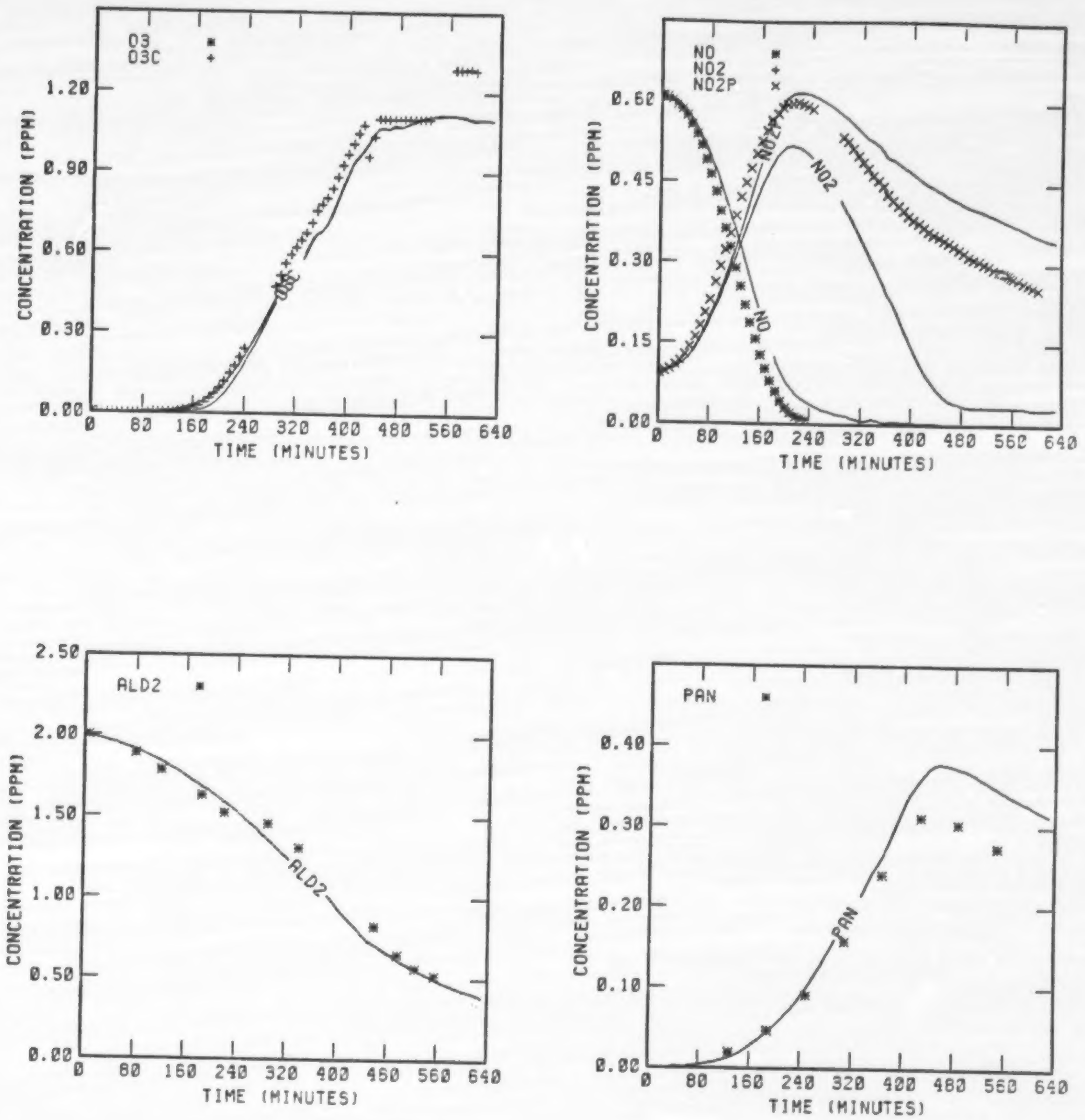

SIMULATION RESULTS FOR
UNCB 81778

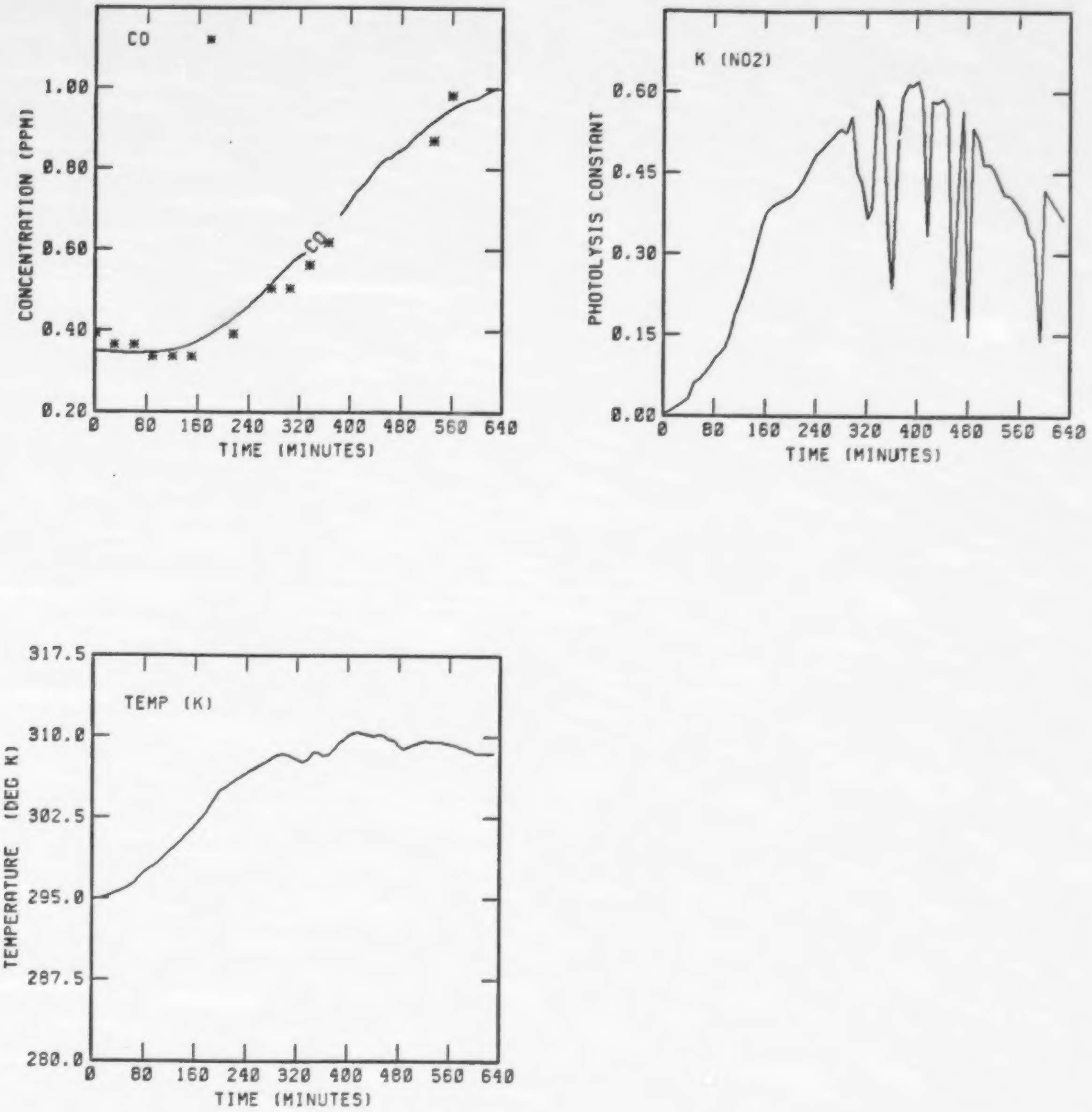

SIMULATION RESULTS FOR
UNCB 81778

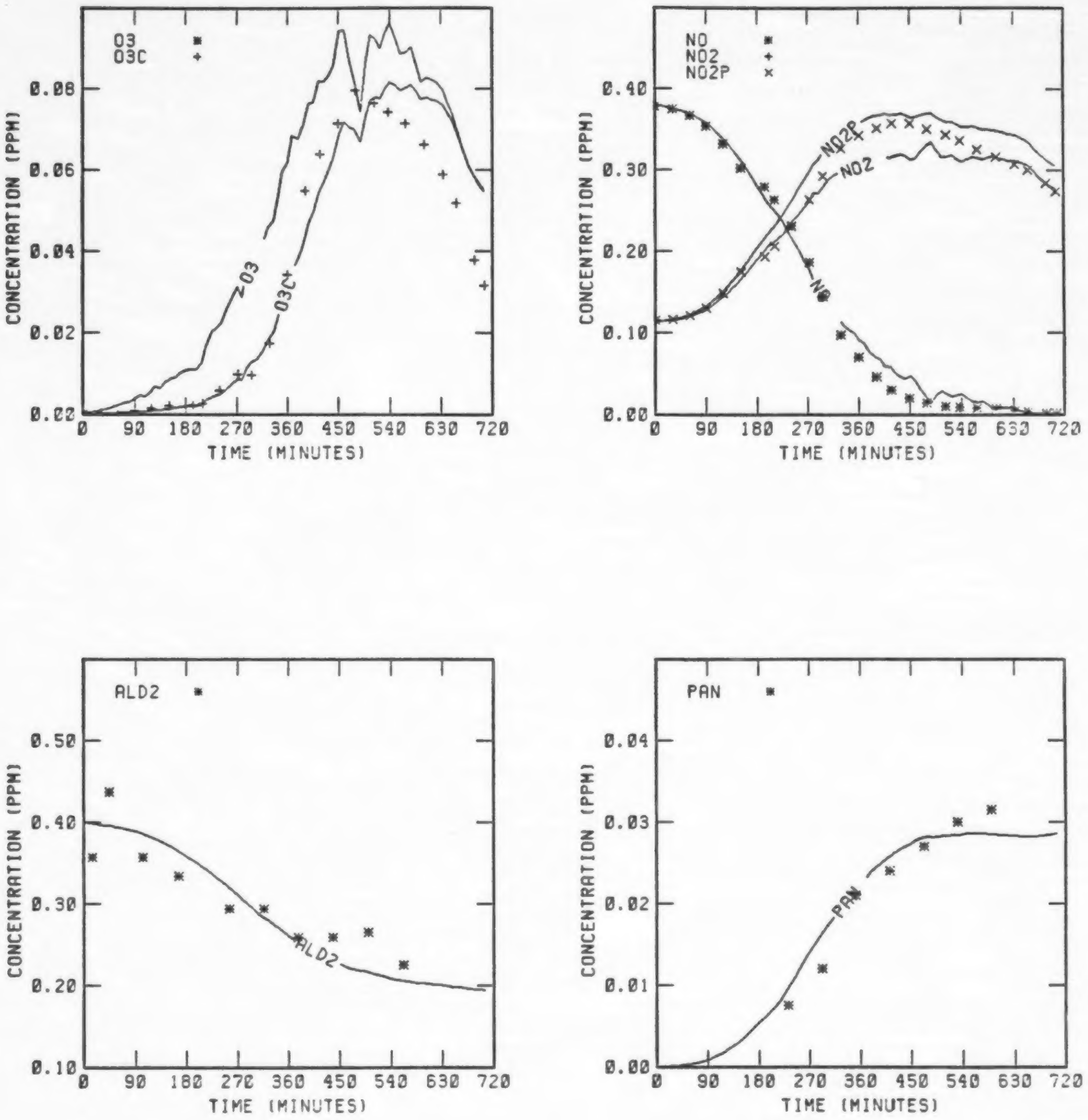

SIMULATION RESULTS FOR
UNCR 101378

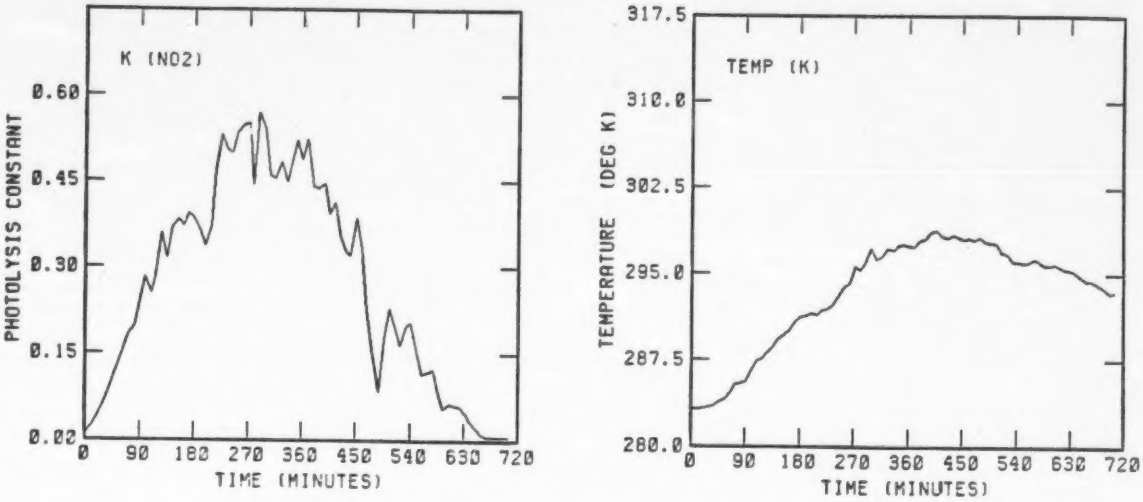

SIMULATION RESULTS FOR
UNCR 101378

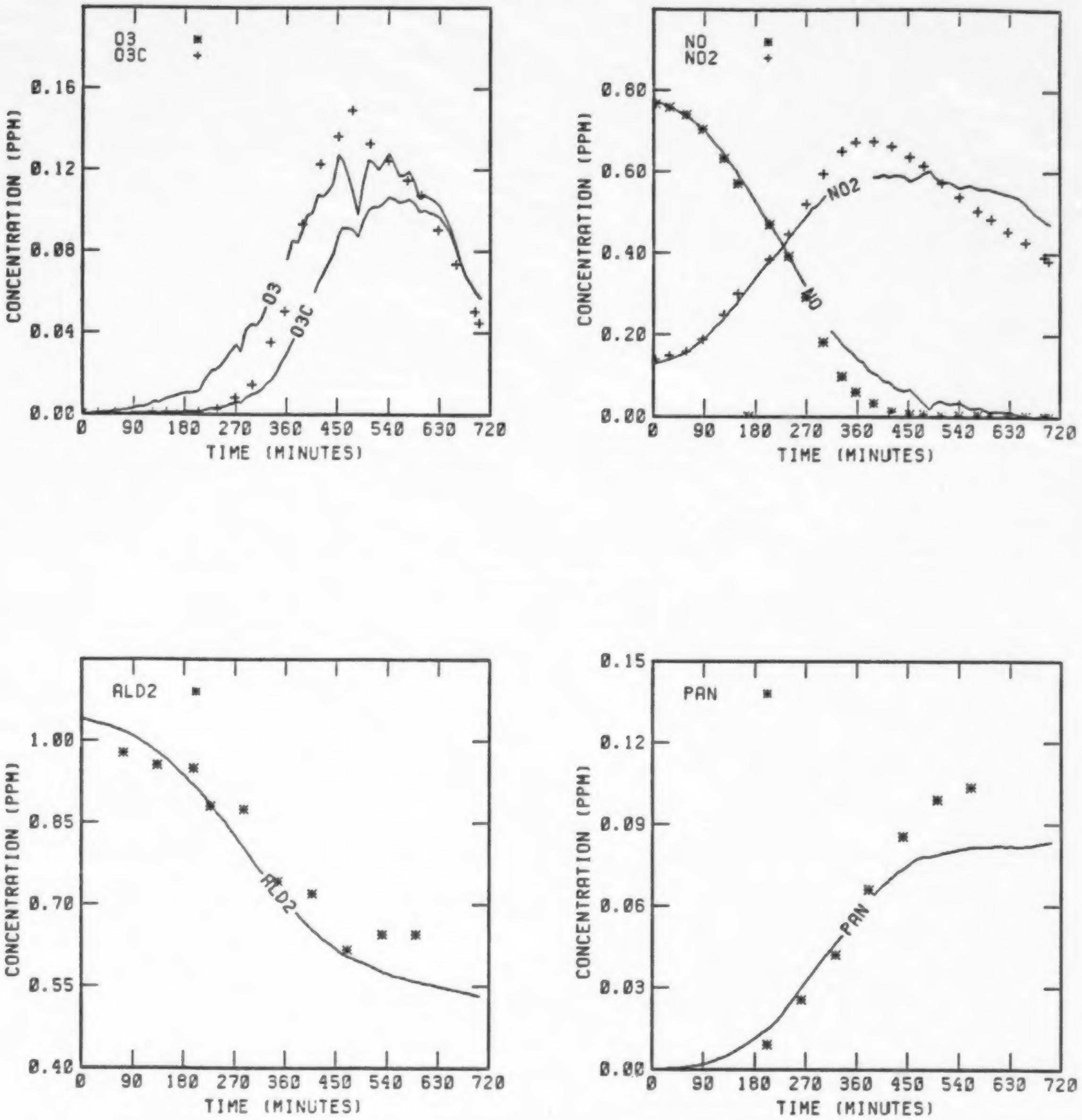

SIMULATION RESULTS FOR
UNCB 101378

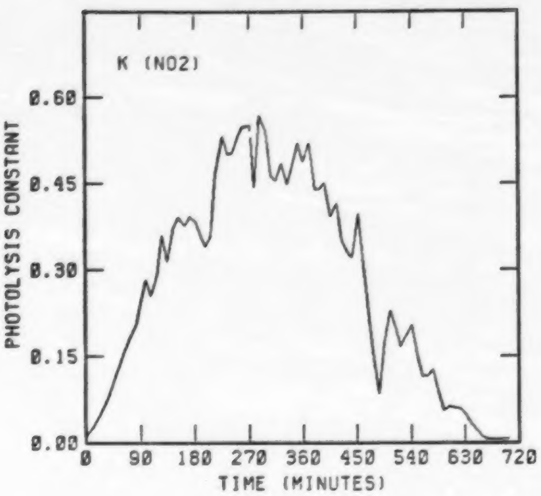

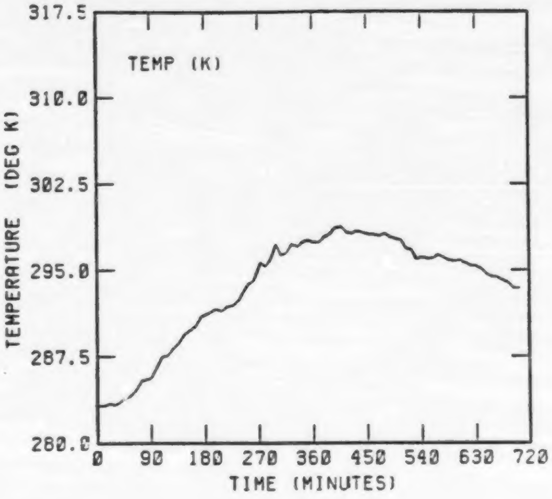

SIMULATION RESULTS FOR
UNCB 101378

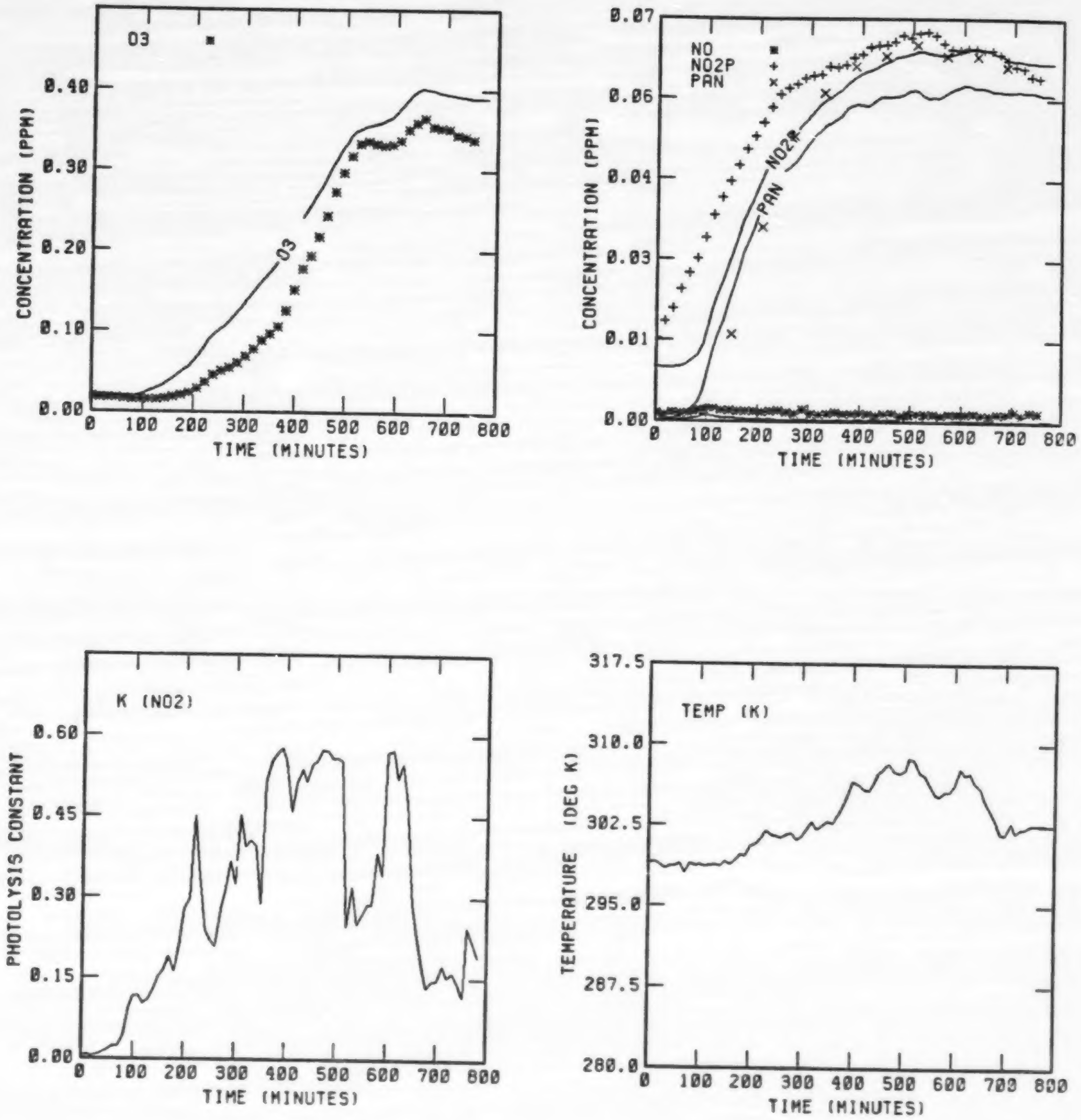

SIMULATION RESULTS FOR
UNCR 72179

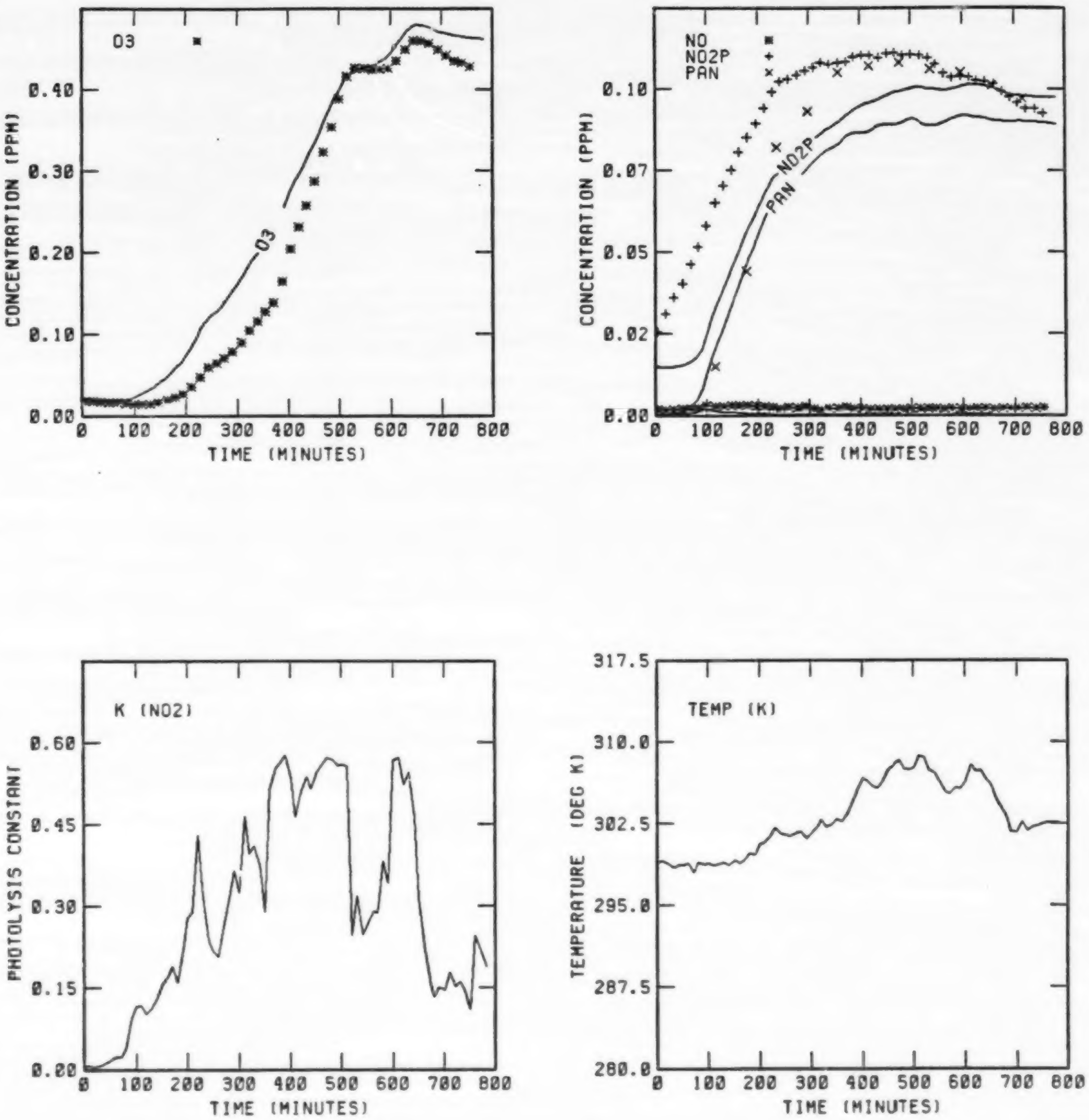

SIMULATION RESULTS FOR
UNCB 72179

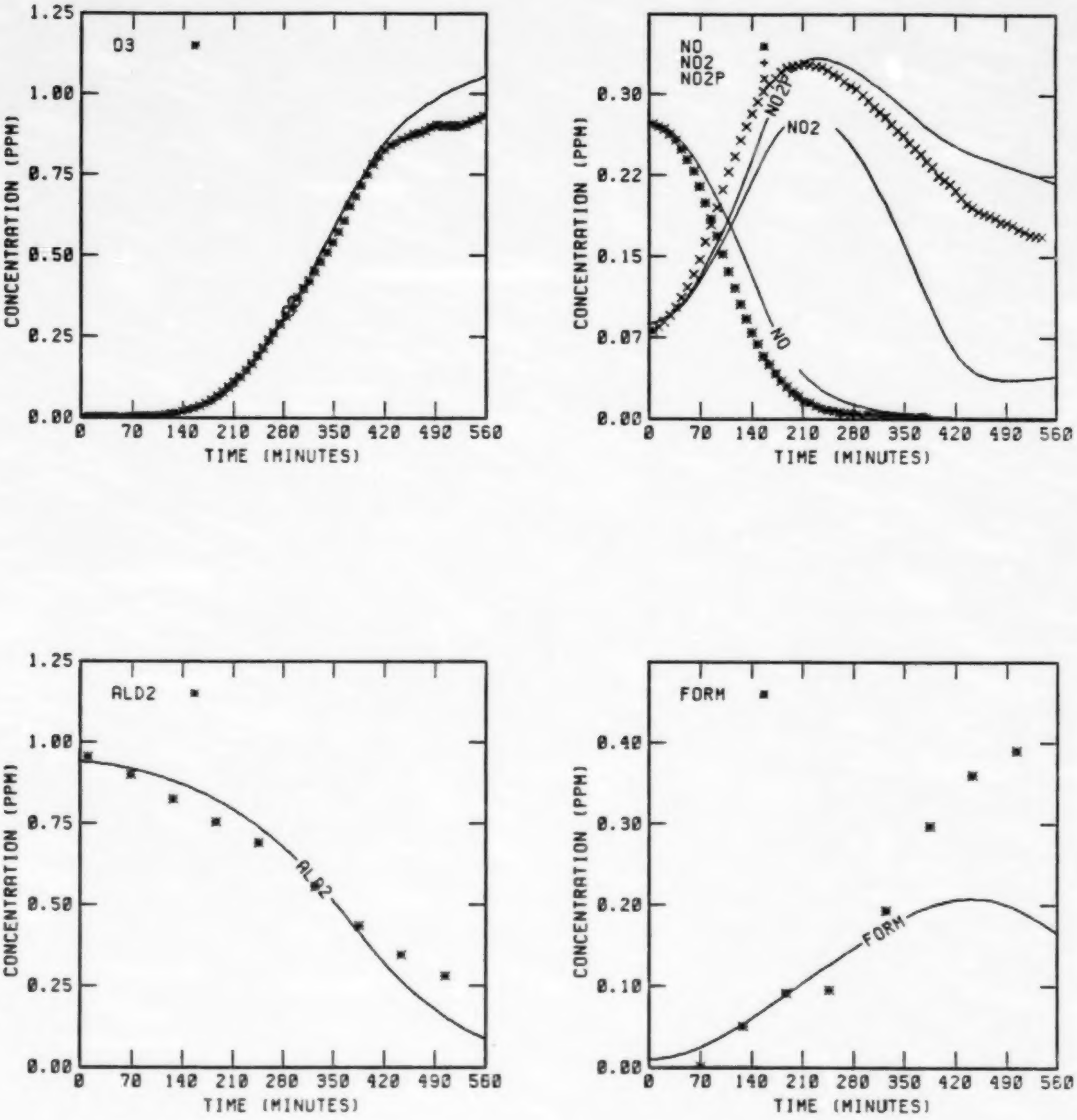

SIMULATION RESULTS FOR
UNCR 80179

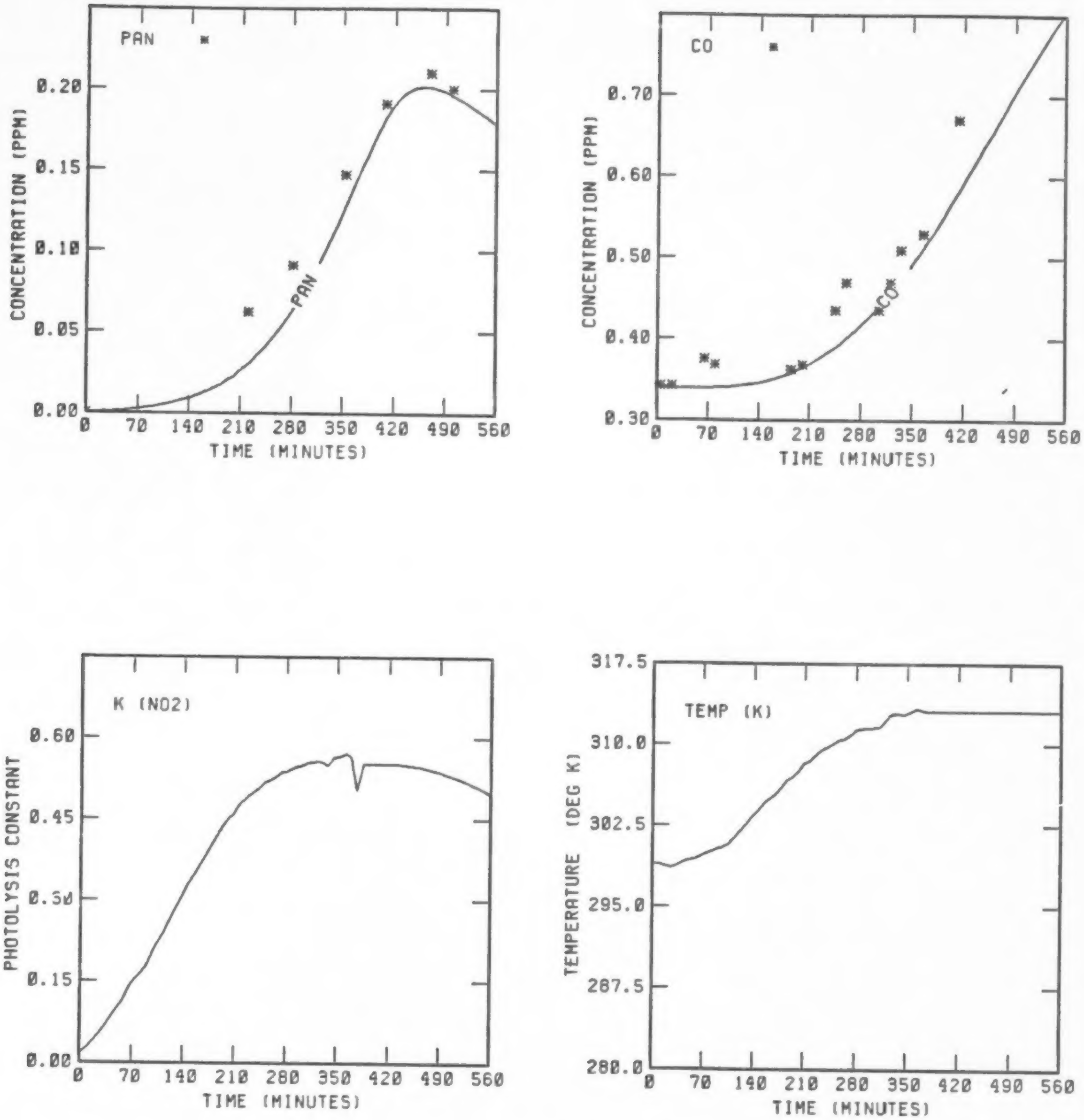

SIMULATION RESULTS FOR
UNCR 80179

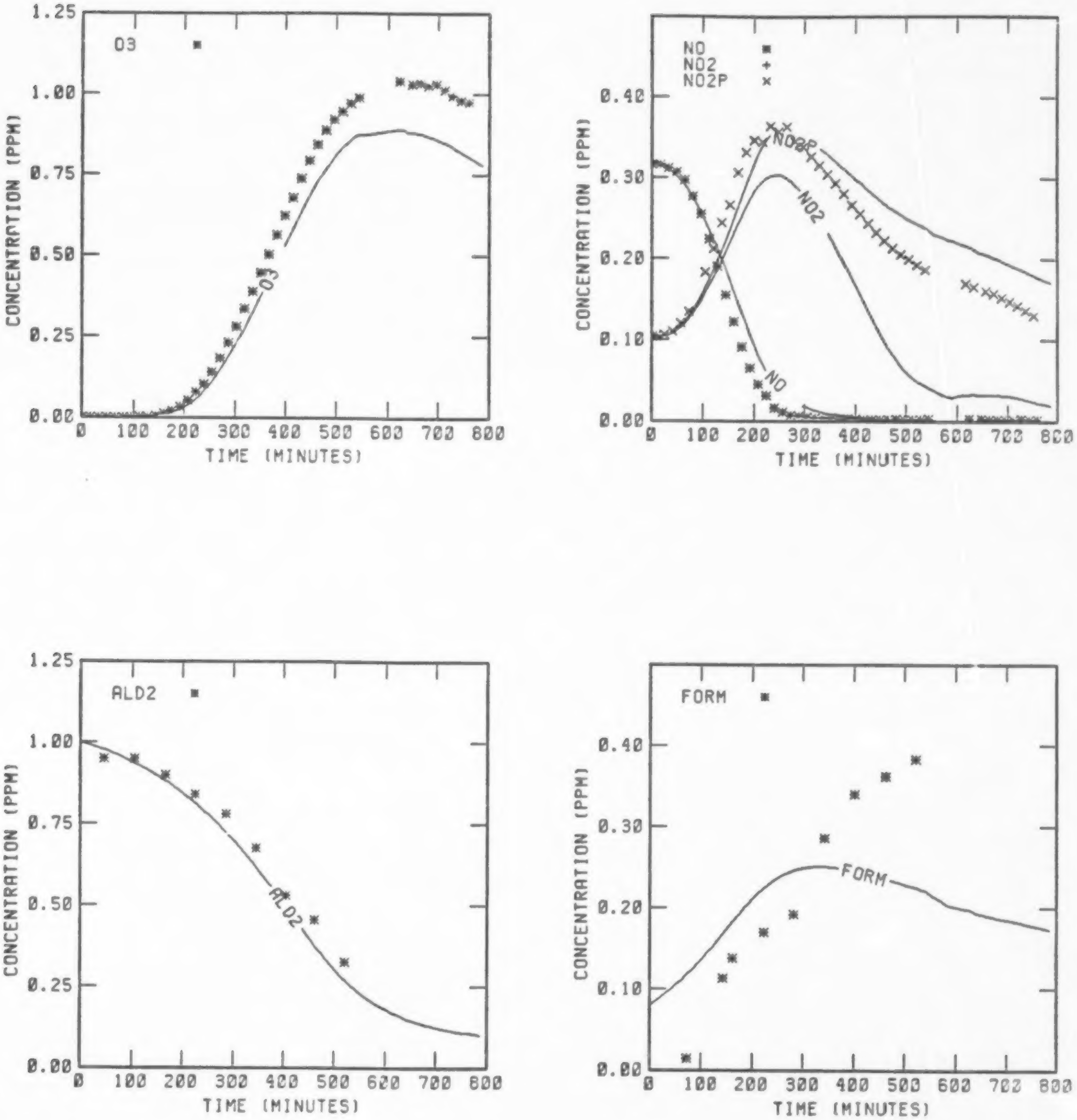

SIMULATION RESULTS FOR
UNCR 80880

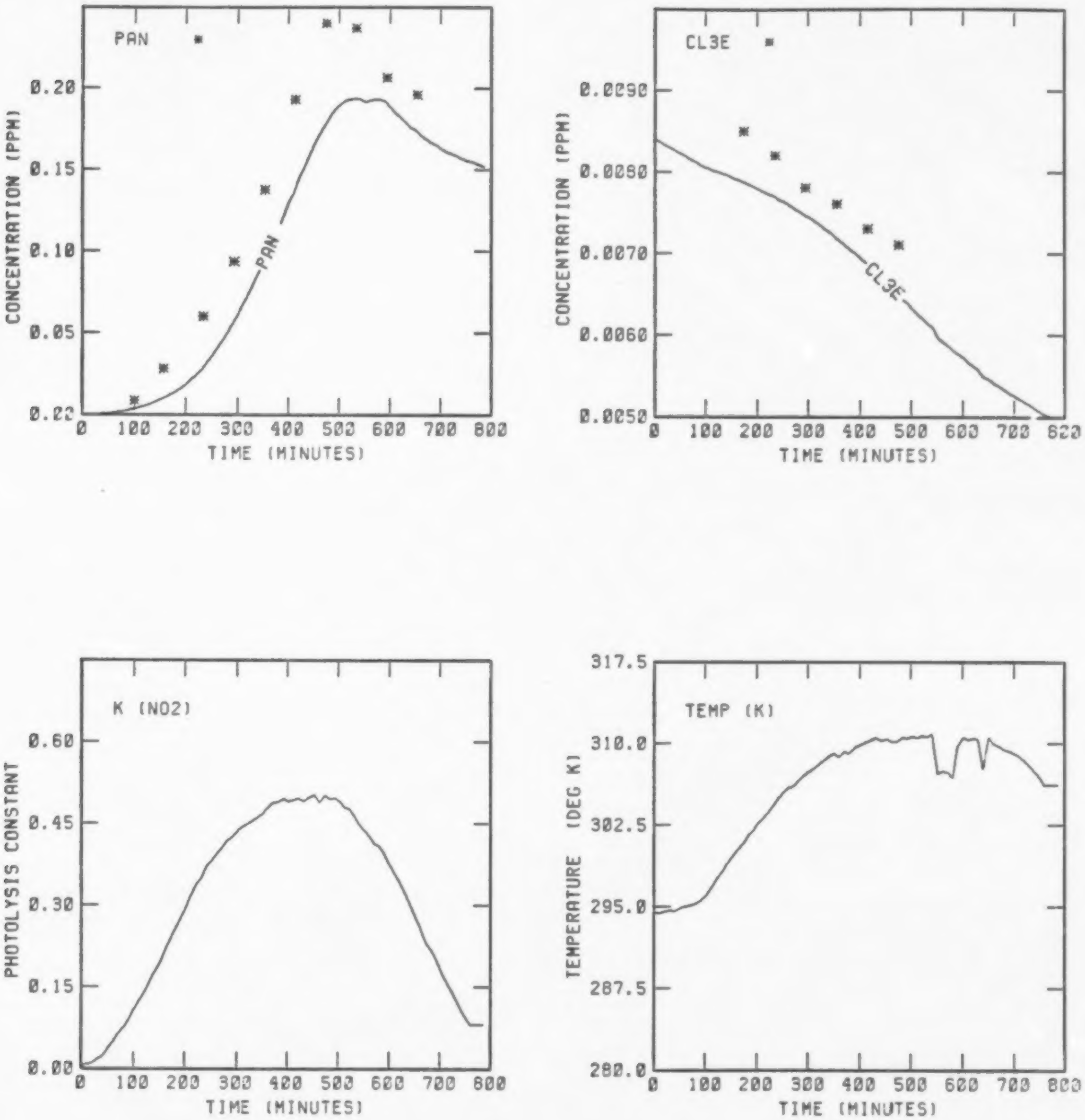

SIMULATION RESULTS FOR
UNCR 80880

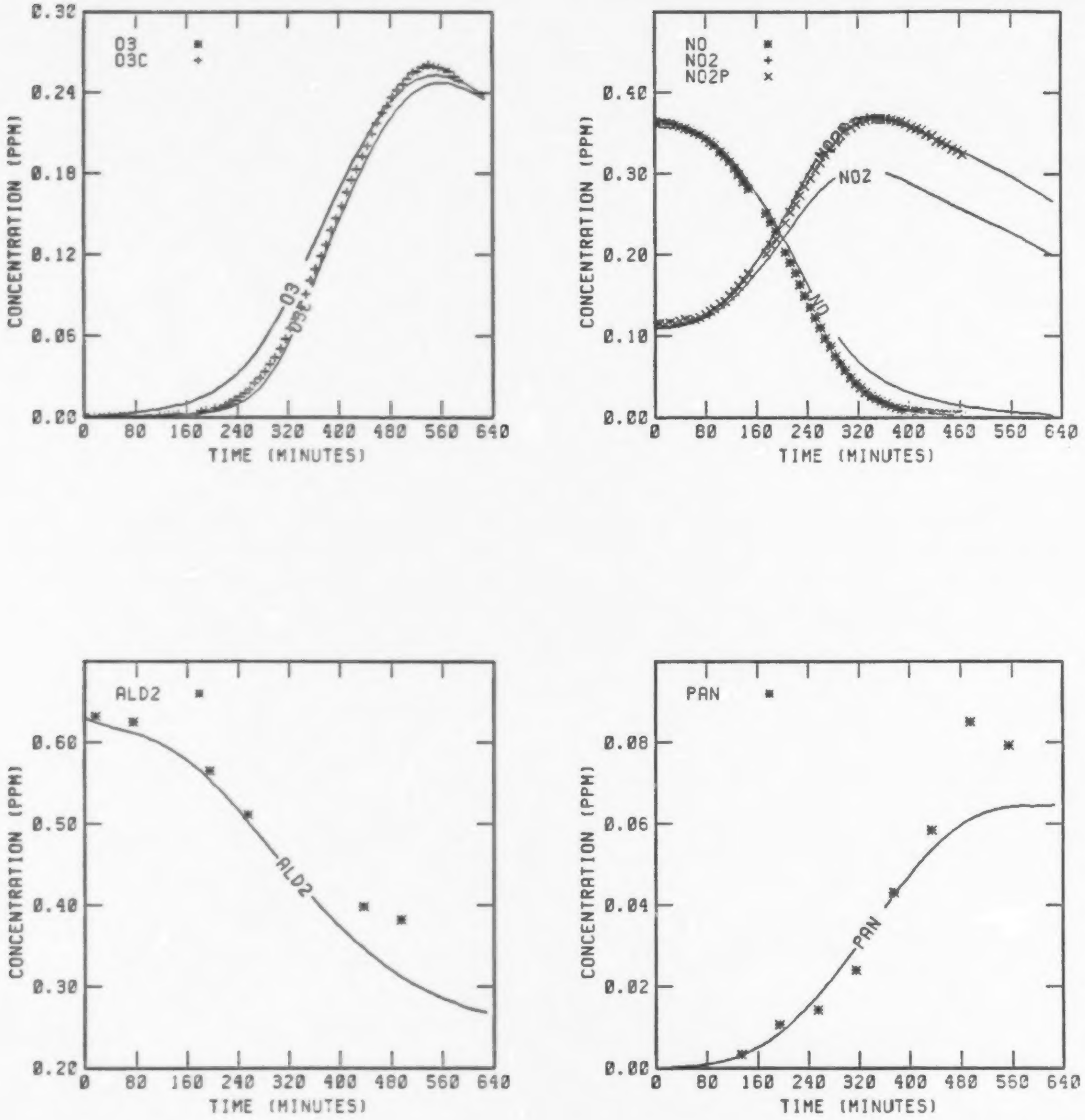

SIMULATION RESULTS FOR
UNCR 101278

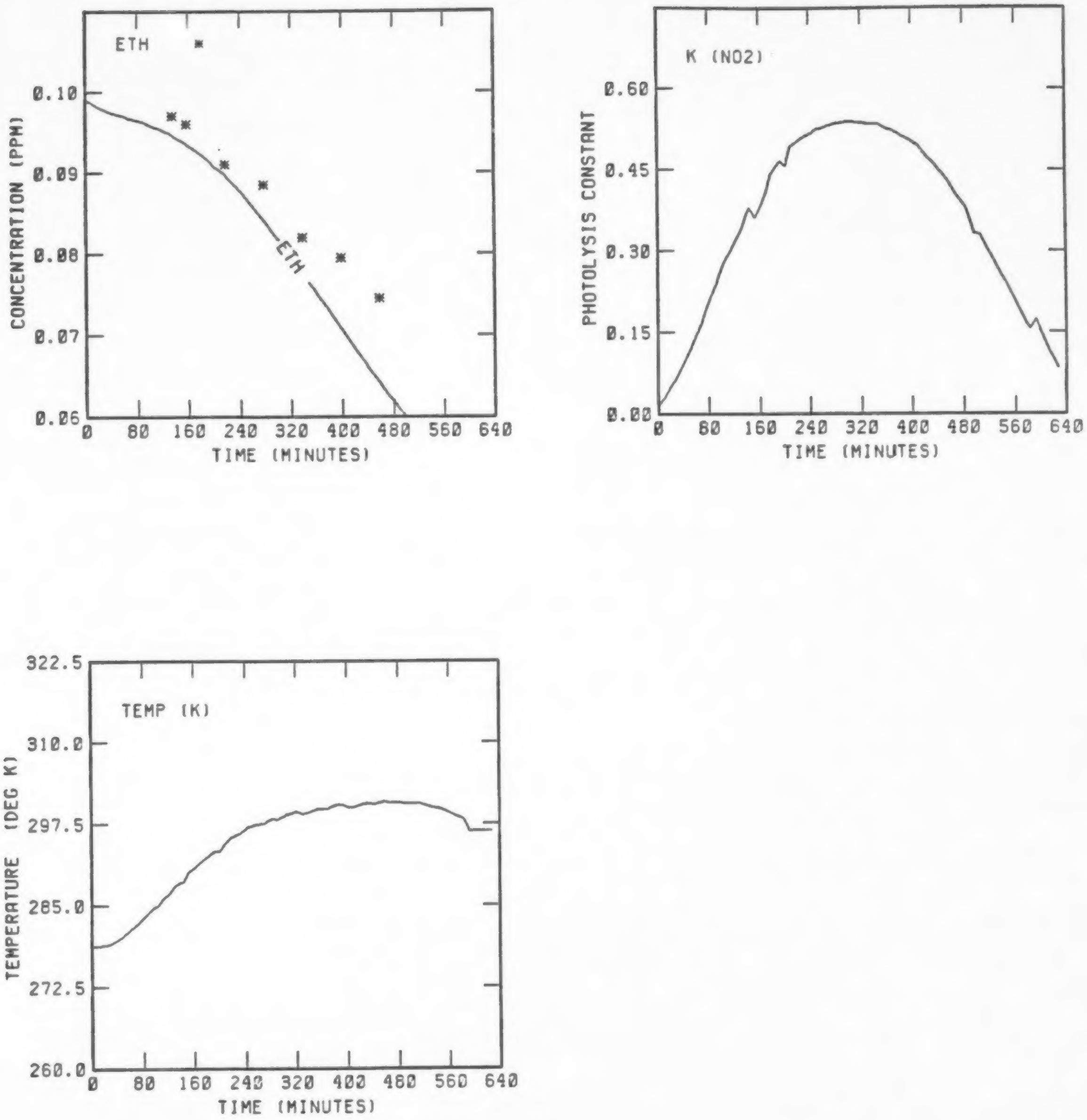

SIMULATION RESULTS FOR
UNCR 101278

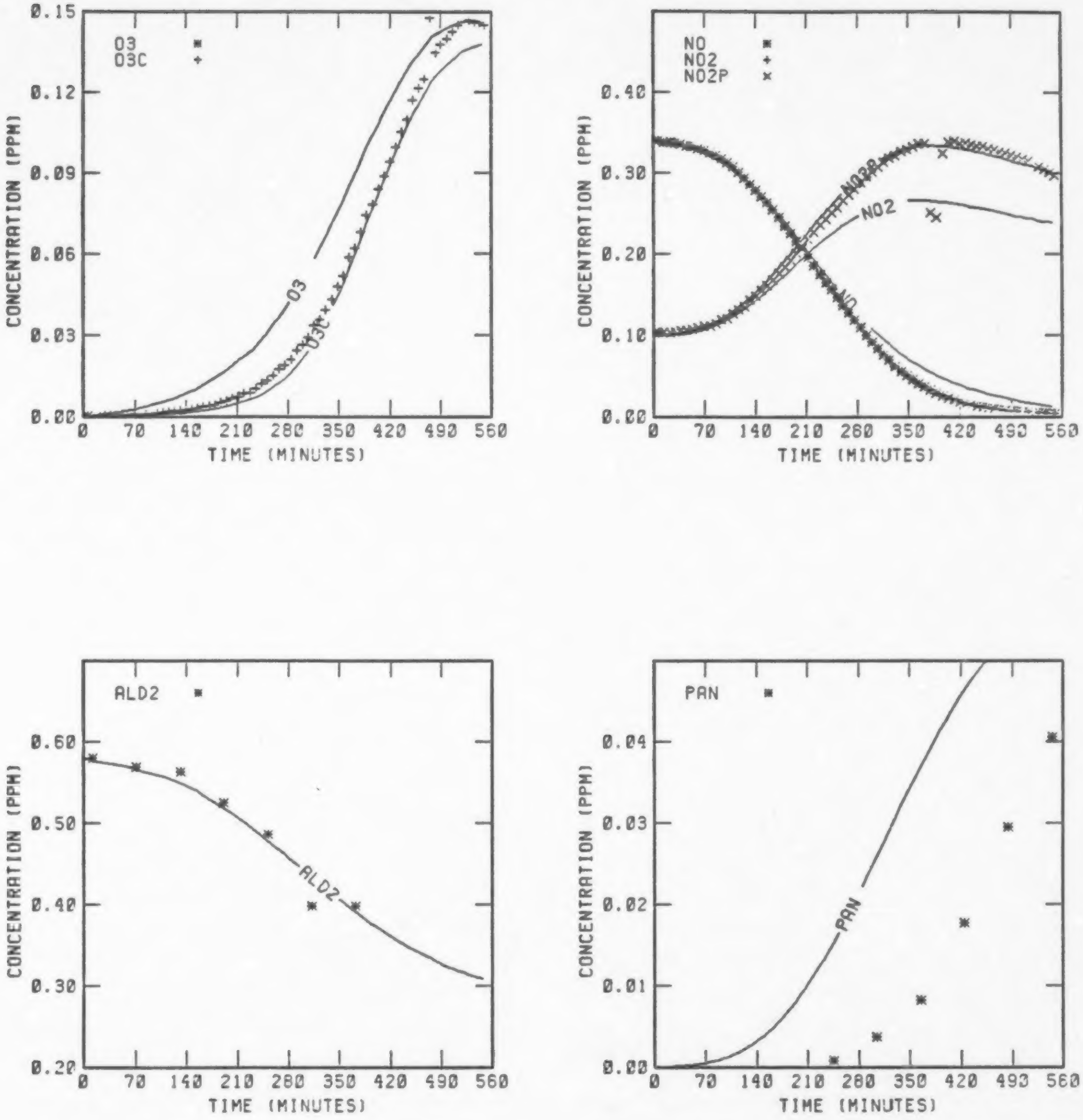

SIMULATION RESULTS FOR
UNCR 102578

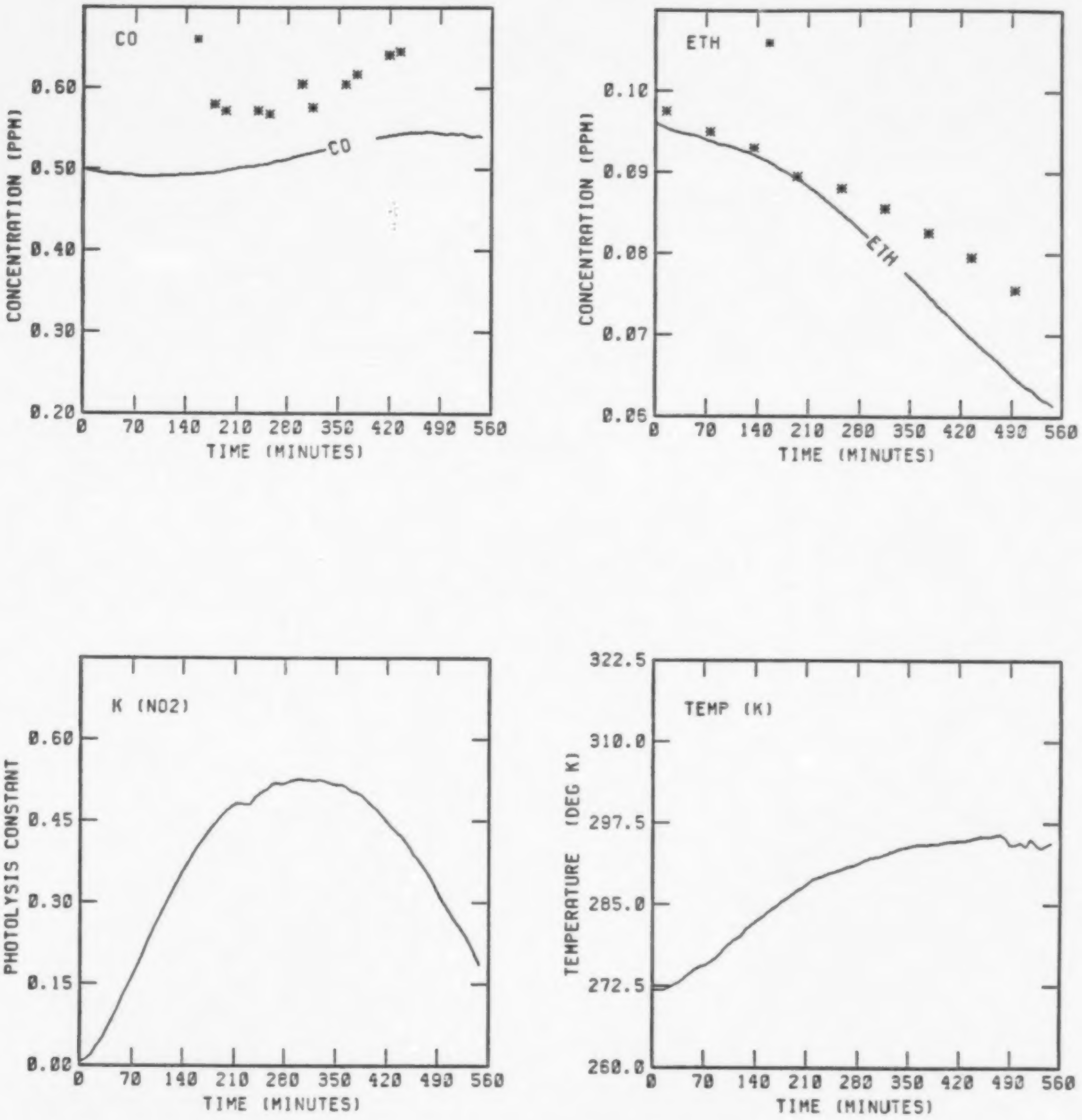

SIMULATION RESULTS FOR
UNCR 102578

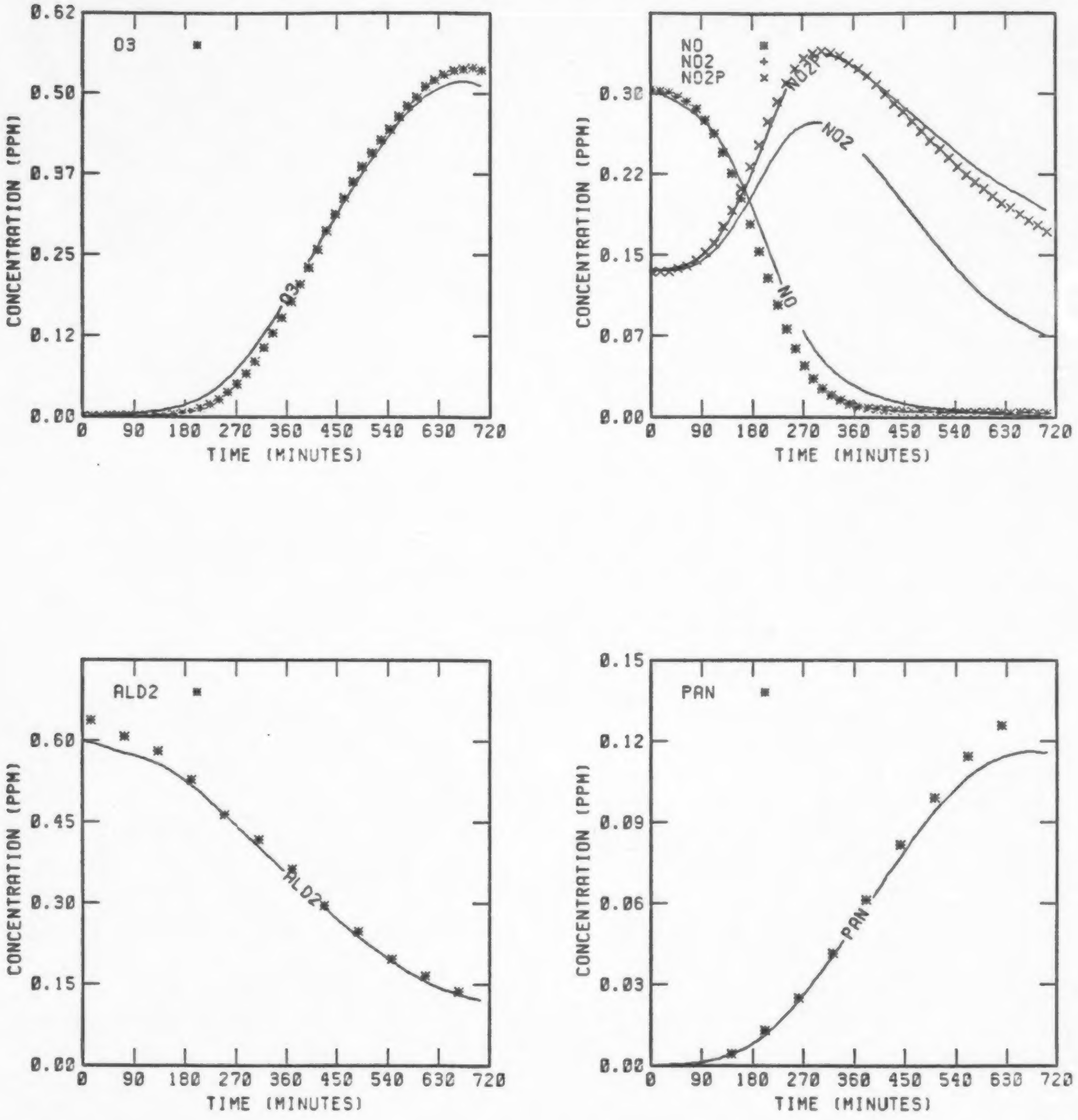

SIMULATION RESULTS FOR
UNCB 81679

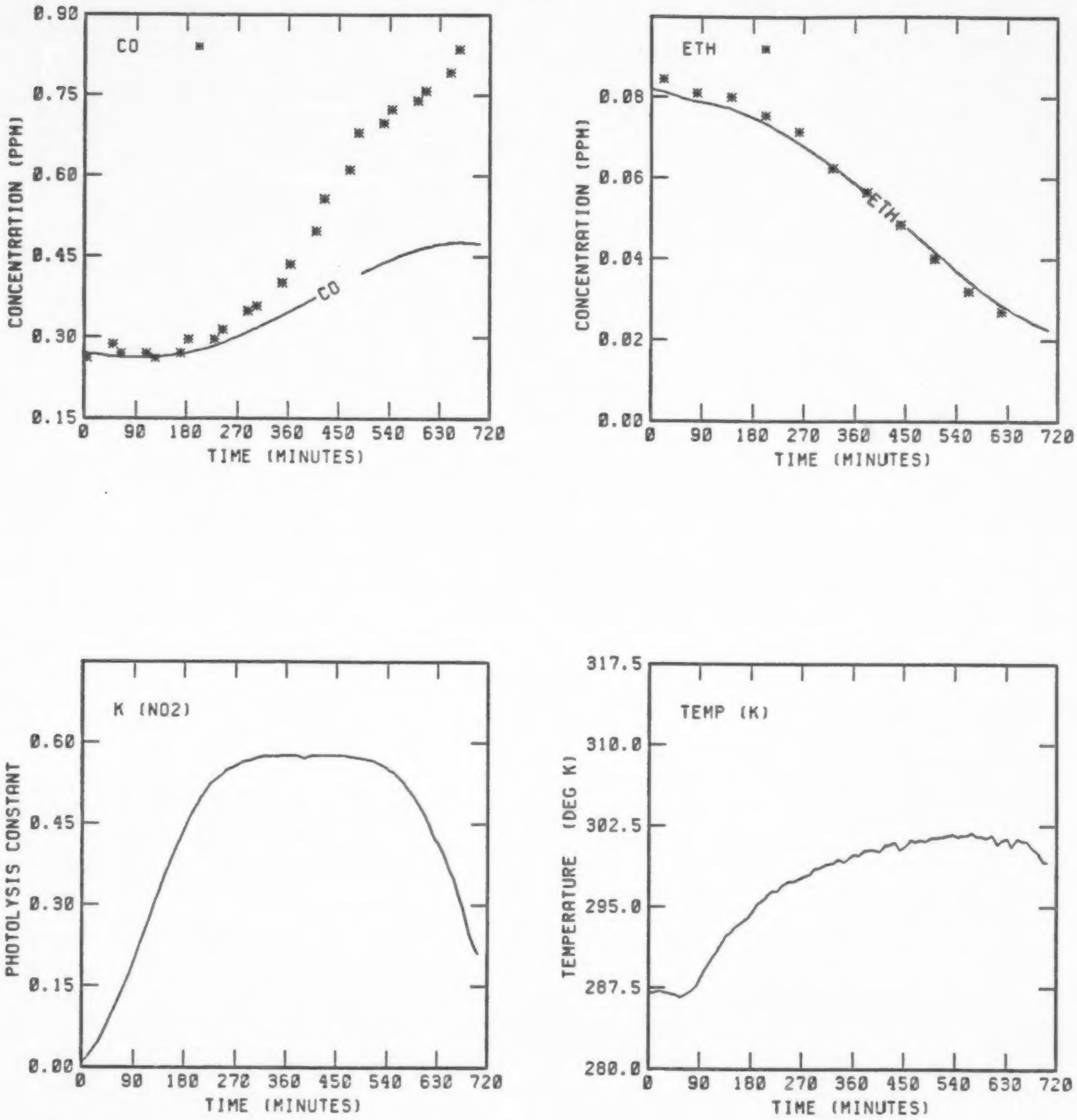

SIMULATION RESULTS FOR
UNCB 81679

Appendix C

SIMULATION RESULTS FOR THE UNC ETHENE EXPERIMENTS

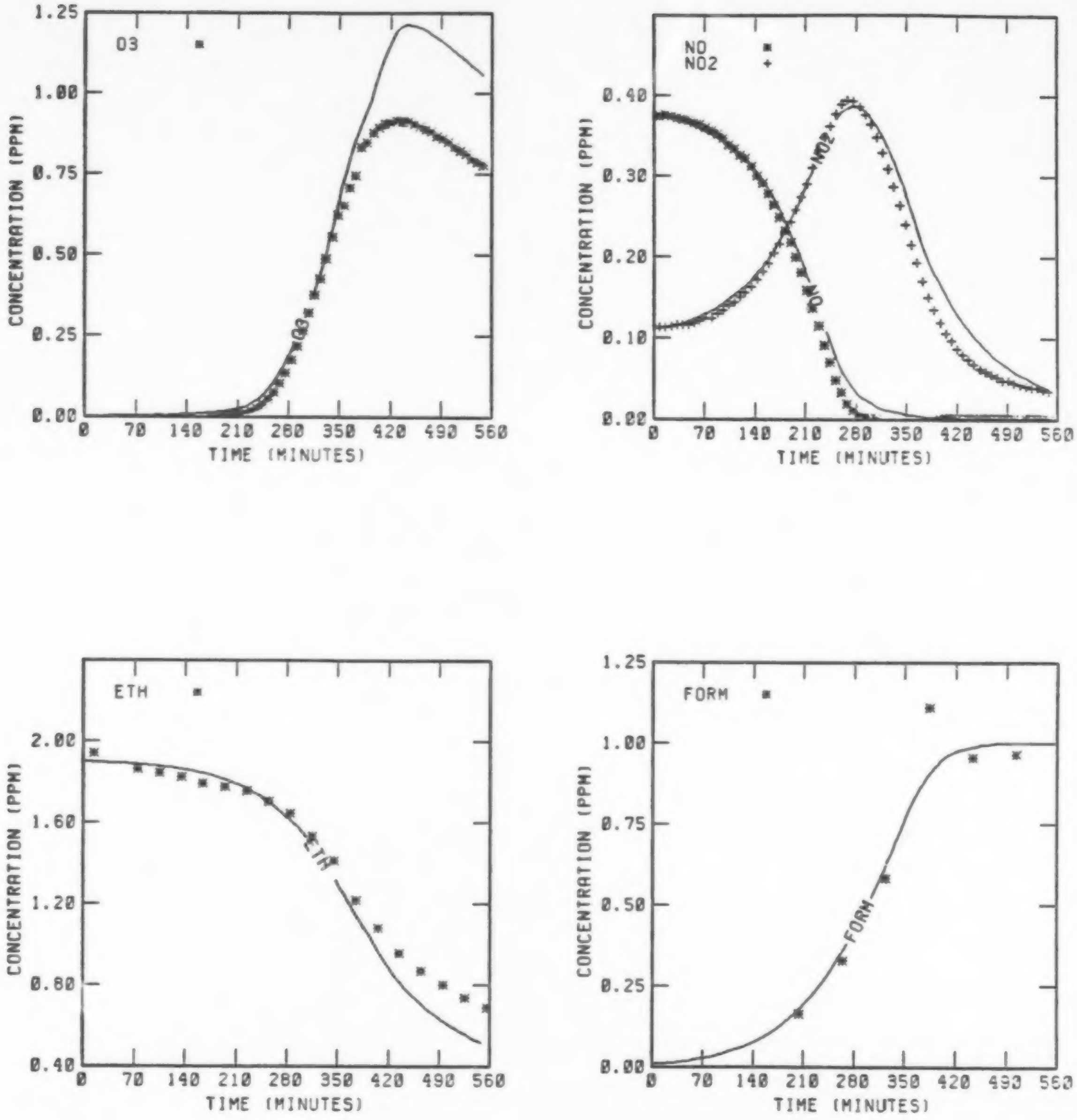

SIMULATION RESULTS FOR
UNCR 101877

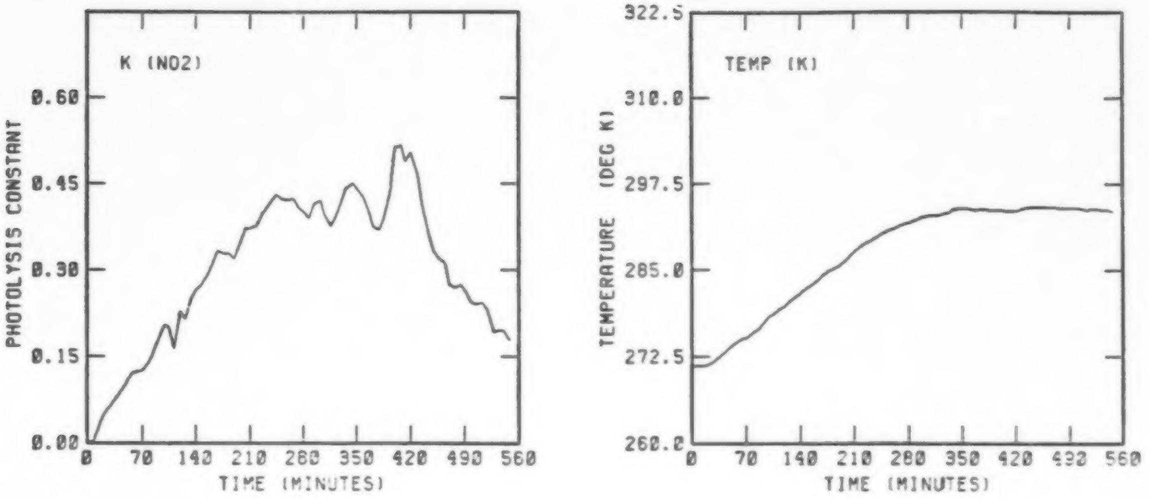

SIMULATION RESULTS FOR
UNCR 101877

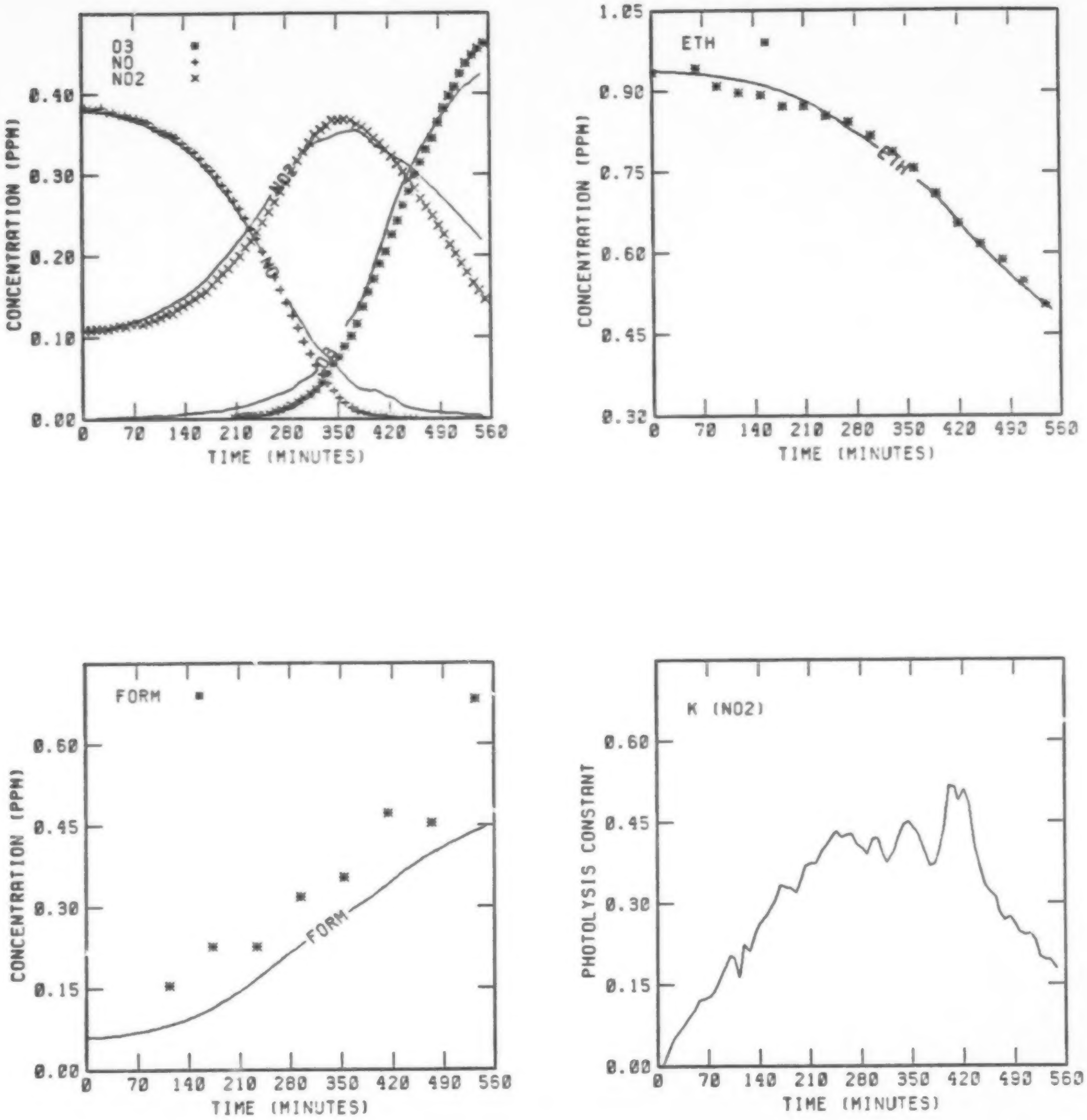

SIMULATION RESULTS FOR
UNCB 101877

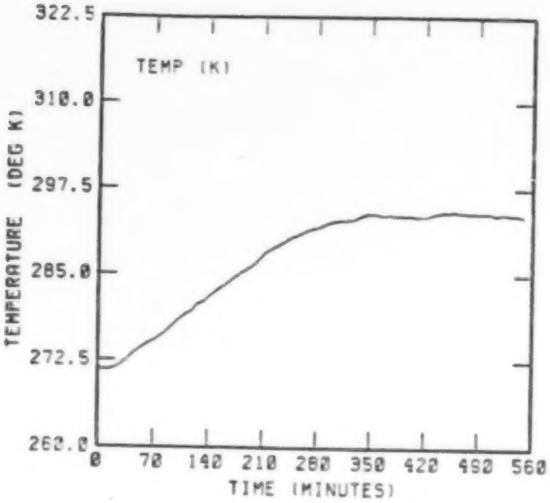

SIMULATION RESULTS FOR
UNCB 101877

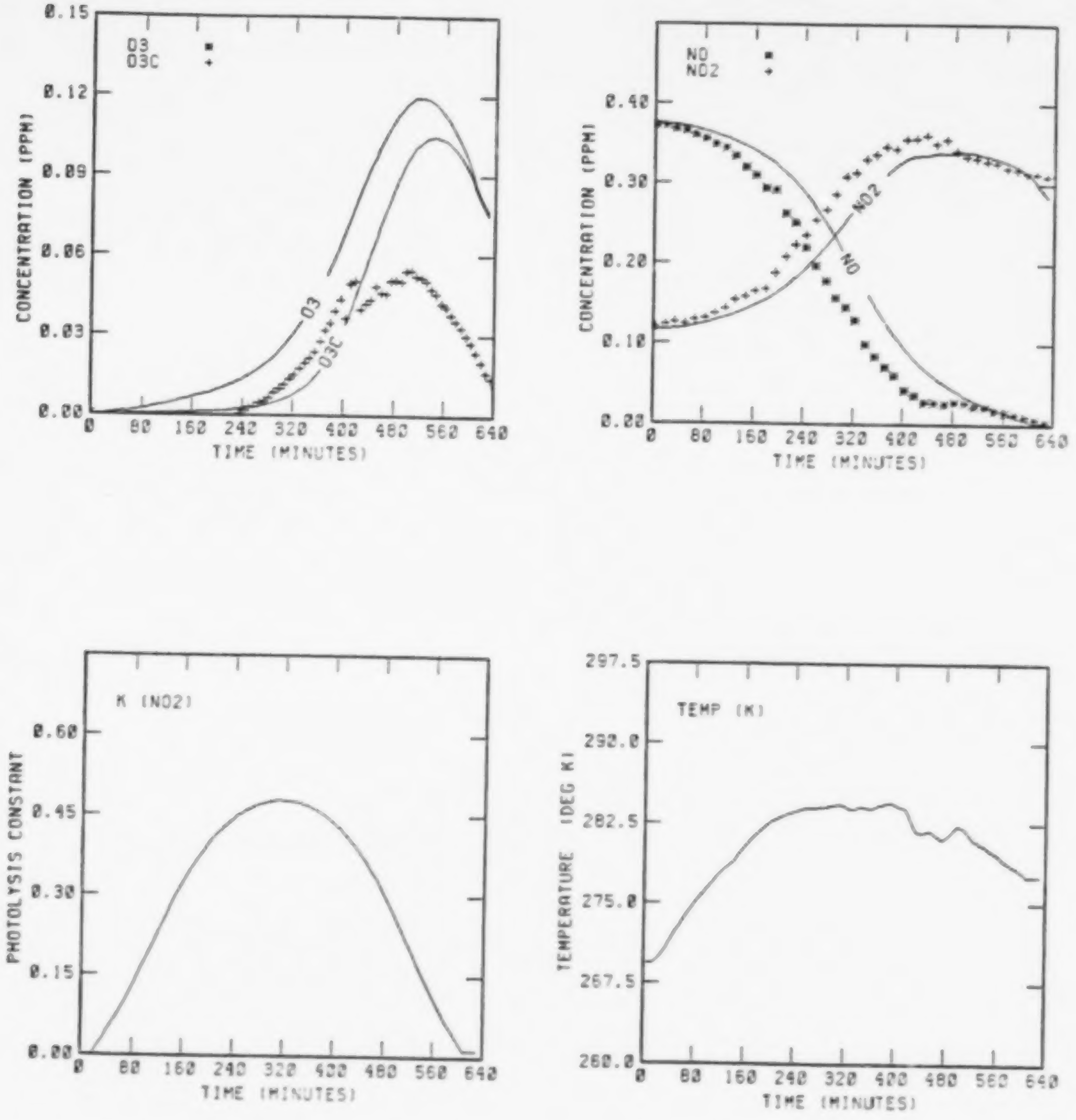

SIMULATION RESULTS FOR
UNCR 111277

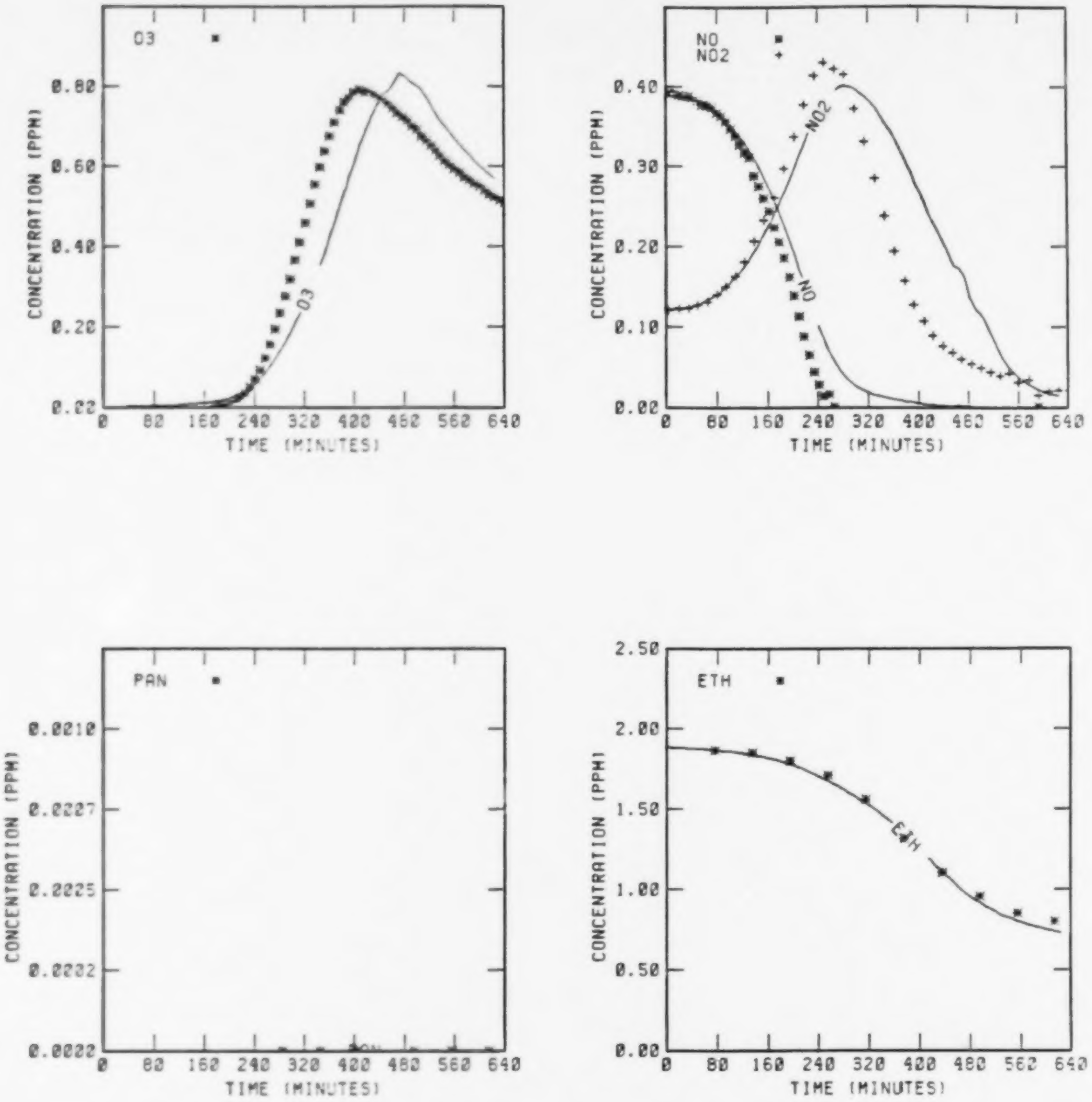

SIMULATION RESULTS FOR
UNCR 111977

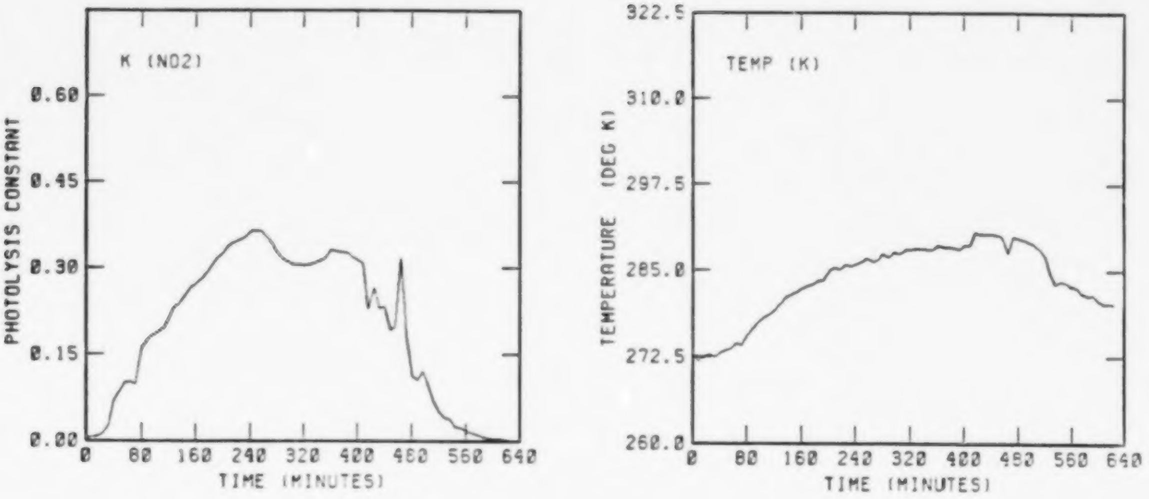

SIMULATION RESULTS FOR
UNCR 111977

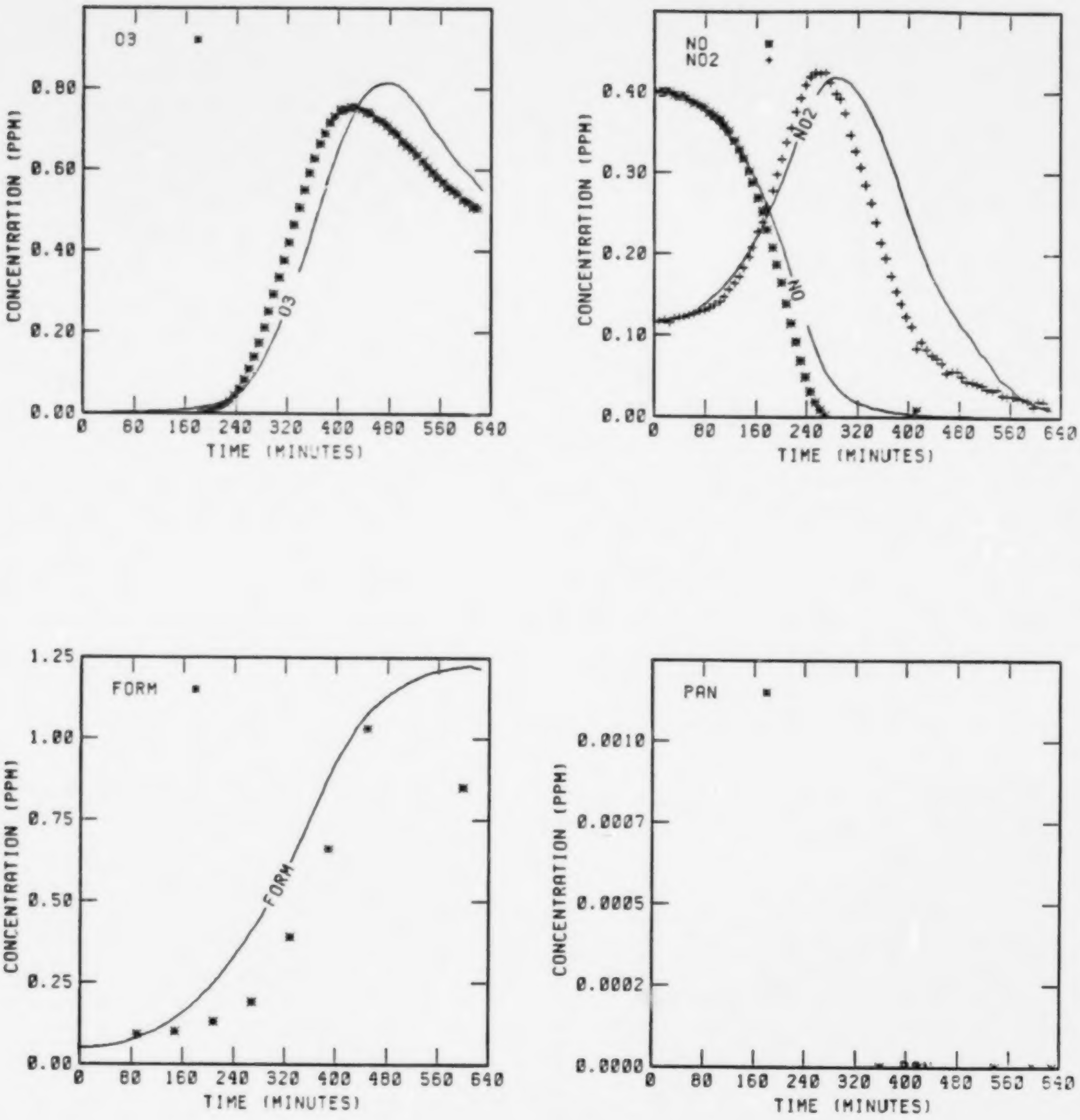

SIMULATION RESULTS FOR
UNCR 112077

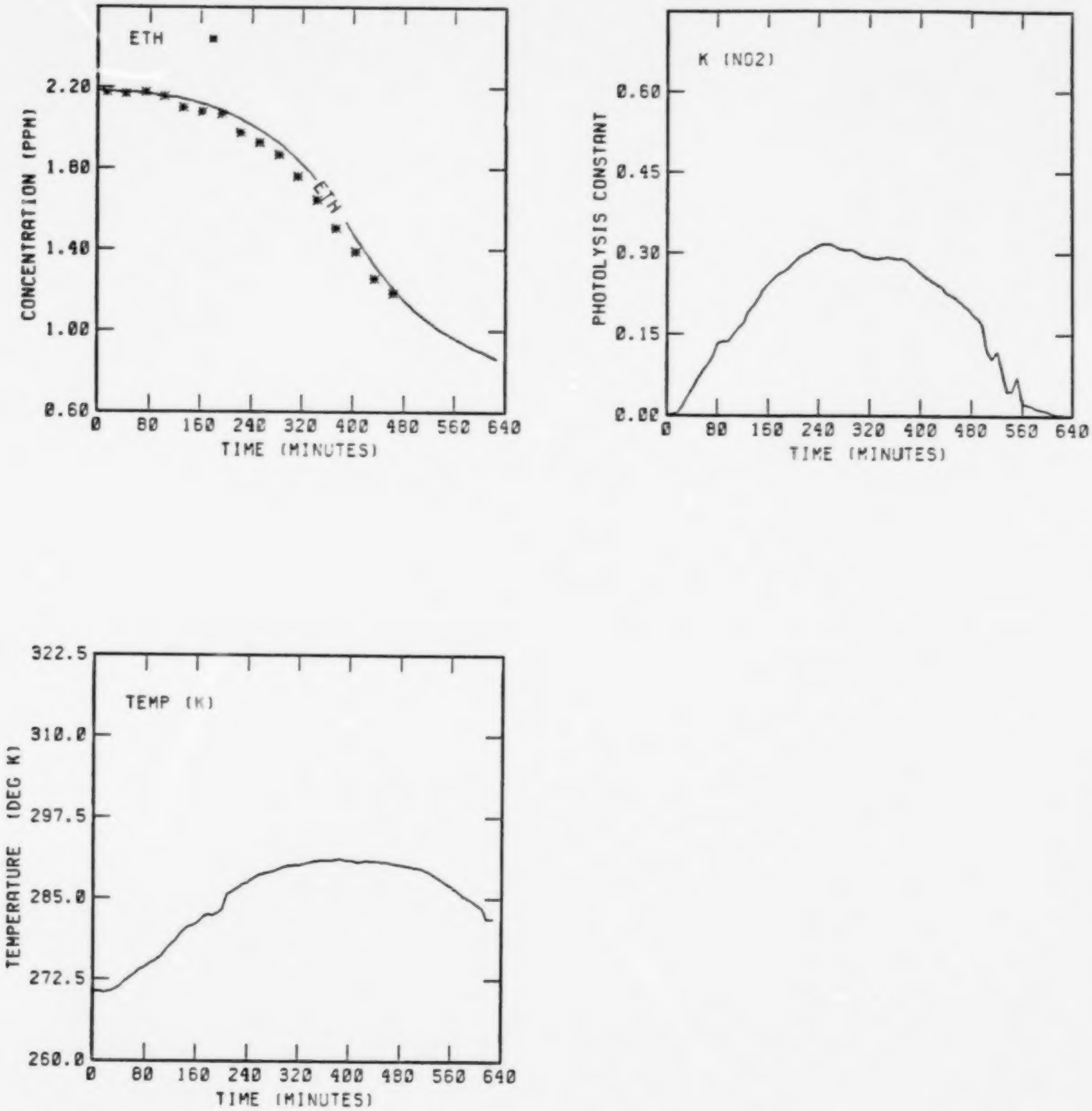

SIMULATION RESULTS FOR
UNCR 112077

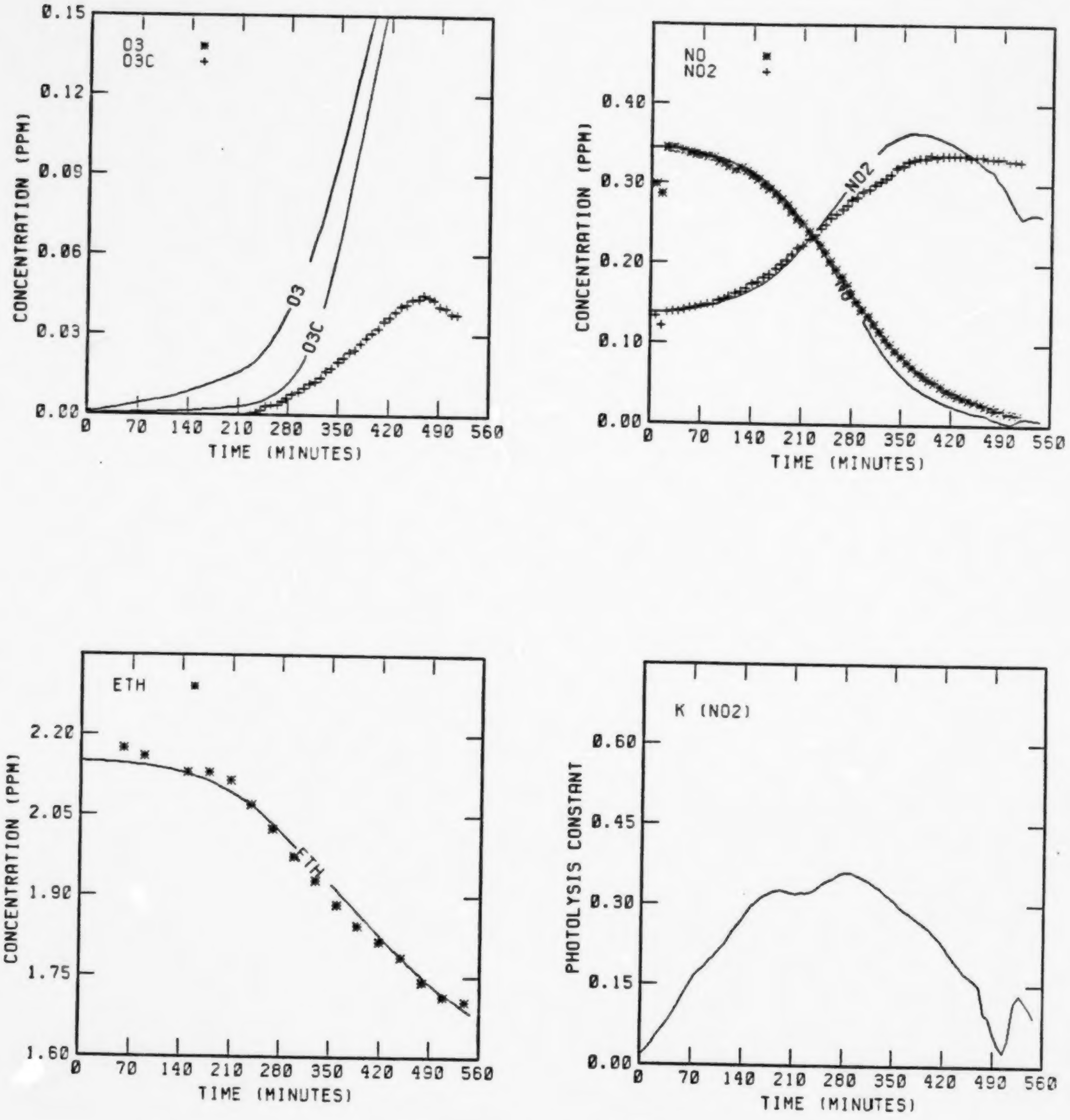

SIMULATION RESULTS FOR
UNCB 11078

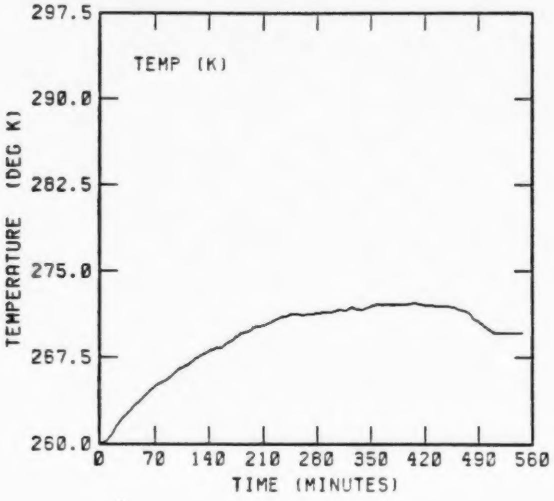

SIMULATION RESULTS FOR
UNCB 11078

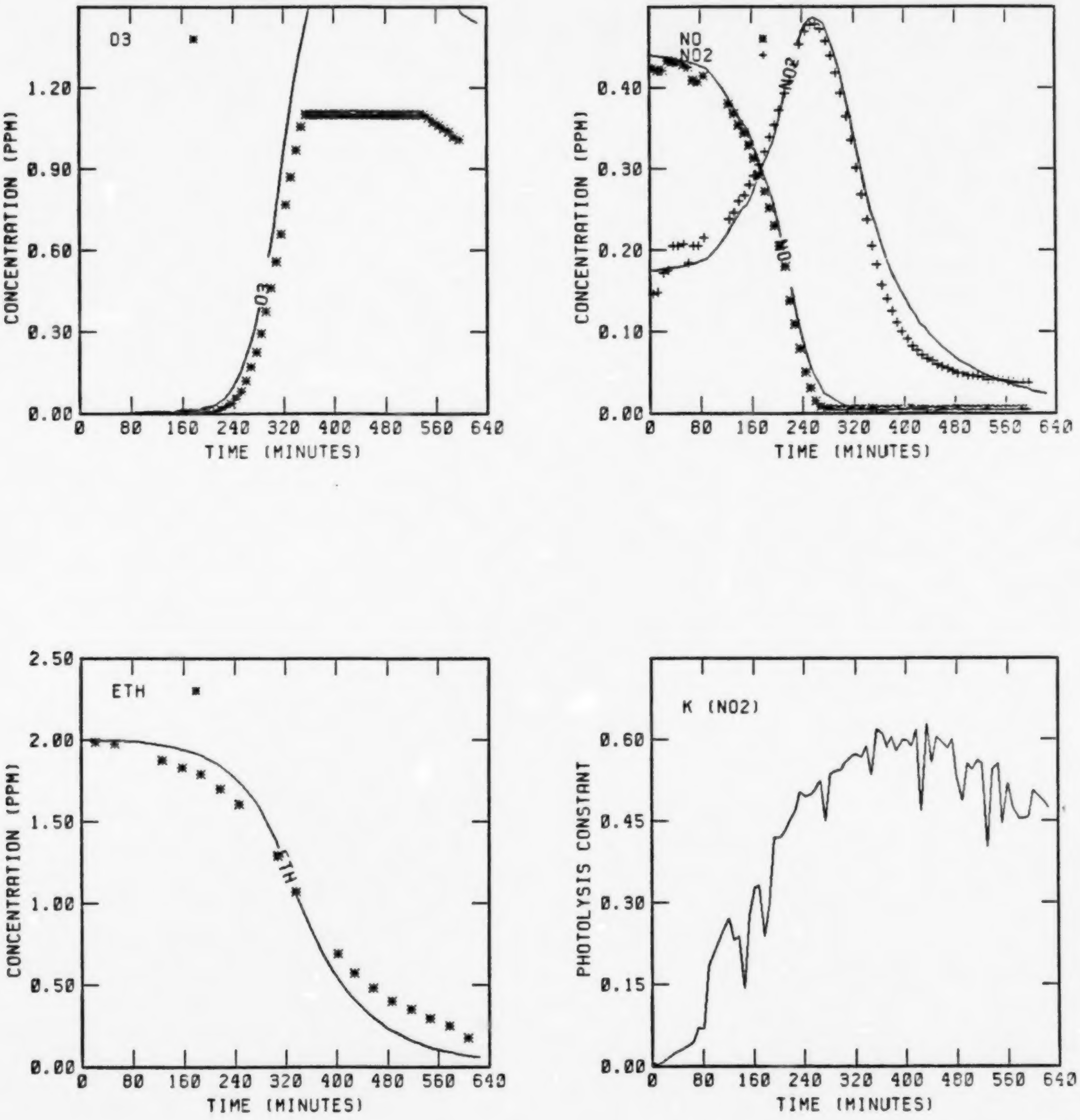

SIMULATION RESULTS FOR
UNCR 61678

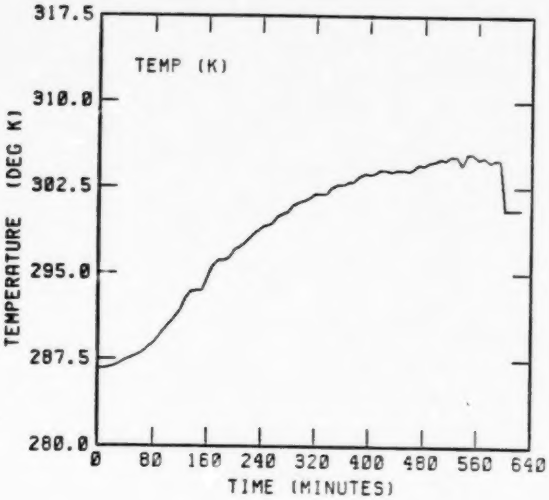

SIMULATION RESULTS FOR
UNCR 61678

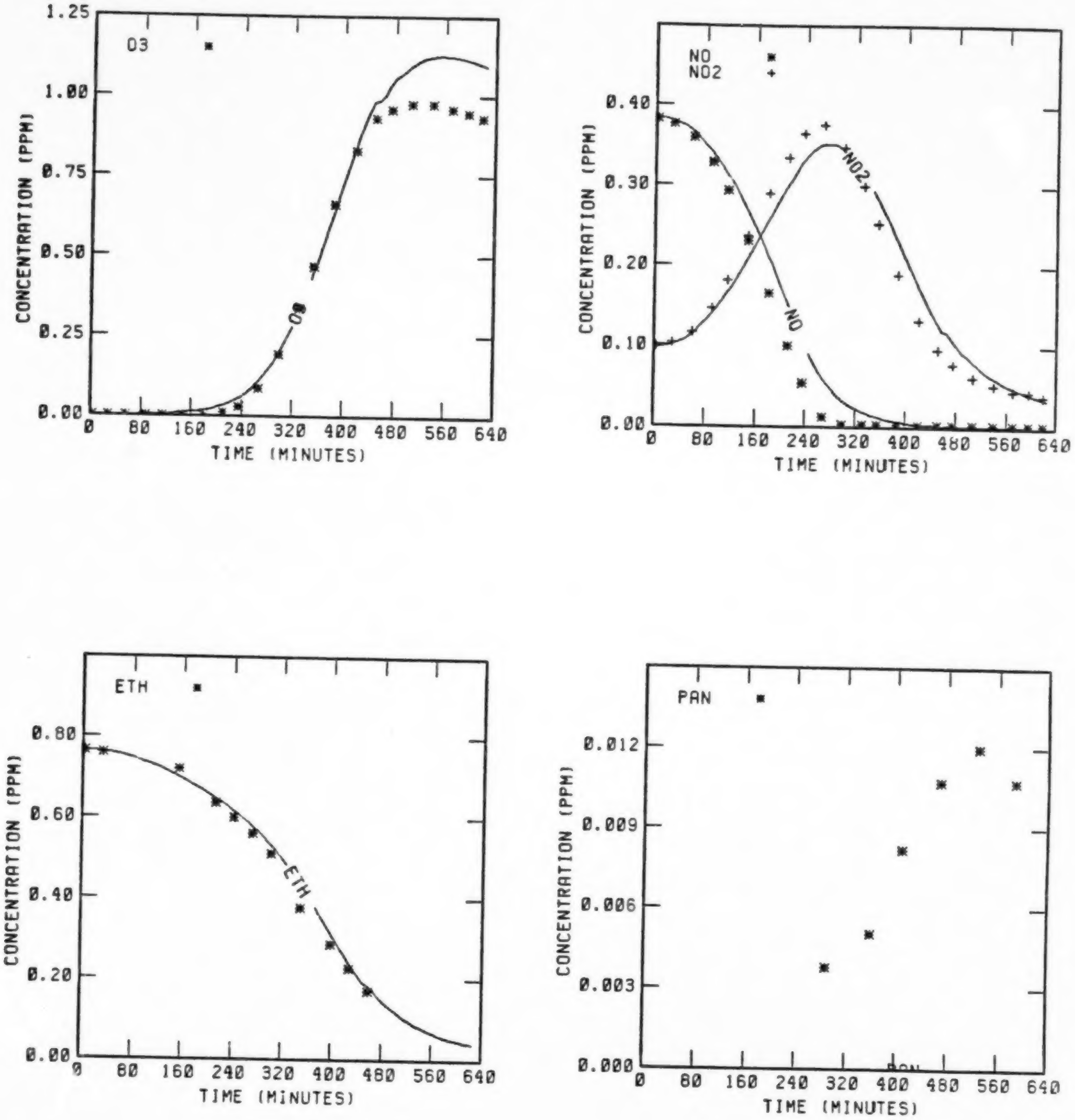

SIMULATION RESULTS FOR
UNCB 63078

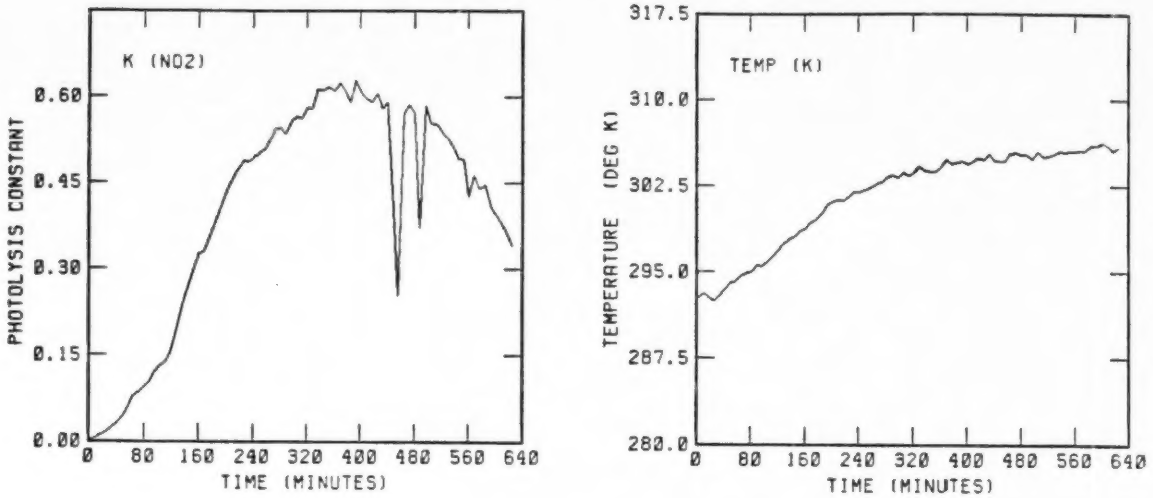

SIMULATION RESULTS FOR
UNCB 63078

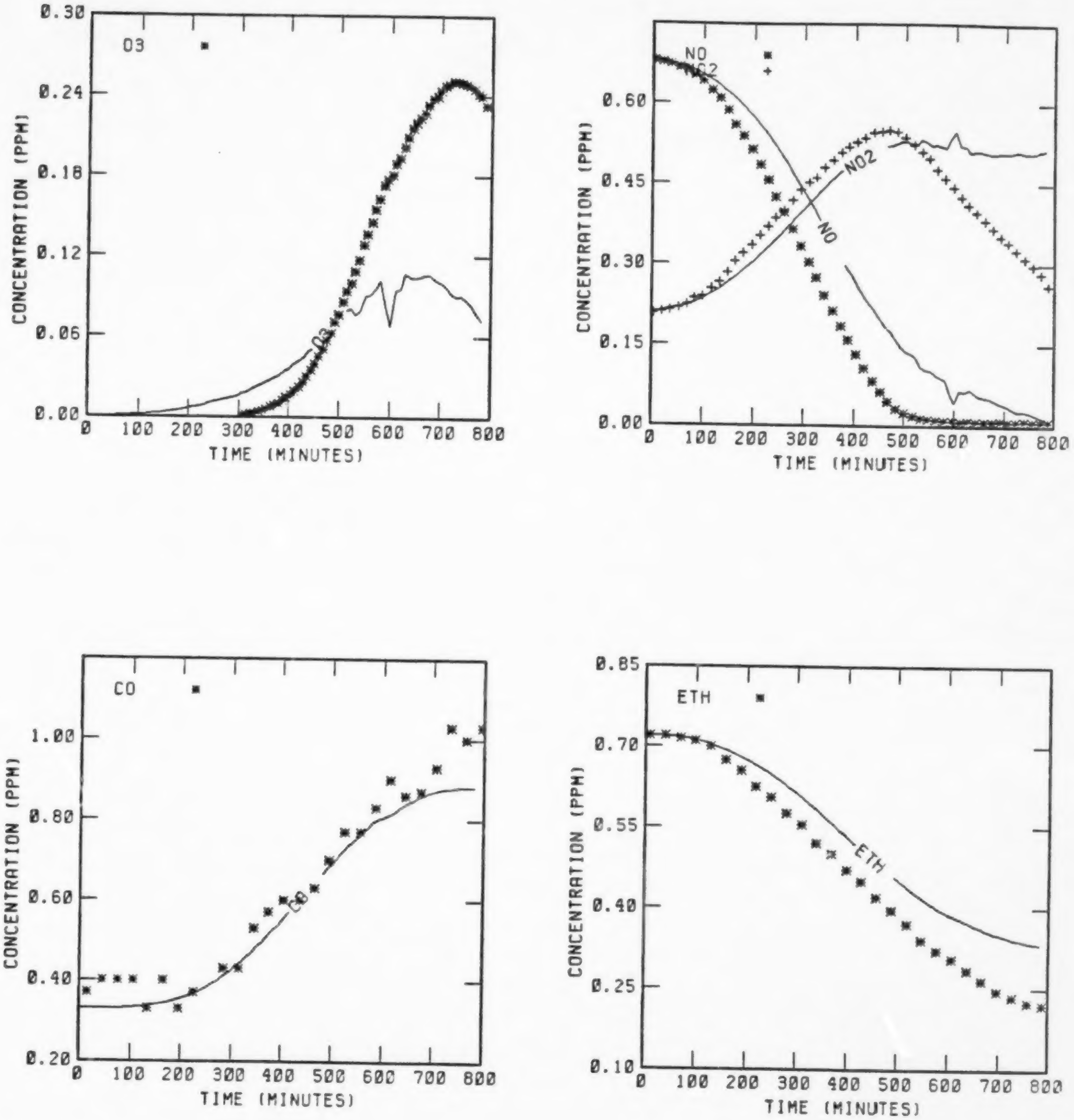

SIMULATION RESULTS FOR
UNCR 70178

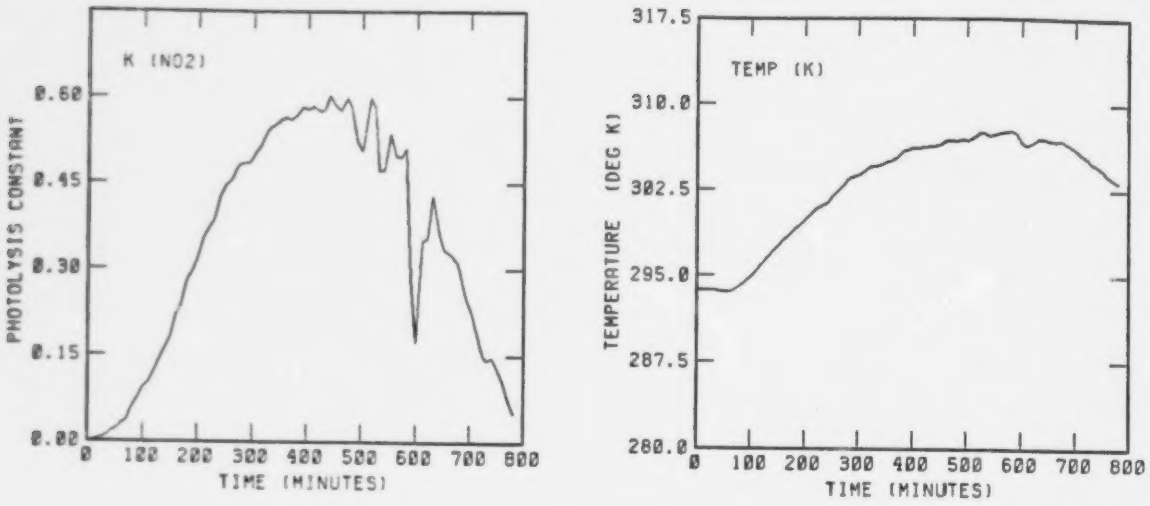

SIMULATION RESULTS FOR
UNCR 70178

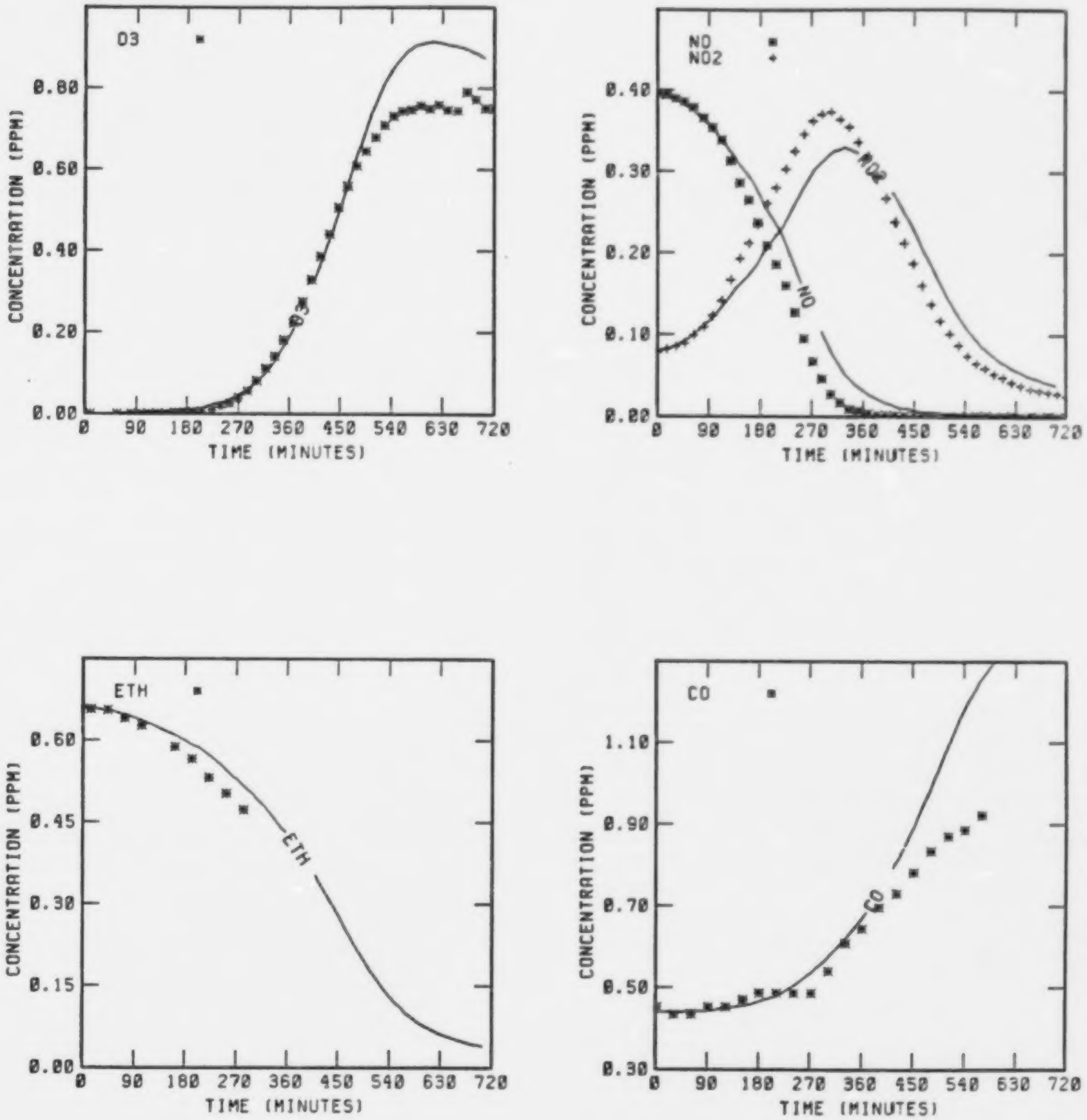

SIMULATION RESULTS FOR
UNCR 73078

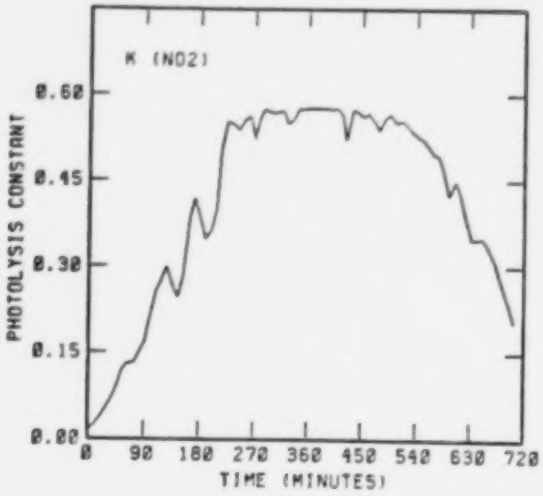

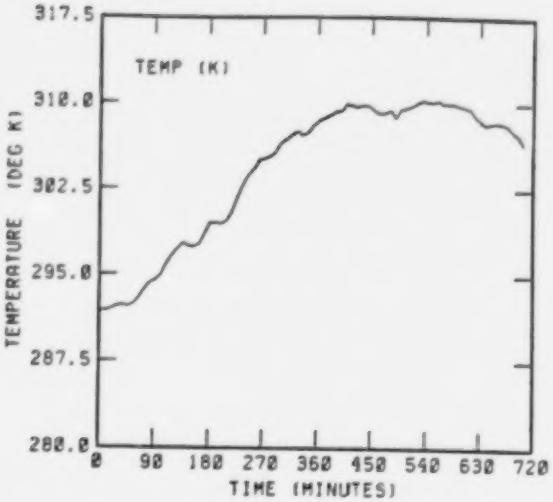

SIMULATION RESULTS FOR
UNCR 73078

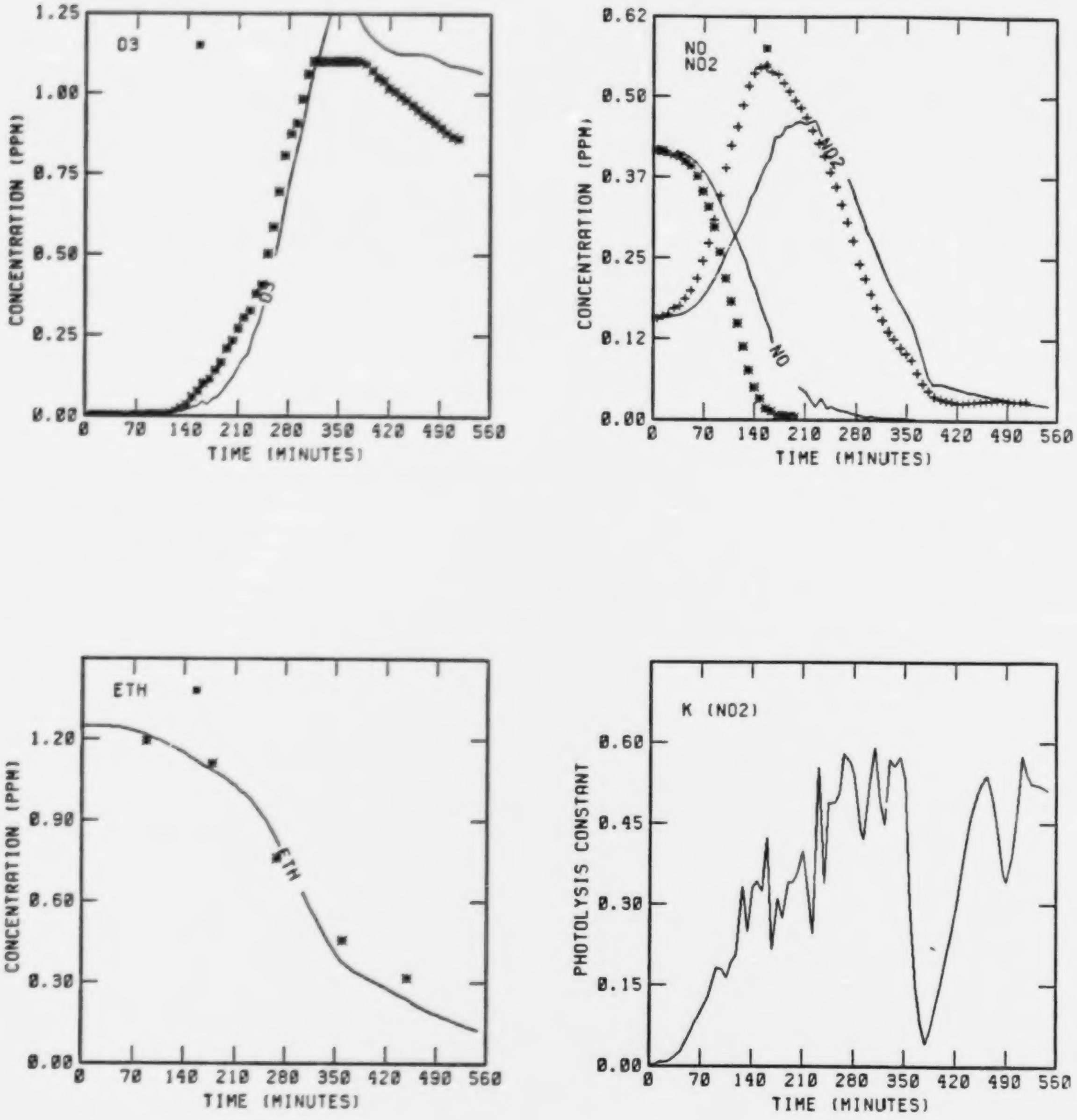

SIMULATION RESULTS FOR
UNCB 80678

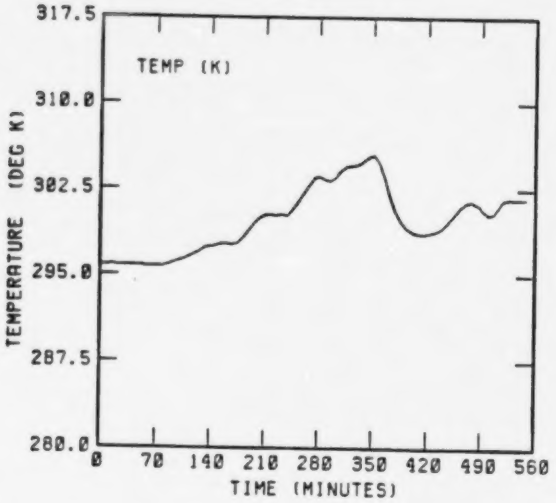

SIMULATION RESULTS FOR
UNCB 80678

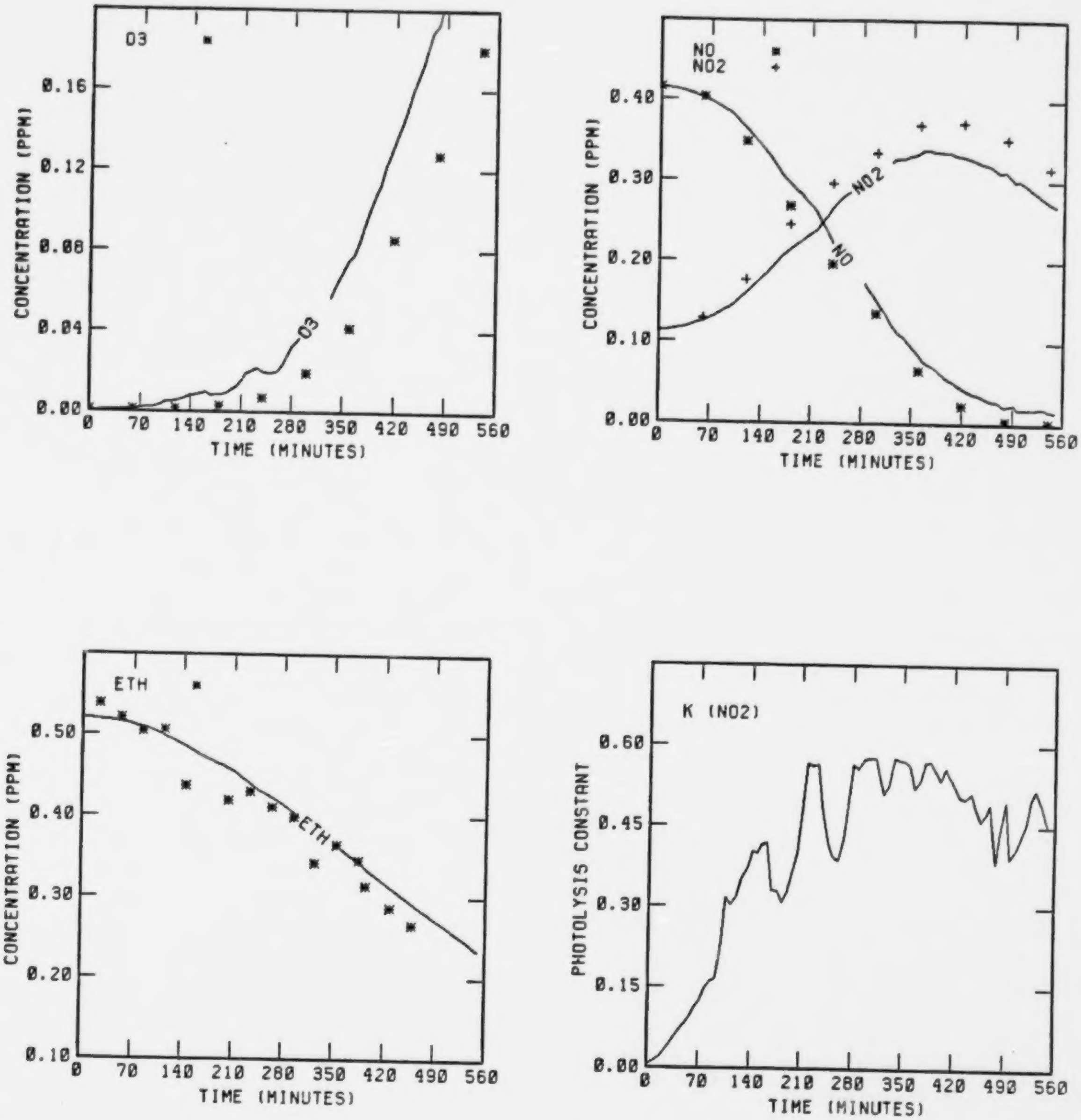

SIMULATION RESULTS FOR
UNCR 81078

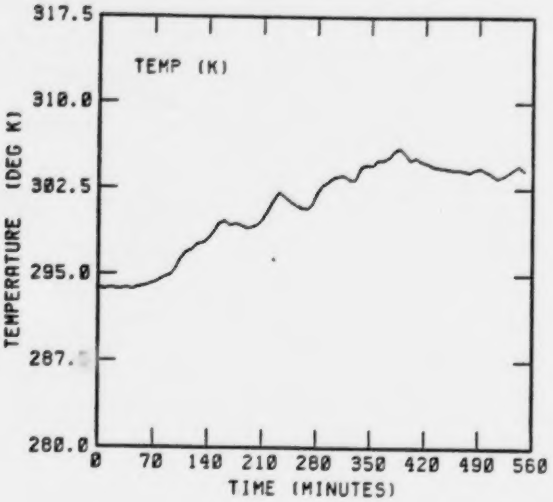

SIMULATION RESULTS FOR
UNCR 81078

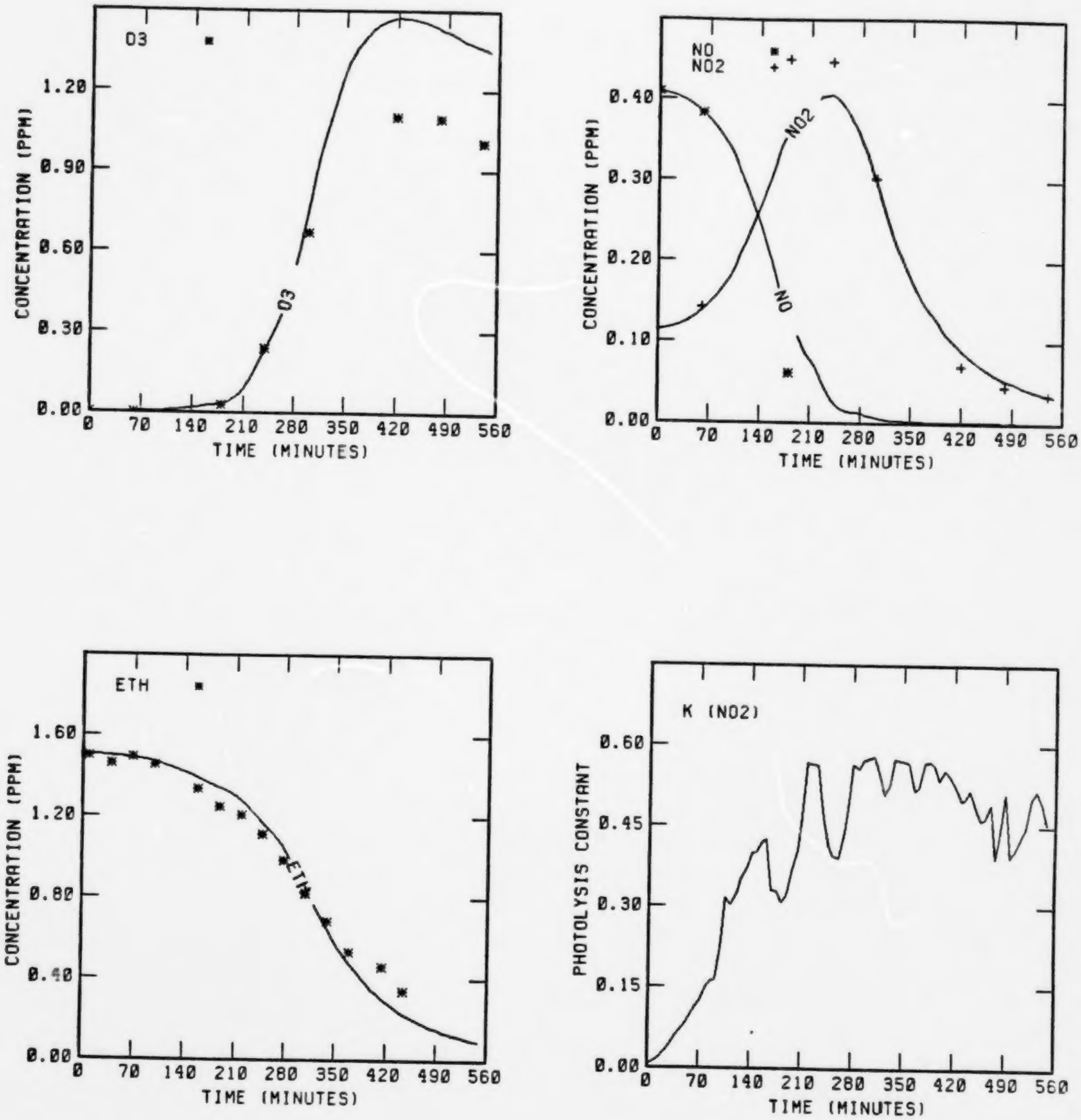

SIMULATION RESULTS FOR
UNCB 81078

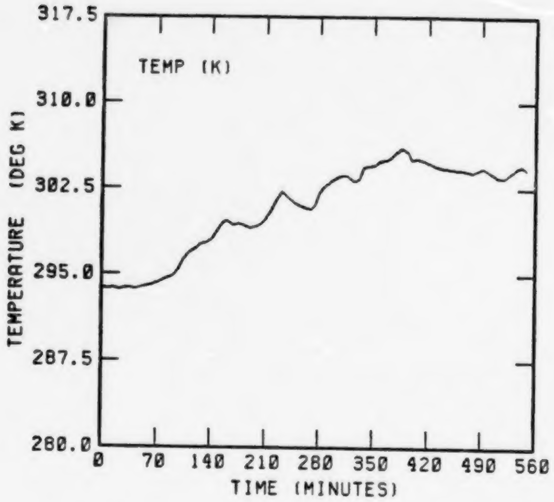

SIMULATION RESULTS FOR
UNCB 81078

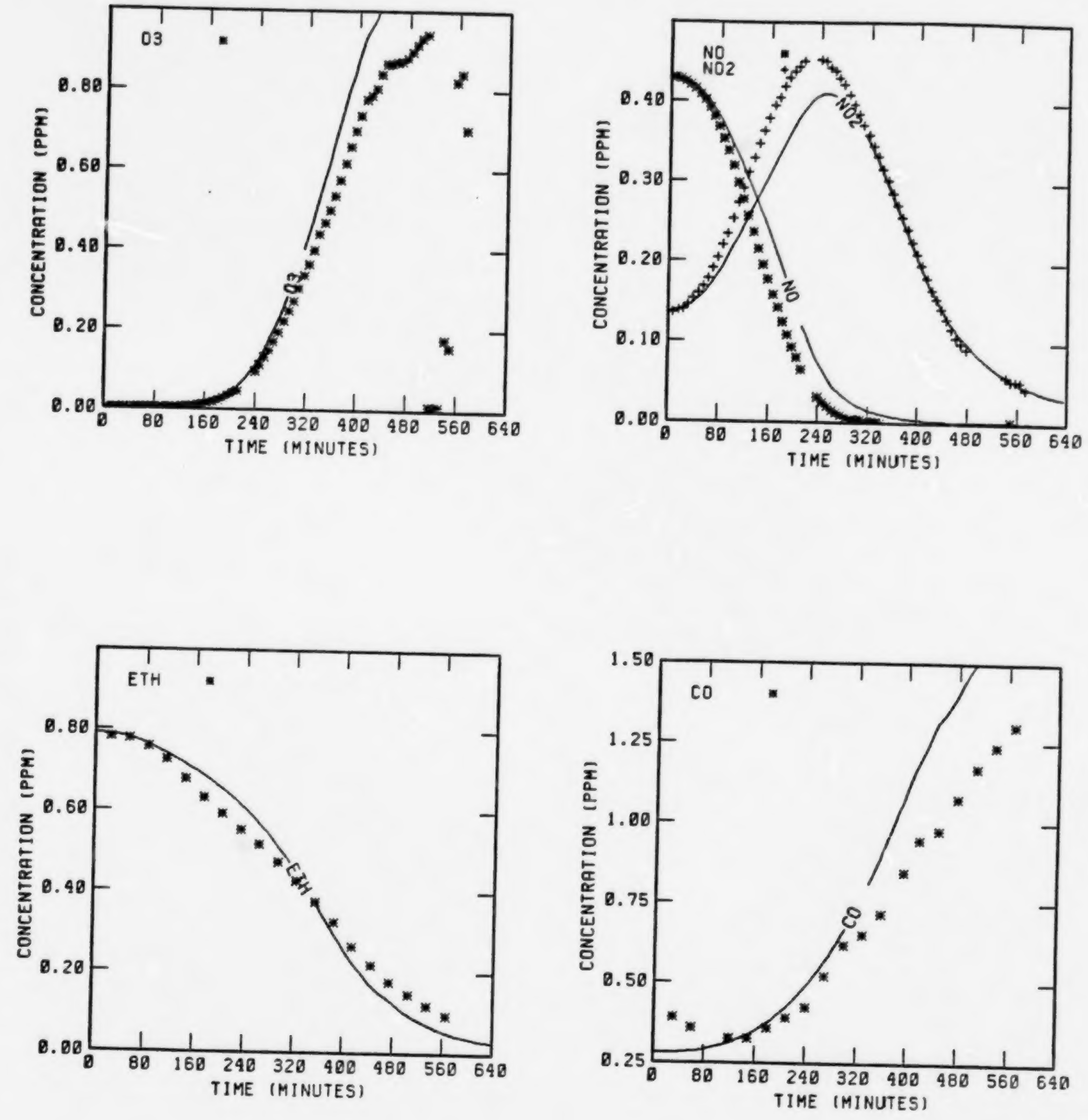

SIMULATION RESULTS FOR
UNCB 81578

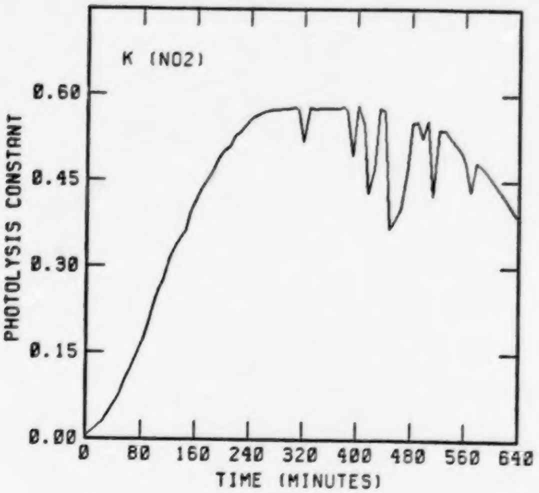

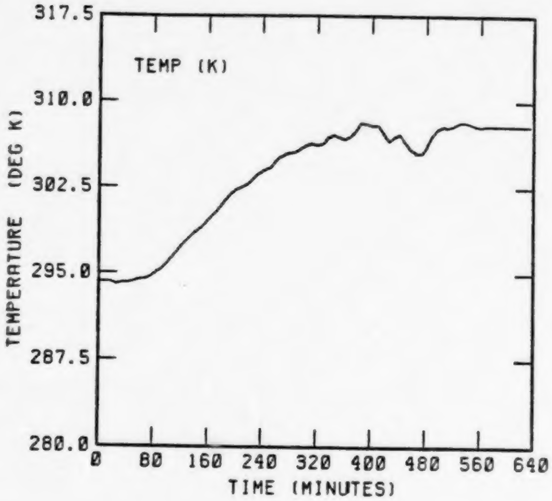

SIMULATION RESULTS FOR
UNCB 81578

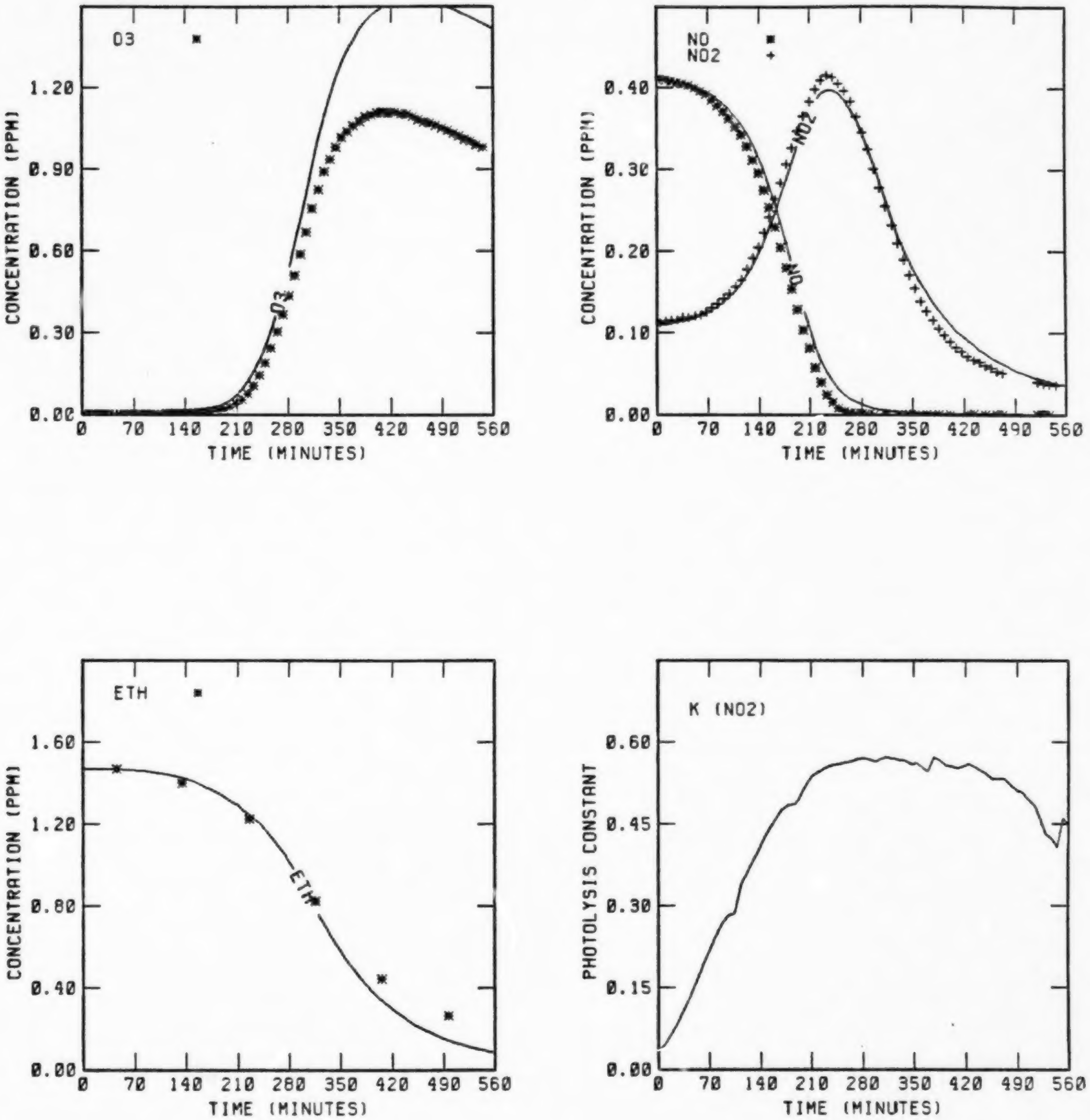

SIMULATION RESULTS FOR
UNCR 82378

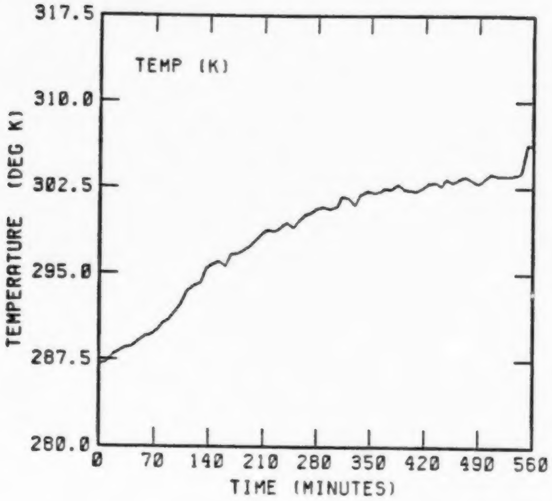

SIMULATION RESULTS FOR
UNCR 82378

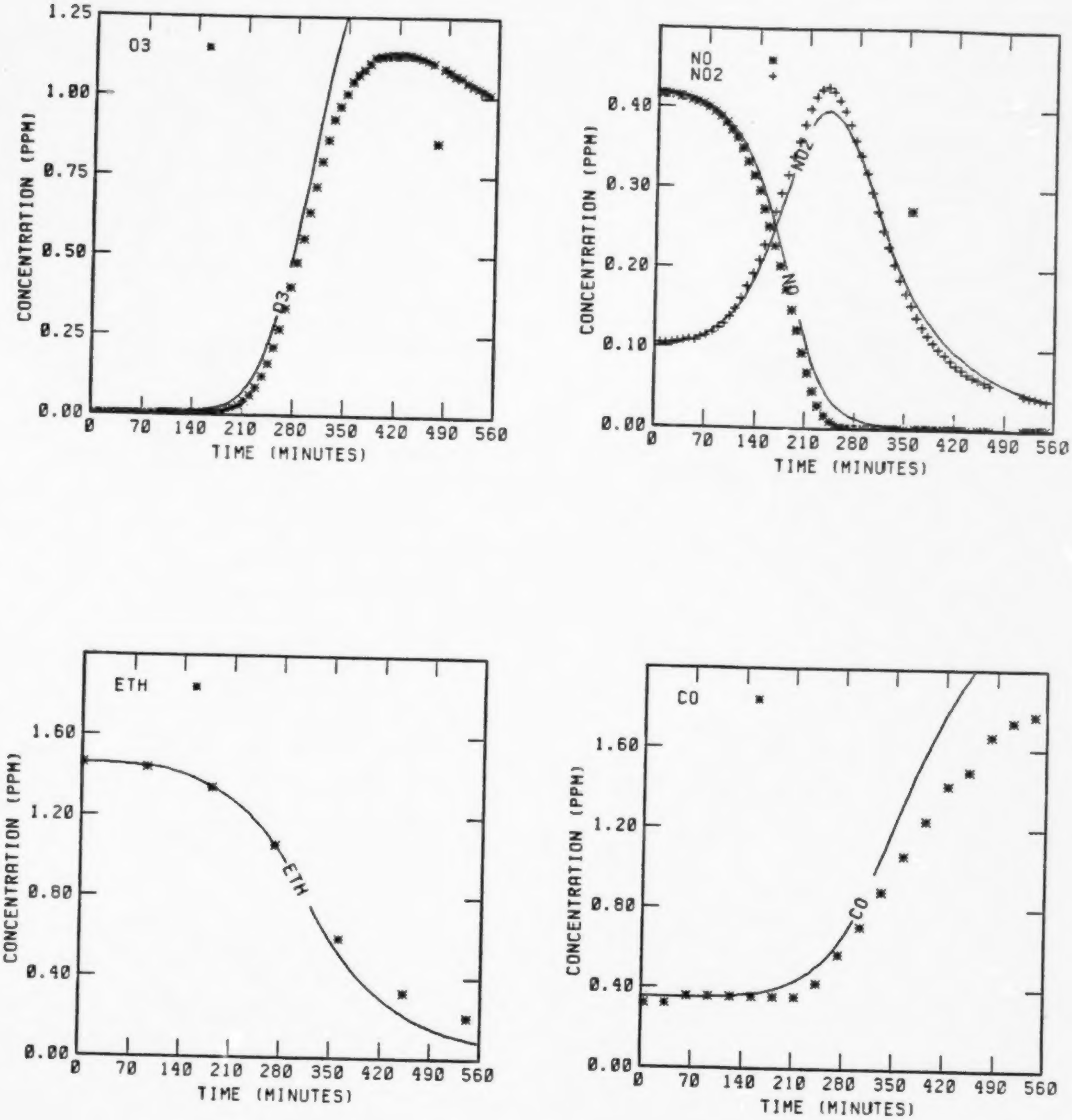

SIMULATION RESULTS FOR
UNCB 82378

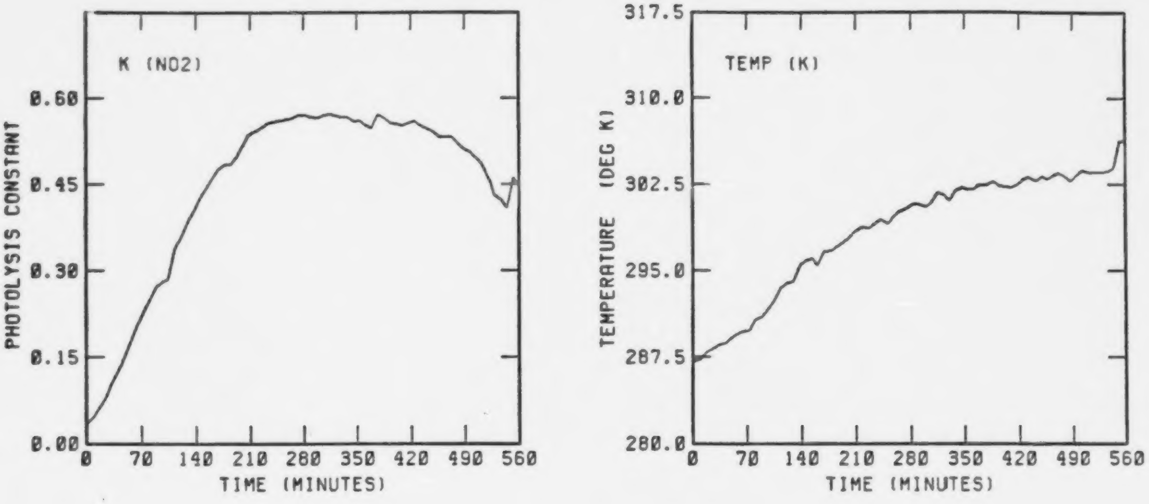

SIMULATION RESULTS FOR
UNCB 82378

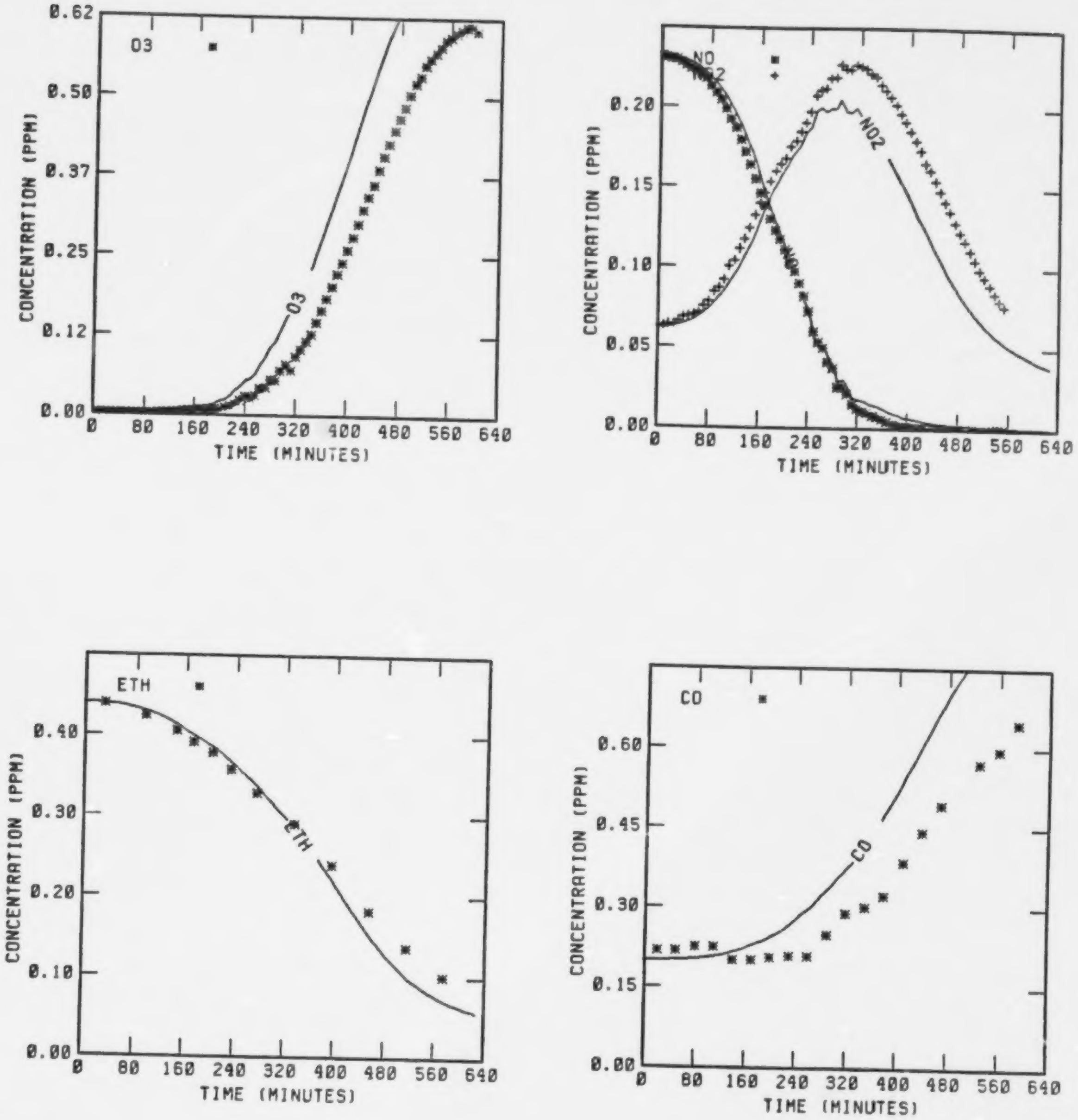

SIMULATION RESULTS FOR
UNCB 91478

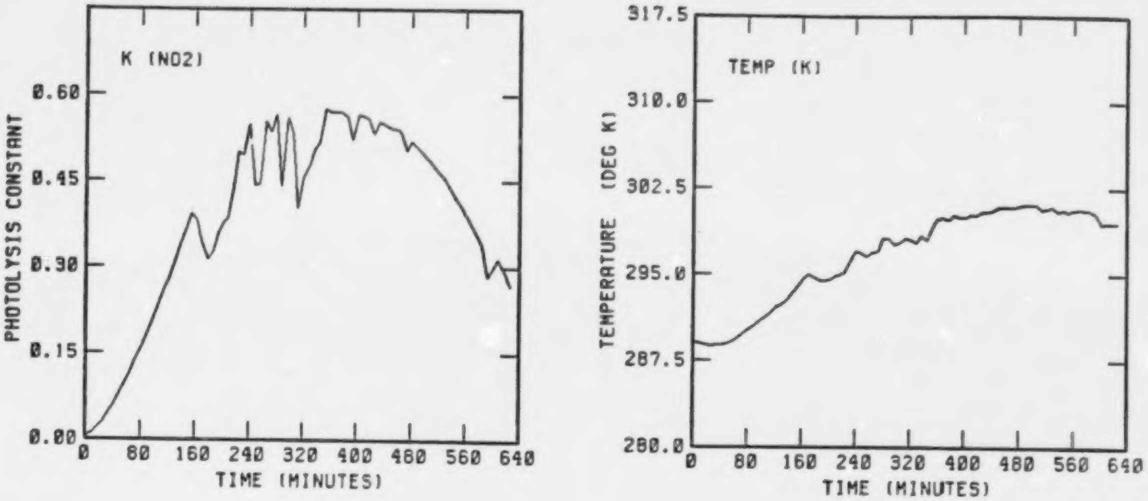

SIMULATION RESULTS FOR
UNCB 91478

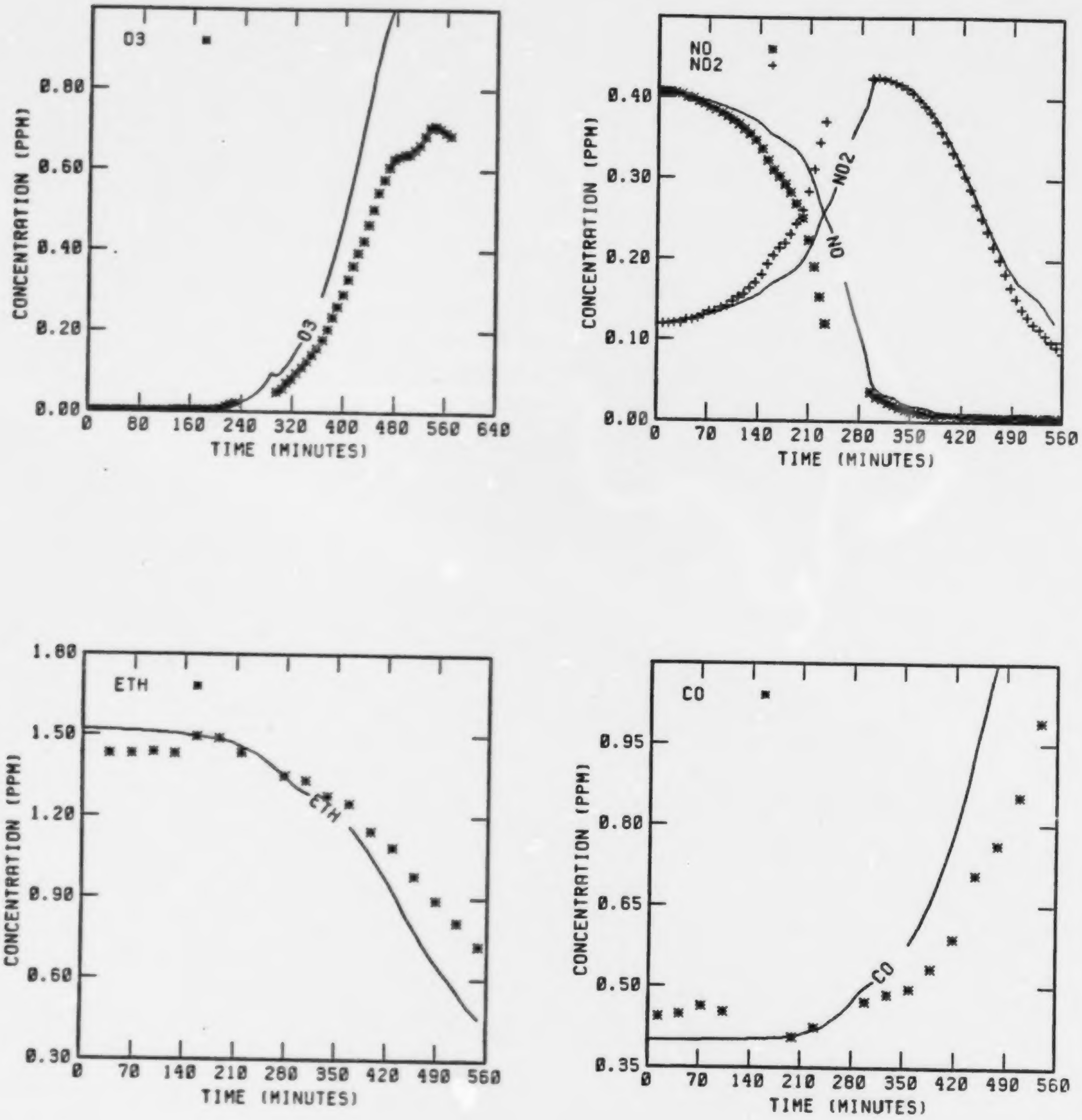

SIMULATION RESULTS FOR
UNCR 91578

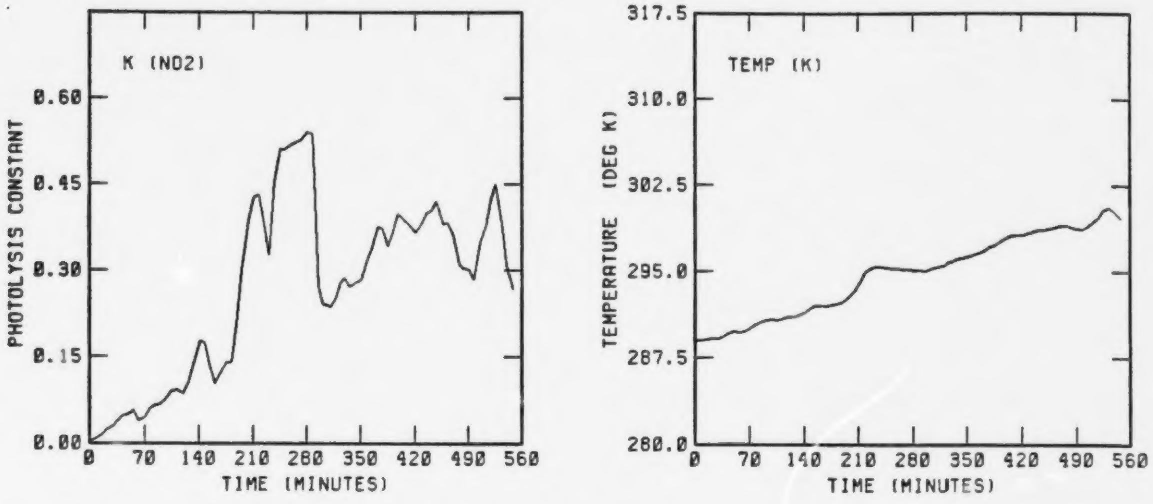

SIMULATION RESULTS FOR
UNCR 91578

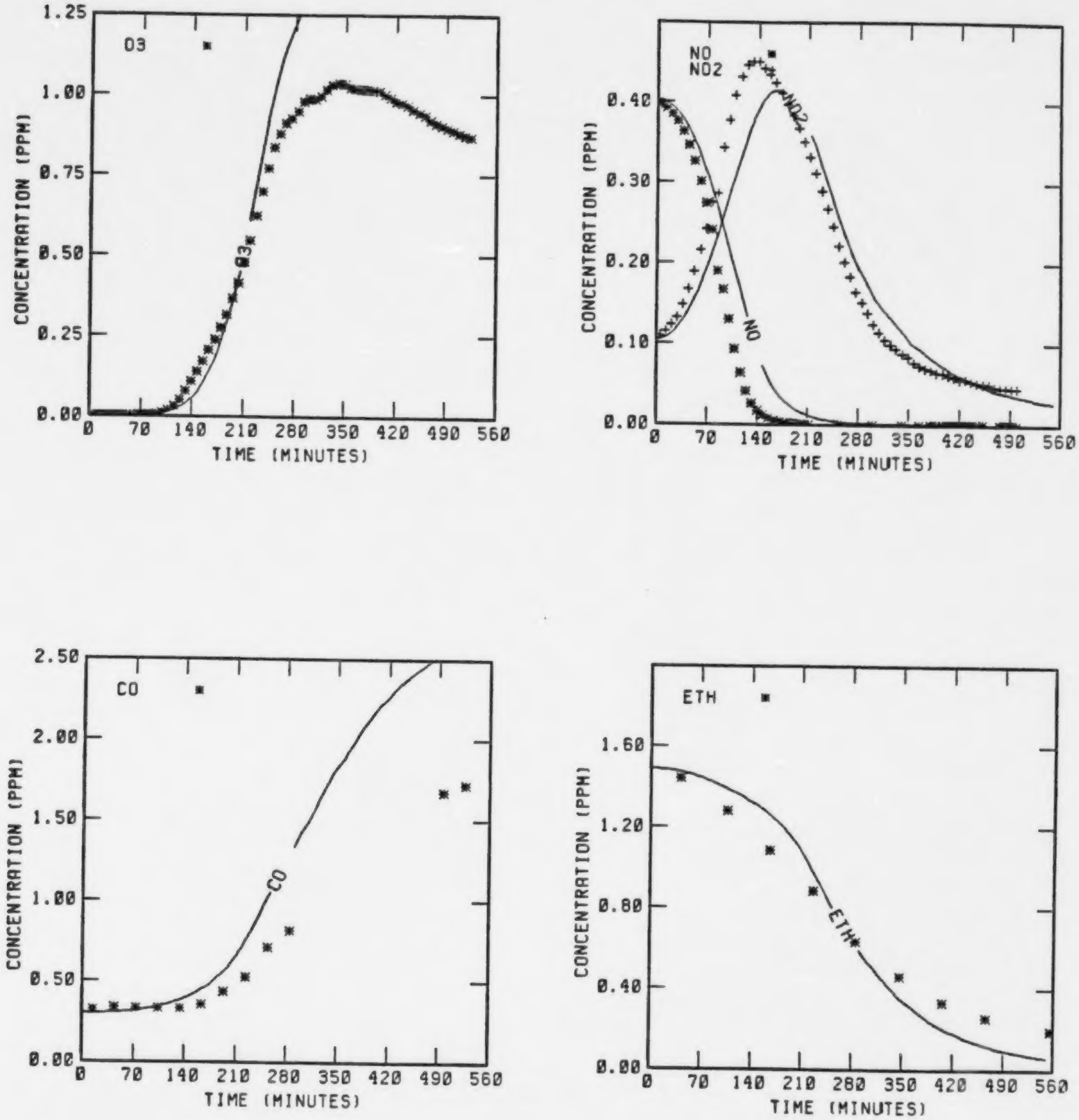

SIMULATION RESULTS FOR
UNCR 91878

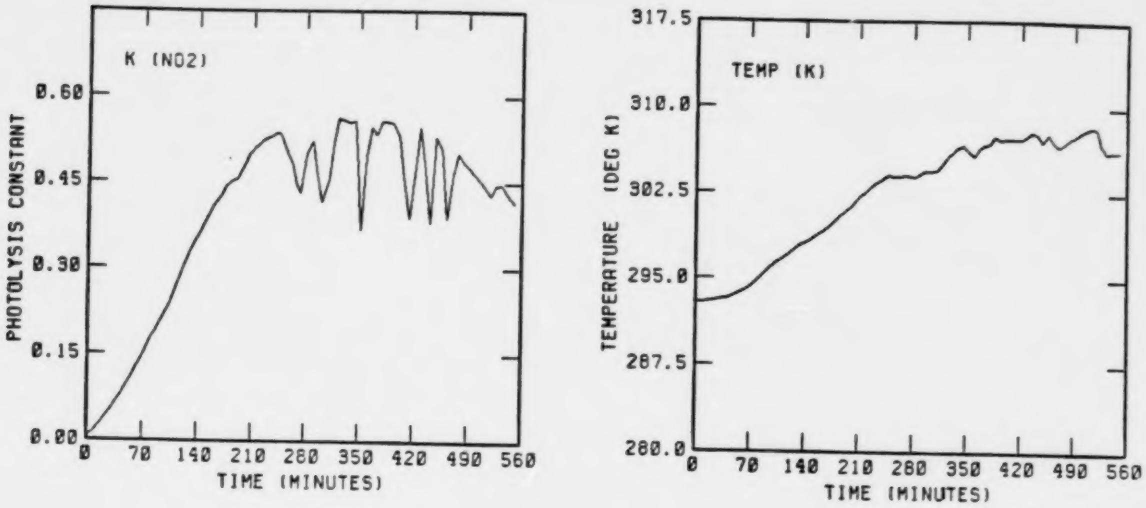

SIMULATION RESULTS FOR
UNCR 91878

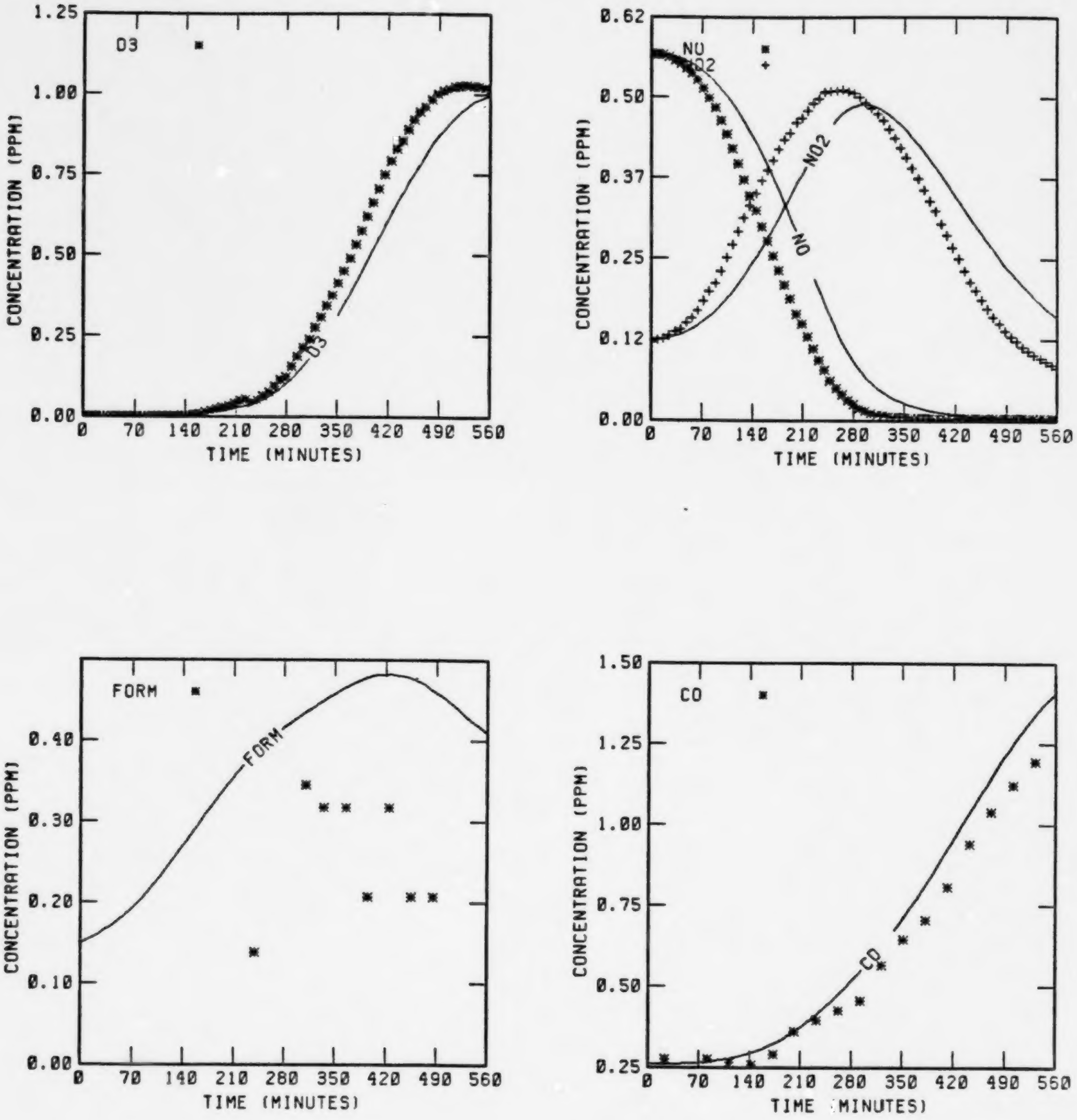

FIGURE . SIMULATION RESULTS FOR
UNCR 91978

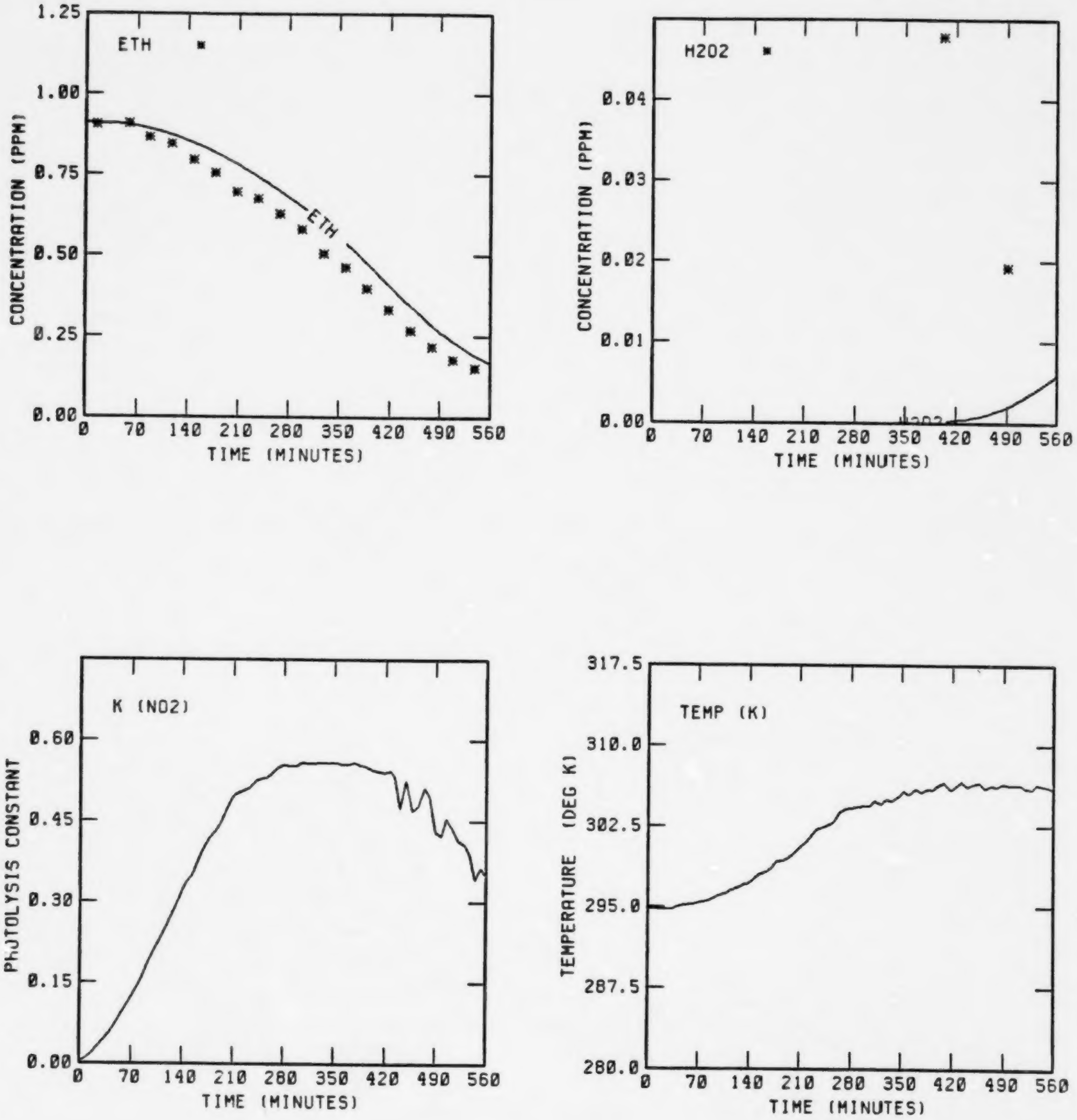

SIMULATION RESULTS FOR
UNCR 91978

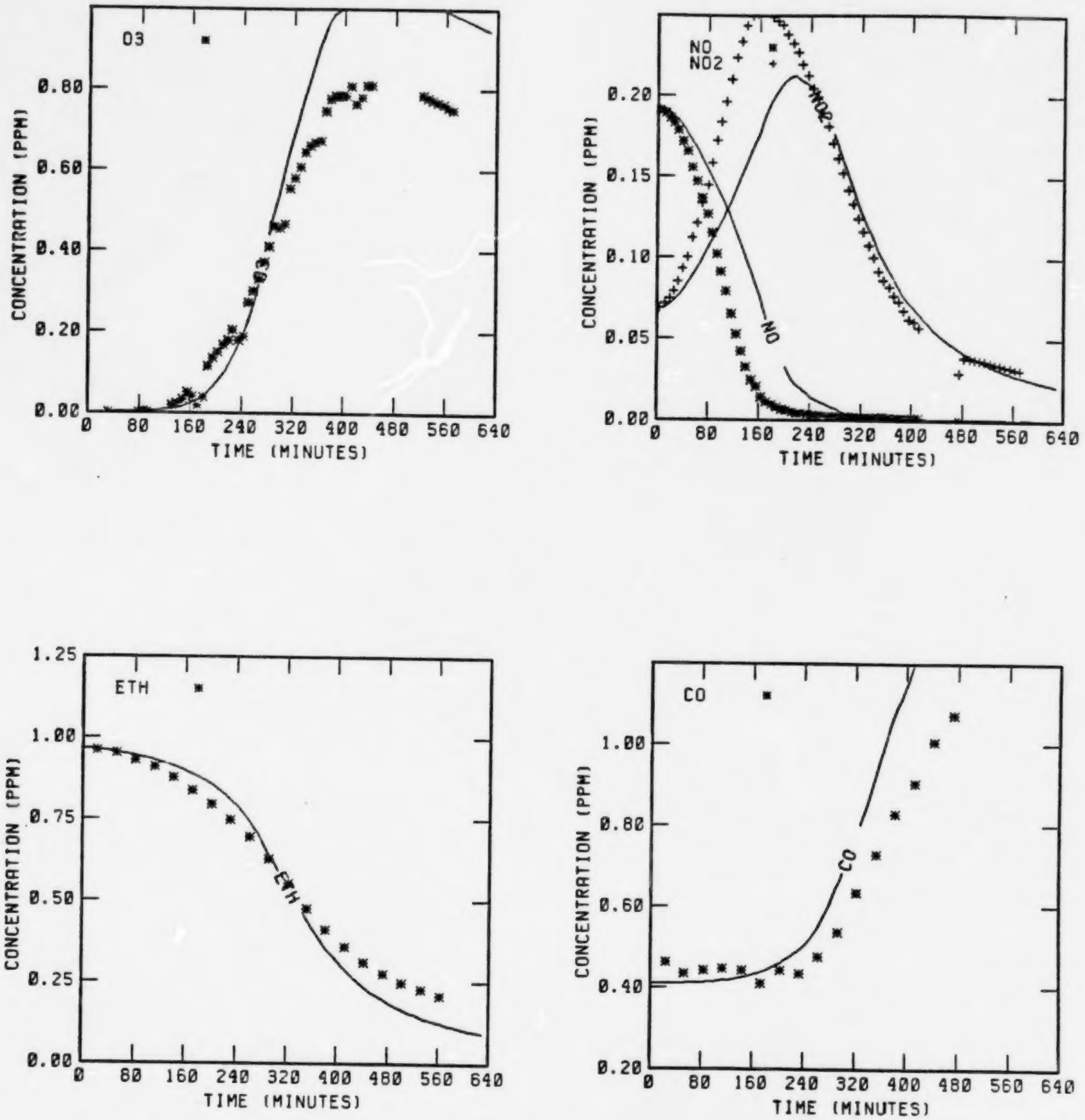

SIMULATION RESULTS FOR
UNCR 92178

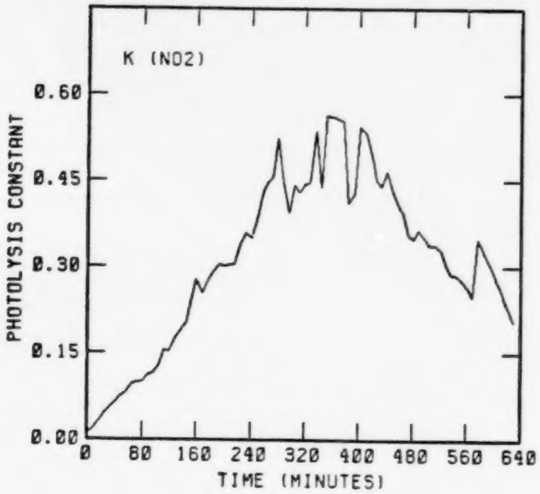

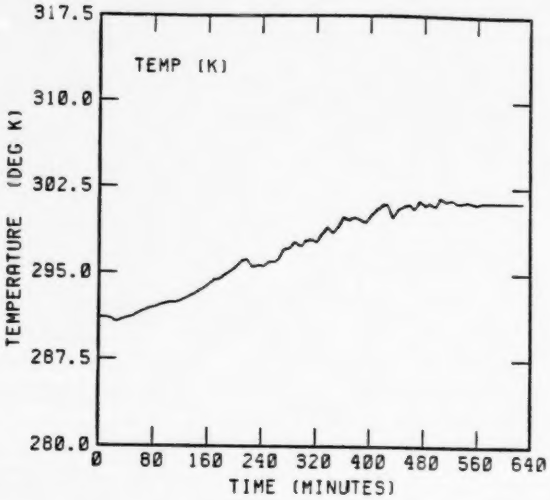

SIMULATION RESULTS FOR
UNCR 92178

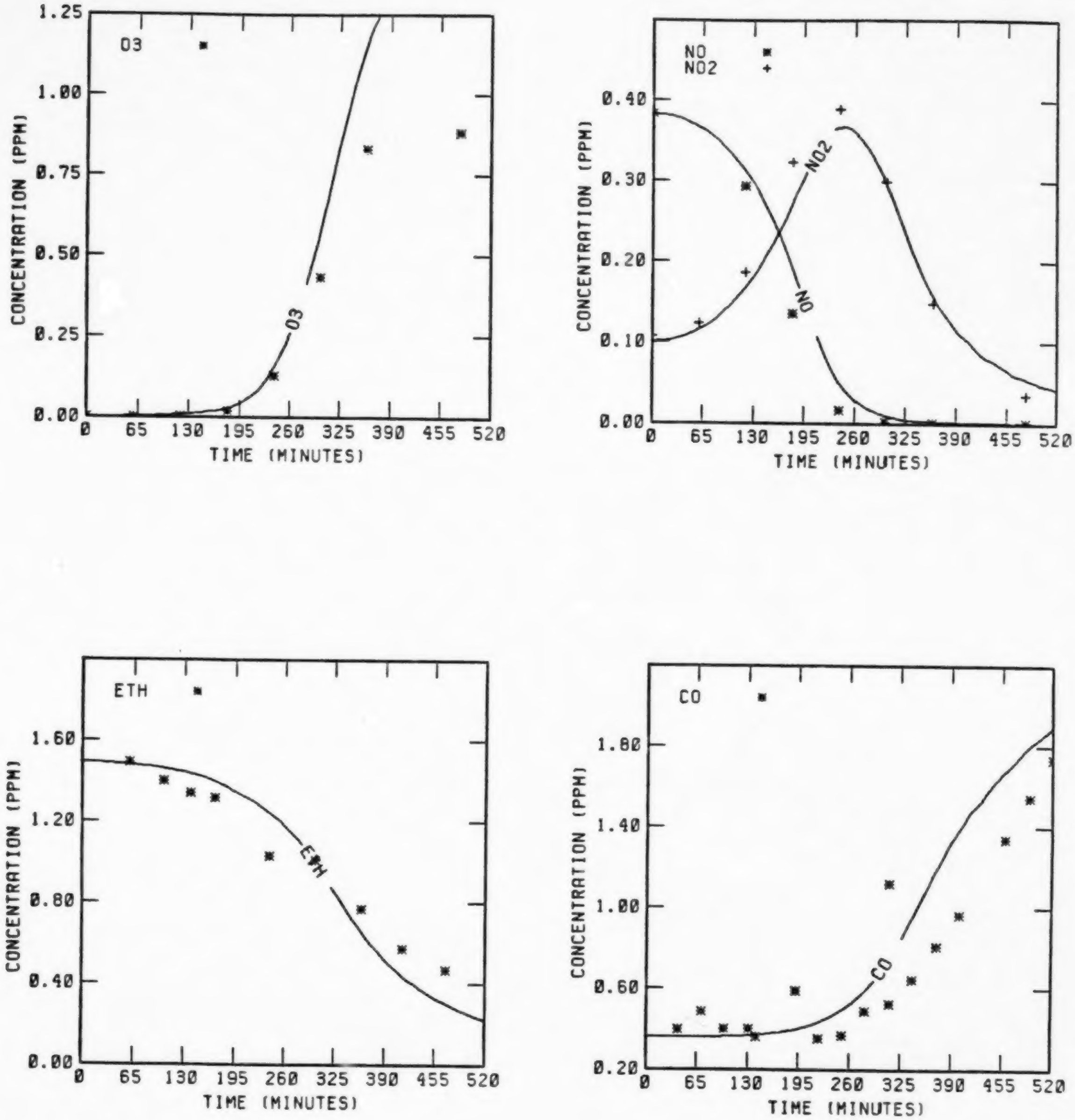

SIMULATION RESULTS FOR
UNCB 100278

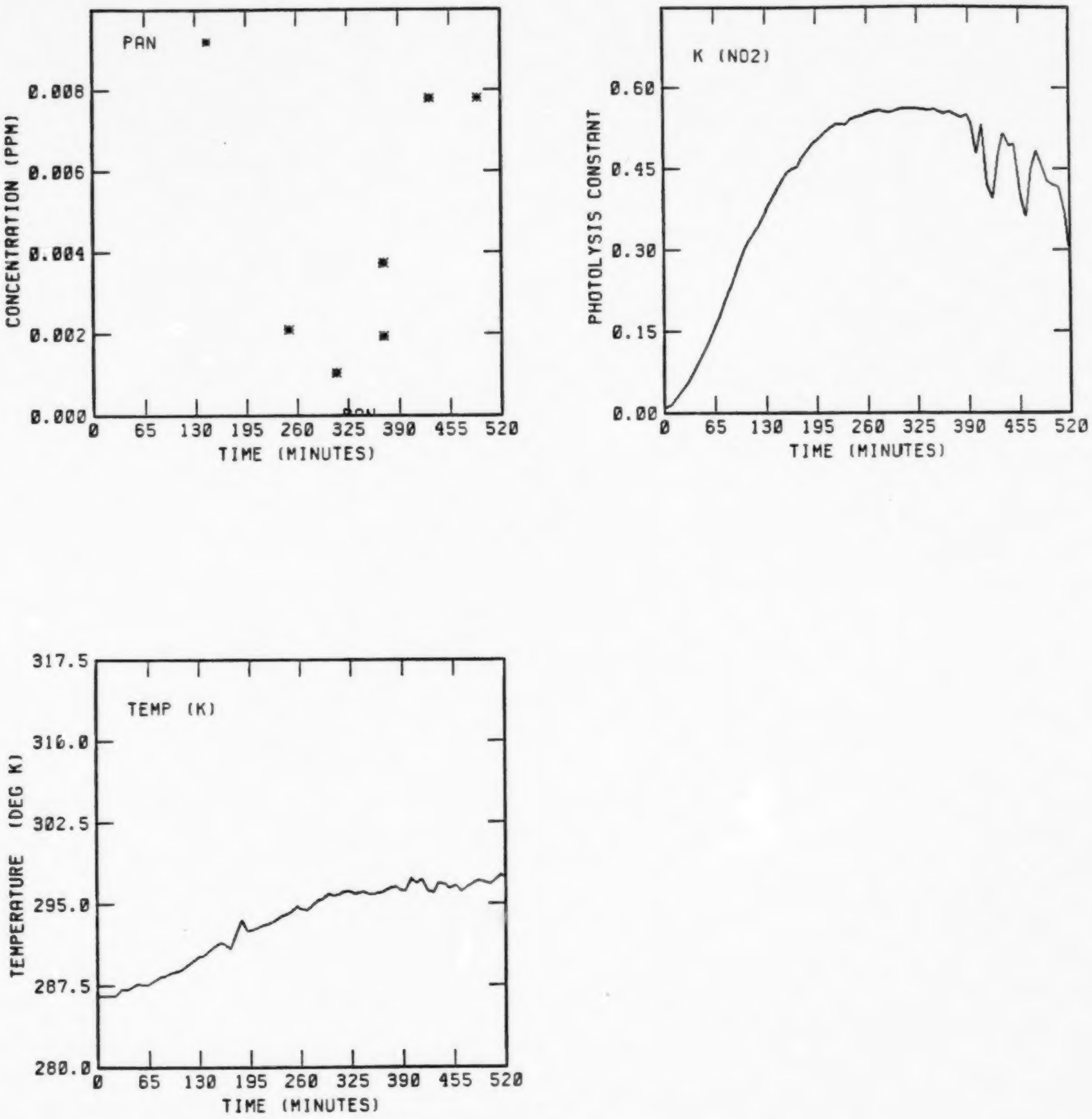

SIMULATION RESULTS FOR
UNCB 100278

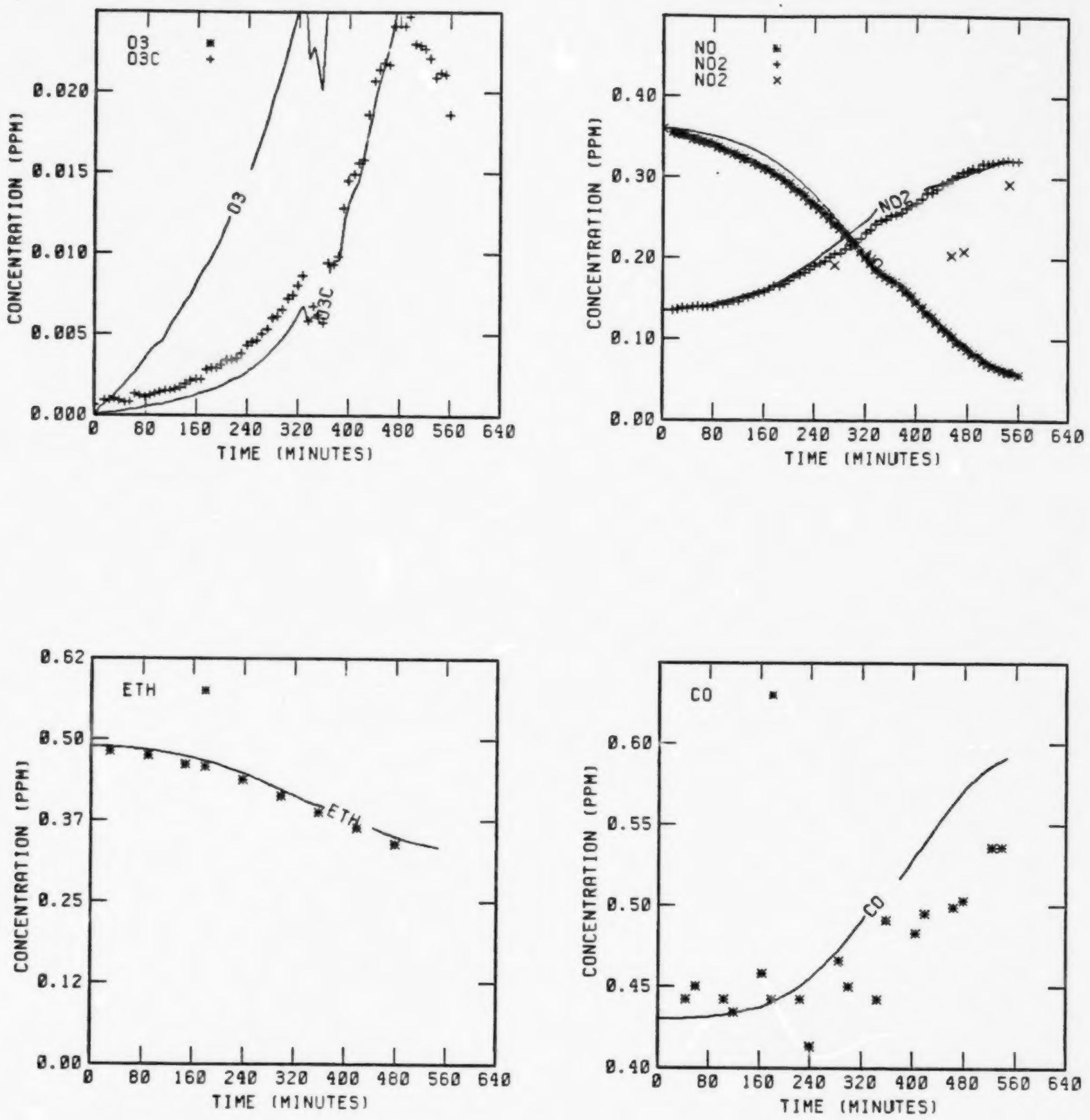

SIMULATION RESULTS FOR
UNCR 100378

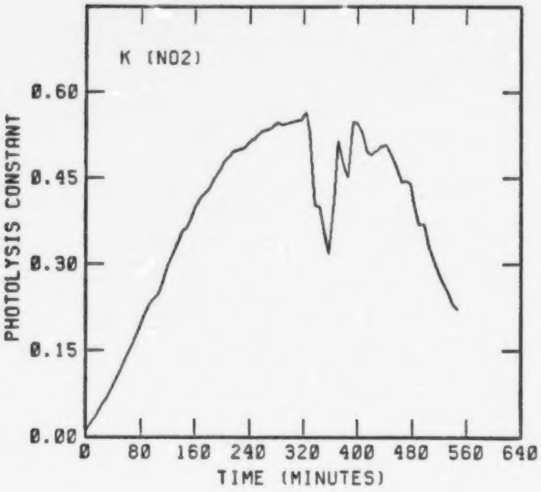

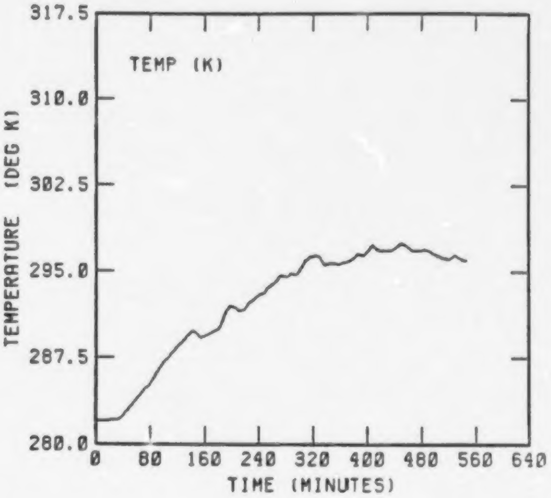

SIMULATION RESULTS FOR
UNCR 100378

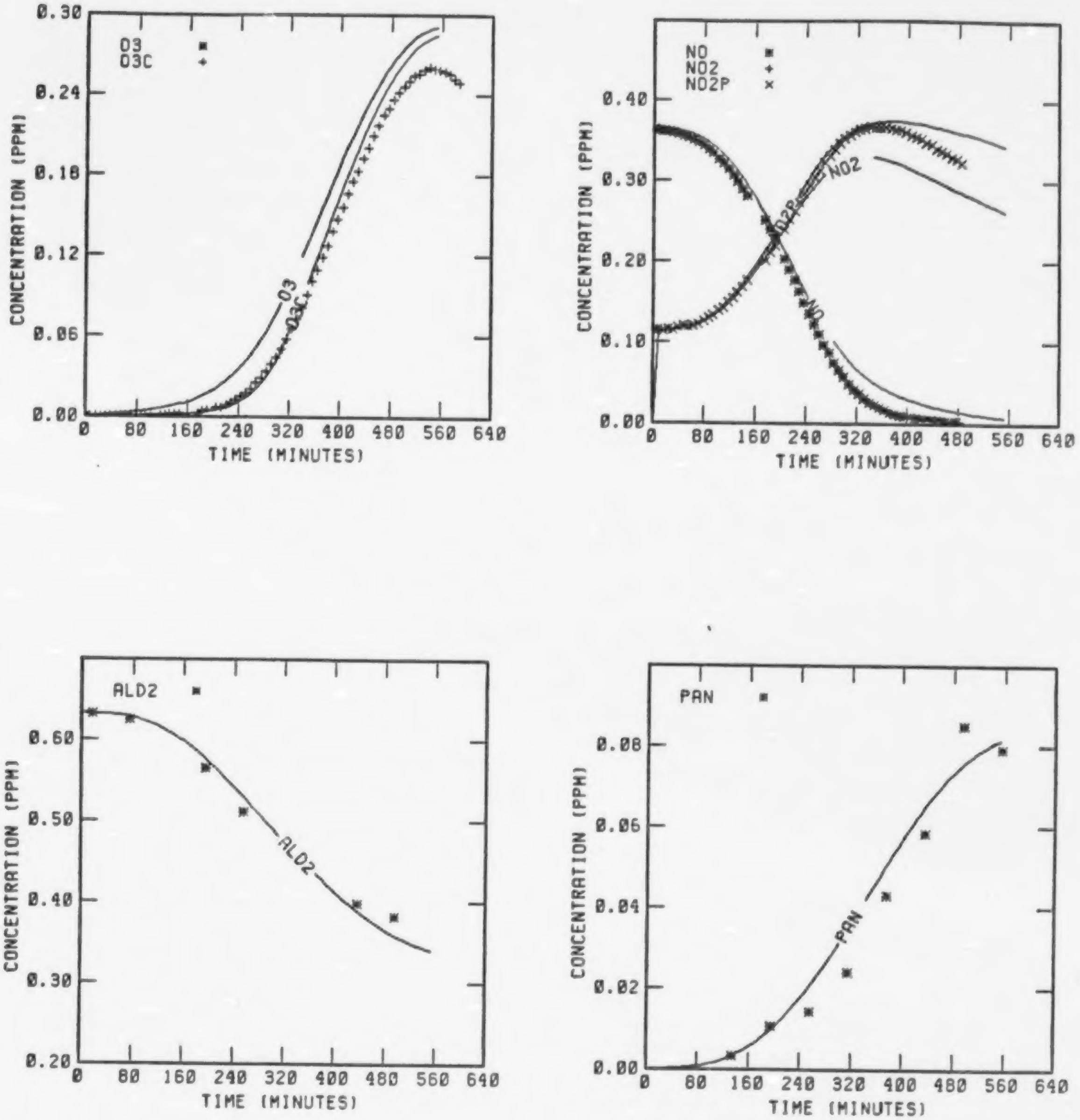

SIMULATION RESULTS FOR
UNCR 101278

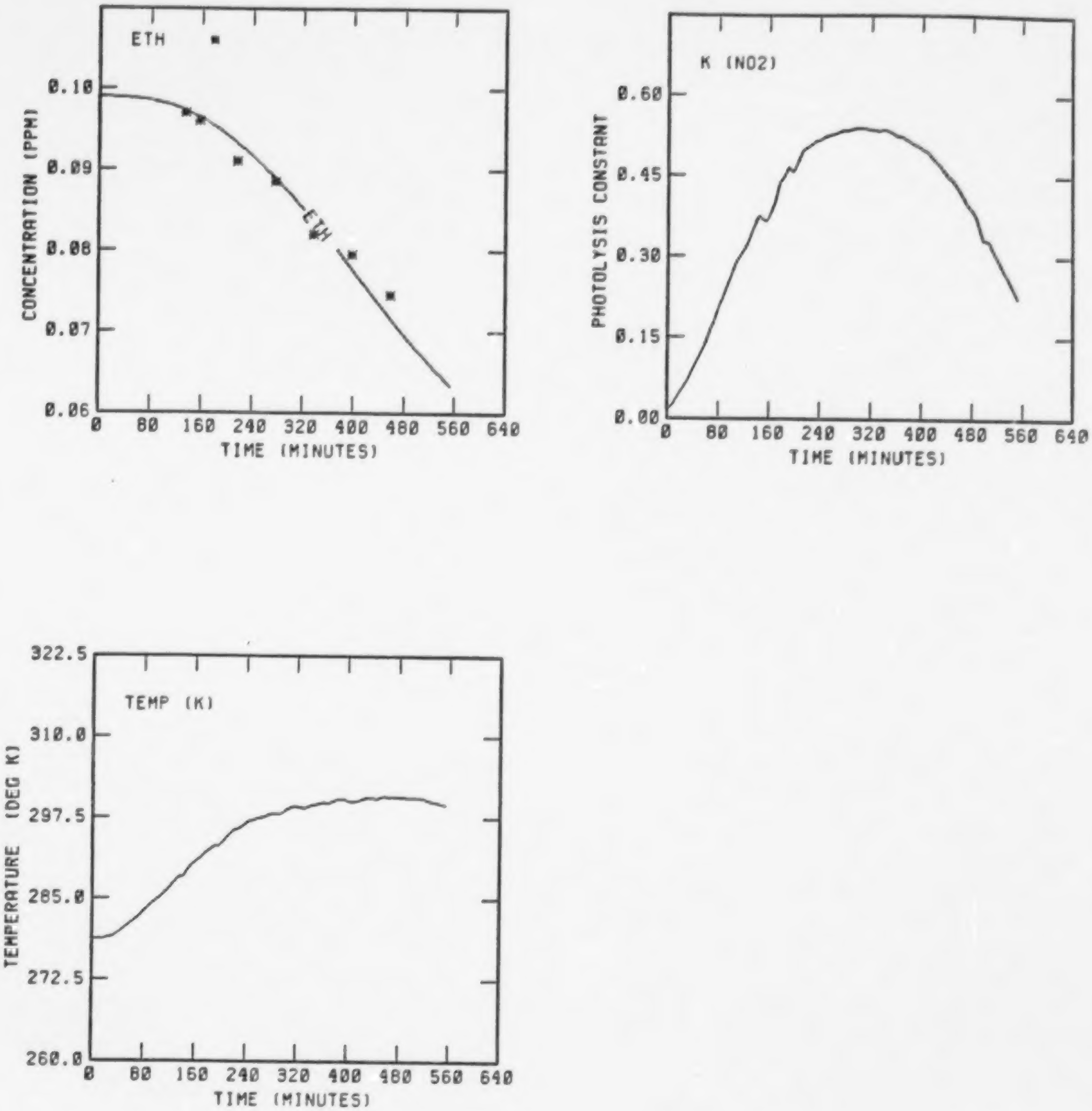

SIMULATION RESULTS FOR
UNCR 101278

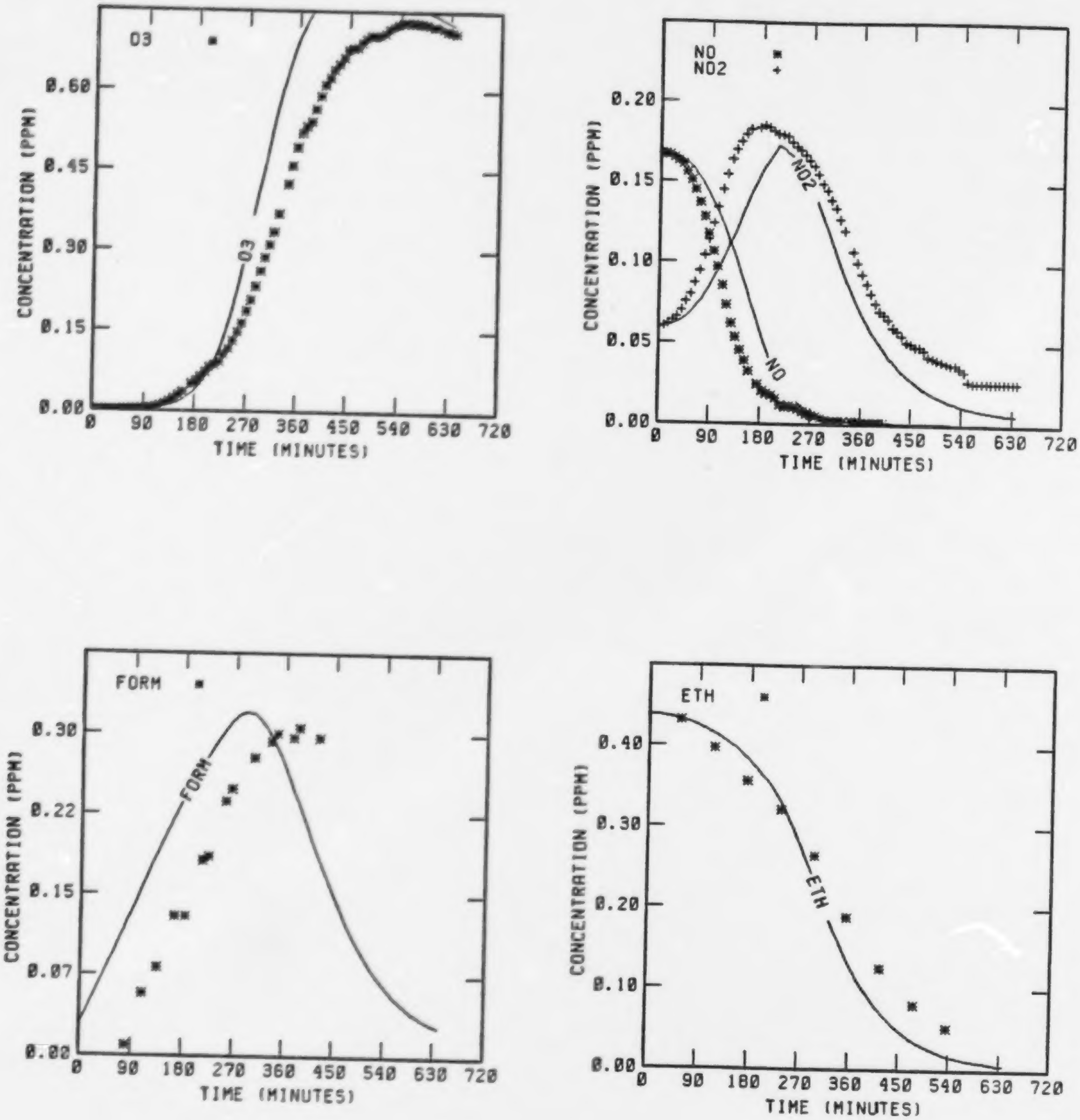

SIMULATION RESULTS FOR
UNCR 80479

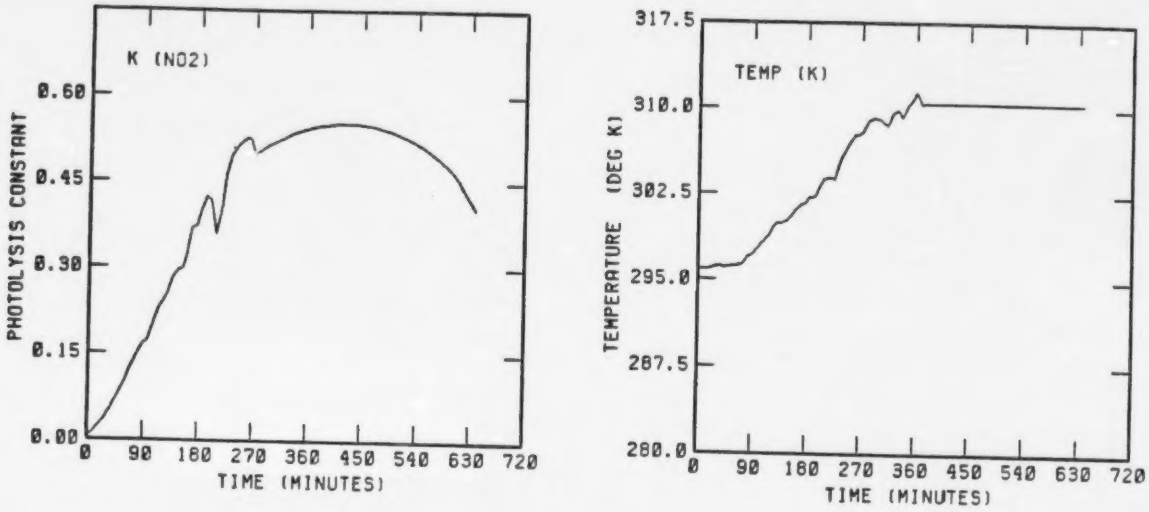

SIMULATION RESULTS FOR
UNCR 80479

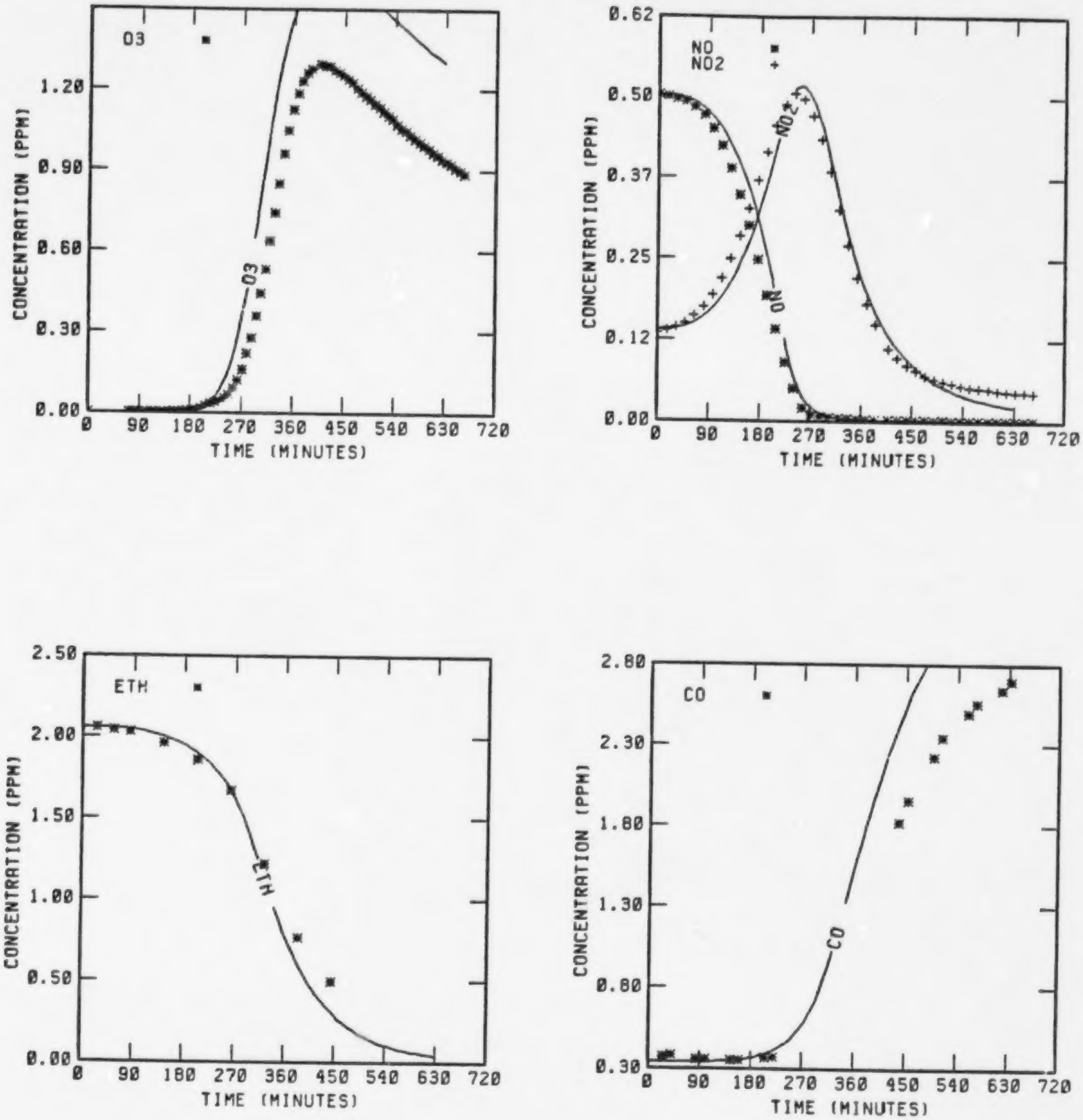

SIMULATION RESULTS FOR
UNCR 80579

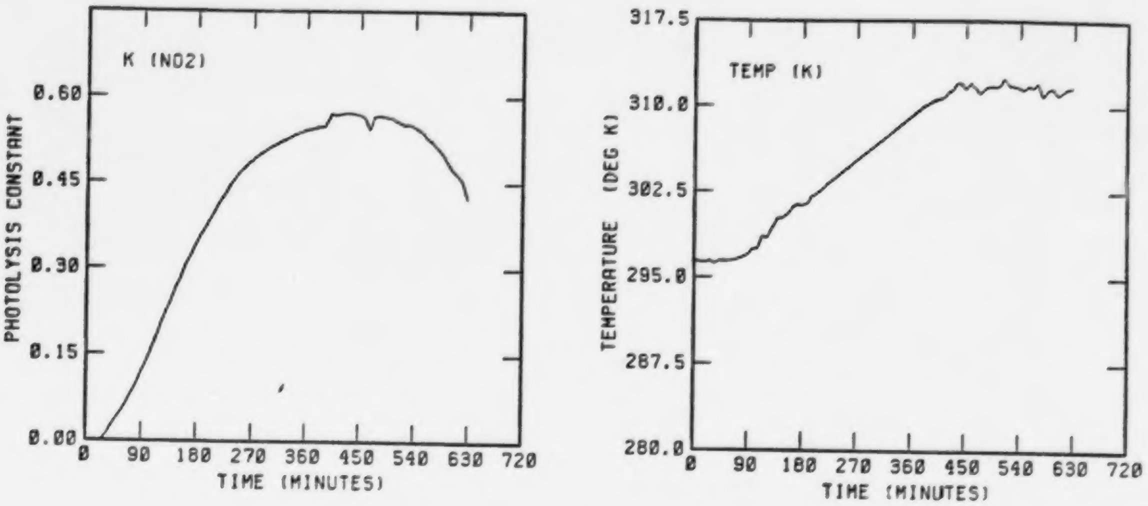

SIMULATION RESULTS FOR
UNCR 80579

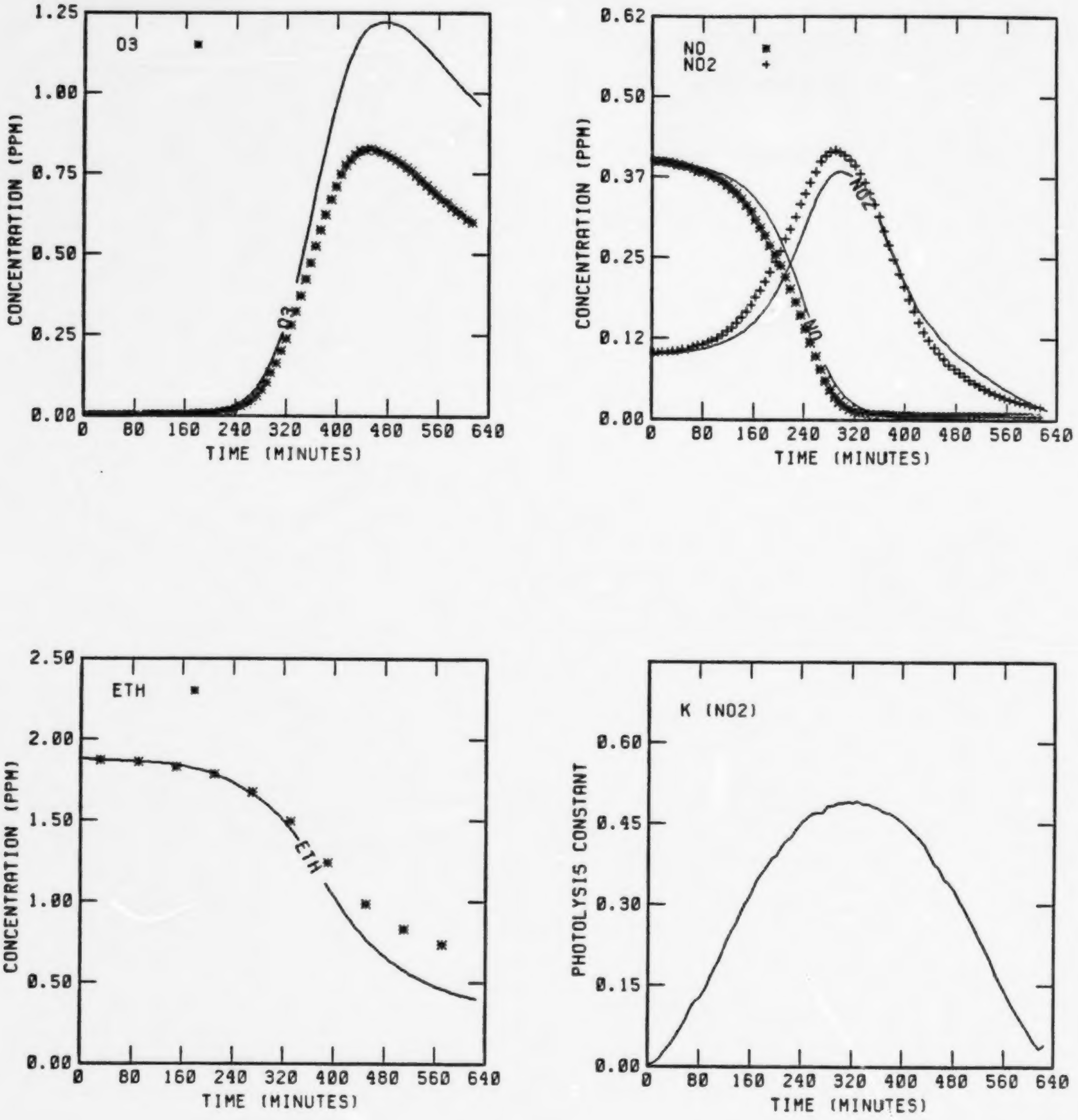

SIMULATION RESULTS FOR
UNCR 103179

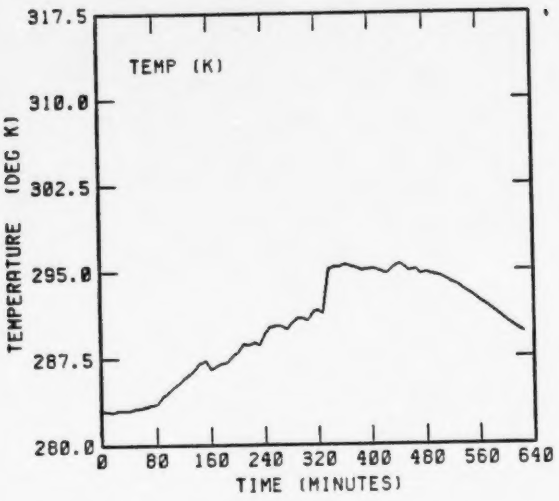

SIMULATION RESULTS.FOR
UNCR 103179

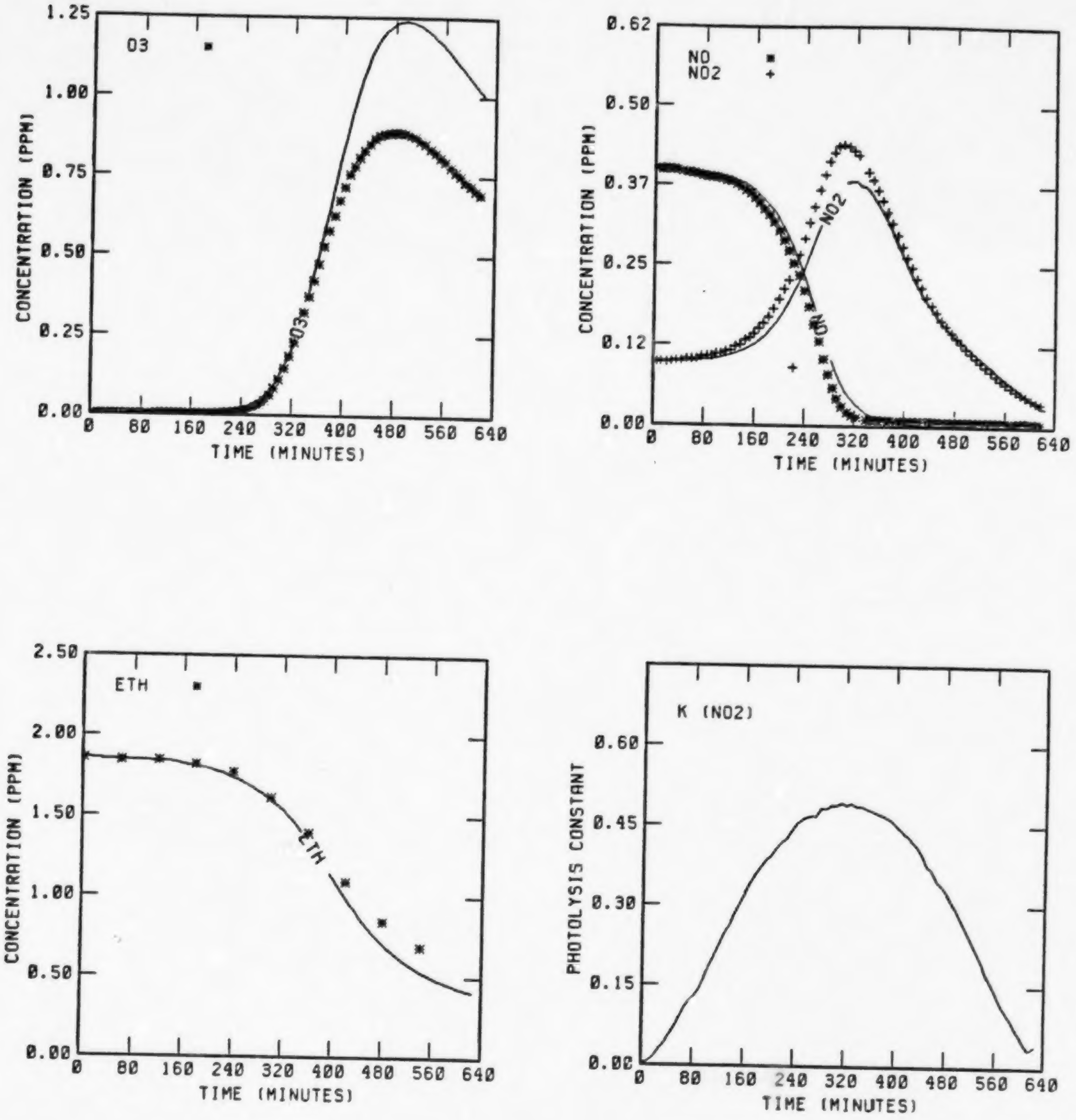

SIMULATION RESULTS FOR
UNCB 103179

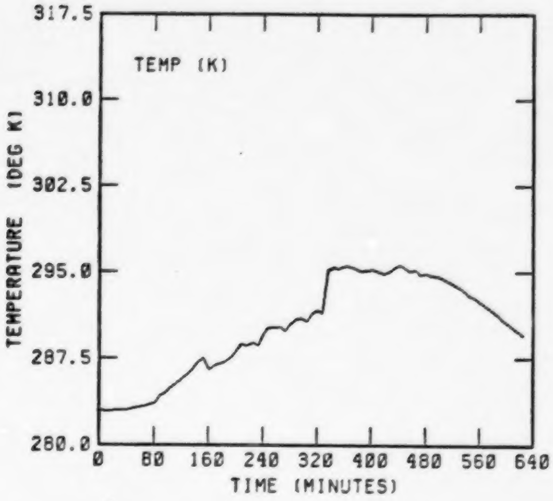

SIMULATION RESULTS FOR
UNCB 103179

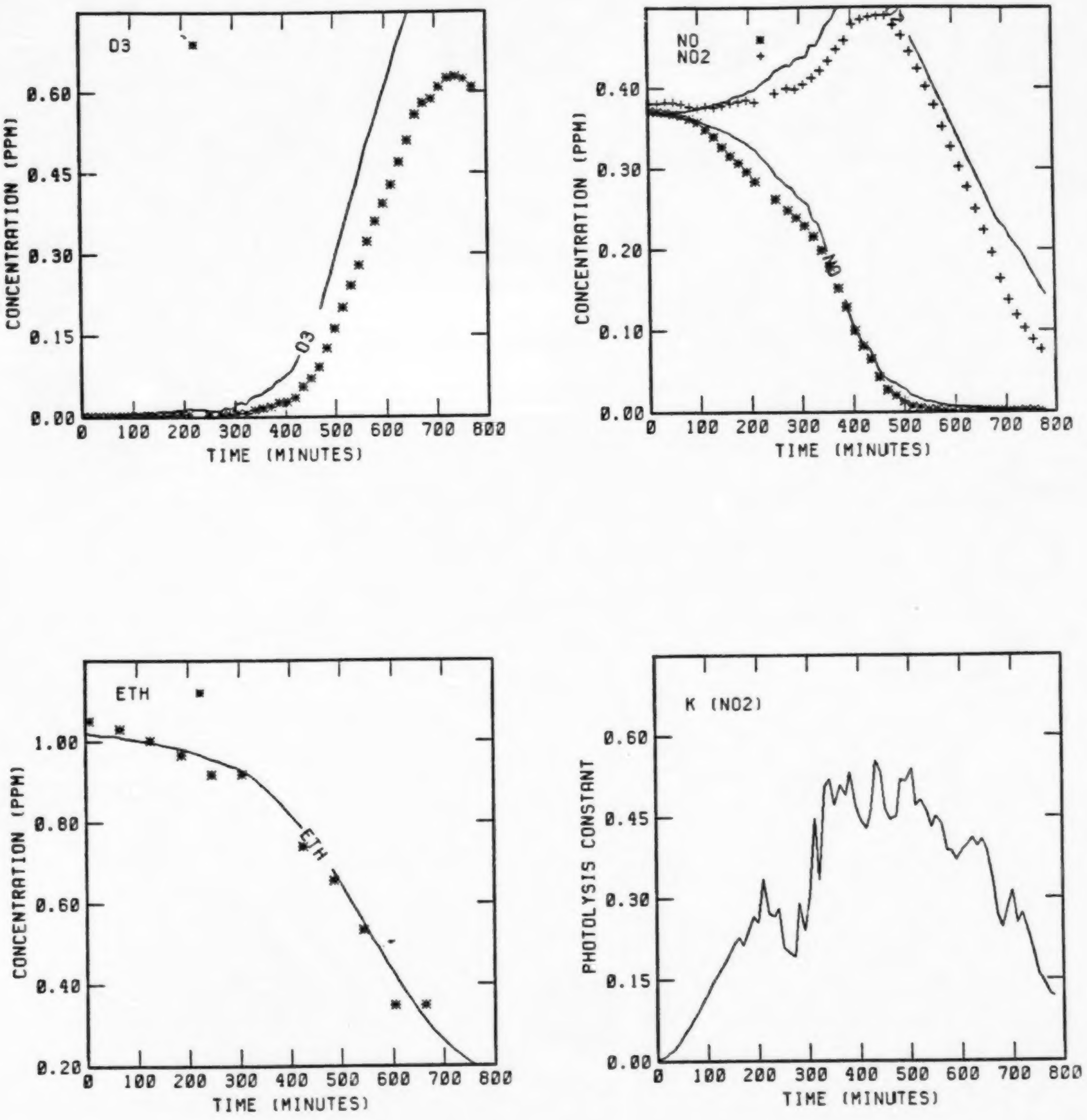

SIMULATION RESULTS FOR
UNCR 70880

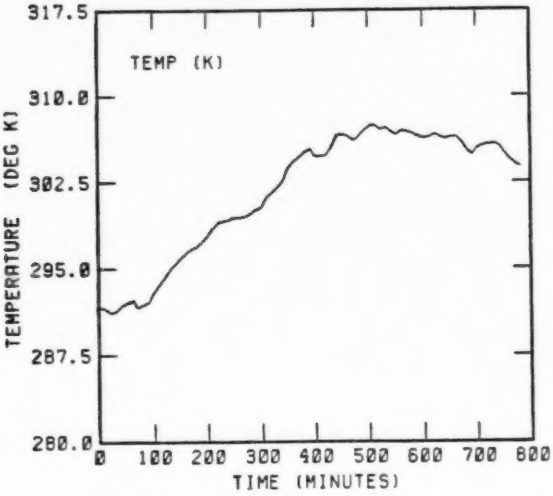

SIMULATION RESULTS FOR
UNCR 70880

Appendix D

SIMULATION RESULTS FOR THE
UNC TOLUENE AND M-XYLENE
EXPERIMENTS

Toluene

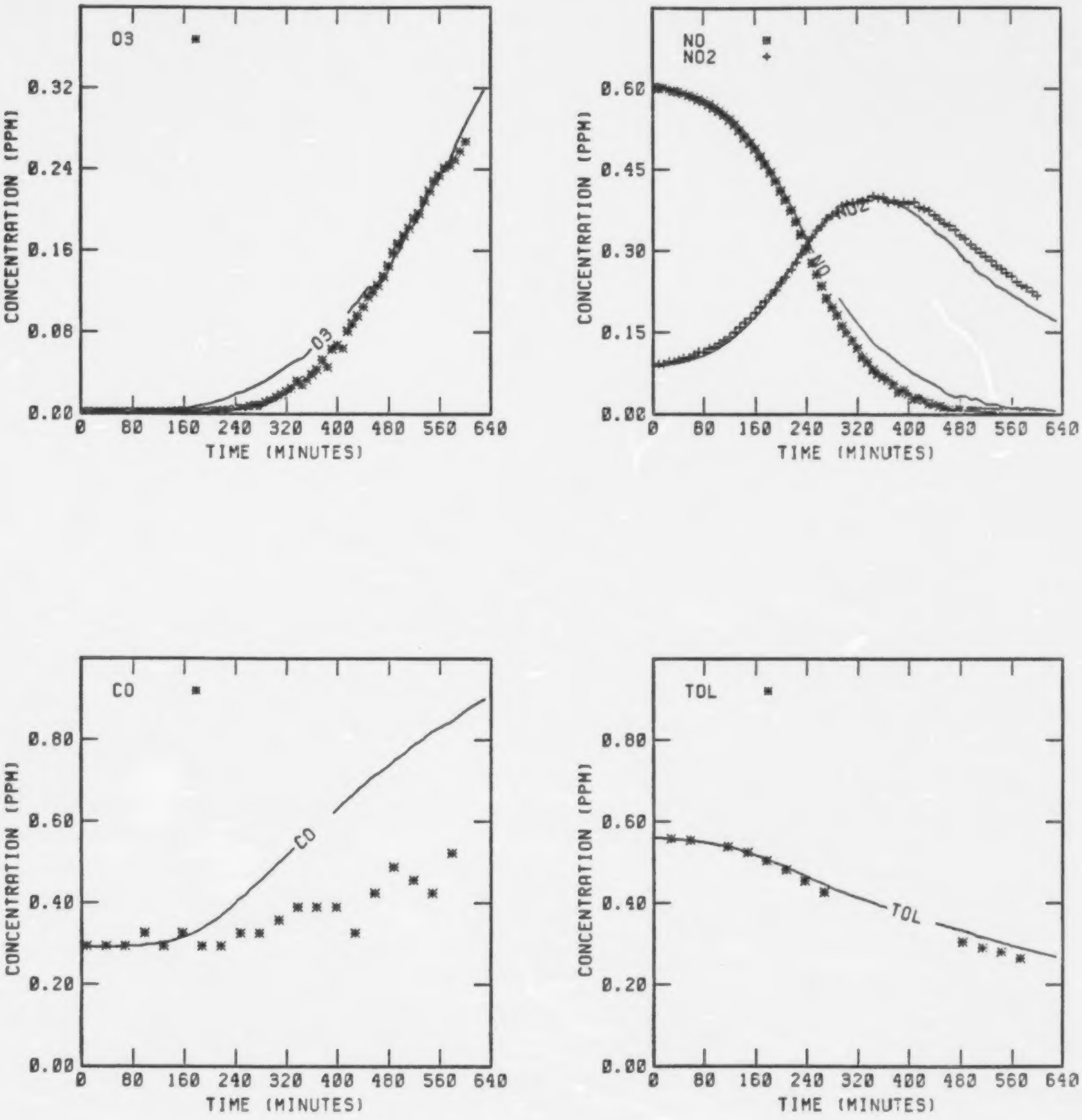

SIMULATION RESULTS FOR
UNCB 81678

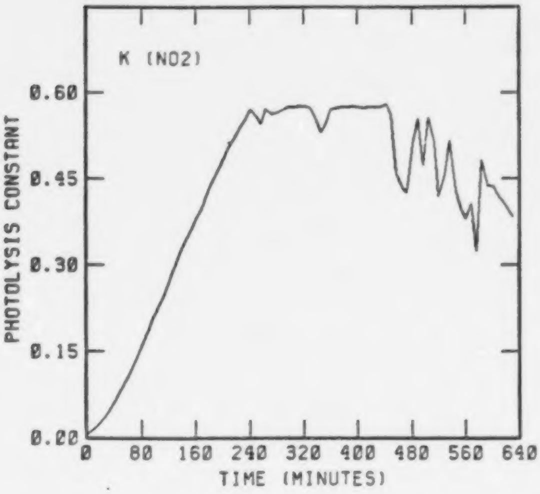

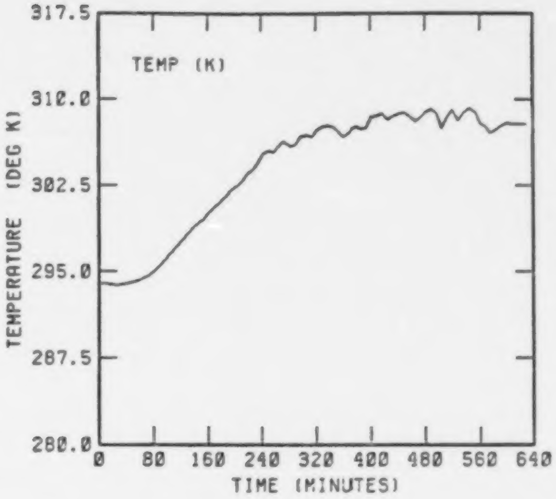

SIMULATION RESULTS FOR
UNCB 81678

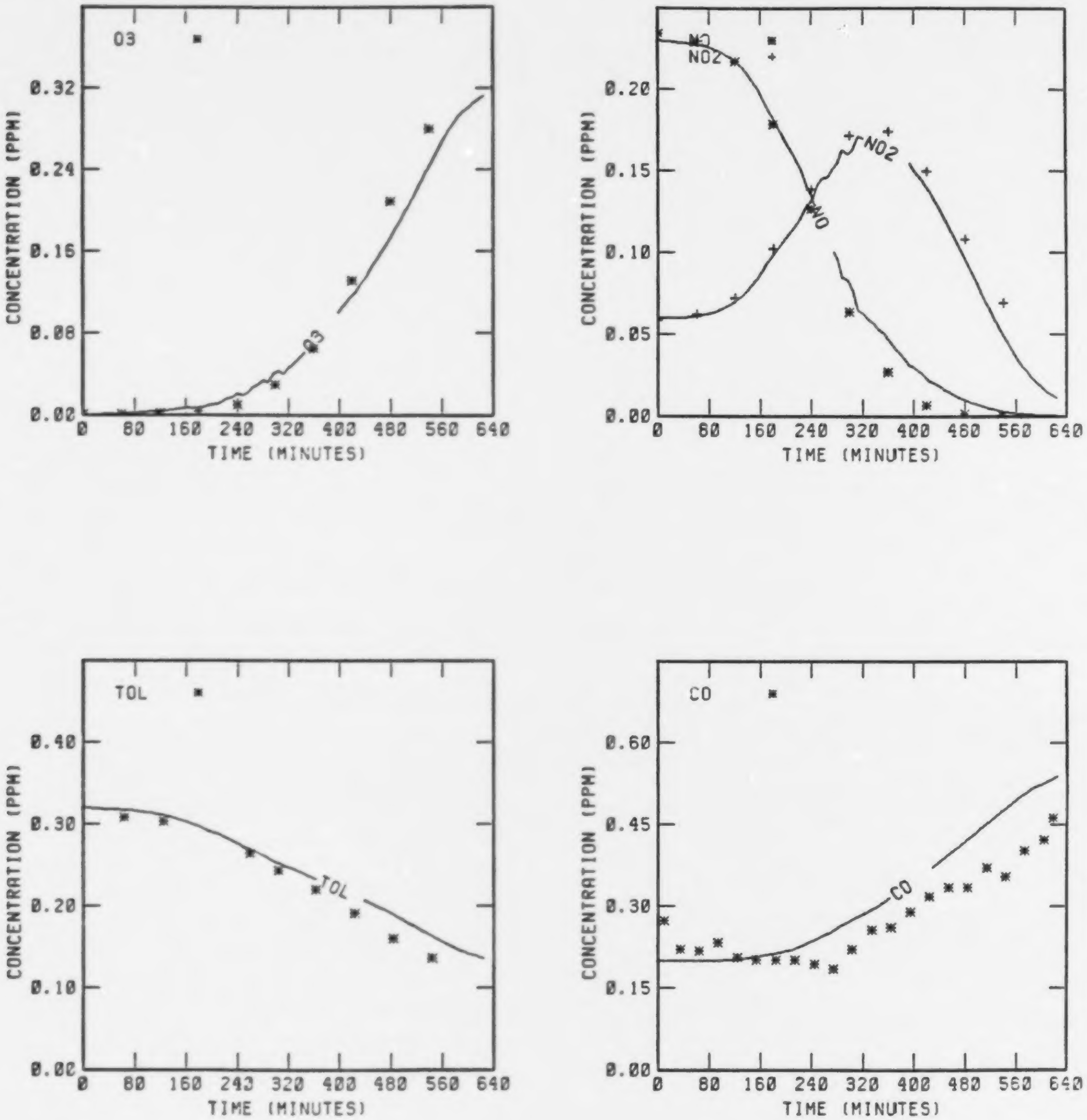

SIMULATION RESULTS FOR
UNCR 91478

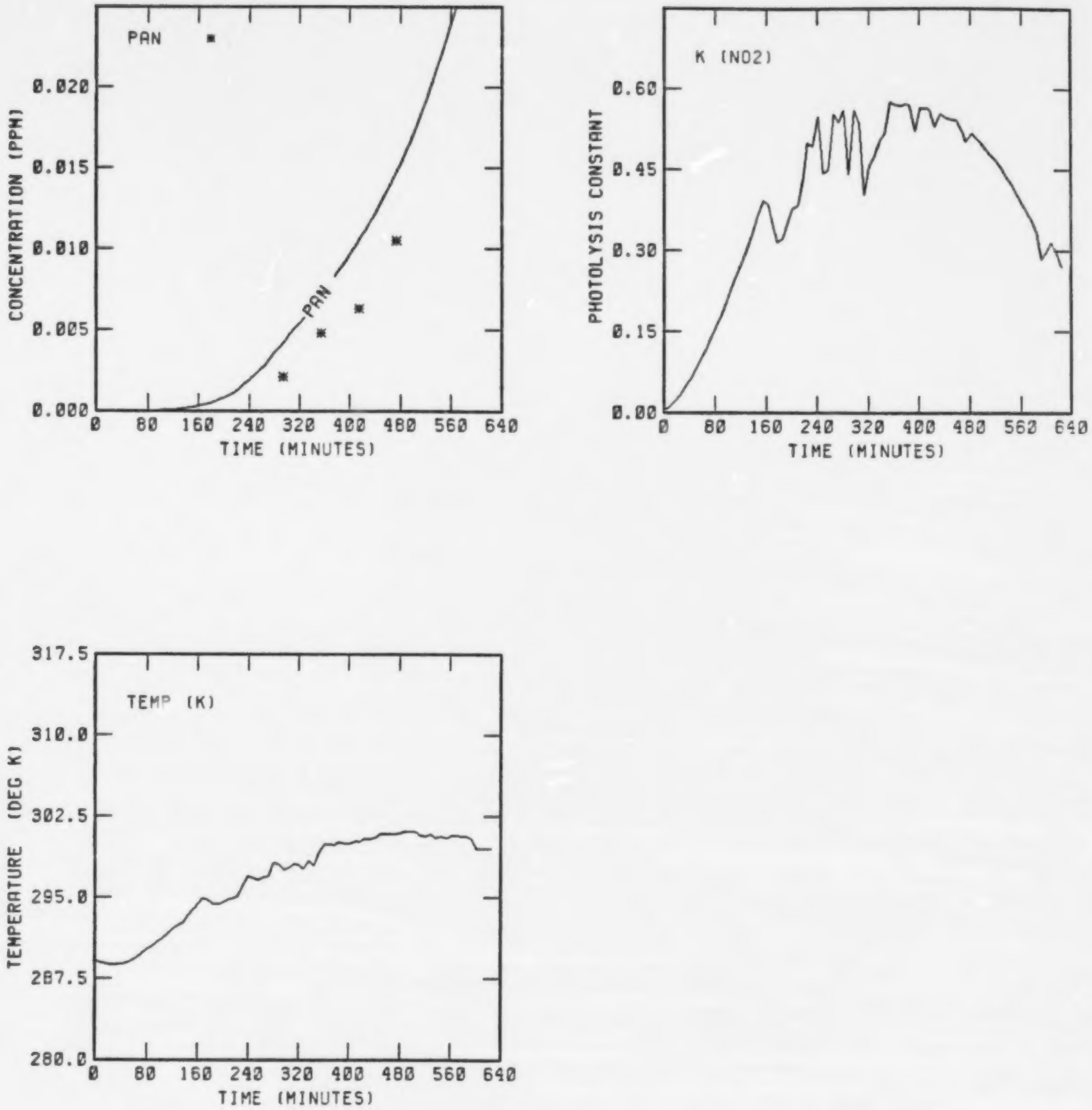

SIMULATION RESULTS FOR
UNCR 91478

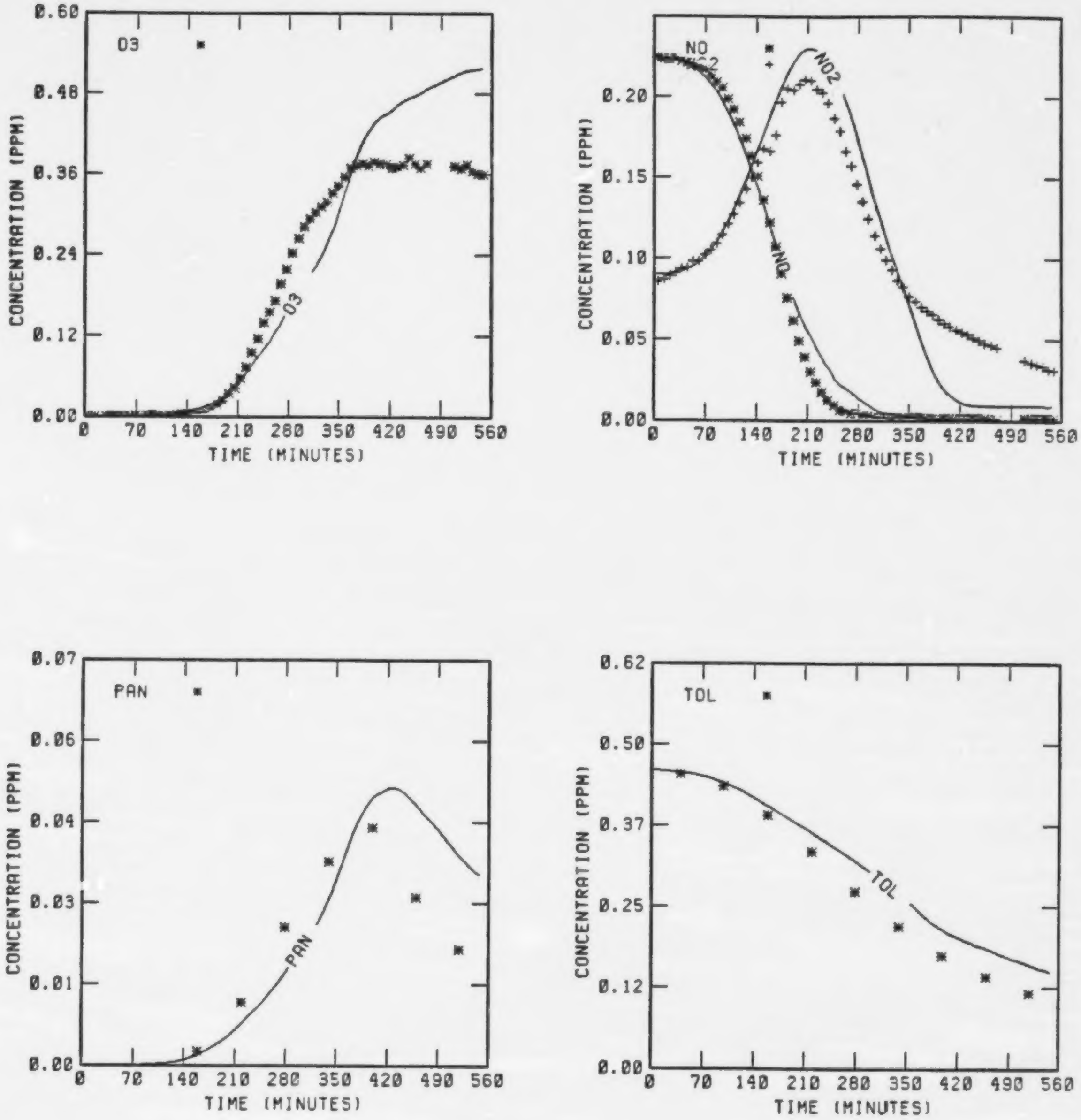

SIMULATION RESULTS FOR
UNCR 81180

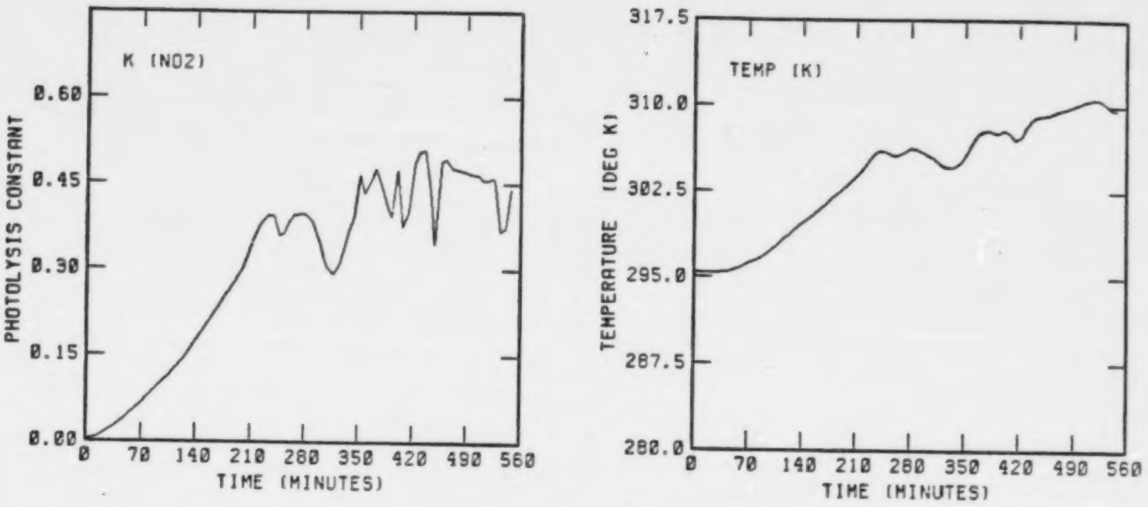

SIMULATION RESULTS FOR
UNCR 81180

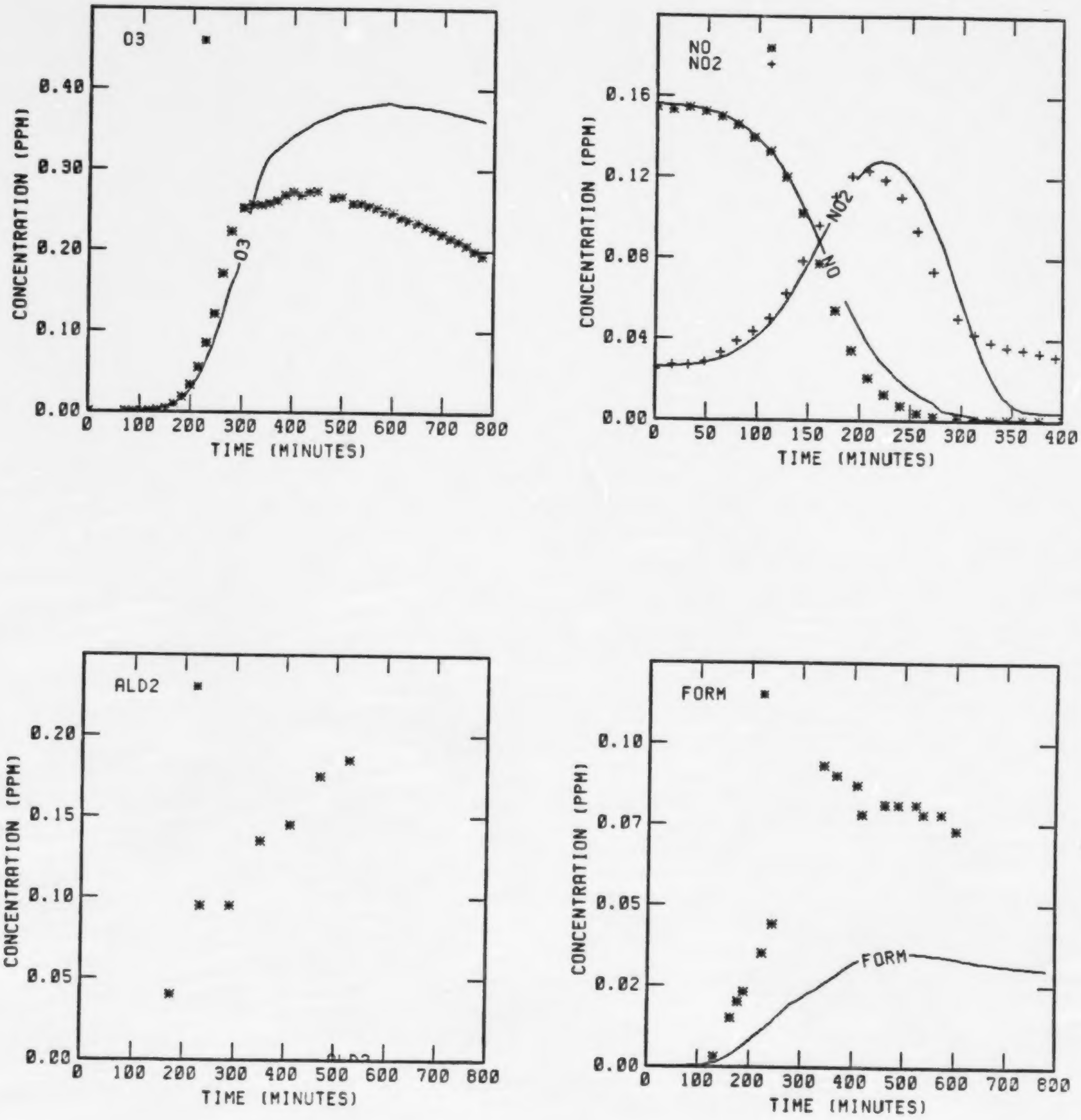

SIMULATION RESULTS FOR
UNCR 73080

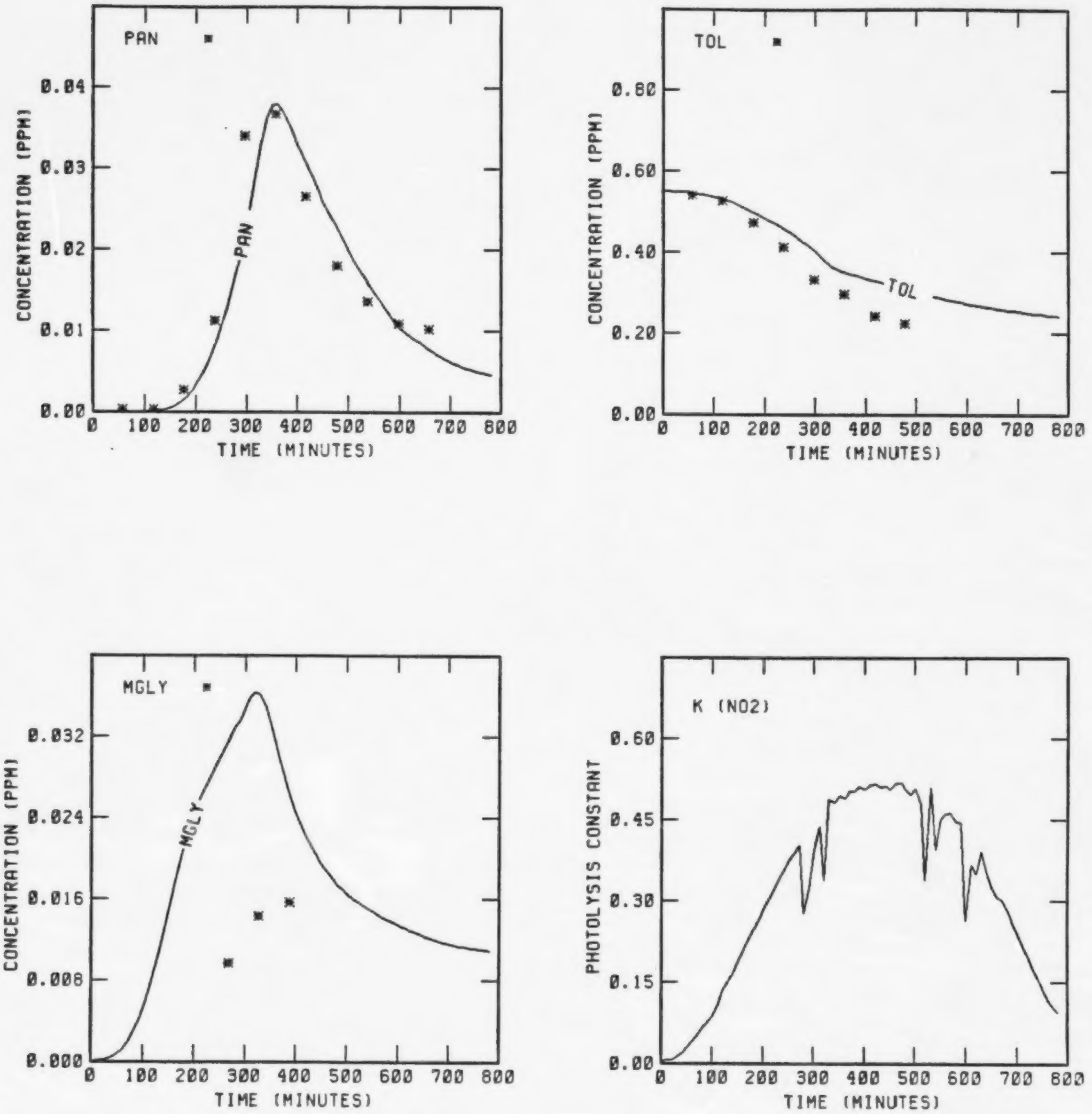

SIMULATION RESULTS FOR
UNCR 73080

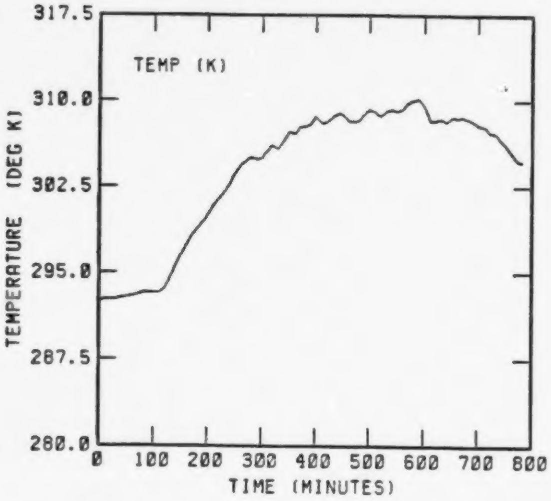

SIMULATION RESULTS FOR
UNCR 73080

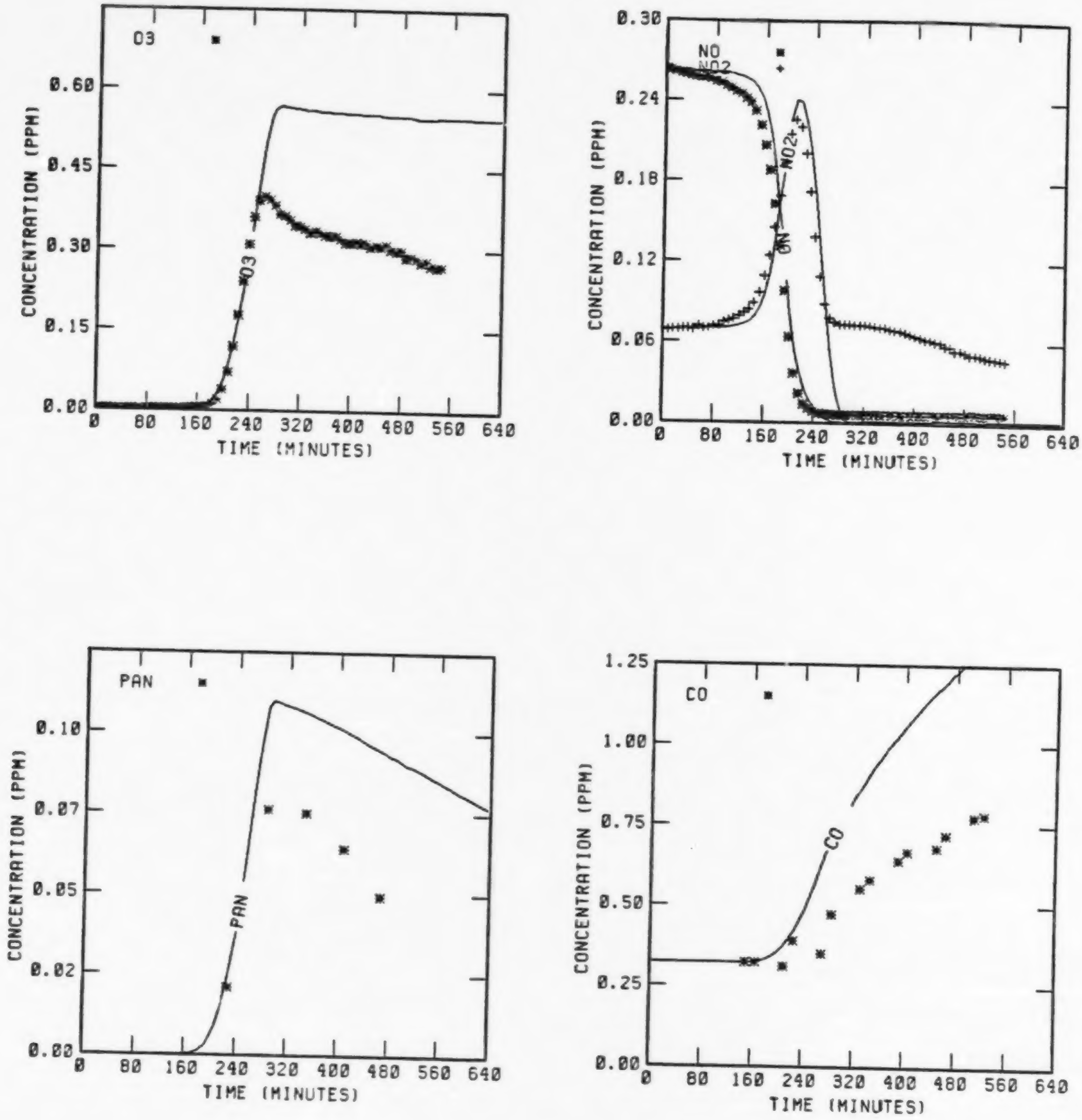

SIMULATION RESULTS FOR
UNCB 62779

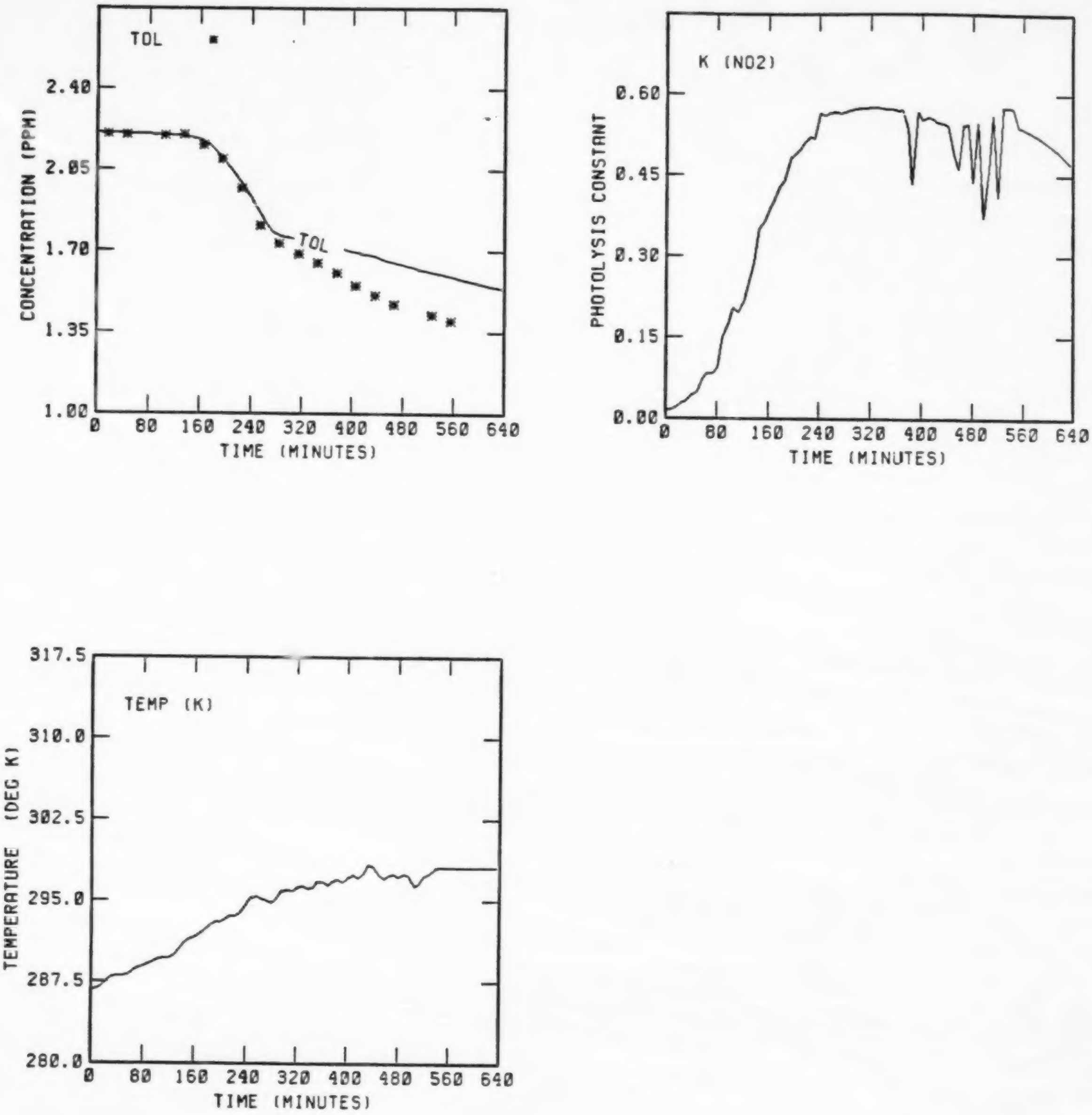

SIMULATION RESULTS FOR
UNCB 62779

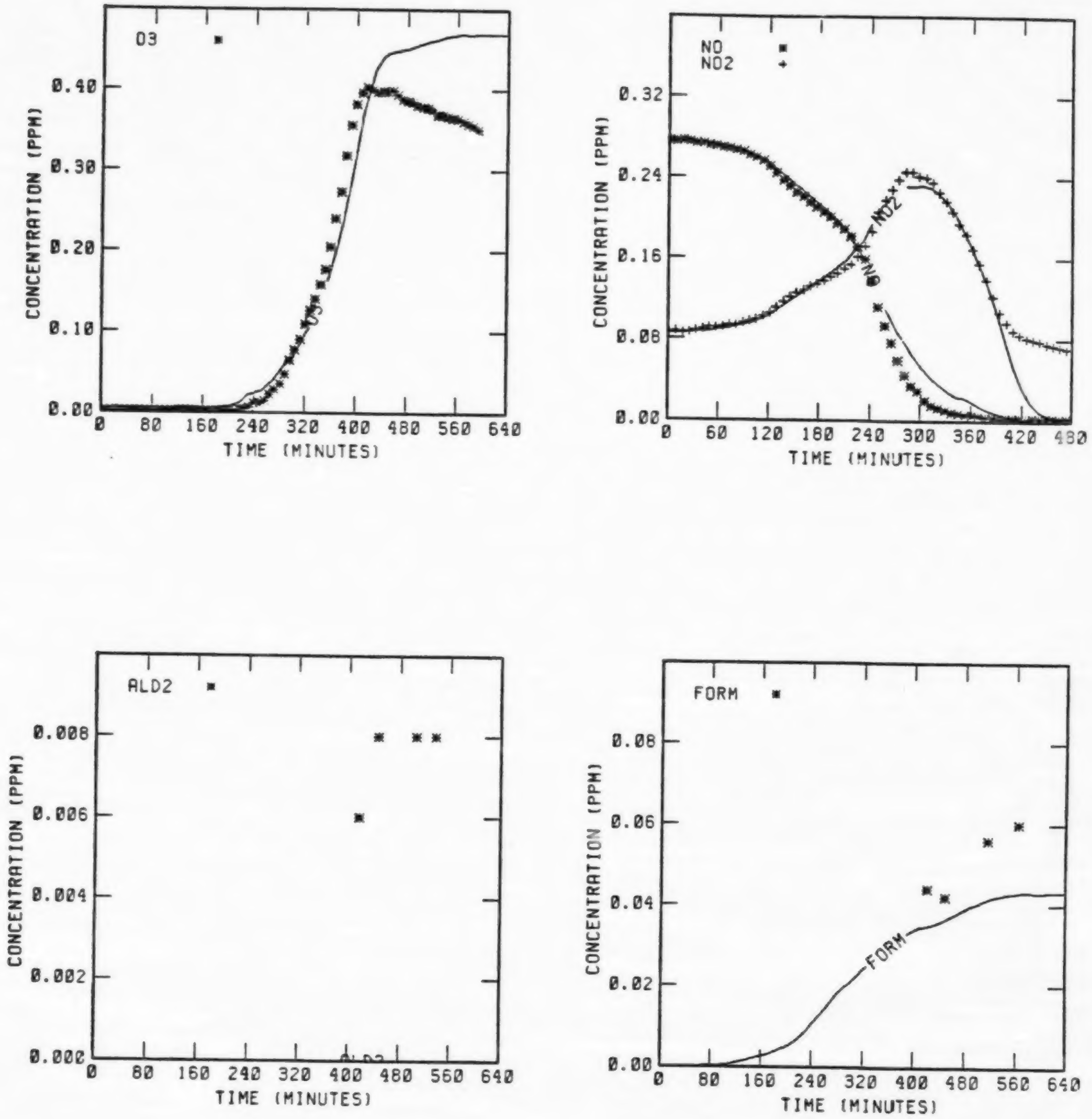

SIMULATION RESULTS FOR
UNCB 81579

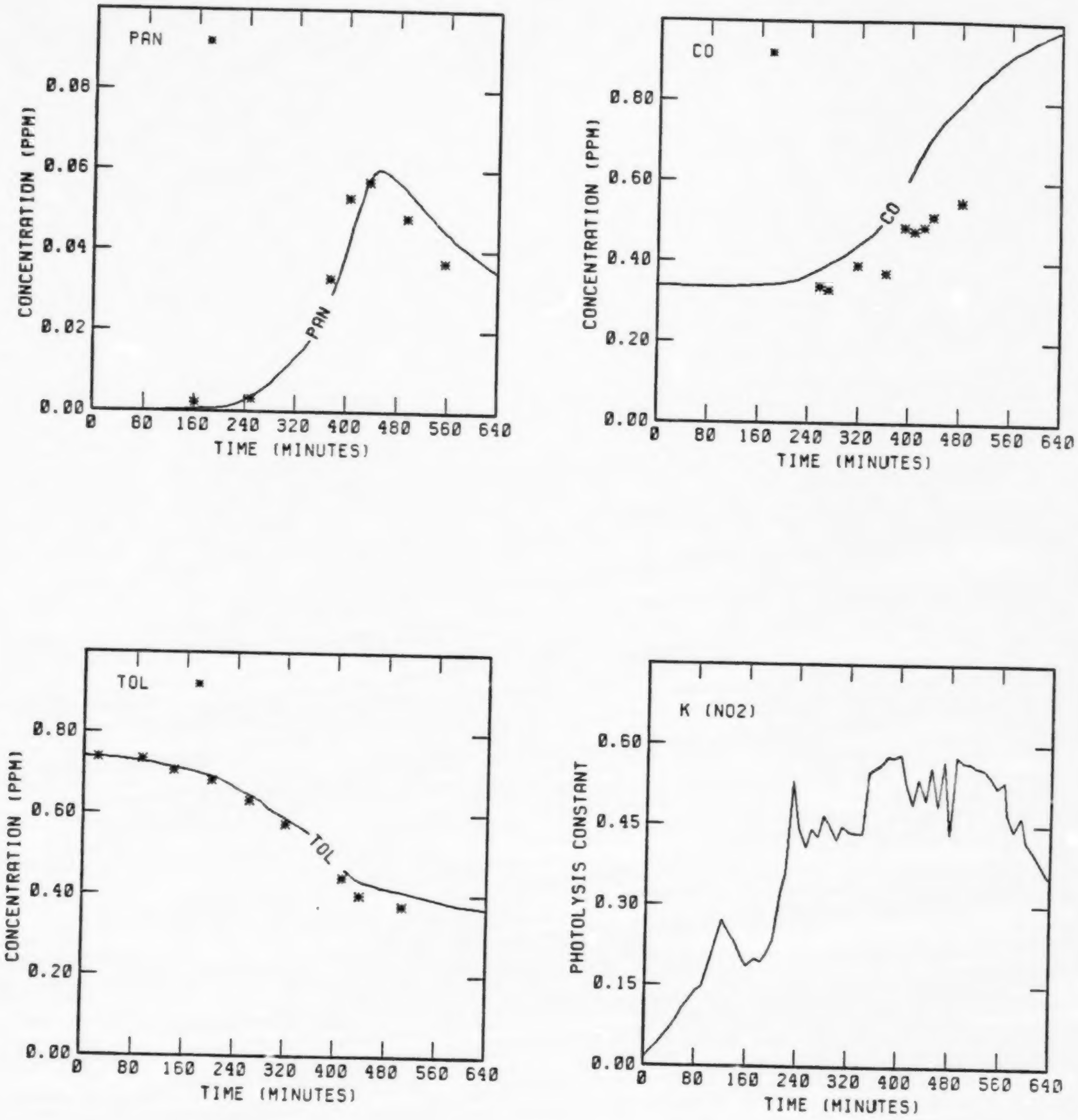

FIGURE . SIMULATION RESULTS FOR
UNCB 81579

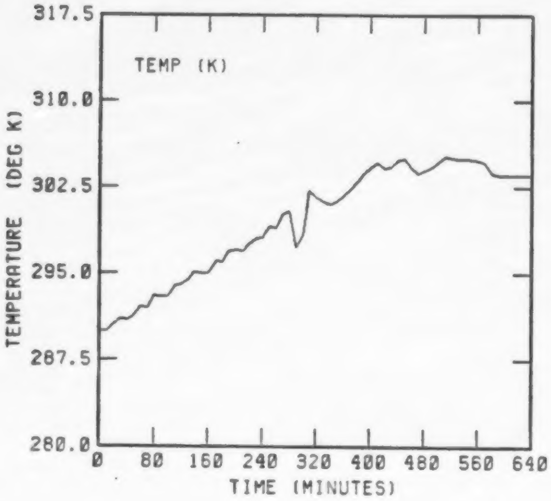

SIMULATION RESULTS FOR
UNCB 81579

M-xylene

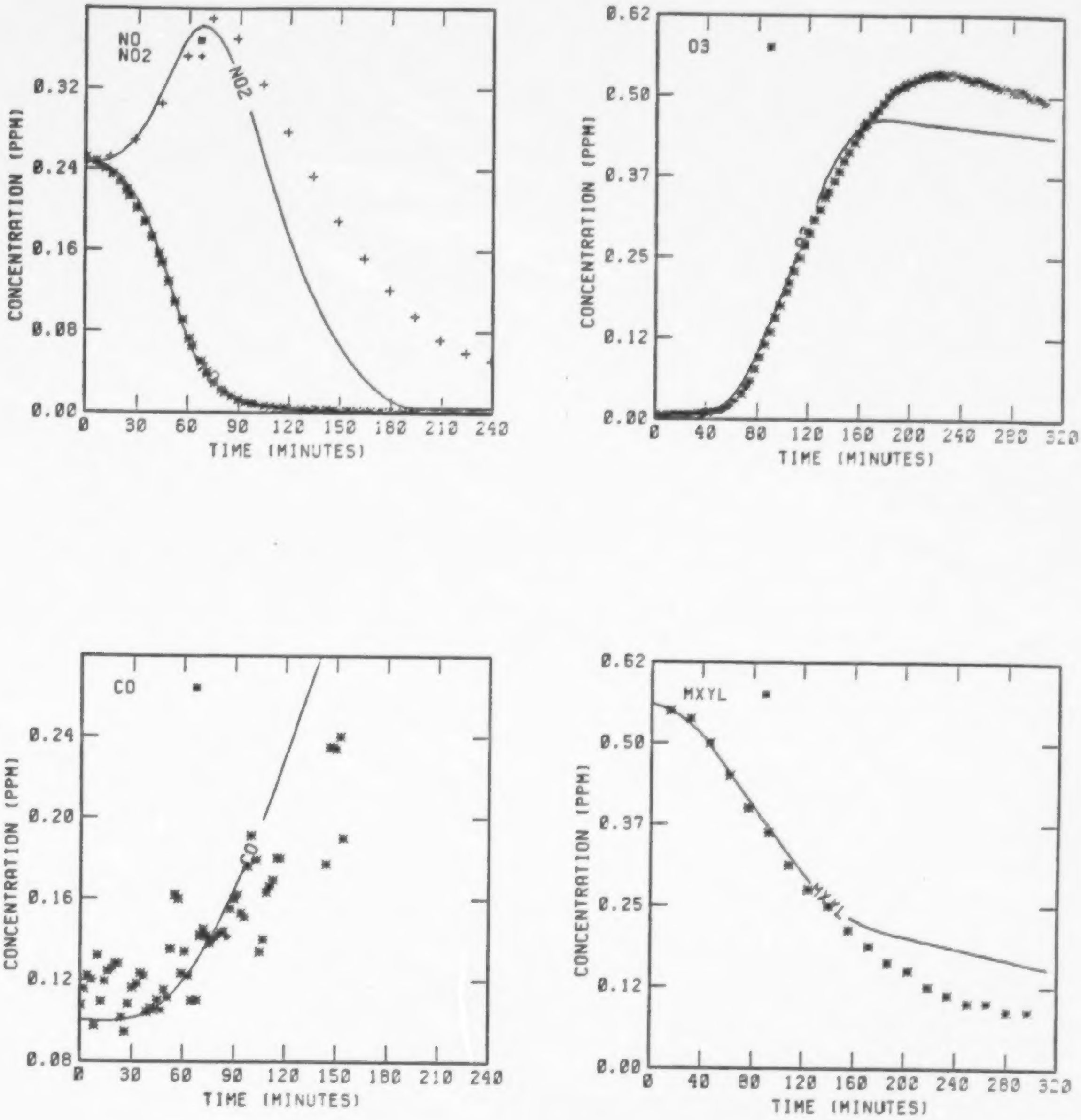

SIMULATION RESULTS FOR
AVOC22

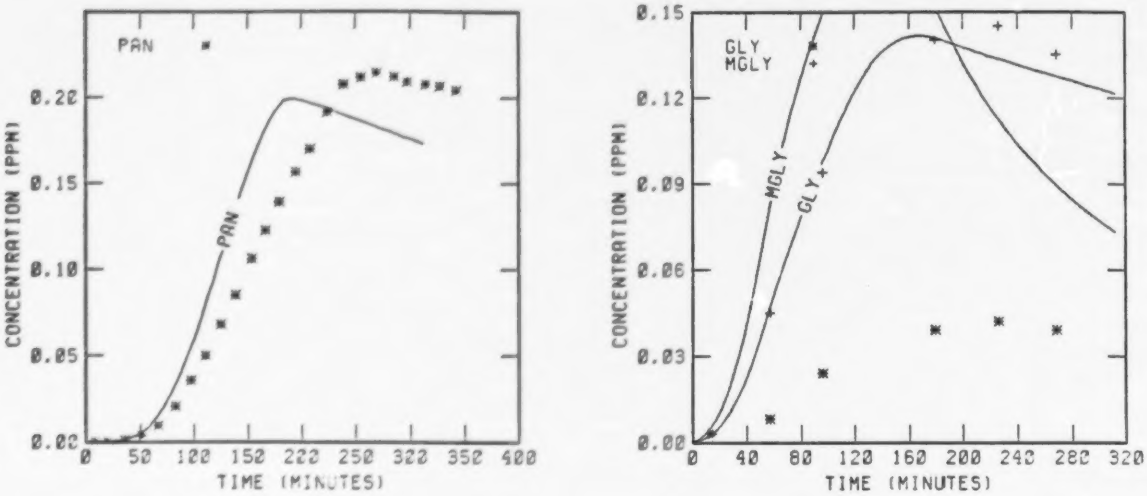

SIMULATION RESULTS FOR
AVOC22

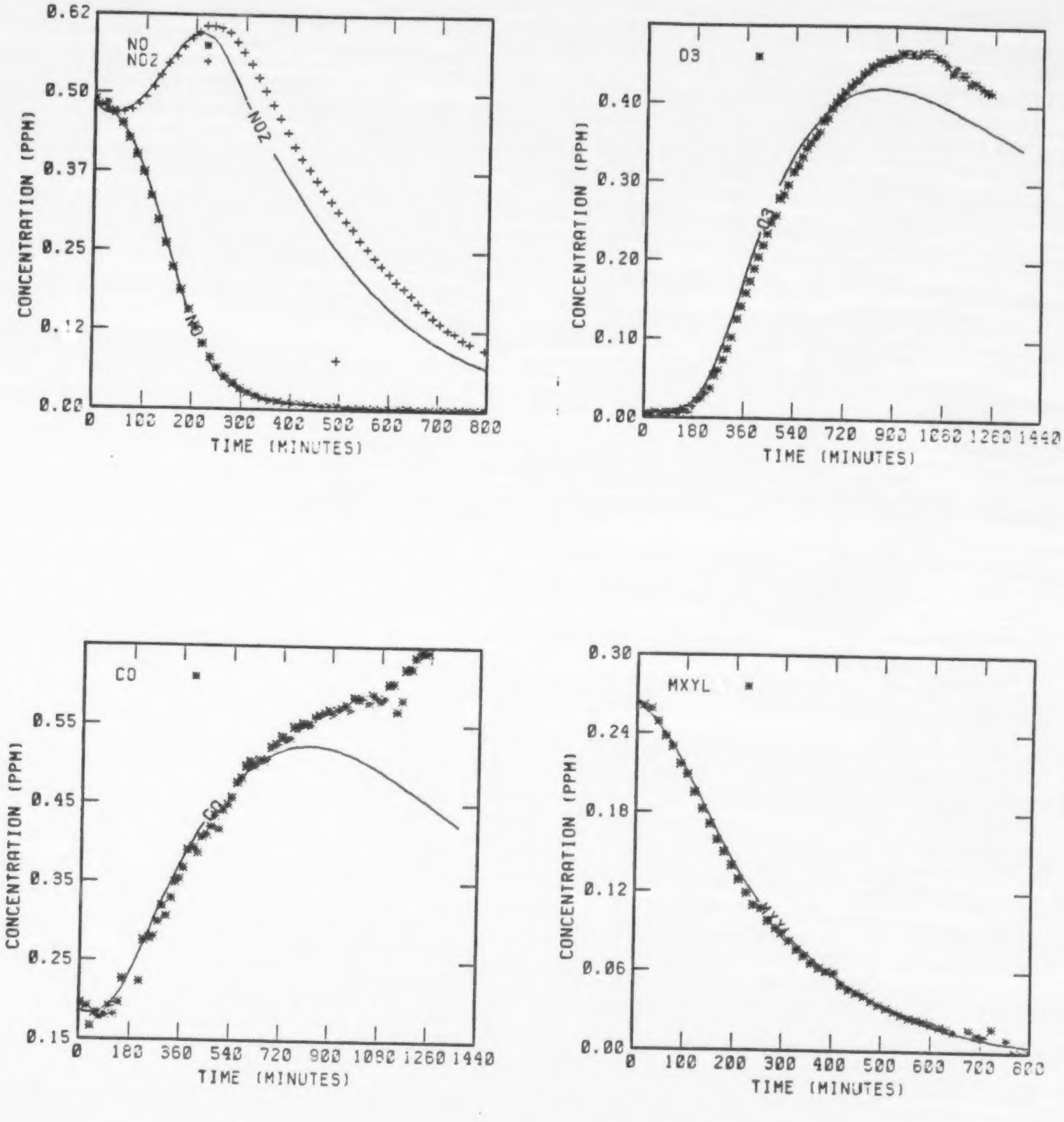

SIMULATION RESULTS FOR
AVOC26

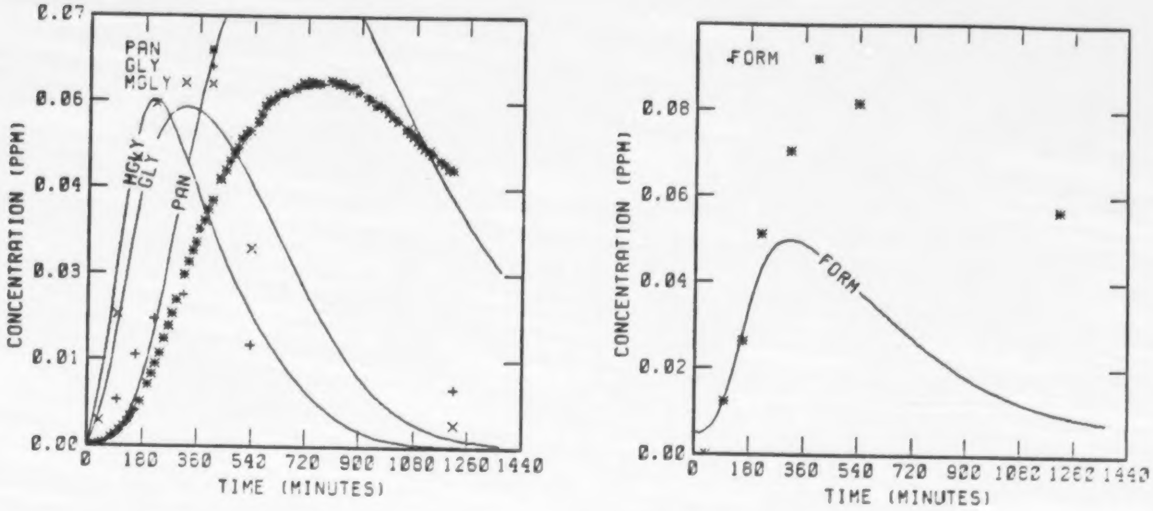

SIMULATION RESULTS FOR
AVOC26

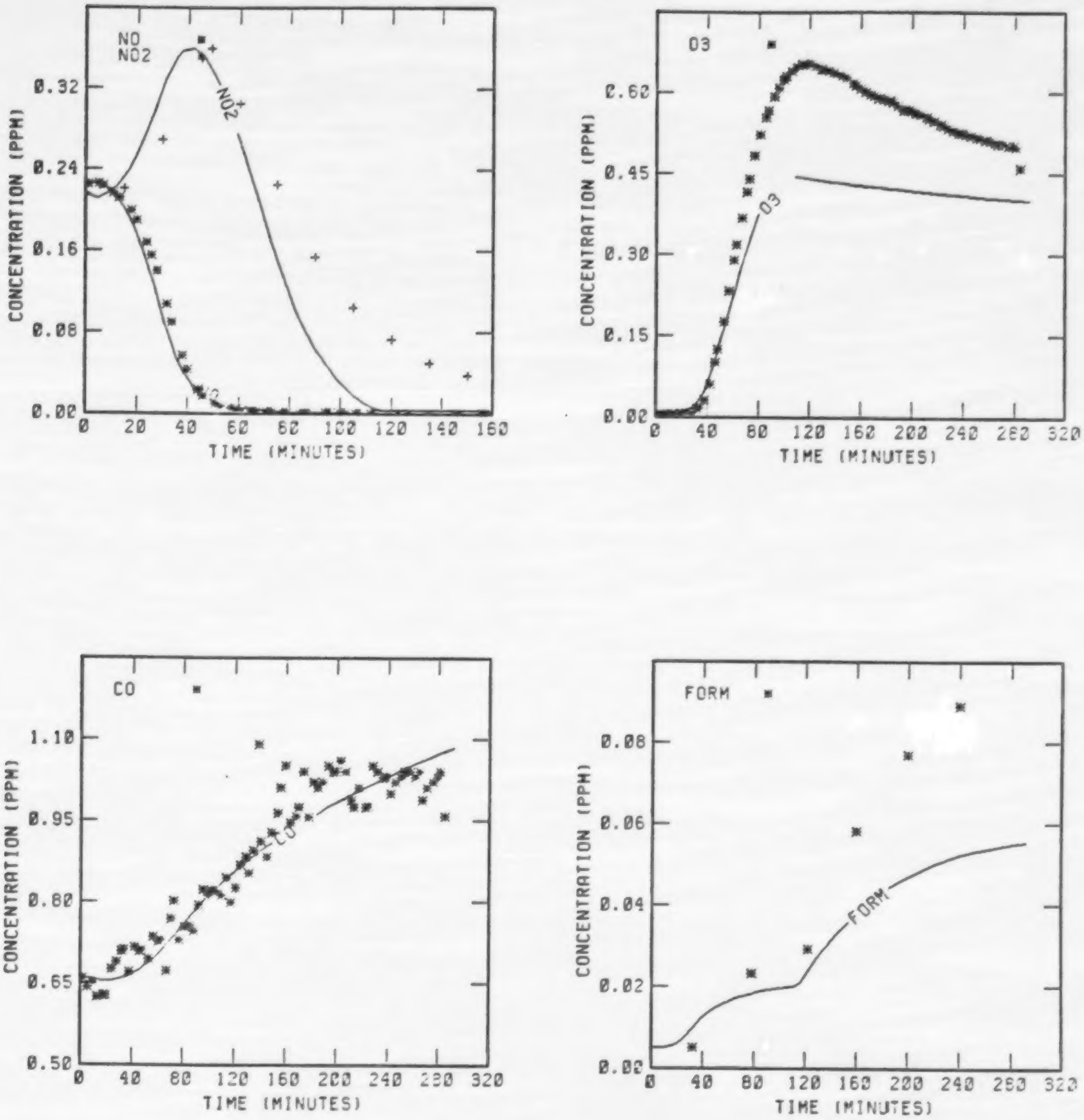

SIMULATION RESULTS FOR
AVOC8

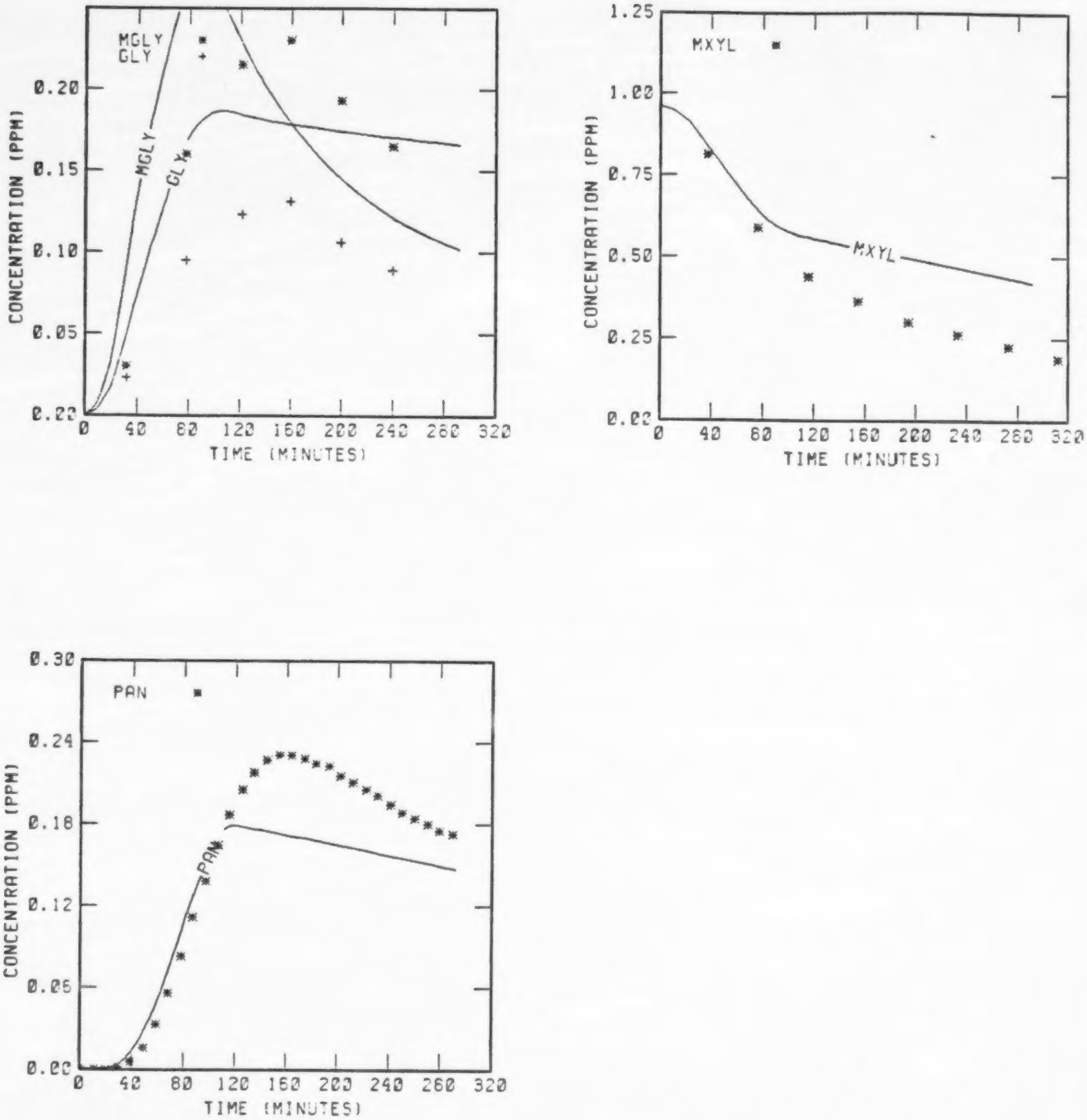

SIMULATION RESULTS FOR
AVOC8

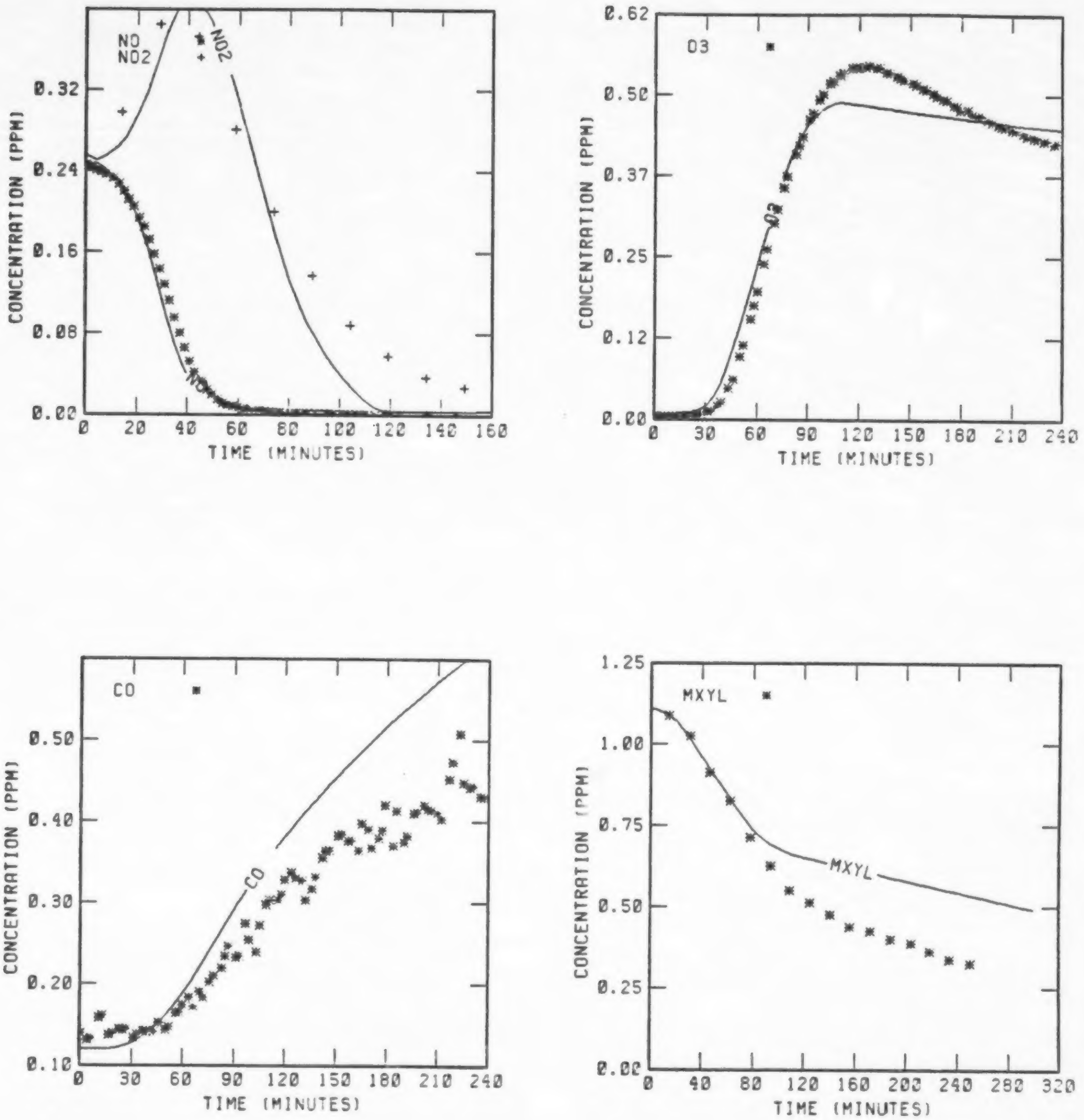

SIMULATION RESULTS FOR
AVOC21

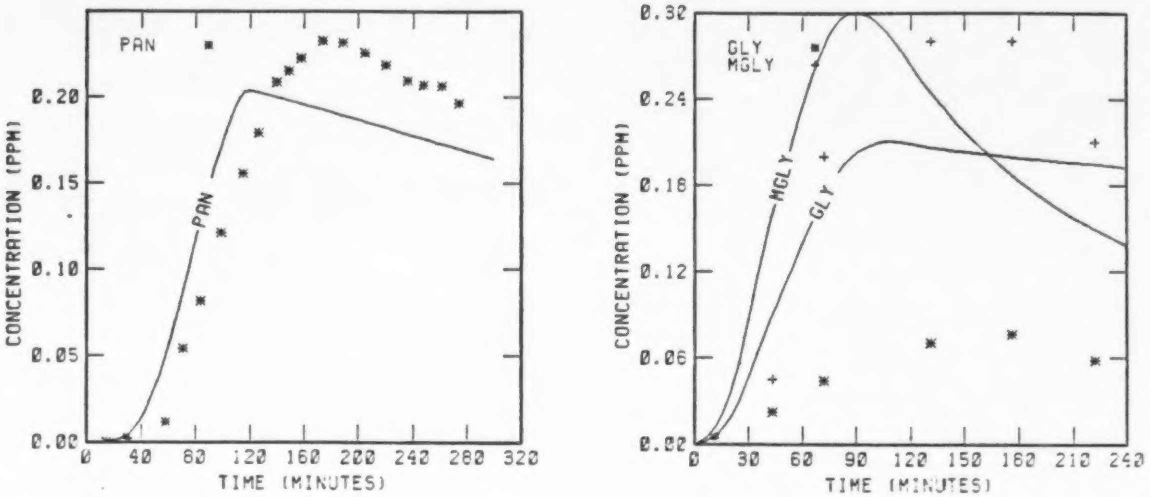

SIMULATION RESULTS FOR
AVOC21

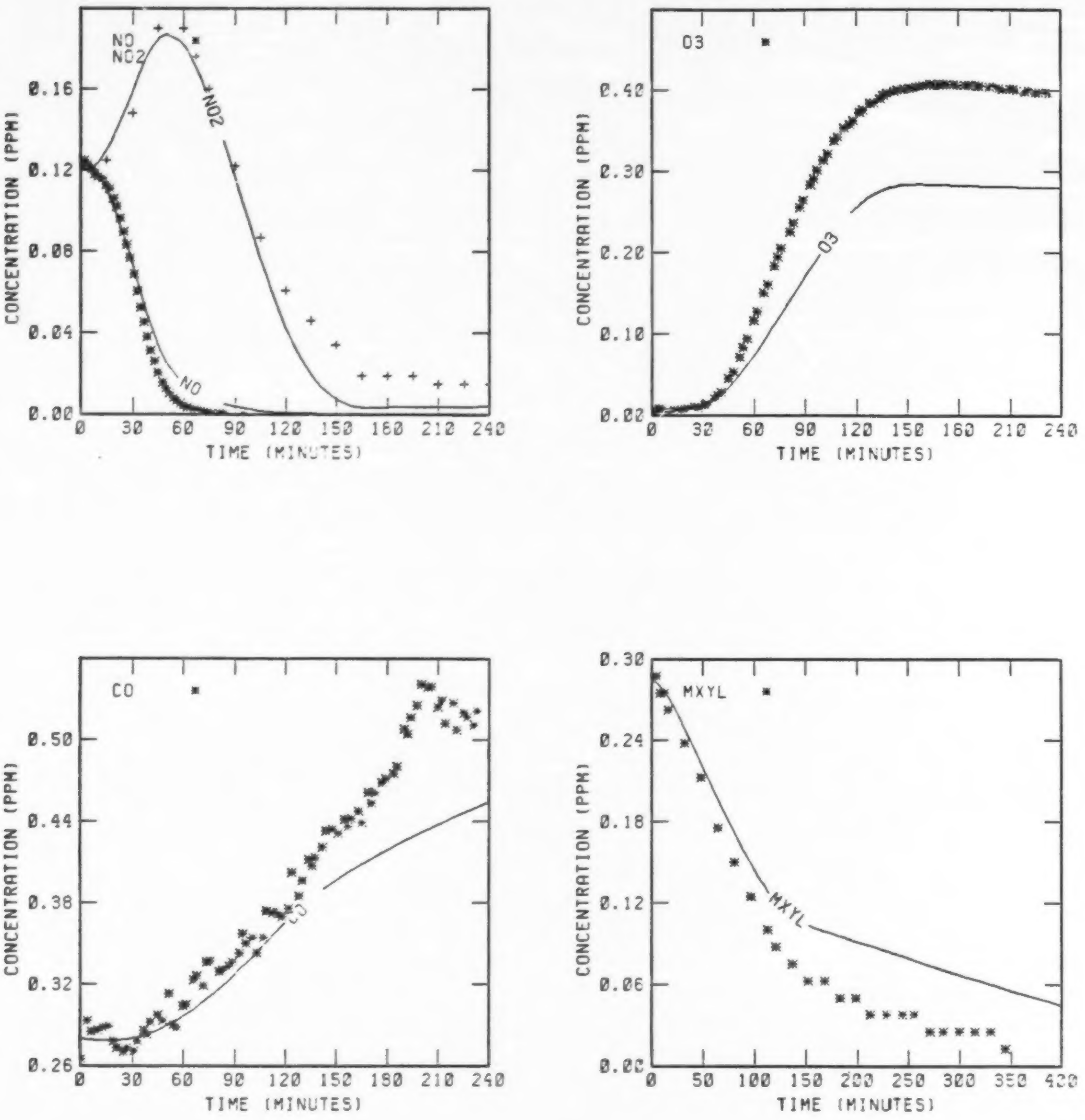

SIMULATION RESULTS FOR
AVOC24

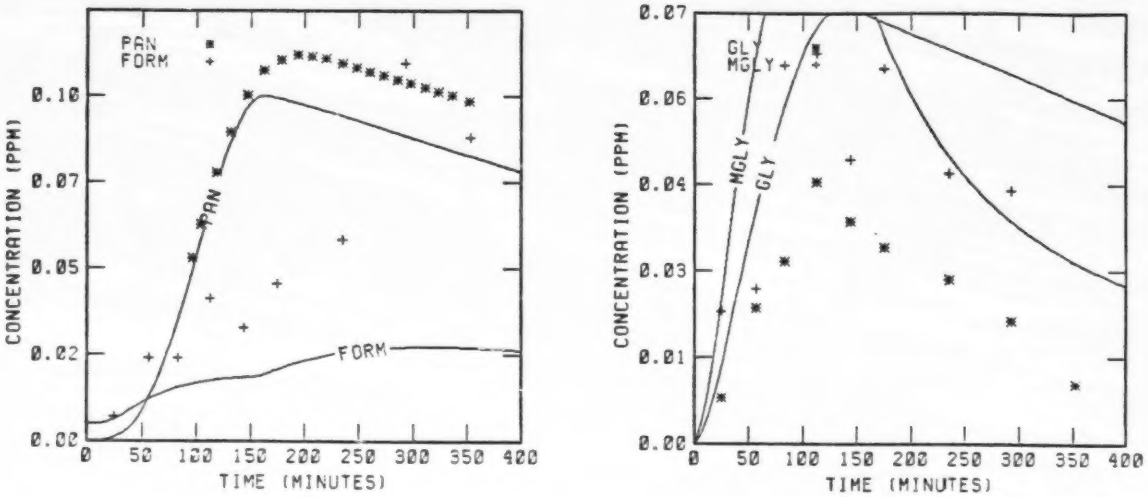

SIMULATION RESULTS FOR
AVOC24